Enhanced Air Transportation Modeling Techniques for Capacity Problems

Thomas Louis Spencer

Dissertation submitted to the Faculty of the
Virginia Polytechnic Institute and State University
in partial fulfillment of the requirements for the degree of

Doctor of Philosophy
in
Civil Engineering

Antonio A. Trani, Chair
Montasir M. Abbas
Barbara M. P. Fraticelli
Pamela M. Murray-Tuite

August 1, 2016
Blacksburg, Virginia

Keywords: Air Transportation, Runway Occupancy Time, Bayesian Inference, Airport Capacity, Hierarchical Regression, Flight Planning, Unmanned Aerial Systems

Enhanced Air Transportation Modeling Techniques for Capacity Problems

Thomas Louis Spencer

(ABSTRACT)

Effective and efficient air transportation systems are crucial to a nation's economy and connectedness. These systems involve capital-intensive facilities and equipment and move millions of people and tonnes of freight every day. As air traffic has continued to increase, the systems necessary to ensure safe and efficient operation will continue to grow more and more complex. Hence, it is imperative that air transport analysts are equipped with the best tools to properly predict and respond to expected air transportation operations. This dissertation aims to improve on those tools currently available to air transportation analysts, while offering new ones.

Specifically, this thesis will offer the following: 1) A model for predicting arrival runway occupancy times (AROT); 2) a model for predicting departure runway occupancy times (DROT); and 3) a flight planning model. This thesis will also offer an exploration of the uses of unmanned aerial vehicles for providing wireless communications services.

For the predictive models of AROT and DROT, we fit hierarchical Bayesian regression models to the data, grouped by aircraft type using airport physical and aircraft operational parameters as the regressors. Recognizing that many existing air transportation models require distributions of AROT and DROT, Bayesian methods are preferred since their output are distributions that can be directly inputted into air transportation modeling programs. Additionally, we exhibit how analysts will be able to decouple AROT and DROT predictions from the traditional 4 or 5 groupings of aircraft currently in use.

Lastly, for the flight planning model, we present a 2-D model using presently available wind data that provides wind-optimal flight routings. We improve over current models by allowing free-flight unconnected to pre-existing airways and by offering finer resolutions over the current 2.5 degree norm.

This work was generously supported by the Federal Aviation Administration (FAA) and the National Aeronautics and Space Administration (NASA).

This work made use of NCEP Reanalysis data provided by the NOAA/OAR/ESRL PSD, Boulder, Colorado, USA from their website at http://www.esrl.noaa.gov/psd/.

Dedication

I am happy to dedicate this dissertation to my grandparents, Louise and Jerry Riley and Laura Lee and Thomas Spencer, who were unable to be with me as I completed this work. They each gave so much to secure a future that they would not see and I hope this dissertation would make them proud.

Acknowledgments

Though the PhD is typically a solitary endeavor, I am so grateful that I was fortunate to have never been alone during my program. I want to thank God for the incredible opportunity to be able to study a subject I love at a place I love with such amazing people. I will never know why He chose to bless me so fully but I am forever thankful and grateful.

I would also like to acknowledge those who supported, encouraged, and fortified me throughout my four years at Virginia Tech. Please know that I am deeply grateful for all that you have done and continue to do.

Specifically, I want to express my heartfelt gratitude to Dr. Antonio Trani for his invaluable guidance and faith in me during my program. His awesome knowledge and command of the field is equally matched by his patience and genuine kindness. Truly, Dr. Trani represents the ideal of what an advisor should be and I am forever grateful for his guidance and mentorship. I also want to thank my committee members: Dr. Montasir Abbas, Dr. Barbara Fraticelli, and Dr. Pamela Murray-Tuite. The constructive comments and strong encouragement they provided during this process was indispensable and helped in strengthening my final product. I have learned so much from each of them.

I also want to acknowledge all of the friends I made during my time at Virginia Tech: Mani Venkat Sai Kumar Ala, Osama Alsalous, Eugene Amarh, Moises Bobadilla, Craig Bryant, Edwin Freire Burgos, Adil Bari Cheema, Saloni Chirania, Andy Edwardes, Şafak Ergişli, Dr. Zheng Fan, Razieh Farzad, Christian Figueroa, Aldo Gargiulo, Aswin Gunnam, Arman Izadi, Kianoush Kompany, Dr. Tao Li, Clara Liranzo, Yanqi Liang, Milko Maykowskyj, Giulio Menciotti, Fabrizio Meroni, Navid Mirmohammadsadeghi, Nadezhda Morozova, Alexandra Noble, Dr. SungKwan Ku, Freddie Salado Martinez, Rahul Padalkar, Carlos Mantilla Pena, Davide Pu, Julio Roa, Alejandra Rosado, Dr. John Sangster, Jorge Alejandro Schmidt,

Shivesh Shrestha, Nida Syed, Nikolaos Tsikas, Qichao Wang, Nazana Weeks, Donia Zaheri, Yang Zhang and so many others. Each of these folks made my Virginia Tech experience so vibrant and fun.

I also want to thank Marie-Dumesle Mercier, Esq. Words cannot do justice to how much you mean to me, nor can they adequately describe the positive impact you have had on my life. I love you dearly and thank you for your love before, during, and beyond my program.

Finally, this section would not be complete without acknowledging my family, especially my parents. To my father, Dr. Michael G. Spencer, thank you for demonstrating a standard of excellence and professionalism in your work and unbridled passion for something you love. You gave me a great model for being a high-performing, self-aware, and intelligent engineer and proud Black man. To my mother, Linda L. Riley, Esq., you have been my model of indomitable spirit and strength through life's challenges and have demonstrated the power of undying faith and trust in God in the face of adversity. You have also shown me how one loves unconditionally. Thank you for your undying support through everything and for always being there to cheer me on.

To everyone, in short...THANK YOU!

Contents

List of Figures

List of Tables

Abbreviations & Acronyms

A306 Airbus A300-600.

A319 Airbus A319-100.

A320 Airbus A320-200.

A321 Airbus A321-200.

A332 Airbus A330-200.

A333 Airbus A330-300.

A343 Airbus A340-300.

A346 Airbus A340-600.

A388 Airbus A380-800.

ADS-B Automatic Dependent Surveillance - Broadcast.

ANOMS Airport Noise and Operations Monitoring System.

AROT Arrival Runway Occupancy Time.

ASDE-X Airport Surface Detection Equipment, Model X.

ASOS Automated Surface Observing System.

ASPM Aviation System Performance Metrics.

AT72 Aerer da Trasporto Regionale/Avions de transport régional ATR-72.

ATC Air Traffic Control.

B190 Beechcraft 1900.

B350 Beechcraft 350 Super King Air.

B712 Boeing 712-200.

B732 Boeing 737-200.

B733 Boeing 737-300.

B734 Boeing 737-400.

B735 Boeing 737-500.

B736 Boeing 737-600.

B737 Boeing 737-700.

B738 Boeing 737-800.

B739 Boeing 737-900.

B744 Boeing 747-400.

B748 Boeing 747-8.

B752 Boeing 757-200.

B753 Boeing 757-300.

B762 Boeing 767-200.

B763 Boeing 767-300.

B764 Boeing 767-400.

B772 Boeing 777-200.

B77L Boeing 777-200LR.

B77W Boeing 777-300ER.

B788 Boeing 787-8.

BADA Base of Aircraft Data.

BE20 Beechcraft Beech 200 Super King Air.

BE40 Beechcraft Beech 400 Beechjet.

BE99 Beechcraft Beech 99 Airliner.

BE9L Beechcraft Beech 90 King Air.

C172 Cessna 172 Skyhawk.

C208 Cessna 208 Grand Caravan.

C402 Cessna 402 Businessliner.

C525 Cessna 525 CitationJet.

C550 Cessna 550 Citation 2.

C560 Cessna 560 Citation 5 Ultra.

C56X Cessna 560X Citation Excel.

C680 Cessna 680 Citation Sovereign.

C750 Cessna 750 Citation X.

CL30 Bombardier Challenger 300.

CL60 Bombardier Challenger 600.

CRJ2 Bombardier CRJ-200.

CRJ7 Bombardier CRJ-700.

CRJ9 Bombardier CRJ-900.

DC10 Douglas DC-10.

DC95 Douglas DC-9-50.

DH8A de Havilland Canada DHC-8-100.

DH8B de Havilland Canada DHC-8-200.

DH8C de Havilland Canada DHC-8-300.

DH8D de Havilland Canada DHC-8-400.

DOT U.S. Department of Transportation.

DROT Departure Runway Occupancy Time.

E120 Embraer EMB-120 Brasilia.

E135 Embraer ERJ-135.

E145 Embraer ERJ-145.

E170 Embraer ERJ-170.

E190 Embraer ERJ-190.

E45X Embraer EMB-145XR.

E50P Embraer EMB-500.

E55P Embraer EMB-505 Phenom 300.

F2TH Dassault Falcon 2000.

F900 Dassault Falcon 900.

FAA Federal Aviation Administration.

FAR 77 Title 14, Chapter 1, Subchapter E, Part 77 of the Federal Code.

GALX IAI Gulfstream G200.

GLEX Bombardier Global Express.

GLF4 Gulfstream IV.

GLF5 Gulfstream V.

GPS Global Positioning System.

H25B British Aerospace 125-700/800.

HALE High Altitude, Long Endurance.

LJ35 Learjet 35.

LJ45 Learjet 45.

LJ60 Learjet 60.

MCMC Markov chain Monte Carlo.

MD11 McDonnell Douglas MD11.

MD82 McDonnell Douglas MD82.

MD83 McDonnell Douglas MD83.

MD88 McDonnell Douglas MD88.

MD90 McDonnell Douglas MD90.

NAS National Airspace System.

NASA National Aeronautics and Space Administration.

NASR National Airspace System Resource.

NFDC National Flight Data Center.

PA31 Piper PA-31.

PC12 Pilatus PC-12 Eagle.

RECAT Wake Turbulence Recategorization.

RNP Required Navigation Performance.

ROT Runway Occupancy Time.

SF34 Saab 340.

SH36 Short Brothers Short SD3-360.

SR22 Cirrus SR-22.

SW4 Fairchild Swearingen Metroliner.

UAS Unmanned Aerial Systems.

Chapter 1

Introduction

1.1 Background

The development and expansion of air transportation systems has ushered in previously unparalleled levels of economic, social and cultural connectivity worldwide. Air transportation allows for the rapid global movement of people between cities and nations and goods between markets. As such, due to the jobs created and the economic growth spurred, air transportation systems are vital to the prosperity and growth of nations.

Demand for air transportation continues to grow unabated, despite the significant shocks of terrorism, economic recession, spikes in oil prices and airline financial weakness. As illustrated in Figure 1.1, world annual traffic has increased 85% since the September 11^{th} terrorist attacks (ICAO, 2015). Furthermore, global air passenger numbers are estimated to more than double from around 3.5 billion to 7.3 billion owing to an estimated annual growth rate of 4.1% through 2034 (IATA, 2014).

Capital-intensive aircraft, substantial airport infrastructure and millions of employees comprise air transportation systems worldwide and managers and analysts are continually compelled to seek new efficiencies in system operations. To this end, robust modeling and simulation capabilities are essential in supporting both improvements to and expansion of air transportation systems. Simulation and modeling allows air transport managers and stakeholders to measure systemwide behavior, evaluate the effectiveness of proposed

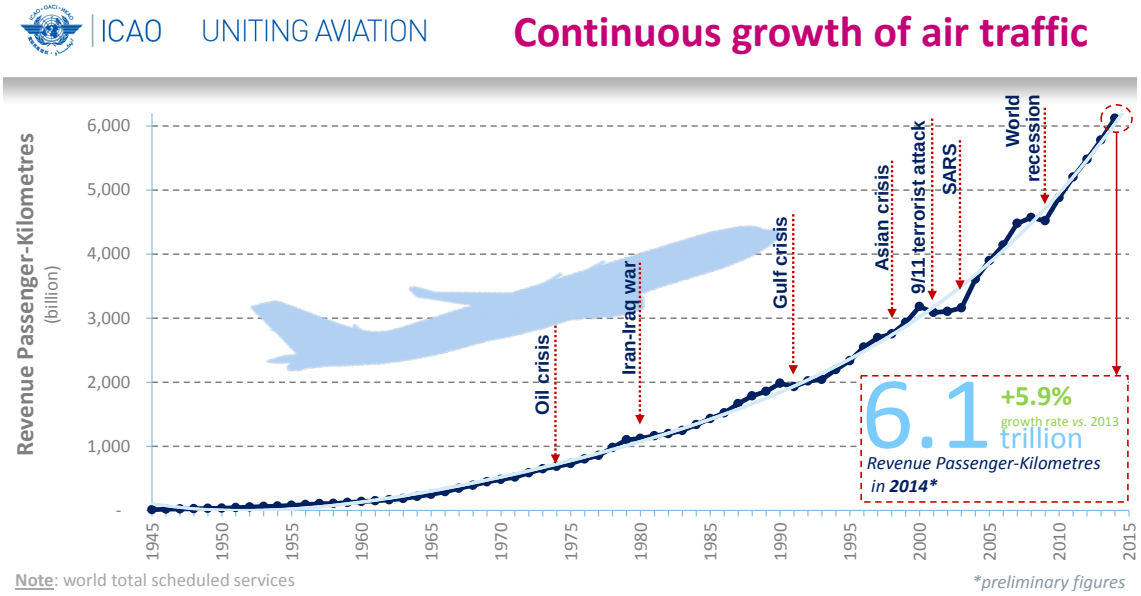

Figure 1.1: Continuous Growth of Air Traffic. Source: (ICAO, 2015)

operational changes and adjustments and provide realistic estimates of the associated costs incurred through changes to the air transportation system.

Generally, the time horizons in air transportation system modeling efforts extend far into the future. This is oftentimes necessary, given that air fleets generally change over periods of months and air transportation infrastructure is added and expanded over periods of years. Additionally, analysts must consider socioeconomic changes in the flying public that might directly affect air transportation demand. However, analysts cannot preclude changes and shocks to air transportation systems that have immediate effect and require immediate attention. Terrorist incidents such as the Pan Am 103 bombing and the September 11$^{\text{th}}$ attacks have resulted in swift changes to the air transportation security operating regime. Weather and environmental events such as the 2010 Eyjafjallajökull volcano eruption have resulted in severe worldwide disruptions to air travel. Geopolitical changes can also be fast-moving and disruptive to air transportation as can global health challenges such as the SARS and avian bird flu pandemics. Thus, simulation and modeling efforts of air transportation systems must be not only effective over long-time horizons but also flexible to account for events having more immediate effects.

The variety of demands placed on air transportation analysts supports the argument made by the Committee on Aeronautics Research and Technology for Vision 2050 that:

> modeling of the air transportation system is best accomplished by a suite of system models. (Transportation Research Board and National Research Council, 2003).

These models would range from detailed, long-run-time system component level models to fast-time systemwide models. Though self-contained, these models should provide and accept input from other available models in order to more completely describe the air transportation system (Transportation Research Board and National Research Council, 2003).

1.2 Research Motivation

Air transportation systems are being modified and redeveloped to allow for new levels of complexity and efficiency. Currently, the FAA is in the midst of rolling out the Next Generation Air Transportation System (NextGen), which is a set of evolving Air Traffic Control (ATC) and aircraft navigation technologies designed to move the American ATC system from a ground-based system to a satellite-based system. The development of NextGen has resulted in the need to estimate the capacity benefits expected from the program in order to justify the estimated $40 billion dollar cost (Carey, 2013) of full implementation.

Air transportation operating paradigms also evolve with changing aircraft fleet mixes, aircraft sizes, and improved surveillance technology. One significant change in progress is the decade-long Wake Turbulence Recategorization (RECAT) joint effort by the U.S. Federal Aviation Administration (FAA), the U.S. Department of Transportation (DOT) and EUROCONTROL. The RECAT refers to the move from five wake turbulence separation categories to six, which increases potential wake combinations from 25 to 36 and will directly impact runway demand analyses. Along with the RECAT, the FAA is also currently implementing Automatic Dependent Surveillance - Broadcast (ADS-B), which refers to a satellite-based aircraft surveillance system based on Global Positioning System (GPS) technology (FAA, 2015). When fully implemented, ADS-B will allow for reduced

separation distances and reduced reliance upon preset airways for flight navigation and ATC.

Finally, air transportation systems are being adapted to make use of an explosion of previously unavailable data and a marked increase in available computational power. Analysts now have access to detailed information on hourly airport throughput rates through the FAA Aviation System Performance Metrics (ASPM) database. Additionally, radar data are freely available from the FAA, noise data is available through Airport Noise and Operations Monitoring System (ANOMS) installations and ground movement data are provided through Airport Surface Detection Equipment, Model X (ASDE-X) installations at many airports.

Given the advances in technology, the increased quality and quantity of air transportation data available to researchers, new operational paradigms and increased available computational power, new simulation models and methods must be developed and existing simulation models must be advanced to meet the new demands of air transportation systems.

1.3 Objective

The purpose of this research effort is to identify areas of improvement in existing models, to develop and demonstrate new models for air transportation analyses, and to consider potential air transportation related issues and objectives that might be addressed with future technologies and methodologies. Three areas of research are considered: 1) Runway Capacity, 2) Flight Planning and 3) Unmanned Aerial Vehicles. Four computer models have been developed as a result of this research utilizing MATLAB. These models are 1) a model predicting Arrival Runway Occupancy Time (AROT) by aircraft type and airport physical parameters, 2) a model predicting Departure Runway Occupancy Time (DROT) by aircraft type and airport physical parameters, 3) a model predicting departure take-off roll distance by aircraft type and airport physical parameters, and 4) a flight planning model based on the principle of free-flight that can estimate wind-optimal flight routes.

1.4 Organization of the Dissertation

This dissertation will outline the research done and models created using the following structure:

- Chapter 2 provides a brief overview of the Bayesian methodology utilized in forming the models presented.
- Chapter 3 outlines the sources of the data used in this thesis and methods for their extraction.
- Chapter 4 concerns Runway Occupancy Time (ROT). In this chapter, a literature review outlining treatments and usage of runway occupancy time will be presented. Next, an overview of the model form applied will be provided. Finally, the two models developed will be presented.
- Chapter 5 deals with Flight Planning. This chapter will contain a review of the literature concerning flight planning methodology and practice. Next, an overview of the flight planning model will be presented and an simulation of its application is demonstrated.
- Chapter 6 regards an investigation of utilizing unmanned aerial systems for wireless communications applications. Scenarios envisioned will be discussed as well potential operational difficulties and solutions to these difficulties.
- Chapter 7 will conclude this dissertation.

Chapter 2

Bayesian Methodology

This chapter provides a brief overview of the Bayesian methodology utilized in our model production. In forming the predictive regression models, we find that the Bayesian methodology offers a number of advantages over the classical (frequentist) approach, which we outline below.

2.1 Comparison to the Classical Approach

The Bayesian approach provides inferences about parameters θ in terms of probability statements, i.e., Figure 2.1, which are conditional on the observed data. In contrast, a classical inference on a parameter θ will offer a point estimate of the true value of θ along with additional statistics such as the standard error and confidence interval. Visually, the information provided in the Bayesian result is richer. For example, an analyst is able to detect skewness, kurtosis, and multimodality. More fundamentally, the Bayesian result directly describes the variability in the parameter θ given the data. The classical result presumes a fixed parameter θ and describes the variability in the data itself while using this variability to give a sense of the precision of the point estimate of the value of θ.

With regards to forming a predictive model, in the classical approach one would utilize prediction intervals. For a prediction interval, we make the necessary assumptions of normally distributed errors, statistical independence of the errors, homoscedasticity and

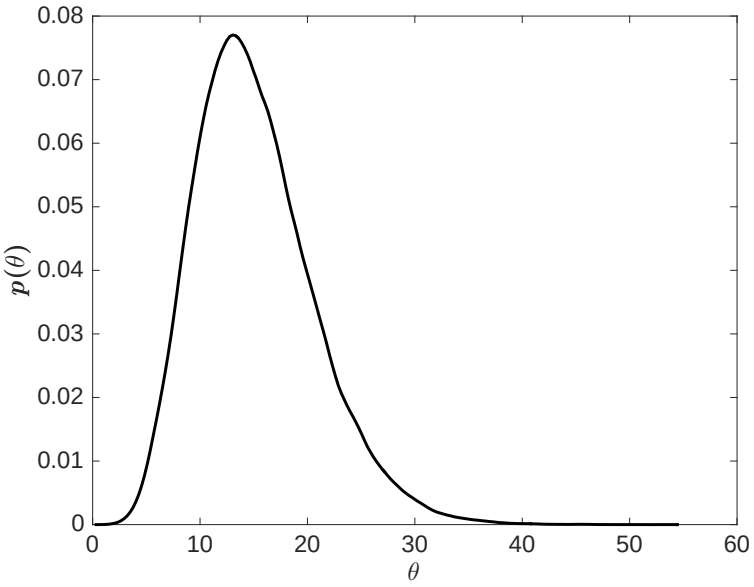

Figure 2.1: Example of a Bayesian Posterior Distribution for a Parameter Inference

linearity of the relationship between the dependent and independent variables. If these assumptions hold, then for a set of p parameter estimates $\hat{\beta}_0, \hat{\beta}_1, \hat{\beta}_2, \ldots, \hat{\beta}_p$ and n observations, the $100\,(1-\alpha)\,\%$ prediction interval for a new prediction y_{new} given a $p \times 1$ vector of new predictors $\mathbf{X}_{new}$ is

$$y_{new} \pm t_{n-p,\alpha/2} \sqrt{MSE \left(1 + \mathbf{X}_{new}^T \left(\mathbf{X}^T \mathbf{X}\right)^{-1} \mathbf{X}_{new}\right)} \tag{2.1}$$

where MSE is the mean squared error given by

$$\frac{\left(\boldsymbol{y} - \mathbf{X}\hat{\boldsymbol{\beta}}\right)^T \left(\boldsymbol{y} - \mathbf{X}\hat{\boldsymbol{\beta}}\right)}{(n-p)} \tag{2.2}$$

Prediction intervals rely on the four aforementioned assumptions being valid, particularly the assumption of homoscedasticity and normality of errors. Should these be violated, the prediction intervals can be misleading. In contrast, the Bayesian approach provides methods to construct predictive distributions for new observations. The performance of these distributions do not rely on assumptions of normality or homoscedasticity and analysts can directly sample from these distributions, once formed.

2.2 Brief Overview of Bayesian Inference

2.2.1 Fundamentals

Probabilities can be considered surrogates for the strength of one's belief or the level of information available about unknown quantities. If given additional relevant information about an unknown quantity, one might update the probability to reflect ones updated beliefs in light of this new information (Kruschke, 2015). The Bayesian approach provides a formal method for updating beliefs given new information by way of Bayes' rule, which is:

$$p(\theta|y) = \frac{p(y|\theta)p(\theta)}{p(y)} \tag{2.3}$$

Bayes' rule consists of four components. For the numerator, we start with the *prior distribution*, $p(\theta)$, which describes through a probability distribution ones pre-existing knowledge, or lack thereof, of the parameter θ. If we consider the prior distribution to encapsulate our initial beliefs about the parameter θ, we can view the *posterior distribution*, $p(\theta|y)$, as our updated beliefs for θ, conditional on having observed the data y. The way in which our beliefs are updated is through the *likelihood function*, $p(y|\theta)$ (Hoff, 2009).

Bayesian inference obeys the likelihood principle, which holds that for inference about θ, after the data y are observed, all relevant information is contained in the likelihood function for the observed y. Additionally, two likelihood functions contain the same information about θ if they are proportional to each other (Berger and Wolpert, 1988).

The denominator term, $p(y)$, represents the probability of having observed one's data y. Also referred to as the marginal distribution of y, this is the integral of the product of $p(y|\theta)\,p(\theta)$ over all possible values of θ within the parameter space Θ. It is given as

$$p(y) = \int_{\Theta} p(y|\theta)p(\theta)d\theta \tag{2.4}$$

Regardless of the value of θ, for a fixed y, $p(y)$ will be constant and can be considered a normalizing constant that ensures that $p(\theta|y)$ is a proper probability density (i.e., sums to 1). Therefore, since we are primarily interested in inference on θ, we can utilize an equivalent

form of Equation 2.3 known as the unnormalized posterior density, which is given as

$$p(\theta|y) \propto p(y|\theta)p(\theta) \tag{2.5}$$

These two equations, equations 2.3 and 2.5, form the fundamental basis of Bayesian inference (Hoff, 2009).

2.2.2 Prediction

Bayesian inference contains two predictive distributions for making predictive inferences. The *prior predictive distribution* describes the distribution of unknown but observable data y before the actual data are observed. To obtain the prior predictive distribution, we integrate the joint probability distribution of y and θ, $p(y, \theta)$, over all possible values of θ as illustrated below.

$$p(y) = \int_{\Theta} p(y, \theta) d\theta \tag{2.6}$$

Recognizing that the joint distribution of y and θ can be written as

$$p(y, \theta) = p(y|\theta)p(\theta) \tag{2.7}$$

we see that the prior predictive distribution is equal to the marginal distribution of y (Hoff, 2009).

The *posterior predictive distribution* refers to the distribution of unknown but observable data $\tilde{y}$ conditional on having already observed your dataset y. We form the posterior predictive distribution by integrating the joint probability density of $\tilde{y}$ and θ, conditional on the observed data y, over θ as follows.

$$p(\tilde{y}|y) = \int p(\tilde{y}, \theta|y) d\theta \tag{2.8}$$

Rewriting $p(\tilde{y}, \theta|y)$ as the product of $p(\tilde{y}|\theta, y)p(\theta|y)$, we recognize the posterior distribution term $p(\theta|y)$. Furthermore, if we assume conditional independence of y and $\tilde{y}$ given θ, then it follows that $p(\tilde{y}|\theta, y) = p(\tilde{y}|\theta)$ (Gelman et al., 2014). Therefore, we can represent the

posterior predictive distribution as

$$p(\tilde{y}|y) = \int p(\tilde{y}|\theta)p(\theta|y)d\theta \tag{2.9}$$

We see that this is the integral over θ of the product of the likelihood function of θ for $\tilde{y}$ and the posterior distribution of θ conditional on the observed data y (Hoff, 2009).

2.2.3 Extension to Classical Linear Regression

The Bayesian methodology can be readily extended to classical regression models as demonstrated below. We first consider the normal linear model, given by

$$\boldsymbol{y} = \mathbf{X}\boldsymbol{\beta} + \boldsymbol{\varepsilon} \tag{2.10}$$

with

$$\boldsymbol{\varepsilon} \sim \mathrm{N}(0, \sigma^2) \tag{2.11}$$

The vector $\boldsymbol{\varepsilon}$ represents the vector of observation errors, which are generally assumed to follow a normal distribution with zero mean and constant variance (σ^2) (Hoff, 2009).

Focusing on the response vector $\boldsymbol{y}$, its conditional expectation given the predictor vector $\mathbf{X}$, $\mathbb{E}[\boldsymbol{y}|\mathbf{X}]$, is $\mathbf{X}\boldsymbol{\beta} = \beta_1 x_{i1} + \cdots + \beta_k x_{ik}$ and its variance is σ^2. Since the errors follow a normal distribution, this implies that

$$y_i \sim \mathrm{N}(\beta_1 x_{i1} + \cdots + \beta_k x_{ik}, \sigma^2) \tag{2.12}$$

Using vector notation, we can equivalent express $\boldsymbol{y}$ as a multivariate normal distribution, namely

$$p(\boldsymbol{y}|\mathbf{X}, \boldsymbol{\beta}, \sigma^2) \sim \text{multivariate normal}(\mathbf{X}\boldsymbol{\beta}, \sigma^2\mathbf{I}) \tag{2.13}$$

where $\mathbf{I}$ is the identity matrix (Hoff, 2009).

As with the classical linear regression model, the desired outputs are the least squares estimators of the coefficients in the coefficient vector $\boldsymbol{\beta}$ and of σ^2. Thus, under a Bayesian approach, the joint posterior distribution of $\boldsymbol{\beta}$ and σ^2 given $\mathbf{X}$ and $\boldsymbol{y}$ is desired. Written out,

this is

$$p(\boldsymbol{\beta}, \sigma^2 | \mathbf{X}, \boldsymbol{y}) \tag{2.14}$$

and is proportional to

$$p(\boldsymbol{\beta}, \sigma^2 | \mathbf{X}, \boldsymbol{y}) \propto p(\mathbf{X}, \boldsymbol{y} | \boldsymbol{\beta}, \sigma^2) p(\boldsymbol{\beta}, \sigma^2) \tag{2.15}$$

In order to form the joint posterior, we can utilize a common tool in Bayesian inference, known as the Gibbs Sampler. The Gibbs Sampler is a Markov-Chain Monte Carlo algorithm that can approximate the joint posterior distribution by sampling from each full conditional distribution of the joint posterior sequentially. Upon convergence of the Gibbs Sampler, it can be shown that the equilibrium distribution to which it converges is exactly the joint posterior distribution desired (Hoff, 2009).

For equation 2.15, we can utilize the Chain Rule of Probability to factor it into the following

$$p(\boldsymbol{\beta}, \sigma^2 | \mathbf{X}, \boldsymbol{y}) \propto p(\sigma^2) p(\boldsymbol{\beta} | \sigma^2) p(\boldsymbol{y} | \mathbf{X}, \boldsymbol{\beta}, \sigma^2) p(\mathbf{X} | \boldsymbol{\beta}, \sigma^2) \tag{2.16}$$

The regressors are assumed to be constant or, if varying, assumed to follow a density with a parameter independent of the regression model parameters $(\boldsymbol{\beta}, \sigma^2)$. As such, the regression model can proceed by considering only the conditional density $p(\boldsymbol{y} | \mathbf{X}, \boldsymbol{\beta}, \sigma^2)$ and ignoring the density $p(\mathbf{X} | \boldsymbol{\beta}, \sigma^2)$ (Congdon, 2006). Therefore, we can represent the joint posterior as

$$p(\boldsymbol{\beta}, \sigma^2 | \mathbf{X}, \boldsymbol{y}) \propto p(\sigma^2) p(\boldsymbol{\beta} | \sigma^2) p(\boldsymbol{y} | \mathbf{X}, \boldsymbol{\beta}, \sigma^2) \tag{2.17}$$

If we assume that the prior densities of $\boldsymbol{\beta}$ and σ^2 are unrelated, then their joint prior density $p(\boldsymbol{\beta}, \sigma^2) = p(\boldsymbol{\beta}) p(\sigma^2)$. Since we assume that the the prior densities of $\boldsymbol{\beta}$ and σ^2 are independent, this also implies that $p(\boldsymbol{\beta} | \sigma^2) = p(\boldsymbol{\beta})$. Thus, equation 2.17 becomes

$$p(\boldsymbol{\beta}, \sigma^2 | \mathbf{X}, \boldsymbol{y}) \propto p(\sigma^2) p(\boldsymbol{\beta}) p(\boldsymbol{y} | \mathbf{X}, \boldsymbol{\beta}, \sigma^2) \tag{2.18}$$

To find the full conditional for a specific parameter, we only consider the terms containing the sought-after parameter of interest. Thus, for the full conditionals for $\boldsymbol{\beta}$ and σ^2, we have

$$p(\boldsymbol{\beta} | \boldsymbol{y}, \mathbf{X}, \sigma^2) \propto p(\boldsymbol{y} | \mathbf{X}, \boldsymbol{\beta}, \sigma^2) p(\boldsymbol{\beta}) \tag{2.19}$$

$$p(\sigma^2 | \boldsymbol{y}, \mathbf{X}, \boldsymbol{\beta}) \propto p(\boldsymbol{y} | \mathbf{X}, \boldsymbol{\beta}, \sigma^2) p(\sigma^2) \tag{2.20}$$

With our distribution for $p(\boldsymbol{y}|\mathbf{X}, \boldsymbol{\beta}, \sigma^2)$ defined, a Bayesian analysis would proceed by first specifying prior distributions on $\boldsymbol{\beta}$ and σ^2 and solving for each respective posterior distribution (Gelman et al., 2014).

Construction of the Gibbs Sampler would then proceed as follows. First, specify starting values of $\boldsymbol{\beta}$ and σ^2 as $\boldsymbol{\beta}^{(0)}$ and $\sigma^{2(0)}$. Next, sample $\boldsymbol{\beta}^{(1)} \sim p(\boldsymbol{\beta}|\boldsymbol{y}, \mathbf{X}, \sigma^{2(0)})$ using $\sigma^{2(0)}$. Then, sample $\sigma^{2(1)} \sim p(\sigma^2|\boldsymbol{y}, \mathbf{X}, \boldsymbol{\beta}^{(1)})$ using $\boldsymbol{\beta}^{(1)}$. Keep repeating this process and updating the parameters for a sufficient number of iterations until the parameters convergence (Hoff, 2009).

2.3 Potential Drawbacks

Before moving forward, it is important to consider many of the criticisms associated with Bayesian methods as well as many of the approaches used to overcome these criticisms.

One major objection to Bayesian methods concerns the arguably subjective choices that are necessary for Bayesian inference. As explained earlier, the selection of a prior probability distribution that, in combination with the likelihood function, will generally determine the form and shape of the posterior distribution. However, there are no set or agreed upon principles for choosing a prior distribution and improper selections can potentially lead to misleading results (Gelman, 2008).

In practice, many researchers address this issue by utilizing what are referred to as *non-informative priors*. These are prior distributions that are considered to hold little or no prior information about the parameters and represent an analyst's lack of previous knowledge of the parameters to be estimated. Additionally, when sufficient data are available, prior probability selections will not affect the outcome since the likelihood function will dominate the solution. Regardless of the prior used, the answer will be the same (Gelman et al., 2014).

Bayesian computations can be computationally expensive, especially for models having large numbers of parameters. Furthermore, Bayesian methods can often involve high-dimensional integration, which can be computationally taxing. Depending on the model complexity, hours and even days can elapse before results are available.

This criticism is, in a sense, also a benefit of Bayesian inference as it is capable of

addressing problems that are often inaccessible using classical methods. Furthermore, with new computational tools specifically designed for Bayesian inference and ever-increasing computational power available to analysts, the computational expense continues to be less and less of an issue.

2.4 Hierarchical Modeling Approach

Many of the models presented make use of a hierarchical modeling approach in forming the regression coefficients. The power of hierarchical regression lie in its ability to estimate effects on a response variable that might vary within a group of individual data points as well as between differing groups of data points. Furthermore, an additional draw of hierarchical modeling is that for hierarchically structured data, hierarchical modeling outperforms classical linear regression in its predictive accuracy (Gelman, 2006).

Simple linear regression on hierarchical data can usually result in one of two cases: (1) complete pooling of the data and (2) no pooling of the data. Under simple linear regression, complete pooling of the data fully ignores any group-level differences in individual data points. For example, consider if we wished to form a regression model that predicts average salary by years of education and age for individuals within the entire United States. A potential grouping of the data may be by individual state as each state in the United States might have different costs of living, major industries, and other state-level factors that would affect the average salary observed. Complete pooling would completely ignore any state-level differences in the individual data points.

Conversely, taking individual regressions for each group rejects the possibility of any similarity between groups. Referring to the average salary regression model example, it may be that the effects of education and age on average salary are generally similar across all 50 states, albeit to varying degrees. Individual regressions would reject this possibility.

Hierarchical regression represents a middle ground as it allows for partial pooling of the data. In this scheme, while individual regressions are performed for each group, these regressions consider two sources of error, one for error within each group and one for error between the groups. This approach is especially useful when group-level sample sizes are

small as it allows for information from larger groups to be "borrowed" for smaller groups. Consider the average salary regression model. If one state-level sample was small, potentially insignificant or nonsensical effects may result from an individual state-level regression. However, with a hierarchical regression model, each state is assumed to have some underlying similarity with each other the state. The effects for states with larger sample sizes will have greater influence in the model and will affect the effects estimated for smaller state

Estimation of hierarchical models in a non-Bayesian context is usually performed using either full maximum likelihood or restricted maximum likelihood methods. For each of these methods, a number of algorithms including the expectation-maximization (EM) algorithm and iterative generalized least squares (IGLS) have been proposed. In contrast, Bayesian estimation of hierarchical models is performed using Markov chain Monte Carlo (MCMC) methods, including the Gibbs Sampler referenced earlier (Dedrick et al., 2009).

Bayesian estimation has the advantage of not being dependent on normality assumptions and asymptotic results. Additionally, Bayesian methods can better handle complex problems that would be difficult to address using the classical approach (Hox and Robert, 2010). Thus, we proceed with the Bayesian methodology.

What follows is a description of the Bayesian hierarchical linear regression model utilized for many of the models presented.

2.4.1 Bayesian Hierarchical Linear Regression Model

For the Bayesian hierarchical linear regression model, the desired outputs are the distributions of each group-level regression coefficient vector $\boldsymbol{\beta_j}$, the mean vector from which the group-level betas are drawn, $\boldsymbol{\Phi}$, the covariance matrix of the distribution from which the group-level betas are drawn, Σ, and the within-group variance of the group-level responses, σ_j^2. Figure 2.2 illustrates the hierarchical structure of the model to be formed (Hoff, 2009).

The joint posterior distribution to be determined for $\boldsymbol{\beta_1}, \ldots, \boldsymbol{\beta_j}$, $\boldsymbol{\Phi}$, Σ, and $\sigma_1^2, \ldots, \sigma_j^2$

given $\boldsymbol{X_1}, \ldots, \boldsymbol{X_j}$ and $\boldsymbol{y_1}, \ldots, \boldsymbol{y_j}$ is desired. Written out, this is

$$p(\boldsymbol{\beta_1}, \ldots, \boldsymbol{\beta_j}, \boldsymbol{\Phi}, \Sigma, \sigma_1^2, \ldots, \sigma^2 | \boldsymbol{X_1}, \ldots, \boldsymbol{X_j}, \boldsymbol{y_1}, \ldots, \boldsymbol{y_j}) \tag{2.21}$$

In describing both the within-group and between-group heterogeneity, we utilize an ordinary regression model, assuming that the residuals follow a normal distribution with zero-mean and group-level variance σ_j^2. We express the within-group sampling model as

$$\boldsymbol{y_j} = \boldsymbol{X_j}\boldsymbol{\beta_j} + \boldsymbol{\epsilon_j}, \{\boldsymbol{\epsilon_j}\} \sim \text{i.i.d. normal}(0, \sigma_j^2) \tag{2.22}$$

Similarly, for the between-group sampling model, we describe the between-group heterogeneity with a multivariate normal distribution with mean $\boldsymbol{\Phi}$ and covariance matrix Σ. We express the between-group sampling model as

$$\boldsymbol{\beta_1}, \ldots, \boldsymbol{\beta_j} \sim \text{i.i.d. multivariate normal}(\boldsymbol{\Phi}, \Sigma) \tag{2.23}$$

Equation 2.23 implies that we will utilize a multivariate normal prior distribution for $\boldsymbol{\beta_1}, \ldots, \boldsymbol{\beta_j}$. For the remaining parameters, $\boldsymbol{\Phi}, \Sigma,$ and $\sigma_1^2, \ldots, \sigma_j^2$, we utilize multivariate normal, an inverse-Wishart and inverse-gamma priors respectively. In all four cases, we will exploit the fact that the priors chosen are semiconjugate with respect to the sampling distribution (Hoff, 2009).

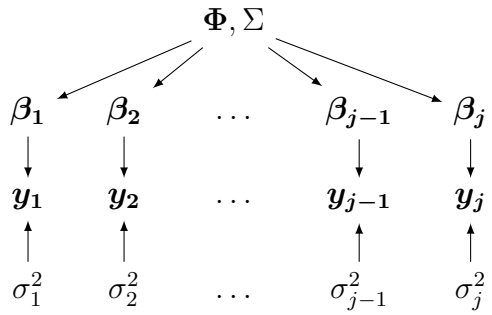

Figure 2.2: A Graphical Representation of the Bayesian Hierarchical Regression Model with Group-Specific Variances

In order to form the joint posterior, the Gibbs Sampler can be utilized, provided that

we can sample from the full conditional distributions. What follows is a presentation of the detailed form of the full conditional distributions necessary for the Gibbs Sampler to compute the joint posterior of our Bayesian hierarchical linear regression model.

Full Conditionals for $\boldsymbol{\beta_1}, \ldots, \boldsymbol{\beta_j}$

As implied by Equation 2.23, each regression coefficient vector $\boldsymbol{\beta_j}$ is assumed to be independent and identically distributed. Thus, we can compute the full conditional for each regression coefficient vector independently.

Each conditional distribution for $\boldsymbol{\beta_j}$

$$p(\boldsymbol{\beta_j}|\boldsymbol{y_j}, \boldsymbol{X_j}, \boldsymbol{\Phi}, \sigma_j^2, \Sigma) \tag{2.24}$$

can be shown to have a multivariate normal distribution with

$$\text{Var}\left[(\boldsymbol{\beta_j}|\boldsymbol{y_j}, \boldsymbol{X_j}, \boldsymbol{\Phi}, \sigma_j^2, \Sigma)\right] = (\Sigma^{-1} + \boldsymbol{X_j}^T\boldsymbol{X_j}/\sigma_j^2)^{-1} \tag{2.25}$$

$$\mathbb{E}\left[(\boldsymbol{\beta_j}|\boldsymbol{y_j}, \boldsymbol{X_j}, \boldsymbol{\Phi}, \sigma_j^2, \Sigma)\right] = (\Sigma^{-1} + \boldsymbol{X_j}^T\boldsymbol{X_j}/\sigma_j^2)^{-1}(\Sigma^{-1}\boldsymbol{\Phi} + \boldsymbol{X_j}^T\boldsymbol{y_j}/\sigma_j^2) \tag{2.26}$$

as its variance and mean respectively (Hoff, 2009).

Full Conditionals for $\sigma_1^2, \ldots, \sigma_j^2$

We assume that each group j has its own specific error variance σ_j^2, independent of those for other groups. Therefore, we can compute each full conditional distribution for σ_j^2 separately.

Each full conditional distribution for σ_j^2

$$p(\sigma_j^2|\boldsymbol{y_j}, \boldsymbol{X_j}, \boldsymbol{\Phi}, \boldsymbol{\beta_j}) \tag{2.27}$$

is given as an inverse-gamma distribution having a shape parameter defined by

$$\frac{\nu_0 + n_j}{2} \tag{2.28}$$

and a scale parameter defined by

$$\frac{\nu_0\sigma_{j,0}^2 + \text{SSR}_j}{2} \tag{2.29}$$

For the shape parameter, ν_0 can be interpreted as the sample size of prior observations while n_j is the sample size of group j. The initial value of σ_j^2 is given by $\sigma_{j,0}^2$ while

$$\sum_{i=1}^{n_j}(y_{ij} - \boldsymbol{\beta_j}^T\boldsymbol{x}_{i,j})^2 \tag{2.30}$$

is the sum of squared residuals (SSR_j) of each group j (Hoff, 2009).

Full Conditional for $\boldsymbol{\Phi}$

The third conditional distribution for $\boldsymbol{\Phi}$

$$p(\boldsymbol{\Phi}|\boldsymbol{\beta_1}, \ldots, \boldsymbol{\beta_j}, \Sigma) \tag{2.31}$$

can be demonstrated to follow a multivariate normal distribution with a mean and variance of

$$\mathbb{E}\left[(\boldsymbol{\beta_1}, \ldots, \boldsymbol{\beta_j}, \Sigma)\right] = (\Lambda_0^{-1} + J\Sigma^{-1})^{-1}(\Lambda_0^{-1}\boldsymbol{\mu}_0 + J\Sigma^{-1}\bar{\boldsymbol{\beta}}) \tag{2.32}$$

$$\text{Var}\left[(\boldsymbol{\beta_1}, \ldots, \boldsymbol{\beta_j}, \Sigma)\right] = (\Lambda_0^{-1} + J\Sigma^{-1})^{-1} \tag{2.33}$$

For the mean and variance, J is the number of groups considered while Λ_0 refers to the prior covariance matrix. The term, $\bar{\boldsymbol{\beta}}$, is equal to

$$\bar{\boldsymbol{\beta}} = \frac{1}{J}\sum \boldsymbol{\beta_j} \tag{2.34}$$

and refers to the vector average of the beta coefficient vectors of all J group (Hoff, 2009).

Full Conditional for Σ

The fourth conditional distribution for Σ

$$p(\Sigma|\boldsymbol{\Phi}, \boldsymbol{\beta_1}, \ldots, \boldsymbol{\beta_j}) \tag{2.35}$$

can be shown to be an Inverse-Wishart distribution having degrees of freedom equal to

$$\eta_0 + J \tag{2.36}$$

and a scale matrix equal to

$$[\mathbf{S}_0 + \mathbf{S}_{\boldsymbol{\Phi}}] \tag{2.37}$$

The degrees of freedom parameters can be interpreted to be the posterior sample size of the covariance matrix, where J is the total number of groups and η_0 is the prior sample size. Likewise, the scale matrix can be considered to be the sum of the data residual sum of squares, given by

$$\sum_{j=1}^{J} (\boldsymbol{\beta_j} - \boldsymbol{\Phi})(\boldsymbol{\beta_j} - \boldsymbol{\Phi})^T \tag{2.38}$$

and the prior residual sum of squares (Hoff, 2009).

Chapter 3

Model Data

This chapter describes the data sources and methods utilized for extraction of or collection of the data that form the models presented in the following chapters.

3.1 Data Sources

The data underpinning both the runway occupancy time models, the departure distance model and the runway exit utilization model came from the fusion of four sources: (1) ASDE-X Surveillance Data, (2) measurements performed using Google Earth, (3) FAA databases and (4) the Automated Surface Observing System. From the surveillance data, a total of 407,660 departure tracks and 467,095 arrival tracks were extracted. These data were provided by the Federal Aviation Administration and t he large majority of the surveillance data are for observations performed throughout October 2013, with additional data taken on various dates in March 2012, May 2012, June 2012, July 2012, October 2012, December 2012, and January 2013. Listed in Table 3.1 are the parameters gathered from the dataset.

Table 3.1: List of Data Parameters extracted from Dataset.

Lift-Off Velocity	Threshold Crossing Velocity
Runway Length	Runway Heading
Exit Taxiway Angle	Airport Altitude
Exit Taxiway Location	Turn Distance on Exit
Perpendicular Distance to Exit Taxiway Hold Bar	Headwind on Departure
Wheels-Up Location on Departure	Departure Roll Distance
Departure Runway Occupancy Time	Arrival Runway Occupancy Time
Average Deceleration on Landing	Displaced Threshold Length
Touchdown Distance	Runway Width

3.1.1 PDARS/ASDE-X

Data parameters were taken from Airport Surface Detection Equipment, Model X ASDE-X System installations at the airports listed in Table 3.2. The original purpose of the ASDE-X system was for runway safety but the surface surveillance data it has provided has allowed for considerable characterization and description of various airport surface movements and associated factors such as surface aircraft emissions and departure queuing (Runnels, 2008). ASDE-X data are produced through data fusion of five data sources: (1) Surface surveillance radar, (2) Multilateration sensors, (3) Airport Surveillance Radars, (4) Automatic Dependent Surveillance - Broadcast (ADS-B) sensors, and (5) the Terminal Automation System (FAA, 2014). The resulting dataset provides 4-D (space and time) aircraft position and identification information to air traffic control (ATC) tower displays.

Table 3.2: List of Airports for which Data were sourced from ASDE-X Installations.

Airport Name	Airport Code
Atlanta Hartsfield-Jackson International Airport	ATL
General Edward Lawrence Logan International Airport (Boston)	BOS
Charlotte Douglas International Airport	CLT
Ronald Reagan Washington National Airport	DCA
Denver International Airport	DEN
Dallas/Fort Worth International Airport	DFW
Detroit Metropolitan Wayne County Airport	DTW
Newark Liberty International Airport	EWR
Fort Lauderdale-Hollywood International Airport	FLL
Honolulu International Airport	HNL
Washington Dulles International Airport	IAD
Houston George Bush Intercontinental Airport	IAH
John F. Kennedy International Airport (New York)	JFK
McCarran International Airport (Las Vegas)	LAS
Los Angeles International Airport	LAX
LaGuardia Airport (New York)	LGA
Orlando International Airport	MCO
Chicago Midway International Airport	MDW
Miami International Airport	MIA
Minneapolis-Saint Paul International Airport	MSP
Chicago O'Hare International Airport	ORD
Philadelphia International Airport	PHL
Phoenix Sky Harbor International Airport	PHX
San Diego International Airport	SAN
Seattle Tacoma International Airport	SEA
Salt Lake City International Airport	SLC
Lambert-St. Louis International Airport	STL

Using the ASDE-X data, the following data parameters were extracted: (1) Lift-Off Velocity on Departure, (2) Runway Threshold Crossing Velocity on Arrival, (3) the Straight-Line Distance travelled from the Runway Threshold to the Exit Taxiway on Arrival, (4) the Wheels-Up Location, (5) the Departure Roll Distance, (6) the AROT, (7) the DROT, (8) the Average Deceleration on Landing and (9) the Touchdown Distance.

3.1.2 Google Earth

Google Earth is a digital mapping software product that arose from technology originally developed by Keyhole, a digital mapping company. Released in June 2005, Google Earth allows users to interactively explore locations and perform measurements directly on mapped images almost anywhere in the world (Google, 2015). Using this functionality, the following parameters were measured: (1) Turn Distance from Start of Turn to Exit Hold Line, (2), Runway Exit Angle, and (3) Runway Exit Distance from Runway Edge.

3.1.3 FAA Databases

The FAA makes available to the public a wealth of aeronautical data through its National Flight Data Center (NFDC), including data updated every 56-days through its freely available 56-day National Airspace System Resource (NASR) Subscription. Airport facility data, including (1) Runway Lengths, (2) Runway Widths, (3) Runway Headings, and (4) Displaced Threshold Lengths, were extracted from the Airports and Other Landing Facilities (APT) text file found in this database.

3.1.4 Automated Surface Observing System (ASOS) Data

Data on windspeeds were sourced from the U.S. National Oceanic and Atmospheric Administration's Automated Surface Observing System (ASOS). The more than 900 ASOS sites report parameters such as wind speed, wind direction, temperature and dew point, and precipitation accumulation. Though most of the data are reported at hourly intervals, data such as wind speeds are available at one minute temporal resolution (NOAA, 2014). Using this data, we found the Headwind on Departure.

3.2 Data Collection Methods

3.2.1 Defining Departure and Arrival Runway Occupancy Time

Before moving to describe the data collection methodologies, it is important to establish how the departure runway occupancy time (DROT) and arrival runway occupancy time (AROT), two of the response variables for models to be presented, are defined. In this section, the definitions of DROT and AROT utilized in this study are presented.

Departure Runway Occupancy Time

A commonly used definition of DROT is provided by EUROCONTROL, which defines DROT as

> the time interval between crossing the hold stop bar and the main gear lifting off the runway (EUROCONTROL, 2003)

and decomposes the DROT into four elements: (1) the line-up time, (2) the wait time, (3) the reaction time of the flight crew to ATC take-off clearance, and (4) the take-off time.

The line-up time refers to the time needed for the aircraft to cross the hold stop bar and align with the runway centerline. This time will depend, in part, on the taxi speed used in the alignment phase. It will also depend on the position of the hold stop bar, which can vary by the runway entrance used and by the runway used. The wait time is the time interval from when the aircraft has successfully aligned with the runway centerline to when ATC grants clearance for take-off. Depending on the current state of aircraft operations, the time to clearance can vary greatly and is fully at the discretion of ATC. The reaction time parameter refers to the time from when ATC take-off clearance is granted to when the pilot begins moving to begin the take-off roll. This can depend on pilot awareness, time needed for final cabin preparations, or even the clarity of the communication received from ATC. Finally, the take-off time refers to the elapsed time from when the take-off roll begins to when the main gear lifts off the runway. This time will generally comprise the majority of the total DROT and is subject to far fewer exogenous and unmeasurable factors. Therefore,

for the purposes of the two predictive models, this time is taken as the departure runway occupancy time.

Arrival Runway Occupancy Time

The AROT is defined as

> the time interval between the aircraft crossing the threshold and its tail vacating the runway (EUROCONTROL, 2003).

Unlike for DROT, fewer external factors contribute to variations in the AROT. The primary variation arises from the pilot's choice of runway exit taxiway. Subject to the performance constraints of the aircraft, a pilot's choice of runway exit taxiway will inform the degree to which braking is applied upon touchdown. However, the choice of exit taxiway can be accounted for in the regression model. Thus, the definition of AROT is taken directly as that given by EUROCONTROL.

3.2.2 Lift-Off Velocity on Departure, Departure Roll Distance, Wheels-Up Location and DROT

For a departure track extracted from the ASDE-X data, a representative plot of the velocity values estimated while the aircraft is on the runway is given in Figure 3.1

Three phases of the departure movement can be identified. The first is the taxi phase which is the relatively flat starting portion of the velocity trace shaded in salmon. During this phase, the aircraft is entering the runway and aligning itself with the runway centerline in preparation for takeoff. The second phase is the take-off roll phase shaded in green. This phase starts from the point at which the aircraft velocity begins to sharply increase. At the point when the aircraft begins its rotation, its translational velocity begins to vary depending, in part, on the angle of attack of the aircraft, the headwind, and the proportion of engine thrust in the translational direction among other factors. The point at which the aircraft lifts off the runway ends the take-off roll and begins the third phase, the lift-off phase, which is shaded in yellow.

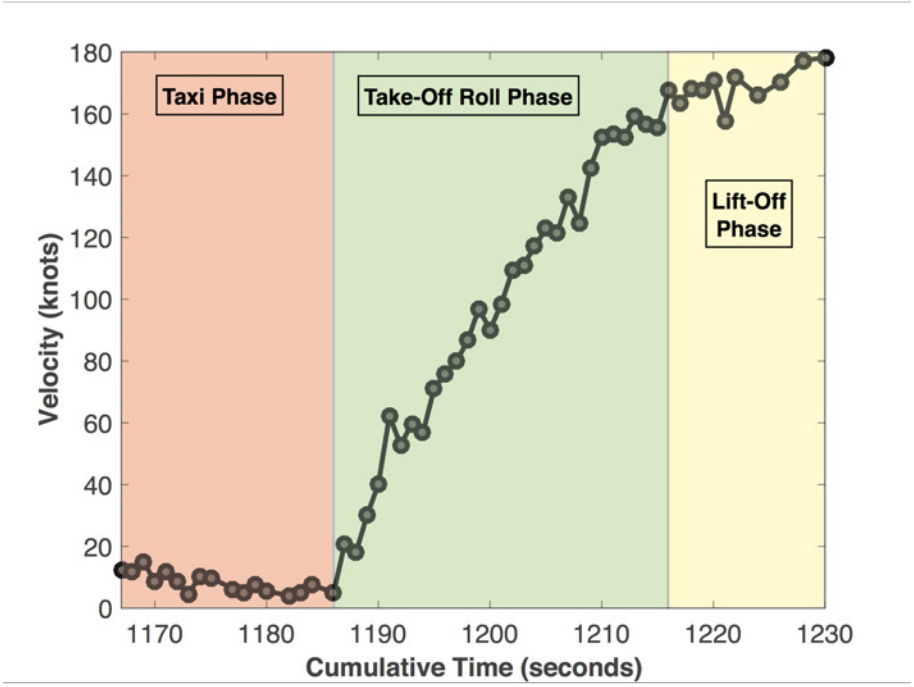

Figure 3.1: Representative Plot of Velocity Values for a Departure Movement (CRJ2 Departing Runway 27 at San Diego)

The DROT is taken to be the time in which the aircraft is in the take-off roll phase. In order to determine the start and end of the take-off roll phase, a number of heuristics combined with low-pass moving average filters were used and are described below.

Start of Take-Off Roll

The runway on which the movement was occurring was first modeled as a rectangle and all track points contained with the runway polygon were identified. Using these track points and their associated time stamps and coordinate data, the successive distances between each track point and the associated headings relative to true North were computed. Next, the offset angles relative to the runway centerline for each successive track point pair were calculated and these were used to compute the straight-line distances traveled on the departure runway. With these straight-line distances, associated straight-line velocities and acceleration values were determined.

The velocities, acceleration values and headings were subsequently smoothed using a moving average filter. This filter type was chosen given that the moving average filter is optimal for reducing noise in a time domain encoded signal while retaining a sharp step response (Smith, 1999). Few published guidelines exist for choosing the span of the moving average filter. Therefore, a span of 7 was chosen by trial and error through observing the loss in signal compared to the reduction in noise. The chosen span of 7 reduces the noise in the signal by a factor of approximately 2.64 ($\sqrt{7}$). Figures 3.2 and 3.3 illustrate examples of the smoothed velocity and acceleration profile.

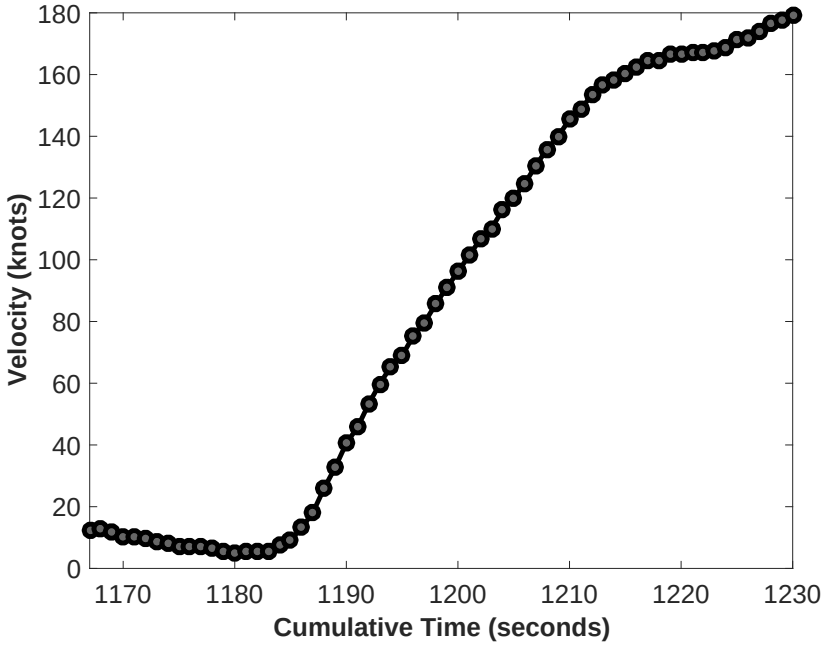

Figure 3.2: Illustration of Smoothed Straight-Line Velocity Profile for (CRJ2 Departing Runway 27 at San Diego)

The next step was to determine the maximum value of acceleration and its associated ordered index in the track points. As the aircraft accelerates, the drag force increases resulting in a gradually lower maximum possible acceleration. Therefore, we assume that the largest acceleration during the take-off roll is achieved during the take-off run, not long after the start of the take-off roll.

Once the maximum acceleration was located, the time stamp associated with this point was called t_m while the acceleration value was called m. Next, preceding values of acceleration

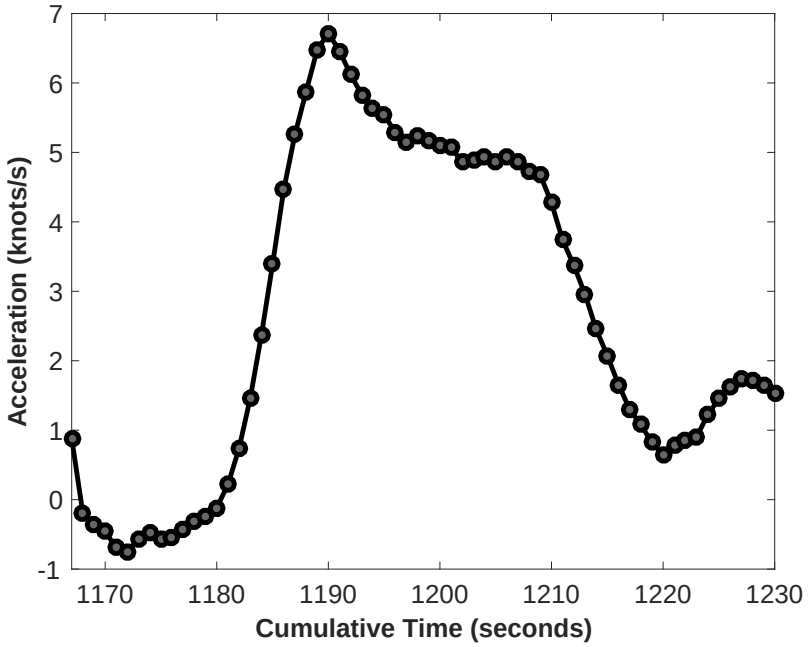

Figure 3.3: Illustration of Smoothed Straight-Line Acceleration Profile for (CRJ2 Departing Runway 27 at San Diego)

were examined until the track point having an acceleration sufficiently close to zero was located. "Sufficiently close" was initially assumed to be a value less than or equal to 0.2 knots/s. Owing to remaining noise in the acceleration data, a value of 0.2 knots/s or less may not be found. If no such value was initially found, the floor was incremented higher by 0.1 knots/s and the process repeated. The maximum possible floor value allowed for was 0.8 knots/s. Once a track point "sufficiently close" to zero was located, the time stamp associated with this point was called t_a while the acceleration value was called s.

After locating t_a, a 4^{th}-degree polynomial function for acceleration, a, as a function of time, t, was fit to the acceleration data spanning from time stamp t_a to t_m. Figure 3.4 illustrates the 4^{th}-degree polynomial fit to the data. The form of the polynomial function is as follows:

$$a = f(t) = \alpha_1(t - t_m)^4 + \alpha_2(t - t_m)^3 + \alpha_3(t - t_m)^2 + \alpha_4(t - t_m) + m \tag{3.1}$$

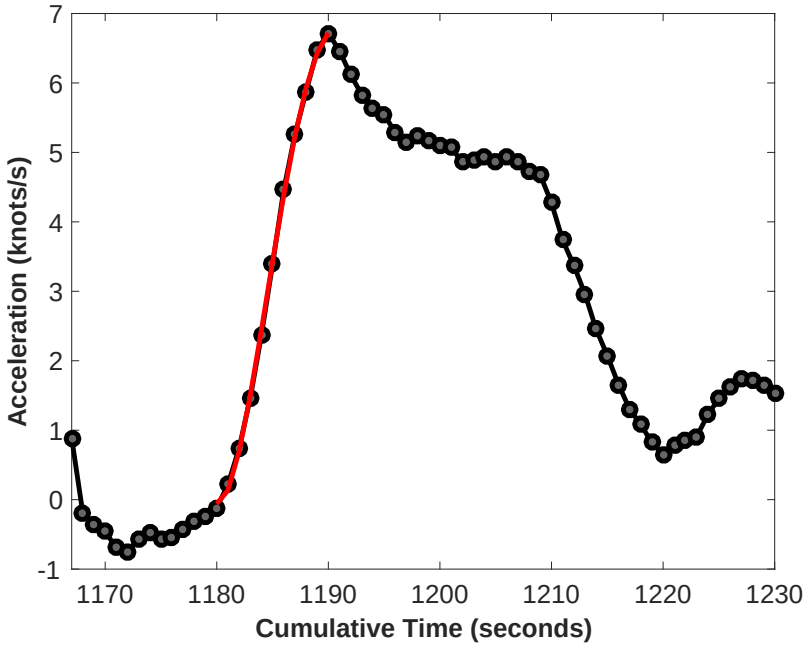

Figure 3.4: Illustration of Smoothed Straight-Line Acceleration Profile with Fitted Polynomial Function for (CRJ2 Departing Runway 27 at San Diego)

Once the coefficients of (3.1) are determined, we then take the first derivative to locate the critical points, giving us:

$$\dot{a} = f'(t) = 4\alpha_1(t - t_m)^3 + 3\alpha_2(t - t_m)^2 + 2\alpha_3(t - t_m) + \alpha_4 \tag{3.2}$$

To estimate the start of the take-off roll, we set as candidate times the real-valued roots and critical points of (3.1). We then apply the following heuristics in the following order:

- **Heuristic 1**: Given a set of candidate roots and a set of critical points of (3.1), find the minimum-valued candidate of t in each set that is greater than t_a. Find the minimum value of the two minimums and choose this as the starting point of the take-off roll provided that the acceleration at the time value is both positive and less than or equal to 0.4 knots/s.

- **Heuristic 2**: If either the acceleration at the minimum value determined in Heuristic 1 exceeds 0.4 knots/s or if no qualifying candidate values of the starting point exist,

Heuristic 1 will fail. If Heuristic 1 fails, select from the set of critical points of (3.1) the minimum value of t, which can be up to 2 seconds behind t_a and has an associated value of acceleration that is both positive and less than or equal to 0.4 knots/s.

For a departure movement, pilots generally enter the departure runway and align the aircraft with the runway centerline. Usually, once the alignment movement concludes, the aircraft remains at rest until given clearance from ATC. Alternatively, a pilot may receive departure clearance prior to entering the runway and may choose to perform a rolling takeoff. In a rolling takeoff, the aircraft does not stop when it enters the runway. Once the aircraft is aligned, take-off thrust settings are engaged and the plane begins its take-off roll. Heuristic 1 utilizes the fitted polynomial function of (3.1) to either find the point of zero acceleration or the last point of minimal acceleration prior to the start of the take-off roll. It looks ahead of t_a to avoid inflating the DROT time and take-off distance since there may be multiple points of zero or near zero acceleration in the line up for take-off. Heuristic 1 can fail if the acceleration at t_a is greater than 0.4 knots/s and the fitted polynomial function increases monotonically beyond t_a with no inflection in the curve. Should Heuristic 1 fail, Heuristic 2 is used to look behind t_a up to 2 seconds to avoid inflating the DROT and take-off distance.

End of Take-Off Roll

Figure 3.3 is illustrative of the acceleration profiles encountered on departure. As the departure movement begins, the aircraft accelerates to its maximum possible acceleration. The acceleration then trails off due to increased drag force and reduced available thrust. Once the aircraft begins to rotate, the horizontal acceleration drops off significantly as a result of the aircraft translating into its angle of attack and its engines no longer providing solely horizontal thrust. The wheels-up location and conclusion of the take-off roll, therefore, is taken to be the point at which either a saddle point is found in the acceleration profile or the acceleration reaches zero.

In preparation for identifying the wheels-up location, we first extract a point approximately halfway between t_m and the estimated start of the take-off roll, which we call t_{start}. We then locate the point in the latter portion of the acceleration profile, t_e, that has the same acceleration value, which we label as e. Once located, we then fit the

following 5^{th}-degree polynomial function to the points 8 seconds prior to t_e and up to 18 seconds following t_e.

$$a = f(t) = \alpha_1(t - t_e)^5 + \alpha_2(t - t_e)^4 + \alpha_3(t - t_e)^3 + \alpha_4(t - t_e)^2 + \alpha_5(t - t_e) + e \tag{3.3}$$

Figure 3.5 illustrates a 5^{th}-degree polynomial fitted to the latter end of the acceleration track.

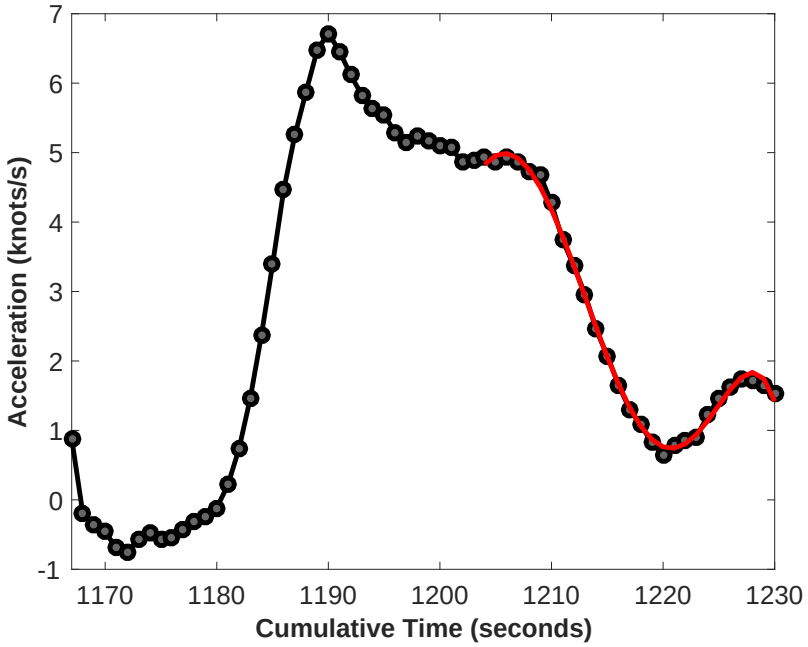

Figure 3.5: Illustration of Smoothed Straight-Line Acceleration Profile with Fitted 5^{th}-Degree Polynomial Function for (CRJ2 Departing Runway 27 at San Diego)

Next, we determine the coefficients of (3.3) and take the first derivative to locate the critical points, giving us:

$$\dot{a} = f'(t) = 5\alpha_1(t - t_e)^4 + 4\alpha_2(t - t_e)^3 + 3\alpha_3(t - t_e)^2 + 2\alpha_4(t - t_e) + \alpha_5 \tag{3.4}$$

To estimate the end of the take-off roll, we set as candidate times the real-valued roots and critical points of (3.3). We then apply the following heuristics in the following order:

- **Heuristic 1**: Given a set of candidate roots and a set of critical points of (3.3), find

the candidate value of t in each set that is greater than e and take the minimum value of the two candidates.

- **Heuristic 2**: If the DROT that would result is less than an assumed minimum value of DROT (15 seconds) for the aircraft, check to see if the value returned from Heuristic 1 corresponds to an acceleration value of less than 1.75 knots/s. If the acceleration value is greater than 1.75 knots/s, reapply Heuristic 1 to estimate the location of the saddle point with the requirement that it correspond to an acceleration value of less than 1.75 knots/s.

Normally, Heuristic 1 was sufficient for estimating the end time of the take-off roll. However, the acceleration profile would sometimes have multiple saddle points occurring at higher values of acceleration that might lead to underestimation of the DROT. Heuristic 2 guards against underestimation of the DROT by providing a feasible floor to the DROT depending on the aircraft type.

Departure Runway Occupancy Time, Wheels-Up Location, Lift-Off Velocity and Departure-Roll Distance

Having estimated the start and end times of the take-off roll, the departure runway occupancy time (DROT) is found as the difference between the end and start time of the take-off roll. To obtain the take-off roll distance and the wheels-up location, we applied numerical integration of the velocity curve with respect to the DROT. Therefore, the take-off roll distance and wheels-up location are found as

$$\text{Take-Off Distance} = \int_{\text{start of take-off roll}}^{\text{end of take-off roll}} v(t)dt \tag{3.5}$$

Lastly, the lift-off velocity was found by evaluating the integral of (3.3) at the difference of the estimated end time of the take-off roll and t_e. Therefore, the lift-off velocity is found to be

$$V_{LO} = \frac{\alpha_1}{6}(\Delta)^6 + \frac{\alpha_2}{5}(\Delta)^5 + \frac{\alpha_3}{4}(\Delta)^4 + \frac{\alpha_4}{3}(\Delta)^3 + \frac{\alpha_5}{2}(\Delta)^2 + a_e(\Delta) + V_e \tag{3.6}$$

where $\Delta =$ end time of take-off roll$-t_e$ and where a_e and V_e are the acceleration and velocity at time t_e respectively.

3.2.3 Headwind on Departure

Having determined the start of the take-off roll, the associated heading corresponding to the nearest track point was assumed to apply to the point of the start of the take-off roll and was used to determine the offset angle relative to the runway centerline. The estimated windspeed corresponding to the nearest track point was also taken as the windspeed corresponding to the start of the take-off roll. Using the offset angle, the horizontal wind component was found.

3.2.4 Runway Threshold Crossing Velocity

For each arrival track, the arrival runway was identified and a rectangular polygon was created to represent that runway. Track points that lay both within and outside the runway polygon were identified. Figure 3.6 illustrates the runway polygon and the track points.

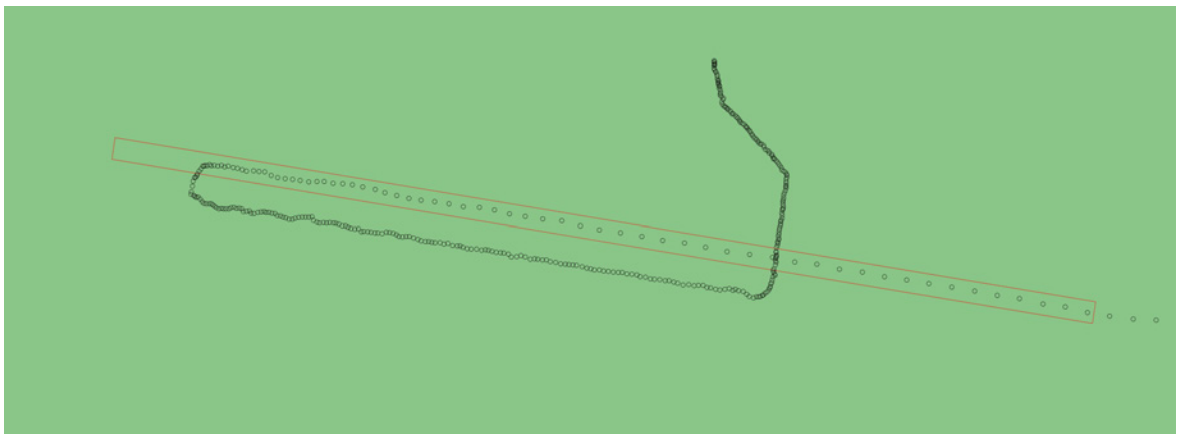

Figure 3.6: Illustration of a Runway Polygon and Arrival Track Points for an Arrival at San Diego International Airport

To produce estimates of velocity, the distance between track point pairs was divided by the difference between track point time stamps, which was generally 1 second.

According to FAA procurement specifications, target data reported to the ASDE-X multiprocessor subsystem must be registered to within ±18 feet of ground truth, i.e., the true location of the target (FAA, 2009). If assuming normally distributed errors, then by

error propagation, this implies that the uncertainty (σ_d) in the distance (d) between the track points would be

$$\sigma_d = \sqrt{2(18 \text{ feet})^2} = 25.46 \text{ feet} \tag{3.7}$$

Assuming a 1 second time difference between the track points, this could result in an error of roughly $\pm$ 15.09 knots (25.46 $\frac{\text{ft}}{\text{s}}$) if assuming that only one measurement was used as the velocity estimate. Therefore, in order to mitigate potential deviation in the velocity estimate, the quotient of an average of multiple distance measurements and an average of multiple time intervals was utilized as the velocity estimate. Assuming that there would be negligible change in the approach velocity 30 seconds from the runway threshold, the first 30 track points outside of the arrival runway polygon for the aircraft on approach were used to create 29 measurements of pairwise distance and 29 time intervals. The advantage of this method is that the uncertainty in the velocity estimate is greatly reduced. For the mean pairwise distance ($\bar{d}$), the uncertainty ($\sigma_{\bar{d}}$) is

$$\sigma_{\bar{d}} = \frac{\sigma}{\sqrt{n}} = \frac{25.46 \text{ feet}}{\sqrt{29}} = 4.73 \text{ feet} \tag{3.8}$$

Since the velocity estimate ($\bar{v}$) is equal to

$$\bar{v} = \frac{\bar{d}}{\bar{t}} \tag{3.9}$$

its fractional uncertainty is equal to

$$\frac{\sigma_{\bar{v}}}{|\bar{v}|} = \sqrt{\left(\frac{\sigma_{\bar{d}}}{\bar{d}}\right)^2 + \left(\frac{\sigma_{\bar{t}}}{\bar{t}}\right)^2} \tag{3.10}$$

If no uncertainty is assumed for the time intervals and a positive velocity estimate is assumed, then the uncertainty in the velocity estimate is found to be

$$\frac{\sigma_{\bar{v}}}{\bar{v}} = \sqrt{\left(\frac{\sigma_{\bar{d}}}{\bar{d}}\right)^2} \Rightarrow \sigma_{\bar{v}} = \frac{\bar{v}\sigma_{\bar{d}}}{\bar{d}} \tag{3.11}$$

Assuming

$$\bar{t} = 1 \text{ second}$$

and with

$$\bar{v} = \frac{\bar{d}}{\bar{t}}$$

$\sigma_{\bar{v}}$ is found to be

$$\sigma_{\bar{v}} = \frac{\bar{d}\sigma_{\bar{d}}}{\bar{t}\bar{d}} = \frac{\sigma_{\bar{d}}}{\bar{t}} = \frac{4.73 \text{ feet}}{1 \text{ second}} = 2.8 \text{ knots} \tag{3.12}$$

and represents a marked improvement in the velocity uncertainty.

3.2.5 Straight-Line Distance from Runway Threshold to Exit and AROT

In determining the arrival runway occupancy time, the track points within the runway on arrival were identified and their respective time stamps were used to calculate the majority of the AROT value. If there was any distance between either the first track point and the closest runway edge or between the last track point and the closest runway edge, this distance was estimated. Figure 3.7 illustrates an example of this for the first track point. The distance (d_1) is the distance between the first runway track point and its immediately preceding track point while distance (d_2) is the distance between the first runway track point and the closest runway edge. Taking the elapsed time between the first track point and the immediately preceding track point ($t_1 - t_2$), a portion of this time equal to $(t_1 - t_2) * (d_2/d_1)$ was estimated. This was similarly done for the last track point within the runway and its immediately succeeding track point. The sum of these two times plus the initial AROT value found earlier became the final AROT value.

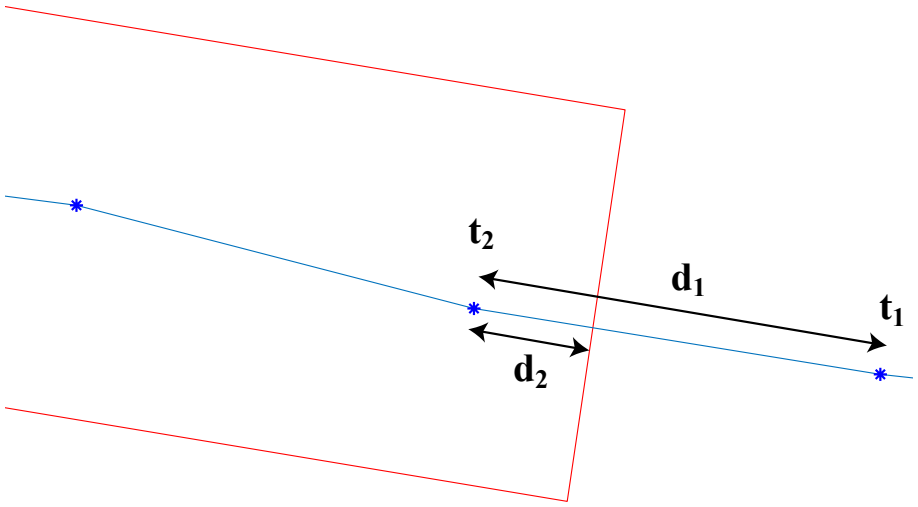

Figure 3.7: Image of First Track Point within Runway and its Immediately Preceding Track Point (A306 Arriving on RW27 at SAN)

In determining the straight-line distance, the track points within the runway on arrival previously identified were used to find the pairwise distances between each set of adjacent track points. The heading between each adjacent pair of track points was also determined. Thus, for n track points, there were $n-1$ pairwise distances and headings. For each heading, the angular offset from the runway centerline heading was determined. Each distance value was mapped to the runway centerline by taking the product of the distance value and the cosine of the angular offset. Any distances between either the first track point and the closest runway edge or between the last track point and the closest runway edge were also similarly mapped to the runway centerline. These distances were then summed and taken as the straight-line distance from the runway edge to the exit taxiway.

3.2.6 Turn Distance, Exit Taxiway Angle, Exit Taxiway Location & Perpendicular Distance to Exit Taxiway Holdbar

Figure 3.8 illustrates the methodology used to measure turn distances and runway exit angles at Los Angeles International Airport (LAX). The runway exit angle was taken as the maximum possible angle between the runway centerline (yellow line in Figure 3.8) and the centerline of the runway exit (red line in Figure 3.8). This angle is exemplified by the blue

curve in Figure 3.8.

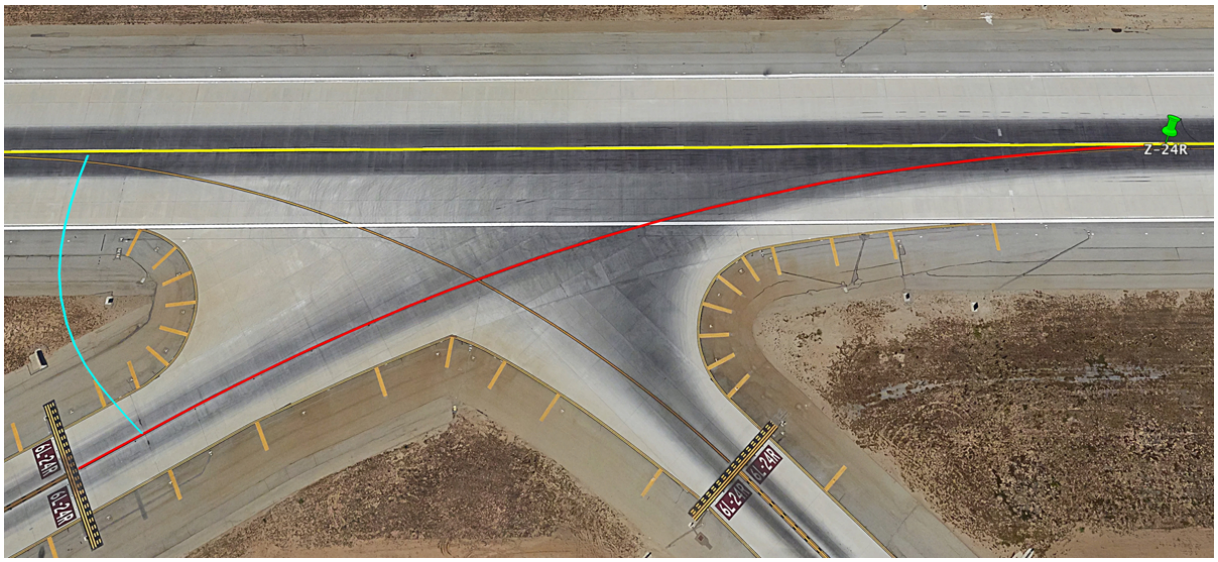

Figure 3.8: Diagram of Turn Distance and Runway Exit Angle Measurements. Source: Google Earth

The total turn distance for an aircraft on arrival is taken to be the distance from the start of the turn to the hold bar, also illustrated by the red line in Figure 3.8. Estimation of the starting point of the turn depended on whether a taxiway centerline extended into the runway. Usually, a taxiway centerline will extend from the point of tangency with the runway centerline up until and beyond the exit hold bar as illustrated in Figure 3.9.

Figure 3.9: Image of Taxiway Centerline at San Francisco International Airport Runway 10L-28R. Source: Google Earth

If a taxiway centerline is present and intersects the runway centerline, the point at which the taxiway centerline first begins to deviate from the runway centerline is taken as the start of the turn. If a taxiway centerline is present but does not extend into the runway, the taxiway centerline was manually projected to an intersection point with the runway centerline taking care to maintain the curvature that might be expected. Similarly, if no taxiway centerline was present, a centerline was manually drawn in Google Earth from the center of the exit hold bar to a projected point of tangency with the runway centerline, making sure match the curvature of the exit boundaries. This point was then taken as the start of the turn.

Once either a real or projected taxiway centerline was established, the straight-line distance from the runway threshold to the intersection of the runway edge and the taxiway centerline was taken as the exit taxiway location. This distance is illustrated by the green line in Figure 3.10.

Figure 3.10: Image of Straight-Line Distance from Runway Threshold to Intersection of Taxiway Centerline and Runway Edge at Chicago O'Hare International Airport Runway 9R-27L. Source: Google Earth

Finally, referencing Figure 3.8, the perpendicular distance to the exit taxiway hold bar is the perpendicular distance relative to the runway centerline in yellow from the runway centerline to the end of the taxiway centerline in red.

3.2.7 Runway Length, Runway Width, Runway Heading & Displaced Threshold Length

These data were extracted from the APT.txt file contained within the FAA 56-day NASR Subscription data.

3.2.8 Airport Altitude

In general, the PDARS/ASDE-X altitude data were very fuzzy and inaccurate usually when viewed during an arrival or departure movement. However, the data were relatively stable otherwise. Thus, in order to estimate the airport altitude, we utilized the runway coordinate data to establish the extent of the airport boundaries. That is, we found the extrema of the runway coordinates and collected all altitude data within these extremes. The most commonly occurring value of altitude was taken as the airport altitude. While the airport altitude data may have been inaccurate, we chose to establish a reference altitude value using the PDARS/ASDE-X data so as to avoid introducing further external uncertainty into the altitude data. This is to say that if, for example, all data were off by 5 feet, then relative to the data's own reference value, the offset would disappear.

3.2.9 Average Deceleration on Arrival & Touchdown Distance

For an arriving aircraft, the runway on which the arrival movement was occurring was first identified. Next, the altitude for each track point during the arrival movement were identified and a low-pass moving average filter with a span of 7 was applied in order to reduce the noise in the signal. Figure 3.11 illustrates a smoothed altitude profile. Having previously estimated the straight-line distances to the runway exit for track points within the runway, these values were used to produce a vector of cumulative distance traversed.

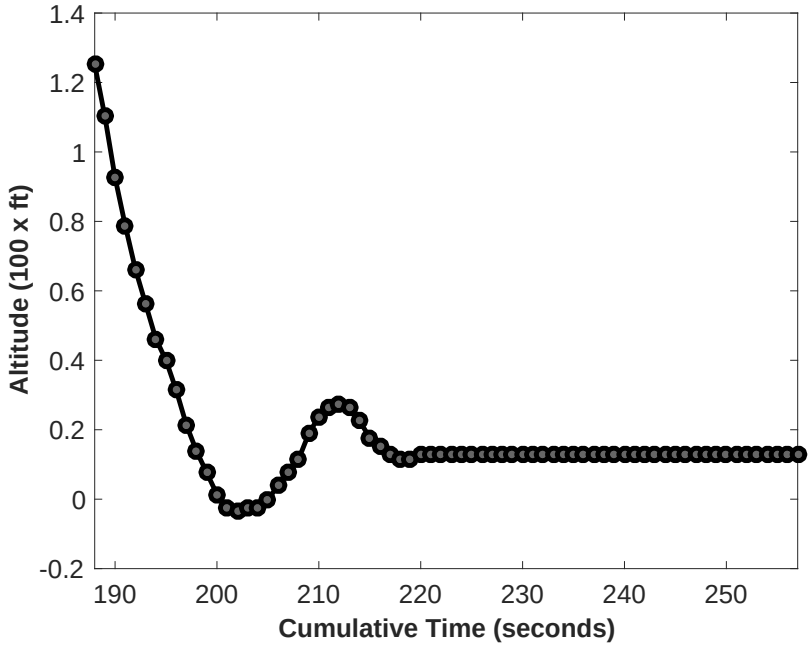

Figure 3.11: Illustration of Smoothed Altitude Profile (A306 Arriving Runway 27 at San Diego)

Using the smoothed altitude profile, the first altitude value corresponding to the first track point within the runway was identified. If the runway has a displaced threshold, then the first track point following that threshold was identified along with its corresponding altitude value. Once the appropriate initial track point was identified, the following track point altitude was examined. If its value was lower than that of the current track point, then the following track point was set as the subject track point. However, if the altitude of the following track point was greater than or equal to the altitude of the current track point,

then the following point up to three points downstream from the subject track point was examined. If no altitude value lower than that of the current track point was identified, then the current track point was taken to be the point of touchdown. The distance of this point from either the runway threshold or the displaced threshold was taken to be the touchdown distance.

Once the point of touchdown was located, the velocities associated with the 15 track points following the touchdown point were utilized to estimate the average deceleration on arrival. This was done on the assumption that an aircraft will decelerate on average for between 10 and 15 seconds following touchdown. A 15 second time window was also utilized to smooth the effects of any errors in the velocity values on the value of the average deceleration.

Chapter 4

Predictive Models of Departure and Arrival Runway Occupancy Time and Take-Off Distance

4.1 Introduction

Runway occupancy time has long been recognized and utilized as one of the critical determinants of runway operational capacity. Consequently, departure and arrival runway occupancy times are utilized in many air transport simulation models in their analyses of airport capacity (LeighFisher, 2012). Oftentimes, air transport simulation models are capable of detailed analyses at the individual aircraft level. However, due to the considerable expense of ROT field collection, data for runway occupancy times are either unavailable or solely available at the aggregate level. Thus, there currently exists a need for reliable runway occupancy time that can be applied by individual aircraft level.

In recognition of this need, we endeavored to produce models of both departure and arrival runway occupancy time, subject to the following design criteria. First, the models should be easily utilized by analysts. Second, the models should depend on data that is either publicly available or acquired with little difficulty. Third, the models should be widely applicable and easily incorporated into existing air transportation simulation models. Finally, the models

should have strong predictive power.

In this chapter, we describe two collections of models that can be used to predict departure and arrival runway occupancy time. The first collection of models predicts both departure runway occupancy time (DROT) and departure roll distance as linear functions of altitude, lift-off velocity, headwind and runway length. The next collection predicts arrival runway occupancy time (AROT) as linear functions of altitude, available landing runway length, straight-line threshold to exit taxiway distance, exit angle, runway threshold crossing velocity and exit turn distance. Each of the models is based on more than four hundred thousand records of aircraft track data collected by a multilateration surveillance system (ASDE-X). Distributions of occupancy times by aircraft type are presented and cross validation of the models demonstrated an expected prediction error that was generally within 10 percent of both average departure runway occupancy times and arrival runway occupancy times at the airports for which data were collected.

The ability to predict by individual aircraft type provides greater fidelity in runway capacity estimates. Additionally, the distributions produced from the models should be readily applicable to existing air transport simulation models, which accept and require probability distributions for modeling runway occupancy time.

4.2 Literature Review

This section presents a review of the role of ROT in airport capacity models as well as various methods for describing and predicting both departure runway occupancy times (DROT) and arrival runway occupancy times (AROT). The goal is to elucidate the reasoning behind the modeling choices made for the predictive models to be presented.

4.2.1 ROT as a Function of Airport Capacity

Runway occupancy time has long been recognized and utilized as one of the critical determinants of runway operational capacity. Among the earliest investigations of runway capacity was a study by Bowen and Pearcey, which modeled arrivals to a single runway using a M/D/1 queueing system (Bowen and Pearcey, 1948). In their model, aircraft

arrivals follow a Poisson distribution with successive aircraft maintaining a fixed time separation. Bowen and Pearcey also assumed the service rate (μ) for the runway is constant, which implies a constant AROT. They determined that the proportion of delayed aircraft was equal to the runway utilization (ρ), measured by the arrival rate (λ) divided by the service rate for arriving aircraft. Written in terms of the AROT, the fraction of delayed aircraft is given as $\lambda \times$AROT. Thus, Bowen and Pearcey's work also demonstrates a positive correlation between higher numbers of delayed arriving aircraft and higher values of AROT (Bowen and Pearcey, 1948).

Horonjeff et al. proposed one of the earliest models to estimate optimal runway exit locations that maximize the landing rate of arriving aircraft. Horonjeff et al. suggested that usage of optimal runway exits would decrease average AROT and increase arrival capacity. In their model, AROT consists of two stochastic parts (1-2) and one deterministic part (3): (1) the time required to decelerate to the design exit speed, (2) the time needed to reach the first exit following deceleration, and (3) the turn-off time. Horonjeff et al. found that optimal exit locations depended heavily on the AROT of the landing aircraft and thus necessitated the development of empirical distributions for the stochastic components of AROT by aircraft type (Horonjeff et al., 1959).

Blumstein also agreed that a more realistic model of AROT would include the relationship between AROT and aircraft type. However, in his airport capacity model, he opted to assume the AROT of a landing aircraft as constant across aircraft types. Nevertheless, Blumstein illustrated the modest effects of AROT on runway operations, showing that variation in AROT from 15 to 30 seconds can affect the number of runway operations possibly by around 5 percent. Reduction of AROT was also found to appreciably increase operations capacity when the runway is used for mixed operations (arrivals and departures) (Blumstein, 1960).

Astholtz et al. highlighted the critical importance of DROT and AROT to runway capacity for runways under mixed operations while also recognizing the influence of runway taxiway design and placement on ROT (Astholz et al., 1970). Astholtz et al. also noted for arrivals-only operations that AROT will become critical as interarrival spacing is further reduced (Astholz et al., 1970).

For a continuous stream of arriving aircraft, Kanafani found that the capacity of the runway is determined by the runway's flow rate,which is the reciprocal of the minimum time

headway between aircraft over the threshold. Kanafani noted that this headway is the larger of either the AROT time or the time resulting from the separation between arriving aircraft. (Kanafani, 1983).

Pavlin et al. quantified the consequences of large ROTs to runway capacity. Pavlin et al. pointed out that excess ROTs of only a few seconds can lead to delays that are one or more orders of magnitude greater than the excess time. These delays can accumulate, ultimately reducing system capacity. Conversely, Pavlin et al. asserted that savings of 5 seconds of ROT per movement can potentially increase system capacity by up to 1.5 hourly movements. (Pavlin et al., 2006).

4.2.2 Measuring ROT and Identifying Its Contributing Factors

Because the use of ROT in determining an airport's capacity requires one to have reasonable values of ROT available, a number of previous efforts aimed to provide guidance on applicable values of ROT. An early study and data collection of ROT by Swedish utilized three hypothetical weight classes (light, medium and heavy jets) in classifying aircraft. Swedish found that while significant differences existed between AROT values for his three weight classes, AROT varied little when aircraft, irrespective of weight, utilized the same runway and exit (Swedish, 1972). Swedish found less variability in DROT values and concluded that time to liftoff did not vary on aircraft type. Swedish noted that the DROT values observed ranged between 25 and 35 seconds for all jet aircraft and between 20 and 25 seconds for all propeller aircraft considered in his study. (Swedish, 1972).

Following Swedish's study, a more extensive survey of AROT was carried out by Koenig of the MITRE Corporation. Though Koenig did not personally collect AROT field data, he utilized a pre-existing database of ROT observations collected by Peat, Marwick, Mitchell and Company. Koenig's study was motivated by the FAA's desire to reduce IFR separation standards. As such, the goal was to get a sense of current AROT parameters to determine whether AROT would inhibit gains to runway capacity achieved through separation standard reduction (Koenig, 1978). Koenig's study was one of the first to identify motivational factors (e.g., minimum time to gate, least number of turns to gate and company procedures) as factors influencing AROT. Koenig found that AROT could differ by as much as 8 seconds

owing to various levels of pilot motivation to exit the runway. Koenig also surmised that given proper pilot motivation towards minimizing AROT and optimal usage of airport exits, existing AROT times could be reduced by as much as 14 seconds (Koenig, 1978).

Koenig's study would be followed by a study by Gosling et al., which had as one of its four objectives, the goal of more completely understanding factors that affect runway occupancy (Gosling et al., 1981). To address this objective, Gosling et al. analyzed a synthesis of ROT data from three databases: (1) FAA airport capacity study data, (2) Transportation Systems Center data, and (3). NASA head-up display simulator data. From these data, typical values of AROTs of large jet transport aircraft (e.g. B727) were found to be in the range of 45 to 65 seconds while for DROTs, typical values were in the range 35 to 50 seconds. (Gosling et al., 1981). Gosling et al. analyses identified aircraft size, airline and pilot motivation, weather and visibility conditions, the presence of landing and navigational aids and approach speed as factors influencing runway occupancy (Gosling et al., 1981).

In a 1979 study, Swedish addressed the feasibility of implementing reduced IFR separations to as low as 2.0 nautical miles on final approach. However, the feasibility of reduced IFR separation rested largely upon whether AROT times were sufficiently low enough or could be reasonably improved to avoid increased ATC controller workload and increased go-around rates for aircraft on approach (Swedish, 1979). Swedish concluded that reduced longitudinal separations of 2.5 nautical miles were possible if mean AROTs were below 50 seconds (Swedish, 1979).

In order to investigate whether current AROT times were below the 50 second threshold that Swedish had previously identified, Weiss and Barrer performed a field study in 1984 at New York LaGuardia, Boston Logan and Newark airports, in which they gathered over 600 observations of AROT at each of the three airports. Weiss and Barrer illustrated that the current AROT times observed were sufficiently low enough to allow for the 2.5 nautical mile longitudinal separation standard (Weiss and Barrer, 1984). Their study was also one of the earliest to break down AROT by runway condition and by airport and aircraft size, illustrating the effects of different ATC regimes, airport layouts, fleet mixes and weather on AROT. Tables 4.1 and 4.2 provide the mean AROTs observed in the Weiss and Barrer study by aircraft type for three airports and by runway condition for two airports.

The results of Weiss and Barrer illustrated that AROT times lower than 50 seconds

Table 4.1: Mean AROT in Seconds by Aircraft Type. Source: (Weiss and Barrer, 1984)

Aircraft Type	LGA	BOS	EWR
Small	43.5	48.7	40.1
Large	46.0	52.1	42.2
Heavy	50.5	56.7	45.6

Table 4.2: Mean AROT in Seconds by Runway Condition. Source: (Weiss and Barrer, 1984)

Runway Condition	LGA	BOS
Dry	45.5	51.5
Wet	47.1	51.5

were being realized and this led the FAA to develop a demonstration program that would implement the reduced separation standard at selected airports. Los Angeles, San Francisco, Atlanta and Dallas-Fort Worth airports were selected as potential candidates for the FAA demonstration program. To verify whether AROT times were below the 50 second maximum, Weiss performed a later field study in 1985, in which AROT data were collected at the candidate airports. While average AROT at San Francisco was too high, Weiss found that mean AROTs at Atlanta, Dallas-Fort Worth and Los Angeles were either below or barely above the 50 second threshold (Weiss, 1985). The mean AROT values at each candidate airport are given in Table 4.3.

Table 4.3: Mean AROTs in Seconds by Airport. Source: (Weiss, 1985)

SFO	LAX	DFW	ATL
57.1	50.7	45.6	41.6

Trani et al. introduced a kinematic computer model known as the Runway Exit Design Interactive Model (REDIM), which simulated the aircraft landing process and applied an optimization algorithm to select the optimal runway exit location. In order to calibrate the model, Trani et al. conducted a videographic data collection of ROT times by specific runway exit taxiway at Washington-Dulles, Atlanta, Washington-National and Charlotte-Douglas Airports. Table 4.4 summarizes their collected ROT data, which were not explicitly assumed

a priori to match any particular probability distribution. (Trani et al., 1995). However, in their kinematic model, Trani et al. utilize a number of intermediate parameters, which are assumed to be normally distributed, in estimating ROT. Consequently, the predicted ROT values, which are formed from the sum of these intermediate parameters, would follow a normal distribution assuming that these intermediate parameters could be considered independent random variables.

Table 4.4: Summary Statistics of Collected ROT Data (in Seconds)by Airport. Source: (Trani et al., 1995)

Airport	Runway	Min	Max	Count	μ	σ
IAD	01R	36.6	72.5	47	53.3	8.63
ATL	08L	39.0	86.0	239	50.7	7.00
DCA	36	34.8	130.4	241	47.6	11.3
CLT	23	33.6	74.8	134	48.0	9.42

A similar tool is described by Barbas et al. of the Spanish engineering firm INECO. They introduce proESTOP (**Es**timador de **T**iempos de **O**cupación de **P**ista), which is capable of estimating AROT and selecting optimal exit taxiways. To validate the model, Barbas et al. collected at Madrid-Barajas airport AROT data, which had a mean of 46.5 seconds and a standard deviation of 7.9 seconds. Barbas et al. claim that proESTOP provide estimates of AROT within the 95% confidence interval around the AROT data sample mean. Additionally, Barbas et al. point out that proESTOP also provides estimates of DROT (Barbas et al., 2007).

4.2.3 Modeling and Prediction of ROT

Field collection of ROT values is not always possible due to its potential expense both in time and money. Consequently, many researchers have sought to develop high fidelity models that can be used to predict ROTs. Perhaps the earliest model assigned to ROTs was provided in a runway capacity study by Bell. In contrast to the 1948 study by Bowen and Pearcey, Bell asserted that arrivals are not necessary Poisson. Regarding ROTs, which Bell called the "holding time", Bell held that DROT and AROT could be modeled using Pearson Type-III distributions (Bell, 1949). However, Bell opted to develop his capacity

model assuming constant ROTs, owing to the "intractable" mathematics associated with the Pearson Type-III distribution. (Bell, 1949).

In a much later study, Lee et al. utilized the NASA Dynamic Runway Occupancy Measurement System (DROMS) to produce a set of current AROT data for studying airport surface operations at Atlanta airport. In their study, analyses centered on determining the factors that influence AROT including aircraft weight, approach velocity, air carrier, and meteorological conditions. Data from DROMS were sorted by runway, exit used, weight class (large, heavy or small), approach speed category (A, B, C, D) and runway conditions (dry, wet, etc.). Over a 15-day period, the DROMS provided AROT for over 3,000 landings. Values of AROT less than 25 seconds were assumed to be incorrect and were omitted. Similarly, values of AROT above 65 seconds were assumed to be aircraft taxiing to specific points at the far end of the runway and were also deleted. Lee et al. concluded that the AROT data fit a normal distribution, having a mean of 44.13 seconds and a standard deviation of 7.46 seconds (Lee et al., 1999).

Haynie investigated the interaction between airport capacity and safety, asserting that levels of safety are influenced by levels of demand on available capacity. In his work, he selected LaGuardia airport in order to demonstrate the safety benefits from potential improvements in capacity. For his study, Haynie collected both landing time interval and AROT data and found that a normal distribution with a mean of 48 seconds and a standard deviation of 8 seconds best-fit his data (Haynie, 2002).

Jeddi examined the factors necessary to maximize the capacity of an airport's landing system. In the course of his work, Jeddi analyzed aircraft track data for Runway 21L at Detroit Metropolitan Wayne County Airport (DTW) and developed a statistical distribution for AROT (Jeddi, 2008). In his analysis, Jeddi divided arrivals into those exiting the runway at the first two exits (early) and those exiting the runway at the latter two exits (late). For the early group of landings, he fit a beta distribution (11.8, 27.9) in the range (20,90) and for the late group of landings, he fit a beta distribution (9.0, 16.6) in the range (30,110). For overall AROT, he summed the two distributions weighted by the percentage composition of landings observed, giving the full distribution of AROT as 0.59 Beta([20,100],11.8, 27.9) + 0.41 Beta([30,120]),9.0, 16.6) (Jeddi, 2008).

Jeddi et al. directly dealt with the inherent uncertainty in factors that influence the

approach process of arriving aircraft. In their study, Jeddi et al. extracted landing time intervals, inter-arrival distances and AROT data from a week's worth of multilateration data at DTW. Under peak periods in IMC conditions, Jeddi et al. fit a Beta distribution to the ROT data having the parameters Beta(25,110;6.1,15.4) with a mean of 49.1 seconds and a standard deviation of 8 seconds. Jeddi et al. then attempted to discern differences between VMC and IMC conditions but found the ROT data for both conditions to have a mean of 49 seconds and a standard deviation of 8 seconds (Jeddi et al., 2006). In a related study in 2009, Jeddi et al. fit two different Beta distributions to ROT data collected at DTW. The first distribution for a mix of small and large aircraft had the parameters 0.62 Beta ([20,90], 11.23,26.33) + 0.38 Beta ([30,110], 13.60,27.39). For a mix of large, B757 and heavy aircraft, the parameters are 0.497 Beta([25,90], 15.75, 40.24) + 0.503 Beta ([30,110], 8.31, 14.72) (Jeddi et al., 2009).

Kumar et al. demonstrated methods for extraction of AROT data from ASDE-X surface track data using Dallas-Fort Worth Airport as a case study. Using three days of ASDE-X surface data, Kumar et al. found the best-fit distribution for all the data to be an Erlang with parameters 20.5 + Erlang(4.51,6). Kumar et al. noted that a normal distribution with mean of 47.5 seconds and standard deviation of 11 seconds fit relatively well once outliers were removed from the dataset. Table 4.5 summarizes their results, broken down by aircraft weight class. (Kumar et al., 2010).

Table 4.5: Summary Statistics of AROT Data (in Seconds) by Aircraft Category. Source: (Kumar et al., 2010)

Weight Class	Count	Min	Max	Median	μ	σ
Small	104	22	115	45	47.6	15.1
Large	1710	21	194	46	47.3	11.6
B757	140	24	82	48	48.5	9.5
Heavy	81	29	92	53	56.4	15.8

Nikoleris investigated differing scenarios for a queueing system under 3-D space and time aircraft operations in order to develop analytical estimates of aircraft delays. In one scenario, Nikoleris sets the runway threshold as the server, thereby making the AROT the service time. The arrival times to the runway threshold have a deterministic portion and stochastic portion, which represents the variability in an aircraft's arrival to the runway threshold.

Depending on the magnitude of the delay, the time at which the arriving aircraft crossed the threshold would be the greater of one of the following: (1) the value of the time delay, (2) the value of any minimum separation headway requirement (3), the value of the time at which the preceding aircraft crossed the threshold plus any minimum separation headway, or (4) the time the preceding aircraft crossed the threshold plus its AROT (Nikoleris, 2011). Nikoleris asserts that a distribution modeling AROT must have a bell-shape and positive skewness. Also, since the service time is dependent on the underlying distributions of either the arrival delay, Nikoleris proposes a Gumbel distribution for each arriving aircraft's ROT (Nikoleris, 2011).

4.2.4 Summary of ROT Models

In order to attain a benchmark of performance for the predictive models to be presented, a summary of the available data from the ROT literature and a summary of the proposed models is provided below in Table 4.6.

Table 4.6: List of Proposed Distributions and Summary Data for AROT and DROT

Author(s)	Year	Distribution	AROT	DROT	Mean	Std. Dev.
Bell	1949	Pearson-Type III	X	X	—	—
Lee et al.	1999	Normal	X	—	44.13	7.46
Haynie	2002	Normal	X	—	48	8
Jeddi et al.	2006	Beta	X	—	49.1	8
Jeddi	2008	Beta	X	—	—	—
Jeddi	2009	Beta	X	—	47	9.3
Kumar et al.	2010	Erlang	X	—	47.5	11
Nikoleris	2011	Gumbel	X	—	—	—

Values of AROT range roughly from 44 to 49 seconds and the average standard deviation of AROT is 8.752 seconds. Unfortunately, no data were available for the mean and standard deviation of Bell's Pearson-Type III distribution, which would have provided some information regarding values of DROT.

4.3 Model Formation

4.3.1 Departure Runway Occupancy Time & Departure Roll Distance Model Variables

The first set of models proposed will consider DROT, represented by the variable $ROTD$, and departure roll distance, represented by $Dist_{TO}$, as linear functions of a combination of altitude above sea level (Alt), horizontal wind velocity ($Wind$), runway length ($Rwlen$) and lift-off velocity (V_{LO}).

Predictions of departure roll distance can be considered indirect predictions of departure runway occupancy time and vice-versa. If we have a departure roll distance and assume an average acceleration (a_{avg}) on take-off or can characterize the acceleration profile, we are able to estimate the departure runway occupancy time by

$$DROT = \sqrt{\frac{2 \times Dist_{TO}}{a_{avg}}} \tag{4.1}$$

assuming zero initial velocity on take-off. Similarly, the take-off distance can be estimated by

$$Dist_{TO} = \frac{1}{2} a_{avg} (DROT)^2 \tag{4.2}$$

What follows is a description of each of the variables as they relate to DROT and take-off distance and the reasoning behind their inclusion.

Altitude above sea level

As an aircraft performs its take-off roll, an air pressure differential forms around the aircraft wings and begins to generate lift force, which is formulated as

$$F_L = \frac{1}{2} \rho v^2 S C_L \tag{4.3}$$

where F_L is the lift force, ρ is the air density, v is the true airspeed, S is the planform area and C_L is the lift coefficient. The air density is a function of atmospheric pressure (p), air

temperature (T) and the mean molar mass of the air (M). Using the ideal gas law, air density is calculated as

$$\rho = \frac{pM}{RT} \tag{4.4}$$

where R is the ideal gas constant. The mean molar mass is determined by

$$M = \frac{\sum(n_i M_i)}{\sum(n_i)} \tag{4.5}$$

where n_i and M_i are the density and molecular weight of the i^{th} component of air. Between sea level and altitudes around 80 km, which are well beyond the operating range of any jet aircraft, the fractional composition of each air component is assumed to remain constant, thereby making the mean molecular mass constant (COESA, 1976). For an altitude h above sea level, T can be approximated as

$$T = T_0 - Lh \tag{4.6}$$

where T_0 is the sea level standard temperature and L is the temperature lapse rate. The pressure at altitude h above sea level is given as

$$p = p_0 \left(1 - \frac{Lh}{T_0}\right)^{\frac{gM}{RL}} \tag{4.7}$$

with p_0 equal to sea level standard atmospheric pressure and g being acceleration due to gravity. Therefore, if we combine (4.3), (4.4), (4.6) and (4.7), the generated lift force can be formulated as

$$F_L = \frac{v^2 p_0 M S C_L \left(1 - \frac{Lh}{T_0}\right)^{\frac{gM}{RL}}}{2R(T_o - Lh)} \tag{4.8}$$

If we take the first derivative with respect to the altitude h, we find $\frac{dF_L}{dh}$ to be

$$\frac{dF_L}{dh} = -\frac{v^2 p_0 M S L C_L \left(\frac{gM}{LR} - 1\right) \left(1 - \frac{Lh}{T_0}\right)^{\frac{gM}{RL} - 2}}{2RT_0^2} \tag{4.9}$$

Equation 4.9 demonstrates that the lift force decreases with increasing altitude h above sea level. Consequently, at higher altitudes, aircraft on take-off will generally need to utilize

additional runway to reach a higher velocity before beginning the take-off rotation. The extra runway length utilized will increase both the departure runway occupancy time and the departure roll distance. Therefore, since altitude has a likely positive effect on DROT and departure roll distance, we include altitude above sea level, represented by the variable *Alt*, as a potential DROT and take-off distance model variable.

Lift-Off Velocity

Takeoff distance for a departing aircraft consists of two parts, the ground run and the horizontal distance from when the aircraft leaves the ground to when it reaches 35 feet. To determine the ground roll, we balance the equations of motion on the aircraft as it rolls down the runway. The vertical forces are the aircraft's lift force (F_L) generated by its wings, the aircraft's weight (mg), and its resulting normal force (N). The horizontal forces are the thrust provided by the aircraft's engines (T_r), the resultant drag force due to the aircraft's motion (F_D), and the rolling friction experienced by the aircraft's tires during takeoff ($N\mu_r$), where μ_r is the coefficient of rolling friction.

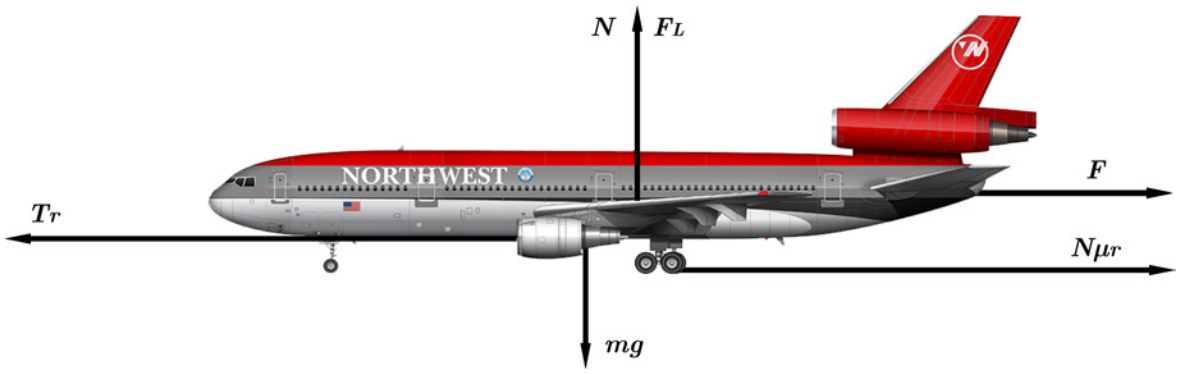

Figure 4.1: Force Balance on Departure. Base Image Source: (Scott, 2016)

If we assume a level runway, the aircraft's vertical forces balance as

$$F_L + N = mg \tag{4.10}$$

and the aircraft's horizontal forces balance as

$$ma = T_r - F_D - N\mu_r \tag{4.11}$$

The drag force is given as

$$F_D = \frac{1}{2}\rho v^2 S C_D \tag{4.12}$$

where C_D is the drag coefficient. Combining equations (4.10), (4.12), and (4.3), we have

$$ma = T_r - \frac{1}{2}\rho v^2 S C_D - (mg - \frac{1}{2}\rho v^2 S C_L)\mu_r \tag{4.13}$$

With $W = mg$ and after simplifying, we have

$$a = \frac{dv}{dt} = \frac{T_r g}{W} - g\mu_r - \frac{g\rho S(C_D - C_L\mu_r)}{2W}v^2 \tag{4.14}$$

As illustrated by (4.3), the lift force is a function of true airspeed v and increases as the airspeed increases. The relationship between thrust and airspeed varies depending on the engine type and environmental factors such as air density and temperature. For turbojet engines, the thrust varies little with airspeed while for piston engines, the thrust will decrease linearly assuming a constant-pitch propeller (Phillips, 2010). For turbofan engines, the thrust is considered to vary parabolically with airspeed. (Phillips, 2010). Figure 4.2 illustrates how thrust available varies with airspeed.

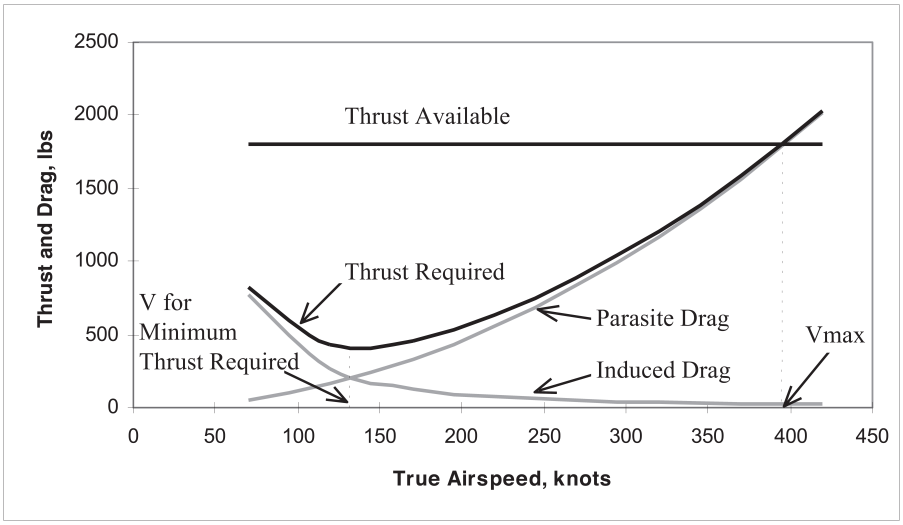

Figure 4.2: Thrust Available and Thrust Required for a Subsonic Jet Aircraft Source: (Brandt et al., 2004).

Assuming the following parabolic relationship

$$T_r = A + Bv + Cv^2 \tag{4.15}$$

where A, B, and C are experimentally determined coefficients depending on the specific engine, we can write (4.14) as

$$\frac{dv}{dt} = \frac{gA}{W} + \frac{gBv}{W} + \frac{gCv^2}{W} - \frac{g\rho S\left(C_D - C_L\mu_r\right)v^2}{2W} - g\mu_r \tag{4.16}$$

To determine the time for the ground run, we first rearrange (4.16) as

$$dt = \frac{2W}{2gA - 2Wg\mu_r + 2gBv + v^2\left(2gC - g\rho S\left(C_D - C_L\mu_r\right)\right)}dv \tag{4.17}$$

If we let $\beta = 2gA - 2Wg\mu_r$, $\xi = 2gB$, and $\lambda = 2gC - g\rho S\left(C_D - C_L\mu_r\right)$, (4.17) becomes

$$dt = \frac{2W}{\beta + \xi v + \lambda v^2}dv \tag{4.18}$$

Integrating with respect to v and assuming zero initial airspeed gives

$$t = \frac{4W}{\sqrt{4\beta\lambda - \xi^2}} \arctan\left(\frac{\xi + 2\lambda v}{\sqrt{4\beta\lambda - \xi^2}}\right) \tag{4.19}$$

Provided the denominator remains positive, the ground run time monotonically increases with v, albeit at a non-constant and decreasing rate. Therefore, since the lift-off velocity represents the final velocity achieved during the ground run phase and has direct bearing on the time in ground run and the DROT, lift-off velocity, represented by the variable V_{LO}, is considered for the DROT models. It also follows that greater time spent in the ground run translates to a longer take-off roll. We explore this further later, but also include V_{LO} in our model of take-off distance.

Horizontal Wind Component

Implicit in (4.19) is the presumption of zero headwind, thus allowing for the assumption that the airspeed v is equal to the groundspeed v_g. If we now consider a positive constant headwind v_{hw}, (4.19) becomes

$$t = \frac{4W}{\sqrt{4\beta\lambda - \xi^2}} \arctan\left(\frac{\xi + 2\lambda\left(v - v_{hw}\right)}{\sqrt{4\beta\lambda - \xi^2}}\right) \tag{4.20}$$

Taking off against a headwind results in a shorter ground run distance and a takeoff at a lower ground speed since the headwind is also generating lift. Consequently, we include the horizontal wind component, represented by the variable *Wind*, in our model of take-off distance.

As illustrated by (4.20), a positive constant headwind also results in a shorter ground run time relative to the ground run time at zero headwind. Conversely, a tailwind would lead to a longer ground run time. Therefore, since wind directly impacts the DROT, the horizontal wind component is also considered for the DROT model.

Runway Length

Revisiting (4.18), we can represent (4.18) as

$$dt = \frac{2W}{\beta + \xi v + \lambda v^2} dv \Rightarrow \frac{dv}{dt} = \frac{\beta + \xi v + \lambda v^2}{2W} = \frac{dv}{ds}\frac{ds}{dt} \tag{4.21}$$

where s is the ground distance traveled. Assuming a constant headwind component, $ds/dt = v - v_{hw}$, thus giving

$$\frac{dv}{ds} = \frac{\beta + \xi v + \lambda v^2}{2W(v - v_{hw})} \tag{4.22}$$

To determine the ground run length, we can rearrange (4.22) to be

$$ds = \frac{2W(v - v_{hw})}{\beta + \xi v + \lambda v^2} dv \tag{4.23}$$

At the start of the ground run, at zero initial groundspeed, the initial airspeed v will be equal to the headwind v_{hw}. Therefore, we integrate (4.23) from v_{hw} to V_{LO}, our liftoff velocity to obtain the total ground run distance. This results in

$$s = \frac{W}{\lambda}\left[\ln\left(\beta + v\left(\xi + \lambda v\right)\right) - \frac{2\left(\xi + 2\lambda v_{hw}\right)\arctan\left[\frac{\xi + 2\lambda v}{\sqrt{4\beta\lambda - \xi^2}}\right]}{\sqrt{4\beta\lambda - \xi^2}}\right]\Bigg|_{v=v_{hw}}^{v=V_{LO}} \tag{4.24}$$

which equals

$$\begin{aligned} s = {} & \frac{W}{\lambda}\ln\left(\frac{\beta + V_{LO}\left(\xi + \lambda V_{LO}\right)}{\beta + v_{hw}\left(\xi + \lambda v_{hw}\right)}\right) + \\ & \frac{2W\left(\xi + 2\lambda v_{hw}\right)}{\lambda\sqrt{4\beta\lambda - \xi^2}}\left(\arctan\left[\frac{\xi + 2\lambda v_{hw}}{\sqrt{4\beta\lambda - \xi^2}}\right] - \arctan\left[\frac{\xi + 2\lambda V_{LO}}{\sqrt{4\beta\lambda - \xi^2}}\right]\right) \end{aligned} \tag{4.25}$$

Further simplification yields

$$\begin{aligned} s = {} & \frac{W}{\lambda}\ln\left[\left(V_{LO} - v_{hw}\right)\left(\xi + \lambda\left(V_{LO} + v_{hw}\right)\right)\right] \\ & + \frac{4W\left(\xi + 2\lambda v_{hw}\right)}{\lambda\sqrt{4\beta\lambda - \xi^2}}\left(\arctan\left[\frac{\lambda\left(v_{hw} - V_{LO}\right)}{\sqrt{4\beta\lambda - \xi^2}}\right]\right) \end{aligned} \tag{4.26}$$

From equation 4.26, we see that the ground run distance is a function of the horizontal wind component v_{hw}, the lift-off velocity V_{LO}, the weight of the aircraft W and the engine characteristics of the aircraft. Since the available runway length will determine the maximum possible value of the ground run, either the aircraft weight W or the lift-off velocity V_{LO} will have to be adjusted in order to ensure that a takeoff is possible. For example, depending on the aircraft type, a fuel-saving reduced thrust takeoff may not be feasible if the runway length is too small.

As was alluded to earlier, longer ground run times will lead to longer take-off lengths, which are ultimately limited by the available runway length. Therefore, we consider runway length, represented by the variable *RwLen*, for our model of take-off distance. Earlier, we also illustrated how V_{LO} affected the DROT. Since available runway length can potentially set a floor on lift-off velocity, runway length potentially has an indirect effect on DROT. Therefore, runway length is also considered for DROT models.

4.3.2 Arrival Runway Occupancy Time Model Variables

The second collection of models proposed will consider AROT, represented by the variable *ROTA*, as a function of aircraft performance, airport physical parameters and runway geometry. We describe the variables included and the reasoning behind their inclusion as follows.

Altitude above Sea Level

We first consider the forces on an aircraft in descent, displayed in Figure 4.3. During the landing process, an arriving aircraft approaches the runway at a reduced and controlled airspeed and sink rate ($\dot{h}$) to allow for a controlled and gentle touch down on the runway.

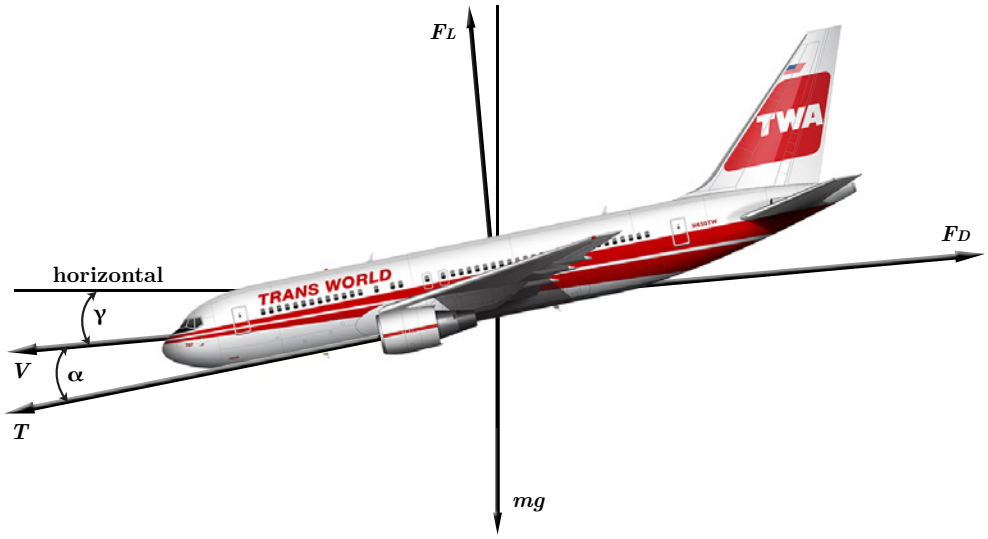

Figure 4.3: Forces acting on an Aircraft in Descent. Base Image Source:(Scott, 2016)

To find the sink rate, we first consider the equations describing an aircraft's motion in a 2-D frame. These are

$$ma = T\cos\alpha - F_D - mg\sin\gamma \tag{4.27}$$

$$\dot{\gamma} = \frac{1}{mv}(T\sin\alpha + F_L - mg\cos\gamma) \tag{4.28}$$

$$\dot{h} = v\sin\gamma \tag{4.29}$$

where γ is the flight path angle, T is the engine thrust produced, and α is the angle of attack. If we assume a steady velocity and a constant flight path angle on approach (generally around -3 degrees), it follows from equations 4.27 and 4.28 that

$$\sin\gamma = \frac{T\cos\alpha - F_D}{mg} \tag{4.30}$$

$$T = \frac{mg\cos\gamma - F_L}{\sin\alpha} \tag{4.31}$$

Therefore, the sink rate can be written as

$$\dot{h} = \frac{v}{mg}(\cot\alpha(mg\cos\gamma - F_L) - F_D) \tag{4.32}$$

Substituting in equations 4.3 and 4.12 into 4.32 gives

$$\dot{h} = \frac{v}{mg}(\cot\alpha(mg\cos\gamma - \frac{1}{2}\rho v^2 AC_L) - \frac{1}{2}\rho v^2 AC_D) \tag{4.33}$$

which can be written as

$$\dot{h} = -\frac{\cot\alpha}{2mg}\rho v^3 AC_L - \frac{1}{2mg}\rho v^3 AC_D + v\cot\alpha\cos\gamma \tag{4.34}$$

Considering the true airspeed v, we recognize that this is also a function of the air density as given by

$$v = EAS\sqrt{\frac{\rho_0}{\rho}} \tag{4.35}$$

where ρ_0 is the air density at sea level and EAS is the equivalent air speed. Consequently, at lower air densities, the true airspeed will be higher. Higher airspeeds lead to higher touchdown speeds and increase the landing roll as more energy has to be absorbed by the brakes, thus demanding the need of a longer runway.

It can be shown that the change in the sink rate with respect to ρ can be shown to be

$$\frac{d\dot{h}}{d\rho} = \frac{EAS^3 A\rho_0^2}{4\rho^2\sqrt{\frac{\rho_0}{\rho}}mg}(C_D + C_L\cot\alpha) - \frac{EAS\rho_0\cos\gamma\cot\alpha}{2\rho^2\sqrt{\frac{\rho_0}{\rho}}} \tag{4.36}$$

Thus, the sink rate $\dot{h}$ is illustrated to be a function of variable parameters such as the air density ρ, the equivalent airspeed EAS, the angle of attack α and the lift and drag coefficients, which can change depending on the flap configuration and angle of attack during approach.

Altitude can serve as a proxy measure of air density since air density decreases with altitude. Therefore, given that a decreased air density will increase approach speeds and will likely affect the landing configuration of arriving aircraft, it is likely that altitude will have a positive effect on the landing roll, which likely translates into a positive effect on AROT. Thus, we include altitude, represented by the variable *Alt*, in our model of AROT.

Runway Threshold Crossing Velocity

The landing distance for an arriving aircraft can be generally divided into two main portions, the flare portion and the landing run. During the flare portion, the aircraft is gliding to its touchdown point with its nose flared in order to regulate its sink rate and allow for a gentle landing. The landing run portion comprises the remainder of the landing distance and can be further subdivided into a first free roll, a braking phase, a second free roll and a turnoff phase (Trani et al., 1995). To estimate the landing roll portion, we apply a force balance, illustrated by Figure 4.4, on the aircraft as it rolls down the runway. The vertical forces are the aircraft's lift force (F_L), the aircraft's weight ($W = mg$), and its resulting normal force (N). The horizontal forces are the thrust provided by the aircraft's engines (T_r), the resultant drag force due to the aircraft's motion (F_D), and the runway rolling friction experienced by the aircraft's tires due to braking ($N\mu_r$), where μ_r is the coefficient of rolling friction. For arrivals, the engine thrust is generally either zero or negative for when reverse thrust is applied to assist with braking.

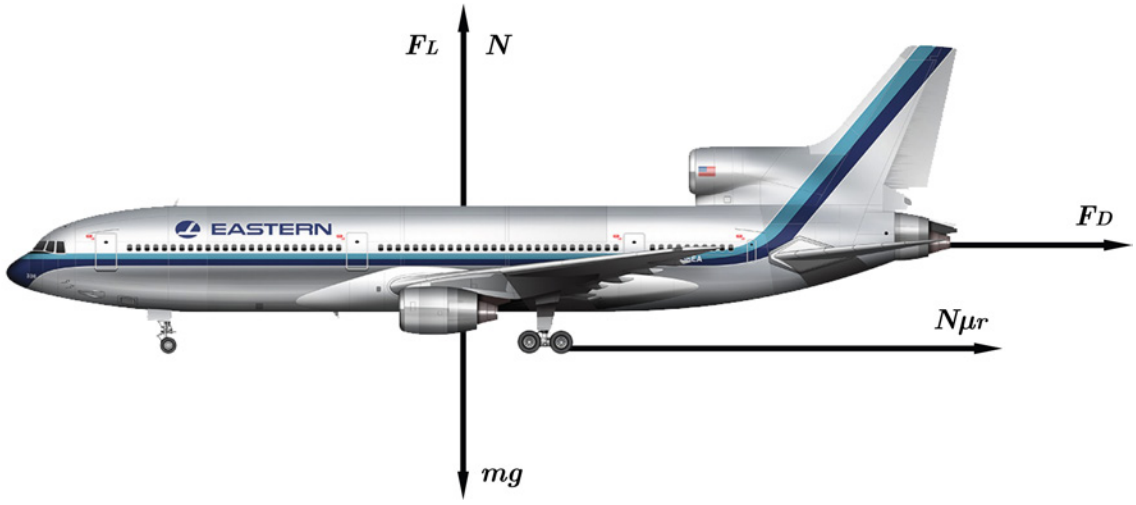

Figure 4.4: Forces Acting on an Aircraft on Landing (Zero Thrust Assumed). Base Image Source, (Scott, 2016).

If we assume a level runway and zero thrust, this results in the aircraft's vertical forces balancing as

$$F_L + N = W \tag{4.37}$$

and the aircraft's horizontal forces balancing as

$$ma = -F_D - N\mu_r \tag{4.38}$$

The drag force is given as

$$\frac{1}{2}\rho v^2 A C_D \tag{4.39}$$

where C_D is the drag coefficient. Combining equations (4.37), (4.39), and (4.3), we have

$$ma = -\frac{1}{2}\rho v^2 A C_D - (W - \frac{1}{2}\rho v^2 A C_L)\mu_r \tag{4.40}$$

With $W = mg$ and after simplifying, we have

$$\frac{dv}{dt} = -g\mu_r - \frac{g\rho A(C_D - C_L\mu_r)}{2W}v^2 \tag{4.41}$$

To determine the time for the ground run, we first rearrange (4.41) as

$$dt = \frac{-2W}{2gW\mu_r + g\rho A(C_D - C_L\mu_r)v^2}dv \tag{4.42}$$

If we let $D = 2gW\mu_r$ and $E = g\rho A(C_D - C_L\mu_r)$, (4.42) becomes

$$dt = \frac{-2W}{D + Ev^2}dv \tag{4.43}$$

Integrating with respect to v and assuming zero final airspeed gives

$$t = \frac{2W}{\sqrt{DE}} \arctan\left(\frac{v\sqrt{E}}{\sqrt{D}}\right) \tag{4.44}$$

Provided that $C_D - C_L\mu_r$ is positive, the ground run time increases with v. Therefore, assuming that the velocity upon touchdown is very close to the threshold crossing velocity, we can infer that the threshold crossing velocity has a direct bearing on the time in the ground run portion. Therefore, we include the threshold crossing velocity, represented by the variable *ThrVel*, in our model of AROT.

Effective Runway Length

Runway Length

The runway length is considered in the model for two reasons. First, assuming normal operations, the length of runway available for landing will ultimately set a practical ceiling on the AROT. That is to say, if an aircraft can safely land on a very short runway and moves toward a runway exit normally, the time spent on the runway will be limited by the available runway length remaining to traverse. Additionally, consideration of the length of runway available should account for the overall expectation that shorter runways will result in smaller AROT values. Second, the length of runway available may potentially have an influence on the variability of AROT values observed. Longer runway lengths will allow for pilots to simply move to the next available exit taxiway should they overshoot an earlier exit. However, shorter runway lengths perhaps demand that pilots brake sufficiently to exit at a certain taxiway lest they have to execute a go-around maneuver. Additionally, fewer exit options might be available for shorter runways. Therefore, for these reasons, we incorporate runway length into our model for AROT.

Displaced Threshold

In Title 14, Chapter 1, Subchapter E, Part 77 of the Federal Code (FAR 77), a number of standards are outlined for determining obstructions to air navigation at civilian and public-use airports. These standards place requirements on the positioning of runways and define the required clearances necessary for safe air navigation in compliance with Federal regulations. As these regulations have evolved, airports that were once in compliance might have found themselves out of compliance. Therefore, a number of airports have been forced to implement displaced thresholds. Displaced thresholds are identified by runway markings and communicate to pilots that they should treat the runway as beginning past the displaced threshold. This effectively reduces the available runway length available to arriving aircraft, as illustrated by Figure 4.5.

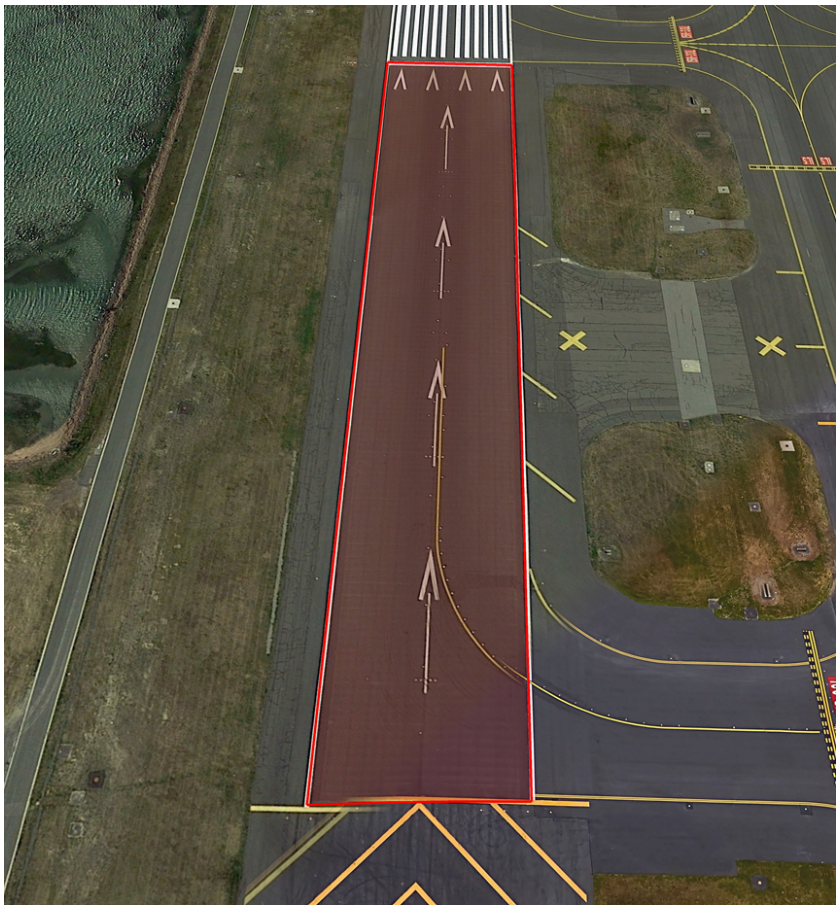

Figure 4.5: Displaced Threshold Shaded in Red at Boston-Logan Airport Runway 15R. Source: Google Earth.

Extending the logic for the inclusion of runway length into the model, since displaced threshold affect the effective length of the runway, it stands to reason that a displaced threshold might affect the AROT.

In order to consider both the runway length and the displaced threshold, we define the effective runway length, represented by the variable *EffRwLen*, as the runway length minus the displaced threshold length. We include *EffRwLen* in our model for AROT.

Exit Angle

As specified by the FAA, exit taxiways should

> permit free flow to the parallel taxiway or at least to a point where the aircraft is completely clear of the hold line. (Federal Aviation Administration, 2014a).

Generally, exit taxiways are set at angles of 90°, 45° or 30° relative to the runway centerline. Runway exit taxiways having an angle of 30° with the runway centerline are often considered high-speed exit taxiways provided that they meet other design criteria (Federal Aviation Administration, 2014a). Considerable research efforts have demonstrated that 30° exits allow for arriving aircraft to exit at higher speeds, thus reducing AROT and increasing airport capacity. Following from this logic, we assume that exit taxiway angles in general have an effect on exit speeds and, by extension, AROT. Therefore, we include exit angle, represented by the variable *ExitAng*, in our model for AROT.

Turn Distance

The turn distance refers to the distance from when the aircraft begins its exit movement to the point where it crosses the hold line. As indicated earlier, the point where the aircraft is clear of the hold line is the point where the aircraft is considered to have fully exited the runway. Generally, longer turn distances should lead to longer AROT except in the case where the exit is a high-speed exit. However, since exit angle is controlled for in the model, it seems reasonable to also consider runway exit turn distance. Therefore, we include turn distance, represented by the variable *TurnDist*, in our model for AROT.

Exit Distance from Runway Threshold

This distance refers to the straight-line distance from the physical runway threshold to the point where an aircraft would begin turning to utilize a specific exit taxiway. This distance will account for the distance in which an aircraft performs its flare maneuver, its free-roll phases and the majority of its deceleration. Figure 4.6 illustrates this distance.

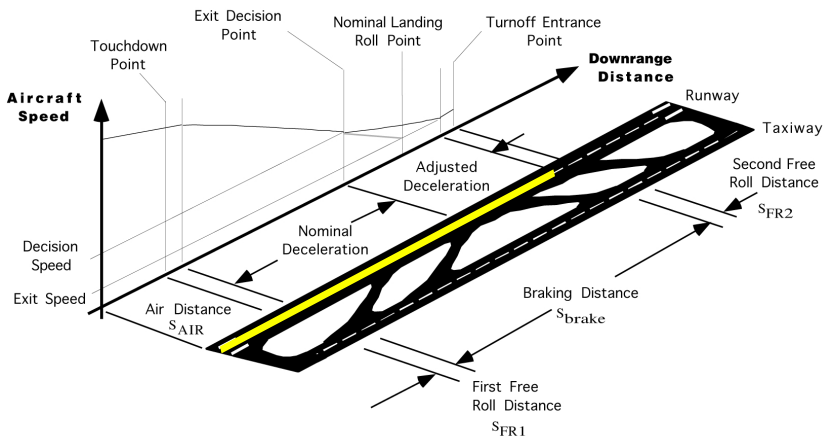

Figure 4.6: Exit Distance from Runway Threshold Indicated in Yellow. Source of Original Picture: (Trani et al., 1995).

Generally, shorter values of exit distance from runway threshold should result in lower values of AROT. Therefore, we include exit distance from runway threshold, represented by the variable $DTTE$, in our model for AROT.

4.4 Models Proposed

We specify 21 models for this analysis. Models 1a, 1b, and 1c are classical fully-pooled linear regression models of $ROTD$, $Dist_{TO}$ and $ROTA$ respectively. They are estimated using ordinary least squares (OLS) and utilize the full set of regressors suggested for $ROTA$, $ROTD$, and $Dist_{TO}$, respectively.

Models 2a, 2b, and 2c are classical fixed-effects regression models, which include the full set of regressors suggested for $ROTD$, $Dist_{TO}$, and $ROTA$ respectively. These models are estimated using the least-squares dummy variable estimator with dummies specified for 84 of the 85 aircraft types considered.

Models 3a, 3b, and 3c are classical mixed-effects regression models, which include the full set of regressors suggested for $ROTD$, $Dist_{TO}$, and $ROTA$ respectively. Similarly, models 4a, 4b, and 4c are classical mixed-effects regression models but utilize the following reduced regressor sets specified in Table 4.7. These models are estimated through maximum

likelihood and we assume normally distributed errors at each level of the model for both sets of mixed-effects models.

Lastly, models 5a, 5b, and 5c are Bayesian hierarchical regression models, which include the full set of regressors suggested for $ROTD$, $Dist_{TO}$, and $ROTA$. Likewise, models 6a, 6b, and 6c are Bayesian hierarchical regression models but utilize the reduced regressor sets specified in Table 4.7.

Table 4.7: Regressor Sets for Mixed-Effects and Hierarchical Bayesian Models

Response	Full Set	Reduced Set
$ROTA$	*Alt*, *DTTE*, *ExitAng* *TurnDist*, *EffRwLen*, *ThrVel*	*Alt*, *DTTE*, *ExitAng* *TurnDist*, *EffRwLen*
$ROTD$	*Wind*, V_{LO}, *RwLen*, *Alt*	*Wind*, V_{LO}, *RwLen*
$Dist_{TO}$	*Wind*, V_{LO}, *RwLen*, *Alt*	*Wind*, V_{LO}, *RwLen*

To estimate the Bayesian models, we utilize a Gibbs Sampler using the full conditional probability distributions introduced in Chapter 2. The Gibbs Sampler is set up as follows. First, a vector of initial parameters ($\Psi^{(0)} = \{\boldsymbol{\beta}_j^{(0)}, \boldsymbol{\Phi}^{(0)}, \Sigma^{(0)}, \sigma_j^{2(0)}\}$) is established. Using this starting point, a sample vector ($\Psi^{(s)} = \{\boldsymbol{\beta}_j^{(s)}, \boldsymbol{\Phi}^{(s)}, \Sigma^{(s)}, \sigma_j^{2(s)}\}$) is generated from $\Phi^{(s-1)}$ using the following sampling order:

1. Sample $\boldsymbol{\Phi}^{(s)} \sim p(\boldsymbol{\Phi}|\boldsymbol{Y_j}, \boldsymbol{X_j}, \Sigma^{(s-1)}, \sigma_j^{2(s-1)}, \boldsymbol{\beta_j}^{(s-1)})$
2. Sample $\Sigma^{(s)} \sim p(\Sigma|\boldsymbol{Y_j}, \boldsymbol{X_j}, \boldsymbol{\Phi}^{(s)}, \sigma_j^{2(s-1)}, \boldsymbol{\beta_j}^{(s-1)})$
3. Sample $\boldsymbol{\beta_j}^{(s)} \sim p(\boldsymbol{\beta_j}|\boldsymbol{Y_j}, \boldsymbol{X_j}, \Sigma^{(s)}, \sigma_j^{2(s-1)}, \boldsymbol{\Phi}^{(s)})$
4. Sample $\sigma_j^{2(s)} \sim p(\sigma_j^2|\boldsymbol{Y_j}, \boldsymbol{X_j}, \Sigma^{(s)}, \boldsymbol{\Phi}^{(s)}, \boldsymbol{\beta_j}^{(s)})$

The initial parameters and hyperparameters were stipulated as the following:

$$
\begin{aligned}
\boldsymbol{\beta_j}^{(0)} &= (\boldsymbol{X_j}^T \boldsymbol{X_j})^{-1}(\boldsymbol{X_j}^T \boldsymbol{Y}) \\
\boldsymbol{\Phi}^{(0)} &= (\boldsymbol{X}^T \boldsymbol{X})^{-1}(\boldsymbol{X}^T \boldsymbol{Y}) \\
\sigma_j^{2(0)} = (\sigma_{j,0}^2)^{(0)} &= \frac{(\boldsymbol{Y_j} - \boldsymbol{X_j}\boldsymbol{\beta_j})^T(\boldsymbol{Y_j} - \boldsymbol{X_j}\boldsymbol{\beta_j})}{n_j - p} \\
n_j &= \text{number of samples in group } j \\
p &= \text{number of parameters estimated} \\
\eta_0 &= p + 2 \\
\nu_0 &= 1 \\
\boldsymbol{\mu_0} &= \frac{1}{g}\sum \boldsymbol{\beta_j} \\
J &= \text{number of groups} \\
\Lambda_0{}^{(0)} = \frac{1}{g}(Q_G \boldsymbol{X}^T)^T(Q_G \boldsymbol{X}^T) \text{ e.g. } Q_2 &= \begin{bmatrix} 1 & 0 \\ 0 & 1 \end{bmatrix} - \frac{1}{2}\begin{bmatrix} 1 & 1 \\ 1 & 1 \end{bmatrix} \\
\mathbf{S}_0{}^{(0)} &= \frac{1}{g}(Q_G \boldsymbol{X}^T)^T(Q_G \boldsymbol{X}^T)
\end{aligned}
\tag{4.45}
$$

4.5 Model Data Summary

Figures 4.7 through 4.11 illustrate the dispersion of the data utilized in the predictive models of DROT and take-off roll distance. As illustrated by Figure 4.7, the bulk of the lift-off velocities ranged from 120 to 200 knots and displayed a somewhat normal shape with a very heavy left tail. Headwinds on departure were oftentimes nonexistent, with zero headwinds accounting for approximately fifteen of all departure data. The majority of headwinds and tailwinds ranged between from 0 to 10 knots in magnitude as illustrated by Figure 4.8.

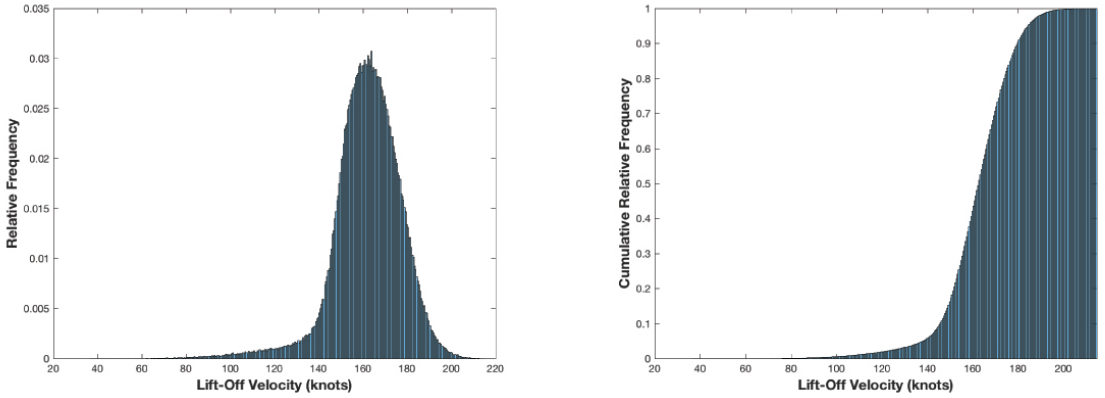

Figure 4.7: Histogram and Cumulative Histogram of Lift-Off Velocities on Departure Runways

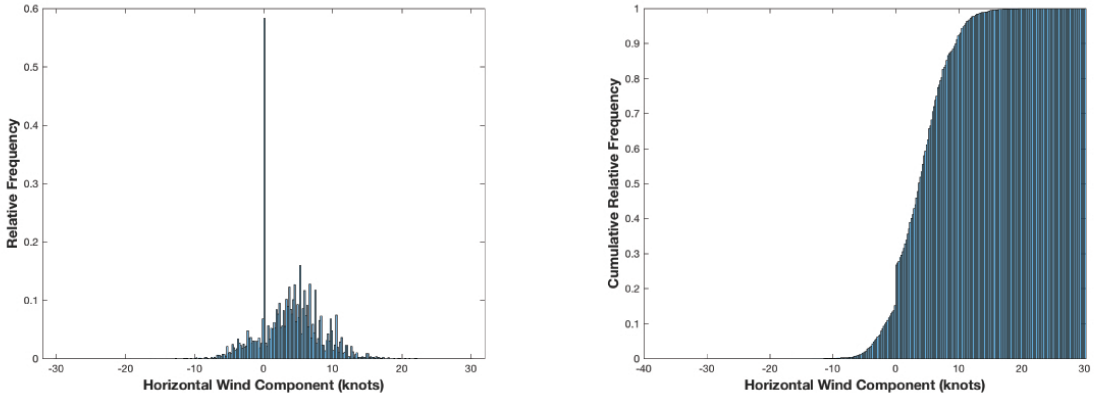

Figure 4.8: Histogram and Cumulative Histogram of Horizontal Wind Components at Departure Runways

Departure runway lengths can be grouped into three ranges of roughly equal size: (1) 4,000 ft. to 10,000 ft., (2) 10,000 ft. to 12,000 ft., and (3) greater than 12,000 ft. The greatest concentrations of runways occurred at lengths of around 10,000 ft and around 12,000 ft.

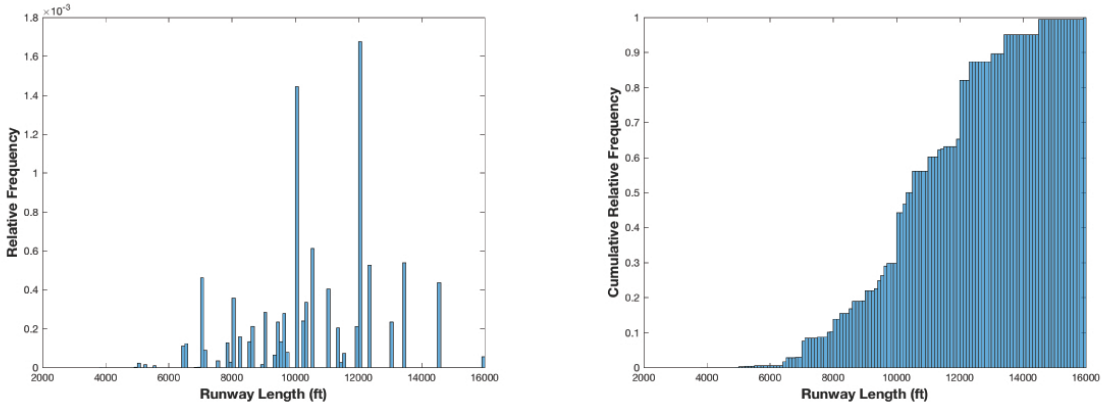

Figure 4.9: Histogram and Cumulative Histogram of Runway Lengths for Departure Runways

Almost sixty percent of airport altitudes for departures were either at or less than 500 feet and an additional thirty-five percent were at altitudes greater than 500 feet but less than 1,000 feet. The remaining airport altitudes were at altitudes greater than 4,000 feet.

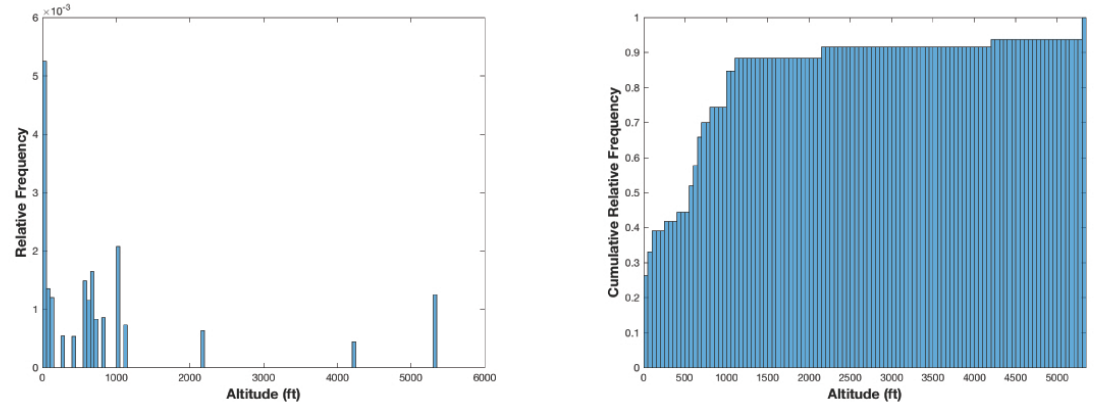

Figure 4.10: Histogram and Cumulative Histogram of Airport Altitudes for Departure Movements

The distributions of departure runway occupancy times illustrated in Figure 4.11 represent a final sample of 402,462 departure movements. From the original sample, we were unable to completely parse the regressor data parameters for 5,198 of the departure tracks. This was due to either missing data in the data record or other errors that could not be corrected. As

such, these were discarded from further consideration and represented approximately 1.28% of the original sample.

Departure runway occupancy time values had a somewhat normal shape with a mean of 47.74 seconds and a standard deviation of 6.49 seconds. From the historical values described in Koenig's study, these values are somewhat high. However, given that Koenig's study involved a sample of generally smaller aircraft, if might be reasonable to expect the DROT values to trend upward with the advent of larger and larger aircraft.

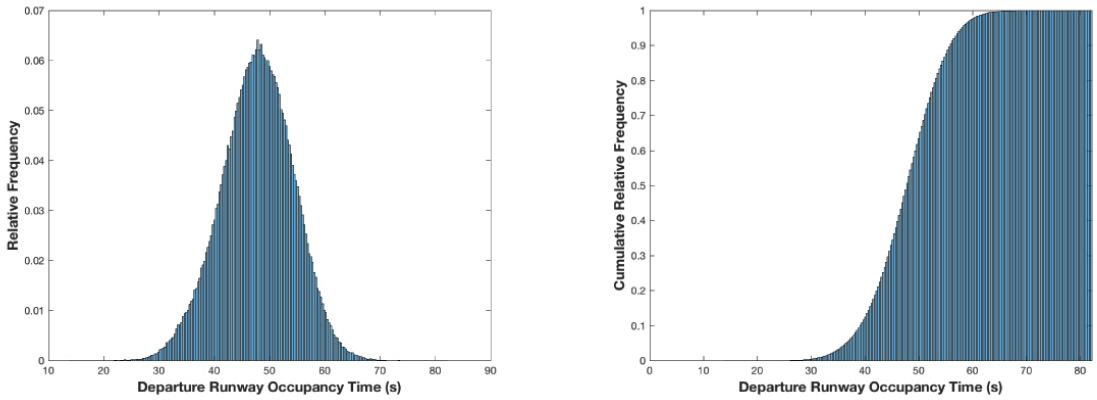

Figure 4.11: Histogram and Cumulative Histogram of Departure Runway Occupancy Times for Departure Movements

Figures 4.12 through 4.18 illustrate the dispersion of the data utilized in the predictive model of arrival runway occupancy time. As seen by Figure 4.12 approximately sixty-five percent of airport altitudes were at or less than 1,000 ft. and an additional twenty percent were at greater than 1,000 ft. but less than 4,000 ft. The remaining airport altitudes were at altitudes greater than 4,000 ft.

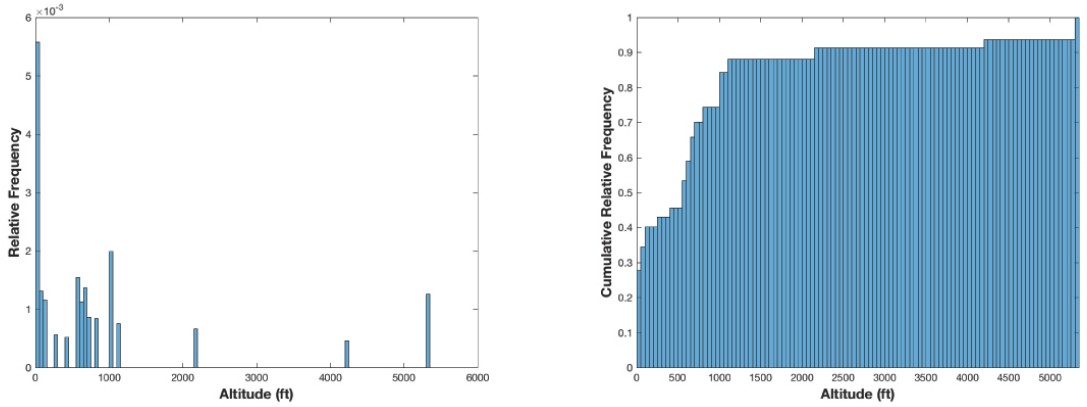

Figure 4.12: Histogram and Cumulative Histogram of Airport Altitudes for Arrival Movements

Effective runway lengths can be broken down by quartiles into the following ranges: (1) 8,400 feet and less, (2) 8,400 to 9,000 feet, (3) 9,000 to 11,095 feet, and (4) lengths greater than 11,095 feet.

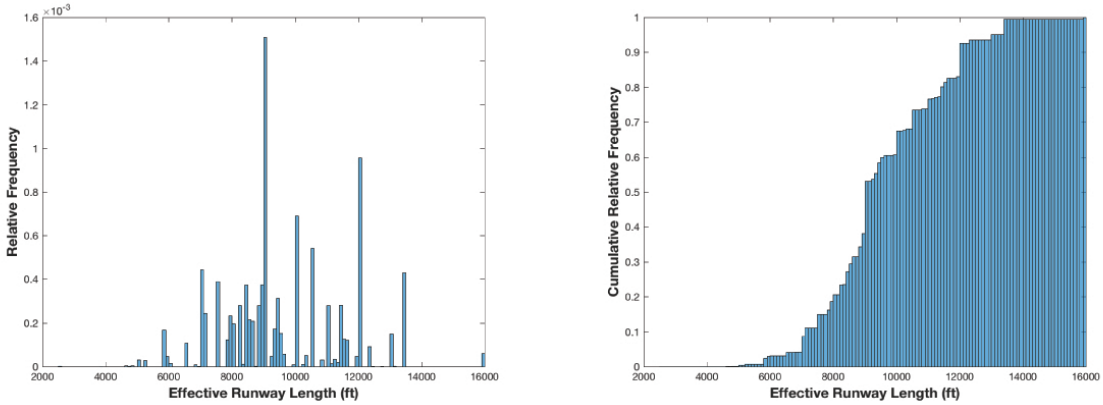

Figure 4.13: Histogram and Cumulative Histogram of Effective Runway Lengths for Arrival Movements

Straight-line exit distances for exits utilized generally ranged from around 4,000 ft to as high as 10,000 ft. As compared with the runway lengths utilized, there was considerably more variability in the exit distances of exits utilized.

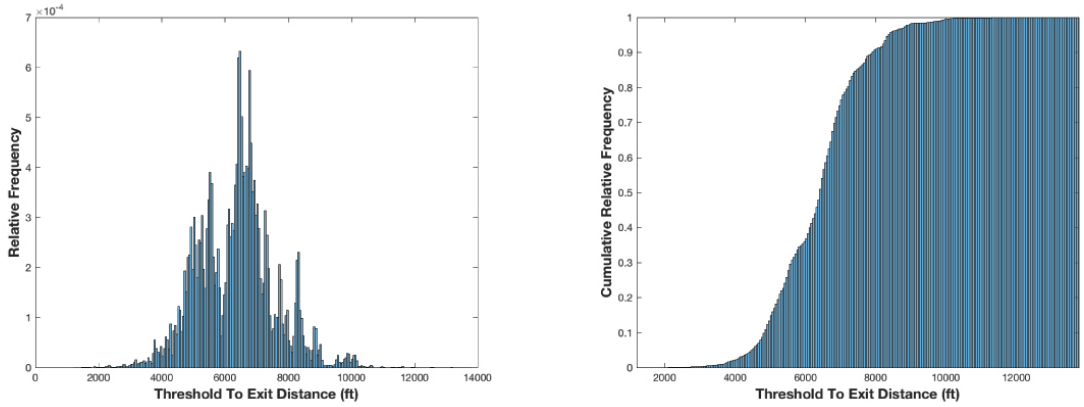

Figure 4.14: Histogram and Cumulative Histogram of Threshold To Exit Distance for Arrival Movements

The distribution of threshold crossing velocities have a roughly normal shape centered at a mean of 135.22 knots and a standard deviation of 11.43 knots.

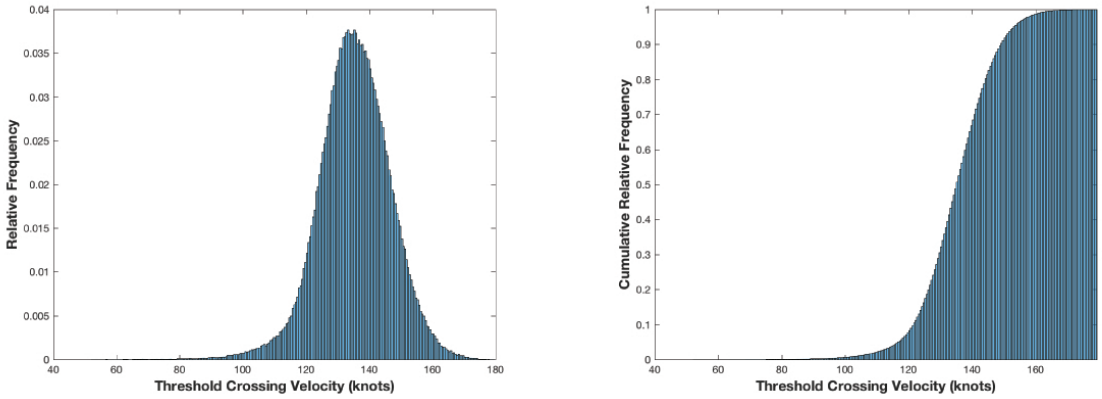

Figure 4.15: Histogram and Cumulative Histogram of Threshold Crossing Velocities for Arrival Movements

Lengths of turn distances generally ranged from between 300 ft to 1,400 ft. There are approximately three modes in the data at around 400 ft., 900 ft., and 1,350 ft.

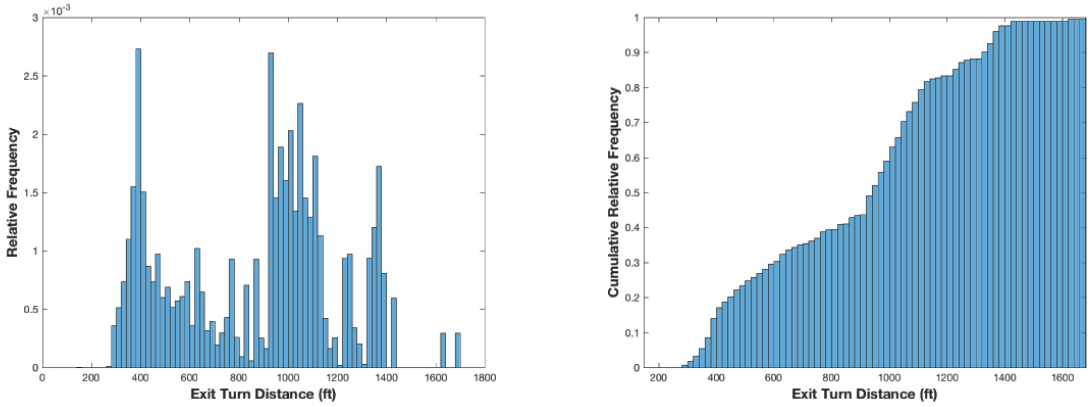

Figure 4.16: Histogram and Cumulative Histogram of Exit Turn Distances for Arrival Movements

Approximately fifty percent of the exit angles encountered are 30° exit angles. An additional twenty-five percent range between greater than 30° to less than 90°. Fifteen percent of the exits are right-angled exits and the remainder of the exits are obtuse-angled exits.

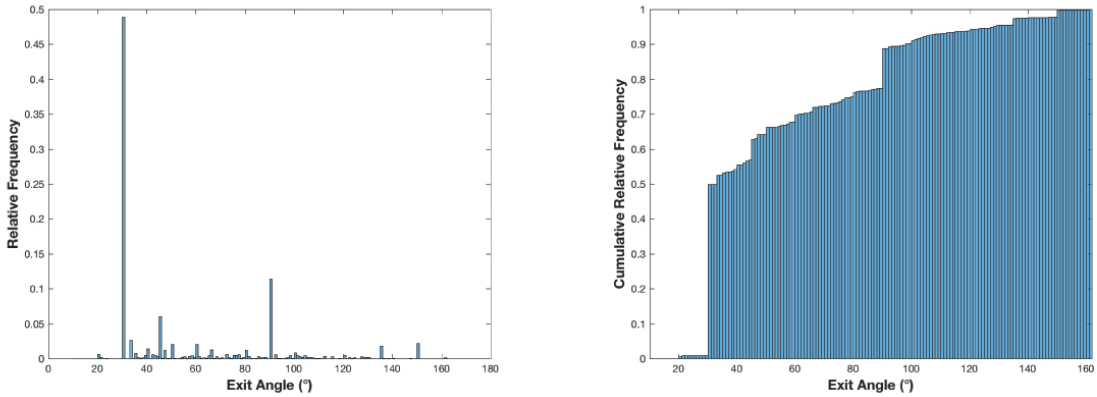

Figure 4.17: Histogram and Cumulative Histogram of Exit Angles for Arrival Movements

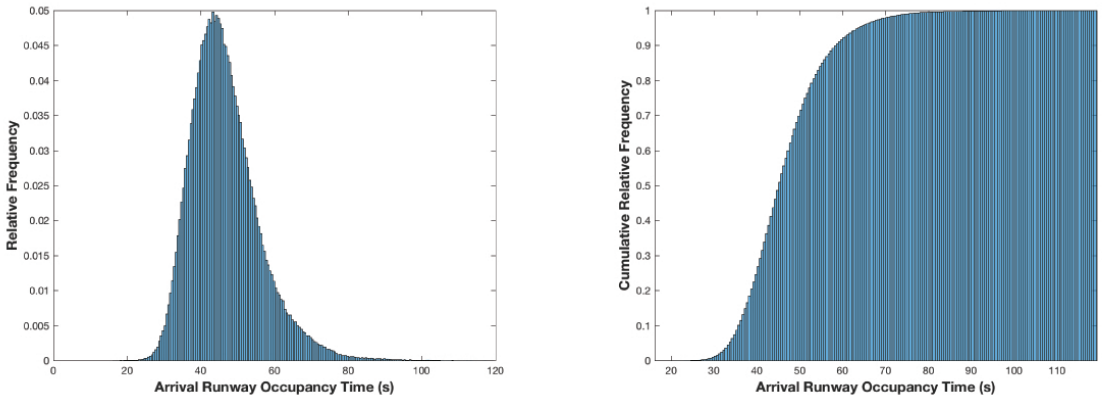

Figure 4.18: Histogram and Cumulative Histogram of Arrival Runway Occupancy Times for Arrival Movements

As seen from Figure 4.18, Arrival Runway Occupancy Times range from approximately 20 seconds to a maximum of 120 seconds. The maximum value was set so as to avoid involving outliers in the predictive model. For example, excessive arrival runway occupancy times could result from cases where an aircraft is forced to taxi on the runway to a previous runway exit. In performing this filtering, 15,386 samples were removed from an initial dataset of 467,095, representing around 3.29% of the original sample.

The distribution of Arrival Runway Occupancy Time values demonstrated a positive skewness of 1.0236 and a kurtosis of 5.22. Compared to a normal, the right tail of the distribution of AROT approaches zero more slowly. The mean of the data is 46.57 seconds with a standard deviation of 9.37 seconds. Compared to historical values from the 2010 study by Kumar et al., the 1999 study by Lee et al., and from the studies by Jeddi et al., the mean value of the data lay well within the ranges of those studies. Additionally, the standard deviation almost exactly matches that gleaned from the Jeddi study of 2009, despite our dataset being far greater. This gives confidence in the data extraction and filtering methods as we proceed.

Table 4.8 provides summary statistics of the regressors and response variables for the departure and arrival models.

Table 4.8: Summary Statistics of the Regressor and Response Variables

	unit	# obs.	Mean	Std.	Skewness	Kurtosis	Min	Max	Mode
Departure Model Variables									
Horizontal Wind Component	knots	402462	3.756	4.329	0.105	3.17	-30.2035	30.2035	0
Lift-Off Velocity	knots	402462	161.99	15.32	-1.0305	6.55	36.72	214.57	151.37
Runway Length	feet	402462	10593	2010.98	-0.1044	2.739	3859	16000	10000
Airport Altitude	feet	402462	872.94	1363.29	2.472	8.155	6	5350	13
Departure Model Response Variables									
DROT	sec.	402462	47.74	6.49	-0.1213	2.997	13.83	82.17	46
Departure Roll Distance	feet	402462	6970.8	1431.63	-0.03123	3.097	538.58	12875.8	6663.52
Arrival Model Variables									
Airport Altitude	feet	451709	871.8	1375.37	2.441	7.978	6	5350	13
Effective Runway Length	feet	451709	9580.15	1906.9	0.3753	3.012	2557	16000	9000
Runway Threshold Velocity	knots	451709	135.22	11.43	-0.3815	4.554	52.46	179.33	137.96
Exit Angle	deg.	451709	53.47	32.65	1.293	3.702	10	162	30
Exit Turn Distance	feet	451709	864.39	340.06	-0.0696	1.962	148	1682	962
Threshold to Exit Distance	feet	451709	6355.23	1217.31	0.2554	3.65	1210.7	13776.7	6688.87
Arrival Model Response Variables									
DROT	sec.	451709	46.57	9.37	1.0236	5.22	16.18	119.28	48

Table 4.9 lists the aircraft types and sample sizes represented in the dataset for the arrival and departure models. The aircraft were chosen such that a minimum sample size of 200 was ensured. In total, 85 different aircraft types are represented in the data for both the arrival and departure models.

Table 4.9: List of Aircraft Types and Sample Sizes for the Departure and Arrival Models

Aircraft Type	Departure Model Sample	Arrival Model Sample	Aircraft Type	Departure Model Sample	Arrival Model Sample
A306	946	1157	C680	521	648
A319	22939	26169	C750	871	1042
A320	31277	34729	CL30	778	967
A321	7431	8453	CL60	730	849
A332	1824	2070	CRJ2	37727	42653
A333	1517	1679	CRJ7	20454	21708
A343	458	491	CRJ9	11921	13175
A346	360	387	DC10	879	1073
A388	217	414	DC95	1508	1656
AT72	312	371	DH8A	2571	3290
B190	2742	3106	DH8B	805	899
B350	236	291	DH8C	1284	1529
B712	8300	9272	DH8D	5534	6232
B732	270	390	E120	2740	3044
B733	7026	7910	E135	7323	8159
B734	2060	2327	E145	25502	27317
B735	444	482	E170	14762	17765
B736	266	377	E190	7970	9109
B737	33251	37071	E45X	7138	7746
B738	33510	37383	E50P	211	268
B739	5987	6543	E55P	220	283
B744	2581	2831	F2TH	659	846
B748	403	453	F900	440	505
B752	21910	23687	GALX	494	566
B753	2614	2816	GLEX	295	336
B762	1513	1661	GLF4	999	1197
B763	6226	6817	GLF5	608	760
B764	881	980	H25B	1023	1279
B772	3322	3461	LJ35	322	410
B77L	505	534	LJ45	481	600
B77W	1737	1843	LJ60	359	434
B788	335	388	MD11	1482	1743
BE20	464	615	MD82	6956	7955
BE40	607	749	MD83	6135	6933
BE99	349	421	MD88	10992	12195
BE9L	310	450	MD90	5358	5957
C172	224	368	PA31	485	607
C208	1466	1888	PC12	493	662
C402	1814	2413	SF34	1400	1672
C525	211	295	SH36	224	263
C550	266	343	SR22	208	247
C560	510	689	SW4	734	829
C56X	1245	1527			

4.6 Model Results

We present the estimation results for each of the models by response variable in Tables 4.10 through 4.12. For the classical models (model numbers 1a, 1b, and 1c), the table reports the estimated coefficients means and standard errors, the adjusted-R^2, and the deviance. We include the deviance since it is a metric of model fit, applicable to both classical and Bayesian models. The deviance is defined as

$$D = 2\left(\log \mathcal{L}_s(\hat{\boldsymbol{\beta}}) - \log \mathcal{L}_m(\hat{\boldsymbol{\beta}})\right) \tag{4.46}$$

where $\log \mathcal{L}_s(\hat{\boldsymbol{\beta}})$ is the maximized log-likelihood of the saturated model and $\log \mathcal{L}_m(\hat{\boldsymbol{\beta}})$ is the maximized log-likelihood of the fitted model. The saturated model refers to the model for which a parameter is defined for every observation leading to a perfect model fit. Thus, the deviance measures the difference between the predicted values of our fitted model and those predicted by the saturated model, the most complete model one can fit. Lower values of deviance indicate better model fit. For the classical fixed-effects model (model numbers 2a, 2b, and 2c), the table reports the parameter coefficients and their standard errors, t-statistics and p-values and does not report the aircraft specific indicator coefficients. The mixed-effects model results (model numbers 3a, 3b, 3c, 4a, 4b, and 4c) include the same information while the Bayesian model results (model numbers 5a, 5b, 5c, 6a, 6b, and 6c) only include the fixed effect coefficient values and standard errors. Regarding the Bayesian results, the coefficient mean values are the posterior mean values and their associated posterior standard deviations after accounting for burn-in.

The Bayesian model results also include estimates of the Deviance Information Criterion (DIC), which is a parameter often utilized in Bayesian model selection. The DIC is defined as

$$\text{DIC} = D(\bar{\theta}) + 2p_D \tag{4.47}$$

where $D(\bar{\theta})$ is the deviance evaluated at the posterior mean vector and $2p_D$ is the effective number of parameters. The value of p_D can be computed as

$$p_D = \bar{D} - D(\bar{\theta}) \tag{4.48}$$

where $\bar{D}$ is the computed deviance $D(\theta)$ averaged over the posterior samples of θ (Spiegelhalter et al., 2002). The DIC is used as it is especially suited for comparison hierarchical Bayesian models and their ability to predict out-of-sample responses. Lower values of DIC indicate better model fit.

We first consider the classical fully-pooled models. Despite all coefficients being significant, for all three response variables, the classical fully-pooled models are immediately recognized as having the poorest model performance. The difference in performance is considerable and strongly suggests that difference between individual aircraft types are significant. Results from the classical fixed-effects models bear this out and offer considerably improved performance over the fully-pooled models. Furthermore, the coefficients in all of the fixed-effects models are significant to the 5% significance level as evidenced by the p-values.

For the mixed-effects models, the deviance and R^2 parameters both generally suggest improved model fit to the data relative to the fixed-effects models. The notable exception is with Model 4c relative to Model 2c. The marked drop in model fit statistics seems to suggest that the variable for Threshold Velocity should be included in the AROT model.

Table 4.10: Estimation Results for Models of Departure Runway Occupancy Time

	Model 1a	Model 2a	Model 3a	Model 4a	Model 5a	Model 6a
Coefficient						
Altitude	3.38E-05	-1.04E-04	9.24E-06	—	3.21E-03	—
std. error	5.31E-06	5.09E-06	7.32E-05	—	4.16E-04	—
t-statistic	6.37	-20.44	0.126	—	—	—
p-value	1.85E-10	7.93E-93	0.8995	—	—	—
Lift-Off Velocity	0.2681	0.3593	0.327	0.3257	0.325	0.323
std. error	4.91E-04	7.69E-04	0.0069	0.007	2.15E-03	2.18E-03
t-statistic	545.88	467.25	47.35	46.52	—	—
p-value	0.00	0.00	0.00	0.00	—	—
Runway Length	8.31E-04	6.84E-04	4.76E-04	4.60E-04	4.73E-04	4.23E-04
std. error	3.70E-06	3.33E-06	4.78E-05	4.59E-05	1.46E-05	1.27E-05
t-statistic	224.73	205.45	9.96	10.01	—	—
p-value	0.00	0.00	2.31E-23	1.37E-23	—	—
Horz. Wind Component	0.1011	0.1733	0.1663	0.1632	0.166	0.163
std. error	0.0016	0.0015	0.0072	0.0073	2.37E-03	2.42E-03
t-statistic	61.37	113.68	23.13	22.25	—	—
p-value	0.00	0.00	3.10E-118	1.46E-109	—	—
Intercept	-4.9054	-23.146	-11.113	-10.638	-10.707	-9.857
std. error	0.0797	0.1756	0.7706	0.765	0.304	0.33
t-statistic	-61.57	-131.78	-14.42	-13.91	—	—
p-value	0.00	0.00	3.90E-47	5.46E-44	—	—
Model Fit Statistics						
Adjusted-R^2	0.5498	0.6679	0.6826	0.6794	—	—
Deviance	2.3264E+06	2.2038E+06	2.1875E+06	2.1912E+06	2.1757E+06	2.7950E+06
DIC	—	—	—	—	2.1767E+06	2.1804E+06

Table 4.11: Estimation Results for Models of Departure Take-Off Distance

	Model 1b	Model 2b	Model 3b	Model 4b	Model 5b	Model 6b
Coefficient						
Altitude	4.93E-02	2.01E-03	6.21E-03	—	0.431	—
std. error	6.03E-04	7.96E-04	9.69E-03	—	7.44E-02	—
t-statistic	239.54	2.518	0.640	—	—	—
p-value	0.00	0.012	0.522	—	—	—
Lift-Off Velocity	72.64	96.773	89.021	88.73	88.374	88.339
std. error	8.01E-02	0.1204	0.974	1.052	0.382	0.38
t-statistic	907.29	803.75	91.41	84.35	—	—
p-value	0.00	0.00	0.00	0.00	—	—
Runway Length	0.144	0.119	8.76E-02	8.73E-02	8.45E-02	8.39E-02
std. error	6.03E-04	5.22E-04	7.93E-03	7.84E-03	2.06E-03	2.08E-03
t-statistic	239.54	227.62	11.05	11.14	—	—
p-value	0.00	0.00	2.15E-28	8.55E-29	—	—
Horz. Wind Component	7.764	27.354	27.134	26.68	26.766	26.544
std. error	0.269	0.239	1.195	1.170	0.349	0.348
t-statistic	28.91	114.57	22.71	22.80	—	—
p-value	1.38E-183	0.00	4.59E-114	5.88E-115	—	—
Intercept	-6398.3	-5869.7	-8604.3	-8553.9	-8494.70	-8467.29
std. error	12.99	40.06	119.72	150.03	67.09	67.207
t-statistic	-492.63	-146.52	-71.87	-57.02	—	—
p-value	0.00	0.00	0.00	0.00	—	—
Model Fit Statistics						
Adjusted-R^2	0.7541	0.8327	0.8436	0.8420	—	—
Deviance	6.4265E+06	6.2716E+06	6.2466E+06	6.2504E+06	6.2172E+06	6.2211E+06
DIC	—	—	—	—	6.2182E+06	6.2219E+06

Table 4.12: Estimation Results for Models of Arrival Runway Occupancy Time

	Model 1c	Model 2c	Model 3c	Model 4c	Model 5c	Model 6c
Coefficient						
Altitude	8.55E-05	5.42E-05	4.32E-04	-2.04E-04	-1.41E-02	-1.59E-02
std. error	6.30E-06	6.41E-06	1.39E-04	1.43E-04	3.08E-03	3.23E-03
t-statistic	13.56	8.46	3.10	-1.43	—	—
p-value	7.21E-42	2.80E-17	1.93E-03	0.15	—	—
Exit Dist. from Threshold	7.6E-03	7.5E-03	8.2E-03	7.4E-03	8.19E-03	7.48E-03
std. error	7.46E-06	7.30E-06	1.04E-04	1.03E-04	2.50E-05	2.42E-05
t-statistic	1017.9	1032.8	78.53	72.63	—	—
p-value	0.00	0.00	0.00	0.00	—	—
Effective Runway Length	-1.73E-04	-1.94E-04	-3.38E-04	-3.01E-04	-3.63E-04	-3.33E-04
std. error	4.65E-06	4.43E-06	6.28E-05	6.52E-05	1.59E-05	1.68E-05
t-statistic	-37.28	-43.70	-5.39	-4.62	—	—
p-value	1.16E-303	0.00	7.12E-08	3.83E-06	—	—
Exit Angle	0.026	1.84E-02	1.25E-02	1.2E-02	1.16E-02	1.13E-02
std. error	3.09E-04	2.88E-04	2.4E-03	2.5E-03	6.45E-04	6.72E-04
t-statistic	84.12	63.82	5.28	4.75	—	—
p-value	0.00	0.00	1.31E-07	2.07E-06	—	—
Threshold Velocity	-0.299	-0.295	-0.291	—	-0.292	—
std. error	7.43E-04	8.91E-04	6.3E-03	—	1.67E-03	—
t-statistic	-401.67	-330.99	-46.58	—	—	—
p-value	0.00	0.00	0.00	—	—	—
Turn Distance	-5.3E-03	-5.1E-03	-6.1E-03	-6.4E-03	-6.19E-03	-6.42E-03
std. error	3.22E-05	3.02E-05	3.18E-04	3.20E-04	8.33E-05	8.16E-05
t-statistic	-163.97	-168.32	-19.29	-20	—	—
p-value	0.00	0.00	6.97E-83	6.06E-89	—	—
Intercept	43.423	46.957	44.958	11.861	45.255	12.100
std. error	9.98E-02	0.302	0.916	0.752	0.265	0.204
t-statistic	434.92	155.54	49.09	15.78	—	—
p-value	0.00	0.00	0.00	4.16E-56	—	—
Model Fit Statistics						
Adjusted-R^2	0.7241	0.7649	0.7761	0.7191	—	—
Deviance	2.7216E+06	2.6493E+06	2.6299E+06	2.7321E+06	2.5959E+06	2.7058E+06
DIC	—	—	—	—	2.5973E+06	2.7069E+06

Considering the coefficient effects, for the departure models, we see that with the exception of Model 2a, altitude consistently has a positive effect on both DROT and Departure Take-Off Distance. This is inline with expectations given that higher altitudes require longer take-off rolls due to decreased air density. Similarly, lift-off velocity effects are positive given that longer take-off rolls requiring longer occupancy times are needed to reach increased lift-off velocities. Runway length positively affects take-off distance and occupancy time, however this is probably the result of longer take-off times and distance being associated with longer runways in general. The runway length itself provides a ceiling on departure distance and occupancy time but does not determine the amount of time and distance an

aircraft needs to successfully depart. However, longer runways may arguably provide pilots with the opportunity to utilize reduced thrust take-offs as a means of saving fuel. In that sense, the availability of extra runway length would lead to longer take-off distances and occupancy times overall as pilots take advantage of the extra length. Lastly, the positive effect of horizontal wind is in keeping with expectations. A headwind blows in the direction opposite to the direction of motion and would be negative. Thus, negative winds would result in lower take-off distances and occupancy times, as we would expect.

Looking at the arrival models, the coefficient effects generally match theoretical expectations. As suggested earlier, threshold velocity appears to be a significant predictor of arrival runway occupancy time, judging by the noticeable drop in model fit when omitted. Higher threshold velocities generally result in lower arrival runway occupancy times since the airplane is moving faster towards its eventual exit. Longer turn distances aid in reducing arrival runway occupancy times as they allow pilots to exit at higher speeds from the runway. Thus, the expected effect of turn distance is negative as borne out in the results. The positive effect of exit angle reflects the fact that for an aircraft to turn safely, it will need to reduce speed on arrival, thereby increasing arrival runway occupancy time. As the exit angle steepens, the needed reduction in speed increases. Longer runways appear to decrease arrival runway occupancy time and this may be because longer runways permit faster approaches. Threshold to exit distance would logically result in higher occupancy times since the aircraft must travel further to exit.

Lastly, regarding the effect of altitude, we see a contrast between the positive effect in Model 3c and the negative effects in Models 4c, 5c, and 6c. The expected effect is negative as higher altitudes lead to increased approach speeds due to the lower air density. As outlined earlier, increased approach speeds generally result in lower arrival runway occupancy times. Furthermore, we notice that for both models 3c and 4c, the effects are very close to zero and are considerably smaller in magnitude relative to their Bayesian model counterparts.

To further explore this discrepancy in the effects of altitude, we tested for correlation between threshold crossing velocity and altitude to determine whether high multicollinearity was impacting the altitude effect. We found a correlation coefficient of 0.2757 with a confidence interval of [0.2730, 0.2784] and a p-value of less than 0.001. This indicates that the correlation coefficient value is statistically significant and would lead us

to reject the null hypothesis of the correlation coefficient being zero (SAS Institute Inc., 2016). However, despite there being nonzero correlation, a correlation of 0.2757 would be considered small (Cohen, 1998). Thus, we rule out excessive correlation as explaining the discrepancy in the effects of altitude.

Comparing the Bayesian models to the classical mixed-effects models, we see that the Bayesian coefficient estimates are generally tighter with smaller standard errors relative to the mixed-effects coefficients. Interestingly, we see that the coefficients for Altitude in mixed-effects Models 3a and 3b are insignificant to the 5% significance level, whereas for Bayesian models, the effects of Altitude remain significant.

To explore this discrepancy further, we investigate whether Altitude should be treated as a fixed-effect. Thus, for Models 3a and 3b, we test the significance of the standard deviation for Altitude in the random-effects covariance matrix. For Model 3a, we find the standard deviation of the Altitude random effect to have a mean of 0.000635 with a 95% confidence interval of [0.000519, 0.000777]. For Model 3b, we find the standard deviation of the Altitude random effect to have a mean of 0.0828 with a 95% confidence interval of [0.0686, 0.0998]. These results do not seem to indicate that treating Altitude as a random effect is improper. However, as further exploration, we recomputed Models 3a and 3b holding Altitude as a fixed effect. The results are given in Table 4.13.

As can be seen, the coefficients for Altitude, when treated solely as a fixed effect, were significant for both recomputed Models 3a and 3b. However, for recomputed Model 3a, the effect of Altitude went negative, which is not in line with theoretical expectations. Higher altitudes generally lead to longer departure runway occupancy times. For recomputed Model 3b, the effect of altitude is almost three times that of original Model 3b and remains positive. However, we note that the R^2 value of recomputed Model 3b decreased in comparison to original Model 3b while the deviance of recomputed Model 3b increased in comparison to original Model 3b. Thus, while the Altitude fixed effect coefficient is significant, the recomputed model is actually inferior to original Model 3b. This is further highlighted by the fact that there is no evidence to suggest that an Altitude random effect is improper.

If we consider Bayesian models 5a and 5b, we see ample evidence of no issue with treating Altitude as a random effect. First, we note again that both Altitude fixed effect

coefficients are significant since the standard errors would not create an interval inclusive of zero. Additionally, from examining the Deviance statistics, we see that both models outperform their original and recomputed mixed-model counterparts. For the arrival runway occupancy time models, we see that the effects of Altitude are more substantial in Models 5c and 6c as compared to Models 3c and 4c, suggesting the improved capability of the Bayesian models to fully characterize the effects of the regressor variables on the response variables. Given the large sample sizes, the estimation results for the mixed-effects and Bayesian models should be similar and this is borne out in the results. However, the thinner standard errors and better model fits favor the Bayesian models. Nevertheless, we will further explore the benefits of each of the models, by assessing their predictive power in the next section.

Table 4.13: Results of Recomputation of Models 3a and 3b and Comparison with Models 3a, 3b, 5a and 5b

	Model 3a (redo)	Model 3b (redo)	Model 3a	Model 3b	Model 5a	Model 5b
Coefficient						
Altitude	-1.21E-04	1.86E-03	9.24E-06	6.21E-03	3.21E-03	0.431
std. error	5.29E-06	8.2E-04	7.32E-05	9.69E-03	4.16E-04	7.44E-02
t-statistic	-22.76	-2.271	0.126	0.640	—	—
p-value	1.26E-114	0.023	0.8995	0.522	—	—
Lift-Off Velocity	0.329	88.693	0.327	89.021	0.325	88.374
std. error	0.0068	1.067	0.0069	0.974	2.15E-03	0.382
t-statistic	48.45	83.147	47.35	91.41	—	—
p-value	0.00	0.00	0.00	0.00	—	—
Runway Length	4.74E-04	8.71E-02	4.76E-04	8.76E-02	4.73E-04	8.45E-02
std. error	4.50-05	7.92E-03	4.78E-05	7.93E-03	1.46E-05	2.06E-03
t-statistic	10.53	11.00	9.96	11.05	—	—
p-value	6.07E-26	3.95E-28	2.31E-23	2.15E-28	—	—
Horz. Wind Component	0.164	26.669	0.1663	27.134	0.166	26.766
std. error	0.007	1.189	0.0072	1.195	2.37E-03	0.349
t-statistic	23.37	22.44	23.13	22.71	—	—
p-value	1.15E-120	2.07E-111	3.10E-118	4.59E-114	—	—
Intercept	-11.171	-8546.5	-11.113	-8604.3	-10.707	-8494.70
std. error	0.7653	149.33	0.7706	119.72	0.304	67.09
t-statistic	-14.60	-57.23	-14.42	-71.87	—	—
p-value	3.05E-48	0.00	3.90E-47	0.00	—	—
Model Fit Statistics						
Adjusted-R^2	0.6798	0.8420	0.6826	0.8436	—	—
Deviance	2.1907E+06	6.2503E+06	2.1875E+06	6.2466E+06	2.1757E+06	6.2172E+06
DIC	—	—	—	—	2.1767E+06	6.2182E+06

4.7 Model Diagnostics

Since we are interested in constructing predictive models, it is critical to estimate the predictive power to guide our final choice of model. In order to gauge the predictive power of the models, five-fold cross-validations were performed. Despite the overall large size of the dataset, cross-validation was utilized since for some aircraft types, the sample sizes were relatively small. Cross-validation is preferred since it does not require that data be partitioned into a separate training set and a separate test set, which is eventually discarded.

For the Bayesian models, 250,000 replications were used to fit each fold to the fold training data. The first 30% of the observations were discarded as burnin replications and the root mean square error (RMSE) was estimated. The RMSE is defined as

$$\text{RMSE} = \sqrt{\frac{1}{n}\sum_{i=1}^{n}(\hat{Y}_i - Y_i)^2} \tag{4.49}$$

The RMSE was chosen as the performance metric since it is universally applicable for the classical and Bayesian models and since it returns a measurement of error in the units of the response variable. Smaller values indicate superior predictive performance. Tables A.1 through A.18 illustrate the full set of cross-validation results for each model by individual aircraft type. Tables 4.14 through 4.16 provide a comparison of the RMSE for each model by individual aircraft type. The values for the best performing models are bolded.

4.7.1 DROT Models

For the DROT models, Models 1a and 2a clearly exhibit inferior predictive performance. In no instance did either model provide the lowest RMSE. Regarding the models with the reduced regressor set (Models 4a and 6a), the mixed-model returned the lowest RMSE for 5 out of 85 aircraft types and tied for the lowest with Model 3a for 8 out of 85 aircraft types. Similarly, Model 6a tied for the lowest RMSE with Model 5a for 5 out of 85 aircraft and did not uniquely return the lowest RMSE. The clear top performer was Model 5a, which returned the lowest RMSE for 55 out of 85 aircraft types. It's closest competitor is Model 3a,

which produced the lowest RMSE for 33 out of 85 aircraft types. However, combined with its tighter coefficient estimates and lower deviance, we conclude that Model 5a represents a superior predictive model of DROT.

Table 4.14: Comparison of Root Mean Square Errors for DROT Models

Aircraft Type	Model 1a	Model 2a	Model 3a	Model 4a	Model 5a	Model 6a
A306	5.79	3.73	3.83	3.83	**3.60**	3.61
A319	3.80	3.54	3.45	**3.45**	3.52	3.52
A320	3.24	3.19	3.19	3.20	**3.18**	3.19
A321	3.55	3.33	3.28	3.28	**3.24**	3.25
A332	6.23	3.84	3.97	3.98	**3.82**	**3.82**
A333	6.04	3.73	**3.59**	**3.59**	3.63	3.63
A343	13.32	4.42	4.35	4.37	**4.27**	4.29
A346	6.50	4.66	4.10	4.11	**4.09**	4.11
A388	12.19	5.03	**3.90**	3.92	4.57	4.66
AT72	5.58	3.41	3.23	3.23	**3.10**	3.17
B190	5.45	4.14	4.12	4.12	**4.06**	4.07
B350	4.13	4.03	4.42	4.46	**3.74**	3.81
B712	3.93	3.07	**3.02**	3.04	3.04	3.05
B732	6.33	4.42	4.48	4.47	**4.11**	4.14
B733	4.01	3.82	**3.65**	3.69	3.76	3.81
B734	3.48	3.26	3.14	3.14	**3.09**	3.10
B735	3.88	3.74	3.73	3.84	**3.62**	3.71
B736	4.91	4.56	3.51	3.76	**3.08**	3.40
B737	4.20	4.10	**4.03**	4.06	4.04	4.07
B738	4.09	4.06	**3.93**	3.95	**3.93**	3.95
B739	3.68	3.48	3.36	3.36	**3.34**	**3.34**
B744	7.17	4.70	4.71	4.71	**4.67**	**4.67**
B748	7.65	5.16	4.85	4.86	**4.69**	4.71
B752	4.01	3.56	3.57	3.58	**3.54**	3.55
B753	3.78	3.70	**3.53**	**3.53**	3.59	3.60

Aircraft Type	Model 1a	Model 2a	Model 3a	Model 4a	Model 5a	Model 6a
B762	3.53	3.47	3.42	3.43	**3.34**	3.35
B763	4.25	3.97	3.98	3.99	**3.92**	**3.92**
B764	3.06	2.83	**2.74**	2.75	2.80	2.81
B772	4.18	3.53	3.54	3.55	**3.44**	3.46
B77L	3.71	3.91	3.78	3.77	**3.59**	3.60
B77W	3.37	3.61	3.36	3.36	**3.27**	3.28
B788	6.33	5.22	5.00	5.16	**4.82**	4.90
BE20	5.31	4.85	5.09	5.09	**4.73**	4.75
BE40	7.44	3.93	3.67	3.71	**3.47**	3.51
BE99	4.56	4.08	**3.58**	3.71	3.59	3.80
BE9L	5.85	4.64	4.73	4.74	**4.25**	4.30
C172	10.16	5.20	**4.64**	4.69	4.82	4.83
C208	10.45	5.10	**4.99**	**4.99**	**4.99**	5.00
C402	7.67	4.81	4.56	4.57	**4.45**	4.46
C525	6.58	5.66	**4.73**	4.83	4.92	4.97
C550	6.33	6.06	**5.05**	**5.05**	5.36	5.47
C560	9.47	5.38	4.74	4.75	**4.65**	4.66
C56X	8.94	3.89	**3.41**	3.42	3.60	3.60
C680	9.74	3.95	**3.39**	**3.39**	3.64	3.65
C750	9.33	3.98	**3.61**	3.65	3.81	3.86
CL30	8.74	3.35	3.26	3.26	**3.19**	3.21
CL60	9.98	3.86	3.88	3.89	**3.74**	3.76
CRJ2	3.86	3.72	**3.69**	**3.69**	3.70	3.70
CRJ7	3.77	3.81	**3.72**	3.75	3.73	3.75
CRJ9	3.53	3.36	3.32	3.35	**3.26**	3.30
DC10	4.40	4.31	4.25	4.26	**4.18**	4.23
DC95	3.10	2.73	2.66	2.66	**2.60**	2.62
DH8A	3.94	2.98	**2.60**	**2.60**	2.66	2.66
DH8B	2.85	2.70	**2.56**	2.57	2.63	2.66

Aircraft Type	Model 1a	Model 2a	Model 3a	Model 4a	Model 5a	Model 6a
DH8C	4.45	3.73	3.53	3.54	**3.39**	3.40
DH8D	5.31	3.50	3.50	3.50	**3.43**	3.44
E120	3.92	3.60	3.48	3.59	**3.38**	3.47
E135	3.74	3.57	3.49	3.54	**3.47**	3.51
E145	4.02	3.72	3.68	3.70	**3.66**	3.68
E170	3.46	3.34	**3.23**	3.24	3.26	3.27
E190	3.33	3.21	3.14	3.14	**3.13**	**3.13**
E45X	5.16	4.85	**4.66**	4.80	4.71	4.84
E50P	3.85	3.71	**2.92**	3.00	3.35	3.48
E55P	9.58	2.85	2.76	2.77	**2.54**	2.57
F2TH	7.95	4.75	4.68	4.71	**4.39**	4.41
F900	7.91	4.48	4.62	4.66	**4.23**	4.24
GALX	10.48	3.97	**3.72**	3.73	3.76	3.80
GLEX	7.93	4.58	**4.17**	**4.17**	4.37	4.45
GLF4	10.21	4.70	**4.33**	**4.33**	4.38	4.42
GLF5	8.37	5.24	4.79	4.80	**4.62**	4.65
H25B	7.98	4.73	**4.41**	**4.41**	4.48	4.51
LJ35	10.91	5.33	4.96	4.96	**4.72**	4.75
LJ45	6.13	3.63	**3.34**	3.35	3.36	3.45
LJ60	13.13	4.25	**3.75**	3.77	3.82	3.83
MD11	7.46	4.08	4.39	4.40	**4.00**	4.03
MD82	4.10	3.83	**3.70**	**3.70**	**3.70**	3.71
MD83	4.11	3.8	**3.69**	**3.69**	3.70	3.71
MD88	3.92	3.54	3.43	3.47	**3.39**	3.43
MD90	3.26	3.13	3.20	3.21	**3.09**	3.11
PA31	6.64	4.66	4.67	4.70	**4.43**	4.44
PC12	7.70	4.94	**4.26**	4.33	4.58	4.69
SF34	3.83	3.70	3.73	3.74	**3.57**	3.60
SH36	9.21	5.26	5.10	5.13	**4.62**	4.66

Aircraft Type	Model 1a	Model 2a	Model 3a	Model 4a	Model 5a	Model 6a
SR22	7.48	5.11	4.97	4.97	**4.69**	4.75
SW4	4.96	5.02	4.98	5.26	**4.60**	4.82

4.7.2 Departure Take-Off Distance Models

For the Departure Take-Off Distance models, Models 1b, 2b and 6b never returned the lowest RMSE. Regarding Model 4b with the reduced regressor set, the mixed-model returned the lowest RMSE for 12 out of 85 aircraft types. It should be noted that for these instances, the differences with Model 3b were often very slight. Regarding Model 3b, it returned the lowest RMSE for 26 out of 85 aircraft types. In contrast, Model 5b returned the lowest RMSE for 47 out of 85 aircraft types. This is perhaps somewhat misleading since if Model 4b were removed from consideration, Model 3b would provide the lowest RMSE for 48 out of 85 aircraft types. However, a clear difference exists between Model 5b and 3b in regards to the widths of the standard errors of the coefficient estimates. As seen in Table 4.11, for the majority of the coefficients, Model 5b returns standard errors that are roughly a third of the size of those returned by Model 3b. Model 5b also has a lower deviance. Therefore, we favor Model 5b over Model 3b for prediction of Departure Take-Off Distance.

Table 4.15: Comparison of Root Mean Square Errors for Departure Take-Off Distance Models

Aircraft Type	Model 1b	Model 2b	Model 3b	Model 4b	Model 5b	Model 6b
A306	1235.20	464.22	403.19	**401.14**	427.04	428.62
A319	515.73	480.64	**473.45**	476.69	473.95	477.71
A320	463.01	397.68	**385.95**	386.41	393.08	393.62
A321	540.44	437.99	**411.07**	411.62	414.24	414.81
A332	755.71	522.28	521.64	522.47	**516.27**	517.18
A333	661.63	459.20	444.11	**443.69**	455.03	455.62
A343	1847.57	680.61	646.30	640.65	**636.26**	640.64
A346	961.05	701.06	739.89	734.91	**609.04**	611.10

Aircraft Type	Model 1b	Model 2b	Model 3b	Model 4b	Model 5b	Model 6b
A388	1606.87	670.52	604.46	598.23	**596.96**	599.43
AT72	724.26	410.07	386.13	384.57	**334.33**	342.49
B190	831.37	696.24	662.63	662.57	**657.22**	657.56
B350	630.38	597.37	544.70	**538.17**	548.91	556.23
B712	607.25	517.72	**491.34**	496.93	506.96	511.65
B732	696.23	534.29	607.51	604.81	**496.78**	502.79
B733	662.18	599.25	**557.47**	561.58	576.59	580.00
B734	550.45	483.84	471.92	471.39	**459.75**	460.09
B735	634.23	550.52	543.66	551.17	**537.29**	544.99
B736	613.31	564.83	411.27	410.86	**401.68**	406.40
B737	675.53	643.98	**631.33**	632.44	636.69	637.42
B738	754.55	707.38	676.57	679.92	**675.93**	679.23
B739	650.26	589.14	**549.96**	550.18	550.14	550.30
B744	1050.42	764.10	757.39	758.21	**746.83**	747.75
B748	1112.40	829.56	827.83	833.99	**755.32**	765.98
B752	664.63	549.26	551.63	551.69	**547.17**	547.53
B753	643.63	618.87	587.54	**587.22**	588.46	588.64
B762	551.55	563.35	546.41	546.80	**520.16**	521.37
B763	735.81	627.50	**629.64**	630.26	614.35	615.50
B764	587.73	489.12	482.91	482.98	**469.36**	470.74
B772	677.44	578.43	**571.41**	572.88	571.53	573.14
B77L	613.18	611.82	585.36	586.03	**565.88**	566.60
B77W	587.35	624.91	574.27	575.15	**569.09**	572.30
B788	852.07	769.14	837.77	853.89	**724.89**	735.31
BE20	804.69	658.28	682.52	688.47	**630.03**	634.93
BE40	1105.36	671.80	561.11	560.54	**546.05**	552.76
BE99	642.72	616.58	**485.78**	493.09	524.16	539.12
BE9L	919.69	539.64	**455.73**	455.89	473.57	475.36
C172	2035.29	658.01	349.28	**322.40**	377.94	385.48

Aircraft Type	Model 1b	Model 2b	Model 3b	Model 4b	Model 5b	Model 6b
C208	1637.63	516.67	**442.90**	443.69	444.47	445.32
C402	1418.69	533.10	498.73	499.52	**495.69**	496.02
C525	957.13	894.56	**710.37**	727.03	767.34	780.17
C550	983.32	998.85	780.24	**770.79**	861.66	876.04
C560	1475.66	933.57	779.27	777.45	**771.88**	773.44
C56X	1313.84	663.37	**573.41**	578.90	586.94	588.87
C680	1459.13	696.89	615.57	613.70	**578.14**	580.69
C750	1294.88	701.65	**637.58**	643.49	669.92	678.26
CL30	1285.45	537.48	479.51	**479.12**	484.36	485.93
CL60	1532.21	656.75	**618.28**	621.71	630.65	633.65
CRJ2	670.73	612.96	**602.94**	603.12	608.20	608.25
CRJ7	614.83	623.16	**601.62**	609.99	607.78	614.52
CRJ9	632.94	569.17	557.19	567.98	**548.77**	558.64
DC10	721.04	660.66	697.69	696.48	**638.98**	647.47
DC95	667.90	353.66	333.46	332.73	**330.65**	334.38
DH8A	779.52	427.14	330.10	328.63	**319.83**	320.73
DH8B	317.32	329.41	**279.49**	276.81	287.45	287.91
DH8C	705.27	520.46	445.16	446.74	**426.52**	431.08
DH8D	826.08	583.14	529.55	**529.53**	531.30	531.68
E120	563.29	508.99	497.68	502.50	**477.07**	481.23
E135	645.03	579.54	564.91	571.17	**553.64**	562.72
E145	738.52	622.83	**606.65**	610.06	607.73	610.45
E170	470.43	429.95	**414.71**	420.37	417.68	422.41
E190	474.75	430.80	420.99	422.07	**417.26**	417.86
E45X	986.00	838.47	829.05	853.07	**815.18**	836.67
E50P	554.04	550.99	**471.04**	474.53	489.92	512.64
E55P	1371.37	465.23	359.95	**358.37**	359.56	364.44
F2TH	1141.94	781.50	696.60	**694.56**	703.43	706.19
F900	1161.00	683.02	633.75	632.21	**607.40**	609.21

Aircraft Type	Model 1b	Model 2b	Model 3b	Model 4b	Model 5b	Model 6b
GALX	1573.58	687.70	662.47	661.74	**651.73**	654.04
GLEX	1284.95	746.10	756.72	757.80	**704.63**	709.14
GLF4	1629.34	786.71	746.44	745.80	**720.93**	731.00
GLF5	1348.30	876.32	816.75	817.13	**753.68**	759.24
H25B	1188.26	801.66	**754.18**	754.39	771.13	775.40
LJ35	1567.44	884.75	834.27	832.38	**776.67**	780.95
LJ45	946.53	608.52	**561.76**	561.80	562.82	572.17
LJ60	2012.53	749.75	641.40	**640.19**	672.09	673.43
MD11	1320.56	728.82	743.48	744.40	**696.86**	704.76
MD82	731.83	621.11	**569.80**	571.14	571.77	575.67
MD83	724.84	622.93	**556.49**	558.51	580.54	584.20
MD88	603.64	482.13	470.50	471.21	**463.20**	464.98
MD90	568.78	475.67	488.13	488.09	**472.09**	472.41
PA31	1027.17	647.70	570.40	570.13	**558.68**	562.93
PC12	1197.18	547.04	**443.74**	447.40	447.23	472.09
SF34	530.42	480.76	483.88	485.53	**442.60**	444.09
SH36	1216.46	570.92	544.73	543.79	**487.26**	498.80
SR22	1334.00	559.35	459.95	446.55	**404.12**	410.54
SW4	748.60	745.28	**658.67**	685.37	674.28	701.44

4.7.3 AROT Models

For the AROT models, Models 1c, 2c and 6c never returned the lowest RMSE and Model 4c represented the lowest RMSE for 1 aircraft type. Between Models 3c and 5c, each produced the lowest RMSE for 42 out of 85 aircraft types. The primary difference between the two models is the coefficient for Altitude. Model 3c holds that higher altitudes lead to higher arrival runway occupancy times, which is contrary to theory. Furthermore, Model 5c returns tighter coefficient estimates and also has a lower deviance. For these reasons, we set Model 5c as the preferred predictive model of arrival runway occupancy time.

Table 4.16: Comparison of Root Mean Square Predictive Errors for AROT Models

Aircraft Type	Model 1c	Model 2c	Model 3c	Model 4c	Model 5c	Model 6c
A306	8.55	7.37	7.31	7.52	**6.94**	7.35
A319	4.27	4.16	**4.07**	4.72	4.13	4.75
A320	4.44	4.34	**4.29**	4.73	4.30	4.75
A321	4.45	4.43	4.43	4.90	**4.42**	4.87
A332	7.01	6.64	**5.81**	6.16	6.46	6.79
A333	6.71	6.19	6.20	6.61	**6.11**	6.57
A343	8.50	7.37	**5.75**	6.23	6.84	7.60
A346	7.18	5.96	6.36	6.76	**5.68**	6.19
A388	13.38	10.73	**8.46**	8.48	8.68	8.80
AT72	5.00	4.97	4.82	5.92	**4.25**	4.97
B190	5.69	5.28	5.23	5.95	**5.15**	5.87
B350	9.17	6.47	5.75	5.88	**5.62**	6.06
B712	3.89	3.37	3.24	3.87	**3.18**	3.80
B732	3.74	3.37	3.14	3.18	**3.01**	3.44
B733	3.99	3.94	**3.82**	4.33	3.87	4.44
B734	4.53	4.51	**4.38**	4.72	4.42	4.79
B735	4.19	4.12	4.20	4.64	**3.83**	4.26
B736	4.52	4.21	**3.56**	4.20	3.65	4.50
B737	4.10	4.08	4.05	4.56	**4.04**	4.55
B738	4.67	4.59	**4.50**	5.02	4.58	5.11
B739	4.96	4.76	**4.50**	5.11	4.65	5.24
B744	10.92	7.91	7.45	7.71	**7.49**	8.04
B748	16.42	10.52	9.20	9.40	**8.86**	9.02
B752	4.90	4.91	**4.85**	5.37	4.88	5.43
B753	5.00	4.92	4.67	5.45	**4.65**	5.36
B762	6.11	5.98	5.92	6.35	**5.78**	6.32
B763	6.04	6.02	6.07	6.51	**5.88**	6.35
B764	5.79	5.56	5.04	5.57	**5.26**	5.67

Aircraft Type	Model 1c	Model 2c	Model 3c	Model 4c	Model 5c	Model 6c
B772	7.17	6.34	**6.00**	6.53	6.20	6.84
B77L	8.89	7.70	5.97	**5.89**	6.12	6.31
B77W	8.01	5.78	5.69	6.38	**5.49**	6.23
B788	10.92	7.72	**6.50**	7.03	6.60	7.07
BE20	10.11	7.49	**6.50**	7.06	6.78	7.34
BE40	6.95	6.01	**5.16**	5.42	5.75	6.15
BE99	8.92	6.51	**5.14**	5.78	5.51	5.91
BE9L	10.42	7.24	**6.55**	7.37	6.74	7.34
C172	11.80	9.73	9.51	10.18	**7.66**	8.97
C208	8.27	6.65	6.69	7.62	**6.31**	7.15
C402	7.63	6.18	**4.72**	5.22	5.14	5.63
C525	7.15	6.42	6.00	6.66	**5.78**	6.29
C550	8.52	7.13	**5.22**	5.30	6.47	6.92
C560	7.39	6.51	6.27	6.81	**6.21**	6.83
C56X	6.10	5.59	5.68	6.01	**5.38**	5.76
C680	6.10	5.72	5.59	5.97	**5.29**	5.76
C750	6.39	5.73	**5.32**	5.80	5.58	6.07
CL30	5.81	5.22	**4.79**	5.34	5.01	5.56
CL60	7.38	6.23	**5.83**	6.08	5.91	6.24
CRJ2	3.77	3.72	**3.68**	4.33	3.70	4.37
CRJ7	3.96	3.89	**3.77**	4.45	3.83	4.50
CRJ9	4.11	3.96	**3.82**	4.45	3.90	4.49
DC10	10.54	7.69	**6.66**	6.93	7.22	7.56
DC95	3.93	3.13	3.06	3.73	**3.05**	3.76
DH8A	4.55	4.59	**4.02**	4.54	4.21	4.72
DH8B	4.52	3.98	**3.39**	3.83	3.55	3.92
DH8C	4.37	3.67	**3.52**	3.86	3.58	4.05
DH8D	5.17	5.10	**4.91**	5.69	4.97	5.66
E120	4.49	4.37	**3.96**	4.63	3.98	4.55

Aircraft Type	Model 1c	Model 2c	Model 3c	Model 4c	Model 5c	Model 6c
E135	4.51	4.20	**3.84**	4.20	3.91	4.28
E145	4.47	4.35	4.25	4.71	**4.18**	4.65
E170	4.02	3.78	3.74	4.26	**3.72**	4.22
E190	4.47	4.20	4.16	4.56	**4.09**	4.49
E45X	4.31	4.28	4.28	4.71	**4.17**	4.65
E50P	6.87	6.13	6.22	6.48	**5.12**	5.73
E55P	5.90	5.59	5.31	5.47	**5.04**	5.28
F2TH	6.77	5.90	5.89	6.40	**5.71**	6.21
F900	6.79	6.09	5.99	6.33	**5.75**	6.37
GALX	7.39	6.01	**5.54**	6.05	5.70	6.24
GLEX	5.99	5.72	6.48	7.36	**5.27**	5.81
GLF4	8.64	6.74	**6.37**	6.65	6.45	6.77
GLF5	7.63	6.29	6.28	6.68	**6.09**	6.68
H25B	8.22	6.42	6.20	6.68	**6.15**	6.68
LJ35	9.99	7.53	8.03	7.90	**7.03**	7.24
LJ45	6.45	5.87	**5.40**	5.53	5.68	5.88
LJ60	9.09	7.07	**6.33**	6.51	6.75	6.90
MD11	11.10	8.29	8.34	8.76	**7.87**	8.33
MD82	4.31	3.71	3.71	4.15	**3.68**	4.17
MD83	4.46	3.86	**3.72**	4.27	3.82	4.33
MD88	4.60	3.43	3.35	3.91	**3.33**	3.97
MD90	4.12	3.77	3.71	4.31	**3.68**	4.27
PA31	9.11	7.07	**6.39**	7.31	6.61	7.57
PC12	7.94	6.46	6.13	7.26	**5.93**	6.92
SF34	5.14	4.91	4.82	5.27	**4.69**	5.21
SH36	7.79	6.92	**5.67**	6.31	5.82	6.71
SR22	7.17	6.52	**5.16**	6.23	5.45	6.41
SW4	9.18	7.03	7.11	7.93	**6.66**	7.31

4.8 Full Model Coefficient Estimates by Individual Aircraft Type

In this section, we present the full set of model coefficient estimates for each individual aircraft type considered in Tables 4.17 through 4.45. We provide the 95% highest posterior density intervals (HPDI) for each coefficient, giving the locations of the 2.5%, the 50% and the 97.5% percentiles as well as the posterior mean and standard deviations.

The HPDI are a form of credible intervals, which are the Bayesian analogs to classical confidence intervals. Credible intervals give the bounds within which a parameter has a probability p of being. That is, If the probability of a number n being between a and b is 0.8, then $[a, b]$ is an 80% credible interval.

It should be noted that credible intervals are not unique and different approaches for defining preferred credible intervals exist. The credible interval that represents the narrowest possible interval for a unimodal distribution is known as the highest posterior density interval.

4.8.1 Departure Runway Occupancy Time Model

Table 4.17: Highest Posterior Density Intervals for Departure Runway Occupancy Time Model 5a Parameters, β_j for A306 - AT72

A306 (Count = 946)

Parameter	Percentile (%), β_j				Std.
	2.5	50	97.5	Mean	Dev.
Alt	-2.51E-04	-8.87E-05	6.30E-05	-9.36E-05	7.99E-05
V_{LO}	0.307	0.339	0.370	0.338	0.016
RwLen	7.88E-05	2.38E-04	3.88E-04	2.32E-04	7.90E-05
Wind	0.064	0.128	0.190	0.126	0.032
Constant	-19.837	-14.418	-9.341	-14.592	2.678

A319 (Count = 22,939)

Parameter	Percentile(%), β_j				Std.
	2.5	50	97.5	Mean	Dev.
Alt	-1.03E-05	2.52E-05	5.94E-05	2.40E-05	1.78E-05
V_{LO}	0.359	0.366	0.372	0.366	0.003
RwLen	7.48E-04	7.75E-04	8.01E-04	7.74E-04	1.34E-05
Wind	0.135	0.147	0.159	0.147	0.006
Constant	-19.971	-18.912	-17.938	-18.943	0.520

A320 (Count = 31,277)

Parameter	Percentile (%), β_j				Std.
	2.5	50	97.5	Mean	Dev.
Alt	-2.05E-04	-1.78E-04	-1.51E-04	-1.78E-04	1.38E-05
V_{LO}	0.336	0.341	0.346	0.341	0.002
RwLen	6.36E-04	6.56E-04	6.75E-04	6.55E-04	9.98E-06
Wind	0.148	0.157	0.166	0.157	0.005
Constant	-15.986	-15.233	-14.518	-15.258	0.376

A321 (Count = 7,431)

Parameter	Percentile(%), β_j				Std.
	2.5	50	97.5	Mean	Dev.
Alt	-1.76E-04	-8.90E-05	-6.61E-06	-9.19E-05	4.34E-05
V_{LO}	0.256	0.267	0.277	0.266	0.005
RwLen	8.49E-04	9.01E-04	9.48E-04	8.99E-04	2.55E-05
Wind	0.084	0.107	0.128	0.106	0.011
Constant	-8.428	-6.623	-4.985	-6.681	0.881

A332 (Count = 1,824)

Parameter	Percentile (%), β_j				Std.
	2.5	50	97.5	Mean	Dev.
Alt	-3.86E-04	-8.66E-05	1.93E-04	-9.63E-05	1.48E-04
V_{LO}	0.328	0.351	0.371	0.350	0.011
RwLen	7.01E-04	8.27E-04	9.41E-04	8.24E-04	6.12E-05
Wind	0.138	0.186	0.230	0.184	0.023
Constant	-17.826	-14.040	-10.551	-14.166	1.854

A333 (Count = 1,517)

Parameter	Percentile(%), β_j				Std.
	2.5	50	97.5	Mean	Dev.
Alt	-1.03E-03	-4.41E-04	1.05E-04	-4.60E-04	2.90E-04
V_{LO}	0.253	0.278	0.301	0.277	0.012
RwLen	3.52E-04	4.95E-04	6.30E-04	4.91E-04	7.07E-05
Wind	0.020	0.069	0.116	0.067	0.024
Constant	-1.492	2.573	6.419	2.440	2.019

A343 (Count = 458)

Parameter	Percentile (%), β_j				Std.
	2.5	50	97.5	Mean	Dev.
Alt	-2.31E-03	-1.01E-03	2.32E-04	-1.05E-03	6.47E-04
V_{LO}	0.397	0.451	0.502	0.449	0.027
RwLen	8.02E-04	1.13E-03	1.43E-03	1.12E-03	1.61E-04
Wind	0.138	0.253	0.364	0.249	0.058
Constant	-32.928	-23.912	-15.509	-24.177	4.439

A346 (Count = 360)

Parameter	Percentile(%), β_j				Std.
	2.5	50	97.5	Mean	Dev.
Alt	-8.13E-04	-1.81E-04	4.13E-04	-2.01E-04	3.12E-04
V_{LO}	0.226	0.262	0.297	0.261	0.018
RwLen	1.28E-03	1.58E-03	1.86E-03	1.58E-03	1.48E-04
Wind	0.145	0.261	0.372	0.258	0.058
Constant	-14.940	-7.707	-0.990	-7.926	3.559

A388 (Count = 217)

Parameter	Percentile (%), β_j				Std.
	2.5	50	97.5	Mean	Dev.
Alt	-8.42E-03	-4.81E-03	-1.47E-03	-4.91E-03	1.77E-03
V_{LO}	0.424	0.471	0.516	0.470	0.024
RwLen	2.13E-04	6.57E-04	1.08E-03	6.42E-04	2.21E-04
Wind	0.165	0.305	0.436	0.300	0.069
Constant	-31.760	-23.592	-16.095	-23.834	3.985

AT72 (Count = 312)

Parameter	Percentile(%), β_j				Std.
	2.5	50	97.5	Mean	Dev.
Alt	-2.52E-02	3.08E-01	6.18E-01	2.97E-01	1.64E-01
V_{LO}	0.243	0.326	0.404	0.324	0.041
RwLen	-1.38E-03	-5.57E-04	1.96E-04	-5.83E-04	4.02E-04
Wind	0.089	0.199	0.302	0.196	0.054
Constant	-16.618	-0.985	14.114	-1.498	7.830

Table 4.18: Highest Posterior Density Intervals for Departure Runway Occupancy Time Model 5a Parameters, β_j for B190 - B738

B190 (Count = 2,742)

Parameter	Percentile (%), β_j				Std.
	2.5	50	97.5	Mean	Dev.
Alt	5.07E-05	1.48E-04	2.40E-04	1.44E-04	4.84E-05
V_{LO}	0.313	0.328	0.342	0.328	0.007
RwLen	1.29E-04	2.39E-04	3.43E-04	2.35E-04	5.48E-05
Wind	0.135	0.169	0.201	0.168	0.017
Constant	-12.927	-10.712	-8.581	-10.787	1.109

B350 (Count = 236)

Parameter	Percentile(%), β_j				Std.
	2.5	50	97.5	Mean	Dev.
Alt	8.82E-05	7.88E-04	1.45E-03	7.67E-04	3.47E-04
V_{LO}	0.267	0.333	0.393	0.331	0.032
RwLen	3.30E-04	5.63E-04	7.83E-04	5.56E-04	1.15E-04
Wind	0.091	0.219	0.338	0.215	0.063
Constant	-21.452	-12.488	-4.130	-12.753	4.417

B712 (Count = 8,300)

Parameter	Percentile (%), β_j				Std.
	2.5	50	97.5	Mean	Dev.
Alt	-6.00E-04	-4.67E-04	-3.40E-04	-4.71E-04	6.65E-05
V_{LO}	0.337	0.347	0.356	0.347	0.005
RwLen	8.79E-04	9.22E-04	9.63E-04	9.20E-04	2.15E-05
Wind	0.163	0.181	0.199	0.181	0.009
Constant	-23.137	-21.546	-20.062	-21.596	0.787

B732 (Count = 270)

Parameter	Percentile(%), β_j				Std.
	2.5	50	97.5	Mean	Dev.
Alt	-8.57E-03	1.42E-03	1.07E-02	1.11E-03	4.94E-03
V_{LO}	0.262	0.328	0.391	0.326	0.033
RwLen	-3.47E-03	-1.79E-03	-2.64E-04	-1.83E-03	8.14E-04
Wind	-0.037	0.100	0.227	0.096	0.068
Constant	-8.818	14.694	36.822	13.948	11.635

B733 (Count = 7,026)

Parameter	Percentile (%), β_j				Std.
	2.5	50	97.5	Mean	Dev.
Alt	-4.95E-04	-4.27E-04	-3.65E-04	-4.29E-04	3.31E-05
V_{LO}	0.346	0.358	0.368	0.357	0.006
RwLen	1.03E-03	1.09E-03	1.14E-03	1.09E-03	2.85E-05
Wind	0.154	0.178	0.200	0.177	0.012
Constant	-23.261	-21.422	-19.685	-21.478	0.914

B734 (Count = 2,060)

Parameter	Percentile(%), β_j				Std.
	2.5	50	97.5	Mean	Dev.
Alt	2.95E-04	7.57E-04	1.18E-03	7.45E-04	2.25E-04
V_{LO}	0.221	0.242	0.261	0.241	0.010
RwLen	4.64E-04	5.72E-04	6.72E-04	5.69E-04	5.31E-05
Wind	0.131	0.171	0.210	0.170	0.020
Constant	-2.913	0.752	4.288	0.639	1.835

B735 (Count = 444)

Parameter	Percentile (%), β_j				Std.
	2.5	50	97.5	Mean	Dev.
Alt	-9.55E-04	-6.62E-04	-3.84E-04	-6.70E-04	1.46E-04
V_{LO}	0.351	0.388	0.423	0.387	0.018
RwLen	3.92E-04	6.09E-04	8.13E-04	6.02E-04	1.07E-04
Wind	0.119	0.211	0.299	0.208	0.046
Constant	-27.978	-21.603	-15.793	-21.788	3.105

B736 (Count = 266)

Parameter	Percentile(%), β_j				Std.
	2.5	50	97.5	Mean	Dev.
Alt	-6.84E-03	-5.34E-03	-3.92E-03	-5.39E-03	7.46E-04
V_{LO}	-4.94E-04	0.063	0.124	0.061	0.032
RwLen	2.36E-03	3.70E-03	4.95E-03	3.66E-03	6.60E-04
Wind	-0.233	-0.131	-0.033	-0.134	0.051
Constant	-5.882	7.772	20.420	7.340	6.721

B737 (Count = 33,251)

Parameter	Percentile (%), β_j				Std.
	2.5	50	97.5	Mean	Dev.
Alt	-3.92E-04	-3.58E-04	-3.27E-04	-3.59E-04	1.66E-05
V_{LO}	0.406	0.412	0.418	0.412	0.003
RwLen	8.81E-04	9.03E-04	9.25E-04	9.02E-04	1.13E-05
Wind	0.162	0.174	0.186	0.174	0.006
Constant	-29.313	-28.334	-27.422	-28.365	0.482

B738 (Count = 33,510)

Parameter	Percentile(%), β_j				Std.
	2.5	50	97.5	Mean	Dev.
Alt	-3.64E-04	-3.27E-04	-2.92E-04	-3.29E-04	1.84E-05
V_{LO}	0.292	0.298	0.302	0.297	0.003
RwLen	1.17E-03	1.20E-03	1.22E-03	1.20E-03	1.14E-05
Wind	0.138	0.149	0.160	0.149	0.005
Constant	-13.977	-13.090	-12.279	-13.117	0.435

Table 4.19: Highest Posterior Density Intervals for Departure Runway Occupancy Time Model 5a Parameters, β_j for B739 - B77L

B739 (Count = 5,987)

Parameter	Percentile (%), β_j				Std.
	2.5	50	97.5	Mean	Dev.
Alt	-1.25E-04	-5.96E-05	1.88E-06	-6.16E-05	3.24E-05
V_{LO}	0.222	0.236	0.248	0.235	0.007
RwLen	1.02E-03	1.08E-03	1.14E-03	1.08E-03	3.05E-05
Wind	0.076	0.099	0.121	0.098	0.012
Constant	-2.597	-0.229	2.052	-0.313	1.187

B744 (Count = 2,581)

Parameter	Percentile(%), β_j				Std.
	2.5	50	97.5	Mean	Dev.
Alt	-4.11E-04	-1.17E-04	1.59E-04	-1.26E-04	1.46E-04
V_{LO}	0.367	0.383	0.398	0.383	0.008
RwLen	6.70E-04	7.99E-04	9.15E-04	7.96E-04	6.25E-05
Wind	0.188	0.234	0.276	0.232	0.022
Constant	-22.285	-19.228	-16.437	-19.307	1.494

B748 (Count = 403)

Parameter	Percentile (%), β_j				Std.
	2.5	50	97.5	Mean	Dev.
Alt	-3.00E-03	-1.37E-03	1.13E-04	-1.42E-03	7.93E-04
V_{LO}	0.168	0.208	0.246	0.207	0.020
RwLen	9.87E-04	1.32E-03	1.62E-03	1.31E-03	1.62E-04
Wind	-0.139	-0.026	0.080	-0.029	0.056
Constant	-0.748	6.976	14.313	6.721	3.853

B752 (Count = 21,910)

Parameter	Percentile(%), β_j				Std.
	2.5	50	97.5	Mean	Dev.
Alt	-2.99E-04	-2.58E-04	-2.20E-04	-2.60E-04	2.02E-05
V_{LO}	0.348	0.355	0.361	0.355	0.003
RwLen	5.27E-04	5.57E-04	5.85E-04	5.56E-04	1.49E-05
Wind	0.178	0.191	0.203	0.191	0.006
Constant	-19.425	-18.330	-17.270	-18.366	0.549

B753 (Count = 2,614)

Parameter	Percentile (%), β_j				Std.
	2.5	50	97.5	Mean	Dev.
Alt	-2.80E-04	-1.43E-04	-1.17E-05	-1.47E-04	6.84E-05
V_{LO}	0.265	0.284	0.300	0.283	0.009
RwLen	1.19E-03	1.29E-03	1.39E-03	1.29E-03	5.22E-05
Wind	0.097	0.133	0.168	0.132	0.018
Constant	-16.573	-13.539	-10.727	-13.626	1.493

B762 (Count = 1,513)

Parameter	Percentile(%), β_j				Std.
	2.5	50	97.5	Mean	Dev.
Alt	-6.71E-04	-3.24E-04	-2.13E-06	-3.35E-04	1.71E-04
V_{LO}	0.290	0.307	0.323	0.306	0.008
RwLen	1.24E-04	2.29E-04	3.31E-04	2.26E-04	5.29E-05
Wind	0.092	0.135	0.175	0.134	0.021
Constant	-6.960	-3.815	-0.889	-3.908	1.549

B763 (Count = 6,226)

Parameter	Percentile (%), β_j				Std.
	2.5	50	97.5	Mean	Dev.
Alt	-3.71E-04	-2.46E-04	-1.31E-04	-2.50E-04	6.10E-05
V_{LO}	0.407	0.417	0.426	0.416	0.005
RwLen	3.82E-04	4.54E-04	5.20E-04	4.52E-04	3.52E-05
Wind	0.232	0.257	0.281	0.257	0.012
Constant	-29.036	-27.217	-25.491	-27.278	0.905

B764 (Count = 881)

Parameter	Percentile(%), β_j				Std.
	2.5	50	97.5	Mean	Dev.
Alt	-2.76E-04	3.18E-05	3.15E-04	2.24E-05	1.51E-04
V_{LO}	0.319	0.346	0.371	0.345	0.013
RwLen	6.73E-04	8.51E-04	1.02E-03	8.45E-04	8.76E-05
Wind	0.086	0.141	0.193	0.140	0.027
Constant	-22.817	-18.160	-13.848	-18.291	2.288

B772 (Count = 3,322)

Parameter	Percentile (%), β_j				Std.
	2.5	50	97.5	Mean	Dev.
Alt	2.31E-04	3.87E-04	5.33E-04	3.82E-04	7.74E-05
V_{LO}	0.272	0.285	0.297	0.284	0.006
RwLen	7.08E-04	8.00E-04	8.86E-04	7.97E-04	4.55E-05
Wind	0.094	0.124	0.151	0.123	0.015
Constant	-7.412	-5.206	-3.131	-5.274	1.095

B77L (Count = 505)

Parameter	Percentile(%), β_j				Std.
	2.5	50	97.5	Mean	Dev.
Alt	-1.77E-04	6.51E-04	1.46E-03	6.24E-04	4.16E-04
V_{LO}	0.185	0.217	0.247	0.216	0.016
RwLen	9.99E-04	1.32E-03	1.62E-03	1.31E-03	1.59E-04
Wind	0.013	0.093	0.168	0.091	0.040
Constant	-6.110	-0.454	4.939	-0.638	2.812

Table 4.20: Highest Posterior Density Intervals for Departure Runway Occupancy Time Model 5a Parameters, β_j for B77W - C525

B77W (Count = 1,737)

Parameter	Percentile (%), β_j				Std.
	2.5	50	97.5	Mean	Dev.
Alt	-1.40E-03	-7.41E-04	-1.18E-04	-7.62E-04	3.26E-04
V_{LO}	0.161	0.181	0.199	0.180	0.010
RwLen	7.76E-04	8.97E-04	1.01E-03	8.93E-04	5.96E-05
Wind	-0.016	0.022	0.059	0.021	0.019
Constant	8.016	11.883	15.471	11.771	1.901

B788 (Count = 335)

Parameter	Percentile(%), β_j				Std.
	2.5	50	97.5	Mean	Dev.
Alt	-8.38E-04	-4.75E-04	-1.37E-04	-4.86E-04	1.79E-04
V_{LO}	0.130	0.190	0.248	0.189	0.030
RwLen	6.11E-04	9.72E-04	1.30E-03	9.61E-04	1.77E-04
Wind	-0.164	-0.043	0.067	-0.047	0.059
Constant	0.906	12.374	22.965	12.028	5.630

BE20 (Count = 464)

Parameter	Percentile (%), β_j				Std.
	2.5	50	97.5	Mean	Dev.
Alt	-4.61E-04	-1.60E-04	1.21E-04	-1.70E-04	1.48E-04
V_{LO}	0.365	0.408	0.449	0.406	0.022
RwLen	1.66E-04	4.28E-04	6.75E-04	4.20E-04	1.30E-04
Wind	0.150	0.260	0.364	0.256	0.055
Constant	-23.736	-17.917	-12.538	-18.093	2.856

BE40 (Count = 607)

Parameter	Percentile(%), β_j				Std.
	2.5	50	97.5	Mean	Dev.
Alt	9.28E-05	3.77E-04	6.45E-04	3.68E-04	1.41E-04
V_{LO}	0.241	0.270	0.298	0.269	0.015
RwLen	-5.90E-05	8.15E-05	2.16E-04	7.68E-05	7.02E-05
Wind	-0.018	0.053	0.120	0.051	0.035
Constant	-8.568	-4.087	0.083	-4.226	2.207

BE99 (Count = 349)

Parameter	Percentile (%), β_j				Std.
	2.5	50	97.5	Mean	Dev.
Alt	5.18E-04	7.82E-04	1.03E-03	7.74E-04	1.31E-04
V_{LO}	0.276	0.324	0.369	0.322	0.024
RwLen	-5.21E-04	-2.76E-04	-5.18E-05	-2.83E-04	1.20E-04
Wind	0.056	0.178	0.291	0.174	0.060
Constant	-9.524	-3.153	2.952	-3.357	3.182

BE9L (Count = 310)

Parameter	Percentile(%), β_j				Std.
	2.5	50	97.5	Mean	Dev.
Alt	-1.48E-04	3.52E-04	8.20E-04	3.36E-04	2.48E-04
V_{LO}	0.375	0.442	0.505	0.440	0.033
RwLen	-2.67E-04	3.01E-05	3.04E-04	2.09E-05	1.46E-04
Wind	0.296	0.412	0.523	0.408	0.058
Constant	-23.932	-15.912	-8.249	-16.174	4.004

C172 (Count = 224)

Parameter	Percentile (%), β_j				Std.
	2.5	50	97.5	Mean	Dev.
Alt	-2.46E-04	1.57E-04	5.43E-04	1.43E-04	2.02E-04
V_{LO}	0.183	0.253	0.318	0.251	0.034
RwLen	-2.03E-05	3.60E-04	7.20E-04	3.47E-04	1.88E-04
Wind	-0.233	-0.038	0.144	-0.043	0.096
Constant	3.727	10.053	15.765	9.879	3.066

C208 (Count = 1,466)

Parameter	Percentile(%), β_j				Std.
	2.5	50	97.5	Mean	Dev.
Alt	-4.35E-04	-1.43E-04	1.29E-04	-1.52E-04	1.44E-04
V_{LO}	0.410	0.445	0.478	0.444	0.018
RwLen	1.15E-04	2.65E-04	4.04E-04	2.61E-04	7.39E-05
Wind	0.180	0.250	0.315	0.248	0.034
Constant	-10.035	-6.600	-3.309	-6.715	1.721

C402 (Count = 1,814)

Parameter	Percentile (%), β_j				Std.
	2.5	50	97.5	Mean	Dev.
Alt	-7.32E-04	-4.08E-04	-1.10E-04	-4.18E-04	1.59E-04
V_{LO}	0.473	0.511	0.545	0.509	0.018
RwLen	-5.75E-04	-4.22E-04	-2.78E-04	-4.27E-04	7.57E-05
Wind	0.220	0.280	0.335	0.278	0.029
Constant	-17.913	-13.873	-10.142	-13.989	1.985

C525 (Count = 211)

Parameter	Percentile(%), β_j				Std.
	2.5	50	97.5	Mean	Dev.
Alt	-3.41E-04	2.02E-04	7.11E-04	1.85E-04	2.69E-04
V_{LO}	0.180	0.231	0.279	0.230	0.025
RwLen	-8.03E-05	3.00E-04	6.55E-04	2.90E-04	1.87E-04
Wind	-0.008	0.168	0.333	0.163	0.087
Constant	-6.055	2.281	10.255	2.005	4.161

Table 4.21: Highest Posterior Density Intervals for Departure Runway Occupancy Time Model 5a Parameters, β_j for C550 - CRJ9

C550 (Count = 266)

Parameter	Percentile (%), β_j				Std.
	2.5	50	97.5	Mean	Dev.
Alt	2.14E-04	8.34E-04	1.42E-03	8.13E-04	3.07E-04
V_{LO}	0.165	0.216	0.264	0.214	0.025
RwLen	-3.44E-04	1.38E-05	3.48E-04	2.84E-06	1.76E-04
Wind	-0.098	0.062	0.217	0.057	0.080
Constant	0.832	8.436	15.701	8.186	3.791

C560 (Count = 510)

Parameter	Percentile(%), β_j				Std.
	2.5	50	97.5	Mean	Dev.
Alt	-2.73E-04	1.25E-04	5.02E-04	1.12E-04	1.98E-04
V_{LO}	0.178	0.209	0.236	0.208	0.015
RwLen	-4.39E-05	1.65E-04	3.62E-04	1.58E-04	1.04E-04
Wind	0.021	0.121	0.217	0.118	0.050
Constant	-1.892	3.030	7.692	2.872	2.447

C56X (Count = 1,245)

Parameter	Percentile (%), β_j				Std.
	2.5	50	97.5	Mean	Dev.
Alt	-8.68E-05	1.44E-04	3.62E-04	1.37E-04	1.14E-04
V_{LO}	0.275	0.296	0.316	0.296	0.010
RwLen	7.60E-05	1.77E-04	2.70E-04	1.74E-04	4.96E-05
Wind	0.141	0.192	0.241	0.191	0.026
Constant	-14.623	-11.316	-8.240	-11.422	1.630

C680 (Count = 521)

Parameter	Percentile(%), β_j				Std.
	2.5	50	97.5	Mean	Dev.
Alt	-4.98E-04	-8.82E-05	2.89E-04	-1.01E-04	2.01E-04
V_{LO}	0.265	0.296	0.324	0.295	0.015
RwLen	1.10E-04	2.58E-04	3.97E-04	2.54E-04	7.32E-05
Wind	0.110	0.198	0.281	0.195	0.044
Constant	-17.218	-12.562	-8.172	-12.703	2.311

C750 (Count = 871)

Parameter	Percentile (%), β_j				Std.
	2.5	50	97.5	Mean	Dev.
Alt	-9.89E-04	-6.82E-04	-3.90E-04	-6.92E-04	1.53E-04
V_{LO}	0.331	0.360	0.388	0.359	0.015
RwLen	1.80E-04	3.11E-04	4.36E-04	3.07E-04	6.55E-05
Wind	0.170	0.233	0.293	0.231	0.031
Constant	-28.126	-23.308	-18.726	-23.467	2.402

CL30 (Count = 778)

Parameter	Percentile(%), β_j				Std.
	2.5	50	97.5	Mean	Dev.
Alt	-5.14E-04	-2.59E-04	-2.57E-05	-2.67E-04	1.25E-04
V_{LO}	0.305	0.337	0.368	0.336	0.016
RwLen	2.03E-04	3.19E-04	4.31E-04	3.16E-04	5.82E-05
Wind	0.146	0.208	0.266	0.206	0.030
Constant	-24.081	-18.974	-14.204	-19.127	2.520

CL60 (Count = 730)

Parameter	Percentile (%), β_j				Std.
	2.5	50	97.5	Mean	Dev.
Alt	9.27E-05	3.80E-04	6.46E-04	3.71E-04	1.41E-04
V_{LO}	0.279	0.320	0.360	0.319	0.021
RwLen	2.53E-04	3.94E-04	5.26E-04	3.90E-04	6.99E-05
Wind	0.082	0.157	0.228	0.155	0.037
Constant	-25.569	-18.619	-12.159	-18.845	3.430

CRJ2 (Count = 37,727)

Parameter	Percentile(%), β_j				Std.
	2.5	50	97.5	Mean	Dev.
Alt	-1.85E-04	-1.54E-04	-1.25E-04	-1.55E-04	1.55E-05
V_{LO}	0.403	0.409	0.413	0.408	0.003
RwLen	5.23E-04	5.46E-04	5.68E-04	5.45E-04	1.15E-05
Wind	0.163	0.173	0.183	0.173	0.005
Constant	-25.192	-24.379	-23.617	-24.404	0.401

CRJ7 (Count = 20,454)

Parameter	Percentile (%), β_j				Std.
	2.5	50	97.5	Mean	Dev.
Alt	2.69E-04	3.09E-04	3.47E-04	3.08E-04	1.99E-05
V_{LO}	0.236	0.245	0.253	0.244	0.004
RwLen	5.68E-04	5.97E-04	6.24E-04	5.96E-04	1.43E-05
Wind	0.026	0.041	0.055	0.041	0.007
Constant	-0.269	1.115	2.402	1.075	0.683

CRJ9 (Count = 11,921)

Parameter	Percentile(%), β_j				Std.
	2.5	50	97.5	Mean	Dev.
Alt	4.13E-04	4.75E-04	5.31E-04	4.73E-04	3.01E-05
V_{LO}	0.394	0.402	0.409	0.402	0.004
RwLen	4.75E-04	5.12E-04	5.48E-04	5.11E-04	1.88E-05
Wind	0.190	0.206	0.221	0.205	0.008
Constant	-25.744	-24.480	-23.297	-24.519	0.625

Table 4.22: Highest Posterior Density Intervals for Departure Runway Occupancy Time Model 5a Parameters, β_j for DC10 - E170

DC10 (Count = 879)

Parameter	Percentile (%), β_j				Std.
	2.5	50	97.5	Mean	Dev.
Alt	-7.85E-04	-5.29E-04	-2.93E-04	-5.37E-04	1.26E-04
V_{LO}	0.320	0.349	0.377	0.349	0.015
RwLen	1.12E-04	2.96E-04	4.71E-04	2.90E-04	9.17E-05
Wind	0.034	0.112	0.185	0.109	0.038
Constant	-17.398	-12.242	-7.395	-12.398	2.557

DC95 (Count = 1,508)

Parameter	Percentile(%), β_j				Std.
	2.5	50	97.5	Mean	Dev.
Alt	7.92E-04	1.39E-03	1.96E-03	1.37E-03	2.99E-04
V_{LO}	0.389	0.405	0.419	0.404	0.008
RwLen	1.56E-04	2.58E-04	3.57E-04	2.55E-04	5.11E-05
Wind	0.126	0.163	0.199	0.162	0.019
Constant	-25.895	-23.049	-20.377	-23.135	1.405

DH8A (Count = 2,571)

Parameter	Percentile (%), β_j				Std.
	2.5	50	97.5	Mean	Dev.
Alt	-1.38E-04	3.14E-04	7.45E-04	2.99E-04	2.25E-04
V_{LO}	0.276	0.300	0.321	0.299	0.012
RwLen	1.26E-04	1.77E-04	2.23E-04	1.75E-04	2.48E-05
Wind	0.201	0.231	0.261	0.230	0.015
Constant	-4.181	-1.462	1.090	-1.549	1.346

DH8B (Count = 805)

Parameter	Percentile(%), β_j				Std.
	2.5	50	97.5	Mean	Dev.
Alt	-2.44E-03	-1.58E-03	-7.55E-04	-1.61E-03	4.31E-04
V_{LO}	0.263	0.300	0.334	0.298	0.018
RwLen	-9.04E-05	3.40E-04	7.40E-04	3.26E-04	2.12E-04
Wind	0.072	0.130	0.183	0.128	0.028
Constant	-10.041	-3.681	2.272	-3.890	3.144

DH8C (Count = 1,284)

Parameter	Percentile (%), β_j				Std.
	2.5	50	97.5	Mean	Dev.
Alt	-2.14E-04	5.66E-04	1.30E-03	5.42E-04	3.88E-04
V_{LO}	0.448	0.487	0.524	0.485	0.019
RwLen	-6.51E-04	-4.33E-04	-2.34E-04	-4.39E-04	1.06E-04
Wind	0.305	0.369	0.428	0.367	0.032
Constant	-25.008	-19.154	-13.625	-19.349	2.905

DH8D (Count = 5,534)

Parameter	Percentile(%), β_j				Std.
	2.5	50	97.5	Mean	Dev.
Alt	-1.39E-04	-7.03E-05	-3.84E-06	-7.24E-05	3.44E-05
V_{LO}	0.325	0.333	0.340	0.333	0.004
RwLen	3.05E-04	3.70E-04	4.31E-04	3.68E-04	3.20E-05
Wind	0.156	0.177	0.198	0.177	0.011
Constant	-14.686	-13.279	-11.964	-13.321	0.696

E120 (Count = 2,740)

Parameter	Percentile (%), β_j				Std.
	2.5	50	97.5	Mean	Dev.
Alt	4.42E-04	5.33E-04	6.16E-04	5.30E-04	4.44E-05
V_{LO}	0.317	0.341	0.364	0.340	0.012
RwLen	-7.38E-05	2.51E-05	1.19E-04	2.20E-05	4.93E-05
Wind	0.178	0.215	0.248	0.214	0.018
Constant	-11.111	-7.664	-4.417	-7.774	1.710

E135 (Count = 7,323)

Parameter	Percentile(%), β_j				Std.
	2.5	50	97.5	Mean	Dev.
Alt	1.69E-03	1.99E-03	2.27E-03	1.98E-03	1.48E-04
V_{LO}	0.333	0.348	0.362	0.348	0.007
RwLen	3.72E-04	4.09E-04	4.43E-04	4.08E-04	1.82E-05
Wind	0.173	0.195	0.215	0.194	0.011
Constant	-15.014	-12.781	-10.653	-12.851	1.110

E145 (Count = 25,502)

Parameter	Percentile (%), β_j				Std.
	2.5	50	97.5	Mean	Dev.
Alt	-8.57E-04	-7.50E-04	-6.51E-04	-7.54E-04	5.26E-05
V_{LO}	0.417	0.425	0.433	0.425	0.004
RwLen	3.93E-04	4.17E-04	4.41E-04	4.17E-04	1.22E-05
Wind	0.253	0.266	0.278	0.265	0.006
Constant	-24.929	-23.671	-22.496	-23.711	0.623

E170 (Count = 14,762)

Parameter	Percentile(%), β_j				Std.
	2.5	50	97.5	Mean	Dev.
Alt	2.37E-04	3.04E-04	3.67E-04	3.02E-04	3.29E-05
V_{LO}	0.426	0.435	0.444	0.435	0.005
RwLen	6.07E-04	6.38E-04	6.67E-04	6.37E-04	1.53E-05
Wind	0.235	0.250	0.264	0.250	0.007
Constant	-30.719	-29.350	-28.042	-29.394	0.683

Table 4.23: Highest Posterior Density Intervals for Departure Runway Occupancy Time Model 5a Parameters, β_j for E190 - GLF5

E190 (Count = 7,970)

Parameter	Percentile (%), β_j				Std.
	2.5	50	97.5	Mean	Dev.
Alt	-4.92E-05	2.37E-05	9.11E-05	2.16E-05	3.59E-05
V_{LO}	0.388	0.399	0.410	0.399	0.006
RwLen	3.10E-04	3.43E-04	3.74E-04	3.42E-04	1.64E-05
Wind	0.185	0.205	0.223	0.204	0.010
Constant	-22.915	-21.119	-19.443	-21.171	0.887

E45X (Count = 7,138)

Parameter	Percentile(%), β_j				Std.
	2.5	50	97.5	Mean	Dev.
Alt	-7.25E-04	-6.56E-04	-5.93E-04	-6.58E-04	3.36E-05
V_{LO}	0.342	0.359	0.376	0.359	0.009
RwLen	8.34E-04	9.22E-04	1.00E-03	9.20E-04	4.33E-05
Wind	0.158	0.188	0.215	0.187	0.014
Constant	-20.784	-17.904	-15.172	-17.994	1.432

E50P (Count = 211)

Parameter	Percentile (%), β_j				Std.
	2.5	50	97.5	Mean	Dev.
Alt	3.27E-04	6.87E-04	1.03E-03	6.76E-04	1.79E-04
V_{LO}	0.264	0.340	0.411	0.338	0.037
RwLen	-7.31E-05	2.00E-04	4.53E-04	1.92E-04	1.34E-04
Wind	-0.031	0.103	0.233	0.099	0.067
Constant	-19.305	-8.870	1.009	-9.201	5.181

E55P (Count = 220)

Parameter	Percentile(%), β_j				Std.
	2.5	50	97.5	Mean	Dev.
Alt	-3.33E-04	8.50E-05	4.67E-04	7.24E-05	2.04E-04
V_{LO}	0.200	0.257	0.311	0.256	0.028
RwLen	1.95E-04	3.75E-04	5.43E-04	3.70E-04	8.90E-05
Wind	0.056	0.153	0.247	0.150	0.049
Constant	-16.343	-7.855	0.260	-8.139	4.226

F2TH (Count = 659)

Parameter	Percentile (%), β_j				Std.
	2.5	50	97.5	Mean	Dev.
Alt	-7.16E-04	-2.57E-04	1.77E-04	-2.71E-04	2.27E-04
V_{LO}	0.163	0.203	0.240	0.202	0.020
RwLen	2.90E-04	4.71E-04	6.41E-04	4.65E-04	8.95E-05
Wind	-0.024	0.068	0.155	0.065	0.046
Constant	-3.183	3.246	9.164	3.051	3.147

F900 (Count = 440)

Parameter	Percentile(%), β_j				Std.
	2.5	50	97.5	Mean	Dev.
Alt	-8.73E-04	-2.97E-04	2.40E-04	-3.15E-04	2.85E-04
V_{LO}	0.227	0.271	0.312	0.270	0.022
RwLen	1.69E-05	2.31E-04	4.31E-04	2.25E-04	1.06E-04
Wind	0.034	0.133	0.226	0.130	0.049
Constant	-12.409	-5.555	0.919	-5.793	3.404

GALX (Count = 494)

Parameter	Percentile (%), β_j				Std.
	2.5	50	97.5	Mean	Dev.
Alt	5.75E-05	4.61E-04	8.47E-04	4.48E-04	2.01E-04
V_{LO}	0.309	0.351	0.391	0.350	0.021
RwLen	6.43E-05	2.39E-04	4.02E-04	2.34E-04	8.63E-05
Wind	0.159	0.248	0.332	0.245	0.044
Constant	-29.945	-22.955	-16.321	-23.193	3.478

GLEX (Count = 295)

Parameter	Percentile(%), β_j				Std.
	2.5	50	97.5	Mean	Dev.
Alt	-1.67E-03	-8.57E-04	-8.86E-05	-8.83E-04	4.02E-04
V_{LO}	0.221	0.285	0.344	0.283	0.031
RwLen	2.13E-04	4.80E-04	7.27E-04	4.72E-04	1.31E-04
Wind	-0.047	0.091	0.222	0.086	0.069
Constant	-19.372	-9.575	-0.313	-9.897	4.859

GLF4 (Count = 999)

Parameter	Percentile (%), β_j				Std.
	2.5	50	97.5	Mean	Dev.
Alt	2.38E-04	5.22E-04	7.90E-04	5.12E-04	1.41E-04
V_{LO}	0.184	0.212	0.239	0.211	0.014
RwLen	3.03E-04	4.36E-04	5.62E-04	4.32E-04	6.62E-05
Wind	-0.006	0.062	0.127	0.060	0.034
Constant	-5.432	-0.544	4.065	-0.688	2.421

GLF5 (Count = 608)

Parameter	Percentile(%), β_j				Std.
	2.5	50	97.5	Mean	Dev.
Alt	-1.02E-04	3.68E-04	8.06E-04	3.54E-04	2.31E-04
V_{LO}	0.123	0.157	0.189	0.156	0.017
RwLen	4.39E-04	6.38E-04	8.29E-04	6.32E-04	9.97E-05
Wind	-0.066	0.032	0.121	0.029	0.048
Constant	2.864	8.597	14.090	8.412	2.858

Table 4.24: Highest Posterior Density Intervals for Departure Runway Occupancy Time Model 5a Parameters, β_j for H25B - PA31

H25B (Count = 1,023)

Parameter	Percentile (%), β_j				Std.
	2.5	50	97.5	Mean	Dev.
Alt	1.68E-04	4.63E-04	7.44E-04	4.53E-04	1.47E-04
V_{LO}	0.223	0.251	0.276	0.250	0.014
RwLen	3.62E-04	5.08E-04	6.44E-04	5.04E-04	7.20E-05
Wind	0.085	0.155	0.220	0.153	0.034
Constant	-9.954	-5.638	-1.547	-5.776	2.140

LJ35 (Count = 322)

Parameter	Percentile(%), β_j				Std.
	2.5	50	97.5	Mean	Dev.
Alt	-4.66E-04	2.74E-05	4.91E-04	1.12E-05	2.44E-04
V_{LO}	0.127	0.176	0.223	0.175	0.025
RwLen	3.35E-04	6.29E-04	9.06E-04	6.19E-04	1.46E-04
Wind	0.025	0.164	0.299	0.159	0.070
Constant	-4.974	3.382	11.354	3.121	4.161

LJ45 (Count = 481)

Parameter	Percentile (%), β_j				Std.
	2.5	50	97.5	Mean	Dev.
Alt	-1.45E-03	-1.02E-03	-6.32E-04	-1.03E-03	2.09E-04
V_{LO}	0.342	0.384	0.422	0.382	0.020
RwLen	4.66E-05	2.10E-04	3.64E-04	2.04E-04	8.11E-05
Wind	0.164	0.243	0.317	0.241	0.039
Constant	-27.581	-21.297	-15.448	-21.495	3.102

LJ60 (Count = 359)

Parameter	Percentile(%), β_j				Std.
	2.5	50	97.5	Mean	Dev.
Alt	-7.07E-04	-1.86E-04	2.93E-04	-2.02E-04	2.54E-04
V_{LO}	0.189	0.226	0.261	0.224	0.018
RwLen	2.80E-04	5.01E-04	7.02E-04	4.95E-04	1.08E-04
Wind	0.064	0.163	0.257	0.160	0.049
Constant	-12.783	-6.277	-0.170	-6.487	3.230

MD11 (Count = 1,482)

Parameter	Percentile (%), β_j				Std.
	2.5	50	97.5	Mean	Dev.
Alt	-6.89E-04	-4.62E-04	-2.47E-04	-4.70E-04	1.13E-04
V_{LO}	0.415	0.441	0.465	0.440	0.013
RwLen	4.89E-04	6.40E-04	7.79E-04	6.35E-04	7.39E-05
Wind	0.208	0.264	0.317	0.262	0.028
Constant	-44.743	-40.135	-35.704	-40.292	2.304

MD82 (Count = 6,956)

Parameter	Percentile(%), β_j				Std.
	2.5	50	97.5	Mean	Dev.
Alt	2.62E-04	3.83E-04	4.97E-04	3.79E-04	5.99E-05
V_{LO}	0.440	0.450	0.459	0.449	0.005
RwLen	5.11E-04	5.56E-04	5.98E-04	5.54E-04	2.22E-05
Wind	0.255	0.276	0.296	0.275	0.011
Constant	-35.210	-33.526	-31.959	-33.575	0.830

MD83 (Count = 6,135)

Parameter	Percentile (%), β_j				Std.
	2.5	50	97.5	Mean	Dev.
Alt	1.15E-04	2.34E-04	3.44E-04	2.31E-04	5.86E-05
V_{LO}	0.428	0.438	0.448	0.438	0.005
RwLen	6.31E-04	6.77E-04	7.21E-04	6.76E-04	2.30E-05
Wind	0.219	0.241	0.262	0.241	0.011
Constant	-34.023	-32.267	-30.612	-32.322	0.871

MD88 (Count = 10,992)

Parameter	Percentile(%), β_j				Std.
	2.5	50	97.5	Mean	Dev.
Alt	1.30E-03	1.49E-03	1.68E-03	1.49E-03	9.53E-05
V_{LO}	0.434	0.442	0.449	0.442	0.004
RwLen	7.00E-04	7.42E-04	7.82E-04	7.41E-04	2.09E-05
Wind	0.209	0.226	0.244	0.226	0.009
Constant	-34.702	-33.442	-32.243	-33.485	0.628

MD90 (Count = 5,358)

Parameter	Percentile (%), β_j				Std.
	2.5	50	97.5	Mean	Dev.
Alt	-5.20E-04	-4.15E-04	-3.16E-04	-4.18E-04	5.21E-05
V_{LO}	0.319	0.330	0.340	0.329	0.005
RwLen	8.46E-04	9.05E-04	9.61E-04	9.03E-04	2.95E-05
Wind	0.125	0.148	0.169	0.147	0.011
Constant	-18.510	-16.705	-14.948	-16.765	0.908

PA31 (Count = 485)

Parameter	Percentile(%), β_j				Std.
	2.5	50	97.5	Mean	Dev.
Alt	-3.13E-05	2.11E-04	4.32E-04	2.03E-04	1.18E-04
V_{LO}	0.175	0.231	0.283	0.229	0.028
RwLen	-2.50E-04	9.06E-05	4.01E-04	8.16E-05	1.66E-04
Wind	0.022	0.130	0.229	0.126	0.053
Constant	5.202	12.044	18.583	11.808	3.406

Table 4.25: Highest Posterior Density Intervals for Departure Runway Occupancy Time Model 5a Parameters, β_j for PC12 - SW4

PC12 (Count = 493)

Parameter	Percentile (%), β_j				Std.
	2.5	50	97.5	Mean	Dev.
Alt	3.42E-04	6.50E-04	9.34E-04	6.40E-04	1.51E-04
V_{LO}	0.322	0.385	0.443	0.383	0.031
RwLen	-3.15E-04	-6.88E-05	1.60E-04	-7.63E-05	1.21E-04
Wind	0.103	0.226	0.341	0.222	0.061
Constant	-10.008	-3.463	2.697	-3.654	3.242

SF34 (Count = 1,400)

Parameter	Percentile(%), β_j				Std.
	2.5	50	97.5	Mean	Dev.
Alt	7.72E-04	1.39E-03	1.97E-03	1.37E-03	3.06E-04
V_{LO}	0.395	0.430	0.463	0.429	0.018
RwLen	-4.75E-05	9.33E-05	2.26E-04	8.88E-05	6.98E-05
Wind	0.218	0.277	0.333	0.276	0.029
Constant	-25.172	-20.182	-15.404	-20.335	2.490

SH36 (Count = 224)

Parameter	Percentile (%), β_j				Std.
	2.5	50	97.5	Mean	Dev.
Alt	-3.21E-02	-8.99E-04	2.85E-02	-1.82E-03	1.54E-02
V_{LO}	0.340	0.446	0.544	0.443	0.052
RwLen	-1.07E-03	-6.50E-04	-2.47E-04	-6.64E-04	2.10E-04
Wind	0.135	0.316	0.490	0.310	0.090
Constant	-14.413	-1.716	10.167	-2.092	6.268

SR22 (Count = 208)

Parameter	Percentile(%), β_j				Std.
	2.5	50	97.5	Mean	Dev.
Alt	-1.77E-04	3.10E-04	7.68E-04	2.95E-04	2.42E-04
V_{LO}	0.312	0.388	0.461	0.385	0.038
RwLen	-2.47E-04	5.92E-05	3.55E-04	4.91E-05	1.53E-04
Wind	-0.013	0.170	0.345	0.164	0.091
Constant	-11.428	-3.820	3.379	-4.041	3.779

SW4 (Count = 734)

Parameter	Percentile (%), β_j				Std.
	2.5	50	97.5	Mean	Dev.
Alt	5.99E-04	7.96E-04	9.81E-04	7.90E-04	9.76E-05
V_{LO}	0.201	0.244	0.285	0.242	0.021
RwLen	-6.16E-04	-3.52E-04	-1.04E-04	-3.61E-04	1.31E-04
Wind	0.052	0.141	0.228	0.138	0.045
Constant	3.793	10.011	15.768	9.822	3.060

4.8.2 Departure Take-Off Distance Model

Table 4.26: Highest Posterior Density Intervals for Departure Take-Off Distance Model 5b Parameters, β_j for A306 - AT72

A306 (Count = 946)

Parameter	Percentile (%), β_j				Std.
	2.5	50	97.5	Mean	Dev.
Alt	-3.11E-02	-1.18E-02	6.20E-03	-1.24E-02	9.50E-03
V_{LO}	85.517	89.434	93.101	89.313	1.941
RwLen	2.27E-02	4.16E-02	5.95E-02	4.10E-02	9.39E-03
Wind	7.517	15.171	22.476	14.930	3.812
Constant	-9802.812	-9159.193	-8555.623	-9179.934	318.166

A319 (Count = 22,939)

Parameter	Percentile(%), β_j				Std.
	2.5	50	97.5	Mean	Dev.
Alt	4.12E-02	4.59E-02	5.06E-02	4.58E-02	2.40E-03
V_{LO}	94.583	95.511	96.363	95.485	0.454
RwLen	1.21E-01	1.25E-01	1.28E-01	1.25E-01	1.80E-03
Wind	21.133	22.802	24.381	22.752	0.829
Constant	-9975.933	-9833.124	-9701.750	-9837.306	70.103

A320 (Count = 31,277)

Parameter	Percentile (%), β_j				Std.
	2.5	50	97.5	Mean	Dev.
Alt	1.21E-02	1.56E-02	1.88E-02	1.55E-02	1.70E-03
V_{LO}	90.567	91.155	91.701	91.138	0.290
RwLen	1.03E-01	1.05E-01	1.07E-01	1.05E-01	1.23E-03
Wind	21.167	22.351	23.444	22.314	0.581
Constant	-9358.533	-9265.412	-9177.178	-9268.543	46.448

A321 (Count = 7,431)

Parameter	Percentile(%), β_j				Std.
	2.5	50	97.5	Mean	Dev.
Alt	1.32E-02	2.43E-02	3.49E-02	2.40E-02	5.55E-03
V_{LO}	77.504	78.855	80.102	78.817	0.664
RwLen	1.69E-01	1.75E-01	1.81E-01	1.75E-01	3.25E-03
Wind	11.316	14.150	16.882	14.051	1.420
Constant	-8364.757	-8134.215	-7924.901	-8141.528	112.548

A332 (Count = 1,824)

Parameter	Percentile (%), β_j				Std.
	2.5	50	97.5	Mean	Dev.
Alt	9.17E-03	4.97E-02	8.75E-02	4.83E-02	2.00E-02
V_{LO}	94.313	97.319	100.142	97.231	1.488
RwLen	1.34E-01	1.51E-01	1.66E-01	1.50E-01	8.28E-03
Wind	15.824	22.214	28.250	22.018	3.164
Constant	-10694.617	-10182.435	-9710.317	-10199.480	250.892

A333 (Count = 1,517)

Parameter	Percentile(%), β_j				Std.
	2.5	50	97.5	Mean	Dev.
Alt	-2.84E-02	4.55E-02	1.14E-01	4.32E-02	3.64E-02
V_{LO}	90.432	93.611	96.515	93.524	1.551
RwLen	9.09E-02	1.09E-01	1.26E-01	1.08E-01	8.89E-03
Wind	10.711	16.840	22.749	16.628	3.077
Constant	-9627.154	-9115.624	-8631.679	-9132.446	254.021

A343 (Count = 458)

Parameter	Percentile (%), β_j				Std.
	2.5	50	97.5	Mean	Dev.
Alt	-3.43E-01	-1.47E-01	4.03E-02	-1.53E-01	9.78E-02
V_{LO}	108.193	116.425	124.144	116.164	4.071
RwLen	1.65E-01	2.15E-01	2.61E-01	2.13E-01	2.43E-02
Wind	23.078	40.406	57.194	39.807	8.706
Constant	-13663.635	-12301.266	-11031.204	-12341.365	670.757

A346 (Count = 360)

Parameter	Percentile(%), β_j				Std.
	2.5	50	97.5	Mean	Dev.
Alt	-9.14E-02	3.83E-03	9.34E-02	8.86E-04	4.71E-02
V_{LO}	80.395	85.808	91.050	85.623	2.715
RwLen	2.45E-01	2.90E-01	3.32E-01	2.89E-01	2.23E-02
Wind	14.086	31.674	48.290	31.147	8.720
Constant	-10739.301	-9649.592	-8637.844	-9682.693	536.159

A388 (Count = 217)

Parameter	Percentile (%), β_j				Std.
	2.5	50	97.5	Mean	Dev.
Alt	-0.737	-0.267	0.167	-0.281	0.230
V_{LO}	108.720	114.893	120.743	114.708	3.066
RwLen	8.03E-02	1.38E-01	1.93E-01	1.36E-01	2.88E-02
Wind	18.302	36.529	53.558	35.958	9.004
Constant	-12670.512	-11607.117	-10631.220	-11638.558	518.821

AT72 (Count = 312)

Parameter	Percentile(%), β_j				Std.
	2.5	50	97.5	Mean	Dev.
Alt	6.816	43.198	77.334	42.049	18.001
V_{LO}	66.814	75.850	84.317	75.570	4.457
RwLen	-1.61E-01	-7.29E-02	1.07E-02	-7.59E-02	4.40E-02
Wind	10.251	22.332	33.538	21.972	5.924
Constant	-6711.520	-4979.894	-3350.364	-5032.539	856.854

Table 4.27: Highest Posterior Density Intervals for Departure Take-Off Distance Model 5b Parameters, β_j for B190 - B738

B190 (Count = 2,742)

Parameter	Percentile (%), β_j				Std.
	2.5	50	97.5	Mean	Dev.
Alt	-1.89E-02	-3.16E-03	1.19E-02	-3.69E-03	7.85E-03
V_{LO}	88.808	91.240	93.513	91.162	1.204
RwLen	1.33E-02	3.12E-02	4.81E-02	3.05E-02	8.88E-03
Wind	28.191	33.798	39.027	33.628	2.767
Constant	-8433.970	-8074.409	-7729.474	-8086.435	179.719

B350 (Count = 236)

Parameter	Percentile(%), β_j				Std.
	2.5	50	97.5	Mean	Dev.
Alt	-9.03E-02	1.40E-02	1.13E-01	1.09E-02	5.17E-02
V_{LO}	82.268	92.086	101.111	91.802	4.803
RwLen	4.31E-02	7.80E-02	1.11E-01	7.68E-02	1.72E-02
Wind	22.565	41.532	59.273	40.933	9.370
Constant	-9872.869	-8536.308	-7290.050	-8575.901	658.549

B712 (Count = 8,300)

Parameter	Percentile (%), β_j				Std.
	2.5	50	97.5	Mean	Dev.
Alt	-1.58E-01	-1.36E-01	-1.15E-01	-1.37E-01	1.11E-02
V_{LO}	95.726	97.348	98.844	97.300	0.795
RwLen	1.62E-01	1.69E-01	1.76E-01	1.69E-01	3.58E-03
Wind	28.430	31.580	34.518	31.479	1.554
Constant	-11335.433	-11070.042	-10823.027	-11078.350	131.060

B732 (Count = 270)

Parameter	Percentile(%), β_j				Std.
	2.5	50	97.5	Mean	Dev.
Alt	-1.48E+00	-2.85E-01	8.36E-01	-3.23E-01	5.93E-01
V_{LO}	89.916	97.894	105.524	97.633	3.973
RwLen	-2.92E-01	-9.00E-02	9.35E-02	-9.52E-02	9.79E-02
Wind	-15.516	0.979	16.251	0.499	8.111
Constant	-10574.004	-7748.829	-5089.921	-7838.482	1398.061

B733 (Count = 7,026)

Parameter	Percentile (%), β_j				Std.
	2.5	50	97.5	Mean	Dev.
Alt	-5.51E-02	-4.47E-02	-3.51E-02	-4.50E-02	5.08E-03
V_{LO}	95.941	97.714	99.352	97.661	0.873
RwLen	2.03E-01	2.12E-01	2.20E-01	2.12E-01	4.37E-03
Wind	21.832	25.509	28.924	25.392	1.812
Constant	-11401.985	-11119.798	-10853.473	-11128.513	140.279

B734 (Count = 2,060)

Parameter	Percentile(%), β_j				Std.
	2.5	50	97.5	Mean	Dev.
Alt	-1.08E-02	5.79E-02	1.20E-01	5.62E-02	3.35E-02
V_{LO}	76.013	79.098	81.996	78.998	1.524
RwLen	1.01E-01	1.17E-01	1.32E-01	1.16E-01	7.90E-03
Wind	24.612	30.687	36.477	30.482	3.033
Constant	-8107.791	-7563.143	-7036.015	-7579.988	273.080

B735 (Count = 444)

Parameter	Percentile (%), β_j				Std.
	2.5	50	97.5	Mean	Dev.
Alt	-1.15E-01	-7.14E-02	-3.01E-02	-7.27E-02	2.17E-02
V_{LO}	94.772	100.299	105.429	100.135	2.718
RwLen	1.08E-01	1.40E-01	1.71E-01	1.39E-01	1.60E-02
Wind	14.953	28.683	41.843	28.219	6.860
Constant	-11904.790	-10955.762	-10090.792	-10983.266	462.169

B736 (Count = 266)

Parameter	Percentile(%), β_j				Std.
	2.5	50	97.5	Mean	Dev.
Alt	-3.54E-01	-1.55E-01	3.48E-02	-1.62E-01	9.93E-02
V_{LO}	4.44E+01	52.879	61.008	52.601	4.240
RwLen	-9.30E-02	8.51E-02	2.51E-01	7.95E-02	8.79E-02
Wind	-9.015	4.518	17.543	4.081	6.788
Constant	-4712.716	-2894.361	-1209.767	-2951.944	895.067

B737 (Count = 33,251)

Parameter	Percentile (%), β_j				Std.
	2.5	50	97.5	Mean	Dev.
Alt	-2.77E-02	-2.24E-02	-1.74E-02	-2.25E-02	2.61E-03
V_{LO}	99.844	100.860	101.781	100.831	0.494
RwLen	1.50E-01	1.54E-01	1.57E-01	1.54E-01	1.79E-03
Wind	20.716	22.626	24.370	22.569	0.933
Constant	-11156.761	-11002.575	-10858.854	-11007.410	75.928

B738 (Count = 33,510)

Parameter	Percentile(%), β_j				Std.
	2.5	50	97.5	Mean	Dev.
Alt	-6.32E-02	-5.69E-02	-5.08E-02	-5.71E-02	3.18E-03
V_{LO}	90.346	91.244	92.082	91.216	0.444
RwLen	2.24E-01	2.28E-01	2.31E-01	2.27E-01	1.97E-03
Wind	24.319	26.200	27.940	26.145	0.924
Constant	-10435.272	-10282.685	-10143.022	-10287.283	74.803

Table 4.28: Highest Posterior Density Intervals for Departure Take-Off Distance Model 5b Parameters, β_j for B739 - B77L

B739 (Count = 5,987)

Parameter	Percentile (%), β_j				Std.
	2.5	50	97.5	Mean	Dev.
Alt	-5.23E-03	5.58E-03	1.57E-02	5.24E-03	5.34E-03
V_{LO}	76.965	79.167	81.204	79.107	1.080
RwLen	2.40E-01	2.50E-01	2.59E-01	2.49E-01	5.03E-03
Wind	10.771	14.609	18.192	14.496	1.897
Constant	-8781.055	-8390.827	-8014.953	-8404.664	195.591

B744 (Count = 2,581)

Parameter	Percentile(%), β_j				Std.
	2.5	50	97.5	Mean	Dev.
Alt	-7.26E-02	-2.55E-02	1.86E-02	-2.70E-02	2.33E-02
V_{LO}	105.536	108.084	110.433	108.008	1.249
RwLen	1.38E-01	1.58E-01	1.77E-01	1.58E-01	1.00E-02
Wind	32.175	39.393	46.173	39.169	3.566
Constant	-12579.879	-12090.981	-11644.579	-12103.632	238.909

B748 (Count = 403)

Parameter	Percentile (%), β_j				Std.
	2.5	50	97.5	Mean	Dev.
Alt	-6.47E-01	-3.83E-01	-1.43E-01	-3.90E-01	1.28E-01
V_{LO}	74.852	81.301	87.434	81.101	3.218
RwLen	2.24E-01	2.77E-01	3.27E-01	2.76E-01	2.62E-02
Wind	-20.828	-2.558	14.612	-3.134	9.060
Constant	-9656.501	-8406.968	-7220.179	-8448.367	623.293

B752 (Count = 21,910)

Parameter	Percentile(%), β_j				Std.
	2.5	50	97.5	Mean	Dev.
Alt	-2.16E-02	-1.53E-02	-9.31E-03	-1.55E-02	3.13E-03
V_{LO}	93.175	94.167	95.083	94.139	0.487
RwLen	1.03E-01	1.07E-01	1.12E-01	1.07E-01	2.31E-03
Wind	23.977	25.998	27.895	25.931	0.999
Constant	-10160.151	-9987.958	-9827.067	-9993.013	84.869

B753 (Count = 2,614)

Parameter	Percentile (%), β_j				Std.
	2.5	50	97.5	Mean	Dev.
Alt	-1.94E-02	3.10E-03	2.46E-02	2.38E-03	1.12E-02
V_{LO}	84.501	87.510	90.258	87.419	1.470
RwLen	2.36E-01	2.53E-01	2.69E-01	2.53E-01	8.55E-03
Wind	16.359	22.395	28.124	22.189	3.010
Constant	-10843.372	-10346.218	-9885.376	-10360.365	244.596

B762 (Count = 1,513)

Parameter	Percentile(%), β_j				Std.
	2.5	50	97.5	Mean	Dev.
Alt	-9.75E-02	-4.33E-02	6.93E-03	-4.50E-02	2.67E-02
V_{LO}	75.179	77.870	80.366	77.791	1.325
RwLen	4.07E-02	5.72E-02	7.31E-02	5.66E-02	8.27E-03
Wind	1.126	7.871	14.121	7.683	3.322
Constant	-6724.031	-6232.798	-5775.787	-6247.339	241.952

B763 (Count = 6,226)

Parameter	Percentile (%), β_j				Std.
	2.5	50	97.5	Mean	Dev.
Alt	-6.39E-02	-4.44E-02	-2.64E-02	-4.49E-02	9.57E-03
V_{LO}	106.953	108.488	109.950	108.436	0.765
RwLen	7.92E-02	9.04E-02	1.01E-01	9.01E-02	5.52E-03
Wind	33.762	37.797	41.425	37.683	1.961
Constant	-12499.600	-12214.345	-11943.605	-12223.901	142.038

B764 (Count = 881)

Parameter	Percentile(%), β_j				Std.
	2.5	50	97.5	Mean	Dev.
Alt	-6.32E-03	4.53E-02	9.28E-02	4.37E-02	2.53E-02
V_{LO}	96.808	101.310	105.520	101.156	2.228
RwLen	1.71E-01	2.01E-01	2.29E-01	2.00E-01	1.47E-02
Wind	17.503	26.725	35.319	26.428	4.548
Constant	-12876.589	-12096.204	-11371.346	-12118.194	384.011

B772 (Count = 3,322)

Parameter	Percentile (%), β_j				Std.
	2.5	50	97.5	Mean	Dev.
Alt	2.62E-02	5.21E-02	7.64E-02	5.13E-02	1.28E-02
V_{LO}	88.431	90.613	92.624	90.551	1.070
RwLen	1.53E-01	1.68E-01	1.82E-01	1.68E-01	7.55E-03
Wind	13.055	17.953	22.553	17.794	2.423
Constant	-9926.080	-9560.180	-9215.931	-9571.443	181.557

B77L (Count = 505)

Parameter	Percentile(%), β_j				Std.
	2.5	50	97.5	Mean	Dev.
Alt	-6.90E-02	6.07E-02	1.87E-01	5.65E-02	6.51E-02
V_{LO}	72.329	77.296	81.997	77.139	2.467
RwLen	2.45E-01	2.96E-01	3.43E-01	2.94E-01	2.49E-02
Wind	-2.759	9.923	21.496	9.547	6.200
Constant	-9752.911	-8866.870	-8022.152	-8895.657	440.482

Table 4.29: Highest Posterior Density Intervals for Departure Take-Off Distance Model 5b Parameters, β_j for B77W - C525

B77W (Count = 1,737)

Parameter	Percentile (%), β_j				Std.
	2.5	50	97.5	Mean	Dev.
Alt	-3.41E-01	-2.27E-01	-1.18E-01	-2.30E-01	5.69E-02
V_{LO}	67.738	71.112	74.285	71.016	1.671
RwLen	2.01E-01	2.22E-01	2.42E-01	2.21E-01	1.04E-02
Wind	-11.898	-5.148	1.240	-5.357	3.363
Constant	-7520.374	-6846.080	-6220.282	-6865.521	331.597

B788 (Count = 335)

Parameter	Percentile(%), β_j				Std.
	2.5	50	97.5	Mean	Dev.
Alt	-1.12E-01	-5.78E-02	-6.85E-03	-5.94E-02	2.70E-02
V_{LO}	70.212	79.397	88.051	79.116	4.560
RwLen	1.41E-01	1.95E-01	2.45E-01	1.94E-01	2.66E-02
Wind	-13.192	4.924	21.550	4.378	8.864
Constant	-9273.799	-7545.071	-5948.561	-7597.236	848.730

BE20 (Count = 464)

Parameter	Percentile (%), β_j				Std.
	2.5	50	97.5	Mean	Dev.
Alt	-4.45E-02	-3.95E-03	3.39E-02	-5.25E-03	2.00E-02
V_{LO}	92.649	98.436	104.020	98.230	2.899
RwLen	2.33E-02	5.86E-02	9.19E-02	5.75E-02	1.75E-02
Wind	30.459	45.181	59.325	44.695	7.357
Constant	-9441.787	-8657.420	-7932.203	-8681.101	385.011

BE40 (Count = 607)

Parameter	Percentile(%), β_j				Std.
	2.5	50	97.5	Mean	Dev.
Alt	3.36E-02	7.85E-02	1.21E-01	7.70E-02	2.22E-02
V_{LO}	68.079	72.683	77.103	72.534	2.302
RwLen	-1.80E-02	4.17E-03	2.54E-02	3.43E-03	1.11E-02
Wind	1.112	12.422	22.942	12.098	5.588
Constant	-6661.155	-5953.888	-5295.650	-5975.841	348.296

BE99 (Count = 349)

Parameter	Percentile (%), β_j				Std.
	2.5	50	97.5	Mean	Dev.
Alt	3.16E-02	7.06E-02	1.07E-01	6.93E-02	1.93E-02
V_{LO}	74.857	81.943	88.694	81.711	3.529
RwLen	-7.36E-02	-3.75E-02	-4.38E-03	-3.85E-02	1.77E-02
Wind	17.395	35.309	52.050	34.719	8.837
Constant	-6710.688	-5770.655	-4869.838	-5800.752	469.572

BE9L (Count = 310)

Parameter	Percentile(%), β_j				Std.
	2.5	50	97.5	Mean	Dev.
Alt	-5.15E-02	3.86E-03	5.58E-02	2.14E-03	2.75E-02
V_{LO}	89.624	96.971	104.009	96.723	3.670
RwLen	-3.03E-02	2.54E-03	3.30E-02	1.51E-03	1.62E-02
Wind	36.138	49.061	61.314	48.649	6.422
Constant	-8257.624	-7368.585	-6519.672	-7397.646	443.678

C172 (Count = 224)

Parameter	Percentile (%), β_j				Std.
	2.5	50	97.5	Mean	Dev.
Alt	1.42E-02	4.77E-02	7.96E-02	4.65E-02	1.67E-02
V_{LO}	42.973	48.753	54.136	48.582	2.849
RwLen	-1.79E-02	1.36E-02	4.34E-02	1.26E-02	1.56E-02
Wind	-21.399	-5.248	9.787	-5.703	7.948
Constant	-1890.353	-1366.107	-892.659	-1380.477	254.093

C208 (Count = 1,466)

Parameter	Percentile(%), β_j				Std.
	2.5	50	97.5	Mean	Dev.
Alt	-4.48E-02	-1.90E-02	5.49E-03	-1.99E-02	1.28E-02
V_{LO}	76.465	79.620	82.572	79.528	1.564
RwLen	1.48E-02	2.83E-02	4.06E-02	2.79E-02	6.59E-03
Wind	21.676	27.908	33.691	27.721	3.063
Constant	-4638.712	-4332.298	-4039.429	-4342.479	153.325

C402 (Count = 1,814)

Parameter	Percentile (%), β_j				Std.
	2.5	50	97.5	Mean	Dev.
Alt	-5.39E-02	-1.78E-02	1.55E-02	-1.90E-02	1.77E-02
V_{LO}	92.884	97.033	100.886	96.901	2.044
RwLen	-1.54E-02	1.59E-03	1.77E-02	1.04E-03	8.44E-03
Wind	31.490	38.136	44.326	37.918	3.280
Constant	-6934.933	-6484.426	-6068.469	-6497.413	221.310

C525 (Count = 211)

Parameter	Percentile(%), β_j				Std.
	2.5	50	97.5	Mean	Dev.
Alt	3.52E-03	8.63E-02	1.64E-01	8.38E-02	4.10E-02
V_{LO}	65.621	73.472	80.798	73.234	3.884
RwLen	-9.71E-03	4.83E-02	1.02E-01	4.68E-02	2.86E-02
Wind	2.669	29.611	54.706	28.776	13.255
Constant	-7338.307	-6067.163	-4851.384	-6109.210	634.424

Table 4.30: Highest Posterior Density Intervals for Departure Take-Off Distance Model 5b Parameters, β_j for C550 - CRJ9

C550 (Count = 266)

Parameter	Percentile (%), β_j				Std.
	2.5	50	97.5	Mean	Dev.
Alt	2.71E-02	1.27E-01	2.21E-01	1.24E-01	4.94E-02
V_{LO}	59.407	67.578	75.362	67.337	4.065
RwLen	-4.17E-02	1.59E-02	6.96E-02	1.41E-02	2.83E-02
Wind	-15.180	10.605	35.457	9.747	12.900
Constant	-5935.985	-4711.874	-3542.361	-4752.237	610.254

C560 (Count = 510)

Parameter	Percentile(%), β_j				Std.
	2.5	50	97.5	Mean	Dev.
Alt	-4.70E-02	1.90E-02	8.15E-02	1.69E-02	3.28E-02
V_{LO}	62.194	67.310	71.909	67.172	2.481
RwLen	-1.80E-02	1.67E-02	4.95E-02	1.56E-02	1.72E-02
Wind	2.901	19.541	35.424	19.015	8.305
Constant	-6312.759	-5495.663	-4721.517	-5521.890	406.305

C56X (Count = 1,245)

Parameter	Percentile (%), β_j				Std.
	2.5	50	97.5	Mean	Dev.
Alt	-1.15E-02	2.63E-02	6.19E-02	2.51E-02	1.87E-02
V_{LO}	79.793	83.300	86.506	83.203	1.713
RwLen	2.80E-04	1.67E-02	3.19E-02	1.62E-02	8.10E-03
Wind	26.429	34.881	42.832	34.597	4.196
Constant	-8565.573	-8024.759	-7521.822	-8042.105	266.548

C680 (Count = 521)

Parameter	Percentile(%), β_j				Std.
	2.5	50	97.5	Mean	Dev.
Alt	-7.16E-02	-6.41E-03	5.36E-02	-8.38E-03	3.20E-02
V_{LO}	73.926	78.800	83.296	78.654	2.393
RwLen	-2.62E-03	2.10E-02	4.30E-02	2.03E-02	1.17E-02
Wind	29.076	43.103	56.389	42.666	6.976
Constant	-8252.127	-7511.216	-6812.576	-7533.713	367.797

C750 (Count = 871)

Parameter	Percentile (%), β_j				Std.
	2.5	50	97.5	Mean	Dev.
Alt	-1.75E-01	-1.21E-01	-6.97E-02	-1.23E-01	2.69E-02
V_{LO}	99.579	104.724	109.657	104.554	2.575
RwLen	2.92E-02	5.22E-02	7.42E-02	5.15E-02	1.15E-02
Wind	38.814	49.899	60.494	49.541	5.529
Constant	-12755.362	-11900.581	-11102.561	-11927.272	422.300

CL30 (Count = 778)

Parameter	Percentile(%), β_j				Std.
	2.5	50	97.5	Mean	Dev.
Alt	-7.40E-02	-3.51E-02	5.47E-04	-3.63E-02	1.91E-02
V_{LO}	83.037	88.057	92.770	87.903	2.485
RwLen	2.97E-02	4.75E-02	6.44E-02	4.69E-02	8.87E-03
Wind	31.228	40.433	49.448	40.113	4.647
Constant	-9885.429	-9106.489	-8378.908	-9129.851	384.265

CL60 (Count = 730)

Parameter	Percentile (%), β_j				Std.
	2.5	50	97.5	Mean	Dev.
Alt	-9.62E-03	3.90E-02	8.43E-02	3.76E-02	2.39E-02
V_{LO}	79.494	86.504	93.134	86.290	3.487
RwLen	4.80E-02	7.20E-02	9.44E-02	7.13E-02	1.19E-02
Wind	18.776	31.631	43.404	31.285	6.275
Constant	-10588.571	-9410.236	-8315.223	-9448.521	581.484

CRJ2 (Count = 37,727)

Parameter	Percentile(%), β_j				Std.
	2.5	50	97.5	Mean	Dev.
Alt	-1.87E-03	3.27E-03	8.10E-03	3.10E-03	2.55E-03
V_{LO}	103.026	103.876	104.670	103.849	0.419
RwLen	8.57E-02	8.95E-02	9.31E-02	8.94E-02	1.89E-03
Wind	24.322	25.982	27.548	25.932	0.825
Constant	-10827.992	-10694.071	-10568.630	-10698.164	66.088

CRJ7 (Count = 20,454)

Parameter	Percentile (%), β_j				Std.
	2.5	50	97.5	Mean	Dev.
Alt	6.31E-02	6.96E-02	7.58E-02	6.93E-02	3.24E-03
V_{LO}	74.083	75.511	76.868	75.463	0.713
RwLen	1.05E-01	1.09E-01	1.14E-01	1.09E-01	2.32E-03
Wind	1.321	3.740	5.970	3.667	1.189
Constant	-6651.535	-6427.804	-6216.348	-6434.575	111.240

CRJ9 (Count = 11,921)

Parameter	Percentile(%), β_j				Std.
	2.5	50	97.5	Mean	Dev.
Alt	9.50E-02	1.05E-01	1.15E-01	1.05E-01	5.06E-03
V_{LO}	104.478	105.811	107.054	105.769	0.657
RwLen	9.67E-02	1.03E-01	1.09E-01	1.03E-01	3.15E-03
Wind	31.932	34.664	37.244	34.576	1.354
Constant	-11641.792	-11429.412	-11230.260	-11435.990	105.147

Table 4.31: Highest Posterior Density Intervals for Departure Take-Off Distance Model 5b Parameters, β_j for DC10 - E170

DC10 (Count = 879)

Parameter	Percentile (%), β_j				Std.
	2.5	50	97.5	Mean	Dev.
Alt	-1.17E-01	-7.79E-02	-4.19E-02	-7.92E-02	1.92E-02
V_{LO}	93.246	97.721	101.976	97.577	2.230
RwLen	2.88E-02	5.70E-02	8.37E-02	5.61E-02	1.40E-02
Wind	6.371	18.186	29.390	17.822	5.871
Constant	-10482.770	-9695.056	-8953.498	-9718.920	390.879

DC95 (Count = 1,508)

Parameter	Percentile(%), β_j				Std.
	2.5	50	97.5	Mean	Dev.
Alt	-2.66E-01	-1.90E-01	-1.17E-01	-1.93E-01	3.81E-02
V_{LO}	101.975	103.966	105.798	103.907	0.973
RwLen	4.04E-02	5.33E-02	6.59E-02	5.29E-02	6.52E-03
Wind	25.126	29.918	34.486	29.761	2.386
Constant	-11261.428	-10898.795	-10558.244	-10909.731	179.021

DH8A (Count = 2,571)

Parameter	Percentile (%), β_j				Std.
	2.5	50	97.5	Mean	Dev.
Alt	1.06E-02	6.51E-02	1.17E-01	6.33E-02	2.71E-02
V_{LO}	61.918	64.718	67.351	64.626	1.387
RwLen	3.30E-02	3.91E-02	4.47E-02	3.89E-02	2.98E-03
Wind	18.992	22.695	26.213	22.570	1.841
Constant	-4383.586	-4055.978	-3748.522	-4066.462	162.153

DH8B (Count = 805)

Parameter	Percentile(%), β_j				Std.
	2.5	50	97.5	Mean	Dev.
Alt	-9.77E-02	-2.90E-03	8.87E-02	-6.09E-03	4.76E-02
V_{LO}	65.340	69.416	73.252	69.287	2.018
RwLen	2.15E-03	4.97E-02	9.39E-02	4.81E-02	2.34E-02
Wind	10.467	16.856	22.755	16.669	3.132
Constant	-5744.996	-5042.717	-4385.563	-5065.777	347.115

DH8C (Count = 1,284)

Parameter	Percentile (%), β_j				Std.
	2.5	50	97.5	Mean	Dev.
Alt	1.42E-01	2.41E-01	3.33E-01	2.37E-01	4.89E-02
V_{LO}	101.185	106.075	110.774	105.908	2.447
RwLen	-1.22E-01	-9.50E-02	-6.98E-02	-9.57E-02	1.34E-02
Wind	45.778	53.845	61.348	53.591	3.979
Constant	-8848.914	-8111.332	-7414.710	-8135.817	366.039

DH8D (Count = 5,534)

Parameter	Percentile(%), β_j				Std.
	2.5	50	97.5	Mean	Dev.
Alt	-1.02E-02	3.85E-04	1.07E-02	5.48E-05	5.32E-03
V_{LO}	80.543	81.827	82.994	81.788	0.627
RwLen	5.19E-02	6.20E-02	7.14E-02	6.16E-02	4.96E-03
Wind	22.146	25.509	28.714	25.401	1.679
Constant	-7647.394	-7429.744	-7226.219	-7436.115	107.670

E120 (Count = 2,740)

Parameter	Percentile (%), β_j				Std.
	2.5	50	97.5	Mean	Dev.
Alt	2.98E-02	4.26E-02	5.43E-02	4.22E-02	6.26E-03
V_{LO}	87.851	91.216	94.473	91.101	1.691
RwLen	-1.19E-02	2.07E-03	1.54E-02	1.64E-03	6.96E-03
Wind	35.096	40.236	44.953	40.085	2.514
Constant	-7993.606	-7507.550	-7049.451	-7522.999	241.213

E135 (Count = 7,323)

Parameter	Percentile(%), β_j				Std.
	2.5	50	97.5	Mean	Dev.
Alt	3.20E-01	3.68E-01	4.13E-01	3.67E-01	2.37E-02
V_{LO}	95.123	97.515	99.729	97.440	1.171
RwLen	4.97E-02	5.56E-02	6.11E-02	5.54E-02	2.90E-03
Wind	31.388	34.874	38.130	34.769	1.715
Constant	-9567.792	-9211.360	-8871.744	-9222.530	177.165

E145 (Count = 25,502)

Parameter	Percentile (%), β_j				Std.
	2.5	50	97.5	Mean	Dev.
Alt	-1.47E-01	-1.29E-01	-1.13E-01	-1.30E-01	8.72E-03
V_{LO}	109.824	111.182	112.468	111.141	0.676
RwLen	5.42E-02	5.82E-02	6.21E-02	5.81E-02	2.02E-03
Wind	43.171	45.263	47.224	45.196	1.035
Constant	-11343.672	-11134.950	-10939.880	-11141.580	103.356

E170 (Count = 14,762)

Parameter	Percentile(%), β_j				Std.
	2.5	50	97.5	Mean	Dev.
Alt	6.86E-02	7.71E-02	8.51E-02	7.68E-02	4.22E-03
V_{LO}	104.137	105.323	106.440	105.284	0.588
RwLen	7.66E-02	8.06E-02	8.43E-02	8.05E-02	1.95E-03
Wind	35.529	37.414	39.178	37.352	0.931
Constant	-11080.074	-10904.725	-10737.314	-10910.345	87.476

Table 4.32: Highest Posterior Density Intervals for Departure Take-Off Distance Model 5b Parameters, β_j for E190 - GLF5

E190 (Count = 7,970)

Parameter	Percentile (%), β_j				Std.
	2.5	50	97.5	Mean	Dev.
Alt	1.13E-02	2.10E-02	3.00E-02	2.07E-02	4.79E-03
V_{LO}	98.815	100.382	101.846	100.331	0.775
RwLen	6.54E-02	6.98E-02	7.40E-02	6.97E-02	2.19E-03
Wind	28.506	31.094	33.503	31.017	1.274
Constant	-10445.901	-10205.928	-9982.058	-10212.932	118.518

E45X (Count = 7,138)

Parameter	Percentile(%), β_j				Std.
	2.5	50	97.5	Mean	Dev.
Alt	-1.24E-01	-1.12E-01	-1.01E-01	-1.13E-01	5.82E-03
V_{LO}	107.509	110.505	113.380	110.402	1.500
RwLen	1.41E-01	1.56E-01	1.70E-01	1.56E-01	7.49E-03
Wind	34.733	39.723	44.500	39.550	2.485
Constant	-12478.072	-11979.755	-11507.036	-11995.332	247.691

E50P (Count = 211)

Parameter	Percentile (%), β_j				Std.
	2.5	50	97.5	Mean	Dev.
Alt	5.45E-02	1.08E-01	1.59E-01	1.07E-01	2.66E-02
V_{LO}	70.836	82.232	92.721	81.877	5.583
RwLen	8.77E-03	4.94E-02	8.71E-02	4.82E-02	2.00E-02
Wind	3.108	23.099	42.505	22.429	10.037
Constant	-8231.367	-6676.331	-5204.294	-6725.710	771.963

E55P (Count = 220)

Parameter	Percentile(%), β_j				Std.
	2.5	50	97.5	Mean	Dev.
Alt	-1.08E-02	4.77E-02	1.02E-01	4.58E-02	2.87E-02
V_{LO}	63.836	71.908	79.449	71.671	3.973
RwLen	3.65E-03	2.91E-02	5.28E-02	2.84E-02	1.25E-02
Wind	11.663	25.425	38.639	24.979	6.881
Constant	-7688.984	-6492.183	-5347.851	-6532.128	595.872

F2TH (Count = 659)

Parameter	Percentile (%), β_j				Std.
	2.5	50	97.5	Mean	Dev.
Alt	-9.24E-02	-1.87E-02	5.11E-02	-2.09E-02	3.65E-02
V_{LO}	60.806	67.292	73.193	67.099	3.155
RwLen	5.88E-02	8.79E-02	1.15E-01	8.70E-02	1.44E-02
Wind	2.211	17.071	30.990	16.605	7.356
Constant	-6821.792	-5788.512	-4837.432	-5819.790	505.785

F900 (Count = 440)

Parameter	Percentile(%), β_j				Std.
	2.5	50	97.5	Mean	Dev.
Alt	-1.10E-01	-2.68E-02	5.02E-02	-2.94E-02	4.09E-02
V_{LO}	69.202	75.573	81.498	75.380	3.140
RwLen	3.36E-03	3.42E-02	6.29E-02	3.32E-02	1.52E-02
Wind	12.217	26.426	39.705	25.974	7.011
Constant	-7686.276	-6701.209	-5770.773	-6735.491	489.218

GALX (Count = 494)

Parameter	Percentile (%), β_j				Std.
	2.5	50	97.5	Mean	Dev.
Alt	-3.48E-02	3.51E-02	1.02E-01	3.28E-02	3.49E-02
V_{LO}	88.393	95.638	102.576	95.400	3.620
RwLen	1.60E-02	4.63E-02	7.46E-02	4.54E-02	1.50E-02
Wind	30.426	45.768	60.455	45.308	7.685
Constant	-11929.022	-10718.237	-9569.231	-10759.553	602.495

GLEX (Count = 295)

Parameter	Percentile(%), β_j				Std.
	2.5	50	97.5	Mean	Dev.
Alt	-2.34E-01	-1.04E-01	1.92E-02	-1.08E-01	6.45E-02
V_{LO}	72.048	82.219	91.643	81.932	4.997
RwLen	3.07E-02	7.34E-02	1.13E-01	7.22E-02	2.10E-02
Wind	4.373	26.446	47.554	25.691	11.006
Constant	-9755.563	-8185.542	-6700.986	-8237.290	778.761

GLF4 (Count = 999)

Parameter	Percentile (%), β_j				Std.
	2.5	50	97.5	Mean	Dev.
Alt	5.91E-02	1.06E-01	1.50E-01	1.04E-01	2.33E-02
V_{LO}	65.662	70.312	74.721	70.153	2.313
RwLen	4.88E-02	7.08E-02	9.17E-02	7.01E-02	1.09E-02
Wind	1.469	12.810	23.567	12.438	5.642
Constant	-7540.427	-6724.950	-5970.236	-6747.553	400.257

GLF5 (Count = 608)

Parameter	Percentile(%), β_j				Std.
	2.5	50	97.5	Mean	Dev.
Alt	2.06E-02	9.70E-02	1.68E-01	9.47E-02	3.76E-02
V_{LO}	54.292	59.815	64.953	59.648	2.714
RwLen	8.01E-02	1.13E-01	1.44E-01	1.11E-01	1.62E-02
Wind	-10.226	5.762	20.237	5.332	7.783
Constant	-5988.167	-5056.234	-4163.174	-5086.291	464.635

Table 4.33: Highest Posterior Density Intervals for Departure Take-Off Distance Model 5b Parameters, β_j for H25B - PA31

H25B (Count = 1,023)

Parameter	Percentile (%), β_j				Std.
	2.5	50	97.5	Mean	Dev.
Alt	1.72E-02	6.79E-02	1.16E-01	6.63E-02	2.53E-02
V_{LO}	78.164	82.928	87.356	82.785	2.341
RwLen	6.03E-02	8.55E-02	1.09E-01	8.47E-02	1.24E-02
Wind	19.137	31.196	42.307	30.851	5.886
Constant	-9203.259	-8460.447	-7756.374	-8484.252	368.372

LJ35 (Count = 322)

Parameter	Percentile(%), β_j				Std.
	2.5	50	97.5	Mean	Dev.
Alt	-1.27E-01	-4.53E-02	3.12E-02	-4.79E-02	4.03E-02
V_{LO}	60.065	68.313	76.001	68.060	4.056
RwLen	6.75E-02	1.16E-01	1.62E-01	1.14E-01	2.41E-02
Wind	17.056	39.974	62.213	39.221	11.514
Constant	-8043.352	-6663.835	-5347.986	-6706.932	686.889

LJ45 (Count = 481)

Parameter	Percentile (%), β_j				Std.
	2.5	50	97.5	Mean	Dev.
Alt	-2.03E-01	-1.31E-01	-6.61E-02	-1.33E-01	3.49E-02
V_{LO}	91.698	98.678	105.115	98.483	3.424
RwLen	1.21E-02	3.94E-02	6.53E-02	3.85E-02	1.36E-02
Wind	30.152	43.466	55.891	43.072	6.575
Constant	-11151.488	-10100.389	-9121.652	-10133.712	518.925

LJ60 (Count = 359)

Parameter	Percentile(%), β_j				Std.
	2.5	50	97.5	Mean	Dev.
Alt	-9.13E-02	-2.71E-05	8.38E-02	-2.84E-03	4.46E-02
V_{LO}	69.708	76.122	82.306	75.910	3.216
RwLen	2.60E-02	6.48E-02	1.00E-01	6.38E-02	1.89E-02
Wind	18.227	35.554	51.980	35.008	8.588
Constant	-9255.939	-8116.886	-7047.497	-8153.487	565.483

MD11 (Count = 1,482)

Parameter	Percentile (%), β_j				Std.
	2.5	50	97.5	Mean	Dev.
Alt	-1.48E-01	-1.09E-01	-7.12E-02	-1.10E-01	1.97E-02
V_{LO}	112.799	117.262	121.402	117.133	2.197
RwLen	1.09E-01	1.36E-01	1.60E-01	1.35E-01	1.29E-02
Wind	32.228	41.991	51.221	41.693	4.853
Constant	-16210.494	-15406.892	-14634.174	-15434.231	401.711

MD82 (Count = 6,956)

Parameter	Percentile(%), β_j				Std.
	2.5	50	97.5	Mean	Dev.
Alt	7.03E-02	8.90E-02	1.07E-01	8.84E-02	9.25E-03
V_{LO}	119.073	120.590	122.050	120.537	0.761
RwLen	8.36E-02	9.06E-02	9.71E-02	9.03E-02	3.43E-03
Wind	42.515	45.787	48.936	45.676	1.637
Constant	-14482.797	-14222.340	-13980.392	-14229.953	128.340

MD83 (Count = 6,135)

Parameter	Percentile (%), β_j				Std.
	2.5	50	97.5	Mean	Dev.
Alt	6.24E-02	8.11E-02	9.84E-02	8.06E-02	9.19E-03
V_{LO}	116.387	118.038	119.531	117.991	0.803
RwLen	1.06E-01	1.13E-01	1.20E-01	1.13E-01	3.61E-03
Wind	38.555	42.029	45.325	41.926	1.727
Constant	-14277.000	-14001.632	-13742.124	-14010.337	136.629

MD88 (Count = 10,992)

Parameter	Percentile(%), β_j				Std.
	2.5	50	97.5	Mean	Dev.
Alt	9.14E-02	1.18E-01	1.42E-01	1.17E-01	1.30E-02
V_{LO}	109.693	110.704	111.676	110.671	0.506
RwLen	1.09E-01	1.15E-01	1.20E-01	1.14E-01	2.85E-03
Wind	36.216	38.673	41.002	38.596	1.220
Constant	-12950.730	-12778.404	-12614.474	-12784.363	85.904

MD90 (Count = 5,358)

Parameter	Percentile (%), β_j				Std.
	2.5	50	97.5	Mean	Dev.
Alt	-3.28E-02	-1.67E-02	-1.53E-03	-1.72E-02	7.96E-03
V_{LO}	90.260	91.923	93.497	91.865	0.826
RwLen	1.34E-01	1.43E-01	1.52E-01	1.43E-01	4.51E-03
Wind	21.175	24.695	27.983	24.586	1.736
Constant	-10222.619	-9946.429	-9678.094	-9955.560	138.812

PA31 (Count = 485)

Parameter	Percentile(%), β_j				Std.
	2.5	50	97.5	Mean	Dev.
Alt	7.88E-03	3.85E-02	6.65E-02	3.76E-02	1.50E-02
V_{LO}	57.356	64.414	71.029	64.218	3.484
RwLen	-3.73E-02	5.82E-03	4.50E-02	4.69E-03	2.10E-02
Wind	7.923	21.541	34.092	21.129	6.697
Constant	-4029.801	-3164.498	-2337.443	-3194.376	430.812

Table 4.34: Highest Posterior Density Intervals for Departure Take-Off Distance Model 5b Parameters, β_j for PC12 - SW4

PC12 (Count = 493)

Parameter	Percentile (%), β_j				Std.
	2.5	50	97.5	Mean	Dev.
Alt	1.72E-02	6.79E-02	1.16E-01	6.63E-02	2.53E-02
V_{LO}	72.314	78.546	84.316	78.365	3.064
RwLen	-2.04E-02	3.95E-03	2.66E-02	3.20E-03	1.20E-02
Wind	8.963	21.113	32.526	20.747	6.003
Constant	-5322.753	-4675.293	-4065.733	-4694.246	320.809

SF34 (Count = 1,400)

Parameter	Percentile(%), β_j				Std.
	2.5	50	97.5	Mean	Dev.
Alt	-1.27E-01	-4.53E-02	3.12E-02	-4.79E-02	4.03E-02
V_{LO}	89.787	94.196	98.306	94.053	2.176
RwLen	-6.56E-03	1.09E-02	2.75E-02	1.04E-02	8.68E-03
Wind	26.967	34.344	41.241	34.125	3.639
Constant	-8492.273	-7872.221	-7278.444	-7891.145	309.464

SH36 (Count = 224)

Parameter	Percentile (%), β_j				Std.
	2.5	50	97.5	Mean	Dev.
Alt	-2.03E-01	-1.31E-01	-6.61E-02	-1.33E-01	3.49E-02
V_{LO}	85.948	97.345	107.920	96.998	5.591
RwLen	-8.74E-02	-4.23E-02	8.77E-04	-4.39E-02	2.25E-02
Wind	8.895	28.239	46.953	27.574	9.686
Constant	-7465.230	-6104.143	-4830.465	-6144.513	671.794

SR22 (Count = 208)

Parameter	Percentile(%), β_j				Std.
	2.5	50	97.5	Mean	Dev.
Alt	-9.13E-02	-2.71E-05	8.38E-02	-2.84E-03	4.46E-02
V_{LO}	65.539	72.101	78.361	71.868	3.270
RwLen	-1.06E-02	1.56E-02	4.10E-02	1.47E-02	1.31E-02
Wind	12.969	28.625	43.627	28.125	7.827
Constant	-4646.752	-3994.332	-3377.054	-4013.324	324.033

SW4 (Count = 734)

Parameter	Percentile (%), β_j				Std.
	2.5	50	97.5	Mean	Dev.
Alt	-1.48E-01	-1.09E-01	-7.12E-02	-1.10E-01	1.97E-02
V_{LO}	75.284	81.518	87.512	81.312	3.125
RwLen	-1.16E-01	-7.76E-02	-4.12E-02	-7.88E-02	1.91E-02
Wind	15.765	28.871	41.518	28.444	6.579
Constant	-6173.212	-5264.079	-4422.286	-5291.756	447.402

4.8.3 Arrival Runway Occupancy Time Model

Table 4.35: Highest Posterior Density Intervals for Arrival Runway Occupancy Time Model 5c Parameters, β_j for A306 - A346

A306 (Count = 1,157)

Parameter	Percentile (%), β_j				Std.
	2.5	50	97.5	Mean	Dev.
Alt	-5.59E-04	-5.59E-04	-5.59E-04	-5.59E-04	-5.59E-04
DTTE	8.57E-03	8.88E-03	9.17E-03	8.87E-03	1.53E-04
ExitAng	1.98E-03	1.96E-02	3.61E-02	1.91E-02	8.69E-03
EffRwLen	1.41E-04	4.12E-04	6.68E-04	4.03E-04	1.34E-04
ThrVel	-3.61E-01	-3.05E-01	-2.54E-01	-3.07E-01	2.74E-02
TurnDist	-7.79E-03	-6.04E-03	-4.38E-03	-6.10E-03	8.69E-04
Constant	28.240	35.734	42.837	35.483	3.722

A319 (Count = 26,169)

Parameter	Percentile(%), β_j				Std.
	2.5	50	97.5	Mean	Dev.
Alt	-2.46E-04	-2.02E-04	-1.61E-04	-2.03E-04	2.17E-05
DTTE	7.64E-03	7.70E-03	7.76E-03	7.70E-03	3.03E-05
ExitAng	1.69E-02	1.92E-02	2.13E-02	1.91E-02	1.13E-03
EffRwLen	-2.71E-05	9.90E-06	4.43E-05	8.76E-06	1.82E-05
ThrVel	-3.40E-01	-3.33E-01	-3.26E-01	-3.33E-01	3.62E-03
TurnDist	-5.27E-03	-5.02E-03	-4.79E-03	-5.03E-03	1.21E-04
Constant	44.104	45.004	45.882	44.973	0.454

A320 (Count = 34,729)

Parameter	Percentile (%), β_j				Std.
	2.5	50	97.5	Mean	Dev.
Alt	-2.49E-04	-2.07E-04	-1.68E-04	-2.09E-04	2.09E-05
DTTE	7.37E-03	7.42E-03	7.47E-03	7.42E-03	2.57E-05
ExitAng	1.50E-02	1.69E-02	1.87E-02	1.69E-02	9.49E-04
EffRwLen	-7.35E-05	-3.91E-05	-6.02E-06	-4.03E-05	1.72E-05
ThrVel	-3.07E-01	-3.00E-01	-2.93E-01	-3.00E-01	3.44E-03
TurnDist	-3.84E-03	-3.67E-03	-3.50E-03	-3.67E-03	8.71E-05
Constant	41.200	42.147	43.019	42.119	0.464

A321 (Count = 8,453)

Parameter	Percentile(%), β_j				Std.
	2.5	50	97.5	Mean	Dev.
Alt	-1.17E-04	3.68E-06	1.18E-04	-2.08E-08	6.00E-05
DTTE	7.18E-03	7.31E-03	7.42E-03	7.30E-03	6.02E-05
ExitAng	1.33E-02	1.73E-02	2.10E-02	1.72E-02	1.96E-03
EffRwLen	-1.75E-04	-9.78E-05	-2.47E-05	-1.00E-04	3.84E-05
ThrVel	-3.02E-01	-2.88E-01	-2.75E-01	-2.88E-01	6.84E-03
TurnDist	-5.81E-03	-5.35E-03	-4.92E-03	-5.37E-03	2.26E-04
Constant	41.797	43.803	45.744	43.736	1.009

A332 (Count = 2,070)

Parameter	Percentile (%), β_j				Std.
	2.5	50	97.5	Mean	Dev.
Alt	-8.69E-04	-3.84E-04	8.60E-05	-4.00E-04	2.43E-04
DTTE	7.79E-03	8.08E-03	8.36E-03	8.07E-03	1.43E-04
ExitAng	8.90E-03	1.96E-02	2.99E-02	1.92E-02	5.36E-03
EffRwLen	-1.12E-03	-9.26E-04	-7.43E-04	-9.32E-04	9.63E-05
ThrVel	-3.62E-01	-3.19E-01	-2.76E-01	-3.20E-01	2.20E-02
TurnDist	-7.75E-03	-6.73E-03	-5.78E-03	-6.76E-03	5.02E-04
Constant	48.415	54.600	60.290	54.419	3.037

A333 (Count = 1,679)

Parameter	Percentile(%), β_j				Std.
	2.5	50	97.5	Mean	Dev.
Alt	3.66E-04	1.34E-03	2.25E-03	1.31E-03	4.80E-04
DTTE	7.73E-03	8.09E-03	8.43E-03	8.07E-03	1.79E-04
ExitAng	9.27E-03	2.09E-02	3.17E-02	2.05E-02	5.72E-03
EffRwLen	-5.15E-04	-2.96E-04	-8.43E-05	-3.03E-04	1.10E-04
ThrVel	-4.33E-01	-3.85E-01	-3.39E-01	-3.86E-01	2.41E-02
TurnDist	-5.42E-03	-4.36E-03	-3.38E-03	-4.39E-03	5.20E-04
Constant	48.364	55.300	61.841	55.071	3.438

A343 (Count = 491)

Parameter	Percentile (%), β_j				Std.
	2.5	50	97.5	Mean	Dev.
Alt	2.46E-03	4.90E-03	7.16E-03	4.83E-03	1.20E-03
DTTE	7.83E-03	8.48E-03	9.09E-03	8.46E-03	3.22E-04
ExitAng	1.27E-02	3.84E-02	6.24E-02	3.76E-02	1.27E-02
EffRwLen	-1.47E-03	-1.05E-03	-6.51E-04	-1.06E-03	2.08E-04
ThrVel	-6.23E-01	-5.18E-01	-4.18E-01	-5.21E-01	5.24E-02
TurnDist	-8.84E-03	-6.05E-03	-3.44E-03	-6.14E-03	1.38E-03
Constant	64.536	80.018	94.322	79.565	7.606

A346 (Count = 387)

Parameter	Percentile(%), β_j				Std.
	2.5	50	97.5	Mean	Dev.
Alt	-1.87E-03	-4.04E-04	9.80E-04	-4.48E-04	7.28E-04
DTTE	8.09E-03	8.96E-03	9.77E-03	8.93E-03	4.30E-04
ExitAng	-1.75E-02	6.60E-03	3.00E-02	5.78E-03	1.21E-02
EffRwLen	-1.11E-03	-5.75E-04	-6.86E-05	-5.93E-04	2.67E-04
ThrVel	-4.67E-01	-3.74E-01	-2.87E-01	-3.77E-01	4.61E-02
TurnDist	-6.30E-03	-4.03E-03	-1.96E-03	-4.09E-03	1.11E-03
Constant	38.018	53.614	68.548	53.112	7.778

Table 4.36: Highest Posterior Density Intervals for Arrival Runway Occupancy Time Model 5c Parameters, β_j for A388 - B734

A388 (Count = 414)

Parameter	Percentile (%), β_j				Std.
	2.5	50	97.5	Mean	Dev.
Alt	-1.31E-03	-1.31E-03	-1.31E-03	-1.31E-03	-1.31E-03
DTTE	6.68E-03	7.74E-03	8.74E-03	7.71E-03	5.25E-04
ExitAng	5.21E-02	9.30E-02	1.32E-01	9.16E-02	2.03E-02
EffRwLen	-5.57E-03	-4.56E-03	-3.59E-03	-4.60E-03	5.06E-04
ThrVel	-2.78E-01	-1.33E-01	6.86E-04	-1.38E-01	7.10E-02
TurnDist	-1.83E-02	-1.42E-02	-1.04E-02	-1.44E-02	2.03E-03
Constant	49.344	74.537	98.219	73.743	12.432

AT72 (Count = 371)

Parameter	Percentile(%), β_j				Std.
	2.5	50	97.5	Mean	Dev.
Alt	-1.76E+00	-1.26E+00	-7.86E-01	-1.27E+00	2.48E-01
DTTE	9.75E-03	1.10E-02	1.21E-02	1.09E-02	6.10E-04
ExitAng	-1.03E-01	-5.65E-02	-1.22E-02	-5.80E-02	2.32E-02
EffRwLen	-2.14E-03	-1.74E-03	-1.34E-03	-1.75E-03	2.04E-04
ThrVel	-4.21E-01	-3.59E-01	-3.00E-01	-3.61E-01	3.08E-02
TurnDist	-1.96E-02	-1.21E-02	-4.84E-03	-1.23E-02	3.78E-03
Constant	58.567	68.245	77.228	67.949	4.770

B190 (Count = 3,106)

Parameter	Percentile (%), β_j				Std.
	2.5	50	97.5	Mean	Dev.
Alt	2.47E-04	4.00E-04	5.43E-04	3.95E-04	7.58E-05
DTTE	7.08E-03	7.29E-03	7.49E-03	7.28E-03	1.05E-04
ExitAng	-2.90E-02	-1.80E-02	-8.02E-03	-1.83E-02	5.33E-03
EffRwLen	8.83E-05	2.67E-04	4.35E-04	2.61E-04	8.85E-05
ThrVel	-3.02E-01	-2.83E-01	-2.65E-01	-2.84E-01	9.42E-03
TurnDist	-1.27E-02	-1.14E-02	-1.02E-02	-1.15E-02	6.43E-04
Constant	45.706	48.259	50.690	48.177	1.273

B350 (Count = 291)

Parameter	Percentile(%), β_j				Std.
	2.5	50	97.5	Mean	Dev.
Alt	-1.34E-03	-2.78E-04	7.20E-04	-3.11E-04	5.25E-04
DTTE	8.56E-03	9.41E-03	1.02E-02	9.38E-03	4.14E-04
ExitAng	-1.67E-02	1.46E-02	4.38E-02	1.37E-02	1.55E-02
EffRwLen	-5.89E-04	-2.24E-04	1.19E-04	-2.36E-04	1.81E-04
ThrVel	-3.00E-01	-2.26E-01	-1.54E-01	-2.29E-01	3.70E-02
TurnDist	-8.09E-03	-4.06E-03	-2.80E-04	-4.18E-03	1.99E-03
Constant	25.559	35.084	43.815	34.793	4.659

B712 (Count = 9,272)

Parameter	Percentile (%), β_j				Std.
	2.5	50	97.5	Mean	Dev.
Alt	-8.30E-04	-6.75E-04	-5.29E-04	-6.79E-04	7.70E-05
DTTE	7.92E-03	8.02E-03	8.11E-03	8.02E-03	4.78E-05
ExitAng	4.11E-03	7.35E-03	1.03E-02	7.26E-03	1.59E-03
EffRwLen	1.30E-04	1.77E-04	2.22E-04	1.75E-04	2.35E-05
ThrVel	-3.39E-01	-3.28E-01	-3.18E-01	-3.29E-01	5.21E-03
TurnDist	-7.13E-03	-6.74E-03	-6.37E-03	-6.75E-03	1.94E-04
Constant	40.698	42.092	43.409	42.048	0.692

B732 (Count = 390)

Parameter	Percentile(%), β_j				Std.
	2.5	50	97.5	Mean	Dev.
Alt	1.02E-02	2.49E-02	3.91E-02	2.44E-02	7.36E-03
DTTE	7.89E-03	8.59E-03	9.25E-03	8.57E-03	3.46E-04
ExitAng	-2.82E-02	-6.22E-03	1.46E-02	-6.92E-03	1.09E-02
EffRwLen	-1.05E-03	-7.47E-04	-4.52E-04	-7.57E-04	1.54E-04
ThrVel	-2.46E-01	-2.06E-01	-1.68E-01	-2.08E-01	2.00E-02
TurnDist	-1.46E-02	-1.12E-02	-7.96E-03	-1.13E-02	1.71E-03
Constant	31.279	36.619	41.633	36.458	2.634

B733 (Count = 7,910)

Parameter	Percentile (%), β_j				Std.
	2.5	50	97.5	Mean	Dev.
Alt	-1.97E-04	-1.18E-04	-4.43E-05	-1.21E-04	3.90E-05
DTTE	6.99E-03	7.08E-03	7.17E-03	7.08E-03	4.59E-05
ExitAng	8.83E-03	1.25E-02	1.60E-02	1.24E-02	1.85E-03
EffRwLen	7.49E-05	1.36E-04	1.94E-04	1.34E-04	3.05E-05
ThrVel	-2.92E-01	-2.80E-01	-2.70E-01	-2.81E-01	5.60E-03
TurnDist	-4.73E-03	-4.29E-03	-3.89E-03	-4.31E-03	2.15E-04
Constant	39.802	41.373	42.859	41.323	0.781

B734 (Count = 2,327)

Parameter	Percentile(%), β_j				Std.
	2.5	50	97.5	Mean	Dev.
Alt	-5.83E-04	7.02E-05	6.86E-04	4.99E-05	3.24E-04
DTTE	6.68E-03	6.92E-03	7.16E-03	6.92E-03	1.21E-04
ExitAng	2.51E-02	3.50E-02	4.42E-02	3.46E-02	4.86E-03
EffRwLen	-1.51E-04	3.86E-05	2.09E-04	3.34E-05	9.21E-05
ThrVel	-2.85E-01	-2.59E-01	-2.35E-01	-2.60E-01	1.29E-02
TurnDist	-5.72E-03	-4.72E-03	-3.78E-03	-4.75E-03	4.97E-04
Constant	35.873	40.092	43.941	39.972	2.056

Table 4.37: Highest Posterior Density Intervals for Arrival Runway Occupancy Time Model 5c Parameters, β_j for B735 - B752

B735 (Count = 482)

Parameter	Percentile (%), β_j				Std.
	2.5	50	97.5	Mean	Dev.
Alt	1.79E-04	1.79E-04	1.79E-04	1.79E-04	1.79E-04
DTTE	7.00E-03	7.37E-03	7.72E-03	7.36E-03	1.85E-04
ExitAng	-4.07E-03	1.21E-02	2.70E-02	1.17E-02	7.94E-03
EffRwLen	-5.23E-04	-2.74E-04	-3.44E-05	-2.82E-04	1.24E-04
ThrVel	-2.57E-01	-2.14E-01	-1.75E-01	-2.15E-01	2.11E-02
TurnDist	-7.60E-03	-5.89E-03	-4.23E-03	-5.95E-03	8.59E-04
Constant	28.947	35.303	41.430	35.100	3.187

B736 (Count = 377)

Parameter	Percentile(%), β_j				Std.
	2.5	50	97.5	Mean	Dev.
Alt	1.44E-03	2.66E-03	3.82E-03	2.63E-03	6.07E-04
DTTE	6.71E-03	7.42E-03	8.09E-03	7.39E-03	3.52E-04
ExitAng	-2.68E-02	3.42E-03	3.23E-02	2.43E-03	1.51E-02
EffRwLen	-2.02E-03	-7.09E-04	5.11E-04	-7.48E-04	6.45E-04
ThrVel	-4.41E-01	-3.84E-01	-3.29E-01	-3.86E-01	2.85E-02
TurnDist	-1.52E-02	-1.18E-02	-8.60E-03	-1.19E-02	1.69E-03
Constant	55.251	65.540	75.207	65.240	5.104

B737 (Count = 37,071)

Parameter	Percentile (%), β_j				Std.
	2.5	50	97.5	Mean	Dev.
Alt	-2.26E-04	-1.87E-04	-1.51E-04	-1.89E-04	1.89E-05
DTTE	7.22E-03	7.27E-03	7.31E-03	7.27E-03	2.33E-05
ExitAng	1.94E-02	2.12E-02	2.29E-02	2.11E-02	8.97E-04
EffRwLen	1.37E-04	1.65E-04	1.93E-04	1.64E-04	1.43E-05
ThrVel	-2.94E-01	-2.88E-01	-2.82E-01	-2.88E-01	2.90E-03
TurnDist	-4.98E-03	-4.76E-03	-4.55E-03	-4.77E-03	1.09E-04
Constant	40.153	40.915	41.646	40.890	0.381

B738 (Count = 37,383)

Parameter	Percentile(%), β_j				Std.
	2.5	50	97.5	Mean	Dev.
Alt	1.28E-04	1.74E-04	2.16E-04	1.73E-04	2.25E-05
DTTE	7.16E-03	7.21E-03	7.26E-03	7.21E-03	2.44E-05
ExitAng	1.60E-02	1.82E-02	2.03E-02	1.82E-02	1.09E-03
EffRwLen	-2.18E-04	-1.90E-04	-1.63E-04	-1.91E-04	1.42E-05
ThrVel	-2.92E-01	-2.85E-01	-2.80E-01	-2.86E-01	2.96E-03
TurnDist	-5.11E-03	-4.89E-03	-4.69E-03	-4.90E-03	1.05E-04
Constant	44.213	45.086	45.884	45.061	0.427

B739 (Count = 6,543)

Parameter	Percentile (%), β_j				Std.
	2.5	50	97.5	Mean	Dev.
Alt	7.26E-05	1.72E-04	2.64E-04	1.69E-04	4.89E-05
DTTE	7.31E-03	7.44E-03	7.56E-03	7.44E-03	6.50E-05
ExitAng	1.93E-02	2.56E-02	3.17E-02	2.54E-02	3.17E-03
EffRwLen	1.59E-04	2.40E-04	3.17E-04	2.37E-04	4.04E-05
ThrVel	-3.20E-01	-3.05E-01	-2.91E-01	-3.05E-01	7.32E-03
TurnDist	-7.31E-03	-6.72E-03	-6.13E-03	-6.74E-03	3.00E-04
Constant	42.154	44.436	46.593	44.365	1.137

B744 (Count = 2,831)

Parameter	Percentile(%), β_j				Std.
	2.5	50	97.5	Mean	Dev.
Alt	7.88E-04	1.26E-03	1.71E-03	1.24E-03	2.35E-04
DTTE	8.00E-03	8.30E-03	8.59E-03	8.29E-03	1.50E-04
ExitAng	5.23E-02	6.60E-02	7.87E-02	6.55E-02	6.73E-03
EffRwLen	-1.01E-03	-8.11E-04	-6.33E-04	-8.17E-04	9.60E-05
ThrVel	-3.92E-01	-3.56E-01	-3.23E-01	-3.58E-01	1.75E-02
TurnDist	-8.32E-03	-7.22E-03	-6.17E-03	-7.25E-03	5.52E-04
Constant	54.390	59.939	65.091	59.780	2.732

B748 (Count = 453)

Parameter	Percentile (%), β_j				Std.
	2.5	50	97.5	Mean	Dev.
Alt	7.14E-03	1.00E-02	1.28E-02	9.95E-03	1.45E-03
DTTE	8.80E-03	9.47E-03	1.01E-02	9.45E-03	3.31E-04
ExitAng	-5.64E-02	-1.56E-02	2.19E-02	-1.67E-02	2.00E-02
EffRwLen	-2.69E-03	-2.08E-03	-1.52E-03	-2.10E-03	3.00E-04
ThrVel	-3.10E-01	-1.95E-01	-8.62E-02	-1.99E-01	5.70E-02
TurnDist	-1.70E-02	-1.30E-02	-9.17E-03	-1.31E-02	1.99E-03
Constant	33.236	51.283	68.626	50.670	9.019

B752 (Count = 23,687)

Parameter	Percentile(%), β_j				Std.
	2.5	50	97.5	Mean	Dev.
Alt	3.51E-05	9.51E-05	1.50E-04	9.33E-05	2.93E-05
DTTE	7.50E-03	7.57E-03	7.64E-03	7.57E-03	3.46E-05
ExitAng	3.30E-02	3.60E-02	3.89E-02	3.59E-02	1.52E-03
EffRwLen	-1.98E-04	-1.51E-04	-1.07E-04	-1.52E-04	2.33E-05
ThrVel	-3.42E-01	-3.33E-01	-3.24E-01	-3.33E-01	4.44E-03
TurnDist	-4.59E-03	-4.30E-03	-4.03E-03	-4.31E-03	1.41E-04
Constant	45.451	46.704	47.895	46.664	0.623

Table 4.38: Highest Posterior Density Intervals for Arrival Runway Occupancy Time Model 5c Parameters, β_j for B753 - B788

B753 (Count = 2,816)

Parameter	Percentile (%), β_j				Std.
	2.5	50	97.5	Mean	Dev.
Alt	1.28E-05	1.28E-05	1.28E-05	1.28E-05	1.28E-05
DTTE	8.69E-03	8.91E-03	9.12E-03	8.90E-03	1.12E-04
ExitAng	-7.98E-03	9.96E-04	9.57E-03	7.09E-04	4.47E-03
EffRwLen	-3.50E-04	-2.06E-04	-7.01E-05	-2.10E-04	7.14E-05
ThrVel	-3.99E-01	-3.74E-01	-3.50E-01	-3.75E-01	1.25E-02
TurnDist	-9.11E-03	-8.24E-03	-7.42E-03	-8.26E-03	4.30E-04
Constant	46.845	50.393	53.694	50.279	1.746

B762 (Count = 1,661)

Parameter	Percentile(%), β_j				Std.
	2.5	50	97.5	Mean	Dev.
Alt	1.32E-03	1.98E-03	2.60E-03	1.96E-03	3.24E-04
DTTE	7.38E-03	7.68E-03	7.96E-03	7.67E-03	1.49E-04
ExitAng	-3.16E-04	1.22E-02	2.39E-02	1.18E-02	6.19E-03
EffRwLen	-1.10E-03	-8.79E-04	-6.82E-04	-8.85E-04	1.06E-04
ThrVel	-3.52E-01	-3.16E-01	-2.83E-01	-3.17E-01	1.77E-02
TurnDist	-7.25E-03	-6.18E-03	-5.17E-03	-6.21E-03	5.31E-04
Constant	49.388	55.239	60.572	55.065	2.840

B763 (Count = 6,817)

Parameter	Percentile (%), β_j				Std.
	2.5	50	97.5	Mean	Dev.
Alt	2.17E-06	1.93E-04	3.67E-04	1.88E-04	9.32E-05
DTTE	7.46E-03	7.60E-03	7.74E-03	7.60E-03	7.01E-05
ExitAng	3.12E-02	3.76E-02	4.36E-02	3.74E-02	3.16E-03
EffRwLen	-3.81E-04	-2.84E-04	-1.95E-04	-2.87E-04	4.74E-05
ThrVel	-3.28E-01	-3.09E-01	-2.92E-01	-3.10E-01	9.24E-03
TurnDist	-7.67E-03	-7.08E-03	-6.54E-03	-7.10E-03	2.89E-04
Constant	45.125	47.966	50.603	47.877	1.397

B764 (Count = 980)

Parameter	Percentile(%), β_j				Std.
	2.5	50	97.5	Mean	Dev.
Alt	4.58E-04	1.04E-03	1.60E-03	1.03E-03	2.91E-04
DTTE	5.83E-03	6.18E-03	6.52E-03	6.17E-03	1.76E-04
ExitAng	9.90E-03	2.29E-02	3.46E-02	2.25E-02	6.31E-03
EffRwLen	-6.39E-04	-3.51E-04	-7.38E-05	-3.61E-04	1.44E-04
ThrVel	-3.37E-01	-2.89E-01	-2.46E-01	-2.91E-01	2.32E-02
TurnDist	-7.05E-03	-5.76E-03	-4.54E-03	-5.81E-03	6.39E-04
Constant	45.507	53.616	61.286	53.351	4.018

B772 (Count = 3,461)

Parameter	Percentile (%), β_j				Std.
	2.5	50	97.5	Mean	Dev.
Alt	8.70E-05	3.61E-04	6.17E-04	3.53E-04	1.35E-04
DTTE	8.27E-03	8.50E-03	8.71E-03	8.49E-03	1.13E-04
ExitAng	2.58E-03	1.04E-02	1.77E-02	1.02E-02	3.85E-03
EffRwLen	-5.49E-04	-4.21E-04	-2.99E-04	-4.25E-04	6.39E-05
ThrVel	-4.24E-01	-3.95E-01	-3.67E-01	-3.96E-01	1.44E-02
TurnDist	-7.48E-03	-6.66E-03	-5.89E-03	-6.68E-03	4.06E-04
Constant	54.463	58.527	62.381	58.393	2.023

B77L (Count = 534)

Parameter	Percentile(%), β_j				Std.
	2.5	50	97.5	Mean	Dev.
Alt	-1.27E-03	2.28E-04	1.64E-03	1.82E-04	7.40E-04
DTTE	8.34E-03	8.96E-03	9.55E-03	8.94E-03	3.07E-04
ExitAng	3.47E-02	6.24E-02	8.75E-02	6.16E-02	1.35E-02
EffRwLen	-5.37E-04	-1.55E-04	2.09E-04	-1.68E-04	1.90E-04
ThrVel	-2.83E-01	-2.01E-01	-1.25E-01	-2.04E-01	4.02E-02
TurnDist	-1.60E-02	-1.30E-02	-1.03E-02	-1.31E-02	1.45E-03
Constant	16.969	29.715	41.765	29.300	6.324

B77W (Count = 1,843)

Parameter	Percentile (%), β_j				Std.
	2.5	50	97.5	Mean	Dev.
Alt	1.42E-03	2.87E-03	4.26E-03	2.82E-03	7.23E-04
DTTE	8.31E-03	8.70E-03	9.07E-03	8.69E-03	1.95E-04
ExitAng	-3.49E-03	6.98E-03	1.67E-02	6.66E-03	5.17E-03
EffRwLen	-1.53E-03	-1.30E-03	-1.08E-03	-1.30E-03	1.13E-04
ThrVel	-4.76E-01	-4.37E-01	-4.00E-01	-4.38E-01	1.94E-02
TurnDist	-6.04E-03	-5.04E-03	-4.12E-03	-5.07E-03	4.90E-04
Constant	66.593	72.686	78.477	72.498	3.032

B788 (Count = 388)

Parameter	Percentile(%), β_j				Std.
	2.5	50	97.5	Mean	Dev.
Alt	-1.67E-03	-1.03E-03	-4.38E-04	-1.05E-03	3.15E-04
DTTE	8.90E-03	9.80E-03	1.06E-02	9.77E-03	4.46E-04
ExitAng	6.45E-02	1.01E-01	1.35E-01	9.98E-02	1.79E-02
EffRwLen	4.84E-05	6.24E-04	1.17E-03	6.05E-04	2.85E-04
ThrVel	-4.81E-01	-3.64E-01	-2.54E-01	-3.67E-01	5.76E-02
TurnDist	-4.57E-03	-1.83E-03	6.96E-04	-1.91E-03	1.34E-03
Constant	15.170	31.513	47.426	30.950	8.214

Table 4.39: Highest Posterior Density Intervals for Arrival Runway Occupancy Time Model 5c Parameters, β_j for BE20 - C525

BE20 (Count = 615)

Parameter	Percentile (%), β_j				Std.
	2.5	50	97.5	Mean	Dev.
Alt	-3.31E-04	-3.31E-04	-3.31E-04	-3.31E-04	-3.31E-04
DTTE	9.24E-03	9.78E-03	1.03E-02	9.77E-03	2.67E-04
ExitAng	-9.81E-03	1.42E-02	3.71E-02	1.34E-02	1.20E-02
EffRwLen	-6.27E-04	-2.54E-04	9.49E-05	-2.66E-04	1.84E-04
ThrVel	-2.99E-01	-2.47E-01	-2.00E-01	-2.49E-01	2.53E-02
TurnDist	-7.42E-03	-4.61E-03	-1.94E-03	-4.69E-03	1.40E-03
Constant	29.171	36.104	42.621	35.892	3.434

BE40 (Count = 749)

Parameter	Percentile(%), β_j				Std.
	2.5	50	97.5	Mean	Dev.
Alt	-2.25E-04	2.29E-04	6.50E-04	2.16E-04	2.23E-04
DTTE	8.21E-03	8.66E-03	9.08E-03	8.65E-03	2.24E-04
ExitAng	3.34E-03	2.11E-02	3.83E-02	2.05E-02	8.91E-03
EffRwLen	-6.78E-04	-4.29E-04	-1.92E-04	-4.38E-04	1.24E-04
ThrVel	-3.21E-01	-2.68E-01	-2.17E-01	-2.70E-01	2.65E-02
TurnDist	-7.28E-03	-5.28E-03	-3.43E-03	-5.35E-03	9.80E-04
Constant	34.263	40.738	46.940	40.530	3.242

BE99 (Count = 421)

Parameter	Percentile (%), β_j				Std.
	2.5	50	97.5	Mean	Dev.
Alt	-4.94E-04	-1.32E-04	2.06E-04	-1.43E-04	1.79E-04
DTTE	8.70E-03	9.35E-03	9.96E-03	9.33E-03	3.20E-04
ExitAng	-1.84E-02	1.11E-02	3.87E-02	1.03E-02	1.46E-02
EffRwLen	-4.22E-04	-1.03E-04	1.99E-04	-1.14E-04	1.58E-04
ThrVel	-2.45E-01	-1.89E-01	-1.37E-01	-1.90E-01	2.74E-02
TurnDist	-6.27E-03	-3.40E-03	-7.21E-04	-3.49E-03	1.42E-03
Constant	21.961	29.300	36.291	29.063	3.658

BE9L (Count = 450)

Parameter	Percentile(%), β_j				Std.
	2.5	50	97.5	Mean	Dev.
Alt	-5.15E-04	1.07E-04	6.98E-04	8.87E-05	3.09E-04
DTTE	8.16E-03	8.73E-03	9.27E-03	8.72E-03	2.85E-04
ExitAng	-2.67E-02	4.11E-03	3.31E-02	3.14E-03	1.53E-02
EffRwLen	-9.13E-04	-4.11E-04	6.29E-05	-4.27E-04	2.49E-04
ThrVel	-3.21E-01	-2.61E-01	-2.05E-01	-2.63E-01	2.97E-02
TurnDist	-1.00E-02	-6.64E-03	-3.43E-03	-6.75E-03	1.70E-03
Constant	38.518	46.189	53.445	45.954	3.819

C172 (Count = 368)

Parameter	Percentile (%), β_j				Std.
	2.5	50	97.5	Mean	Dev.
Alt	-9.10E-04	-4.07E-04	7.18E-05	-4.24E-04	2.50E-04
DTTE	1.18E-02	1.27E-02	1.35E-02	1.27E-02	4.28E-04
ExitAng	-3.51E-02	-5.76E-03	2.14E-02	-6.66E-03	1.44E-02
EffRwLen	-1.31E-03	-8.37E-04	-3.91E-04	-8.53E-04	2.35E-04
ThrVel	-5.07E-01	-4.29E-01	-3.57E-01	-4.32E-01	3.81E-02
TurnDist	-8.16E-03	-8.45E-04	6.06E-03	-1.08E-03	3.63E-03
Constant	42.536	50.188	57.349	49.963	3.779

C208 (Count = 1,888)

Parameter	Percentile(%), β_j				Std.
	2.5	50	97.5	Mean	Dev.
Alt	-4.45E-04	-1.52E-04	1.28E-04	-1.62E-04	1.46E-04
DTTE	7.34E-03	7.56E-03	7.76E-03	7.55E-03	1.07E-04
ExitAng	1.12E-03	1.30E-02	2.43E-02	1.27E-02	5.90E-03
EffRwLen	-4.28E-04	-2.58E-04	-9.98E-05	-2.63E-04	8.38E-05
ThrVel	-2.17E-01	-2.00E-01	-1.83E-01	-2.00E-01	8.68E-03
TurnDist	-6.56E-03	-5.21E-03	-3.92E-03	-5.25E-03	6.73E-04
Constant	37.003	39.559	42.020	39.475	1.281

C402 (Count = 2,413)

Parameter	Percentile (%), β_j				Std.
	2.5	50	97.5	Mean	Dev.
Alt	5.11E-04	8.28E-04	1.12E-03	8.18E-04	1.56E-04
DTTE	9.34E-03	9.51E-03	9.66E-03	9.50E-03	8.04E-05
ExitAng	-5.84E-03	5.50E-03	1.61E-02	5.15E-03	5.62E-03
EffRwLen	-6.41E-04	-5.03E-04	-3.75E-04	-5.08E-04	6.80E-05
ThrVel	-2.40E-01	-2.20E-01	-2.00E-01	-2.20E-01	1.02E-02
TurnDist	-8.20E-03	-6.67E-03	-5.24E-03	-6.71E-03	7.53E-04
Constant	33.288	35.788	38.098	35.713	1.228

C525 (Count = 295)

Parameter	Percentile(%), β_j				Std.
	2.5	50	97.5	Mean	Dev.
Alt	-3.65E-04	1.78E-04	6.82E-04	1.60E-04	2.68E-04
DTTE	8.30E-03	9.00E-03	9.65E-03	8.98E-03	3.44E-04
ExitAng	-1.87E-02	1.00E-02	3.69E-02	9.11E-03	1.42E-02
EffRwLen	-6.34E-04	-2.56E-04	1.01E-04	-2.68E-04	1.88E-04
ThrVel	-3.23E-01	-2.52E-01	-1.82E-01	-2.54E-01	3.59E-02
TurnDist	-6.54E-03	-3.40E-03	-3.53E-04	-3.51E-03	1.58E-03
Constant	26.523	35.431	43.931	35.149	4.445

Table 4.40: Highest Posterior Density Intervals for Arrival Runway Occupancy Time Model 5c Parameters, β_j for C550 - CRJ2

C550 (Count = 343)

Parameter	Percentile (%), β_j				Std.
	2.5	50	97.5	Mean	Dev.
Alt	-1.93E-04	-1.93E-04	-1.93E-04	-1.93E-04	-1.93E-04
DTTE	8.27E-03	9.01E-03	9.69E-03	8.99E-03	3.62E-04
ExitAng	-3.63E-02	-7.13E-03	1.99E-02	-7.95E-03	1.43E-02
EffRwLen	-3.28E-04	8.69E-05	4.75E-04	7.40E-05	2.05E-04
ThrVel	-3.40E-01	-2.56E-01	-1.78E-01	-2.59E-01	4.13E-02
TurnDist	-1.05E-02	-7.31E-03	-4.33E-03	-7.41E-03	1.57E-03
Constant	27.601	37.732	47.398	37.392	5.050

C560 (Count = 689)

Parameter	Percentile(%), β_j				Std.
	2.5	50	97.5	Mean	Dev.
Alt	-2.40E-04	2.08E-04	6.34E-04	1.93E-04	2.23E-04
DTTE	8.35E-03	8.79E-03	9.20E-03	8.77E-03	2.17E-04
ExitAng	-6.23E-03	1.31E-02	3.14E-02	1.25E-02	9.62E-03
EffRwLen	-8.10E-04	-5.45E-04	-2.98E-04	-5.53E-04	1.30E-04
ThrVel	-3.78E-01	-3.22E-01	-2.70E-01	-3.24E-01	2.75E-02
TurnDist	-5.24E-03	-3.13E-03	-1.16E-03	-3.20E-03	1.04E-03
Constant	40.185	46.661	52.797	46.457	3.229

C56X (Count = 1,527)

Parameter	Percentile (%), β_j				Std.
	2.5	50	97.5	Mean	Dev.
Alt	-2.91E-04	2.85E-05	3.25E-04	1.84E-05	1.57E-04
DTTE	8.46E-03	8.77E-03	9.05E-03	8.76E-03	1.52E-04
ExitAng	8.74E-03	1.92E-02	2.91E-02	1.89E-02	5.20E-03
EffRwLen	-5.84E-04	-4.32E-04	-2.86E-04	-4.37E-04	7.61E-05
ThrVel	-3.07E-01	-2.71E-01	-2.37E-01	-2.73E-01	1.78E-02
TurnDist	-4.77E-03	-3.52E-03	-2.35E-03	-3.55E-03	6.16E-04
Constant	34.194	38.477	42.499	38.341	2.121

C680 (Count = 648)

Parameter	Percentile(%), β_j				Std.
	2.5	50	97.5	Mean	Dev.
Alt	-5.07E-04	5.47E-05	5.86E-04	3.82E-05	2.78E-04
DTTE	8.54E-03	8.98E-03	9.39E-03	8.97E-03	2.16E-04
ExitAng	2.37E-02	4.05E-02	5.61E-02	3.99E-02	8.26E-03
EffRwLen	-3.13E-04	-9.00E-05	1.17E-04	-9.67E-05	1.10E-04
ThrVel	-3.36E-01	-2.82E-01	-2.30E-01	-2.83E-01	2.72E-02
TurnDist	-6.33E-03	-4.42E-03	-2.61E-03	-4.47E-03	9.48E-04
Constant	28.709	34.884	40.653	34.697	3.040

C750 (Count = 1,042)

Parameter	Percentile (%), β_j				Std.
	2.5	50	97.5	Mean	Dev.
Alt	1.45E-04	5.48E-04	9.28E-04	5.35E-04	2.00E-04
DTTE	7.80E-03	8.17E-03	8.51E-03	8.15E-03	1.83E-04
ExitAng	-7.36E-03	5.90E-03	1.84E-02	5.48E-03	6.57E-03
EffRwLen	-5.24E-04	-3.21E-04	-1.28E-04	-3.27E-04	1.01E-04
ThrVel	-3.43E-01	-2.97E-01	-2.54E-01	-2.98E-01	2.26E-02
TurnDist	-6.85E-03	-5.30E-03	-3.86E-03	-5.35E-03	7.66E-04
Constant	39.799	45.713	51.298	45.528	2.926

CL30 (Count = 967)

Parameter	Percentile(%), β_j				Std.
	2.5	50	97.5	Mean	Dev.
Alt	-4.33E-04	-7.81E-05	2.58E-04	-8.93E-05	1.77E-04
DTTE	8.38E-03	8.76E-03	9.11E-03	8.75E-03	1.86E-04
ExitAng	-1.55E-02	-2.21E-03	9.86E-03	-2.59E-03	6.47E-03
EffRwLen	-5.27E-04	-3.41E-04	-1.65E-04	-3.47E-04	9.25E-05
ThrVel	-3.27E-01	-2.87E-01	-2.48E-01	-2.88E-01	2.01E-02
TurnDist	-8.88E-03	-7.30E-03	-5.82E-03	-7.35E-03	7.81E-04
Constant	38.703	43.764	48.493	43.607	2.492

CL60 (Count = 849)

Parameter	Percentile (%), β_j				Std.
	2.5	50	97.5	Mean	Dev.
Alt	1.38E-04	5.73E-04	9.79E-04	5.59E-04	2.15E-04
DTTE	8.11E-03	8.58E-03	9.02E-03	8.57E-03	2.31E-04
ExitAng	-1.46E-02	3.00E-04	1.43E-02	-1.15E-04	7.35E-03
EffRwLen	-1.04E-03	-7.95E-04	-5.69E-04	-8.02E-04	1.19E-04
ThrVel	-3.17E-01	-2.63E-01	-2.13E-01	-2.65E-01	2.64E-02
TurnDist	-6.03E-03	-4.33E-03	-2.72E-03	-4.38E-03	8.44E-04
Constant	36.951	43.956	50.486	43.737	3.465

CRJ2 (Count = 42,653)

Parameter	Percentile(%), β_j				Std.
	2.5	50	97.5	Mean	Dev.
Alt	8.09E-05	1.15E-04	1.47E-04	1.14E-04	1.69E-05
DTTE	7.61E-03	7.66E-03	7.70E-03	7.66E-03	2.30E-05
ExitAng	2.01E-02	2.16E-02	2.30E-02	2.16E-02	7.24E-04
EffRwLen	-4.31E-04	-4.04E-04	-3.80E-04	-4.05E-04	1.31E-05
ThrVel	-3.26E-01	-3.21E-01	-3.17E-01	-3.21E-01	2.49E-03
TurnDist	-4.51E-03	-4.32E-03	-4.15E-03	-4.33E-03	9.31E-05
Constant	47.611	48.314	48.966	48.293	0.346

Table 4.41: Highest Posterior Density Intervals for Arrival Runway Occupancy Time Model 5c Parameters, β_j for CRJ7 - DH8D

CRJ7 (Count = 21,708)

Parameter	Percentile (%), β_j				Std.
	2.5	50	97.5	Mean	Dev.
Alt	-1.82E-04	-1.82E-04	-1.82E-04	-1.82E-04	-1.82E-04
DTTE	7.76E-03	7.83E-03	7.88E-03	7.82E-03	3.07E-05
ExitAng	6.15E-03	8.36E-03	1.04E-02	8.29E-03	1.10E-03
EffRwLen	-2.25E-04	-1.88E-04	-1.53E-04	-1.89E-04	1.83E-05
ThrVel	-3.40E-01	-3.33E-01	-3.26E-01	-3.33E-01	3.66E-03
TurnDist	-4.50E-03	-4.25E-03	-4.01E-03	-4.26E-03	1.24E-04
Constant	45.539	46.519	47.470	46.484	0.493

CRJ9 (Count = 13,175)

Parameter	Percentile(%), β_j				Std.
	2.5	50	97.5	Mean	Dev.
Alt	-1.64E-04	-8.67E-05	-1.47E-05	-8.91E-05	3.81E-05
DTTE	7.23E-03	7.32E-03	7.40E-03	7.32E-03	4.18E-05
ExitAng	1.57E-02	1.89E-02	2.17E-02	1.88E-02	1.54E-03
EffRwLen	-2.84E-04	-2.26E-04	-1.70E-04	-2.27E-04	2.91E-05
ThrVel	-3.18E-01	-3.09E-01	-3.00E-01	-3.09E-01	4.76E-03
TurnDist	-3.46E-03	-3.15E-03	-2.86E-03	-3.16E-03	1.52E-04
Constant	43.612	45.015	46.329	44.972	0.694

DC10 (Count = 1,073)

Parameter	Percentile (%), β_j				Std.
	2.5	50	97.5	Mean	Dev.
Alt	-6.70E-04	-2.18E-04	2.10E-04	-2.32E-04	2.25E-04
DTTE	7.96E-03	8.27E-03	8.56E-03	8.26E-03	1.54E-04
ExitAng	-2.98E-02	-1.02E-02	7.74E-03	-1.08E-02	9.55E-03
EffRwLen	2.58E-04	5.67E-04	8.58E-04	5.58E-04	1.53E-04
ThrVel	-3.03E-01	-2.51E-01	-2.03E-01	-2.53E-01	2.55E-02
TurnDist	-1.11E-02	-9.28E-03	-7.54E-03	-9.33E-03	9.11E-04
Constant	30.239	37.952	45.451	37.679	3.887

DC95 (Count = 1,656)

Parameter	Percentile(%), β_j				Std.
	2.5	50	97.5	Mean	Dev.
Alt	-2.94E-03	-2.05E-03	-1.22E-03	-2.07E-03	4.38E-04
DTTE	7.60E-03	7.88E-03	8.13E-03	7.87E-03	1.35E-04
ExitAng	-1.12E-02	-1.44E-03	7.86E-03	-1.76E-03	4.86E-03
EffRwLen	-5.61E-04	-3.28E-04	-1.14E-04	-3.35E-04	1.14E-04
ThrVel	-3.51E-01	-3.28E-01	-3.06E-01	-3.29E-01	1.14E-02
TurnDist	-7.79E-03	-6.54E-03	-5.39E-03	-6.57E-03	6.11E-04
Constant	45.431	49.353	53.090	49.221	1.954

DH8A (Count = 3,290)

Parameter	Percentile (%), β_j				Std.
	2.5	50	97.5	Mean	Dev.
Alt	-1.47E-03	-6.90E-04	3.85E-05	-7.15E-04	3.85E-04
DTTE	8.67E-03	8.90E-03	9.12E-03	8.89E-03	1.17E-04
ExitAng	1.78E-02	2.40E-02	2.97E-02	2.38E-02	3.03E-03
EffRwLen	-9.46E-04	-8.04E-04	-6.69E-04	-8.08E-04	7.08E-05
ThrVel	-2.67E-01	-2.49E-01	-2.33E-01	-2.50E-01	8.56E-03
TurnDist	-1.10E-02	-9.87E-03	-8.88E-03	-9.90E-03	5.33E-04
Constant	37.338	39.452	41.436	39.386	1.048

DH8B (Count = 899)

Parameter	Percentile(%), β_j				Std.
	2.5	50	97.5	Mean	Dev.
Alt	1.83E-03	3.34E-03	4.76E-03	3.29E-03	7.47E-04
DTTE	7.21E-03	7.50E-03	7.79E-03	7.49E-03	1.47E-04
ExitAng	-1.77E-02	-8.23E-03	3.73E-04	-8.50E-03	4.61E-03
EffRwLen	-2.71E-05	2.07E-04	4.24E-04	2.00E-04	1.15E-04
ThrVel	-2.38E-01	-2.08E-01	-1.80E-01	-2.09E-01	1.49E-02
TurnDist	-6.36E-03	-4.95E-03	-3.64E-03	-5.00E-03	6.94E-04
Constant	25.548	29.602	33.470	29.476	2.015

DH8C (Count = 1,529)

Parameter	Percentile (%), β_j				Std.
	2.5	50	97.5	Mean	Dev.
Alt	4.38E-04	1.13E-03	1.79E-03	1.11E-03	3.44E-04
DTTE	7.09E-03	7.35E-03	7.59E-03	7.34E-03	1.28E-04
ExitAng	3.61E-03	1.23E-02	2.09E-02	1.20E-02	4.40E-03
EffRwLen	-4.15E-04	-1.12E-04	1.69E-04	-1.21E-04	1.49E-04
ThrVel	-2.60E-01	-2.36E-01	-2.14E-01	-2.37E-01	1.17E-02
TurnDist	-7.17E-03	-6.34E-03	-5.56E-03	-6.36E-03	4.10E-04
Constant	31.957	35.835	39.519	35.705	1.927

DH8D (Count = 6,232)

Parameter	Percentile(%), β_j				Std.
	2.5	50	97.5	Mean	Dev.
Alt	-1.67E-04	-5.32E-05	5.05E-05	-5.66E-05	5.55E-05
DTTE	6.56E-03	6.71E-03	6.86E-03	6.71E-03	7.61E-05
ExitAng	-1.81E-02	-1.08E-02	-4.06E-03	-1.10E-02	3.60E-03
EffRwLen	2.93E-04	3.94E-04	4.90E-04	3.91E-04	5.02E-05
ThrVel	-3.23E-01	-3.08E-01	-2.94E-01	-3.09E-01	7.18E-03
TurnDist	-8.59E-03	-7.94E-03	-7.32E-03	-7.96E-03	3.25E-04
Constant	46.387	48.426	50.318	48.363	1.005

Table 4.42: Highest Posterior Density Intervals for Arrival Runway Occupancy Time Model 5c Parameters, β_j for E120 - E55P

E120 (Count = 3,044)

Parameter	Percentile (%), β_j				Std.
	2.5	50	97.5	Mean	Dev.
Alt	-1.82E-04	-1.82E-04	-1.82E-04	-1.82E-04	-1.82E-04
DTTE	7.76E-03	7.83E-03	7.88E-03	7.82E-03	3.07E-05
ExitAng	6.15E-03	8.36E-03	1.04E-02	8.29E-03	1.10E-03
EffRwLen	-2.25E-04	-1.88E-04	-1.53E-04	-1.89E-04	1.83E-05
ThrVel	-3.40E-01	-3.33E-01	-3.26E-01	-3.33E-01	3.66E-03
TurnDist	-4.50E-03	-4.25E-03	-4.01E-03	-4.26E-03	1.24E-04
Constant	45.539	46.519	47.470	46.484	0.493

E135 (Count = 8,159)

Parameter	Percentile(%), β_j				Std.
	2.5	50	97.5	Mean	Dev.
Alt	-1.64E-04	-8.67E-05	-1.47E-05	-8.91E-05	3.81E-05
DTTE	7.23E-03	7.32E-03	7.40E-03	7.32E-03	4.18E-05
ExitAng	1.57E-02	1.89E-02	2.17E-02	1.88E-02	1.54E-03
EffRwLen	-2.84E-04	-2.26E-04	-1.70E-04	-2.27E-04	2.91E-05
ThrVel	-3.18E-01	-3.09E-01	-3.00E-01	-3.09E-01	4.76E-03
TurnDist	-3.46E-03	-3.15E-03	-2.86E-03	-3.16E-03	1.52E-04
Constant	43.612	45.015	46.329	44.972	0.694

E145 (Count = 27,317)

Parameter	Percentile (%), β_j				Std.
	2.5	50	97.5	Mean	Dev.
Alt	-6.70E-04	-2.18E-04	2.10E-04	-2.32E-04	2.25E-04
DTTE	7.96E-03	8.27E-03	8.56E-03	8.26E-03	1.54E-04
ExitAng	-2.98E-02	-1.02E-02	7.74E-03	-1.08E-02	9.55E-03
EffRwLen	2.58E-04	5.67E-04	8.58E-04	5.58E-04	1.53E-04
ThrVel	-3.03E-01	-2.51E-01	-2.03E-01	-2.53E-01	2.55E-02
TurnDist	-1.11E-02	-9.28E-03	-7.54E-03	-9.33E-03	9.11E-04
Constant	30.239	37.952	45.451	37.679	3.887

E170 (Count = 17,765)

Parameter	Percentile(%), β_j				Std.
	2.5	50	97.5	Mean	Dev.
Alt	-2.94E-03	-2.05E-03	-1.22E-03	-2.07E-03	4.38E-04
DTTE	7.60E-03	7.88E-03	8.13E-03	7.87E-03	1.35E-04
ExitAng	-1.12E-02	-1.44E-03	7.86E-03	-1.76E-03	4.86E-03
EffRwLen	-5.61E-04	-3.28E-04	-1.14E-04	-3.35E-04	1.14E-04
ThrVel	-3.51E-01	-3.28E-01	-3.06E-01	-3.29E-01	1.14E-02
TurnDist	-7.79E-03	-6.54E-03	-5.39E-03	-6.57E-03	6.11E-04
Constant	45.431	49.353	53.090	49.221	1.954

E190 (Count = 9,109)

Parameter	Percentile (%), β_j				Std.
	2.5	50	97.5	Mean	Dev.
Alt	-1.47E-03	-6.90E-04	3.85E-05	-7.15E-04	3.85E-04
DTTE	8.67E-03	8.90E-03	9.12E-03	8.89E-03	1.17E-04
ExitAng	1.78E-02	2.40E-02	2.97E-02	2.38E-02	3.03E-03
EffRwLen	-9.46E-04	-8.04E-04	-6.69E-04	-8.08E-04	7.08E-05
ThrVel	-2.67E-01	-2.49E-01	-2.33E-01	-2.50E-01	8.56E-03
TurnDist	-1.10E-02	-9.87E-03	-8.88E-03	-9.90E-03	5.33E-04
Constant	37.338	39.452	41.436	39.386	1.048

E45X (Count = 7,746)

Parameter	Percentile(%), β_j				Std.
	2.5	50	97.5	Mean	Dev.
Alt	1.83E-03	3.34E-03	4.76E-03	3.29E-03	7.47E-04
DTTE	7.21E-03	7.50E-03	7.79E-03	7.49E-03	1.47E-04
ExitAng	-1.77E-02	-8.23E-03	3.73E-04	-8.50E-03	4.61E-03
EffRwLen	-2.71E-05	2.07E-04	4.24E-04	2.00E-04	1.15E-04
ThrVel	-2.38E-01	-2.08E-01	-1.80E-01	-2.09E-01	1.49E-02
TurnDist	-6.36E-03	-4.95E-03	-3.64E-03	-5.00E-03	6.94E-04
Constant	25.548	29.602	33.470	29.476	2.015

E50P (Count = 268)

Parameter	Percentile (%), β_j				Std.
	2.5	50	97.5	Mean	Dev.
Alt	4.38E-04	1.13E-03	1.79E-03	1.11E-03	3.44E-04
DTTE	7.09E-03	7.35E-03	7.59E-03	7.34E-03	1.28E-04
ExitAng	3.61E-03	1.23E-02	2.09E-02	1.20E-02	4.40E-03
EffRwLen	-4.15E-04	-1.12E-04	1.69E-04	-1.21E-04	1.49E-04
ThrVel	-2.60E-01	-2.36E-01	-2.14E-01	-2.37E-01	1.17E-02
TurnDist	-7.17E-03	-6.34E-03	-5.56E-03	-6.36E-03	4.10E-04
Constant	31.957	35.835	39.519	35.705	1.927

E55P (Count = 283)

Parameter	Percentile(%), β_j				Std.
	2.5	50	97.5	Mean	Dev.
Alt	-1.67E-04	-5.32E-05	5.05E-05	-5.66E-05	5.55E-05
DTTE	6.56E-03	6.71E-03	6.86E-03	6.71E-03	7.61E-05
ExitAng	-1.81E-02	-1.08E-02	-4.06E-03	-1.10E-02	3.60E-03
EffRwLen	2.93E-04	3.94E-04	4.90E-04	3.91E-04	5.02E-05
ThrVel	-3.23E-01	-3.08E-01	-2.94E-01	-3.09E-01	7.18E-03
TurnDist	-8.59E-03	-7.94E-03	-7.32E-03	-7.96E-03	3.25E-04
Constant	46.387	48.426	50.318	48.363	1.005

Table 4.43: Highest Posterior Density Intervals for Arrival Runway Occupancy Time Model 5c Parameters, β_j for F2TH - LJ60

F2TH (Count = 846)

Parameter	Percentile (%), β_j				Std.
	2.5	50	97.5	Mean	Dev.
Alt	-3.89E-04	-3.89E-04	-3.89E-04	-3.89E-04	-3.89E-04
DTTE	8.26E-03	8.70E-03	9.12E-03	8.69E-03	2.21E-04
ExitAng	-1.59E-02	-1.36E-03	1.26E-02	-1.84E-03	7.29E-03
EffRwLen	-4.59E-04	-2.26E-04	-2.38E-06	-2.34E-04	1.16E-04
ThrVel	-3.58E-01	-3.08E-01	-2.60E-01	-3.09E-01	2.50E-02
TurnDist	-9.86E-03	-8.05E-03	-6.35E-03	-8.11E-03	8.96E-04
Constant	40.378	46.747	52.888	46.546	3.190

F900 (Count = 505)

Parameter	Percentile(%), β_j				Std.
	2.5	50	97.5	Mean	Dev.
Alt	-8.33E-04	-1.11E-04	5.73E-04	-1.31E-04	3.59E-04
DTTE	7.95E-03	8.48E-03	8.97E-03	8.46E-03	2.59E-04
ExitAng	-1.25E-02	7.03E-03	2.55E-02	6.44E-03	9.68E-03
EffRwLen	-5.06E-04	-1.86E-04	1.13E-04	-1.96E-04	1.58E-04
ThrVel	-3.53E-01	-2.93E-01	-2.35E-01	-2.95E-01	3.01E-02
TurnDist	-1.00E-02	-7.63E-03	-5.36E-03	-7.71E-03	1.19E-03
Constant	36.585	44.503	51.838	44.259	3.885

GALX (Count = 1,197)

Parameter	Percentile (%), β_j				Std.
	2.5	50	97.5	Mean	Dev.
Alt	-8.39E-05	4.88E-04	1.03E-03	4.71E-04	2.84E-04
DTTE	8.16E-03	8.65E-03	9.11E-03	8.64E-03	2.44E-04
ExitAng	-2.26E-02	-4.88E-03	1.14E-02	-5.42E-03	8.68E-03
EffRwLen	-7.13E-04	-4.08E-04	-1.19E-04	-4.17E-04	1.51E-04
ThrVel	-3.58E-01	-2.97E-01	-2.40E-01	-2.99E-01	3.00E-02
TurnDist	-1.06E-02	-8.26E-03	-6.15E-03	-8.33E-03	1.13E-03
Constant	40.645	48.354	55.854	48.097	3.879

GLF5 (Count = 760)

Parameter	Percentile(%), β_j				Std.
	2.5	50	97.5	Mean	Dev.
Alt	-4.44E-04	5.33E-04	1.45E-03	5.02E-04	4.84E-04
DTTE	7.99E-03	8.63E-03	9.23E-03	8.62E-03	3.18E-04
ExitAng	-1.19E-02	8.93E-03	2.84E-02	8.30E-03	1.03E-02
EffRwLen	-8.73E-04	-5.10E-04	-1.76E-04	-5.21E-04	1.78E-04
ThrVel	-3.71E-01	-2.98E-01	-2.25E-01	-3.00E-01	3.72E-02
TurnDist	-9.48E-03	-6.62E-03	-4.01E-03	-6.70E-03	1.40E-03
Constant	36.154	45.021	53.647	44.707	4.461

H25B (Count = 1,279)

Parameter	Percentile (%), β_j				Std.
	2.5	50	97.5	Mean	Dev.
Alt	2.21E-04	6.11E-04	9.86E-04	5.98E-04	1.95E-04
DTTE	7.99E-03	8.38E-03	8.74E-03	8.36E-03	1.90E-04
ExitAng	-2.57E-02	-1.08E-02	3.01E-03	-1.12E-02	7.34E-03
EffRwLen	-7.27E-04	-4.90E-04	-2.70E-04	-4.97E-04	1.17E-04
ThrVel	-2.97E-01	-2.50E-01	-2.06E-01	-2.52E-01	2.33E-02
TurnDist	-9.97E-03	-8.23E-03	-6.60E-03	-8.28E-03	8.58E-04
Constant	39.028	45.394	51.363	45.202	3.151

LJ35 (Count = 410)

Parameter	Percentile(%), β_j				Std.
	2.5	50	97.5	Mean	Dev.
Alt	-1.32E-04	4.18E-04	9.22E-04	4.00E-04	2.69E-04
DTTE	8.28E-03	8.79E-03	9.26E-03	8.78E-03	2.49E-04
ExitAng	-1.02E-02	8.21E-03	2.59E-02	7.58E-03	9.21E-03
EffRwLen	-2.86E-04	1.59E-05	3.02E-04	6.70E-06	1.50E-04
ThrVel	-4.17E-01	-3.58E-01	-3.03E-01	-3.60E-01	2.92E-02
TurnDist	-9.01E-03	-6.79E-03	-4.71E-03	-6.86E-03	1.10E-03
Constant	41.825	49.307	56.228	49.082	3.681

LJ45 (Count = 600)

Parameter	Percentile (%), β_j				Std.
	2.5	50	97.5	Mean	Dev.
Alt	2.81E-04	6.56E-04	1.02E-03	6.44E-04	1.88E-04
DTTE	8.84E-03	9.24E-03	9.61E-03	9.23E-03	1.97E-04
ExitAng	-7.40E-03	5.06E-03	1.68E-02	4.70E-03	6.16E-03
EffRwLen	-5.00E-04	-2.97E-04	-1.07E-04	-3.03E-04	1.00E-04
ThrVel	-3.88E-01	-3.42E-01	-2.99E-01	-3.43E-01	2.26E-02
TurnDist	-8.22E-03	-6.67E-03	-5.17E-03	-6.72E-03	7.77E-04
Constant	42.908	48.550	53.709	48.383	2.757

LJ60 (Count = 434)

Parameter	Percentile(%), β_j				Std.
	2.5	50	97.5	Mean	Dev.
Alt	-6.68E-04	-2.55E-05	5.79E-04	-4.48E-05	3.18E-04
DTTE	6.53E-03	7.21E-03	7.83E-03	7.19E-03	3.33E-04
ExitAng	1.09E-02	4.14E-02	6.96E-02	4.05E-02	1.50E-02
EffRwLen	-2.74E-04	2.01E-04	6.46E-04	1.85E-04	2.35E-04
ThrVel	-1.97E-01	-1.16E-01	-4.09E-02	-1.19E-01	3.99E-02
TurnDist	-6.16E-03	-3.20E-03	-4.23E-04	-3.30E-03	1.47E-03
Constant	11.783	23.324	33.917	22.999	5.647

Table 4.44: Highest Posterior Density Intervals for Arrival Runway Occupancy Time Model 5c Parameters, β_j for MD11 - SF34

MD11 (Count = 1,743)

Parameter	Percentile (%), β_j				Std.
	2.5	50	97.5	Mean	Dev.
Alt	-3.06E-04	-3.06E-04	-3.06E-04	-3.06E-04	-3.06E-04
DTTE	7.68E-03	8.21E-03	8.71E-03	8.19E-03	2.63E-04
ExitAng	-2.34E-03	1.65E-02	3.38E-02	1.59E-02	9.24E-03
EffRwLen	-4.72E-04	-1.99E-04	5.47E-05	-2.07E-04	1.35E-04
ThrVel	-2.88E-01	-2.18E-01	-1.55E-01	-2.20E-01	3.38E-02
TurnDist	-7.99E-03	-5.81E-03	-3.75E-03	-5.88E-03	1.08E-03
Constant	25.629	34.552	42.840	34.281	4.390

MD82 (Count = 7,955)

Parameter	Percentile(%), β_j				Std.
	2.5	50	97.5	Mean	Dev.
Alt	-6.61E-04	2.05E-04	1.02E-03	1.77E-04	4.28E-04
DTTE	7.15E-03	7.78E-03	8.40E-03	7.76E-03	3.19E-04
ExitAng	-2.26E-02	2.47E-03	2.59E-02	1.66E-03	1.24E-02
EffRwLen	-8.61E-04	-4.66E-04	-9.36E-05	-4.78E-04	1.96E-04
ThrVel	-2.64E-01	-1.80E-01	-1.01E-01	-1.83E-01	4.16E-02
TurnDist	-1.09E-02	-8.10E-03	-5.43E-03	-8.19E-03	1.40E-03
Constant	26.885	38.832	50.148	38.459	5.925

MD83 (Count = 6,933)

Parameter	Percentile (%), β_j				Std.
	2.5	50	97.5	Mean	Dev.
Alt	-1.70E-04	2.32E-04	5.97E-04	2.21E-04	1.97E-04
DTTE	8.07E-03	8.39E-03	8.69E-03	8.38E-03	1.60E-04
ExitAng	3.15E-03	2.25E-02	4.00E-02	2.20E-02	9.40E-03
EffRwLen	-4.29E-04	-1.74E-04	6.47E-05	-1.82E-04	1.26E-04
ThrVel	-4.19E-01	-3.67E-01	-3.19E-01	-3.69E-01	2.55E-02
TurnDist	-1.18E-02	-1.02E-02	-8.65E-03	-1.02E-02	8.03E-04
Constant	51.146	59.287	67.000	59.039	4.048

MD88 (Count = 12,195)

Parameter	Percentile(%), β_j				Std.
	2.5	50	97.5	Mean	Dev.
Alt	5.38E-05	1.78E-04	2.98E-04	1.74E-04	6.23E-05
DTTE	7.41E-03	7.49E-03	7.57E-03	7.49E-03	4.22E-05
ExitAng	1.40E-03	6.77E-03	1.17E-02	6.61E-03	2.64E-03
EffRwLen	-3.81E-04	-3.42E-04	-3.05E-04	-3.44E-04	1.95E-05
ThrVel	-3.02E-01	-2.90E-01	-2.78E-01	-2.90E-01	6.14E-03
TurnDist	-6.19E-03	-5.66E-03	-5.16E-03	-5.68E-03	2.61E-04
Constant	42.302	44.021	45.641	43.965	0.851

MD90 (Count = 5,957)

Parameter	Percentile (%), β_j				Std.
	2.5	50	97.5	Mean	Dev.
Alt	-4.58E-05	7.98E-05	1.97E-04	7.56E-05	6.19E-05
DTTE	7.25E-03	7.34E-03	7.43E-03	7.34E-03	4.68E-05
ExitAng	-3.58E-03	2.30E-03	7.80E-03	2.13E-03	2.91E-03
EffRwLen	-4.11E-04	-3.67E-04	-3.25E-04	-3.68E-04	2.20E-05
ThrVel	-3.01E-01	-2.88E-01	-2.76E-01	-2.89E-01	6.47E-03
TurnDist	-7.21E-03	-6.65E-03	-6.11E-03	-6.67E-03	2.79E-04
Constant	44.307	46.215	47.942	46.161	0.926

PA31 (Count = 607)

Parameter	Percentile(%), β_j				Std.
	2.5	50	97.5	Mean	Dev.
Alt	-1.62E-03	-1.43E-03	-1.25E-03	-1.44E-03	9.48E-05
DTTE	7.15E-03	7.25E-03	7.35E-03	7.25E-03	5.14E-05
ExitAng	1.91E-02	2.32E-02	2.72E-02	2.31E-02	2.08E-03
EffRwLen	-4.03E-04	-3.25E-04	-2.53E-04	-3.27E-04	3.82E-05
ThrVel	-3.18E-01	-3.09E-01	-3.01E-01	-3.09E-01	4.34E-03
TurnDist	-5.56E-03	-5.16E-03	-4.79E-03	-5.18E-03	1.98E-04
Constant	45.569	46.859	48.114	46.816	0.649

PC12 (Count = 662)

Parameter	Percentile (%), β_j				Std.
	2.5	50	97.5	Mean	Dev.
Alt	1.18E-04	2.58E-04	3.89E-04	2.54E-04	6.91E-05
DTTE	6.82E-03	6.97E-03	7.12E-03	6.97E-03	7.57E-05
ExitAng	1.75E-02	2.38E-02	2.94E-02	2.36E-02	3.04E-03
EffRwLen	7.03E-05	1.97E-04	3.14E-04	1.93E-04	6.24E-05
ThrVel	-3.30E-01	-3.16E-01	-3.03E-01	-3.17E-01	6.93E-03
TurnDist	-7.36E-03	-6.73E-03	-6.13E-03	-6.75E-03	3.15E-04
Constant	44.128	46.325	48.446	46.252	1.101

SF34 (Count = 1,672)

Parameter	Percentile(%), β_j				Std.
	2.5	50	97.5	Mean	Dev.
Alt	-9.08E-04	-5.31E-04	-1.60E-04	-5.44E-04	1.91E-04
DTTE	7.77E-03	8.19E-03	8.58E-03	8.18E-03	2.08E-04
ExitAng	-8.08E-03	1.66E-02	3.87E-02	1.59E-02	1.19E-02
EffRwLen	-9.87E-04	-4.71E-04	5.25E-06	-4.88E-04	2.53E-04
ThrVel	-4.07E-01	-3.52E-01	-3.01E-01	-3.54E-01	2.72E-02
TurnDist	-2.99E-03	2.00E-04	3.24E-03	1.01E-04	1.59E-03
Constant	46.303	52.862	58.933	52.674	3.214

Table 4.45: Highest Posterior Density Intervals for Arrival Runway Occupancy Time Model 5c Parameters, β_j for SH36 - SW4

SH36 (Count = 263)

Parameter	Percentile (%), β_j				Std.
	2.5	50	97.5	Mean	Dev.
Alt	4.05E-05	4.05E-05	4.05E-05	4.05E-05	4.05E-05
DTTE	8.18E-03	8.57E-03	8.95E-03	8.56E-03	1.95E-04
ExitAng	-8.08E-03	8.97E-03	2.48E-02	8.47E-03	8.40E-03
EffRwLen	-7.07E-04	-3.92E-04	-9.62E-05	-4.00E-04	1.56E-04
ThrVel	-3.33E-01	-2.92E-01	-2.55E-01	-2.94E-01	1.99E-02
TurnDist	-4.20E-03	-1.92E-03	2.58E-04	-1.99E-03	1.14E-03
Constant	39.876	44.440	48.721	44.295	2.258

SR22 (Count = 247)

Parameter	Percentile(%), β_j				Std.
	2.5	50	97.5	Mean	Dev.
Alt	-2.81E-03	-2.12E-03	-1.47E-03	-2.14E-03	3.41E-04
DTTE	7.07E-03	7.43E-03	7.76E-03	7.42E-03	1.74E-04
ExitAng	1.98E-02	2.74E-02	3.44E-02	2.72E-02	3.73E-03
EffRwLen	-4.05E-04	-2.50E-04	-9.99E-05	-2.55E-04	7.80E-05
ThrVel	-2.92E-01	-2.65E-01	-2.39E-01	-2.65E-01	1.37E-02
TurnDist	-1.59E-03	-5.68E-04	4.24E-04	-6.01E-04	5.15E-04
Constant	35.814	39.293	42.635	39.181	1.743

SW4 (Count = 829)

Parameter	Percentile (%), β_j				Std.
	2.5	50	97.5	Mean	Dev.
Alt	-3.76E-02	1.57E-02	6.48E-02	1.43E-02	2.61E-02
DTTE	9.43E-03	1.01E-02	1.07E-02	1.01E-02	3.14E-04
ExitAng	-1.40E-01	-9.67E-02	-5.60E-02	-9.81E-02	2.15E-02
EffRwLen	-2.25E-03	-1.60E-03	-1.01E-03	-1.62E-03	3.17E-04
ThrVel	-4.93E-01	-4.00E-01	-3.11E-01	-4.03E-01	4.66E-02
TurnDist	-2.63E-02	-1.99E-02	-1.40E-02	-2.01E-02	3.14E-03
Constant	63.386	77.060	90.251	76.606	6.857

4.9 Posterior Predictive Checks

Having selected Bayesian models for our predictive models, we apply another set of model diagnostics known as posterior predictive checks to verify that the model fits. If the model has a good fit, the observed data should appear plausible when compared against the posterior predictive distribution. If we let y equal the observed data and θ be the vector of parameters, we can define y^{rep} as data that could have been produced if the experiment and model that produced the data y were replicated with parameters θ. Thus, the distribution of y^{rep} is given as

$$p(y^{\text{rep}}|y) = \int p(y^{\text{rep}}|\theta)p(\theta|y)d\theta \tag{4.50}$$

The discrepancy between the model and the data is measured by setting a test statistic or discrepancy measure that is used as a standard when comparing the data to predictive simulations (Gelman et al., 2014). Test statistics should depend only on the data and should summarize the discrepancy between the observed data and the expected observations from

the model with the parameters θ.

For the purposes of this study, we choose the mean of the data as the test statistic.

Once a test statistic is selected, we move to evaluate *posterior predictive p-values*, which are measures of the probability that the replicated data could be more extreme than the observed data. The posterior predictive p-value is defined as

$$p_{post} = \Pr(T(y^{rep}, \theta) \geq T(y, \theta|y) \tag{4.51}$$

where the probability is evaluated over the posterior distribution of θ and the posterior predictive distribution of y^{rep} (Gelman et al., 2014). Computation of the posterior predictive p-value is done through estimating the proportion of instances for which the test statistics of the replicates of the posterior predictive distribution exceed the test statistic of the observed data. As with classical p-values, the range of p_{post} is between 0 and 1. Values at either extreme would suggest poor model fit.

4.9.1 Posterior Predictive P-Values of Models

Table 4.46 illustrates the posterior predictive p-values for each of the aircraft level posterior distributions. Generally, the models fit the data well. However, there were some weaker model fits primarily for aircraft types with low numbers of observations. Additionally, the arrival runway occupancy time model (Model 5c) overall had slightly weaker fits than the departure runway occupancy time and departure take-off distance models, possibly due to the larger number of sources of variance that affect arrival runway occupancy time.

Table 4.46: Posterior Predictive P-Values of Posterior Predictive Distributions for Predictive Models by Individual Aircraft Type

Aircraft Type	Model 5a	Model 5b	Model 5c	Obs.
A306	0.530	0.518	0.431	1157
A319	0.459	0.450	0.469	26169
A320	0.518	0.508	0.466	34729
A321	0.496	0.494	0.501	8453

Aircraft Type	Model 5a	Model 5b	Model 5c	Obs.
A332	0.526	0.531	0.436	2070
A333	0.520	0.517	0.451	1679
A343	0.489	0.502	0.440	491
A346	0.472	0.467	0.439	387
A388	0.622	0.599	0.423	414
AT72	0.478	0.474	0.458	371
B190	0.478	0.475	0.483	3106
B350	0.475	0.462	0.447	291
B712	0.527	0.516	0.450	9272
B732	0.481	0.504	0.359	390
B733	0.507	0.492	0.429	7910
B734	0.493	0.492	0.452	2327
B735	0.482	0.480	0.407	482
B736	0.609	0.526	0.379	377
B737	0.500	0.488	0.443	37071
B738	0.530	0.524	0.433	37383
B739	0.494	0.482	0.472	6543
B744	0.490	0.483	0.455	2831
B748	0.484	0.486	0.448	453
B752	0.513	0.505	0.420	23687
B753	0.507	0.502	0.435	2816
B762	0.463	0.473	0.468	1661
B763	0.529	0.527	0.438	6817
B764	0.513	0.514	0.399	980
B772	0.502	0.498	0.465	3461
B77L	0.503	0.493	0.382	534
B77W	0.519	0.530	0.445	1843
B788	0.478	0.484	0.412	388
BE20	0.483	0.491	0.465	615

Aircraft Type	Model 5a	Model 5b	Model 5c	Obs.
BE40	0.483	0.491	0.457	749
BE99	0.487	0.470	0.420	421
BE9L	0.458	0.442	0.498	450
C172	0.500	0.473	0.495	368
C208	0.476	0.486	0.447	1888
C402	0.488	0.496	0.388	2413
C525	0.469	0.445	0.427	295
C550	0.432	0.447	0.443	343
C560	0.488	0.476	0.444	689
C56X	0.484	0.477	0.447	1527
C680	0.461	0.468	0.435	648
C750	0.466	0.459	0.453	1042
CL30	0.492	0.483	0.431	967
CL60	0.479	0.485	0.463	849
CRJ2	0.501	0.495	0.491	42653
CRJ7	0.459	0.460	0.490	21708
CRJ9	0.518	0.520	0.471	13175
DC10	0.527	0.519	0.425	1073
DC95	0.450	0.444	0.458	1656
DH8A	0.474	0.489	0.382	3290
DH8B	0.499	0.504	0.545	899
DH8C	0.513	0.523	0.447	1529
DH8D	0.407	0.408	0.424	6232
E120	0.411	0.445	0.438	3044
E135	0.496	0.494	0.489	8159
E145	0.493	0.493	0.474	27317
E170	0.481	0.483	0.459	17765
E190	0.489	0.484	0.526	9109
E45X	0.497	0.481	0.493	7746

Aircraft Type	Model 5a	Model 5b	Model 5c	Obs.
E50P	0.498	0.498	0.466	268
E55P	0.514	0.495	0.452	283
F2TH	0.524	0.517	0.415	846
F900	0.443	0.457	0.440	505
GALX	0.476	0.480	0.406	566
GLEX	0.461	0.495	0.417	336
GLF4	0.476	0.479	0.439	1197
GLF5	0.461	0.462	0.462	760
H25B	0.459	0.449	0.444	1279
LJ35	0.484	0.460	0.400	410
LJ45	0.459	0.462	0.432	600
LJ60	0.485	0.482	0.435	434
MD11	0.465	0.461	0.464	1743
MD82	0.490	0.486	0.411	7955
MD83	0.502	0.494	0.404	6933
MD88	0.478	0.477	0.420	12195
MD90	0.499	0.489	0.428	5957
PA31	0.507	0.495	0.468	607
PC12	0.473	0.495	0.423	662
SF34	0.527	0.535	0.479	1672
SH36	0.487	0.478	0.338	263
SR22	0.462	0.466	0.425	247
SW4	0.500	0.495	0.524	829

4.9.2 Visual Comparisons of Data against Posterior Predictive Distributions

For further analysis of the models, it is useful to graphically examine the distribution of the observed data versus that produced by posterior predictive simulations. We provide these comparisons in Figures B.1 through B.45 in the Appendix.

4.10 Application of the Models

As mentioned previously, the models presented can be readily applied to airfield capacity simulation models and airport analysis tools that accept distributions of runway occupancy time. We now demonstrate the usage of the departure and arrival runway occupancy time models in QuickRunSim, a runway capacity model developed at the Air Transportation Systems Laboratory at Virginia Tech.

4.10.1 Overview of QuickRunSim

QuickRunSim is a hybrid analytical and simulation model designed to estimate the throughput capacity of an airport. In the model, random arriving and departing flights are generated to produce an ordered flight schedule and fleet mix. The expected headways of each of the successive aircraft are then used to estimate the throughput capacity of the subject airport.

QuickRunSim considers minimum runway length requirements for aircraft to safely operate on a runway, in order to avoid unrealistic aircraft assignments. It also models VMC and IMC conditions and is capable of handling dependent runway configurations, including: (1) two intersecting runways, (2) two parallel and one intersecting runway and (3) four runways (Pu, 2014).

QuickRunSim operates on a database of 186 individual aircraft types and requires, as one of its input parameters, departure and arrival runway occupancy times for its analysis. The output produced is a Pareto Diagram, illustrating the maximum possible departure-arrival capacity combinations for the airport. Figure 4.19 illustrates an example of this output.

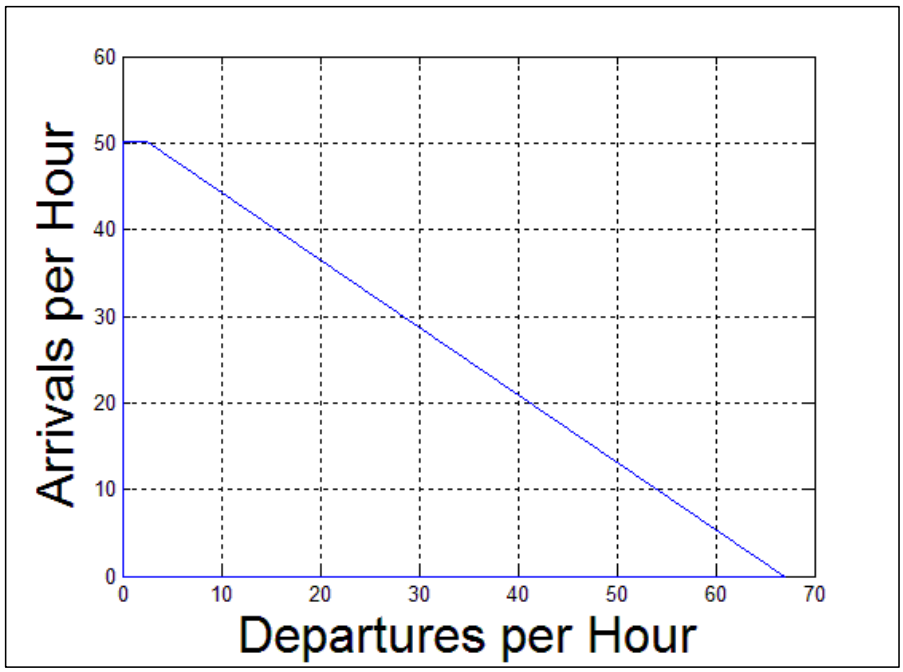

Figure 4.19: Model Output from QuickRunSim, Source (Pu, 2014)

4.10.2 Simulation Studies

To demonstrate the benefits of utilizing individual runway occupancy time data, we ran two groups of scenarios using QuickRunSim, which are defined as follows. For the first group, we considered mixed operations on Runway 01 at Washington Ronald Reagan National Airport. A synthetic schedule of operations was created by the program and consisted of the following aircraft at the following proportions.

Table 4.47: Fleet Mix of Synthetic Schedule by Individual Aircraft Type and RECAT Grouping

Group 1: Scenario 1		
Aircraft Type	Pct. of Fleet Mix	RECAT Group
DH8D	0.403%	D
DH8A	0.597%	E
B712	0.264%	D
B737	10.826%	D
B738	10.242%	D
B735	0.001%	D
B733	0.137%	D
B752	0.565%	D
B753	0.001%	D
CRJ2	20.008%	E
CRJ7	2.570%	E
B739	0.081%	D
CRJ9	2.009%	E
MD82	1.803%	D
MD90	2.162%	D
CR75	0.062%	E
E175	9.406%	E
E135	0.002%	E
E145	2.385%	E
E140	0.151%	E
E170	10.178%	E
E190	9.357%	D
A320	4.479%	D
A319	11.628%	D
A321	0.684%	D
B73E	0.001%	D

Group 1: Scenario 2	
RECAT Group	Pct. of Fleet Mix
A	0.000%
B	0.000%
C	0.000%
D	52.630%
E	47.370%
F	0.000%

Using the departure and arrival runway occupancy time models, we estimated the mean DROT and AROT values for each individual aircraft type. The aircraft type CR75 was mapped to a CRJ9 and the aircraft type B73E was mapped to a B735. Once the values for the individual aircraft types were set, the composite values for RECAT groups D and E were formed by taking the weighted average of the individual types composing each group.

Figures 4.20 and 4.21 illustrate the results of the simulation.

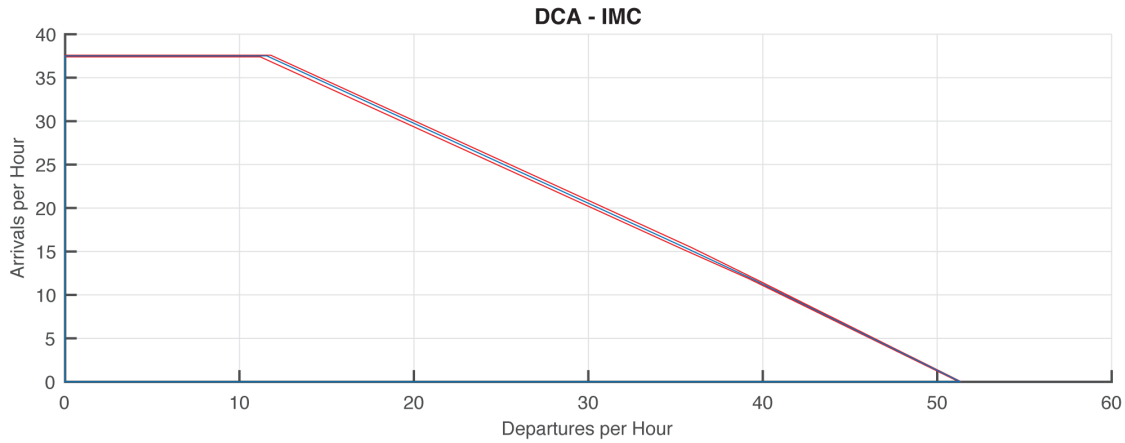

Figure 4.20: Model Output from QuickRunSim utilizing Aircraft-Specific ROT Parameters

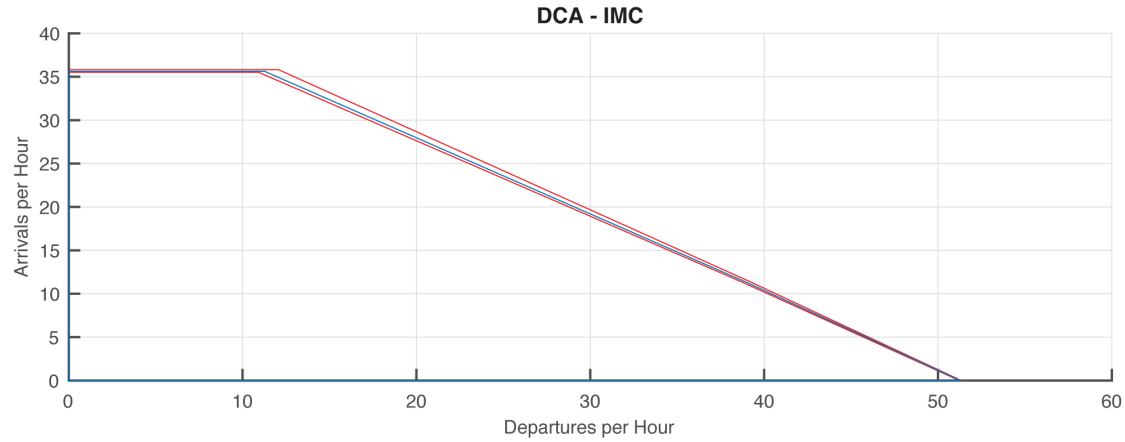

Figure 4.21: Model Output from QuickRunSim utilizing RECAT Grouping Composite ROT Parameters

Before considering the results, it is important to validate the results of the model to ensure that the output is reasonable. Figure 4.22 illustrates the FAA Airport Capacity Profile for DCA under instrument weather conditions. (Federal Aviation Administration, 2014b)

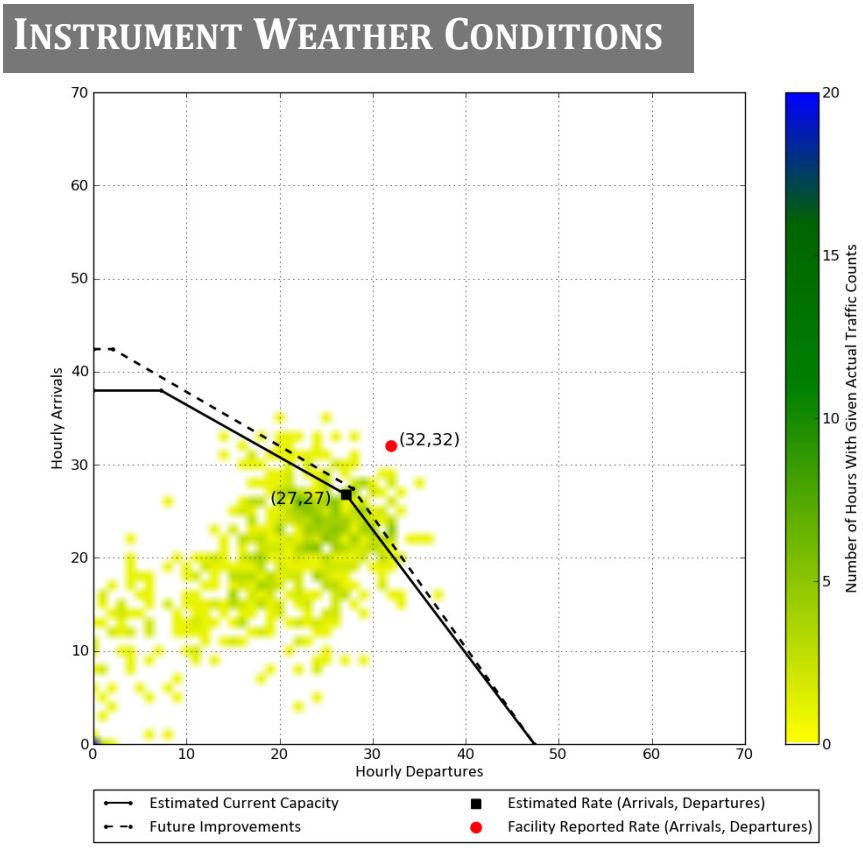

Figure 4.22: Airport Capacity Profile Estimate for Ronald Reagan Washington National Airport under Instrument Weather Conditions. Source: (Federal Aviation Administration, 2014b)

As we can see, the estimates of arrivals-only capacity fall between the estimated current capacity and the projected future improvements. The departures-only capacity is greater than the FAA estimate by roughly 4 operations and the point of even arrivals and departures sits near 24 and 24. While the comparisons are not an exact match, the profiles are somewhat similar.

For the DCA simulation, using aircraft-specific parameters resulted in a gain of 2 additional arrivals for the arrivals-only capacity estimate and also slightly increased the estimate of the maximum number of sequenced departures under mixed operations from 11.25 to 11.55. Increases in mixed operations capacity are arguably due to composite average not being used in the analysis. These averages will generally overestimate the ROT

on at least half of the respective aircraft grouping and mask the considerable variability that exists within many of the RECAT groupings. Figure 4.23 illustrates the variability of AROT for each of the six RECAT groups.

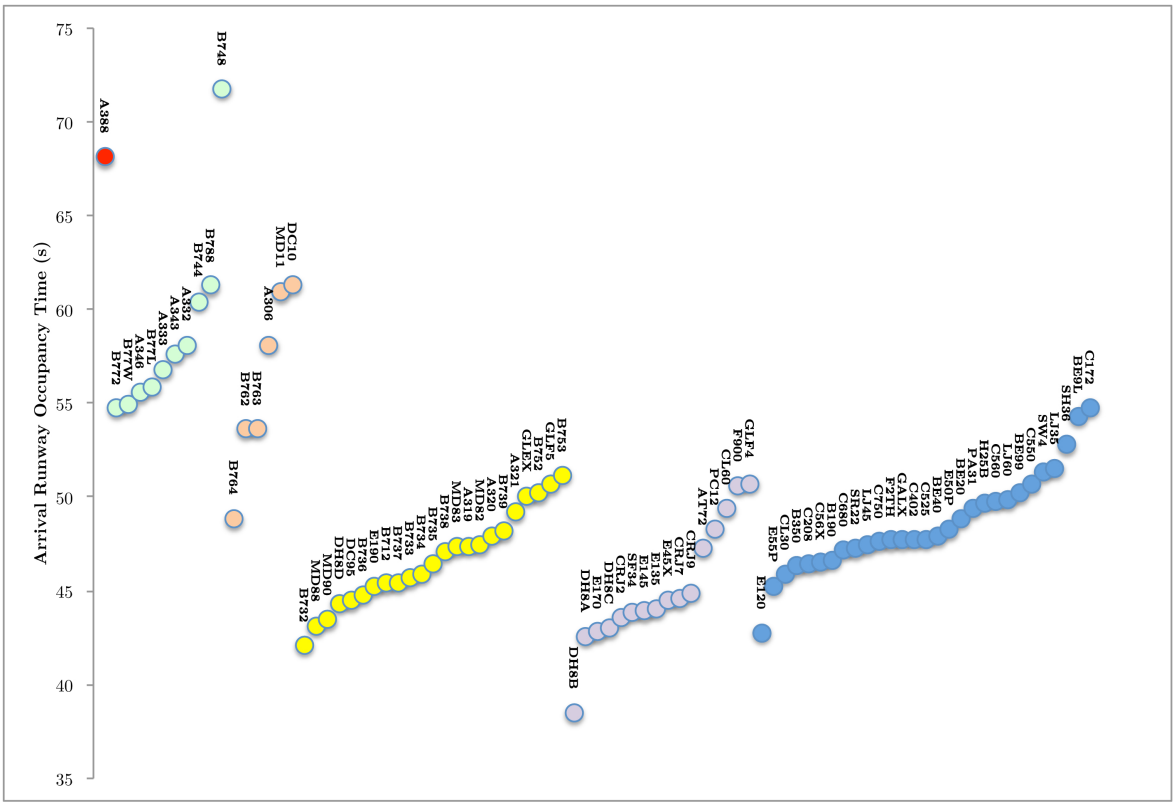

Figure 4.23: Illustration of Differences in AROT by RECAT Grouping. Red = A, Lime = B, Salmon = C, Yellow = D, Lavender = E, Blue = F

Departures-only capacity remains unaffected, likely due to the departure-departure separation requirements being the limiting factor in departure capacity. That is, the minimum separation standard is greater than most if not all DROT values. As such, the separation standards will determine the number of departure operations possible, instead of the DROT.

For our second group of scenarios, we consider mixed operations on Runway 27 at San Diego International Airport having the following proportions of aircraft.

Table 4.48: Fleet Mix of Synthetic Schedule by Individual Aircraft Type and RECAT Grouping

Group 2: Scenario 1						Group 2: Scenario 2	
Aircraft Type	Pct. of Fleet Mix	RECAT Group	Aircraft Type	Pct. of Fleet Mix	RECAT Group	RECAT Group	Pct. of Fleet Mix
C208	2.590%	F	DC93	0.001%	D	A	0.00%
E120	0.808%	F	GLF3	0.005%	E	B	1.25%
DH8D	1.365%	D	GALX	0.007%	F	C	2.55%
LJ75	0.021%	F	G150	0.006%	F	D	82.04%
B712	0.021%	D	MD82	0.416%	D	E	10.72%
CL30	0.001%	F	MD90	0.959%	D	F	3.44%
B737	25.533%	D	GLEX	0.006%	D		
B738	17.309%	D	E175	4.839%	E		
B735	0.001%	D	E135	0.001%	E		
B734	1.080%	D	E145	0.002%	E		
B733	8.386%	D	E170	0.047%	E		
B752	2.644%	D	H25B	0.006%	F		
B753	0.299%	D	LJ45	0.001%	F		
B764	0.005%	C	A306	0.198%	C		
B762	0.304%	C	A310	0.001%	C		
B763	1.830%	C	A320	8.974%	D		
B772	0.393%	B	A332	0.414%	B		
CRJ2	3.535%	E	A319	3.912%	D		
CRJ7	1.901%	E	A321	4.172%	D		
B736	0.009%	D	DC10	0.100%	C		
B739	6.465%	D	DC13	0.056%	F		
DC94	0.001%	D	MD11	0.052%	C		
B773	0.021%	B	GL6T	0.001%	D		
CRJ9	0.396%	E	B744	0.002%	B		
B73E	0.487%	D	B788	0.416%	B		

The aircraft type mappings are as follows: E175 ⇒ E170, B73E ⇒ B735, GL6T ⇒ GLEX, DC13 ⇒ BE99, G150 ⇒ H25B, B773 ⇒ B77W, LJ75 ⇒ LJ45, DC94 ⇒ DC95, DC93 ⇒ DC95, GLF3 ⇒ GLF4.

Figures 4.24 and 4.25 illustrate the results of the simulation while Figure 4.26 illustrates the FAA Airport Capacity Profile for SAN under instrument weather conditions (Federal Aviation Administration, 2014c).

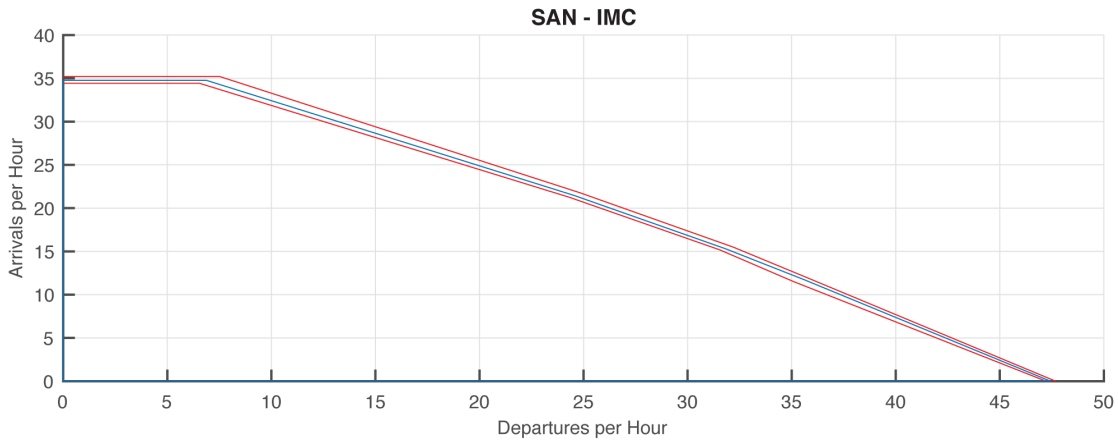

Figure 4.24: Model Output from QuickRunSim utilizing Aircraft-Specific ROT Parameters

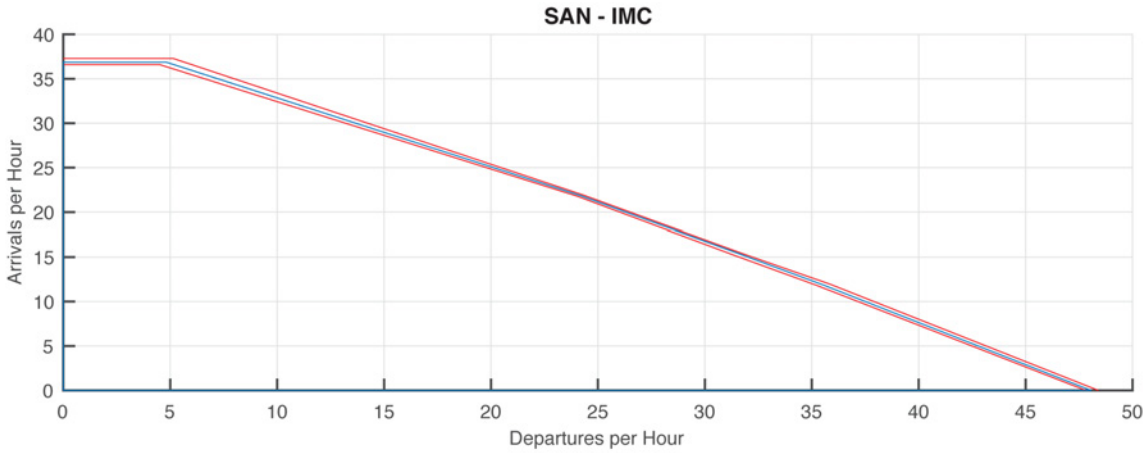

Figure 4.25: Model Output from QuickRunSim utilizing RECAT Grouping Composite ROT Parameters

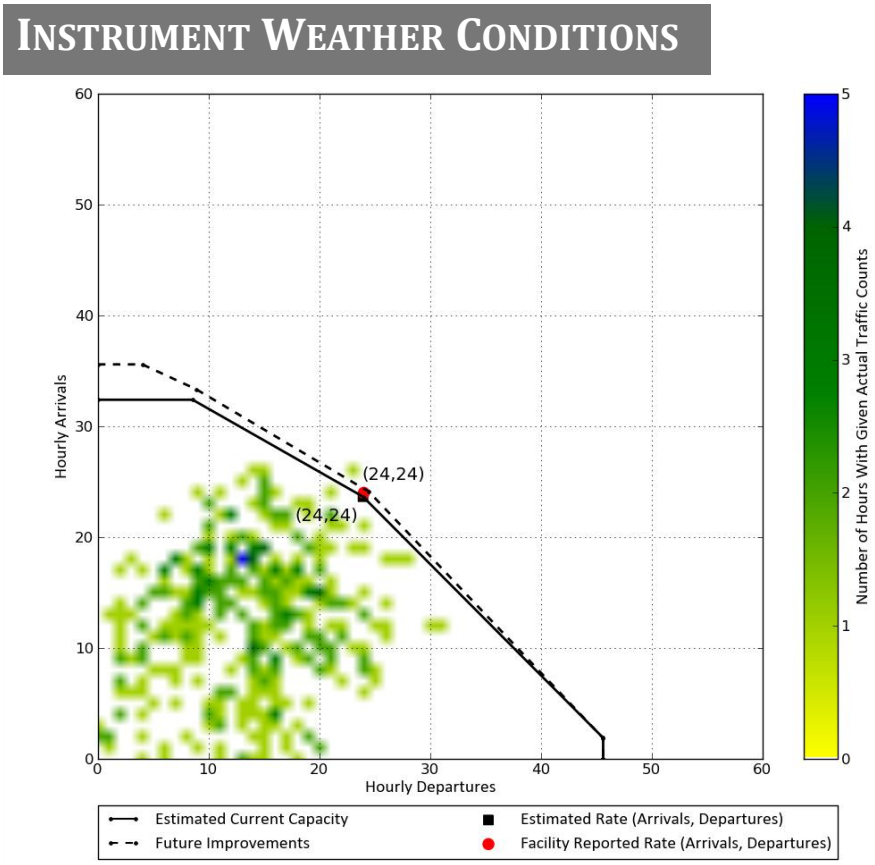

Figure 4.26: Airport Capacity Profile Estimate for San Diego International Airport under Instrument Weather Conditions. Source: (Federal Aviation Administration, 2014c)

The estimates of arrivals-only capacity again fall between the estimated current capacity and the projected future improvements while the departures-only capacity is slightly greater than the FAA estimate. The point of even arrivals and departures sits near 22 and 22 and the maximum number of sequenced departures under 100% arrivals priority also exactly matches that of the FAA estimate. Thus, we conclude that the QuickRunSim output is reasonable when compared against the FAA estimate.

In contrast to the DCA simulation, the use of aircraft-specific parameters resulted in a loss of 2 operations for the arrivals-only capacity estimate while increasing the maximum number of sequenced departures under mixed operations by 2 operations. The SAN simulation further illustrates the problem with using group averages of ROT. Referencing Figure 4.23, we

see that for RECAT Group B, the mean AROT values range from 55 seconds to 72 seconds. It is possible that the drop in arrivals-only capacity relative to the RECAT Pareto Diagram was perhaps the result of a Group B aircraft's AROT having been underestimated with the composite group average AROT. RECAT Group C also exhibits considerable variability and may have also led to the drop in arrivals-only capacity. In short, the SAN simulation illustrates how the use of group averages can lead to overestimates of airport capacity.

4.11 Concluding Remarks

The ACRP 79 proposed classifying Airfield Capacity Evaluation Tools by five levels of sophistication: (1) Table Lookup, (2) Charts, Nomographs and Spreadsheets, (3) Analytical Capacity Models, (4) Airfield Capacity Simulation Models and (5) Aircraft Delay Simulation Models (LeighFisher, 2012). Inputs for models at level 3 and above include arrival and departure runway occupancy times, which are provided by the models presented in this work. The immediate benefit of the predictive models is the ability to move away from aggregate measures of runway occupancy time and take-off distance. This is evident from observing the variability in average departure and arrival runway occupancy times extracted from the data used to produce the models. As illustrated by Figure 4.23, there exist considerable within-group variability that can now be considered in future analyses of runway capacity.

An additional benefit of the models presented is that they now obviate the need for time-consuming and expensive field collection of arrival and departure runway occupancy times. Furthermore, critical "what-if" analyses of runway capacity are now possible when considering new aircraft types that may utilize airports in the future. Analysts now have available, models that can provide departure and arrival runway occupancy times and departure take-off distances with a high degree of predictive accuracy. The additional benefit of utilizing Bayesian predictive models is that the output are in the form of probability distributions that can be readily used in the numerous airfield and airspace simulation models that accept them.

This chapter has described and contributed to the field, three predictive models of arrival and departure runway occupancy times and departure take-off distance. In our opinion,

the aircraft specific and airport specific data produced by these models will ultimately yield more refined and precise analyses of airport capacity.

Chapter 5

A Coplanar Commercial Aircraft Horizontal Flight Trajectory Optimization Model

5.1 Background

Air transportation analysts continue to be consumed with determining new methods and practices that will both provide further gains in operational efficiency and capacity and reduce fuel and operational expense. Fuel costs, in particular, are of acute concern to the industry as changes in fuel prices and consumption can determine whether operations are profitable or loss-making.

A number of new initiatives associated with NextGen, the FAA initiative to modernize the U.S. air transportation system, have been proposed and/or implemented with the express goal of reducing fuel costs and usage. For example, new Required Navigation Performance (RNP) flight procedures have been anticipated to save $60 million dollars a year in fuel costs for Southwest Airlines alone (GreenBiz Editors, 2011). Even greater savings are promised by the eventual move to GPS-based navigation, which it is hoped will free airlines from having to fly along predefined airways. Instead, airlines will be able to route aircraft along optimized flight trajectories from origin to destination. Thus,

determination of these trajectories becomes key to the goals of enhancing airline operational efficiency and minimizing costs.

In this chapter, we present a coplanar flight trajectory optimization model that utilizes available wind and air temperature data to provide optimal trajectories. It is important to note that an "optimal" trajectory will depend on the parameter or collection of parameters to be optimized. For this model, we aim to minimize the total travel time along a route. We also construct a simulation both to demonstrate the model and to investigate the potential benefits of utilizing wind optimal flight trajectories. For this simulation, we construct an airline airline network and compare estimated fuel burn savings for routings along the wind optimal flight trajectories as opposed to the great-circle trajectories.

5.2 Literature Review

The problem of optimally navigating a vehicle within a fluid was first dealt with by Ernst Zermelo through *Zermelo's Navigation Problem*. In 1931, Zermelo first proposed the minimum-time path problem for a boat moving through a region of strong currents (Zermelo, 1931). The goal was to determine an optimal path for a boat navigating in a body of water in presence of water currents and wind. Considered a classic optimal control problem, Zermelo's work is the foundation to which much of the current work on aircraft flight trajectory optimization can be traced.

A solution to Zermelo's problem would later come from Bryson and Ho, who developed a solution technique called neighboring optimal control (NOC) (Bryson and Ho, 1975). Bryson presents the NOC solution for the Zermelo problem with constant wind shear both numerically and analytically (Bryson, 1998). Under the NOC technique, a time-varying feedback control is produced that minimizes a performance index to second order perturbations from a nominal optimal path. However, while the perturbations in the nominally optimal states can be compensated for, errors in the system dynamic model parameters may result in suboptimal performance (Jardin and Bryson, 2001).

Dynamic programming, directed graph and discrete methods have also been utilized in flight trajectory estimation. In the 1950s, R. Dixon Speas and his aviation company offered

clients flight trajectory optimization using discrete dynamic programming. The flight path to be analyzed was divided into discrete regions and wind data were sourced from weather balloons. Lou Reinkins of Lockheed later began offering flight planning services to airlines and private aviators in the 1970s for flights in the United States. His flight plans also utilized directed graph methods (Jardin, 2003). Le Sellier also considers discrete methods in flight trajectory optimization. In his work, he highlights the inefficiencies of flight planning optimization software that utilized, prior to a flight's departure, the Cost Index concept, which is the ratio of the time-related costs incurred by an extra hour of flight to the fuel-price (Le Sellier, 1999). Another discrete method is offered by How and Richards. They present a mixed-integer linear program for aircraft collision avoidance that can also be extended to multiple waypoint flight-path planning (Richards and How, 2002). Devulapalli also demonstrates a discrete method that utilizes the A* algorithm in incorporating flight trajectory constraints placed on commercial aircraft in flight by air traffic regulations (Devulapalli, 2012).

Ng et al. presented an optimization algorithm to provide wind-optimal trajectories that minimized the climatic impact of aircraft in terms of global warming potentials. The optimal trajectory algorithms presented were generated by repeatedly calculating horizontal trajectories for a variety of cruising altitudes. Ng et al. demonstrated time savings and a reduction in climatic impact over great-circle trajectories. However, since the constraints of the optimization included those aimed at minimizing climatic impacts, it is unclear how well the trajectories of Ng et al. would compare against unconstrained wind-optimal trajectories (Ng et al., 2011).

Wickramasinghe et al. approached the issue of 4-D flight trajectory optimization through use of a dynamic programming approach. In their study, they optimized flight trajectories using aircraft operational and performance data, weather forecasts and air traffic control data from which they set operational constraints. Wickramasinghe et al. did not provide speed benchmarks of their process. In estimating the fidelity of their results, they illustrated performance gains over historical flight data, but it is unclear how well their method would perform against strictly optimal flight paths (Wickramasinghe et al., 2012).

Ng et al. next presented a trajectory-optimization algorithm for approximately minimizing aircraft travel time and fuel burn. In their study, they computed minimum-time

routes in wind on multiple horizontal planes and utilized an aircraft fuel burn model for generating fuel-optimal vertical profiles. Ng et al. illustrated a potential savings of up to 3% in fuel burn over flights that operate at a single cruise altitude (Ng et al., 2014).

A heuristic routing algorithm is presented by Hewitt and Broatch, in which routes are constructed in stepwise fashion (Hewitt and Broatch, 1992). In their algorithm, which closely resembled a genetic algorithm, routes were constructed in stepwise fashion so as to minimize the route distance, fuel usage, and other metrics that comprised the total route cost.

Guided by the literature, we aim to demonstrate the feasibility and effectiveness of a general horizontal flight trajectory optimization model, capable of providing wind-optimal flight trajectories at high levels of detail.

5.3 Model Description

In this section, we describe the capabilities of the flight optimization model. Given the necessary inputs, the model will produce wind-optimized flight trajectories at the desired flight levels using the user-selected wind and air temperature data and user-defined routings.

The organization of this section will be as follows. First, we describe the full set of user inputs necessary. Next, we illustrate the underlying methodology and analytical approach utilized by the model in producing wind optimal flight trajectories. Finally, we provide a description of the model output.

5.3.1 Technical Overview

Figure 5.1 displays a high-level operational flow chart that describes the order in which data are loaded and processed and illustrates points at which user input is required.

Route Definition

In executing a flight plan, the first task is to select or define the set of airports that will comprise the origin-destination pairs to be analyzed. Currently, the model has incorporated

more than 7,000 distinct worldwide airports from which users can select. Given either an ICAO or IATA airport code, the model will search the airport database and present any matching results located. Once the user confirms the selection, the model will query whether the user wishes to enter additional airports.

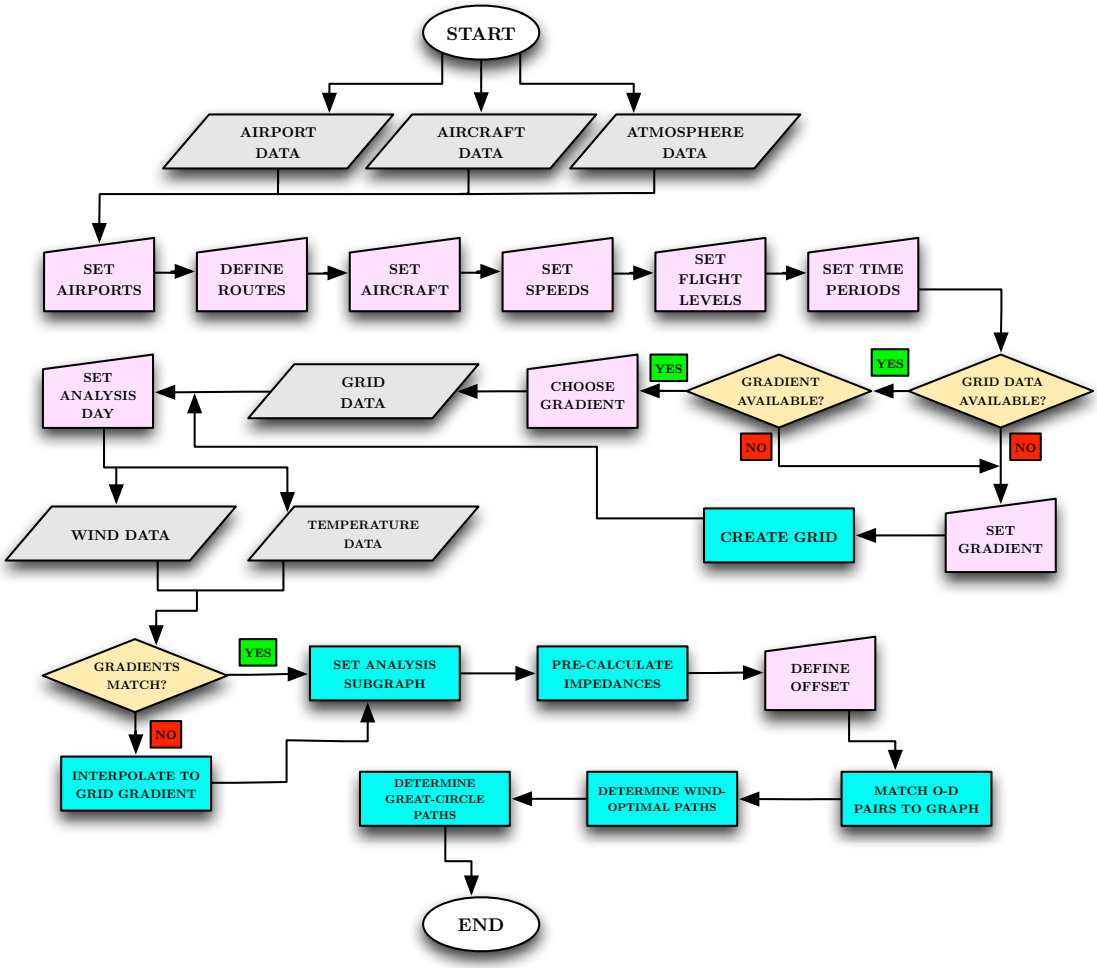

Figure 5.1: Flight Trajectory Model Operational Flowchart

Next, a user defines routings from their set of selected airports. Once these routings are set, the user then assigns aircraft to each routing. Users are able to select from a set of aircraft that correspond to those available in the Base of Aircraft Data (BADA) database.

The user then sets the desired cruise speed, which is assumed to be constant throughout

the flight.

Available Analysis Flight Levels and Time Periods

The NCEP/NCAR Reanalysis Wind Vector and Air Temperature Data contain 17 distinct flight levels corresponding to the atmospheric pressure levels listed in Table 5.1 and 4 distinct daily time periods. The user's choice of flight levels and time periods will determine the Wind and Air Temperature data sets with which the Impedance matrix will be calculated. Users are able to choose any flight level within the range spanned by the 17 flight levels. For flight levels not initially available, linear interpolation is performed to construct an equivalent wind vector field for the chosen flight level or flight levels. Similarly, the air temperature data is also linearly interpolated to match the chosen flight level.

Table 5.1: Atmospheric Pressures (millibars) of Available Flight Levels

1000	925	850	700	600	500	400	300	250
200	150	100	70	50	30	20	10	

Users can choose one or all of the four 6-hour daily time periods for analysis. For each time period chosen, separate analyses will be conducted using a separate full set of flight levels. Table 5.2 lists the time periods available for analysis.

Table 5.2: Available Time Periods for Analysis.

00:00 — 06:00	06:00 — 12:00	12:00 — 18:00	18:00 — 24:00

Formation of Analysis Graph

Once the route data is entered, the flight planning function will search for preformed graph data. If none is available, the function will request that the user enter a separation gradient and will begin formation of a dense rectangular graph on which wind-optimized flight paths will be estimated. Figure 5.2 provides an example of an analysis graph.

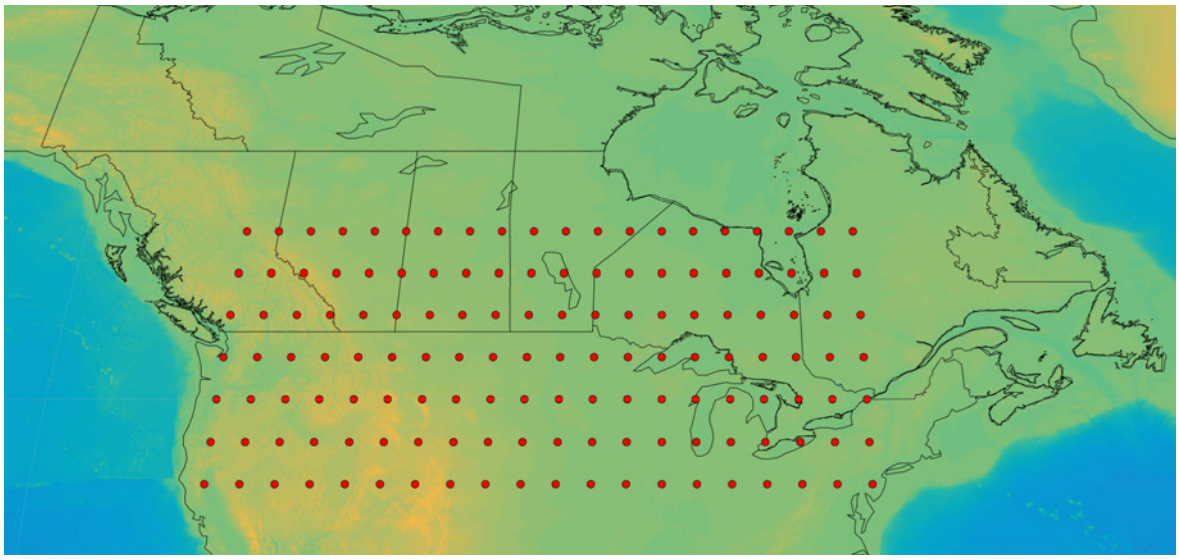

Figure 5.2: Illustration of an Example Analysis Graph covering the Majority of Southern Canada and the Northern United States. Nodes have 2.5 ° spacing in both Latitude and Longitude

For this graph, each node is spaced at 2.5 degrees from each other. Available gradients are those that allow for the division of the globe into an integer value of evenly spaced grid points. Table 5.3 lists the gradients available.

Table 5.3: List of Available Graph Gradients in Degrees

0.50	0.60	0.72
0.75	0.80	0.90
0.96	1.00	1.20
1.25	1.44	1.50
1.60	1.80	2.00
2.25	2.40	2.50

To allow for greater freedom in flight path estimation and to provide for finer solutions, each node within the graph has up to forty-eight unique node-arc connections for forty-eight degrees of freedom as illustrated by Figure 5.3. The node in red illustrates a subject analysis node and the nodes in dark gray illustrate the nodes connected to the analysis node.

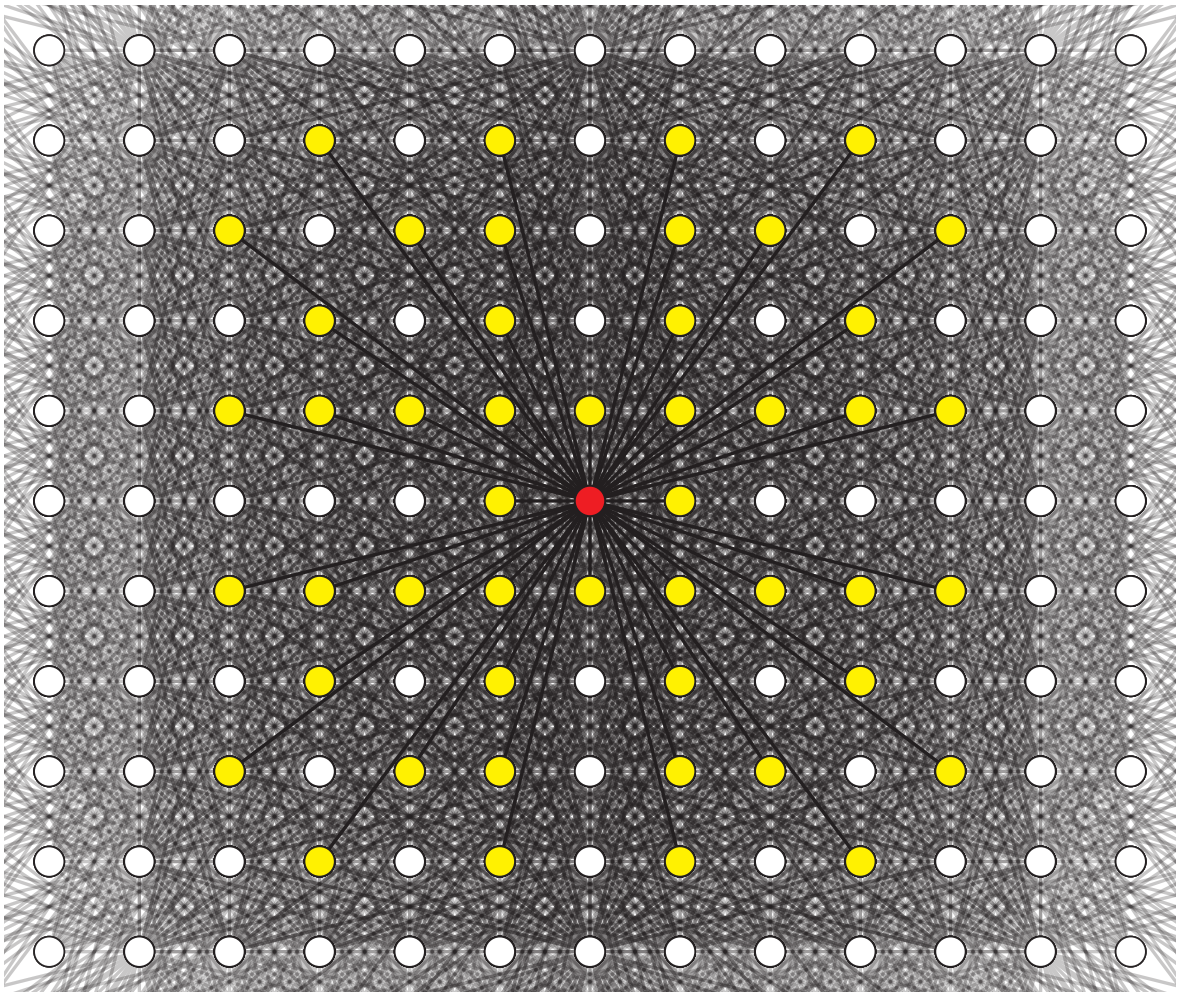

Figure 5.3: Illustration of the Density of the Analysis Graph and the Maximum Available Degrees of Freedom for an Analysis Node

Selection of Wind & Air Temperature Data

The next task is to select the wind and air temperature data corresponding to the user-provided analysis date. The function utilizes raw wind and air temperature data sourced from the NCEP/NCAR Reanalysis 1 Summary dataset (Kalnay et al., 1996). Figures 5.4 and 5.5 provide illustrative examples of the parsed wind and air temperature data.

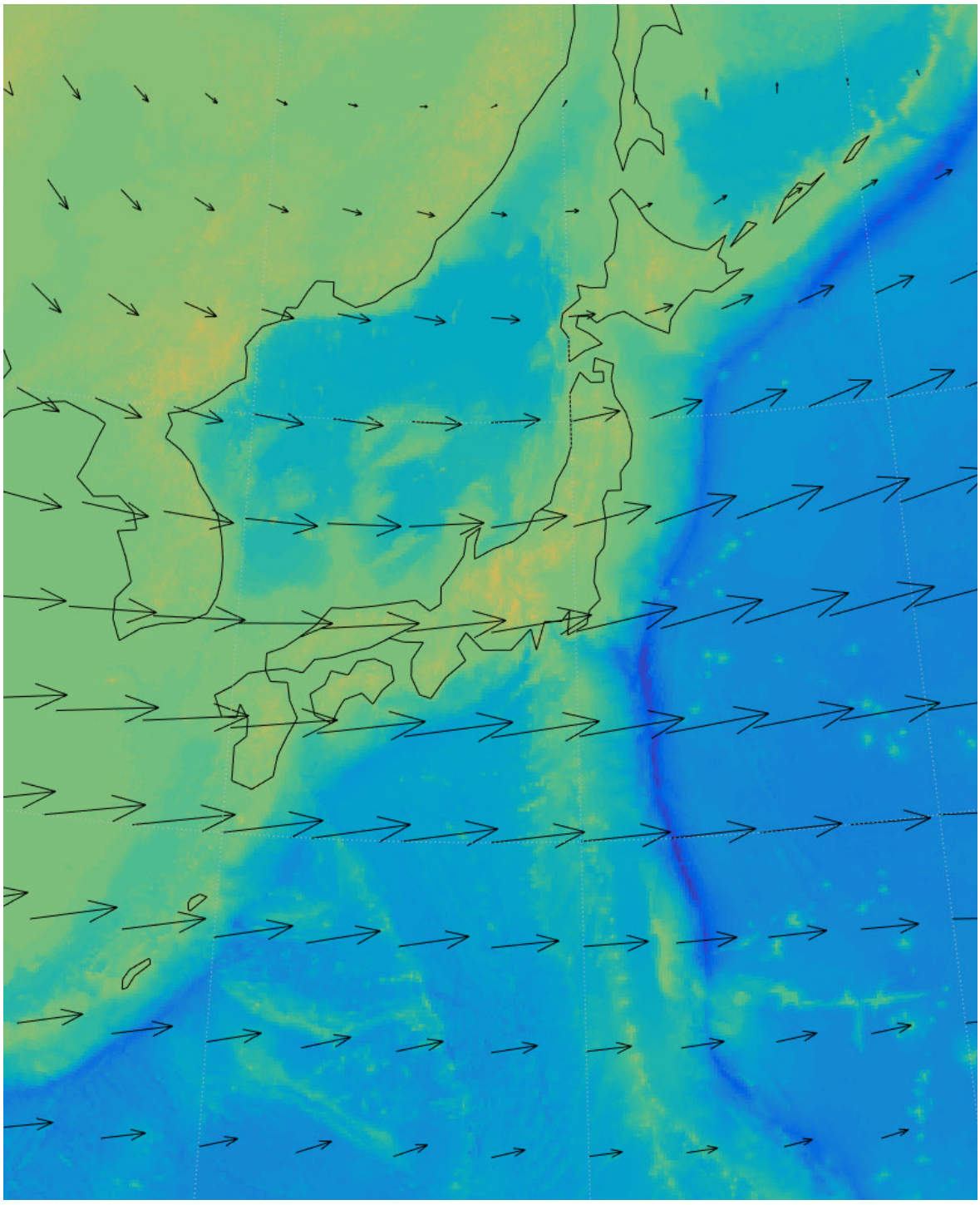

Figure 5.4: Example of Parsed Wind Vector Data centered over Japan

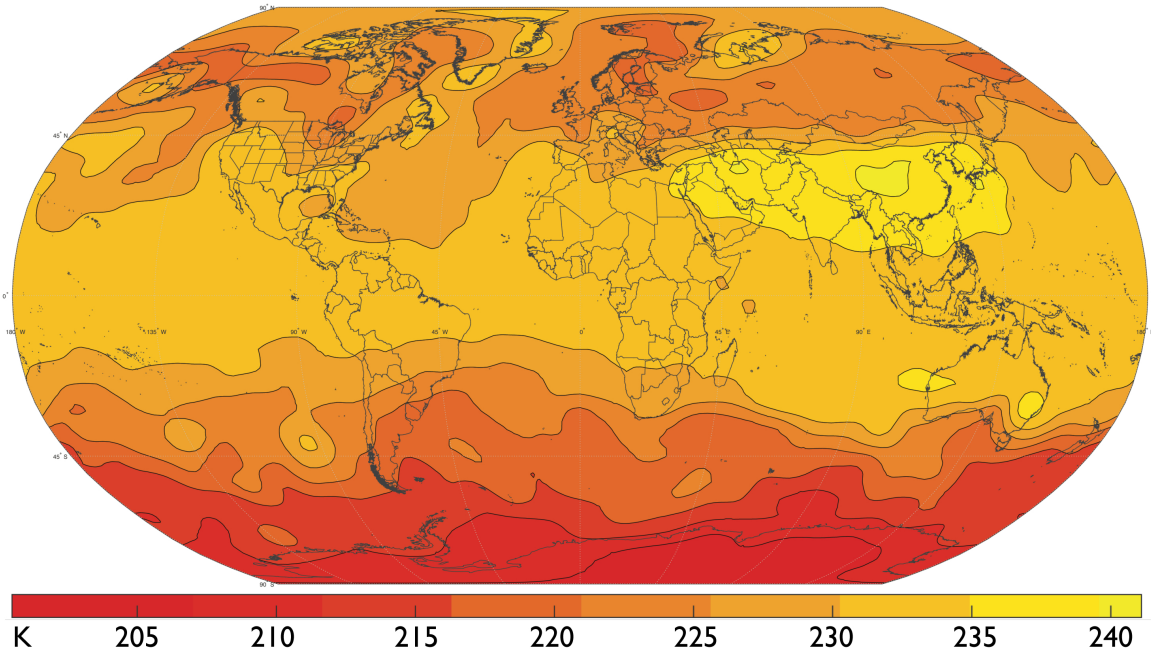

Figure 5.5: Example of Parsed Global Air Temperature Data

The raw NCEP/NCAR Reanalysis data provide global measurements at intervals of 2.5 degrees (roughly 150 nautical miles). Depending on the analysis graph gradient previously chosen, interpolation of the wind and air temperature data may be necessary. Linear interpolation is currently utilized in the interpolation and Figure 5.6 provides an example of interpolation from 2.5° to 0.5°. The quiver arrows in red represent the wind field at 0.5° spacing while the arrows in black represent the original 2.5° spacing.

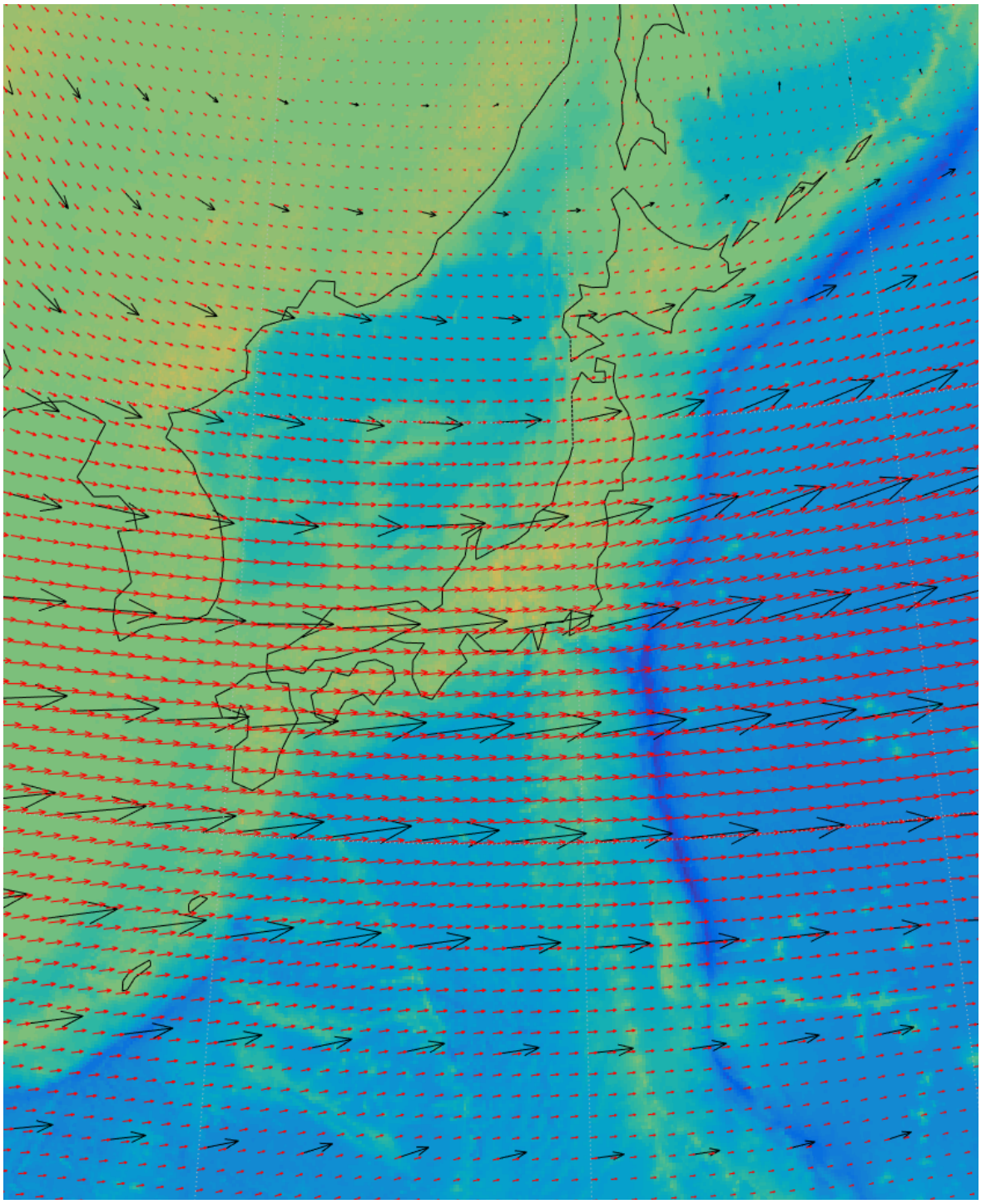

Figure 5.6: Example of Interpolated Wind Vector Data superimposed over Parsed Wind Vector Data centered over Japan

Creation of Analysis Subgraph

A subgraph of the global analysis graph will be utilized both to save processing time and to reduce memory usage. The extent of the subgraph is set by using a subset of airports at the furthest extremes (i.e., the northernmost, southernmost, easternmost and westernmost airports). Great circle routes are determined between each airport in this subset. The locations of the extreme points on these routes will initially determine the boundary edges of the graph. Next, a margin is added to the eastern and western longitude boundaries and the northern and southern latitude boundaries. The formula used to determine the margin was estimated empirically from observing the extent to which actual flight data deviated from great circle routings. Before applying the formulae, the values *DegDistLat* and *DegDistLon* are determined. These respectively correspond to the degree distance between the current northern and southern latitude boundaries and the degree distance between the current eastern and western longitude boundaries. Equations (5.1) and (5.2) outline the formulae used to determine the margins.

$$\text{Latitude Margin} = \frac{10 \times DegDistLat}{84} \tag{5.1}$$

$$\text{Longitude Margin} = \frac{10 \times DegDistLon}{84} \tag{5.2}$$

Pre-calculation of the Impedance Matrix

The flight planning function will calculate an impedance matrix for every combination of flight level and time period chosen. This impedance matrix will mirror the analysis graph in size and connectivity. The impedance on an arc is the resultant wind velocity at the origin node in the direction of the destination node as illustrated by Figure 5.7.

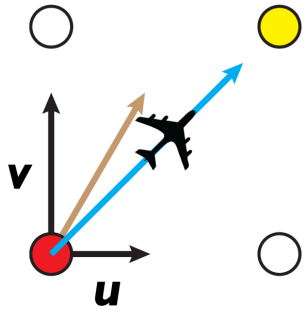

Figure 5.7: Illustration of Resultant Wind Vector

For destination nodes not immediately adjacent to the origin node, the resultant wind velocity is determined piecewise. The resultant wind is first determined to the midpoint(s). At the midpoint, the wind components are taken to be the distance-weighted mean values of the encompassing nodes. These wind components are then used to determine the resultant wind velocity for the next piece until all pieces are calculated. Figure 5.8 demonstrates the piecewise resultant wind vector.

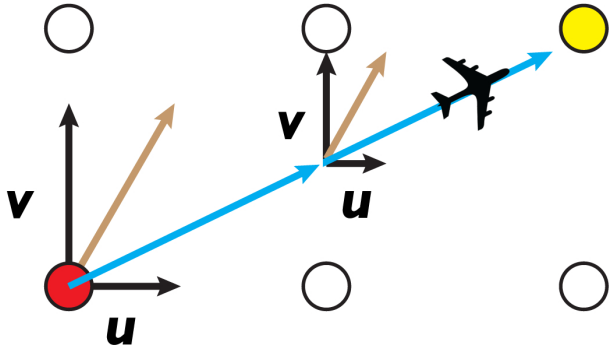

Figure 5.8: Illustration of Piecewise Resultant Wind Vector

In addition to resultant wind vectors, the total distances along arcs connecting origin nodes to destination nodes are calculated. Air temperatures at the origin nodes are also calculated. For destination nodes not adjacent to the origin node, the air temperature is determined at the midpoint(s) to the destination node as the distance-weighted mean of the air temperatures at the encompassing nodes.

The air temperatures T are utilized in determining the speed of sound V_{sound} along the

arc portions. This will be necessary in determining the flight time along the arc. To find the speed of sound, we use

$$V_{sound} = 331.3\sqrt{\frac{T}{273.15}} \text{ m/s} \tag{5.3}$$

where T is in degrees Kelvin.

Match O-D Pairs to Analysis Subgraph

Once the impedances have been pre-calculated, the function begins matching the origin and destination nodes for each defined routing to the analysis subgraph. The user is first asked to define an offset distance in nautical miles from the true origin and destination. This is to account for the time and distance needed to climb to the desired flight level. The function then calculates a great-circle trajectory and sets the starting point of the flight path to be a point spaced at the user-defined offset distance away from the true start along the great-circle trajectory in the direction of the true destination point. Similarly, the ending point of the flight is set to be a point spaced at the user-defined offset distance away from the true destination point along the great-circle trajectory in the direction of the true starting point. The function then locates the closest grid points to the defined starting and ending points. These grid points will represent the start and end of the flight trajectory to be estimated on the analysis subgraph.

Figure 5.9 illustrates the offset starting and ending points, colored yellow and spaced 10 nautical miles away from the true origin and destination, for a flight from Ottawa to Vancouver. Next, Figure 5.9 shows the closest grid points, colored blue, that will be taken as the start and end nodes of the estimated flight trajectory.

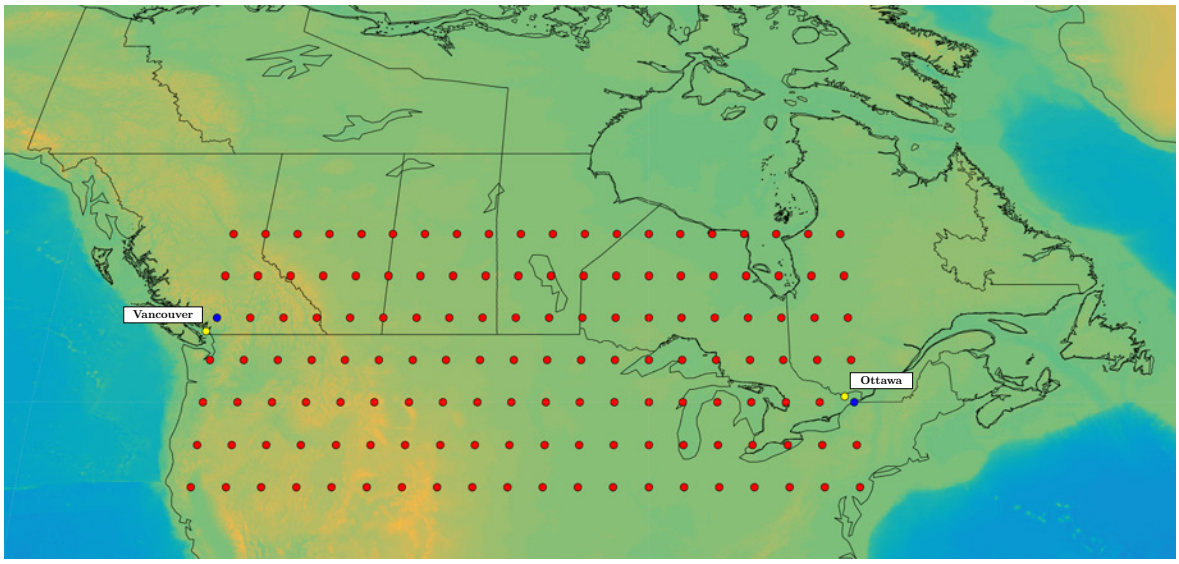

Figure 5.9: Illustration of Offset Start and End Points and Matched Grid Nodes for a flight from Ottawa to Vancouver

5.4 Optimal Flight Plan Construction

With the resultant wind velocity V_{wind}, and the speed of sound on the arc V_{sound} having been pre-calculated, the flight time, FT, on any arc can now be determined. For an arc having a length D, the flight time is given by

$$FT = \frac{D}{V_{wind} + (M \times V_{sound})} \tag{5.4}$$

where M is the user-defined cruise speed in Mach.

In order to construct wind-optimal paths, the function utilizes the A* search algorithm, which we define further below.

5.4.1 A* Search Algorithm

The A* (pronounced as "A star") search algorithm is an informed search algorithm first presented by Hart, Nilsson and Raphael in 1968 (Hart et al., 1968). Starting from an initial

node, the algorithm supposes that there exists an evaluation function $\hat{f}(n)$ for any node n such that an available node having the smallest value of $\hat{f}$ is the node that should be explored next. This evaluation function consists of two parts: the cost from the start node to node n, represented as $g(n)$, and a heuristic estimate of the cost from node n to the goal or end node, represented as $h(n)$. With the evaluation function, the algorithm is defined as follows:

1. Initialize an OPEN and a CLOSED list of nodes
2. Set a node or nodes as goal nodes and put these in the node set T.
3. Set a starting node as node s and mark this node as OPEN. Calculate or assign a value of $\hat{f}(s)$.
4. If the OPEN list is empty, END.
5. Set as node c, the node in the OPEN list with the lowest value of $\hat{f}$.
6. If $c \in T$, END.
7. Remove c from the OPEN list and add to the CLOSED list
8. For each neighbor p of c:
   $g(p)$ is the cost from s to p
   $g(c)$ is the cost from s to c,
   - If p is CLOSED, ignore.
     - Otherwise, calculate $t(p) = g(c) + d(c, p)$ where
       $d(c, p)$ is the cost or distance from c to p.
     - If p is OPEN but $t(p) \geq g(p)$, ignore.
       * Otherwise, if p is not OPEN, set p as OPEN.
       * Set predecessor of p as c and set $g(p) = t(p)$.
       * Calculate for p, $\hat{f}(p) = g(p) + h(p)$ where
         $h(p)$ is the heuristic cost estimate from p to a goal node.
9. Return to 4

5.4.2 Application of the A* Search Algorithm

The behavior of the A* search algorithm is primarily determined by the choice of heuristic and each chosen heuristic should be geared towards the problem to be solved. For the algorithm to successfully return the shortest path, it is necessary that the chosen heuristic be *admissible*. If we set $h^*(n)$ as the actual cost from a node n to the nearest goal node, then we can say a heuristic is admissible on the graph if and only if $h(n) \leq h^*(n)$ for every $n \in G$. which means that it can never overestimate the actual cost to reach the nearest goal node.

For the flight trajectory optimization model, the flight time from a node n to the destination e would be determined as

$$FT_{n \to e} = \frac{GCD_{n \to e}}{V_{wind,avg} + (M \times V_{sound,avg})} \tag{5.5}$$

where $GCD_{n \to e}$ is the great-circle distance from node n to destination e, $V_{wind,avg}$ is the average wind from n to e and $V_{sound,avg}$ is the average speed of sound from n to e. In the presence of zero wind, the flight time would become

$$FT_{n \to e} = \frac{GCD_{n \to e}}{(M \times V_{sound,avg})} \tag{5.6}$$

and in the face of a positive headwind, the flight time becomes

$$FT_{n \to e} = \frac{GCD_{n \to e}}{-V_{wind,avg} + (M \times V_{sound,avg})} \tag{5.7}$$

Since positive headwind would always lead to longer flight times, the zero wind great-circle flight time may be a good heuristic choice since it would never underestimate the flight time. However, if we consider the case where favorable winds (negative headwinds) are present throughout the flight, then (5.6) becomes an overestimate of the true flight time since

$$FT_{n \to e} = \frac{GCD_{n \to e}}{(M \times V_{sound,avg})} > FT_{n \to e} = \frac{GCD_{n \to e}}{V_{wind,avg} + (M \times V_{sound,avg})}$$

One way to address this is to consider the maximum possible favorable resultant wind vector in the direction of travel that exists in the wind vector field that is applicable to our analysis

subgraph. If we label this as $V_{wind,max}$, then the flight time from node n to destination e becomes

$$FT_{n\to e} = \frac{GCD_{n\to e}}{V_{wind,max} + (M \times V_{sound,avg})} \tag{5.8}$$

Additionally, we can utilize the maximum value of V_{sound} which would be obtained from the maximum value of air temperature within the analysis region. Therefore, we have

$$FT_{n\to e} = \frac{GCD_{n\to e}}{V_{wind,max} + (M \times V_{sound,max})} \tag{5.9}$$

Since it follows that

$$\frac{GCD_{n\to e}}{(V_{wind,max} + M \times V_{sound,max})} < \frac{GCD_{n\to e}}{V_{wind,avg} + (M \times V_{sound,avg})} < \frac{GCD_{n\to e}}{-V_{wind,avg} + (M \times V_{sound,avg})}$$

we can utilize (5.9) as an admissible heuristic for the A* search algorithm.

Determining $V_{wind,max}$

For an angle θ relative to the zonal wind vector, a zonal wind magnitude of A and a meridional wind magnitude of B, the resultant wind vector is given as

$$V_{resultant} = A\cos\theta + B\sin\theta \tag{5.10}$$

Figure 5.3 defines the possible arcs for an analysis node and also sets out the possible angles for that arc relative to the zonal wind vector. For example, for the node that sits one gradient multiple to the right of the analysis node and one gradient multiple up from the analysis node, the connecting arc would form an angle of 45° (arctan(1)) relative to the zonal wind vector. Table 5.4 lists all possible combinations of distances (rising distance and running distance) and angles from an analysis node.

The maximum possible tailwind is then found through evaluating all possible combinations of magnitudes of zonal and meridional wind and arc angle for a given wind vector field.

Table 5.4: List of All Possible Angles and Rising and Running Gradient Multiple Distance Combinations for a Connecting Arc relative to the Zonal Wind Vector in an Analysis Subgraph

1:1	(45°)	1:2	(26.57°)	1:3	(18.43°)	1:4	(14.04°)
2:1	(63.43°)	2:3	(33.69°)	3:1	(71.57°)	3:2	(56.31°)
3:4	(36.87°)	4:1	(75.96°)	4:3	(53.13°)	-1:1	(-45°)
-1:2	(-26.57°)	-1:3	(-18.43°)	-1:4	(-14.04°)	-2:1	(-63.43°)
-2:3	(-33.69°)	-3:1	(-71.57°)	-3:2	(-56.31°)	-3:4	(-36.87°)
-4:1	(-75.96°)	-4:3	(-53.13°)	1:-1	(-45°)	1:-2	(-26.57°)
1:-3	(-18.43°)	1:-4	(-14.04°)	2:-1	(-63.43°)	2:-3	(-33.69°)
3:-1	(-71.57°)	3:-2	(-56.31°)	3:-4	(-36.87°)	4:-1	(-75.96°)
4:-3	(-53.13°)	-1:-1	(45°)	-1:-2	(26.57°)	-1:-3	(18.43°)
-1:-4	(14.04°)	-2:-1	(63.43°)	-2:-3	(33.69°)	-3:-1	(71.57°)
-3:-2	(56.31°)	-3:-4	(36.87°)	-4:-1	(75.96°)	-4:-3	(53.13°)

5.4.3 Great-Circle Equivalent Path Construction

For comparison, the function also provides great-circle flight paths that are aligned with the nodes of the analysis subgraph. To do so, the function utilizes the A* algorithm but sets all wind vector values to be zero. The heuristic utilized is

$$FT_{n\to e} = (0.99)\frac{GCD_{n\to e}}{(M \times V_{sound,max})} \tag{5.11}$$

since it will always be true that

$$(0.99)\frac{GCD_{n\to e}}{M \times V_{sound,max})} < \frac{GCD_{n\to e}}{(M \times V_{sound,avg})}$$

5.5 Sample Results

In this section, we illustrate the results of a number of origin-destination (O-D) pairs used to validate the performance of the flight trajectory optimization model. For each of the O-D pairs, we analyzed the flight at approximately 34,000 feet and during the 06:00 - 12:00 daily wind time period for wind from January 4, 2012. Figure 5.10 illustrates the global wind field

for the date and time in question.

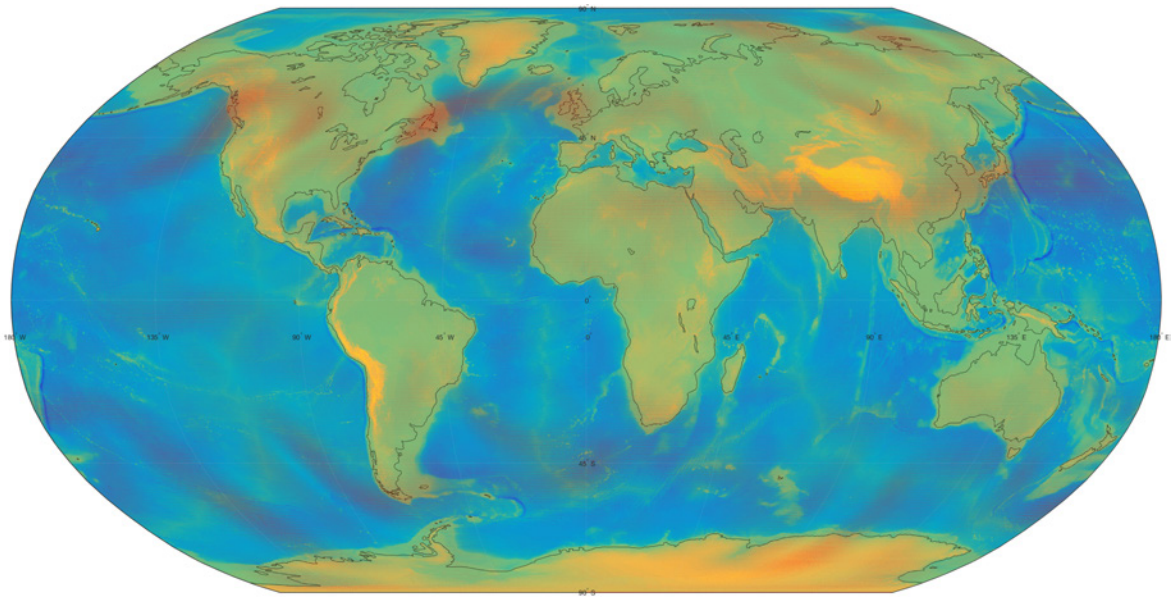

Figure 5.10: Display of the Global Wind Field for January 4th, 2012 for the Time Period 06:00 - 12:00 at a Flight Level of 34,000 feet

5.5.1 Ottawa-Vancouver Origin-Destination Pair

Figure 5.11 illustrates the flight trajectories produced for an A321-200 flying the Ottawa-Vancouver O-D pair at Mach 0.78. As can be seen, both wind optimal paths deviate significantly from the great-circle path. Due to the strong headwind circulating down from the northern Canadian territories, the Ottawa-Vancouver flight path takes a more southerly path and attempts to avoid facing the headwinds directly. We see that the route seems to follow in parallel with the United States - Canada border for the majority of the flight before vectoring towards Vancouver.

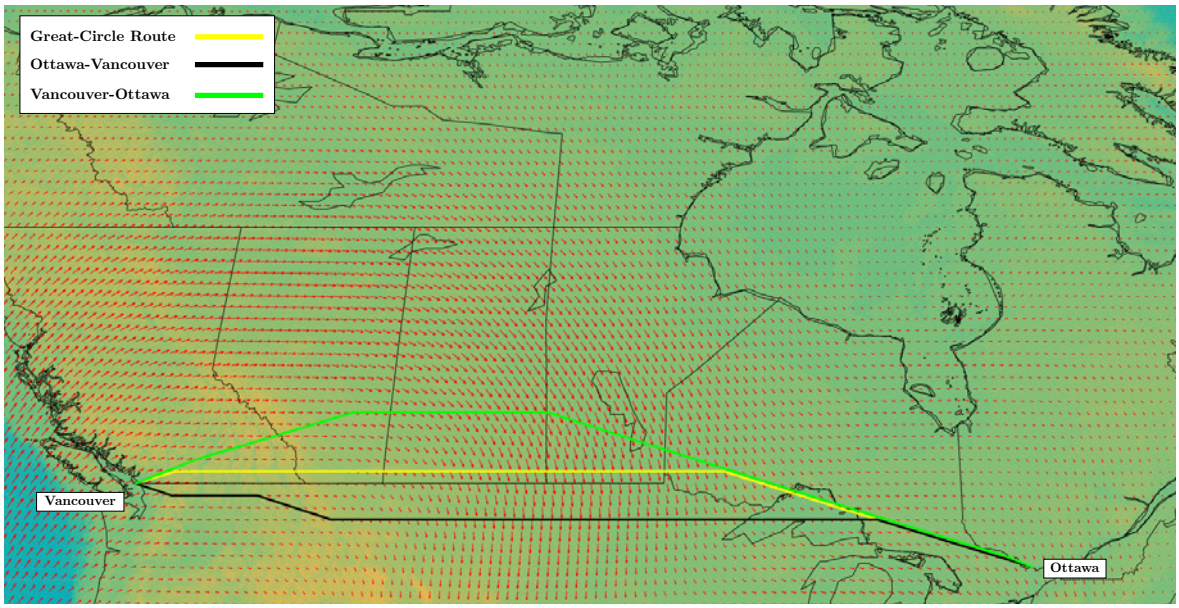

Figure 5.11: Ottawa-Vancouver Origin-Destination Pair with Great-Circle and Wind Optimal Trajectories operated by an Airbus A321-200

In contrast, the Vancouver-Ottawa trajectory is formed to take advantage of the east-flowing tailwind. The flight path quickly tracks to the northeast and follows along the with the curvature of the wind field. It levels off to a straight trajectory near the Alberta - Saskatchewan border before beginning to follow a southeastern heading towards Ottawa. The Vancouver-Ottawa flight essentially rides the tailwind for the entire flight to Ottawa and this is borne out in a comparison of the flight times and flown distances, displayed in Table 5.5. The flight to Ottawa from Vancouver is over an hour shorter than the flight from Vancouver to Ottawa.

If we compare the results of the great-circle routings to the wind-optimal routing, we see that for the Ottawa-Vancouver pair, the saving is roughly 3.98 minutes per flight. For the return leg to Ottawa, the savings is about 5.77 minutes per flight.

Table 5.5: Comparison of Flight Times and Flown Distances for the Ottawa-Vancouver O-D Pair. GC = great-circle, W = wind optimal

Routing	Flight Time (s)	Flown Distance (km)
Ottawa-Vancouver (GC)	17,328	3,531.1
Vancouver-Ottawa (GC)	13,668	3,531.1
Ottawa-Vancouver (W)	17,089	3,598.5
Vancouver-Ottawa (W)	13,322	3,566.6

5.5.2 Salt Lake City - Tokyo Origin-Destination Pair

Figure 5.12 illustrates the flight trajectories produced for a Boeing 777-200ER flying the Salt Lake City-Tokyo O-D pair at Mach 0.84. For this pair, we see that the trajectory from Salt Lake City to Tokyo tracks the great-circle path rather closely. This is primarily due to the presence of little wind along the majority of the route. The complete absence of wind would push the wind optimal trajectory to be the great-circle trajectory and this trend is illustrated by the Salt Lake City-Tokyo trajectory. In contrast, the flight to Salt Lake City comes nowhere near the great-circle path, but instead follows the east flowing tailwind for the entirety of the flight segment from Japan to the west coast of the United States. Once the tailwind begins to die down, we see the flight begin to vector towards Salt Lake City.

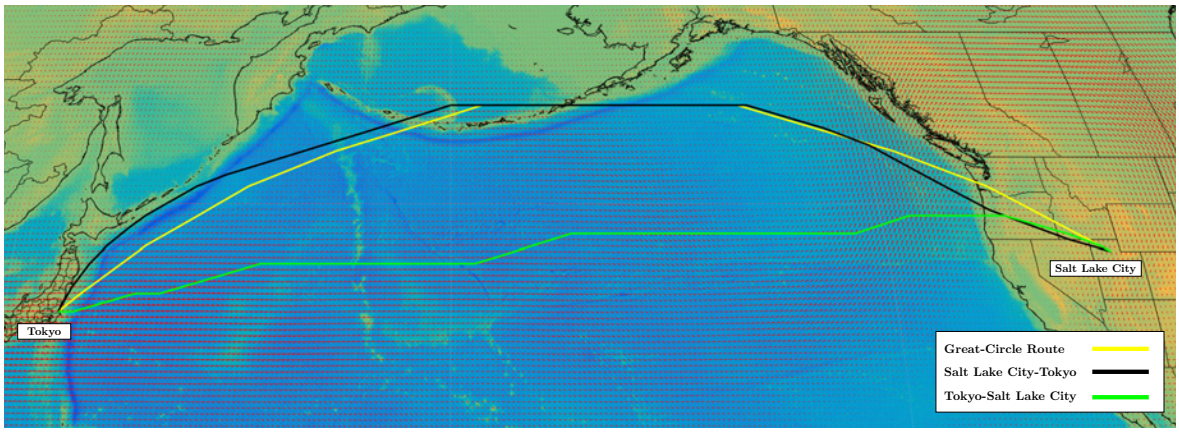

Figure 5.12: Salt Lake City-Tokyo Origin-Destination Pair with Great-Circle and Wind Optimal Trajectories operated by an Boeing 777-200ER

The time savings between the wind optimal and great-circle trajectories on the Tokyo-Salt Lake City leg are considerable. Flying the wind optimal path from Tokyo to Salt Lake City yields a time savings of 25.5 minutes per flight, which is even more striking considering that the distance flown is 458.4 kilometers greater than the great-circle distance. For the Salt Lake City-Tokyo leg, the time savings is not as pronounced at 9.28 minutes per flight. This is to be expected since the wind-optimal and great-circle trajectories are very similar.

Table 5.6: Comparison of Flight Times and Flown Distances for the Salt Lake City-Tokyo O-D Pair. GC = great-circle, W = wind optimal

Routing	Flight Time (s)	Flown Distance (km)
Salt Lake City-Tokyo (GC)	37,814	8,740.4
Tokyo-Salt Lake City (GC)	32,224	8,740.4
Salt Lake City-Tokyo (W)	37,257	8,837.3
Tokyo-Salt Lake City (W)	30,691	9,198.8

5.5.3 Washington - London Origin-Destination Pair

Figure 5.13 illustrates the flight trajectories produced for an A380-800 flying the Washington-London O-D pair at Mach 0.85.

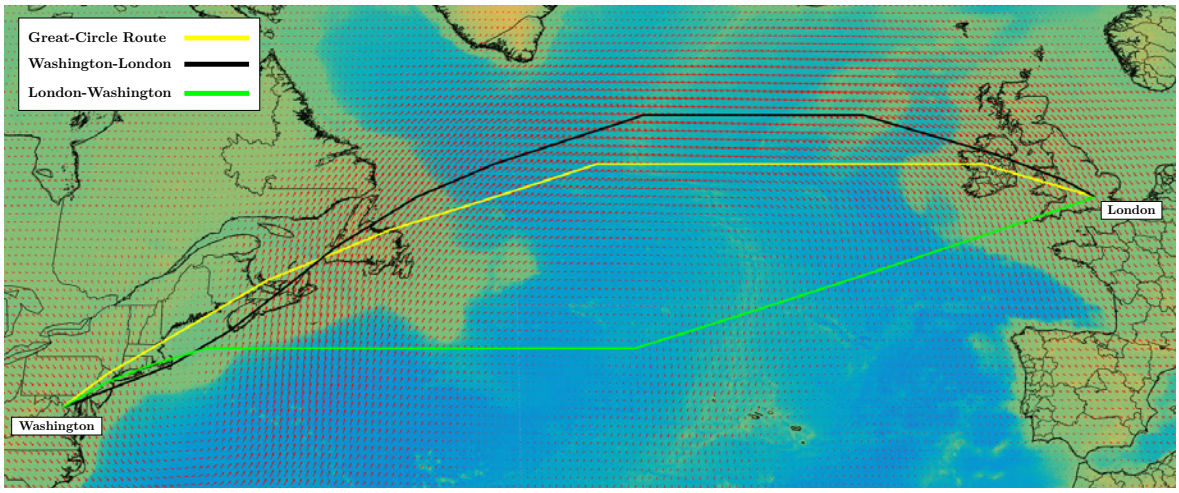

Figure 5.13: Washington-London Origin-Destination Pair with Great Circle and Wind-Optimal Trajectories operated by an Airbus A380-800

While both paths deviate from the great-circle path, the greatest deviation is seen in the London-Washington flight trajectory. This is due to the flight wishing to not only avoid the east-flowing headwind, but to also traverse the atlantic with minimal headwind. As can be seen, the flight path moves well beyond the range of the east-flowing headwind and into airspace with minimal winds. The Washington-London flight trajectory, on the other hand, is produced to fully take advantage of the east-flowing tailwind. As can be seen, its flight path tracks the center of the tailwind almost immediately upon leaving Washington. This routing is highly advantageous as illustrated through a comparison of flight times in Table 5.7. In comparison with the great-circle path, the wind optimal path on the Washington-London leg saves 10.52 minutes per flight. Recognizing the considerable flight traffic from the east coast of the United States to London, we see that with only 6 daily flights, over an hour of time spent in flight is saved by flying the wind optimal trajectory. Furthermore, less time in flight generally implies less fuel burned. Thus, the potential fuel savings are likely significant. These potential savings are even more pronounced on the London-Washington leg. In comparison to the great-circle trajectory, the wind optimal trajectory has a time savings of 69.78 minutes (1.16 hours) per flight despite traveling an extra 452.5 kilometers. With enough traffic, the daily time savings could be measured in days worth of time.

Table 5.7: Comparison of Flight Times and Flown Distances for the Washington-London O-D Pair. GC = great-circle, W = wind optimal

Routing	Flight Time (s)	Flown Distance (km)
Washington-London (GC)	19,728	5,924.1
London-Washington (GC)	29,888	5,924.1
Washington-London (W)	19,097	6,019.8
London-Washington (W)	25,701	6,376.6

5.5.4 Los Angeles - Sydney Origin-Destination Pair

Figure 5.14 illustrates the trajectories for the Los Angeles-Sydney and Sydney-Los Angeles flights.

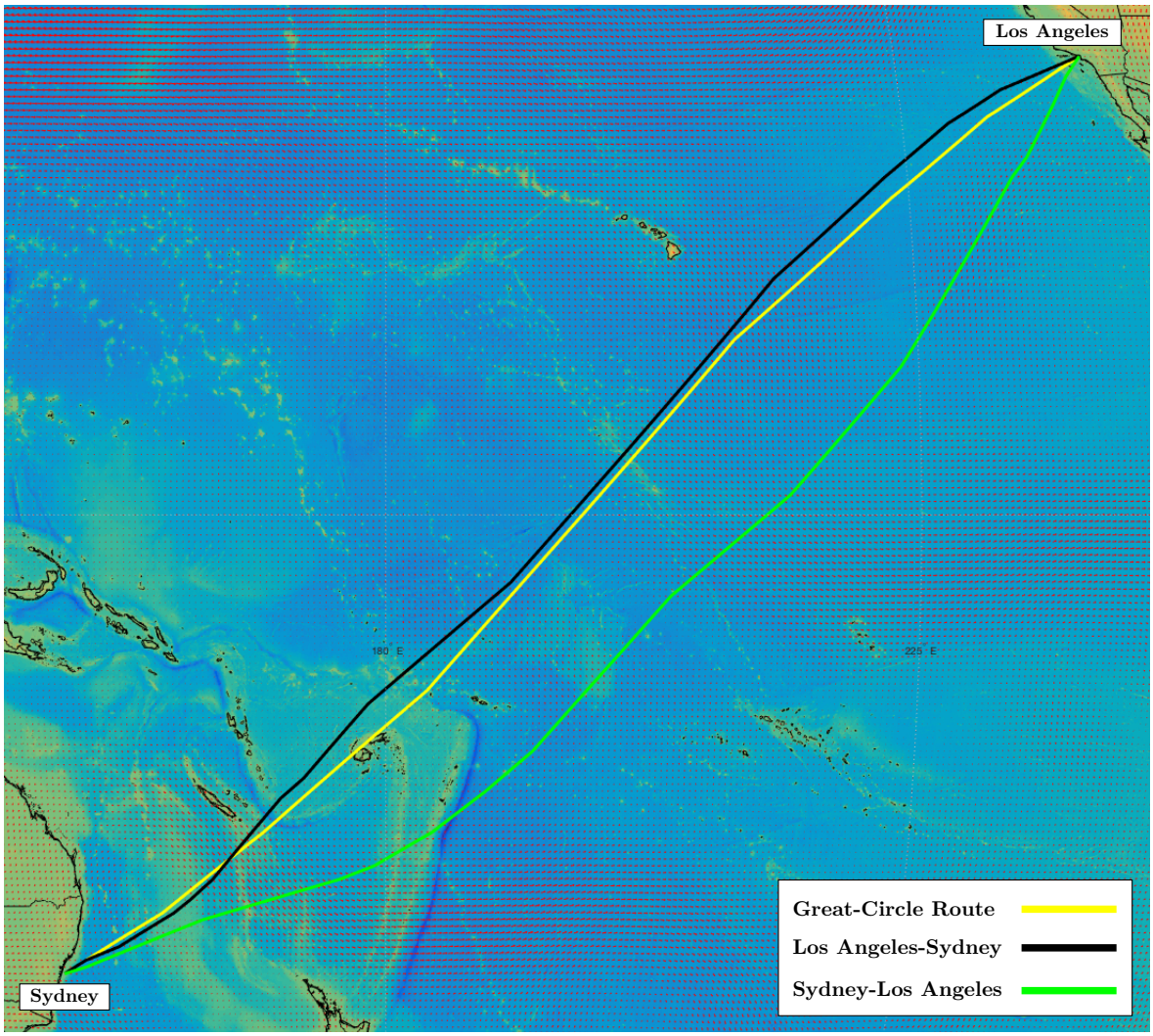

Figure 5.14: Los Angeles-Sydney Origin-Destination Pair with Great Circle and Wind-Optimal Trajectories operated by a Boeing 777-300ER

As can be seen with Figure 5.14 and Table 5.8, the Los Angeles-Sydney great-circle and wind optimal trajectories are very similar, with only a 2.32 minute difference between the two. In contrast, the difference between the great-circle and wind optimal trajectories on the Sydney-Los Angeles leg is 8.77 minutes. We note that despite there being a clear difference in the two Sydney-Los Angeles flight paths, the time savings is rather small when compared with the overall flight time of about 12.8 hours. This demonstrates that while the model is sensitive to the wind field and will produce a wind optimal trajectory, the savings in time

may not be considerable. This is due to the rather gentle wind field over the southern Pacific. Thus, while there is a savings, flight planners may see little benefit to flying an extra 250 kilometers over the Pacific Ocean to only save around 8 minutes of flight time.

Table 5.8: Comparison of Flight Times and Flown Distances for the Los Angeles-Sydney O-D Pair. GC = great-circle, W = wind optimal

Routing	Flight Time (s)	Flown Distance (km)
Los Angeles-Sydney (GC)	47,695	12,043
Sydney-Los Angeles (GC)	46,641	12,043
Los Angeles-Sydney (W)	47,556	12,080
Sydney-Los Angeles (W)	46,115	12,296

5.6 A Benefits Demonstration of the Flight Trajectory Model

We now describe a simulated application of the flight trajectory model described. For this application, we aim to estimate the total fuel saved over all large jet-operated operations within the domestic network of Air Canada. For large-jet operations, we limited our selections to routes operated by the following aircraft in the Air Canada fleet listed in Table 5.9.

Table 5.9: Aircraft considered in forming the Simulated Air Canada Network

Boeing 777-300ER	Boeing 777-200LR	Airbus A330-300
Boeing 787-9	Boeing 787-8	Boeing 767-300ER
Airbus A321-200	Airbus A320-200	Airbus A319-100
Embraer 190	Embraer 175	Bombardier CRJ705
Bombardier CRJ100/200		

Using the Air Canada Timetable of flights for July 21, 2016 to October 23, 2016, we identified the origin-destination pairs served by the aircraft identified in Table 5.9 for Air Canada

domestic operations (Air Canada, 2016). We then applied the Flight Trajectory model for each O-D pair using the aircraft specified.

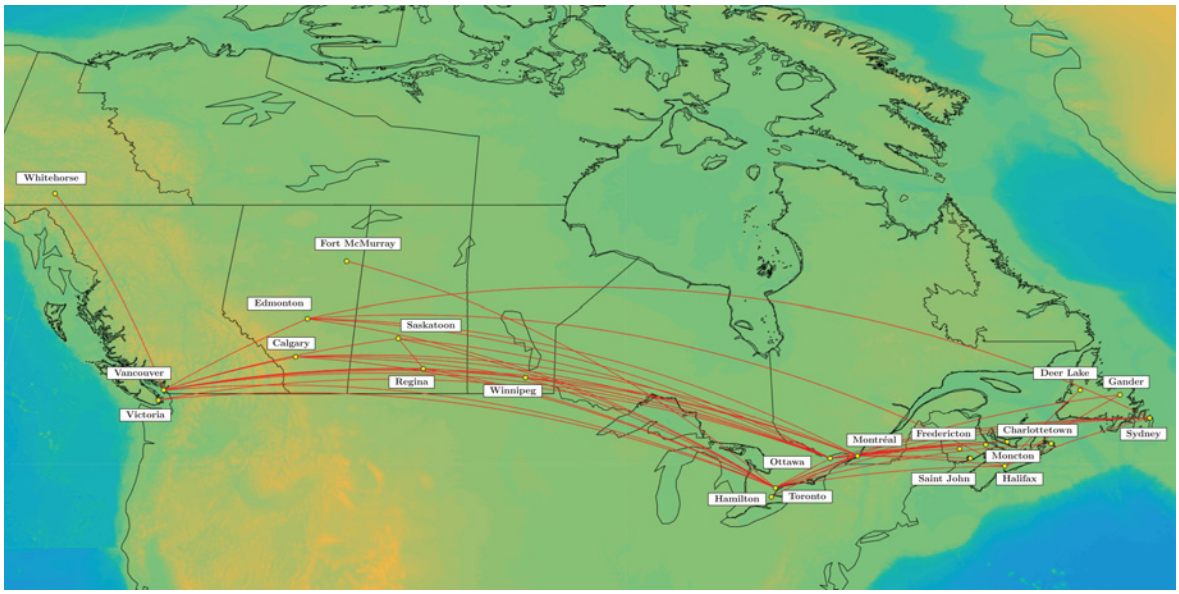

Figure 5.15: Illustration of the Simulated Air Canada Domestic Network

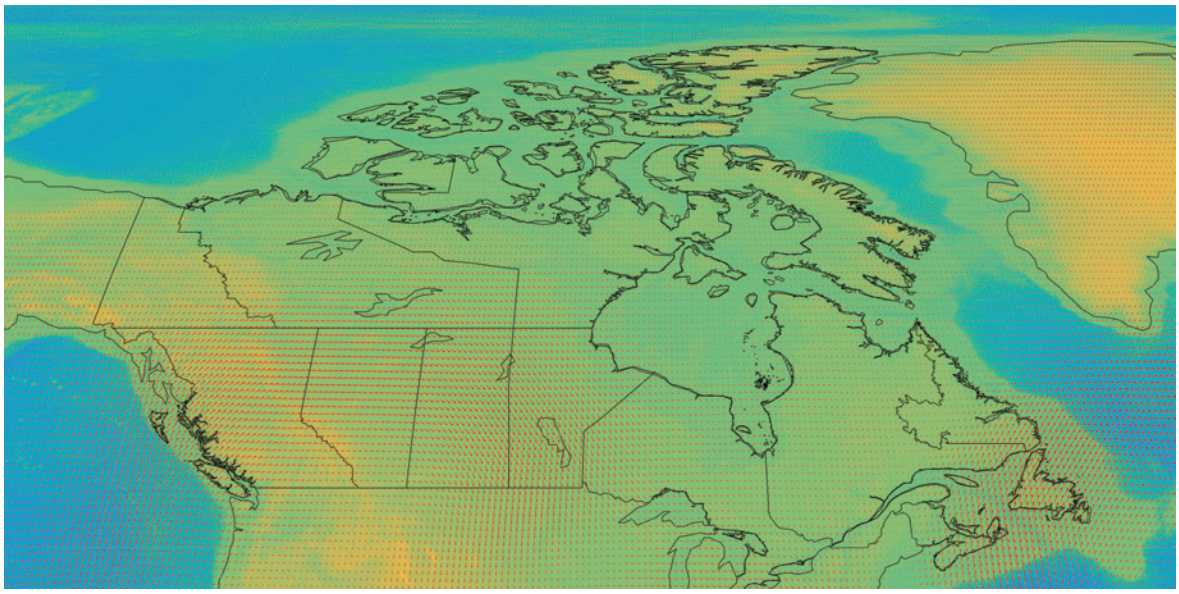

Figure 5.16: Display of the Global Wind Field for January 4th, 2012 for the Time Period 06:00 - 12:00 at a Flight Level of 34,000 feet over Canada

We applied the model for the wind field existing on January 4th, 2012 for the time period from 06:00 - 12:00. Figure 5.15 illustrates the simulated network while Figure 5.16 illustrates the wind field over Canada for the day in question.

The base case for operations assumed that the flights follow the great-circle trajectories. We then compared the estimated fuel burned under the base case against that for when the flights followed the wind-optimal trajectories. In doing the fuel burn analyses described in the following section, aircraft specific parameters were sourced from the BADA database.

5.6.1 Estimation of the Fuel Burned

As seen in Figure 5.17, for an aircraft in level steady cruising flight, the horizontal and vertical forces balance as

$$T \cos \alpha = F_D \tag{5.12}$$

and

$$T \sin \alpha + F_L = mg \tag{5.13}$$

where α is the angle of attack and is generally between zero and three degrees in cruising flight.

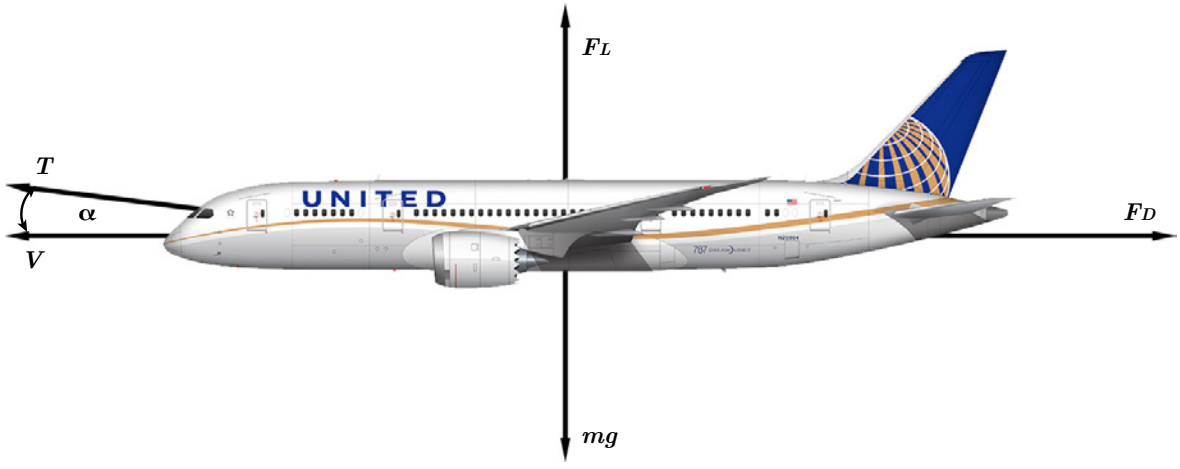

Figure 5.17: Forces on an Aircraft in Steady Level Flight. Base Image Source, (Scott, 2016).

Utilizing the BADA drag polar, the drag force is given as

$$F_D = \frac{1}{2}\rho v^2 S \left(C_{d0} + C_{d2} C_L^2\right) \tag{5.14}$$

where v is the true airspeed of the aircraft, S is the wing surface area, ρ is the air density, and C_{d0} and C_{d2} are the parasitic and induced drag coefficients. With the lift force given as

$$F_L = \frac{1}{2}\rho v^2 S C_L \tag{5.15}$$

we can solve for the lift coefficient by using (5.15) with (5.13) to get

$$C_L = \frac{mg - T\sin\alpha}{\frac{1}{2}\rho v^2 S} \tag{5.16}$$

Putting (5.16) into (5.12), we have

$$\frac{1}{2}\rho v^2 S C_{d0} + \frac{1}{2}\rho v^2 S C_{d2} \left[\frac{mg - T\sin\alpha}{\frac{1}{2}\rho v^2 S}\right]^2 = T\cos\alpha \tag{5.17}$$

Rearranging, we can write (5.17) as

$$T^2 \left(C_{d2}(\sin\alpha)^2\right) - T\left(2C_{d2} W \sin\alpha + \frac{1}{2}\rho v^2 S\cos\alpha\right) + C_{d0}\left(\frac{1}{2}\rho v^2 S\right)^2 + mgC_{d2} = 0 \tag{5.18}$$

Using the quadratic equation, we find T to be

$$T = \frac{-\lambda - \sqrt{\lambda^2 - 4\phi\nu}}{2\phi} \tag{5.19}$$

where $\lambda = \left(2C_{d2} W \sin\alpha + \frac{1}{2}\rho v^2 S\cos\alpha\right)$, $\phi = (C_{d2}(\sin\alpha)^2)$ and $\nu = C_{d0}\left(\frac{1}{2}\rho v^2 S\right)^2 + mgC_{d2}$.

Using the BADA model of the thrust specific fuel consumption (η), the thrust specific fuel consumption parameter is determined as

$$\eta = C_{f1}\left(1 + \frac{v_{TAS}}{C_{f2}}\right) \tag{5.20}$$

where C_{f1} and C_{f2} are thrust specific fuel consumption coefficients. The fuel burned per unit time or fuel burn rate is then the product of the thrust (T) and the thrust specific fuel

consumption (η). That is,

$$\frac{dW}{dt} = -\eta T g \tag{5.21}$$

where W is the weight of the aircraft ($W = mg$).

Assuming that a constant airspeed and angle of attack are maintained, the necessary thrust will change as a function of the weight of the aircraft. As the weight decreases, the thrust needed will lessen, which in turn, will lower the fuel burn rate. Owing to the cyclical nature of the problem, we can estimate the fuel burn iteratively using discrete time steps. The computational algorithm can be outlined as follows.

1. Initialize the Aircraft starting Mass (W_0)
2. Compute the thrust T
3. Compute the fuel burn $\frac{dW}{dt}$
4. Update the aircraft weight $W_t = W_{t-1} + \Delta t(\frac{dW}{dt})$
5. Return to 2

5.6.2 Simulation Time Required & Results

In estimating the total fuel burned during a flight, we repeated the computational algorithm until a total time equal to that of the flight time has elapsed. We assume that the flight flies straight and level at a constant altitude of 34,000 feet and we do not consider any additional factors such as turns in flight or flight level changes. Additionally, we assume a constant attack angle α of 3 degrees.

The total time needed to construct all 204 optimal flight trajectories came out to roughly 1.87 hours. The time for data entry added approximately another 30 minutes, resulting in a total of 2.37 hours spent in constructing the optimal flight trajectories The analyses were performed using seven batches of flights on an Apple iMac Retina 5K with a 4GHz Intel Core i7 quad-core processor and 32 GB of 1600 MHz DDR3 RAM. The simulations were performed using MATLAB 2016a and parallel computing was utilized.

A total of 204 unique flight leg and aircraft type combinations were simulated and are given in Appendix C.1. From the timetable data, these represent 677 daily flights. The total daily fuel saved was found to be 50,927.63 kg. The price of jet fuel as of July 8th, 2016 is estimated to be $ 443.6 U.S. dollars per metric ton (International Air Transport Association (IATA), 2016). Thus, the total estimated savings over this simulated Air Canada domestic network is $ 22,591.50 per day, which translates into $8,245,896.28 per year. As can be seen, this is not an insignificant amount for a rather small domestic network, when compared against those of U.S. carriers. Furthermore, when considering the tight profit margins that many airlines face, there is likely great incentive for airlines to utilize optimal flight path trajectories, especially when achieved with little expense in time.

5.7 Concluding Remarks

In this chapter, we have described the construction of and demonstrate the performance of a 2-D flight trajectory optimization model. This work illustrates how informed search techniques can be utilized to determine wind optimal trajectories using publicly available wind and air temperature data. Furthermore, we have demonstrated that a realistic airline network can be fully analyze with a reasonable expenditure of time and effort. Additionally, we have quantified in dollars, the potential benefits to be gained from utilizing wind optimal flight trajectories.

5.8 Future Development

The logical next steps will be to extend the model to consider four dimensions (altitude and time) and the extension to the four dimensional realm will need to consider a number of technical challenges. Regarding the shortest path algorithm to be utilized, if the A* algorithm is to be kept, an admissible heuristic suitable for 4-D optimization must be discovered or developed. The other primary issue is that of ensuring that sufficient computer memory is available. Under this model framework, a 4-D analysis will likely require a much larger impedance matrix that may considerably tax available computer memory. Strategies for controlling memory usage will be critical, both to ensuring that a

future model can operate on long flights and to ensure reasonable simulation times.

Future developers might also consider the addition of modules to consider convective-weather patterns. Other possible constraints may include consideration of **E**xtended-range **T**win-engine **O**perational **P**erformance **S**tandards (ETOPS) restrictions and instances when certain airspaces are either undesirable or restricted for passage. Organized track systems also might be incorporated into future versions of this model.

Chapter 6

An Investigation of UAS Civilian and Commercial Applications and Potential Airspace Capacity Impacts

6.1 Background

The civil uses and applications of Unmanned Aerial Systems (UAS) continue to advance and increase in both scale and complexity. While having a long history of military-related applications, UAS is expected to expand in a number of areas including: security awareness, disaster response, communications and broadcast services, infrastructure monitoring and commercial photography (Federal Aviation Administration, 2013). However, the increasing utilization of UAS also necessitates the consideration of potential conflicts that these newly introduced vehicles might have with existing commercial and general aviation air traffic. To this end, it is important to consider potential UAS mission profiles and the associated number of UAS vehicles necessary for conducting these missions.

This chapter presents two possible mission scenarios inline with those imagined by the FAA. First, we consider communications and broadcast service delivery by UAS. Second, we apply UAS platforms to damage survey assessment tracking. We estimate the number of UAS vehicles necessary to conduct the communications and broadcast service delivery

mission for a base year and for up to and including 25 years into the future to get a sense of the number of UAS vehicles we might expect to see in the National Airspace System (NAS) in the near future. Finally, we consider the potential impacts to commercial airspace resulting from large-scale UAS vehicle deployment and examine potential ways of mitigating airspace conflicts.

6.2 Description of Assumed Flight Vehicle

For the missions to be analyzed, we assume that they will be performed using what is known as a High Altitude, Long Endurance (HALE) aircraft. The benefits of HALE aircraft are twofold: (1) they can cruise at very high altitudes far above any commercial aircraft traffic and (2) they can stay aloft for days or weeks at a time depending on the specific mission and platform. Furthermore, HALE aircraft lend themselves well to the missions to be analyzed. Early research into such aircraft noted that communications relay missions require long endurance, while surveillance missions require long lines of sight and the ability to transit long distances (Hall et al., 1983).

6.2.1 Aerodynamic Characteristics

We consider a HALE vehicle having similar aerodynamic characteristics to a proposed solar-hybrid vehicle described by Nicolai and Carichner (Nicolai and Carichner, 2010). The physical configuration of the HALE vehicle is shown in Figure 6.1 while the BADA performance files (Trani and Spencer, 2014) for the vehicle are presented in Appendix D. We assume a twin-boom tail configuration with a high aspect ratio wing (36) and a maximum takeoff mass of 2,200 kg. The design L/D ratio is approximately 41 and cruising altitude and speed are assumed to be 60,000 feet and 75 knots, respectively. The vehicle is also limited to a maximum bank angle of 15° to ensure payload safety and stability. Additionally, the vehicle stall speed at cruise is assumed to be 20 knots.

The vehicle will be self-propelled and autonomous. It will be designed to have a mission endurance of 7 days and will be powered by two turbo-charged 30kW electric engines, which draw their power from solar cells mounted on both the wings and the horizontal stabilizer.

We summarize the operational and design parameters of the assumed HALE vehicle in Table 6.1.

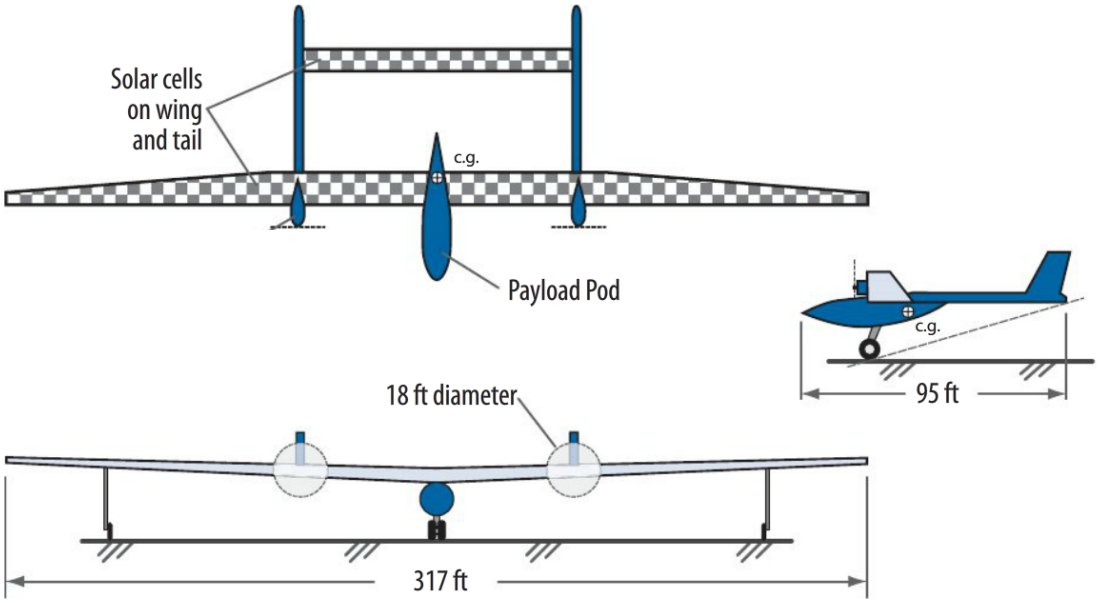

Figure 6.1: Physical Configuration of the UAS HALE Vehicle used for UAS Mission Profile Types. Source for Original Picture: (Nicolai and Carichner, 2010).

Table 6.1: Overview of Aircraft Design and Performance Parameters

Takeoff Mass	2,200 kg
Design L/D Ratio	41
Wing Aspect Ratio	36
Speed	75 kts at 60,000 feet
Mission Endurance	7 days
Total Power Available	40 kW

For our assumed vehicle, we assume a BADA drag polar. The BADA drag polar specification is only an approximation of the drag polar of the vehicle. A cambered airfoil section (such as a Liebeck airfoil design) would be best represented with multiple parameters. However, the BADA specification presented in Appendix Figure D.3 allows

only two parameters as illustrated below.

$$F_D = C_{d0} + C_{d2}C_L^2 \text{ (EUROCONTROL Experimental Centre, 2009)} \tag{6.1}$$

Similarly, the BADA performance characteristic of the engine thrust is only an approximation for the vehicle.

6.2.2 Aircraft Performance

Using the given aircraft parameters, estimates of the climb profile, descent profile, and the rate of climb profile were generated and are presented in Figures 6.2, 6.3 and 6.4, respectively. As can be seen, the HALE vehicle needs more than 250 nautical miles to reach above 50,000 feet and far longer to complete its climb to 60,000 feet. Given its slow cruise speed of 75 knots, this has potential implications for conflicts with commercial air traffic as the vehicle passes through commercial airspace. We consider these further later in this chapter.

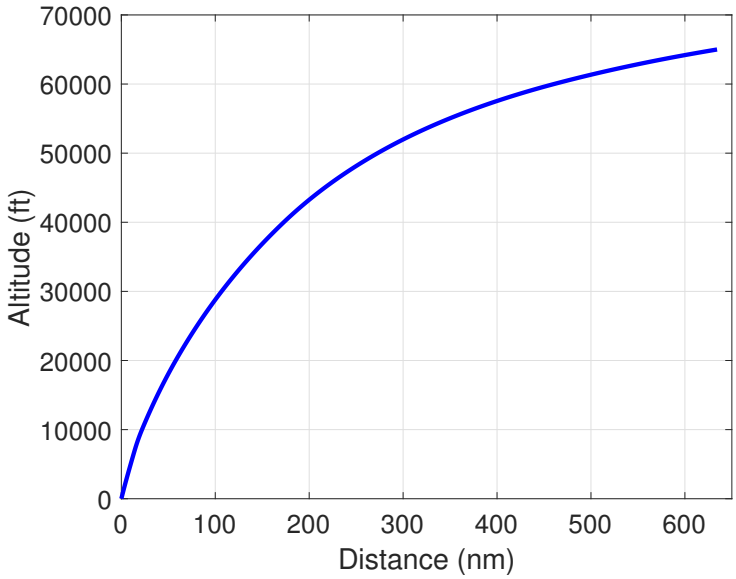

Figure 6.2: Climb Performance for HALE Solar Hybrid Aircraft. Initial Mass is 2,200 kg.

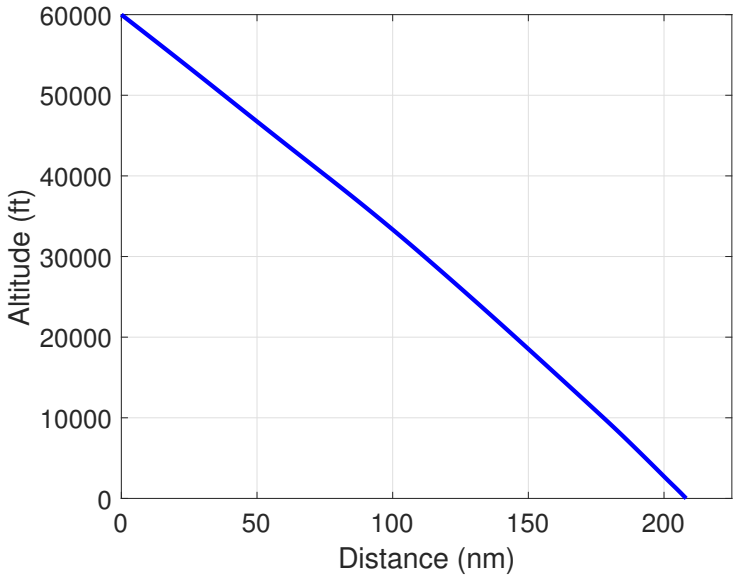

Figure 6.3: Descent Performance for HALE Solar Hybrid Aircraft. Mass is 2,200 kg.

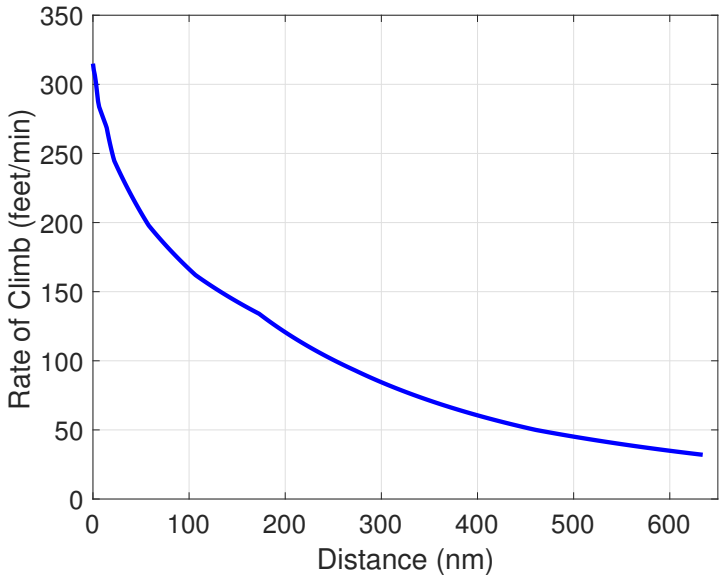

Figure 6.4: Rate of Climb Profile for HALE Solar Hybrid Aircraft. Initial Mass is 2,200 kg.

6.3 Communications and Broadcast Service Delivery

Internet access and wireless communication continues to shift from a convenience to a necessity in modern American life. As evidenced by streaming video-on-demand services, internet banking, and video communications, more and more aspects of life are being shifted to a digital medium. This, in turn, has caused demand for internet access and bandwidth capacity to increase exponentially.

Communications delivery has typically been achieved through physical cell-phone towers, landline trunk cables and orbiting satellites. Recently however, attention has been paid to high altitude platforms as an alternative method of access provisioning and bandwidth delivery. High altitude platforms are appealing due to their relatively easy and incremental deployment. In such a system, a High Altitude Long Endurance vehicle (HALE) would be launched and would loiter over a prescribed area and beam service to end users within its coverage area. These vehicles would fly well above commercial traffic and avoid further congestion of commercial airspace. Furthermore, any additional demand could be met by simply adding additional flights. The concept has been called "flying cell tower" to indicate that HALE vehicles one day could compete with ground cell towers.

6.3.1 Deployment Schemes

High Altitude Platforms (HAPs) allow for considerable flexibility in their deployment and configuration. Though not exhaustive, the three most common deployment schemes for HAPs are: (1) Terrestrial-HAP-Satellite System, (2) Integrated Terrestrial-HAP System and (3) Stand-Alone HAP System (Yang and Mohammed, 2008).

Terrestrial-HAP-Satellite Deployment

Under this configuration, the HAP network compliments existing satellite and terrestrial infrastructure and bidirectional links would exist between each of the three platforms. The HAP network would be deployed below orbiting satellites and would improve satellite performance over the earth by better delivering content to end users. The HAP network could also extend the coverage area of the system much more easily than the terrestrial

network (Yang and Mohammed, 2010).

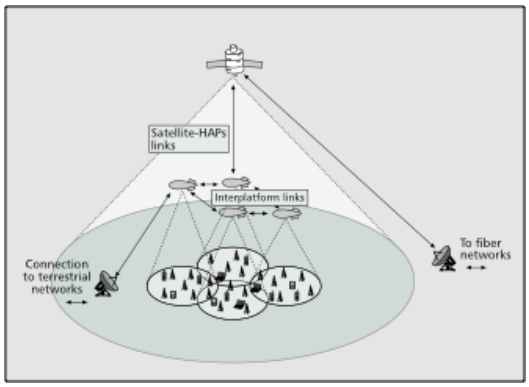

Figure 6.5: Terrestrial-HAP-Setellite Deployment, (Karapantazis and Pavlidou, 2005)

Integrated Terrestrial-HAP Deployment

In this configuration, the HAP network would complement existing terrestrial networks while extending communications reach to areas where terrestrial connectivity is sparse or impractical. Two-way connectivity would be maintained with the existing terrestrial network and the HAP network would project a number of coverage regions or cells over a target population. HAP networks are well-suited for extending ground network coverage and HAP network coverage footprints have been envisioned with radii exceeding 150 kilometers (Yang and Mohammed, 2008).

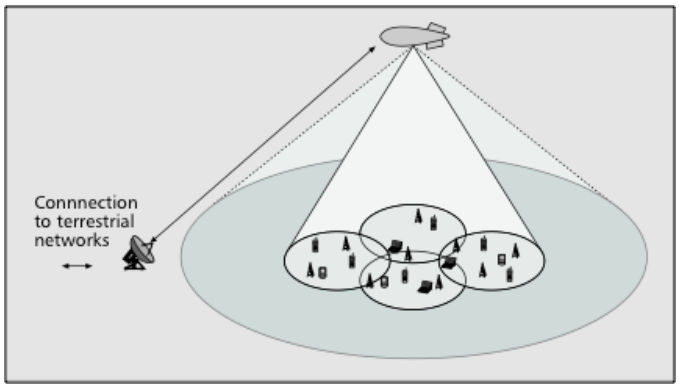

Figure 6.6: Integrated Terrestrial-HAP Deployment, (Karapantazis and Pavlidou, 2005)

Stand-Alone HAP Deployment

This deployment envisions the HAP network as the primary communications delivery platform for end users. Backhaul links would exist between ground base stations and satellites, but interfacing and contact delivery would occur solely between the end user on the ground and the orbiting HAP network. This configuration highlights the benefits of HAP networks and might be suitable for a number of applications including environmental and disaster surveillance and broadband internet delivery (Yang and Mohammed, 2008).

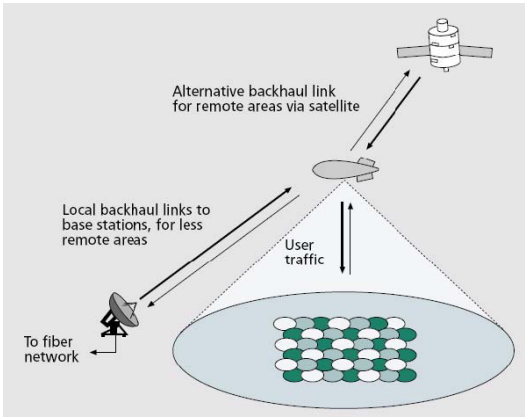

Figure 6.7: Stand-Alone HAP System, (Avilés, 2007)

6.3.2 Mission Description

These missions assumed a stand-alone HAP deployment and were prototyped using the aforementioned HALE solar/electric vehicle. For each individual mission, a total mission time of 7 days was assumed. This includes take-off, travel time to the loiter position, loiter time, travel back to the airport and landing. Additionally, we assumed that all travel to and from the basing airport was non-stop. The HALE missions designed in this analysis would fly circular orbits set at altitudes between 60,000 and 65,000 feet above service areas. HALE vehicles would loiter at 70 knots and all HALE vehicles are assumed to operate in a manner such that they are autonomously de-conflicted with other HALE vehicles.

6.3.3 Methodology

Coverage Area and User Requirements

We assumed a primary mission of providing broadband internet access to customers in metropolitan and micropolitan areas throughout the continental United States, Alaska, Hawaii and Puerto Rico. This analysis included 929 metro- and micropolitan statistical areas, most of which are illustrated in Figure 6.8.

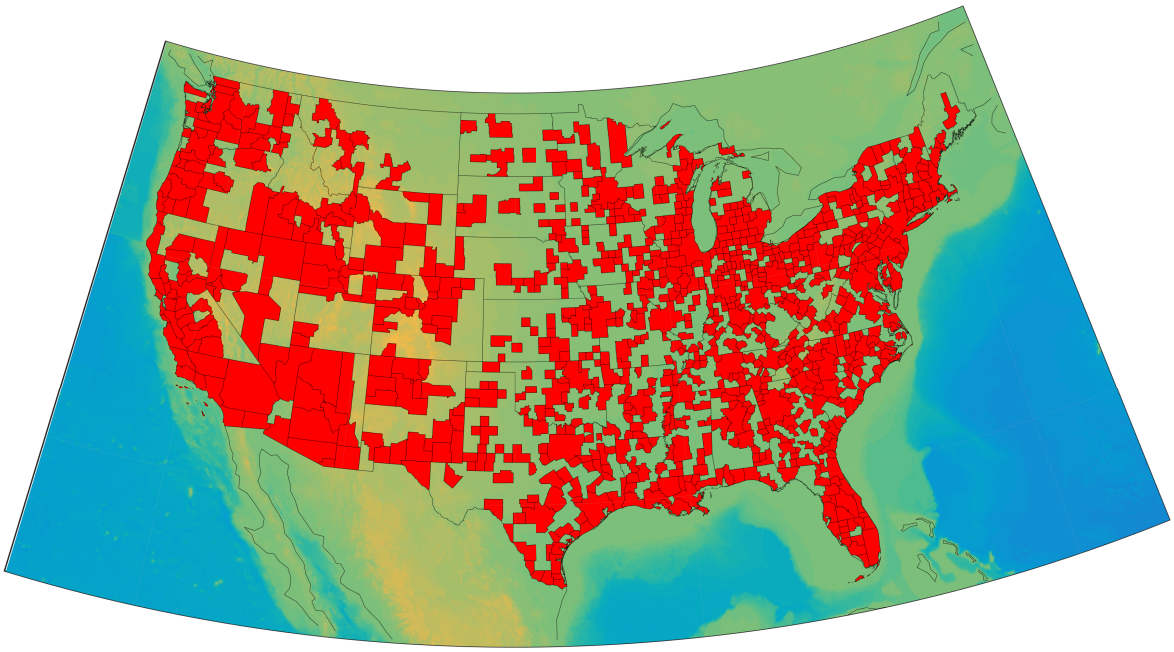

Figure 6.8: Metropolitan and Micropolitan Areas considered, exclusive of Alaska, Hawaii and Puerto Rico

In the base year, we assume that users would demand, on average, a T1-level connection operating at 1.5 Mbps. This bandwidth would be delivered by a series of platforms, each capable of delivering up to 100,000 Mbps (Martin and Colella, 1998) of bandwidth in the base year. We further assume a peak utilization rate of 50%. Under these assumptions, we estimated that each vehicle could support 133,333 users on average, based on the following calculation.

$$\frac{100,000 \text{ Mpbs}}{(1.5 \text{ Mbps/user})\,(0.5 \text{ peak utilization})} = 133,333 \text{ Users} \tag{6.2}$$

We then established our platform operating parameters as follows. We assumed an operating altitude range of 60,000 feet up to a maximum of 65,000 feet. A cruise speed of 70 knots and total mission length of 7 days was established. We also assume a minimum elevation angle of 35° between end-user ground receivers and the orbiting platform.

Figure 6.9 illustrates how the coverage radius is estimated. For aircraft operating a circular orbit, a covered area is one that can have a direct line-of-sight to the orbiting aircraft no matter where the aircraft is in its orbit. Given an elevation angle β, an orbit height of h and an orbit radius R, the radius of the covered area is given in Figure 6.9 as s, which is equal to $h\cos\beta - R$. The base of the shaded triangle in Figure 6.9 is the diameter of the covered region. In order to ensure that no holes exist in the covered region, this necessarily requires that $h\cos\beta$ be greater than R. Additionally, if a greater coverage area is needed, this can be increased by increasing the orbit height of the HALE aircraft assuming a constant elevation angle.

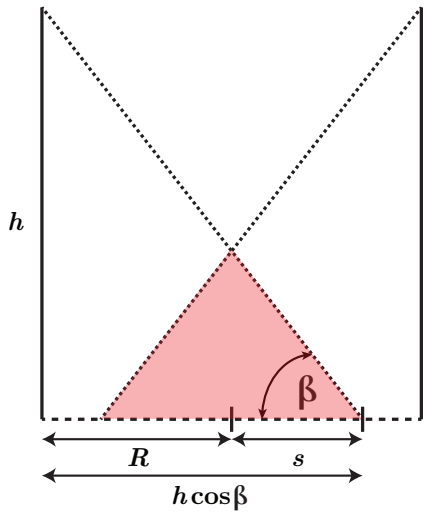

Figure 6.9: Illustration of Coverage Radius (s) as a Function of the Elevation Angle and Orbit Height

UAS Flight Demand Estimation

Analysis was done to efficiently place mission orbits such that they would cover the statistical population area and meet the estimated user demands. We first assumed that each circular orbit has a radius of 2.5 nautical miles ($\sim$ 15,190 feet). At this radius, the necessary bank angle is given by

$$\phi = \arctan\left[\frac{v^2 \cos\gamma}{gR}\right] \tag{6.3}$$

where γ is the flight path angle, v is the airspeed and R is the flight turn radius. Assuming level steady flight, the flight path angle γ would be equal to zero. Therefore, at a cruise speed of 70 knots, the required bank angle ϕ would be $\phi = 1.63°$, which is well below the assumed maximum bank angle of 15°.

Next, to establish the starting number of vehicles required, we first consider the population of the statistical area. Assuming an even population density, we divide the population by the estimated total number of users per platform, as calculated in (6.2). The ceiling of this number gives the minimum number of platforms by population irrespective of platform coverage area.

$$\left\lceil \frac{\text{total population}}{\text{total users per platform}} \right\rceil = \text{minimum number of platforms by population} \tag{6.4}$$

We then divide the total land area of the statistical area by the minimum number of platforms by population (6.4) to get the area that would need to be covered using this number of platforms.

$$\left\lceil \frac{\text{total land area}}{\text{min. number of platforms by pop.}} \right\rceil = \text{needed coverage area per platform} \tag{6.5}$$

However, the assumed operating parameters of the broadcast mission imply a minimum coverage area per platform. With a 2.5 nautical mile orbit, a maximum altitude of 65,000 feet and a minimum elevation angle of 35°, this results in a coverage area of approximately 163.2 square miles. If the needed coverage area determined in (6.5) exceeds this area, we then determine the starting number of platforms by dividing the total land area of the statistical area by the coverage area for a 2.5 nautical mile orbit with a 35° elevation angle at 65,000 feet ($\sim$ 163.2 square miles). The ceiling of the quotient of the land area by the coverage area

is set to be the starting number of platforms required.

$$\left\lceil \frac{\text{total land area}}{\pi \left(\text{coverage radius}\right)^2} \right\rceil = \text{ minimum number of platforms} \tag{6.6}$$

Otherwise, if the needed coverage area from (6.5) did not exceed 163.2 square miles, then (6.6) is determined using the coverage area from (6.5).

The efficient placement of polygons over a geometric area is a type of set-covering problem and arises in many applications. One common example is the problem of placing wireless antennas to serve a given set of customers. If one models each customer as a discrete point and each antenna as a geometric region of service with an associated cost of deployment, then the problem is to place the antennas such that the costs of deployment are minimized.

The geometric set cover problem has direct application for the placement of HALE orbits for delivering broadband communications service. However, most versions of the set-covering problem are known to be NP-hard (Har-Peled and Lee, 2012) and difficult to solve in polynomial time.

Har-Peled proposes the k-center problem as akin to our geometric set cover problem. If we define a *ball* having a radius r around a point $p \in \mathbf{P}$ as the set of points in $\mathbf{P}$ with a distance at most r from p, then the k-center (k-mean) problem can be taken as the problem of covering the points of $\mathbf{P}$ using k balls of minimum or maximum radius (Har-Peled, 2011).

k-Means Clustering Algorithm

The k-means clustering algorithm is an unsupervised learning algorithm that aims to partition n observations into k sets, provided that $k \leq n$. If given a set of observations $\{p_1, p_2, \ldots p_n\}$, the objective of the algorithm is to cluster the observations into sets $\{S_1, S_2, \ldots S_k\}$ such that the sum of the distance functions of each observation to its cluster center, the within-cluster sum of squares, is minimized. The objective function of the algorithm is

$$\sum_{i=1}^{k} \sum_{j=1}^{c_i} \left(\|\mu_i - p_j\|\right)^2 \tag{6.7}$$

where c_i is the number of observations in cluster i and $\|\mu_i - p_j\|$ is the Euclidean distance between the j^{th} observation p_j in cluster i and the cluster center of cluster i, μ_i. The algorithm proceeds as follows. Given an initial set of k means $\{\mu_1^t, \mu_2^t, \ldots, \mu_k^t\}, t = 0$:

1. Assign observations $\{p_1, p_2, \ldots p_n\}$ to the cluster for which the within-cluster sum of squares is minimized. Since the sum of squares is the squared Euclidean distance, this works out to be the closest cluster mean to the observation.

2. With all observations assigned, calculate the new means to be the centroids of the cluster observations.

3. If the cluster assignments no longer change, terminate the algorithm as it has converged. Otherwise return to 1.

We note that for the k-means algorithm, since both steps 1 and 2 optimize the within-cluster sum of squares and since there exists only a finite number of such partitionings, the algorithm is guaranteed to converge to a local optimum. However, it is not guaranteed that the k-means algorithm will return a global optimum (Gowri and Janakiraman, 2015).

Application of the *k*-Means Algorithm

We opted to utilize k-means clustering with an iterative approach in order to place the flight orbits. We first discretized each metropolitan area into a mesh of points spaced 1 nautical mile from one another as exemplified by Figure 6.10.

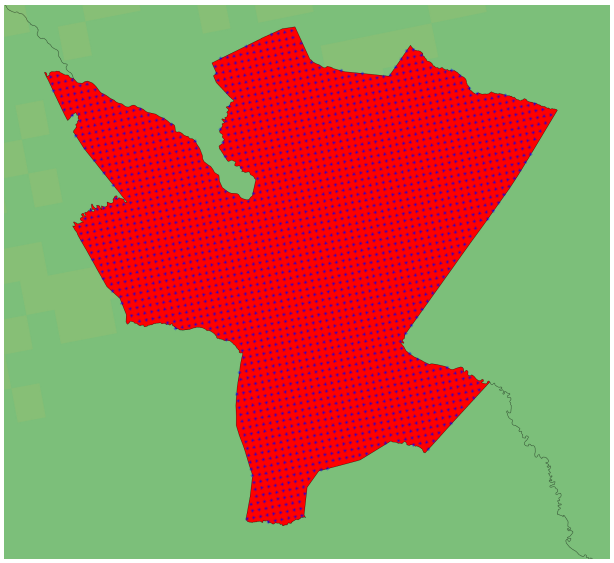

Figure 6.10: Mesh Points for the Augusta, GA-Richmond County, SC Metropolitan Area

We then applied the k-means clustering algorithm to place k centroids of a corresponding platform orbit. The starting value of k is the minimum number of platforms calculated by (6.6) and the starting altitude was assumed to be 60,000 feet. A check was done to ensure that no mesh point within the statistical area was spaced from its closest orbit center at a distance further than the coverage radius for the given altitude. If this check failed, the altitudes of the orbits were incremented upwards by 500 feet. The increased coverage radius was then rechecked against the furthest distance from the closest orbit center. If the check failed again, the altitude was further incremented by 500 feet and the process was repeated until either the check succeeded or until the flight ceiling was reached. If the flight ceiling was reached, the k-means cluster algorithm was rerun with an additional orbit. The entire process was repeated until the distance requirement was met or until an iteration limit was reached. However, solutions were found for all statistical areas prior to reaching the iteration limit. Figure 6.11 illustrates examples of fully covered statistical areas.

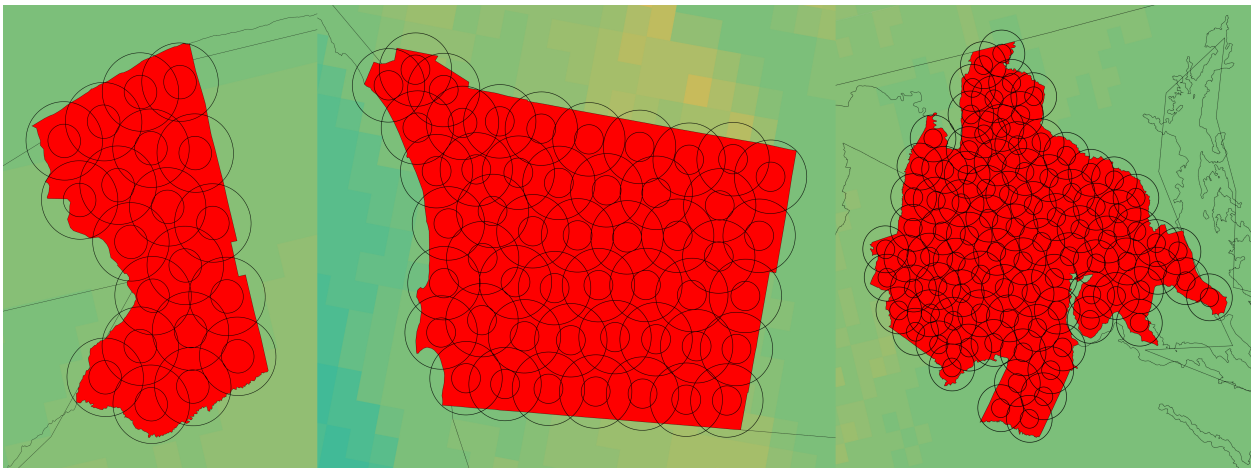

Figure 6.11: Buffalo, NY, San Diego, CA and Washington DC Metropolitan Areas with UAV Coverage (Base Year)

Basing Airports for UAS Missions

Once the location of each flight orbit nationwide was determined, we then proceeded to determine a set of airports from which to launch these missions. The first step was to define a set of suitable airports from among airports in the continental United States, Alaska and Hawaii. Using FAA airport data (Federal Aviation Administration, 2014e), we first chose those that had at least a 6,000 foot by 150 foot runway. We then limited potential airports to public airports and airports having airframe and engine maintenance facilities. This resulted in an initial set of 100 airports, illustrated in Figure 6.12 below.

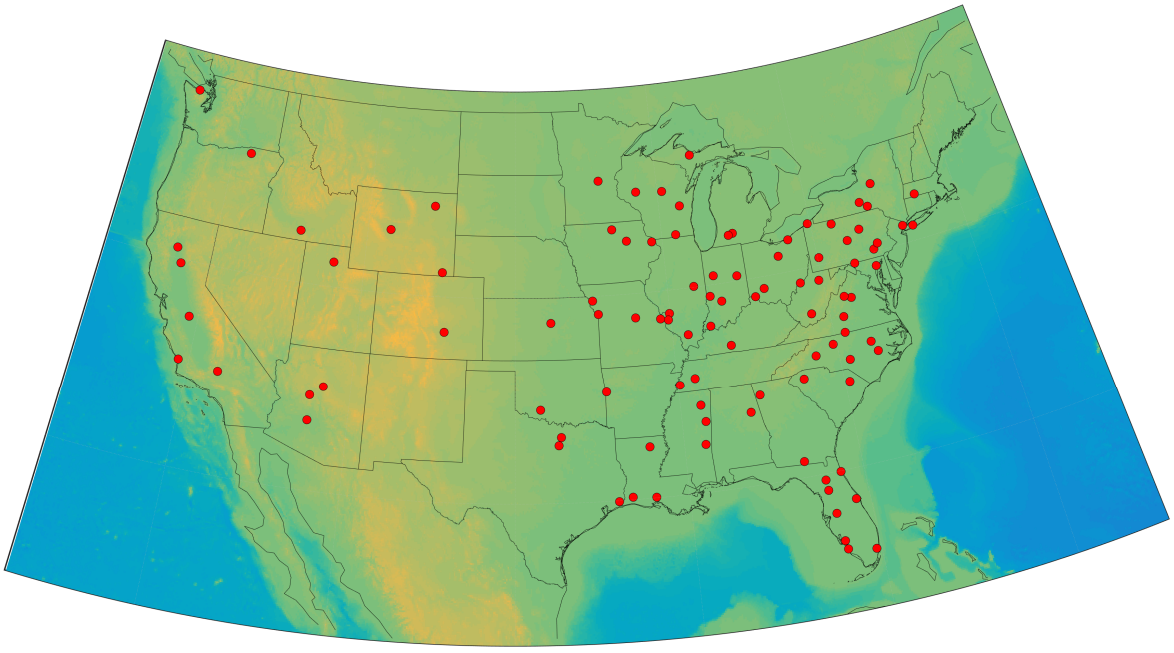

Figure 6.12: Full Set of 100 Suitable Basing Airports for UAV Missions

The next step involved choosing a subset of basing airports from our initial set. For each airport in the initial set, the straight-line distance from the airport centroid to each determined orbit was calculated, resulting in a matrix of $n \times 100$ distances. We then scored each airport by each orbit n. For each orbit, the airport having the shortest distance was assigned a score of 1 for that orbit. Otherwise, it was assigned a zero. We decided on a subset of 30 airports and the 30 airports having the highest cumulative scores were chosen as the basing airport subset. We note that this basing airport subset is not static. This algorithm was carried out for each demand year and certain years had slight modifications to the basing airport subset, owing to additional orbits being assigned to growing metropolitan areas. Illustrated in Figure 6.13 are all basing airports that every appear in a basing airport subset, highlighted in black. As can be seen, a total of 37 unique airports appear, listed in Table 6.2, appear in a basing airport subset.

Table 6.2: Airports appearing in a Basing Airport Subset

#	Airport Codes			Airport Name	City, State
	ICAO	IATA	FAA		
1	KANB	ANB	ANB	Anniston Regional Airport	Anniston, AL
2	KARA	ARA	ARA	Acadiana Regional Airport	New Iberia, LA
3	KBAF	BAF	BAF	Westfield-Barnes Regional Airport	Westfield/Springfield, MA
4	KBKL	BKL	BKL	Burke Lakefront Airport	Cleveland, OH
5	KBPT	BPT	BPT	Jack Brooks Regional Airport	Beaumont/Port Arthur, TX
6	KBTL	BTL	BTL	W. K. Kellogg Airport	Battle Creek, MI
7	KBWG	BWG	BWG	Bowling Green-Warren County Regional	Bowling Green, KY
8	KCIC	CIC	CIC	Chico Municipal Airport	Chico, CA
9	KCLM	CLM	CLM	William R. Fairchild International Airport	Port Angeles, WA
10	KDTO	—	DTO	Denton Municipal Airport	Denton, TX
11	KFLG	FLG	FLG	Flagstaff Pulliam Airport	Flagstaff, AZ
12	KFRG	FRG	FRG	Republic Airport	Farmingdale, NY
13	KFSM	FSM	FSM	Fort Smith Regional Airport	Fort Smith AR
14	KFTW	FTW	FTW	Fort Worth Meacham International Airport	Fort Worth, TX
15	KGYH	GDC	GYH	Donaldson Center Airport	Greenville, SC
16	KGYR	GYR	GYR	Phoenix Goodyear Airport	Goodyear, AZ
17	KHKY	HKY	HKY	Hickory Regional Airport	Hickory, NC
18	KJVL	JVL	JVL	Southern Wisconsin Regional Airport	Janesville, WI
19	KLAF	LAF	LAF	Purdue University Airport	Lafayette, IN
20	KLAL	LAL	LAL	Lakeland Linder Regional Airport	Lakeland, FL
21	KLAW	LAW	LAW	Lawton-Fort Sill Regional Airport	Lawton, OH
22	KMER	MER	MER	Castle Airport	Atwater, CA
23	KMFD	MFD	MFD	Mansfield Lahm Regional Airport	Mansfield, OH
24	KMHV	MHV	MHV	Mojave Airport	Mojave, CA
25	KMTN	MTN	MTN	Martin State Airport	Baltimore, MD
26	KOGD	OGD	OGD	Ogden-Hinckley Airport	Ogden, UT
27	KOPF	OPF	OPF	Opa-Locka Executive Airport	Opa-Locka, FL
28	KPDT	PDT	PDT	Eastern Oregon Regional at Pendleton	Pendleton, OR
29	KPUB	PUB	PUB	Pueblo Memorial Airport	Pueblo, CO
30	KRDG	RDG	RDG	Reading Regional Carl A. Spaatz Field	Reading, PA
31	KRMG	RMG	RMG	Richard B. Russell Airport	Rome, GA
32	KSBP	SBP	SBP	San Luis County Regional Airport	San Luis Obispo, CA
33	KSTC	STC	STC	St. Cloud Regional Airport	St. Cloud, MN
34	KTEB	TEB	TEB	Teterboro Airport	Teterboro, NJ
35	KTWF	TWF	TWF	Magic Valley Regional Airport	Twin Falls, ID
36	KVLD	VLD	VLD	Valdosta Regional Airport	Valdosta, GA
37	PAGS	GST	GST	Port Elizabeth International Airport	Gustavus, AK

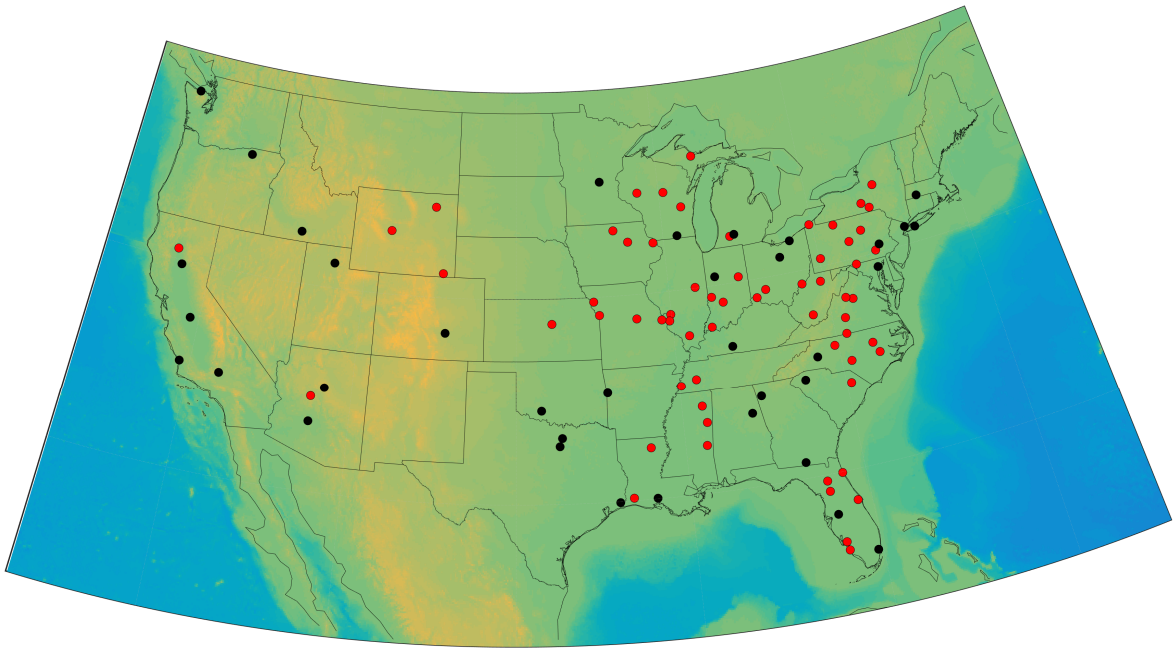

Figure 6.13: Basing Airports that appear in any Basing Airport Subset for UAV Missions

6.3.4 Future Demands for Hale Communications and Relay Missions

Our methodology provides us with a base year estimate of the number of flights necessary to meet the estimated demand. In determining the number of flights necessary for future years, we assumed annual growth factors for platform capacity, peak utilization percentage and average end-user bandwidth demand. The growth factors utilized in the communications and relay analysis are shown in Table 6.3. We assumed that capacity potential would initially be at 100,000 Mbps and steadily increase to 250,000 Mbps by year 25. Similarly, we assumed that average peak utilization rates would increase from 50% to 70% and demand per user from 1.5 Mbps to 7.5 Mbps over the same time frame. The reasoning mainly stems from the assumption that overall demand and peak demand will generally outpace available technical capacity. Additionally, we assumed ambitious growth for bandwidth demand per user in recognition of the continuing expansion of an internet-based world.

Table 6.3: Assumed Growth Factors for Underlying Demand Parameters for Demand Years beyond the Base Year (Demand Year = 0)

Parameter	Estimated Annual Growth Factor
Capacity per Platform	3.73%
Peak Utilization Percentage	$(3.144 \times \log_{50}(\text{Demand Year}))\%$
Minimum End-User Bandwidth Demand	6.65%

We assumed a non-linear decaying annual growth factor for peak utilization percentage owing to population growth and increasing saturation in the internet domain.

We also utilized historical population data to extrapolate annual population growth rates for each metropolitan and micropolitan statistical area (U.S. Census Bureau, Population Division, 2014). We then utilized these growth rates to estimate the total number of users per platform in future years. Figure 6.14 illustrates the projected number of flights needed in the 25^{th} demand year for the same statistical areas as Figure 6.11.

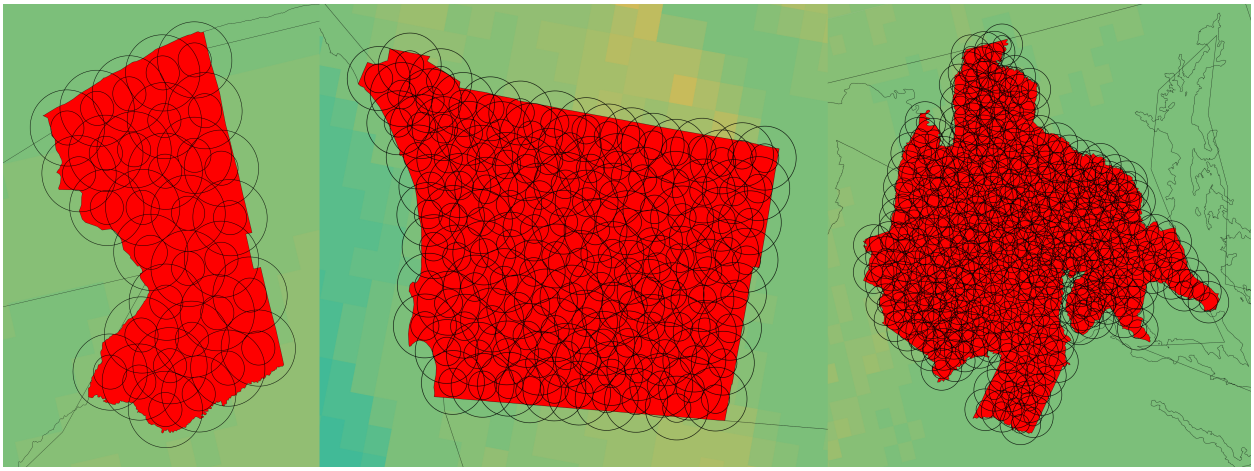

Figure 6.14: Buffalo, NY, San Diego, CA and Washington DC Metropolitan Areas with UAV Coverage (Projected Demand Year 25)

As can be seen, positive population growth and bandwidth demand increases combined with higher levels of peak utilization lead to denser placements of HALE mission orbits over the statistical areas.

Simulated and Iterative Demand Projections

Iterative demand projections were made using the MATLAB implementation of the k-means algorithm and represent the sum total of estimated HALE vehicles needing to be deployed in order to fully serve all considered metropolitan and micropolitan statistical areas.

We also present a simulated demand projection, which is generated as follows. We first assume the base year orbit covering result as the floor of necessary vehicles needed to completely cover all considered statistical areas for the base year. Next, we directly apply the growth rates and factors to the data and recompute the total users that can be served per vehicle. If the number of assigned vehicles is insufficient, we add additional vehicles until the total demand is served. Since we do not consider the placement of these vehicles, we avoid potential overestimates resulting from the k-means algorithm as it is not guaranteed to always converge to a global optimum. Thus, the simulated demand projections can serve as a lower bound for the number of HALE vehicles needing to be deployed. Figure 6.15 illustrates the results from both the simulated and iterative demand projections. As illustrated, future 25 year projections indicate that more than 25,500 HALE vehicles could orbit the skies of American metropolitan and micropolitan areas, from a base of around 22,500. We also see that the simulated and iterative demand estimates are virtually identical.

From the iterative results and simulated results, we found that the total number of flights grows on average at a rate of 0.522% and 0.520% per year, respectively.

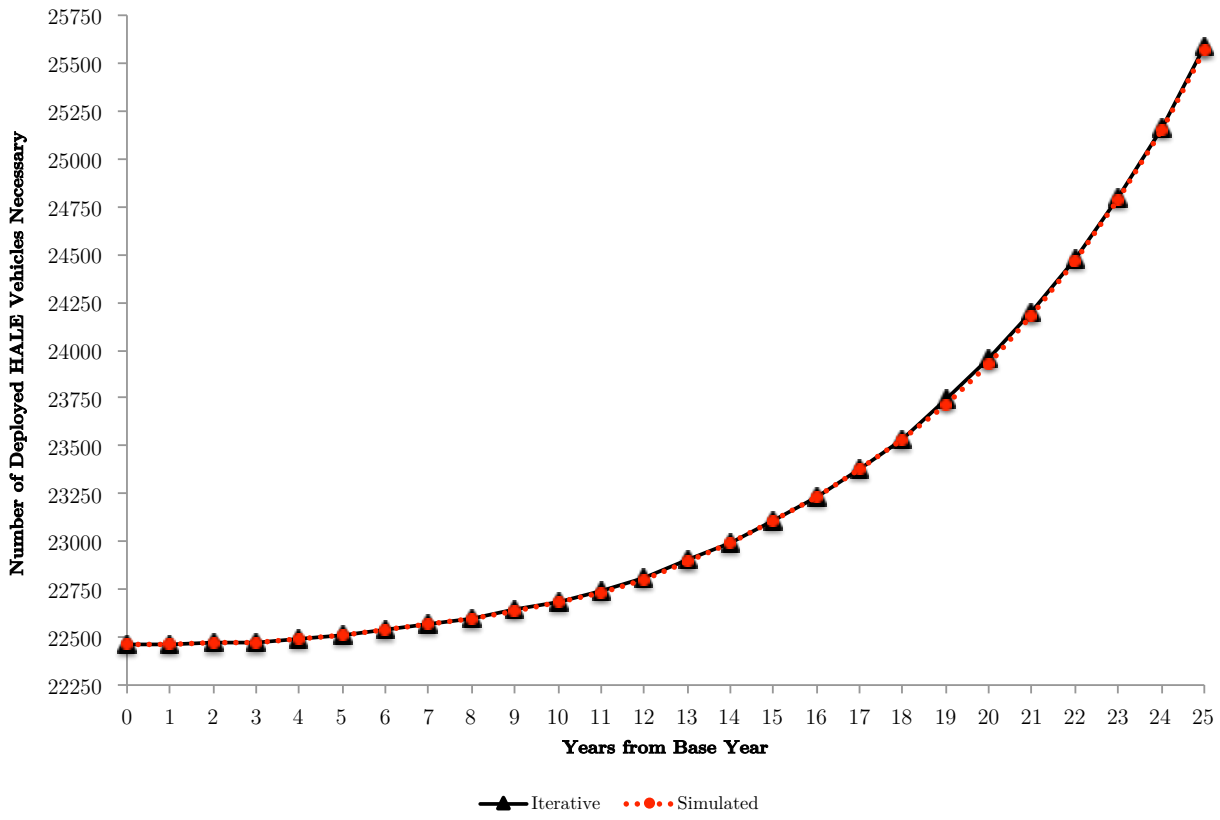

Figure 6.15: Estimated and Simulated Growth in the Number of HALE Vehicles to be Deployed

Sensitivity Analysis

To explore the effects of different end-user bandwidth growth rates and platform capacity growth rates on the number of flights, we simulated 100 different scenarios whereby we changed the growth rates for platform capacity and end-user bandwidth demand while keeping the peak-utilization growth rate the same. Table 6.4 gives the matrix of combinations explored

Table 6.4: Matrix of Combinations of Platform Capacity Growth Rates and End-User Bandwidth Growth Rates

1.5%, 4.0%	2.0%, 4.0%	2.5%, 4.0%	3.0%, 4.0%	3.5%, 4.0%	4.0%, 4.0%	4.5%, 4.0%	5.0%, 4.0%	5.5%, 4.0%	6.0%, 4.0%
1.5%, 4.5%	2.0%, 4.5%	2.5%, 4.5%	3.0%, 4.5%	3.5%, 4.5%	4.0%, 4.5%	4.5%, 4.5%	5.0%, 4.5%	5.5%, 4.5%	6.0%, 4.5%
1.5%, 5.0%	2.0%, 5.0%	2.5%, 5.0%	3.0%, 5.0%	3.5%, 5.0%	4.0%, 5.0%	4.5%, 5.0%	5.0%, 5.0%	5.5%, 5.0%	6.0%, 5.0%
1.5%, 5.5%	2.0%, 5.5%	2.5%, 5.5%	3.0%, 5.5%	3.5%, 5.5%	4.0%, 5.5%	4.5%, 5.5%	5.0%, 5.5%	5.5%, 5.5%	6.0%, 5.5%
1.5%, 6.0%	2.0%, 6.0%	2.5%, 6.0%	3.0%, 6.0%	3.5%, 6.0%	4.0%, 6.0%	4.5%, 6.0%	5.0%, 6.0%	5.5%, 6.0%	6.0%, 6.0%
1.5%, 6.5%	2.0%, 6.5%	2.5%, 6.5%	3.0%, 6.5%	3.5%, 6.5%	4.0%, 6.5%	4.5%, 6.5%	5.0%, 6.5%	5.5%, 6.5%	6.0%, 6.5%
1.5%, 7.0%	2.0%, 7.0%	2.5%, 7.0%	3.0%, 7.0%	3.5%, 7.0%	4.0%, 7.0%	4.5%, 7.0%	5.0%, 7.0%	5.5%, 7.0%	6.0%, 7.0%
1.5%, 7.5%	2.0%, 7.5%	2.5%, 7.5%	3.0%, 7.5%	3.5%, 7.5%	4.0%, 7.5%	4.5%, 7.5%	5.0%, 7.5%	5.5%, 7.5%	6.0%, 7.5%
1.5%, 8.0%	2.0%, 8.0%	2.5%, 8.0%	3.0%, 8.0%	3.5%, 8.0%	4.0%, 8.0%	4.5%, 8.0%	5.0%, 8.0%	5.5%, 8.0%	6.0%, 8.0%
1.5%, 8.5%	2.0%, 8.5%	2.5%, 8.5%	3.0%, 8.5%	3.5%, 8.5%	4.0%, 8.5%	4.5%, 8.5%	5.0%, 8.5%	5.5%, 8.5%	6.0%, 8.5%

As illustrated by Figure 6.16, platform capacity growth has greatest effect on the number of future flights needed.

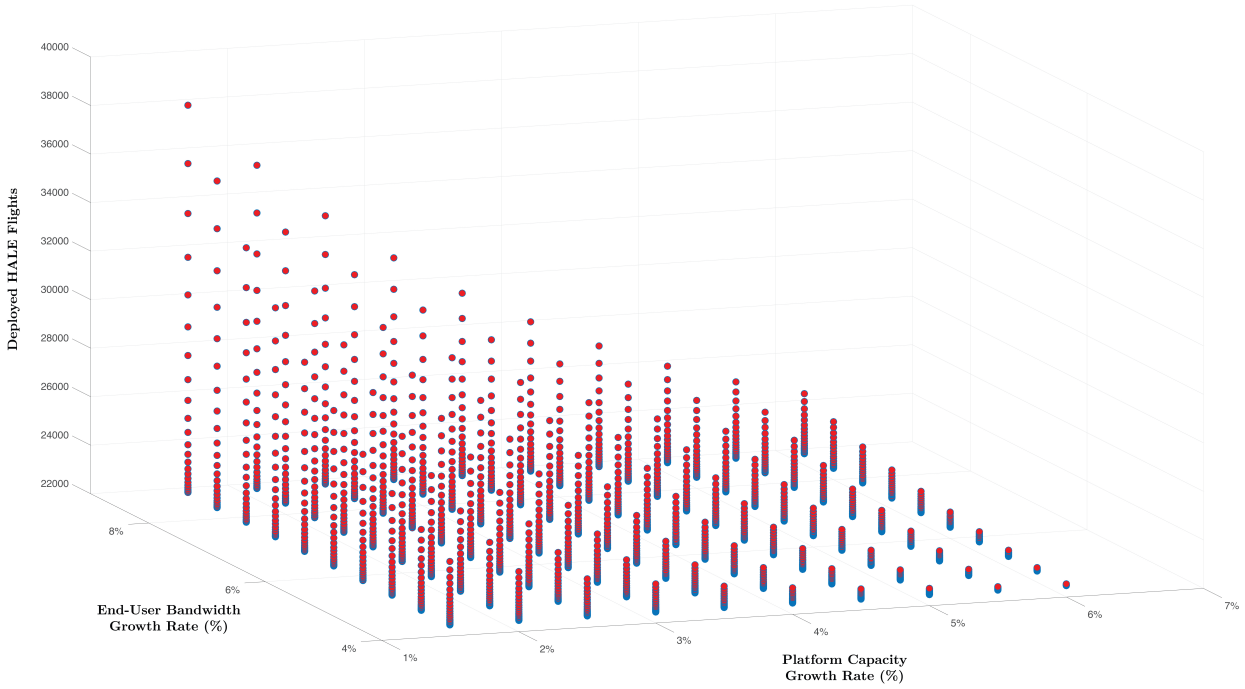

Figure 6.16: Estimated and Simulated Growth in the Number of HALE Vehicles to be Deployed

Even under the most aggressive end-user bandwidth growth assumption, the growth in the number of necessary HALE flight deployments is strongly mitigated with high platform

capacity growth. Table 6.5 provides equivalent annual growth rates for each combination and further illustrates the strong effect of platform capacity growth.

Table 6.5: Matrix of Equivalent Annual Growth Rates in Platforms Deployed for Platform Capacity Growth Rate (Row) and End-User Bandwidth Growth Rate (Column) Combinations

	1.5%	2.0%	2.5%	3.0%	3.5%	4.0%	4.5%	5.0%	5.5%	6.0%
4.0%	0.442%	0.345%	0.265%	0.201%	0.152%	0.110%	0.074%	0.046%	0.026%	0.015%
4.5%	0.555%	0.440%	0.343%	0.265%	0.200%	0.152%	0.110%	0.074%	0.046%	0.027%
5.0%	0.687%	0.551%	0.437%	0.342%	0.264%	0.200%	0.151%	0.110%	0.074%	0.046%
5.5%	0.840%	0.683%	0.547%	0.435%	0.340%	0.262%	0.200%	0.151%	0.110%	0.074%
6.0%	1.011%	0.833%	0.678%	0.543%	0.431%	0.339%	0.261%	0.199%	0.151%	0.110%
6.5%	1.200%	1.003%	0.828%	0.673%	0.540%	0.429%	0.337%	0.261%	0.199%	0.151%
7.0%	1.412%	1.191%	0.994%	0.821%	0.668%	0.536%	0.426%	0.335%	0.260%	0.198%
7.5%	1.643%	1.401%	1.181%	0.987%	0.814%	0.663%	0.533%	0.424%	0.333%	0.258%
8.0%	1.896%	1.629%	1.389%	1.171%	0.980%	0.809%	0.658%	0.530%	0.422%	0.332%
8.5%	2.172%	1.879%	1.615%	1.377%	1.162%	0.972%	0.803%	0.655%	0.527%	0.419%

6.3.5 Concluding Remarks

High altitude vehicles provide an alternative to additional construction of terrestrial delivery systems as well as expensive deployment of satellite delivery systems. Keys to success in the utilization of high altitude vehicles will include managing per-platform operational cost and ensuring efficient deployment and siting of high-altitude vehicles. Effective mission scheduling will also be important to ensure that continuous coverage is maintained while accounting for potential downtime and maintenance. Future work should also consider modeling per-platform costs and account for uneven population densities in metropolitan areas. This will directly affect the deployment of high altitude platforms as well as inform whether such a system would be cost-effective.

6.4 Disaster Survey Assessment

Natural disasters are a great threat to many of the highly populated areas in the world. For example, as seen in Figure 6.17, at least 6,923 tropical cyclone events have approached the densely populated coastal regions of the World over a 165-year period. The United States is no exception and is exposed to 12 tropical cyclones in a typical year. As seen in Figure 6.18, more than 1015 tropical cyclone events have affected the Eastern and Southeastern coasts of the United States for over a century.

The impact of hurricanes cannot be understated. Exemplifying the severity of their destructive power, the five deadliest hurricanes alone have produced close to 15,000 deaths in the United States (Wunderground, 2014). Thus, due to their destructive power, hurricanes require constant monitoring, which is currently performed using satellites and aerial vehicles (i.e., hurricane hunter aircraft). While it is unlikely that hurricane hunter aircraft would be fully converted to unmanned vehicles in the future, there still remains a need to fly above the hurricane event to assess its path, pressure distribution, and other atmospheric parameters that could help predict the hurricane's future path and destructive power. These missions could potentially be carried out by unmanned aerial vehicles.

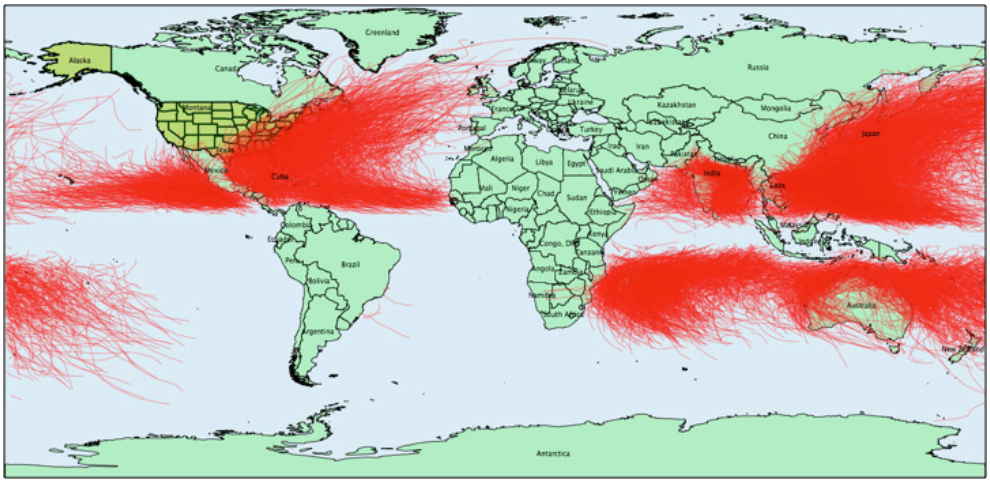

Figure 6.17: Tropical Cyclone Events Worldwide from 1848 to 2014 (6,923 Events). Source of Data for Picture: (National Hurricane Center, 2014).

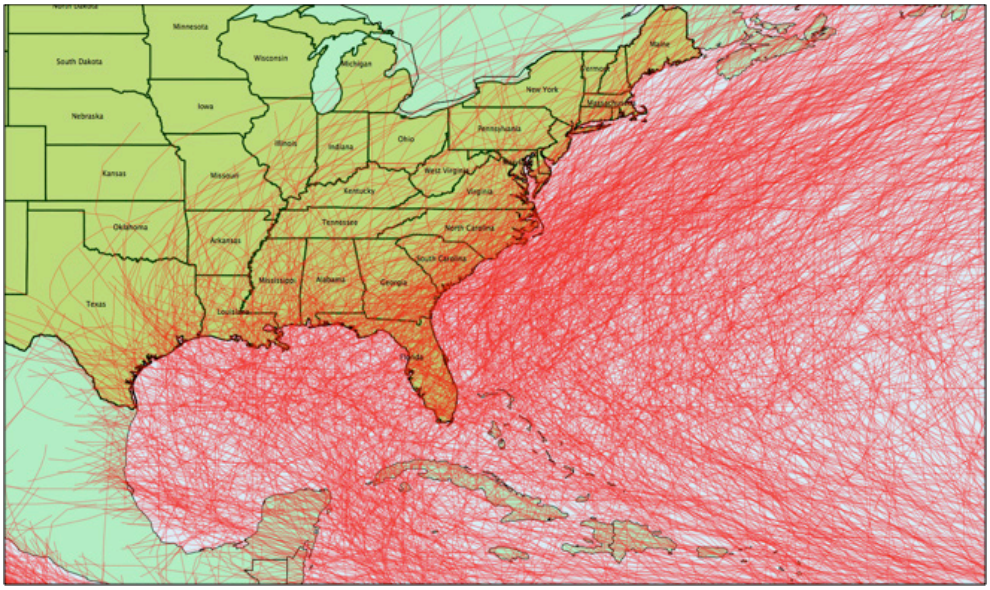

Figure 6.18: Tropical Cyclone Events in the Eastern United States from 1848 to 2014 (1,015 Events). Source of Data for Picture: (National Hurricane Center, 2014).

We consider two mission profiles flown by UAS vehicles for this analysis: a) Over-storm surveillance and b) Over land surveillance and emergency command and control flights. The first mission is flown over the weather and over land to track the hurricane event and thus assess weather characteristics using a high-flying platform. This mission is similar to the flights taken by NASA's Global Hawk RQ-4 missions to track hurricane events as shown in Figure 6.20. The figure shows the approximate tracks flown starting from Wallops Island and moving East to the North Atlantic Ocean for two hurricane events. The mission shows the need for long flight endurance and a high altitude platform.

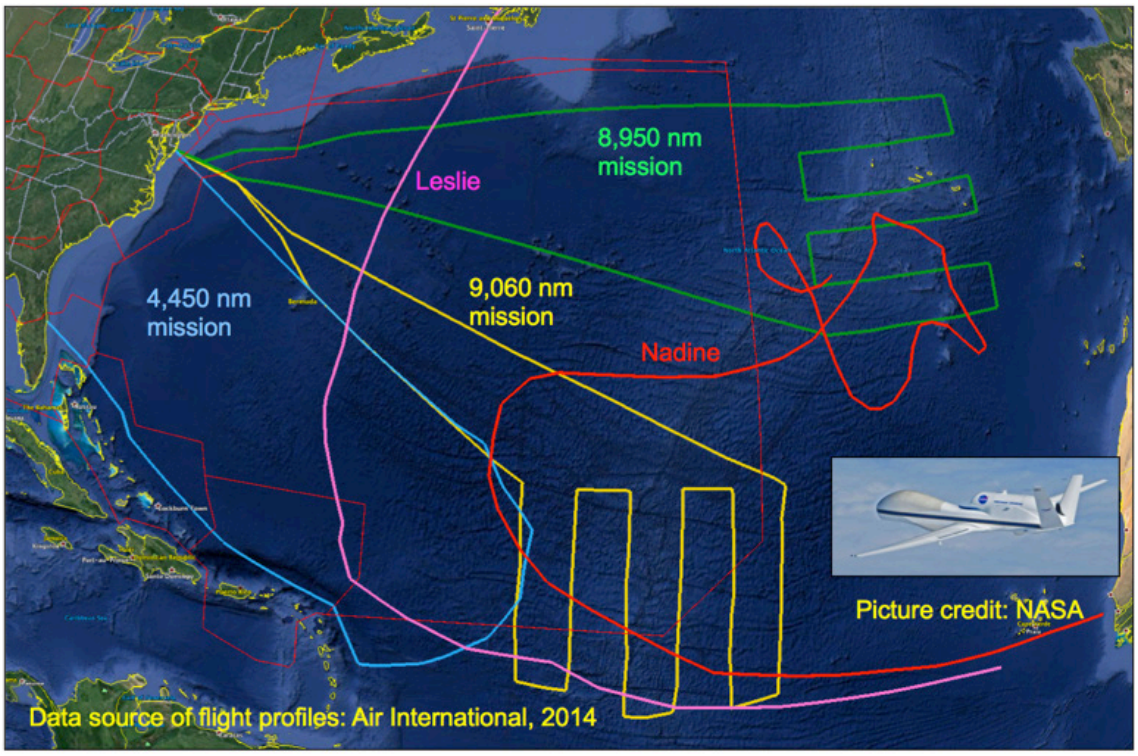

Figure 6.19: Approximate Flight Tracks Flown by NASA Global Hawk Aircraft in Support of Reconaissance Missions for Hurricanes Nadine and Leslie. Source for Picture: (AIR International, 2014).

6.4.1 Mission Profile Design

Two missions are flown using High Altitude and Long Endurance UAS vehicles: a) over-storm and b) disaster command and control and rescue surveillance. These mission profiles are described in the following sections.

Over-Storm Mission Profile

As our illustrative example, we simulated potential disaster relief and surveillance missions for Hurricane Katrina, considered one of the deadliest and most destructive hurricanes to affect the United States. Hurricane Katrina originated over the Bahamas and tracked a path from southern Florida through southeastern Louisiana to as far north as Ohio.

For storm monitoring, the long endurance of the HALE vehicle makes it an idea platform to track and fly over the storm providing important characteristics in the development and movement of a cyclone event well before it hits the coastal areas.

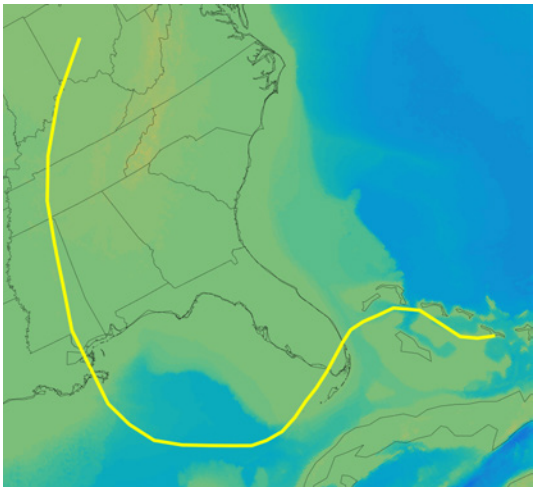

Figure 6.20: Flight Path of Hurricane Katrina. Source of Data: (National Hurricane Center, 2014).

For the over-storm profile, we assume that it follows a regular pattern to track the storm. A potential mission would begin at an airport situated over 600 nautical miles away from the starting point of the storm to be tracked. This is necessary given the slow climb rate of the assumed flight vehicle as illustrated earlier in Figure 6.2 and allows for a direct climb to an altitude and flight ceiling of 65,000 ft. Once the aircraft reaches its intended starting point, it begins tracing a saw-tooth pattern as shown in Figure 6.21.

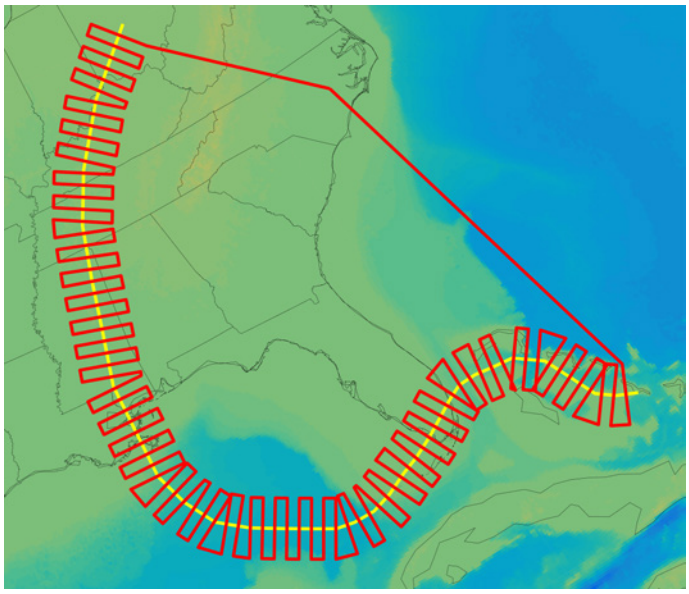

Figure 6.21: Depiction of Sawtooth Tracking Profile over Hurricane Katrina

The saw-tooth pattern is centered on the approximate centerline of the storm. A saw-tooth pattern was assumed for the mission profile both to match prior profiles used for storm tracking and to cover as much of the storm area as possible. This is especially important if the operator intends to deploy drop sondes for collecting atmospheric profiles, humidity and other storm data.

For the surveillance mission depicted in Figure 6.21, the HALE aircraft departs from Kinston Regional Jetport located in Kinston, North Carolina. The aircraft is estimated to travel a total of 11,908 nautical miles from takeoff to touchdown with a total mission time of approximately 170.1 hours ($\propto$ 7.09 days) at a cruise speed of 70 knots.

Disaster Relief Surveillance and Emergency Communication Support

HALE UAS vehicles are particularly suited for disaster relief observation, command and control communications and in general for aerial surveillance of areas affected by natural or man-made disasters. The HALE vehicle has significant endurance to survey large areas of a population center in need for disaster relief support. The HALE vehicle also can orbit at low speed and thus provide a platform for emergency communication and command and control

support after a disaster.

6.4.2 Estimating Platform Capacity and Affected Area

Using hurricane track and average wind speed data, we first identified metropolitan areas that would experience hurricane force winds. The Saffir-Simpson Scale for Hurricane Intensity sets the lower bound for hurricane level winds at 64 knots (Graumann et al., 2005). Furthermore, at its peak strength, hurricane force winds extended outward up to 105 miles (Graumann et al., 2005) from the center. Therefore, for track points having an average wind speed in excess of 64 knots, we considered affected areas as those that fit within a circle having a radius of 105 miles and centered at a qualifying track point. Figure 6.22 illustrates the affected areas determined by this method.

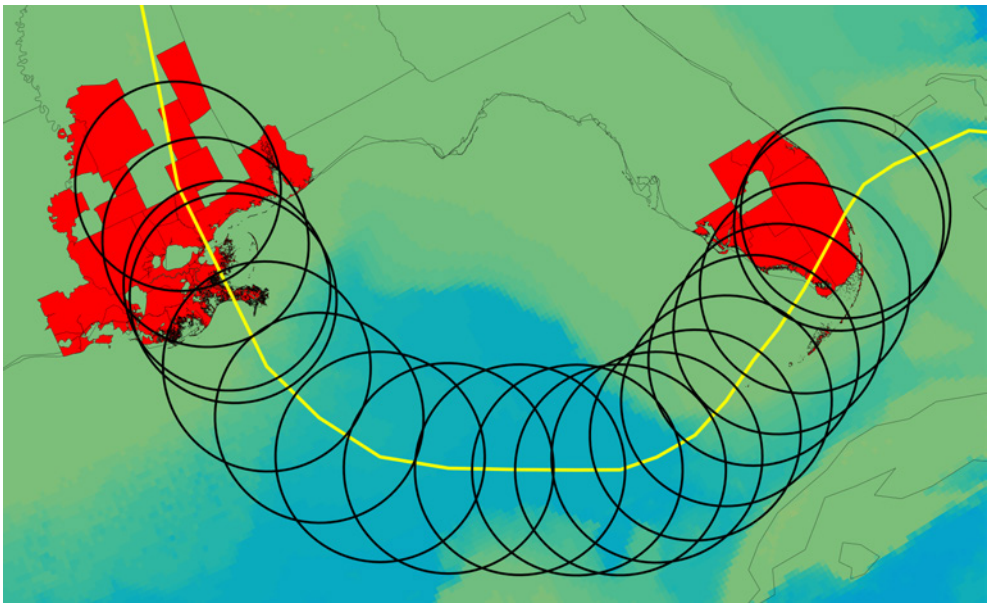

Figure 6.22: Metropolitan Areas determined to be severely impacted by Hurricane Katrina

These areas cover the New Orleans metropolitan area, the Mississippi Gulf Coast and Southern Florida and generally correspond to the areas affected by Hurricane Katrina in 2005.

For estimating average user demand, we assume that affected civilians and emergency

responders will need the ability to send and receive calls, texts and utilize the Global Positioning System. This necessitates an average bandwidth need of between 20-384 kb/s (Karapantazis and Pavlidou, 2005).

Given the emergency conditions, we also assume a relatively high peak utilization rate of 75%, reflecting both the expected high demand on communication systems during emergencies and the need to minimize the risk of lacking sufficient system capacity. We assume the bandwidth will be delivered by a series of platforms, each capable of delivering up to 100,000 Mbps of bandwidth in the base year. Under these assumptions, we estimated that each platform could support 347,222 users on average.

$$\frac{100,000 \text{ Mpbs}}{(0.384 \text{ Mbps/user})\,(0.75 \text{ peak utilization})} = 347,222 \text{ Users} \tag{6.8}$$

We then established our platform operating parameters as follows. We assumed an operating altitude range of 60,000 feet up to a maximum of 65,000 feet, at a cruise speed of 70 knots and total mission length corresponding to the event length (8 days for Hurricane Katrina). Mission length includes the time to takeoff, fly to the loiter area, loiter, cruise to the return airport and land. We also assumed circular flight orbits, each having a radius of 2.5 nautical miles for simplicity, and a maximum look angle of 35° between end-user ground receivers and the orbiting platform. Having established the operating parameters, the flight demand estimation methodology mirrors that of Section 6.3.3.

6.4.3 Flight Demand Estimates

Using the methodology of Section 6.3.3, solutions were found for all of statistical areas prior to reaching the iteration limit. Figure 6.23 illustrates examples of fully covered statistical areas affected by Hurricane Katrina.

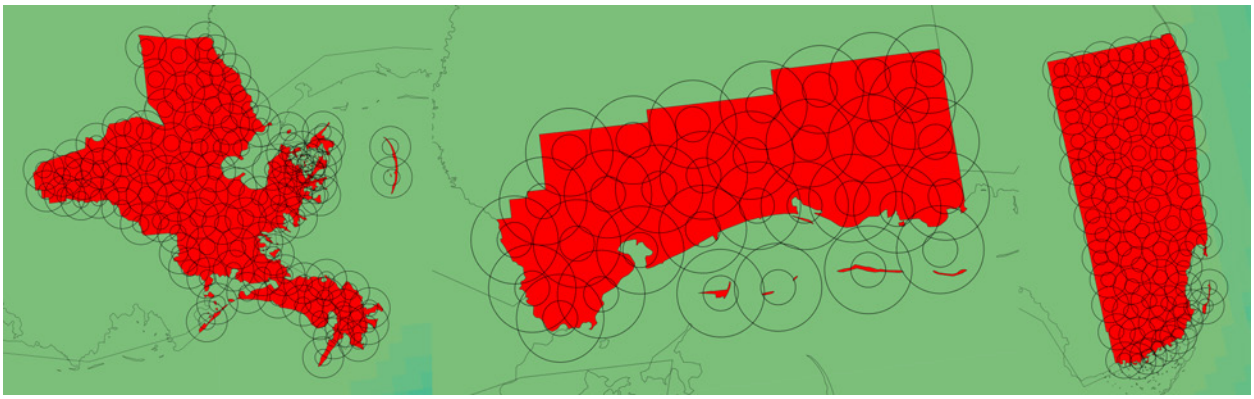

Figure 6.23: Miami, FL, Gulfport-Biloxi, MS, and New Orleans, LA Metropolitan Areas with HALE Coverage

As can be seen, for those three statistical areas, we estimated a total need of 196 damage survey flights and 1 hurricane surveillance flight. As a comparison, for the mission of delivering broadband internet service, we estimated a total of 271 HALE vehicles being necessary to serve the statistical areas.

For the areas affected by Hurricane Katrina, we estimate that a total of 760 flights are needed to fully surveil the affected areas.

6.4.4 Concluding Remarks

In emergency weather situations, high altitude aircraft provide a readily deployable and scalable backup to providing communications and navigational service delivery to disaster areas. HALE platforms are attractive in that they fly above storms and can loiter potentially for the duration of the weather event. One determinant of successful utilization of HALE aircraft is ensuring that the broadcast signal is effectively transmitted through associated cloud cover and other weather-related interference. It will also be important to choose the launch site wisely as it must be situated away from the storm so as to allow for sufficient distance for the HALE aircraft to reach its cruising altitude. Future work might investigate the effects of cloud cover on signal transmission in order to provide more accurate estimates of effective available capacity. This will directly affect the efficacy of a HALE deployment during a weather disaster.

6.5 Airspace Conflict Considerations

The complication to any HALE deployment scheme center on how to move the HALE vehicles to and from their basing airports to their deployment locations. As illustrated by Figures 6.2 and 6.3, HALE vehicles generally are slow moving platforms that have very lengthy climb profiles. While their operational altitudes sit well above commercial traffic, the time and space needed to climb to these altitudes presents a potential challenge in terms of ensuring that no conflicts arise with faster moving commercial and general aviation traffic.

Given the long climb distance and time, one potential workaround is to have the HALE vehicle perform a spiral climb to its cruising altitude before continuing to its loiter position. Similarly, on the return leg, the aircraft could perform an spiral descent maneuver before leveling out and landing at a basing airport. Therefore, it is necessary to determine the amount of airspace implicated during these maneuvers to establish their feasibility.

6.5.1 A Spiraling Climb Maneuver

For the climb maneuver, we assume that the HALE vehicle will perform a steady coordinated turn with a gentle climb angle. The forces during the turn are depicted in Figures 6.24, 6.25, and 6.26.

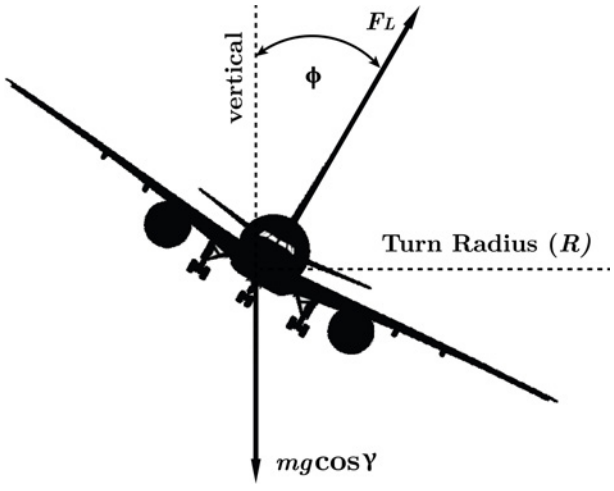

Figure 6.24: Front View of Forces acting on an Aircraft in a Steady Coordinated Turn

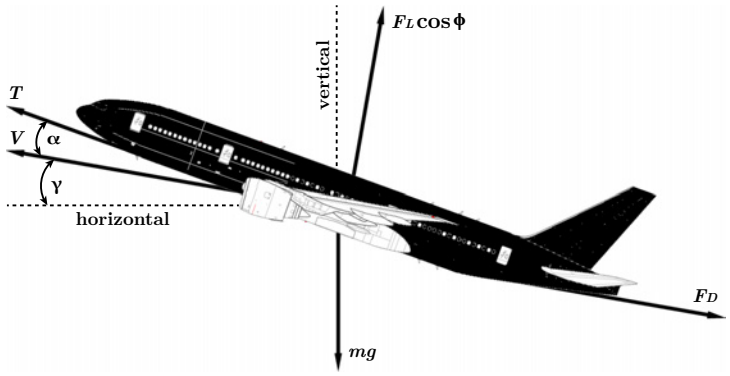

Figure 6.25: Side View of Forces acting on an Aircraft in a Steady Coordinated Turn

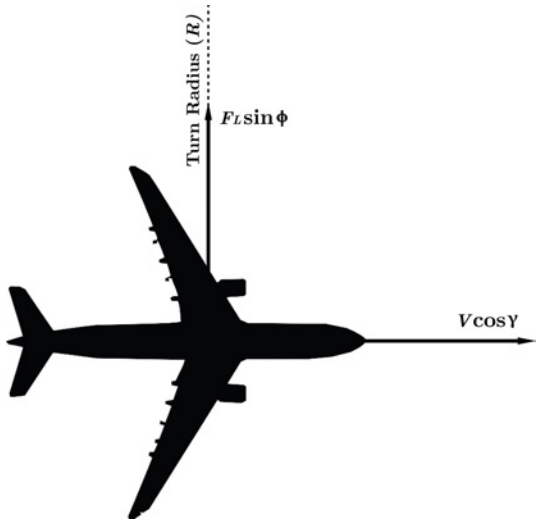

Figure 6.26: Top View of Forces acting on an Aircraft in a Steady Coordinated Turn

From Figure 6.25, we can represent the balanced forces the direction of flight as

$$T \cos \alpha = F_D + mg \sin \gamma \tag{6.9}$$

or as

$$\frac{T \cos \alpha - F_D}{mg} = \sin \gamma \tag{6.10}$$

From (4.29), we see that multiplying $\sin\gamma$ by the airspeed (V) gives the climb rate. Therefore

$$v\left(\frac{T\cos\alpha - F_D}{mg}\right) = \frac{dh}{dt} \tag{6.11}$$

Utilizing the BADA drag polar, the drag force is given as

$$F_D = \frac{1}{2}\rho v^2 S\left(C_{d0} + C_{d2}C_L^2\right) \tag{6.12}$$

Therefore, combining (6.11) with (6.12) gives

$$v\left(\frac{T\cos\alpha - \frac{1}{2}\rho v^2 S\left(C_{d0} + C_{d2}C_L^2\right)}{mg}\right) = \frac{dh}{dt} \tag{6.13}$$

From Figure 6.24, we see that the forces acting on the aircraft in the direction perpendicular to the direction of flight and the radial direction are

$$F_L\cos\phi = mg\cos\gamma \tag{6.14}$$

With the lift force equal to $\rho v^2 S C_L/2$, we can write (6.14) as

$$\frac{1}{2}\rho v^2 S C_L = \frac{mg\cos\gamma}{\cos\phi} \tag{6.15}$$

Solving for the lift coefficient, we have

$$C_L = \frac{2mg\cos\gamma}{\rho v^2 S\cos\phi} \tag{6.16}$$

We can then combine (6.16) with (6.13) to give

$$v\left(\frac{T\cos\alpha - \frac{1}{2}\rho v^2 S\left(C_{d0} + C_{d2}\left(\frac{2mg\cos\gamma}{\rho v^2 S\cos\phi}\right)^2\right)}{mg}\right) = \frac{dh}{dt} \tag{6.17}$$

Given that the HALE vehicle is entirely electric powered, there will be no mass lost due to fuel burn. Therefore, we can assume that the mass (m) remains constant during the flight. Consequently, the climb rate will be a function of the angle of attack (α), the airspeed

(v), the flight path angle (γ), the bank angle (ϕ) and the air density (ρ). Having already accounted for the change in air density for the BADA performance files, if we assume a relatively constant angle of attack and flight path angle, the climb rate becomes a function of the bank angle and is given as

$$\frac{dh/dt}{d\phi} = -\frac{4C_{d2}g^3 m\cos^2\gamma\sec^2\phi\tan\phi}{\rho S v} \tag{6.18}$$

As illustrated by (6.18), increasing the bank angle progressively decreases the climb rate. Figure 6.27 illustrates the unit rate of decrease in the climb rate for bank angles up to 15 degrees.

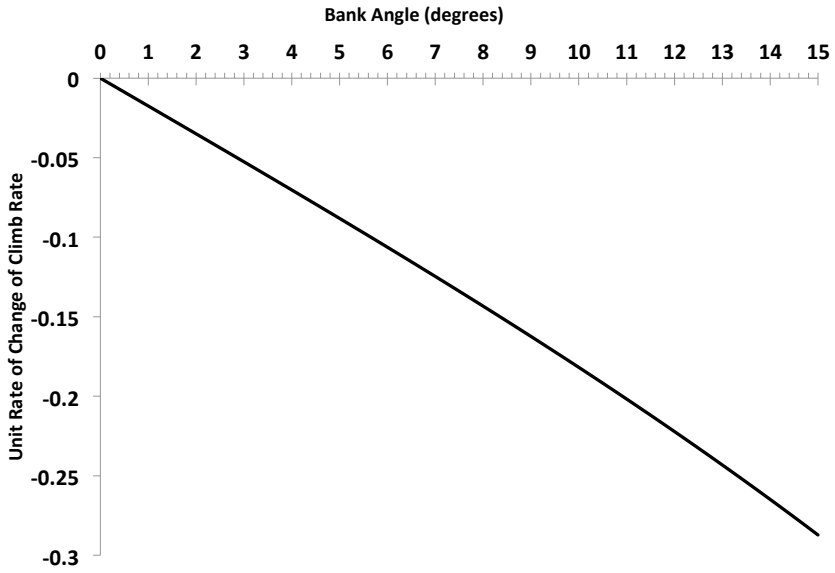

Figure 6.27: Unit Rate of Change of Climb Rate with respect to Bank Angle

For level flight, the bank angle (ϕ) will be equal to zero. Therefore, at level flight, the rate of climb is given as

$$v\left(\frac{T\cos\alpha - \frac{1}{2}\rho v^2 S\left(C_{d0} + C_{d2}\left(\frac{2mg\cos\gamma}{\rho v^2 S}\right)^2\right)}{mg}\right) = \frac{dh}{dt}_{\phi=0} \tag{6.19}$$

Taking the difference of (6.17) and (6.19), we have

$$\frac{2mg\left(\cos\gamma\right)^2 C_{d2}}{\rho S V}\left(\frac{1}{\left(\cos\phi\right)^2}-1\right)=\frac{dh}{dt}_{\phi=0}-\frac{dh}{dt} \tag{6.20}$$

Therefore, for a given bank angle (ϕ), the resultant climb rate will be

$$\frac{dh}{dt}=\frac{dh}{dt}_{\phi=0}-\frac{2mg\left(\cos\gamma\right)^2 C_{d2}}{\rho S V}\left(\frac{1}{\left(\cos\phi\right)^2}-1\right) \tag{6.21}$$

We assume that the flight path angle remains unchanged from that during straight flight. Therefore, since $\sin\gamma$ multiplied by the airspeed yields the climb rate, it follows that

$$\sin\gamma=\frac{\frac{dh}{dt}_{\phi=0}}{v}\Rightarrow\gamma=\arcsin\frac{\frac{dh}{dt}_{\phi=0}}{v} \tag{6.22}$$

The radius of the turn executed can also be determined by considering the forces in the radial direction. From Figure 6.26, we can write

$$F_L\sin\phi=m\frac{\left(v\cos\gamma\right)^2}{R} \tag{6.23}$$

From (6.14), we can write the lift force F_L as

$$F_L=\frac{mg\cos\gamma}{\cos\phi} \tag{6.24}$$

Therefore, with (6.23) and (6.24), we can solve for R as

$$R=\frac{v^2\cos\gamma}{g\tan\phi} \tag{6.25}$$

With (6.22), we can write (6.25) as

$$R=\frac{v^2\sqrt{1-\left(\frac{\frac{dh}{dt}_{\phi=0}}{v}\right)^2}}{g\tan\phi} \tag{6.26}$$

6.5.2 Simulating the Climb Maneuver

As demonstrated, one of the key determinants of the climbing turn maneuver possible is the bank angle (ϕ). Therefore, we first need to determine the bank angles possible given the vehicles performance and weight characteristics.

The bank angle will be limited by the maximum lift coefficient ($C_{L,max}$). To determine $C_{L,max}$, we consider the necessary lift force to maintain the full weight of HALE vehicle in flight at its stall speed (v_{stall}). Therefore, we have

$$F_L = \frac{1}{2}\rho v_{stall}^2 S C_{L,max} \Rightarrow C_{L,max} = \frac{2mg}{\rho v_{stall}^2 S} \tag{6.27}$$

From (6.27), $C_{L,max}$ is found to be 1.399. Next, using (6.16) and (6.22), we determine the maximum possible bank (ϕ_{max}) angle for a given airspeed (v), equivalent zero bank angle rate of climb ($\frac{dh}{dt}_{\phi=0}$) and air density (ρ) to be

$$\phi_{max} = \arccos\left(\frac{2mg\sqrt{1-\left(\frac{\frac{dh}{dt}_{\phi=0}}{v}\right)^2}}{C_{L,max}\rho v^2 S}\right) \tag{6.28}$$

Figure 6.28 illustrates the maximum bank angles possible for the given HALE performance parameters over the range of possible flight levels. However, we mirror the maximum command bank angle of the similar X-HALE vehicle presented by Köthe et al and limit the bank angle to 15 degrees (Köthe et al., 2016).

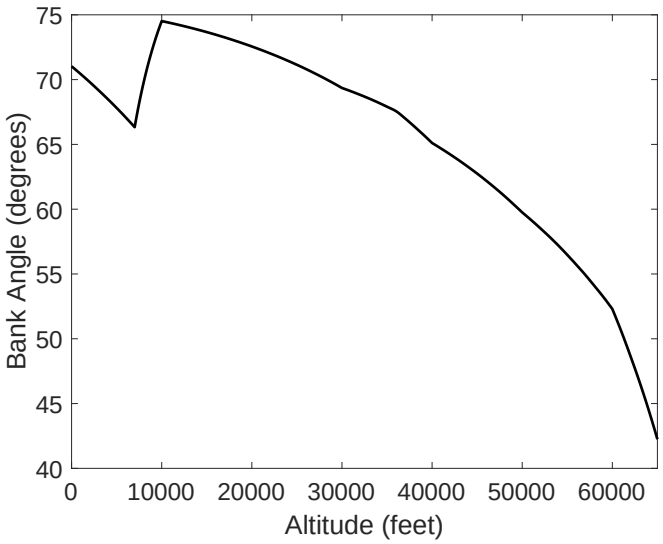

Figure 6.28: Maximum Bank Angles Possible for given Performance Characteristics of the HALE Vehicle

For the climb maneuver, we assume that the climb will not begin until the HALE vehicle reaches an altitude of 5,000 feet. At the time it reaches 5,000 feet, the aircraft will turn at the specified bank angle until it reaches 60,000 feet. The implementation in MATLAB produces the following trajectory, displayed in Figure 6.29. After climbing over a distance of approximately 10 nautical miles to an altitude of 5,000 feet, the HALE aircraft climbs and turns at a constant bank angle of 15 degrees. As the aircraft climbs and increases in airspeed, the turn radius increases and reaches a maximum of 0.33 nautical miles at 60,000 feet.

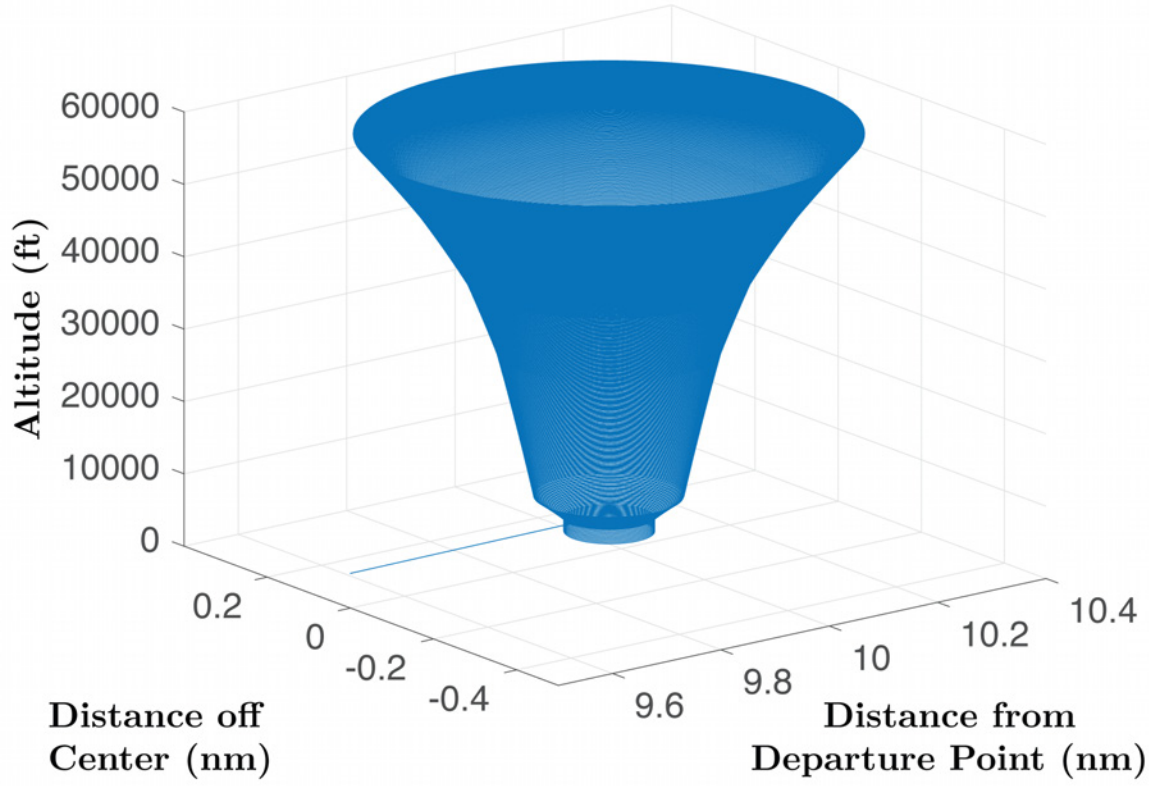

Figure 6.29: Simulated Spiral Up Trajectory for the assumed HALE Aircraft

6.5.3 Airspace Implications

Using the climb profile displayed in Figure 6.2, the climb to 5,000 feet occurs over a distance of approximately 11.43 miles and over a time of about 17.08 minutes. During the spiral up maneuver, an area of 0.453 square miles will be utilized after which the HALE aircraft will be clear of commercial aircraft flight levels and can proceed to its loiter point. The time to complete the spiral up maneuver to 60,000 feet is estimated to be approximately 7.69 hours for a total maneuver time of approximately 8 hours. This compares to a distance of 530 miles and a climb time of approximately 7.31 hours for a direct climb to 60,000 feet. Though the spiral maneuver requires an additional 41 minutes, the airspace implicated is significantly less than that for a direct climb.

6.5.4 Simulating the Descent Maneuver

Similar to the climb maneuver, we also assume that on descent, the aircraft will spiral down until it reaches an altitude of 5,000 feet. At that time, the aircraft will move to begin its approach to the base airport. The analysis for the descent maneuver is similar to that of the climb maneuver. From Figure 6.30, we can represent the force balance on the aircraft in descent as

$$T\cos\alpha + mg\sin\gamma = F_D \tag{6.29}$$

From (6.29) and utilizing the BADA drag polar, we can represent the rate of descent or sink rate as

$$\frac{dh}{dt} = v\left(\frac{\frac{1}{2}\rho v^2 S\left(C_{d0} + C_{d2}\left(\frac{2mg\cos\gamma}{\rho v^2 S\cos\phi}\right)\right) - T\cos\alpha}{mg}\right) \tag{6.30}$$

For level flight, the bank angle (ϕ) will be equal to zero. Therefore, at level flight, the sink rate is given as

$$\frac{dh}{dt}_{\phi=0} = v\left(\frac{\frac{1}{2}\rho v^2 S\left(C_{d0} + C_{d2}\left(\frac{2mg\cos\gamma}{\rho v^2 S}\right)\right) - T\cos\alpha}{mg}\right) \tag{6.31}$$

By differencing (6.30) and (6.31), we can solve for the sink rate as

$$\frac{dh}{dt} = \frac{dh}{dt}_{\phi=0} + \frac{2mg\left(\cos\gamma\right)^2 C_{d2}}{\rho S v}\left(\frac{1}{(\cos\phi)^2} - 1\right) \tag{6.32}$$

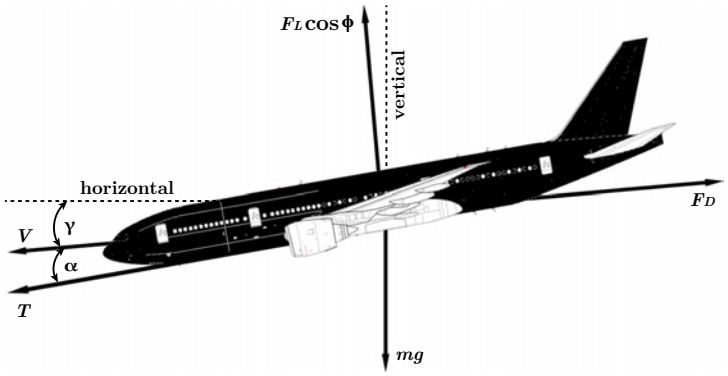

Figure 6.30: Side View of Forces acting on an Aircraft in a Steady Coordinated Turn during Descent

We assume that the flight path angle remains unchanged from that during straight flight. Therefore, since $\sin\gamma$ multiplied by the airspeed yields the sink rate, it follows that

$$\sin\gamma = \frac{\frac{dh}{dt}\,\phi=0}{v} \Rightarrow \gamma = \arcsin\frac{\frac{dh}{dt}\,\phi=0}{v} \tag{6.33}$$

The radius of the turn will also be determined similarly as

$$R = \frac{v^2\sqrt{1-\left(\frac{\frac{dh}{dt}\,\phi=0}{v}\right)^2}}{g\tan\phi} \tag{6.34}$$

The implementation in MATLAB produces the following trajectory, displayed in Figure 6.31. After spiraling down from a starting altitude of 60,000 to an altitude of 5,000 feet, the HALE aircraft continues to its approach vector for the arrival airport. As the aircraft descends, the turn radius becomes smaller, going from a high of 0.453 nautical miles to a minimum of approximately 0.137 nautical miles.

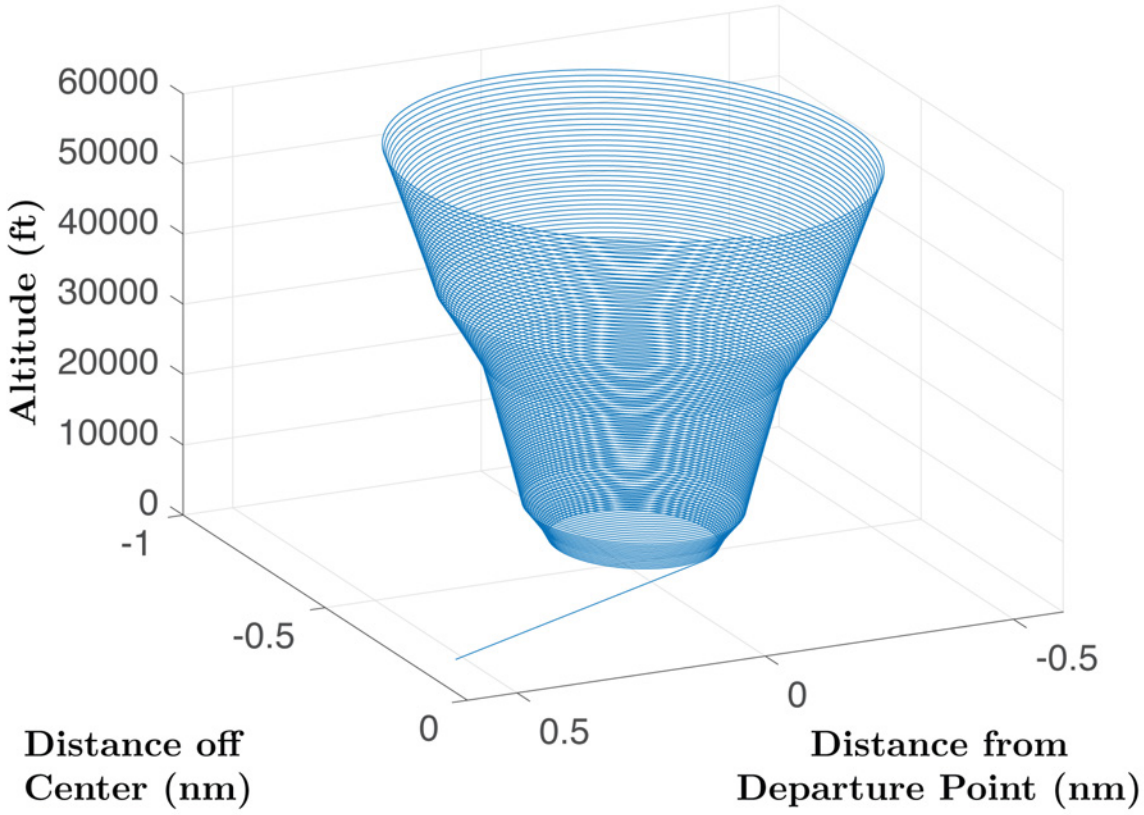

Figure 6.31: Simulated Spiral Down Trajectory for the assumed HALE Aircraft

6.5.5 Airspace Implications

The time to complete the spiral down maneuver is approximately 2.69 hours. Once the spiral down maneuver concludes, the HALE aircraft can descend from 5,000 feet to ground level in a time of 1134 seconds (*sim* 0.315 hours) over a distance of 17.22 miles. This compares against a total time of 2.98 hours for a direct descent over a distance of approximately 240 miles. As we can see, the times of both descent options are similar even though the spiral down maneuver involves significantly less airspace.

6.5.6 Concluding Remarks

In this section, we have demonstrated alternative climb and descent options for HALE aircraft to get to and from their loiter orbits. The maneuvers demonstrated also allow for considerable flexibility as operational conditions would dictate. Aircraft can begin climbs or descents at any altitude and the radii of the turns are also adjustable by changing the bank angle utilized. Finally, HALE operations are minimally penalized by adopting spiral maneuvers in terms of climb and descent time. Unlike the direct climb and descent options, the spiral maneuvers allow for HALE operations to involve significantly less airspace, resulting in easier potential integration into U.S. airspace.

6.6 Summary & Recommendations

In this chapter, we set out to demonstrate the feasibility and required scale for utilizing HALE aircraft for broadcasting communications services both commercially and during weather disasters. We assumed complete coverage of 929 metropolitan and micropolitan statistical areas in the United States, which accounted for approximately 300,645,000 residents as of 2013. In order to fully provide a T-1 internet connection to the covered areas, it was estimated that more than 22,500 HALE vehicle deployments would be necessary.

A consideration not covered in this chapter was that of cost. The procurement, maintenance, operation and deployment of 22,500 individual and autonomous aircraft would represent a considerable endeavor and a potentially considerable start-up cost. Additionally, future work should consider the life-cycle costs of maintaining such an operation and also consider the necessary pricing to end-users.

We also recommend that future work consider the organizational approach for operating such a system. Questions of whether this system should be a public or private operation are essential to determining the ultimate scale, funding mechanisms, and reach of any potential system that would be created. Additionally, the regulatory schemes under which such a system would operate are also critical to address. Since thousands of autonomous vehicles would be injected into U.S. airspace, it is necessary to have clarity on who determines where these vehicles can operate, where they can be stationed, and what measures should be taken

in the event of disasters.

High Altitude Platforms (HAPs) are a potential alternative to wireless communications networks. Their importance resides in the fact that HAPs offer easy and scalable deployment and maintenance while operating well above existing commercial air traffic. Given the promise of HAPs for future communications solutions, this area of research is of considerable importance and should be pursued vigorously.

6.7 Attributions

This work made use of the TIGER/Line Shapefile products, which were sourced from the United States Census Bureau (U.S. Census Bureau, 2014).

Chapter 7

Summary of Contributions and Recommendation for Future Research

7.1 Summary of Results

As this dissertation comes to a close, it is important to review the contributions believed to have been added to the field of Air Transportation as well as provide some concluding remarks and recommendations. To that end, this chapter provides an overview of the thesis and summarizes the additions to the field while also offering some avenues for future research and suggestions for extending this work.

The dissertation demonstrated the application of Bayesian methods and "Big Data" to Air Transportation problems. Despite the dynamic complexity of aircraft operations and flight mechanics, it was demonstrated that for airport operations, Bayesian statistical methods can provide accurate predictions of aircraft behavior and lead to more precise and detailed estimates of airport capacity.

In discussing the runway occupancy time models, it is important to understand what an analyst no longer needs to do regarding runway occupancy time data. No longer does an analyst need to collect field data for every airport needing to be analyzed. These data collections can be timely and expensive. Furthermore, they remain dependent on what is seen during the day(s) of collection. As such, data on certain desired aircraft may not be

collected. With the predictive models of departure and arrival runway occupancy time and distance, there now exists in the field, a methodology to estimate these parameters for 85 individual aircraft types, while accounting for differences in airport runway lengths, airport altitudes, aircraft performance and runway exit geometries.

Given the constant pressure for enhancing capacity, it is essential that base estimates of capacity are accurate. From using the predictive models developed, we observed how using aircraft-level parameters in a capacity model produced different outcomes as compared with aggregated parameters. Furthermore, we saw how the resulting differences revealed both prior overestimates and underestimates of capacity. Our specific examples illustrated a 2-operation change per hour. This is the equivalent to roughly 48 operations daily either assumed to be possible or unrealized.

The flight planning model presented is novel in that it is a fully transparent and working product that can produce wind-optimal flight trajectories. In the dissertation, it was proven that the model is capable of estimating wind-optimal trajectories through the A* algorithm. An heuristic suitable for the A* algorithm and the flight trajectory model was developed and proven to be admissible. Furthermore, all aspects of the flight planning model are fully open to critique and review. Many other flight planning software packages exist. However, these often are "black boxes" that are only available to end users at considerable expense. The model presented in this thesis will be freely available and usable by anyone with an installation of MATLAB. Additionally, it was demonstrated that the presented model can easily be utilized for industrial-scale real world air transportation applications.

Using a simulated domestic network, built from actual schedule data, we demonstrated with the "off the shelf" model presented herein a potential savings of over $8,000,000 dollars in fuel costs annually. It should be noted that the network constructed was relatively small in comparison to the sizable domestic networks of U.S. carriers as well as those of pan-European carriers. Thus, we can likely expect savings that scale with the size of the network.

This dissertation offered readers a glimpse into a possible future where internet access is beamed down from flying unmanned vehicles overhead. We covered the number and placement of these vehicles and offered practical solutions to the potential conflicts with commercial airspace these vehicles might cause.

7.2 Recommendations for Future Research

7.2.1 Further Expand the Predictive Models with Additional Data

The predictive power of the three predictive models can be improved with additional data. Future research should aim to reproduce these models using far more data and even more aircraft types. Additionally, research might consider methods to generalize to new aircraft types not yet in existence to avoid having to reproduce the entire model upon the entry of a new aircraft type into the field.

7.2.2 Extension of the Flight Trajectory Model to 4-D

The flight planning model can be extended to four dimensions, but the difficulty in doing so will be to determine the appropriate optimization and shortest-path algorithms to apply so as to allow for reasonable execution time. If the A* search algorithm is to retained, an admissible heuristic that is both suitable for four-dimensional shortest path searching and efficient will need to be developed.

7.2.3 Consideration of the Economics of UAS Deployment

Future work into the Unmanned Aerial Systems scenario laid out in this dissertation should take a more economics-based approach and consider the potential cost of such a system to further assess its feasibility.

7.2.4 Relax the Assumption of Uniform Population Density and UAS Platform Deployment Scheme

Future research into the Unmanned Aerial Systems scenario should consider actual concentrations of population and relax the assumptions of uniform population. Additionally, the deployment scheme need not be limited to a single variant.

Bibliography

Air Canada (2016). "Air Canada Timetable." Air Canada, <https://services.aircanada.com/portal/rest/timetable/pdf/ac-timetable-en.pdf?locale=en&app_key=AE919FDCC80311DF9BABC975DFD72085> (accessed Jul. 17, 2016).

AIR International (2014). "Weather Sentinel." *AIR International*.

Astholz, P. T., Sheftel, D. J., and Harris, R. M. (1970). "Increasing Runway Capacity." *Proceedings of the IEEE*, 58(3), 300–307.

Avilés, J. C. (2007). "High Altitude Platforms for UMTS." M.S. thesis, Tampere University of Technology, Tampere, Finland (January).

Barbas, C., Vásquez, J., and López, P. (2007). "Development of an Algorithm to Model the Landing Operations, Based on Statistical Analysis of Actual Data Survey (proESTOP)." *Proceedings of the 7th USA/Europe Air Traffic Management Research and Development Seminar*, Barcelona, Spain, Federal Aviation Administration and EUROCONTROL (July).

Bell, G. E. (1949). "Operational Research into Air Traffic Control." *The Journal of the Royal Aeronautical Society*, 53(466), 965–976.

Berger, J. O. and Wolpert, R. L. (1988). *The Likelihood Principle*. Lecture Notes-Monograph Series. Institute of Mathematical Statistics, Hayward, California, 2nd edition.

Blumstein, A. (1960). "An Analytical Investigation of Airport Capacity." *Internal Research TA-1358-G-1*, Cornell Aeronautical Laboratory, Inc., Buffalo, New York (June).

Bowen, E. G. and Pearcey, T. (1948). "Delays in the Flow of Air Traffic." *The Journal of the Royal Aeronautical Society*, 52(456), 799–812.

Brandt, S. A., Stiles, R. J., Bertin, J. J., and Whitford, R. (2004). *Introduction to Aeronautics: A Design Perspective*. American Institute of Aeronautics and Astronautics, Inc., Reston, Virginia, 2nd edition.

Bryson, A. E. (1998). *Dynamic Optimization*. Pearson Education, 1st edition.

Bryson, A. E. and Ho, Y.-C. (1975). *Applied Optimal Control: Optimization, Estimation, and Control*. Taylor & Francis Group, New York, New York, revised edition.

Carey, S. (2013). "The FAA's $40 Billion Adventure." *The Wall Street Journal* <http://www.wsj.com/articles/SB10001424127887323971204578625952559851308>.

Cohen, J. (1998). *Statistical Power Analysis for the Behavioral Sciences*. Lawrence Erlbaum Associates, Hillsdale, New Jersey, 2nd edition.

Congdon, P. (2006). *Bayesian Statistical Modelling*. Wiley Series in Probability and Statistics. John Wiley & Sons, Inc., West Sussex, England, 2nd edition.

Dedrick, R. F., Ferron, J. M., Hess, M. R., Hogarty, K. Y., Kromrey, J. D., Lang, T. R., Niles, J. D., and Lee, R. S. (2009). "Multilevel Modeling: A Review of Methodological Issues and Applications." *Review of Educational Research*, 79(1), 69–102.

Devulapalli, R. (2012). "An Efficient Algorithm for Commercial Aircraft Trajectory Optimization in the Air Traffic System." M.S. thesis, University of Minnesota, Minneapolis, Minnesota (July).

EUROCONTROL (2003). *Enhancing Airside Capacity, the Complete Guide, Edition 2.0*.

EUROCONTROL Experimental Centre (2009). "Base of Aircraft Data (BADA) Aircraft Performance Modelling Report." *Report No. 2009-009*, European Organisation for the Safety of Air Navigation, Brétigny-sur-Orge, France.

Federal Aviation Administration (2009). "National Airspace System (NAS) Subsystem Level Specification for Airport Surface Detection Equipment - Model X (ASDE-X), Version 2.0 Preliminary." Federal Aviation Administration (August).

Federal Aviation Administration (2013). "Integration of Civil Unmanned Aircraft Systems (UAS) in the National Airspace System (NAS) Roadmap." Federal Aviation

Administration, <https://www.faa.gov/uas/media/UAS_Roadmap_2013.pdf> (accessed May 8, 2016).

Federal Aviation Administration (2014a). *Advisory Circular AC 150/5300-13A*.

Federal Aviation Administration (2014b). "Airport Capacity Profile - Ronald Reagan Washington National." Federal Aviation Administration, <http://www.faa.gov/airports/planning_capacity/profiles/media/DCA-Airport-Capacity-Profile-2014.pdf> (July).

Federal Aviation Administration (2014c). "Airport Capacity Profile - San Diego International." Federal Aviation Administration, <http://www.faa.gov/airports/planning_capacity/profiles/media/SAN-Airport-Capacity-Profile-2014.pdf> (July).

Federal Aviation Administration (2014d). "Airport Surface Detection Equipment - Model X (ASDE-X)." Federal Aviation Administration, <https://www.faa.gov/air_traffic/technology/asde-x/> (accessed Sept. 12, 2015).

Federal Aviation Administration (2014e). "Airports and Other Landing Facilities (APT) Legacy (TXT) Data." Federal Aviation Administration, <https://nfdc.faa.gov/xwiki/bin/view/NFDC/56DaySub-2014-07-24> (accessed Aug. 13, 2014).

Federal Aviation Administration (2015). "Automatic Dependent Surveillance-Broadcast (ADS-B)." Federal Aviation Administration, <http://www.faa.gov/nextgen/programs/adsb/> (accessed Sept. 11, 2015). (July).

Gelman, A. (2006). "Multilevel (Hierarchical) Modeling: What It Can and Cannot Do." *Technometrics*, 48(3), 432–435.

Gelman, A. (2008). "Objections to Bayesian Statistics." *Bayesian Analysis*, 3(3), 445–450.

Gelman, A., Carlin, J. B., Stern, H. S., Dunson, D. B., Vehtari, A., and Rubin, D. B. (2014). *Bayesian Data Analysis*. Texts in Statistical Science. CRC Press, Boca Raton, Florida, 3rd edition.

Google (2015). "Our history in depth." Google, <https://www.google.com/about/company/history/> (accessed Oct. 20, 2015).

Gosling, G. D., Kanafani, A., and Hockaday, S. L. (1981). "Measures to Increase Airfield Capacity by Changing Aircraft Runway Occupancy Characteristics." *Research Report N82-22240*, Institute of Transportation Studies, University of California, Berkeley, California (December).

Gowri, J. and Janakiraman, S. (2015). "Edge Detection based on K-Means and Gabor Wavelet Technique." *Proceedings of the International Conference on Interdisciplinary Research in Electronics and Instrumentation Engineering (ICIREIE)*, Association of Scientists, Developers and Faculties, Chennai, India, Association of Scientists, Developers and Faculties, 7–11.

Graumann, A., Houston, T., Lawrimore, J., Levinson, D., Lott, N., McCown, S., Stephens, S., and Wuertz, D. (2005). "Hurricane Katrina: A Climatological Perspective - Preliminary Report." *Technical Report 2005-01*, National Oceanic and Atmospheric Administration, Asheville, North Carolina (October).

GreenBiz Editors (2011). "Southwest to Save $16m in Fuel Costs with NextGen Navigation." GreenBiz Editors, <https://www.greenbiz.com/news/2011/01/11/southwest-save-16-million-fuel-costs-nextgen-navigation> (accessed Sep. 15, 2015). (January).

Hall, D. W., Fortenbach, C. D., Dimiceli, E. V., and Parks, R. W. (1983). "A Preliminary Study of Solar Powered Aircraft and Associated Power Trains." *NASA Contractor Report 3699*, National Aeronautics and Space Administration, Scientific and Technical Information Branch, Washington, D.C. (December).

Har-Peled, S. (2011). *Geometric Approximation Algorithms*. Mathematical Surveys and Monographs. American Mathematical Society, Providence, Rhode Island, 1st edition.

Har-Peled, S. and Lee, M. (2012). "Weighted Geometric Set Cover Problems Revisited." *Journal of Computational Geometry*, 3(1), 65–85.

Hart, P. E., Nilsson, N. J., and Raphael, B. (1968). "A Formal Basis for the Heuristic Determination of Minimum Cost Paths." *IEEE Transactions on Systems Science and Cybernetics*, 4(2), 100–107.

Haynie, C. R. (2002). "An Investigation of Capacity and Safety in Near-Terminal Airspace for Guiding Information Technology Adoption." Ph.D. thesis, George Mason University, Fairfax, Virginia.

Hewitt, C. and Broatch, S. (1992). "A Tactical Navigation and Routing System for Low-Level Flight." *Technical report*, General Electric Company - Marconi Avionics, Rochester, Kent, United Kingdom, Agard, Italy (December).

Hoff, P. D. (2009). *A First Course in Bayesian Statistical Methods*. Springer Science+Business Media, LLC, New York, New York.

Horonjeff, R., Grassi, C., Read, R. R., and Ahlborn, G. (1959). "A Mathematical Model for Locating Exit Taxiways." *Special study*, Institute of Transportation and Traffic Engineering, University of California, Berkeley, California.

Hox, J. J. and Robert, J. K. (2010). *Handbook of Advanced Multilevel Analysis*. European Association of Methodology Series. Routledge, New York, New York, 1st edition.

International Air Transport Association (IATA) (2014). "New IATA Passenger Forecast Reveals Fast-Growing Markets of the Future." International Air Transport Association (IATA), <http://www.iata.org/pressroom/pr/Pages/2014-10-16-01.aspx> (accessed Sept. 11, 2015). Press Release No.: 57, (October).

International Air Transport Association (IATA) (2016). "Fuel Price Analysis." International Air Transport Association (IATA), <http://www.iata.org/publications/economics/fuel-monitor/Pages/price-analysis.aspx> (accessed Jul. 17, 2016). (July).

International Civil Aviation Organization (ICAO) (2015). "Air Transport in Figures - Economic Development at a Glance." International Civil Aviation Organization (ICAO), <http://www.icao.int/sustainability/documents/AirTransport-figures.pdf>. (April). Powerpoint Slides.

Jardin, M. (2003). "Real-Time Conflict-Free Trajectory Optimization." (Presentation), <http://atm2003.eurocontrol.fr/past-seminars/5th-seminar-budapest-hungary-june-2003/papers/paper_027/at_download/presentation> (accessed Jun. 10, 2016). (June).

Jardin, M. R. and Bryson, A. E. (2001). "Neighboring Optimal Aircraft Guidance in Winds." *Journal of Guidance, Control, and Dynamics*, 24(4), 711–715.

Jeddi, B. G. (2008). "A Statistical Separation Standard and Risk-Throughput Modeling of the Aircraft Landing Process." M.S. thesis, George Mason University, Fairfax, Virginia.

Jeddi, B. G., Donahue, G. L., and Shortle, J. F. (2009). "A Statistical Analysis of the Aircraft Landing Process." *Journal of Industrial and Systems Engineering*, 3(3), 152–169.

Jeddi, B. G., Shortle, J. F., and Sherry, L. (2006). "Statistics of the Approach Process at Detroit Metropolitan Wayne County Airport." *Proceedings of the 2nd International Conference on Research in Air Transportation*, Belgrade, Serbia and Montenegro.

Kalnay, E., Kanamitsu, M., Kistler, R., Collins, W., Deaven, D., Gandin, L., Iredell, M., Saha, S., White, G., Woollen, J., Zhu, Y., Leetmaa, A., and Reynolds, R. (1996). "The NCEP/NCAR 40-Year Reanalysis Project." *Bulletin of the American Meteorological Society*, 77, 437–470.

Kanafani, A. (1983). "Operational Procedures to Increase Runway Capacity." *Journal of Transportation Engineering*, 109(3), 414–424.

Karapantazis, S. and Pavlidou, F.-N. (2005). "The Role of High Altitude Platforms Beyond 3G Networks." *IEEE Wireless Communications*, 12(6), 33–41.

Koenig, S. E. (1978). "Analysis of Runway Occupancy Times at Major Airports." *Technical Report FAA-EM-78-9*, The MITRE Corporation, McLean, Virginia (May).

Köthe, A., Luckner, R., Ramirez, P. J. G., Silvestre, F. J., Pang, Z. Y., and Cesnik, C. E. S. (2016). "Development of Robust Flight Control Laws for a Highly Flexible Aircraft in the Frequency Domain." *AIAA Atmospheric Flight Mechanics Conference*, American Institute of Aeronautics and Astronautics, Washington, D.C., AIAA, 1–23. doi:10.2514/6.2016-3394.

Kruschke, J. K. (2015). *Doing Bayesian Data Analysis - A Tutorial with R, JAGS, and Stan*. Academic Press, London, United Kingdom, 2nd edition.

Kumar, V., Sherry, L., and Kicinger, R. (2010). "Runway Occupancy Time Extraction and Analysis Using Surface Track Data." *TRB 89th Annual Meeting Compendium of Papers*, Washington, District of Columbia, Transportation Research Board.

Le Sellier, F. (1999). "Discrete Real-Time Flight Plan Optimization." M.S. thesis, Massachusetts Institute of Technology, Cambridge, Massachusetts (September).

Lee, D. D., Smith, A., Cassell, R., and Abdul-Baki, B. (1999). "NASA Low Visibility Landing and Surface Operations (LVLASO) Runway Occupancy Time (ROT) Analysis." *Proceedings of the 18th Digital Avionics Systems Conference*, Institute of Electrical and Electronics Engineers, St. Louis, Missouri, IEEE.

LeighFisher (2012). "Evaluating Airfield Capacity." *Report No. ACRP Report 79*, Transportation Research Board, Washington, D.C.

Martin, J. N. and Colella, N. J. (1998). "Broadband Wireless Services from High-Altitude Long-Operation (HALO) Aircraft." *Proc. SPIE 3232, Wireless Technologies and Systems: Millimeter-Wave and Optical, 9*, SPIE, Dallas, Texas (January). doi:10.1117/12.301028.

National Hurricane Center (2014). "Atlantic Hurricane Database (HURDAT2) 1851 - 2013." National Hurricane Center, <http://www.nhc.noaa.gov/data/#hurdat> (accessed Dec. 4, 2014).

Ng, H. K., Sridhar, B., and Grabbe, S. (2014). "Optimizing Aircraft Trajectories with Multiple Cruise Altitudes in the Presence of Winds." *Journal of Aerospace Information Systems*, 11(1).

Ng, H. K., Sridhar, B., Grabbe, S., and Chen, N. (2011). "Cross-Polar Aircraft Trajectory Optimization and the Potential Climate Impact." *Proceedings of the IEEE/AIAA 30th Digital Avionics Systems Conference*, Seattle, USA, Institute of Electrical and Electronic Engineers (IEEE) (October).

Nicolai, L. M. and Carichner, G. E. (2010). *Fundamentals of Aircraft and Airship Design - Volume 1 - Aircraft Design.* AIAA Education Series. American Institute of Aeronautics and Astronautics, New York, New York.

Nikoleris, A. N. (2011). "Stochastic Queueing Models for Air Transportation Systems with Scheduled Arrivals." Ph.D. thesis, University of California, Berkeley, Berkeley, California.

Pavlin, S., Žužić, M., and Pavičić, S. (2006). "Runway Occupancy Time as Element of Runway Capacity." *Promet - Traffic&Transportation*, 18(4), 293–299.

Phillips, W. F. (2010). *Mechanics of Flight*. John Wiley & Sons, Inc., Hoboken, New Jersey, 2nd edition.

Pu, D. (2014). "Demand and Capacity Problems in the Next Generation Air Transportation System." M.S. thesis, Virginia Polytechnic Institute and State University, Blacksburg, Virginia (November).

Richards, A. and How, J. P. (2002). "Aircraft Trajectory Planning With Collision Avoidance Using Mixed Integer Linear Programming." *Proceedings of the 2002 American Control Conference*, Institute of Electrical and Electronics Engineers, Anchorage, Alaska, IEEE, 1936 – 1941. doi:10.1109/ACC.2002.1023918.

Runnels, M. H. (2008). "ASDE-X and NextGen Total Airport Management Operations." Online, <http://thehill.com/sites/default/files/Sensis_ATCA_08_Runnels_Total_0.pdf> (accessed Sept. 12, 2015).

SAS Institute Inc. (2016). "Multivariate Platform Options." (Online), <http://www.jmp.com/support/help/Multivariate_Platform_Options.shtml> (accessed Aug. 12, 2016).

Scott (2016). "NOREBBO Stock Illustration and Design." Online, <http://www.norebbo.com/> (accessed Jun. 19, 2016).

Smith, S. W. (1999). *The Scientist and Engineer's Guide to Digital Signal Processing*. California Technical Publishing, San Diego, California, 2nd edition.

Spiegelhalter, D. J., Best, N. G., Carlin, B. P., and van der Linde, A. (2002). "Bayesian Measures of Model Complexity and Fit." *Journal of the Royal Statistical Society: Series B (Statistical Methodology)*, 64(4), 583–639.

Swedish, W. J. (1972). "Some Measures of Aircraft Performance on the Airport Surface." M.S. thesis, Massachusetts Institute of Technology, Cambridge, Massachusetts (May).

Swedish, W. J. (1979). "Evaluation of the Potential for Reduced Longitudinal Spacing on Final Approach." *Technical Report FAA-EM-79-7*, The MITRE Corporation, McLean, Virginia (August).

Trani, A. A., Cao, J., Kim, B. J., Gu, X., Zhong, C. Y., and Tarrago-Trani, M. T. (1995). "Flight Simulations of High Speed Runway Exits." *Report 95-02*, Virginia Polytechnic Institute and State University, Blacksburg, Virginia (June).

Trani, A. A. and Spencer, T. (2014). "UAS Demand Generation and Airspace Performance Impact Prediction." *Communication and Broadcast Relay Mission Report*, Intelligent Automation Incorporated, Rockville, Maryland (October).

Transportation Research Board and National Research Council (2003). *Securing the Future of U.S. Air Transportation: A System in Peril*. The National Academies Press.

U.S. Census Bureau (2014). "2013 TIGER/Line Shapefiles." (machine-readable datafiles), <http://www.census.gov/geo/maps-data/data/tiger-line.html>. (accessed Aug. 12, 2014).

U.S. Census Bureau, Population Division (2014). "Annual Estimates of the Resident Population: April 1, 2010 to July 1, 2013 - United States – Metropolitan and Micropolitan Statistical Area; and for Puerto Rico." (Online), <http://www.census.gov/popest/data/historical/2010s/vintage_2013/metro.html> (accessed Aug. 17, 2014). (March).

U.S. Committee on Extension to the Standard Atmosphere (COESA) (1976). "U.S. Standard Atmosphere, 1976." *Report No. NOAA-S/T 76-1562*, National Oceanic and Atmospheric Administration, National Aeronautics and Space Administration, United States Air Force, Washington, D.C.

U.S. National Oceanic and Atmospheric Administration, National Centers for Environmental Information (2014). "1-Minute ASOS Data." (Public Data Set), <https://www.ncdc.noaa.gov/data-access/land-based-station-data/land-based-datasets/automated-surface-observing-system-asos>.

Weiss, W. E. (1985). "Analysis of Runway Occupancy Time Data Collected at Los Angeles, San Francisco, Atlanta, and Dallas-Fort Worth Airports." *Technical Report FAA-DL5-85-3*, The MITRE Corporation, McLean, Virginia (September).

Weiss, W. E. and Barrer, J. N. (1984). "Analysis of Runway Occupancy Time and Separation Data Collected at La Guardia, Boston, and Newark Airports." *Technical Report FAA-DL5-84-2*, The MITRE Corporation, McLean, Virginia (December).

Wickramasinghe, N. K., Harada, A., and Miyazawa, Y. (2012). "Flight Trajectory Optimization for an Efficient Air Transportation System." *Proceedings of the 28th International Congress of the Aeronautical Sciences*, Brisbane, Australia, International Council of the Aeronautical Sciences (September).

Wunderground (2014). "The 30 Deadliest US Hurricanes / Tropical Cyclones [1851 - 2006]." (Online), <http://www.wunderground.com/resources/severe/severe.asp> (accessed Dec. 10, 2014).

Yang, Z. and Mohammed, A. (2008). "On the Cost-Effective Wireless Broadband Service Delivery from High Altitude Platforms with an Economical Business Model Design." *2008 IEEE 68th Vehicular Technology Conference*, Institute of Electrical and Electronics Engineers, Calgary, Alberta, Canada, IEEE, 1–5. doi:10.1109/VETECF.2008.454.

Yang, Z. and Mohammed, A. (2010). "Wireless Communications from Hugh Alatitude Platforms: Applications, Deployment and Development." *2010 12th IEEE International Conference on Communication Technology (ICCT)*, Institute of Electrical and Electronics Engineers, Nanjing, China, IEEE, 1476–1479.

Zermelo, E. (1931). "Über das Navigationsproblem bei ruhender oder veränderlicher Windverteilung." *Zeitschrift für Angewandte Mathematik und Mechanik*, 11(2).

Appendices

Appendix A

Results of 5-Fold Cross-Validations for Predictive Models

Table A.1: Root Mean Square Error by Aircraft Type for Model 1a

Aircraft Type	Average RMSPE (s)	% of Mean DROT	Aircraft Type	Average RMSE (s)	% of Mean DROT	Aircraft Type	Average RMSE (s)	% of Mean DROT
A306	5.79	12.79	B77L	3.71	6.68	E135	3.74	8.11
A319	3.8	7.89	B77W	3.37	5.92	E145	4.02	8.54
A320	3.24	6.64	B788	6.33	11.48	E170	3.46	7.8
A321	3.55	7.14	BE20	5.31	13.03	E190	3.33	7.26
A332	6.23	11.24	BE40	7.44	19.74	E45X	5.16	10.39
A333	6.04	10.93	BE99	4.56	12.95	E50P	3.85	9.97
A343	13.32	22.52	BE9L	5.85	15.44	E55P	9.58	28.17
A346	6.5	11.7	C172	10.16	32.01	F2TH	7.95	19.82
A388	12.2	20.78	C208	10.45	28.02	F900	7.91	20.55
AT72	5.58	15.86	C402	7.67	20.85	GALX	10.49	27.43
B190	5.45	13.79	C525	6.58	16.64	GLEX	7.93	20.2
B350	4.13	10.8	C550	6.33	15.73	GLF4	10.21	25.7
B712	3.93	8.27	C560	9.47	25.45	GLF5	8.37	20.79
B732	6.33	14.36	C56X	8.94	24.33	H25B	7.98	19.51
B733	4.01	7.88	C680	9.74	27.79	LJ35	10.91	27.71
B734	3.48	7.03	C750	9.33	23.47	LJ45	6.13	15.37
B735	3.88	8.1	CL30	8.74	23.31	LJ60	13.13	34.12
B736	4.91	12.23	CL60	9.98	25.44	MD11	7.46	15.8
B737	4.2	8.97	CRJ2	3.86	8.19	MD82	4.1	7.99
B738	4.09	7.94	CRJ7	3.77	8.17	MD83	4.11	7.89
B739	3.68	6.82	CRJ9	3.53	7.4	MD88	3.92	7.82
B744	7.17	12.7	DC10	4.4	8.88	MD90	3.26	6.6
B748	7.65	13.5	DC95	3.1	6.42	PA31	6.64	17.05
B752	4.01	8.24	DH8A	3.94	11.12	PC12	7.7	20.53
B753	3.78	7.17	DH8B	2.85	7.83	SF34	3.83	9.61
B762	3.53	7.37	DH8C	4.45	11.07	SH36	9.21	21.07
B763	4.25	8.32	DH8D	5.31	13.29	SR22	7.48	22.45
B764	3.06	5.53	E120	3.92	9.88	SW4	4.96	11.87
B772	4.18	7.61						

Table A.2: Root Mean Square Error by Aircraft Type for Model 1b

Aircraft Type	Average RMSPE (ft)	% of Mean $Dist_{TO}$	Aircraft Type	Average RMSPE (ft)	% of Mean $Dist_{TO}$	Aircraft Type	Average RMSE (ft)	% of Mean $Dist_{TO}$
A306	1235.2	19.42	B77L	613.18	6.83	E135	645.03	9.96
A319	515.73	7.53	B77W	587.35	6.29	E145	738.52	10.94
A320	463.01	6.54	B788	852.07	10.34	E170	470.43	7.64
A321	540.44	7.12	BE20	804.69	15.69	E190	474.75	7.44
A332	755.71	9.26	BE40	1105.36	21.54	E45X	986	13.14
A333	661.63	8.18	BE99	642.72	15.91	E50P	554.04	11.58
A343	1847.57	22.24	BE9L	919.69	21.67	E55P	1371.37	30.25
A346	961.05	11.47	C172	2035.29	84.84	F2TH	1141.94	19.54
A388	1606.87	19.7	C208	1637.63	49.68	F900	1161	21.77
AT72	724.26	18.22	C402	1418.69	37.01	GALX	1573.58	27.68
B190	831.37	15.59	C525	957.13	17.91	GLEX	1284.95	23.65
B350	630.38	13.32	C550	983.32	18.45	GLF4	1629.34	27.75
B712	607.25	8.36	C560	1475.66	28.78	GLF5	1348.3	23.6
B732	696.23	10.46	C56X	1313.84	25.71	H25B	1188.26	19.52
B733	662.18	8.52	C680	1459.13	30.88	LJ35	1567.44	25.7
B734	550.45	7.25	C750	1294.88	21.22	LJ45	946.53	17.09
B735	634.23	9.2	CL30	1285.45	24.27	LJ60	2012.53	33.44
B736	613.31	11.42	CL60	1532.21	26.23	MD11	1320.56	17.9
B737	675.53	10.06	CRJ2	670.73	9.63	MD82	731.83	9.52
B738	754.55	9.48	CRJ7	614.83	9.23	MD83	724.84	9.28
B739	650.26	7.62	CRJ9	632.94	8.85	MD88	603.64	8.45
B744	1050.42	12.52	DC10	721.04	9.81	MD90	568.78	7.7
B748	1112.4	13.18	DC95	667.9	9.86	PA31	1027.17	24.7
B752	664.63	9.09	DH8A	779.52	20.29	PC12	1197.18	31.51
B753	643.63	7.6	DH8B	317.32	7.86	SF34	530.42	10.58
B762	551.55	8.13	DH8C	705.27	14.57	SH36	1216.46	24.89
B763	735.81	9.45	DH8D	826.08	15.52	SR22	1334	44.76
B764	587.73	6.6	E120	563.29	11.51	SW4	748.6	13.99
B772	677.44	8						

Table A.3: Root Mean Square Error by Aircraft Type for Model 1c

Aircraft Type	Average RMSE (s)	% of Mean AROT	Aircraft Type	Average RMSE (s)	% of Mean AROT	Aircraft Type	Average RMSE (s)	% of Mean AROT
A306	8.55	14.71	B77L	8.89	15.92	E135	4.51	10.25
A319	4.27	9.01	B77W	8.01	14.58	E145	4.47	10.19
A320	4.44	9.27	B788	10.92	17.82	E170	4.02	9.4
A321	4.45	9.05	BE20	10.11	20.68	E190	4.47	9.88
A332	7.01	12.06	BE40	6.95	14.51	E45X	4.31	9.68
A333	6.71	11.82	BE99	8.92	17.77	E50P	6.87	14.24
A343	8.5	14.76	BE9L	10.42	19.19	E55P	5.9	13.03
A346	7.18	12.92	C172	11.8	21.53	F2TH	6.77	14.2
A388	13.38	19.64	C208	8.27	17.81	F900	6.79	13.4
AT72	5	10.57	C402	7.63	15.97	GALX	7.39	15.48
B190	5.69	12.19	C525	7.15	14.96	GLEX	5.99	11.97
B350	9.17	19.78	C550	8.52	16.81	GLF4	8.64	17.03
B712	3.89	8.57	C560	7.39	14.83	GLF5	7.63	15.07
B732	3.74	8.89	C56X	6.1	13.11	H25B	8.22	16.54
B733	3.99	8.73	C680	6.1	12.92	LJ35	9.99	19.38
B734	4.53	9.85	C750	6.39	13.41	LJ45	6.45	13.6
B735	4.19	9.03	CL30	5.81	12.65	LJ60	9.09	18.23
B736	4.52	10.09	CL60	7.38	14.95	MD11	11.1	18.21
B737	4.1	9.02	CRJ2	3.77	8.65	MD82	4.31	9.09
B738	4.67	9.92	CRJ7	3.96	8.88	MD83	4.46	9.42
B739	4.96	10.29	CRJ9	4.11	9.14	MD88	4.6	10.67
B744	10.92	18.07	DC10	10.54	17.2	MD90	4.12	9.47
B748	16.42	22.87	DC95	3.93	8.84	PA31	9.11	18.45
B752	4.9	9.77	DH8A	4.55	10.68	PC12	7.94	16.43
B753	5	9.76	DH8B	4.52	11.74	SF34	5.14	11.7
B762	6.11	11.39	DH8C	4.37	10.16	SH36	7.79	14.77
B763	6.04	11.25	DH8D	5.17	11.66	SR22	7.17	15.18
B764	5.79	11.86	E120	4.49	10.48	SW4	9.18	17.88
B772	7.17	13.09						

Table A.4: Root Mean Square Error by Aircraft Type for Model 2a

Aircraft Type	Average RMSE (s)	% of Mean DROT	Aircraft Type	Average RMSE (s)	% of Mean DROT	Aircraft Type	Average RMSE (s)	% of Mean DROT
A306	3.73	8.24	B77L	3.91	7.03	E135	3.57	7.75
A319	3.54	7.36	B77W	3.61	6.34	E145	3.72	7.89
A320	3.19	6.55	B788	5.22	9.47	E170	3.34	7.54
A321	3.33	6.69	BE20	4.85	11.89	E190	3.21	7.01
A332	3.84	6.92	BE40	3.93	10.43	E45X	4.85	9.76
A333	3.73	6.74	BE99	4.08	11.58	E50P	3.71	9.6
A343	4.42	7.47	BE9L	4.64	12.26	E55P	2.85	8.37
A346	4.66	8.39	C172	5.2	16.39	F2TH	4.75	11.84
A388	5.03	8.57	C208	5.1	13.68	F900	4.48	11.64
AT72	3.41	9.7	C402	4.81	13.06	GALX	3.97	10.39
B190	4.14	10.48	C525	5.66	14.33	GLEX	4.58	11.67
B350	4.03	10.52	C550	6.06	15.05	GLF4	4.7	11.82
B712	3.07	6.47	C560	5.38	14.47	GLF5	5.24	13.02
B732	4.42	10.03	C56X	3.89	10.58	H25B	4.73	11.57
B733	3.82	7.51	C680	3.95	11.26	LJ35	5.33	13.53
B734	3.26	6.58	C750	3.98	10	LJ45	3.63	9.1
B735	3.74	7.81	CL30	3.35	8.93	LJ60	4.25	11.06
B736	4.56	11.37	CL60	3.86	9.83	MD11	4.08	8.64
B737	4.1	8.77	CRJ2	3.72	7.9	MD82	3.83	7.47
B738	4.06	7.88	CRJ7	3.81	8.26	MD83	3.8	7.31
B739	3.48	6.45	CRJ9	3.36	7.05	MD88	3.54	7.07
B744	4.7	8.32	DC10	4.31	8.7	MD90	3.13	6.34
B748	5.16	9.12	DC95	2.73	5.67	PA31	4.66	11.96
B752	3.56	7.31	DH8A	2.98	8.4	PC12	4.94	13.16
B753	3.7	7.02	DH8B	2.7	7.4	SF34	3.7	9.3
B762	3.47	7.25	DH8C	3.73	9.29	SH36	5.26	12.03
B763	3.97	7.77	DH8D	3.5	8.75	SR22	5.11	15.34
B764	2.83	5.11	E120	3.6	9.08	SW4	5.02	12.02
B772	3.53	6.44						

Table A.5: Root Mean Square Error by Aircraft Type for Model 2b

Aircraft Type	Average RMSE (ft)	% of Mean $Dist_{TO}$	Aircraft Type	Average RMSE (ft)	% of Mean $Dist_{TO}$	Aircraft Type	Average RMSE (ft)	% of Mean $Dist_{TO}$
A306	464.22	7.3	B77L	611.82	6.81	E135	579.54	8.95
A319	480.64	7.02	B77W	624.91	6.69	E145	622.83	9.23
A320	397.68	5.62	B788	769.14	9.33	E170	429.95	6.98
A321	437.99	5.77	BE20	658.28	12.83	E190	430.8	6.75
A332	522.28	6.4	BE40	671.8	13.09	E45X	838.47	11.17
A333	459.2	5.68	BE99	616.58	15.27	E50P	550.99	11.52
A343	680.61	8.19	BE9L	539.64	12.71	E55P	465.23	10.26
A346	701.06	8.37	C172	658.01	27.43	F2TH	781.5	13.37
A388	670.52	8.22	C208	516.67	15.67	F900	683.02	12.81
AT72	410.07	10.31	C402	533.1	13.91	GALX	687.7	12.1
B190	696.24	13.06	C525	894.56	16.74	GLEX	746.1	13.73
B350	597.37	12.62	C550	998.85	18.74	GLF4	786.71	13.4
B712	517.72	7.12	C560	933.57	18.21	GLF5	876.32	15.34
B732	534.29	8.03	C56X	663.37	12.98	H25B	801.66	13.17
B733	599.25	7.71	C680	696.89	14.75	LJ35	884.75	14.51
B734	483.84	6.37	C750	701.65	11.5	LJ45	608.52	10.99
B735	550.52	7.99	CL30	537.48	10.15	LJ60	749.75	12.46
B736	564.83	10.52	CL60	656.75	11.24	MD11	728.82	9.88
B737	643.98	9.59	CRJ2	612.96	8.8	MD82	621.11	8.08
B738	707.38	8.88	CRJ7	623.16	9.35	MD83	622.93	7.98
B739	589.14	6.91	CRJ9	569.17	7.96	MD88	482.13	6.75
B744	764.1	9.11	DC10	660.66	8.99	MD90	475.67	6.44
B748	829.56	9.83	DC95	353.66	5.22	PA31	647.7	15.58
B752	549.26	7.51	DH8A	427.14	11.12	PC12	547.04	14.4
B753	618.87	7.3	DH8B	329.41	8.16	SF34	480.76	9.59
B762	563.35	8.31	DH8C	520.46	10.75	SH36	570.92	11.68
B763	627.5	8.06	DH8D	583.14	10.96	SR22	559.35	18.77
B764	489.12	5.5	E120	508.99	10.4	SW4	745.28	13.92
B772	578.43	6.83						

Table A.6: Root Mean Square Error by Aircraft Type for Model 2c

Aircraft Type	Average RMSE (s)	% of Mean AROT	Aircraft Type	Average RMSE (s)	% of Mean AROT	Aircraft Type	Average RMSE (s)	% of Mean AROT
A306	7.37	12.69	B77L	7.7	13.78	E135	4.2	9.52
A319	4.16	8.78	B77W	5.78	10.53	E145	4.35	9.9
A320	4.34	9.06	B788	7.72	12.59	E170	3.78	8.83
A321	4.43	9.01	BE20	7.49	15.33	E190	4.2	9.29
A332	6.64	11.43	BE40	6.01	12.55	E45X	4.28	9.61
A333	6.19	10.91	BE99	6.51	12.96	E50P	6.13	12.69
A343	7.37	12.79	BE9L	7.24	13.33	E55P	5.59	12.36
A346	5.96	10.72	C172	9.73	17.76	F2TH	5.9	12.37
A388	10.73	15.75	C208	6.65	14.32	F900	6.09	12.02
AT72	4.97	10.51	C402	6.18	12.93	GALX	6.01	12.6
B190	5.28	11.32	C525	6.42	13.45	GLEX	5.72	11.42
B350	6.47	13.96	C550	7.13	14.06	GLF4	6.74	13.29
B712	3.37	7.43	C560	6.51	13.07	GLF5	6.29	12.41
B732	3.37	7.99	C56X	5.59	12.03	H25B	6.42	12.92
B733	3.94	8.62	C680	5.72	12.13	LJ35	7.53	14.62
B734	4.51	9.82	C750	5.73	12.03	LJ45	5.87	12.36
B735	4.12	8.87	CL30	5.22	11.36	LJ60	7.07	14.18
B736	4.21	9.39	CL60	6.23	12.6	MD11	8.29	13.61
B737	4.08	8.99	CRJ2	3.72	8.54	MD82	3.71	7.83
B738	4.59	9.75	CRJ7	3.89	8.72	MD83	3.86	8.16
B739	4.76	9.88	CRJ9	3.96	8.81	MD88	3.43	7.96
B744	7.91	13.09	DC10	7.69	12.54	MD90	3.77	8.67
B748	10.52	14.66	DC95	3.13	7.05	PA31	7.07	14.31
B752	4.91	9.79	DH8A	4.59	10.78	PC12	6.46	13.37
B753	4.92	9.61	DH8B	3.98	10.35	SF34	4.91	11.18
B762	5.98	11.14	DH8C	3.67	8.54	SH36	6.92	13.12
B763	6.02	11.21	DH8D	5.1	11.49	SR22	6.52	13.8
B764	5.56	11.38	E120	4.37	10.21	SW4	7.03	13.7
B772	6.34	11.57						

Table A.7: Root Mean Square Error by Aircraft Type for Model 3a

Aircraft Type	Average RMSE (s)	% of Mean AROT	Aircraft Type	Average RMSE (s)	% of Mean AROT	Aircraft Type	Average RMSE (s)	% of Mean AROT
A306	3.83	8.46	B77L	3.78	6.79	E135	3.49	7.58
A319	3.45	7.17	B77W	3.36	5.89	E145	3.68	7.82
A320	3.19	6.54	B788	5	9.08	E170	3.23	7.29
A321	3.28	6.6	BE20	5.09	12.48	E190	3.14	6.86
A332	3.97	7.16	BE40	3.67	9.75	E45X	4.66	9.36
A333	3.59	6.49	BE99	3.58	10.17	E50P	2.92	7.57
A343	4.35	7.36	BE9L	4.73	12.49	E55P	2.76	8.13
A346	4.1	7.38	C172	4.64	14.63	F2TH	4.68	11.66
A388	3.9	6.64	C208	4.99	13.37	F900	4.62	12.01
AT72	3.23	9.18	C402	4.56	12.4	GALX	3.72	9.73
B190	4.12	10.42	C525	4.73	11.96	GLEX	4.17	10.63
B350	4.42	11.54	C550	5.05	12.54	GLF4	4.33	10.91
B712	3.02	6.37	C560	4.74	12.75	GLF5	4.79	11.91
B732	4.48	10.15	C56X	3.41	9.29	H25B	4.41	10.77
B733	3.65	7.17	C680	3.39	9.67	LJ35	4.96	12.59
B734	3.14	6.33	C750	3.61	9.08	LJ45	3.34	8.39
B735	3.73	7.79	CL30	3.26	8.69	LJ60	3.75	9.76
B736	3.51	8.76	CL60	3.88	9.88	MD11	4.39	9.3
B737	4.03	8.61	CRJ2	3.69	7.82	MD82	3.7	7.2
B738	3.93	7.63	CRJ7	3.72	8.07	MD83	3.69	7.08
B739	3.36	6.23	CRJ9	3.32	6.96	MD88	3.43	6.85
B744	4.71	8.34	DC10	4.25	8.59	MD90	3.2	6.48
B748	4.85	8.56	DC95	2.66	5.52	PA31	4.67	11.99
B752	3.57	7.33	DH8A	2.6	7.33	PC12	4.26	11.35
B753	3.53	6.69	DH8B	2.56	7.02	SF34	3.73	9.35
B762	3.42	7.15	DH8C	3.53	8.79	SH36	5.1	11.68
B763	3.98	7.8	DH8D	3.5	8.75	SR22	4.97	14.93
B764	2.74	4.96	E120	3.48	8.77	SW4	4.98	11.92
B772	3.54	6.45						

Table A.8: Root Mean Square Error by Aircraft Type for Model 3b

Aircraft Type	Average RMSE (ft)	% of Mean $Dist_{TO}$	Aircraft Type	Average RMSE (ft)	% of Mean $Dist_{TO}$	Aircraft Type	Average RMSE (ft)	% of Mean $Dist_{TO}$
A306	403.19	6.34	B77L	585.36	6.52	E135	564.91	8.73
A319	473.45	6.91	B77W	574.27	6.15	E145	606.65	8.99
A320	385.95	5.45	B788	837.77	10.17	E170	414.71	6.73
A321	411.07	5.42	BE20	682.52	13.3	E190	420.99	6.6
A332	521.64	6.39	BE40	561.11	10.94	E45X	829.05	11.05
A333	444.11	5.49	BE99	485.78	12.03	E50P	471.04	9.85
A343	646.3	7.78	BE9L	455.73	10.74	E55P	359.95	7.94
A346	739.89	8.83	C172	349.28	14.56	F2TH	696.6	11.92
A388	604.46	7.41	C208	442.9	13.44	F900	633.75	11.88
AT72	386.13	9.71	C402	498.73	13.01	GALX	662.47	11.65
B190	662.63	12.43	C525	710.37	13.3	GLEX	756.72	13.93
B350	544.7	11.51	C550	780.24	14.64	GLF4	746.44	12.71
B712	491.34	6.76	C560	779.27	15.2	GLF5	816.75	14.29
B732	607.51	9.13	C56X	573.41	11.22	H25B	754.18	12.39
B733	557.47	7.17	C680	615.57	13.03	LJ35	834.27	13.68
B734	471.92	6.21	C750	637.58	10.45	LJ45	561.76	10.14
B735	543.66	7.89	CL30	479.51	9.05	LJ60	641.4	10.66
B736	411.27	7.66	CL60	618.28	10.58	MD11	743.48	10.08
B737	631.33	9.4	CRJ2	602.94	8.66	MD82	569.8	7.41
B738	676.57	8.5	CRJ7	601.62	9.03	MD83	556.49	7.13
B739	549.96	6.45	CRJ9	557.19	7.79	MD88	470.5	6.59
B744	757.39	9.03	DC10	697.69	9.5	MD90	488.13	6.61
B748	827.83	9.81	DC95	333.46	4.92	PA31	570.4	13.72
B752	551.63	7.54	DH8A	330.1	8.59	PC12	443.74	11.68
B753	587.54	6.93	DH8B	279.49	6.92	SF34	483.88	9.65
B762	546.41	8.06	DH8C	445.16	9.19	SH36	544.73	11.15
B763	629.64	8.09	DH8D	529.55	9.95	SR22	459.95	15.43
B764	482.91	5.43	E120	497.68	10.17	SW4	658.67	12.31
B772	571.41	6.75						

Table A.9: Root Mean Square Error by Aircraft Type for Model 3c

Aircraft Type	Average RMSE (s)	% of Mean AROT	Aircraft Type	Average RMSE (s)	% of Mean AROT	Aircraft Type	Average RMSE (s)	% of Mean AROT
A306	7.31	12.58	B77L	5.97	10.69	E135	3.84	8.71
A319	4.07	8.59	B77W	5.69	10.35	E145	4.25	9.67
A320	4.29	8.96	B788	6.5	10.6	E170	3.74	8.74
A321	4.43	9.01	BE20	6.5	13.3	E190	4.16	9.2
A332	5.81	9.99	BE40	5.16	10.77	E45X	4.28	9.6
A333	6.2	10.92	BE99	5.14	10.24	E50P	6.22	12.88
A343	5.75	9.99	BE9L	6.55	12.05	E55P	5.31	11.72
A346	6.36	11.45	C172	9.51	17.35	F2TH	5.89	12.36
A388	8.46	12.42	C208	6.69	14.41	F900	5.99	11.82
AT72	4.82	10.19	C402	4.72	9.89	GALX	5.54	11.6
B190	5.23	11.2	C525	6	12.56	GLEX	6.48	12.94
B350	5.75	12.41	C550	5.22	10.3	GLF4	6.37	12.56
B712	3.24	7.14	C560	6.27	12.59	GLF5	6.28	12.39
B732	3.14	7.45	C56X	5.68	12.21	H25B	6.2	12.47
B733	3.82	8.37	C680	5.59	11.84	LJ35	8.03	15.57
B734	4.38	9.54	C750	5.32	11.17	LJ45	5.4	11.37
B735	4.2	9.05	CL30	4.79	10.44	LJ60	6.33	12.69
B736	3.56	7.94	CL60	5.83	11.81	MD11	8.34	13.68
B737	4.05	8.92	CRJ2	3.68	8.45	MD82	3.71	7.82
B738	4.5	9.55	CRJ7	3.77	8.47	MD83	3.72	7.86
B739	4.5	9.34	CRJ9	3.82	8.5	MD88	3.35	7.77
B744	7.45	12.33	DC10	6.66	10.86	MD90	3.71	8.54
B748	9.2	12.82	DC95	3.06	6.88	PA31	6.39	12.93
B752	4.85	9.67	DH8A	4.02	9.45	PC12	6.13	12.69
B753	4.67	9.13	DH8B	3.39	8.81	SF34	4.82	10.99
B762	5.92	11.03	DH8C	3.52	8.19	SH36	5.67	10.74
B763	6.07	11.31	DH8D	4.91	11.06	SR22	5.16	10.92
B764	5.04	10.32	E120	3.96	9.26	SW4	7.11	13.85
B772	6	10.96						

Table A.10: Root Mean Square Error by Aircraft Type for Model 4a

Aircraft Type	Average RMSE (s)	% of Mean AROT	Aircraft Type	Average RMSE (s)	% of Mean AROT	Aircraft Type	Average RMSE (s)	% of Mean AROT
A306	3.83	8.46	B77L	3.77	6.79	E135	3.54	7.68
A319	3.45	7.17	B77W	3.36	5.89	E145	3.7	7.86
A320	3.2	6.55	B788	5.16	9.36	E170	3.24	7.32
A321	3.28	6.6	BE20	5.09	12.49	E190	3.14	6.86
A332	3.98	7.17	BE40	3.71	9.84	E45X	4.8	9.65
A333	3.59	6.49	BE99	3.71	10.54	E50P	3	7.77
A343	4.37	7.39	BE9L	4.74	12.5	E55P	2.77	8.14
A346	4.11	7.39	C172	4.69	14.77	F2TH	4.71	11.75
A388	3.92	6.68	C208	4.99	13.38	F900	4.66	12.11
AT72	3.23	9.19	C402	4.57	12.43	GALX	3.73	9.75
B190	4.12	10.43	C525	4.83	12.21	GLEX	4.17	10.63
B350	4.46	11.66	C550	5.05	12.55	GLF4	4.33	10.91
B712	3.04	6.4	C560	4.75	12.77	GLF5	4.8	11.92
B732	4.47	10.14	C56X	3.42	9.31	H25B	4.41	10.77
B733	3.69	7.25	C680	3.39	9.68	LJ35	4.96	12.6
B734	3.14	6.34	C750	3.65	9.18	LJ45	3.35	8.4
B735	3.84	8.02	CL30	3.26	8.71	LJ60	3.77	9.8
B736	3.76	9.37	CL60	3.89	9.92	MD11	4.4	9.31
B737	4.06	8.69	CRJ2	3.69	7.83	MD82	3.7	7.22
B738	3.95	7.67	CRJ7	3.75	8.13	MD83	3.69	7.09
B739	3.36	6.23	CRJ9	3.35	7.04	MD88	3.47	6.92
B744	4.71	8.34	DC10	4.26	8.6	MD90	3.21	6.5
B748	4.86	8.58	DC95	2.66	5.52	PA31	4.7	12.06
B752	3.58	7.36	DH8A	2.6	7.33	PC12	4.33	11.56
B753	3.53	6.7	DH8B	2.57	7.05	SF34	3.74	9.38
B762	3.43	7.18	DH8C	3.54	8.79	SH36	5.13	11.74
B763	3.99	7.81	DH8D	3.5	8.75	SR22	4.97	14.93
B764	2.75	4.97	E120	3.59	9.06	SW4	5.26	12.59
B772	3.55	6.48						

Table A.11: Root Mean Square Error by Aircraft Type for Model 4b

Aircraft Type	Average RMSE (ft)	% of Mean $Dist_{TO}$	Aircraft Type	Average RMSE (ft)	% of Mean $Dist_{TO}$	Aircraft Type	Average RMSE (ft)	% of Mean $Dist_{TO}$
A306	401.14	6.31	B77L	586.03	6.52	E135	571.17	8.82
A319	476.69	6.96	B77W	575.15	6.16	E145	610.06	9.04
A320	386.41	5.46	B788	853.89	10.36	E170	420.37	6.82
A321	411.62	5.43	BE20	688.47	13.42	E190	422.07	6.62
A332	522.47	6.4	BE40	560.54	10.92	E45X	853.07	11.37
A333	443.69	5.49	BE99	493.09	12.21	E50P	474.53	9.92
A343	640.65	7.71	BE9L	455.89	10.74	E55P	358.37	7.9
A346	734.91	8.77	C172	322.4	13.44	F2TH	694.56	11.88
A388	598.23	7.33	C208	443.69	13.46	F900	632.21	11.85
AT72	384.57	9.67	C402	499.52	13.03	GALX	661.74	11.64
B190	662.57	12.43	C525	727.03	13.61	GLEX	757.8	13.95
B350	538.17	11.37	C550	770.79	14.46	GLF4	745.8	12.7
B712	496.93	6.84	C560	777.45	15.16	GLF5	817.13	14.3
B732	604.81	9.09	C56X	578.9	11.33	H25B	754.39	12.39
B733	561.58	7.22	C680	613.7	12.99	LJ35	832.38	13.65
B734	471.39	6.21	C750	643.49	10.55	LJ45	561.8	10.15
B735	551.17	8	CL30	479.12	9.05	LJ60	640.19	10.64
B736	410.86	7.65	CL60	621.71	10.64	MD11	744.4	10.09
B737	632.44	9.42	CRJ2	603.12	8.66	MD82	571.14	7.43
B738	679.92	8.54	CRJ7	609.99	9.16	MD83	558.51	7.15
B739	550.18	6.45	CRJ9	567.98	7.94	MD88	471.21	6.6
B744	758.21	9.04	DC10	696.48	9.48	MD90	488.09	6.61
B748	833.99	9.88	DC95	332.73	4.91	PA31	570.13	13.71
B752	551.69	7.54	DH8A	328.63	8.55	PC12	447.4	11.78
B753	587.22	6.93	DH8B	276.81	6.86	SF34	485.53	9.68
B762	546.8	8.06	DH8C	446.74	9.23	SH36	543.79	11.13
B763	630.26	8.1	DH8D	529.53	9.95	SR22	446.55	14.98
B764	482.98	5.43	E120	502.5	10.26	SW4	685.37	12.81
B772	572.88	6.76						

Table A.12: Root Mean Square Error by Aircraft Type for Model 4c

Aircraft Type	Average RMSE (s)	% of Mean AROT	Aircraft Type	Average RMSE (s)	% of Mean AROT	Aircraft Type	Average RMSE (s)	% of Mean AROT
A306	7.52	12.95	B77L	5.89	10.55	E135	4.2	9.54
A319	4.72	9.95	B77W	6.38	11.62	E145	4.71	10.72
A320	4.73	9.87	B788	7.03	11.47	E170	4.26	9.96
A321	4.9	9.95	BE20	7.06	14.44	E190	4.56	10.09
A332	6.16	10.61	BE40	5.42	11.32	E45X	4.71	10.58
A333	6.61	11.64	BE99	5.78	11.5	E50P	6.48	13.42
A343	6.23	10.81	BE9L	7.37	13.56	E55P	5.47	12.07
A346	6.76	12.17	C172	10.18	18.58	F2TH	6.4	13.42
A388	8.48	12.45	C208	7.62	16.41	F900	6.33	12.51
AT72	5.92	12.52	C402	5.22	10.92	GALX	6.05	12.68
B190	5.95	12.75	C525	6.66	13.93	GLEX	7.36	14.7
B350	5.88	12.68	C550	5.3	10.46	GLF4	6.65	13.11
B712	3.87	8.53	C560	6.81	13.67	GLF5	6.68	13.18
B732	3.18	7.55	C56X	6.01	12.93	H25B	6.68	13.43
B733	4.33	9.48	C680	5.97	12.66	LJ35	7.9	15.33
B734	4.72	10.27	C750	5.8	12.18	LJ45	5.53	11.66
B735	4.64	10	CL30	5.34	11.62	LJ60	6.51	13.05
B736	4.2	9.37	CL60	6.08	12.3	MD11	8.76	14.37
B737	4.56	10.04	CRJ2	4.33	9.95	MD82	4.15	8.76
B738	5.02	10.65	CRJ7	4.45	9.98	MD83	4.27	9.01
B739	5.11	10.61	CRJ9	4.45	9.9	MD88	3.91	9.06
B744	7.71	12.75	DC10	6.93	11.3	MD90	4.31	9.92
B748	9.4	13.1	DC95	3.73	8.4	PA31	7.31	14.8
B752	5.37	10.7	DH8A	4.54	10.67	PC12	7.26	15.03
B753	5.45	10.65	DH8B	3.83	9.95	SF34	5.27	12.01
B762	6.35	11.83	DH8C	3.86	8.96	SH36	6.31	11.95
B763	6.51	12.14	DH8D	5.69	12.82	SR22	6.23	13.19
B764	5.57	11.4	E120	4.63	10.81	SW4	7.93	15.45
B772	6.53	11.93						

Table A.13: Root Mean Square Error by Aircraft Type for Model 5a

Aircraft Type	Average RMSE (s)	% of Mean DROT	Aircraft Type	Average RMSE (s)	% of Mean DROT	Aircraft Type	Average RMSE (s)	% of Mean DROT
A306	3.6	7.94	B77L	3.59	6.45	E135	3.47	7.53
A319	3.52	7.3	B77W	3.27	5.74	E145	3.66	7.78
A320	3.18	6.53	B788	4.82	8.74	E170	3.26	7.36
A321	3.24	6.52	BE20	4.73	11.6	E190	3.13	6.82
A332	3.82	6.89	BE40	3.47	9.22	E45X	4.71	9.48
A333	3.63	6.56	BE99	3.59	10.18	E50P	3.35	8.68
A343	4.27	7.21	BE9L	4.25	11.22	E55P	2.54	7.46
A346	4.09	7.35	C172	4.82	15.18	F2TH	4.39	10.95
A388	4.57	7.79	C208	4.99	13.38	F900	4.23	10.99
AT72	3.1	8.82	C402	4.45	12.1	GALX	3.76	9.84
B190	4.06	10.27	C525	4.92	12.45	GLEX	4.37	11.15
B350	3.74	9.77	C550	5.36	13.31	GLF4	4.38	11.01
B712	3.04	6.41	C560	4.65	12.5	GLF5	4.62	11.48
B732	4.11	9.31	C56X	3.6	9.79	H25B	4.48	10.94
B733	3.76	7.38	C680	3.64	10.4	LJ35	4.72	11.98
B734	3.09	6.24	C750	3.81	9.59	LJ45	3.36	8.44
B735	3.62	7.55	CL30	3.19	8.52	LJ60	3.82	9.92
B736	3.08	7.67	CL60	3.74	9.52	MD11	4	8.46
B737	4.04	8.64	CRJ2	3.7	7.84	MD82	3.7	7.21
B738	3.93	7.62	CRJ7	3.73	8.08	MD83	3.7	7.11
B739	3.34	6.19	CRJ9	3.26	6.85	MD88	3.39	6.76
B744	4.67	8.27	DC10	4.18	8.44	MD90	3.09	6.26
B748	4.69	8.28	DC95	2.6	5.39	PA31	4.43	11.38
B752	3.54	7.27	DH8A	2.66	7.49	PC12	4.58	12.2
B753	3.59	6.81	DH8B	2.63	7.21	SF34	3.57	8.97
B762	3.34	6.98	DH8C	3.39	8.43	SH36	4.62	10.58
B763	3.92	7.66	DH8D	3.43	8.6	SR22	4.69	14.09
B764	2.8	5.07	E120	3.38	8.54	SW4	4.6	11.01
B772	3.44	6.28						

Table A.14: Root Mean Square Error by Aircraft Type for Model 5b

Aircraft Type	Average RMSE (ft)	% of Mean $Dist_{TO}$	Aircraft Type	Average RMSE (ft)	% of Mean $Dist_{TO}$	Aircraft Type	Average RMSE (ft)	% of Mean $Dist_{TO}$
A306	427.04	6.72	B77L	565.88	6.3	E135	553.64	8.55
A319	473.95	6.92	B77W	569.09	6.09	E145	607.73	9
A320	393.08	5.55	B788	724.89	8.8	E170	417.68	6.78
A321	414.24	5.46	BE20	630.03	12.28	E190	417.26	6.54
A332	516.27	6.33	BE40	546.05	10.64	E45X	815.18	10.86
A333	455.03	5.63	BE99	524.16	12.98	E50P	489.92	10.24
A343	636.26	7.66	BE9L	473.57	11.16	E55P	359.56	7.93
A346	609.04	7.27	C172	377.94	15.75	F2TH	703.43	12.04
A388	596.96	7.32	C208	444.47	13.48	F900	607.4	11.39
AT72	334.33	8.41	C402	495.69	12.93	GALX	651.73	11.46
B190	657.22	12.33	C525	767.34	14.36	GLEX	704.63	12.97
B350	548.91	11.6	C550	861.66	16.17	GLF4	720.93	12.28
B712	506.96	6.98	C560	771.88	15.05	GLF5	753.68	13.19
B732	496.78	7.46	C56X	586.94	11.49	H25B	771.13	12.67
B733	576.59	7.42	C680	578.14	12.24	LJ35	776.67	12.73
B734	459.75	6.05	C750	669.92	10.98	LJ45	562.82	10.16
B735	537.29	7.8	CL30	484.36	9.15	LJ60	672.09	11.17
B736	401.68	7.48	CL60	630.65	10.79	MD11	696.86	9.45
B737	636.69	9.48	CRJ2	608.2	8.74	MD82	571.77	7.44
B738	675.93	8.49	CRJ7	607.78	9.12	MD83	580.54	7.44
B739	550.14	6.45	CRJ9	548.77	7.67	MD88	463.2	6.49
B744	746.83	8.9	DC10	638.98	8.7	MD90	472.09	6.39
B748	755.32	8.95	DC95	330.65	4.88	PA31	558.68	13.44
B752	547.17	7.48	DH8A	319.83	8.32	PC12	447.23	11.77
B753	588.46	6.94	DH8B	287.45	7.12	SF34	442.6	8.83
B762	520.16	7.67	DH8C	426.52	8.81	SH36	487.26	9.97
B763	614.35	7.89	DH8D	531.3	9.98	SR22	404.12	13.56
B764	469.36	5.27	E120	477.07	9.74	SW4	674.28	12.6
B772	571.53	6.75						

Table A.15: Root Mean Square Error by Aircraft Type for Model 5c

Aircraft Type	Average RMSE (s)	% of Mean AROT	Aircraft Type	Average RMSE (s)	% of Mean AROT	Aircraft Type	Average RMSE (s)	% of Mean AROT
A306	6.94	12.95	B77L	6.12	10.55	E135	3.91	9.54
A319	4.13	9.95	B77W	5.49	11.62	E145	4.18	10.72
A320	4.3	9.87	B788	6.6	11.47	E170	3.72	9.96
A321	4.42	9.95	BE20	6.78	14.44	E190	4.09	10.09
A332	6.46	10.61	BE40	5.75	11.32	E45X	4.17	10.58
A333	6.11	11.64	BE99	5.51	11.5	E50P	5.12	13.42
A343	6.84	10.81	BE9L	6.74	13.56	E55P	5.04	12.07
A346	5.68	12.17	C172	7.66	18.58	F2TH	5.71	13.42
A388	8.68	12.45	C208	6.31	16.41	F900	5.75	12.51
AT72	4.25	12.52	C402	5.14	10.92	GALX	5.7	12.68
B190	5.15	12.75	C525	5.78	13.93	GLEX	5.27	14.7
B350	5.62	12.68	C550	6.47	10.46	GLF4	6.45	13.11
B712	3.18	8.53	C560	6.21	13.67	GLF5	6.09	13.18
B732	3.01	7.55	C56X	5.38	12.93	H25B	6.15	13.43
B733	3.87	9.48	C680	5.29	12.66	LJ35	7.03	15.33
B734	4.42	10.27	C750	5.58	12.18	LJ45	5.68	11.66
B735	3.83	10	CL30	5.01	11.62	LJ60	6.75	13.05
B736	3.65	9.37	CL60	5.91	12.3	MD11	7.87	14.37
B737	4.04	10.04	CRJ2	3.7	9.95	MD82	3.68	8.76
B738	4.58	10.65	CRJ7	3.83	9.98	MD83	3.82	9.01
B739	4.65	10.61	CRJ9	3.9	9.9	MD88	3.33	9.06
B744	7.49	12.75	DC10	7.22	11.3	MD90	3.68	9.92
B748	8.86	13.1	DC95	3.05	8.4	PA31	6.61	14.8
B752	4.88	10.7	DH8A	4.21	10.67	PC12	5.93	15.03
B753	4.65	10.65	DH8B	3.55	9.95	SF34	4.69	12.01
B762	5.78	11.83	DH8C	3.58	8.96	SH36	5.82	11.95
B763	5.88	12.14	DH8D	4.97	12.82	SR22	5.45	13.19
B764	5.26	11.4	E120	3.98	10.81	SW4	6.66	15.45
B772	6.2	11.93						

Table A.16: Root Mean Square Error by Aircraft Type for Model 6a

Aircraft Type	Average RMSE (s)	% of Mean DROT	Aircraft Type	Average RMSE (s)	% of Mean DROT	Aircraft Type	Average RMSE (s)	% of Mean DROT
A306	3.61	7.97	B77L	3.6	6.49	E135	3.51	7.62
A319	3.52	7.3	B77W	3.28	5.75	E145	3.68	7.81
A320	3.19	6.54	B788	4.9	8.9	E170	3.27	7.38
A321	3.25	6.53	BE20	4.75	11.66	E190	3.13	6.82
A332	3.82	6.89	BE40	3.51	9.31	E45X	4.84	9.73
A333	3.63	6.56	BE99	3.8	10.79	E50P	3.48	9.01
A343	4.29	7.26	BE9L	4.3	11.36	E55P	2.57	7.57
A346	4.11	7.39	C172	4.83	15.21	F2TH	4.41	11
A388	4.66	7.94	C208	5	13.4	F900	4.24	11.03
AT72	3.17	9.01	C402	4.46	12.13	GALX	3.8	9.93
B190	4.07	10.3	C525	4.97	12.58	GLEX	4.45	11.34
B350	3.81	9.96	C550	5.47	13.6	GLF4	4.42	11.11
B712	3.05	6.43	C560	4.66	12.53	GLF5	4.65	11.56
B732	4.14	9.4	C56X	3.6	9.8	H25B	4.51	11.02
B733	3.81	7.47	C680	3.65	10.43	LJ35	4.75	12.05
B734	3.1	6.26	C750	3.86	9.7	LJ45	3.45	8.67
B735	3.71	7.75	CL30	3.21	8.56	LJ60	3.83	9.95
B736	3.4	8.48	CL60	3.76	9.58	MD11	4.03	8.53
B737	4.07	8.7	CRJ2	3.7	7.85	MD82	3.71	7.24
B738	3.95	7.66	CRJ7	3.75	8.13	MD83	3.71	7.13
B739	3.34	6.19	CRJ9	3.3	6.92	MD88	3.43	6.84
B744	4.67	8.28	DC10	4.23	8.55	MD90	3.11	6.3
B748	4.71	8.32	DC95	2.62	5.44	PA31	4.44	11.41
B752	3.55	7.3	DH8A	2.66	7.5	PC12	4.69	12.5
B753	3.6	6.82	DH8B	2.66	7.29	SF34	3.6	9.04
B762	3.35	7.01	DH8C	3.4	8.45	SH36	4.66	10.67
B763	3.92	7.67	DH8D	3.44	8.6	SR22	4.75	14.25
B764	2.81	5.07	E120	3.47	8.75	SW4	4.82	11.54
B772	3.46	6.3						

Table A.17: Root Mean Square Error by Aircraft Type for Model 6b

Aircraft Type	Average RMSE (ft)	% of Mean $Dist_{TO}$	Aircraft Type	Average RMSE (ft)	% of Mean $Dist_{TO}$	Aircraft Type	Average RMSE (ft)	% of Mean $Dist_{TO}$
A306	428.62	6.74	B77L	566.6	6.31	E135	562.72	8.69
A319	477.71	6.97	B77W	572.3	6.13	E145	610.45	9.04
A320	393.62	5.56	B788	735.31	8.92	E170	422.41	6.86
A321	414.81	5.47	BE20	634.93	12.38	E190	417.86	6.55
A332	517.18	6.34	BE40	552.76	10.77	E45X	836.67	11.15
A333	455.62	5.64	BE99	539.12	13.35	E50P	512.64	10.71
A343	640.64	7.71	BE9L	475.36	11.2	E55P	364.44	8.04
A346	611.1	7.29	C172	385.48	16.07	F2TH	706.19	12.08
A388	599.43	7.35	C208	445.32	13.51	F900	609.21	11.42
AT72	342.49	8.61	C402	496.02	12.94	GALX	654.04	11.5
B190	657.56	12.33	C525	780.17	14.6	GLEX	709.14	13.05
B350	556.23	11.75	C550	876.04	16.44	GLF4	731	12.45
B712	511.65	7.04	C560	773.44	15.08	GLF5	759.24	13.29
B732	502.79	7.56	C56X	588.87	11.53	H25B	775.4	12.74
B733	580	7.46	C680	580.69	12.29	LJ35	780.95	12.8
B734	460.09	6.06	C750	678.26	11.11	LJ45	572.17	10.33
B735	544.99	7.91	CL30	485.93	9.17	LJ60	673.43	11.19
B736	406.4	7.57	CL60	633.65	10.85	MD11	704.76	9.55
B737	637.42	9.5	CRJ2	608.25	8.74	MD82	575.67	7.49
B738	679.23	8.53	CRJ7	614.52	9.22	MD83	584.2	7.48
B739	550.3	6.45	CRJ9	558.64	7.81	MD88	464.98	6.51
B744	747.75	8.91	DC10	647.47	8.81	MD90	472.41	6.39
B748	765.98	9.07	DC95	334.38	4.93	PA31	562.93	13.54
B752	547.53	7.48	DH8A	320.73	8.35	PC12	472.09	12.43
B753	588.64	6.95	DH8B	287.91	7.13	SF34	444.09	8.86
B762	521.37	7.69	DH8C	431.08	8.9	SH36	498.8	10.21
B763	615.5	7.91	DH8D	531.68	9.99	SR22	410.54	13.77
B764	470.74	5.29	E120	481.23	9.83	SW4	701.44	13.11
B772	573.14	6.77						

Table A.18: Root Mean Square Error by Aircraft Type for Model 6c

Aircraft Type	Average RMSE (ft)	% of Mean AROT	Aircraft Type	Average RMSE (ft)	% of Mean AROT	Aircraft Type	Average RMSE (ft)	% of Mean AROT
A306	7.35	12.95	B77L	6.31	10.55	E135	4.28	9.54
A319	4.75	9.95	B77W	6.23	11.62	E145	4.65	10.72
A320	4.75	9.87	B788	7.07	11.47	E170	4.22	9.96
A321	4.87	9.95	BE20	7.34	14.44	E190	4.49	10.09
A332	6.79	10.61	BE40	6.15	11.32	E45X	4.65	10.58
A333	6.57	11.64	BE99	5.91	11.5	E50P	5.73	13.42
A343	7.6	10.81	BE9L	7.34	13.56	E55P	5.28	12.07
A346	6.19	12.17	C172	8.97	18.58	F2TH	6.21	13.42
A388	8.8	12.45	C208	7.15	16.41	F900	6.37	12.51
AT72	4.97	12.52	C402	5.63	10.92	GALX	6.24	12.68
B190	5.87	12.75	C525	6.29	13.93	GLEX	5.81	14.7
B350	6.06	12.68	C550	6.92	10.46	GLF4	6.77	13.11
B712	3.8	8.53	C560	6.83	13.67	GLF5	6.68	13.18
B732	3.44	7.55	C56X	5.76	12.93	H25B	6.68	13.43
B733	4.44	9.48	C680	5.76	12.66	LJ35	7.24	15.33
B734	4.79	10.27	C750	6.07	12.18	LJ45	5.88	11.66
B735	4.26	10	CL30	5.56	11.62	LJ60	6.9	13.05
B736	4.5	9.37	CL60	6.24	12.3	MD11	8.33	14.37
B737	4.55	10.04	CRJ2	4.37	9.95	MD82	4.17	8.76
B738	5.11	10.65	CRJ7	4.5	9.98	MD83	4.33	9.01
B739	5.24	10.61	CRJ9	4.49	9.9	MD88	3.97	9.06
B744	8.04	12.75	DC10	7.56	11.3	MD90	4.27	9.92
B748	9.02	13.1	DC95	3.76	8.4	PA31	7.57	14.8
B752	5.43	10.7	DH8A	4.72	10.67	PC12	6.92	15.03
B753	5.36	10.65	DH8B	3.92	9.95	SF34	5.21	12.01
B762	6.32	11.83	DH8C	4.05	8.96	SH36	6.71	11.95
B763	6.35	12.14	DH8D	5.66	12.82	SR22	6.41	13.19
B764	5.67	11.4	E120	4.55	10.81	SW4	7.31	15.45
B772	6.84	11.93						

Appendix B

Comparisons of Observed Data against Posterior Predictive Distributions

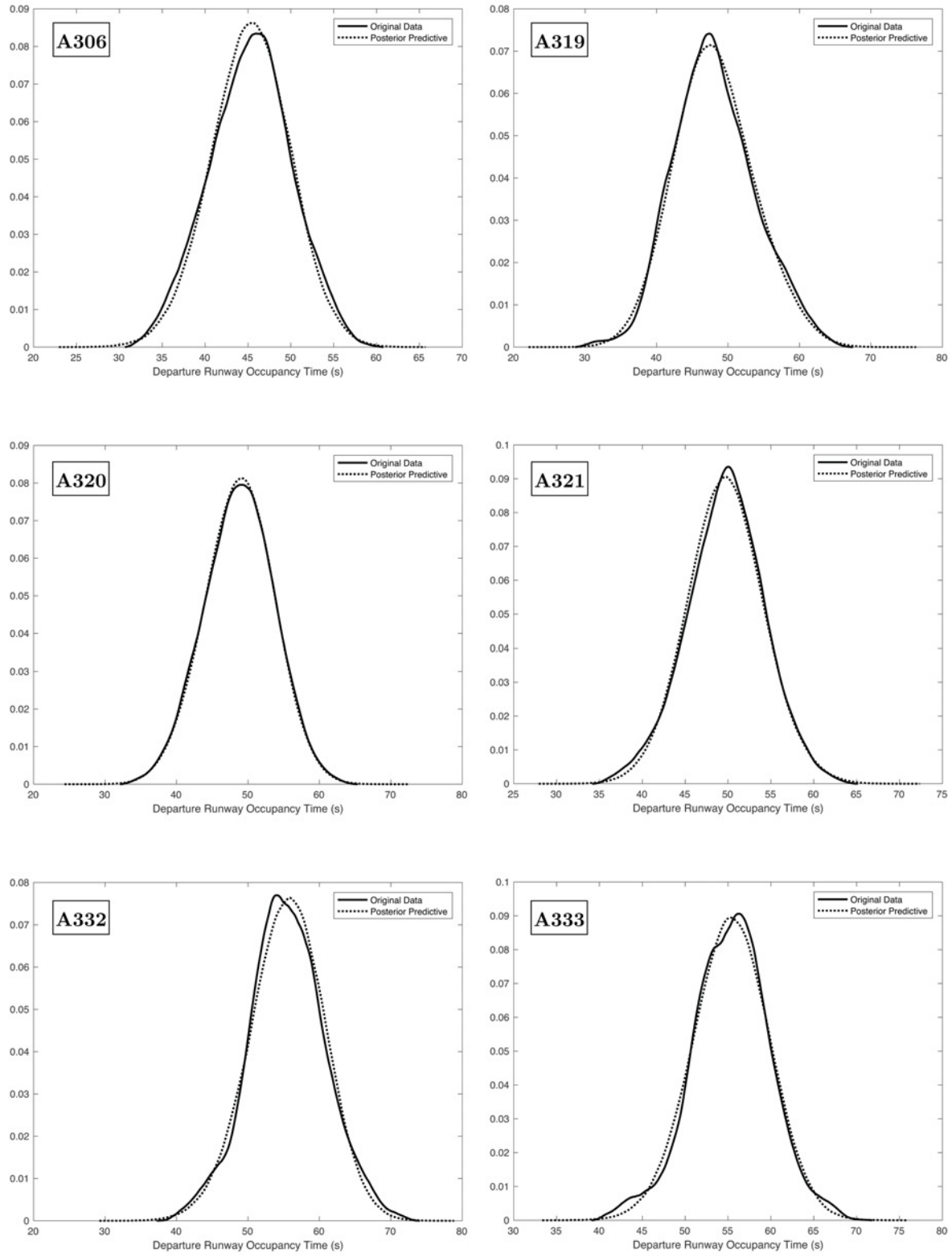

Figure B.1: Comparisons of Observed Data against Posterior Predictive Distributions of Model 5a, A306 - A333.

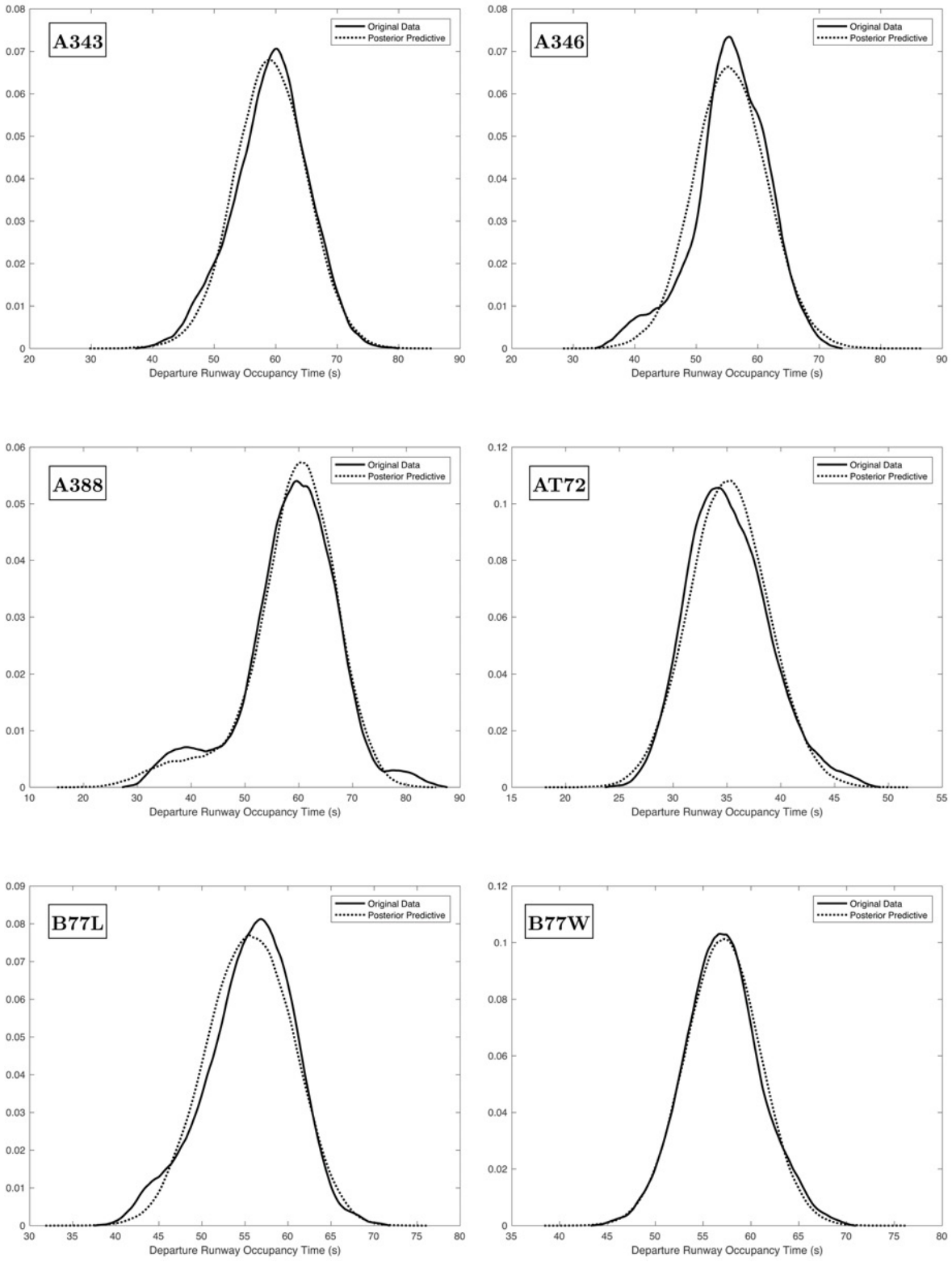

Figure B.2: Comparisons of Observed Data against Posterior Predictive Distributions of Model 5a, A343 - B77W.

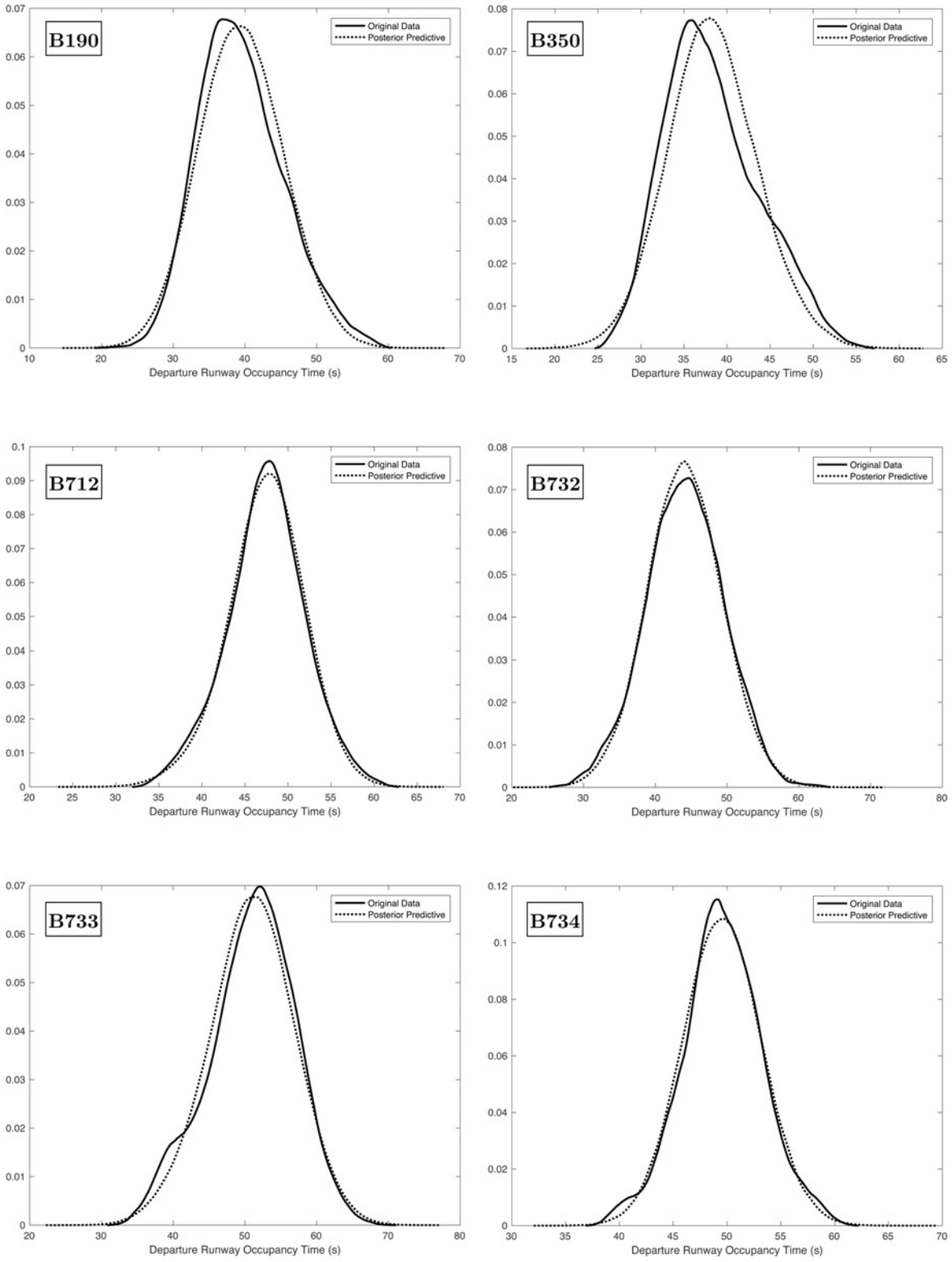

Figure B.3: Comparisons of Observed Data against Posterior Predictive Distributions of Model 5a, B190 - B734.

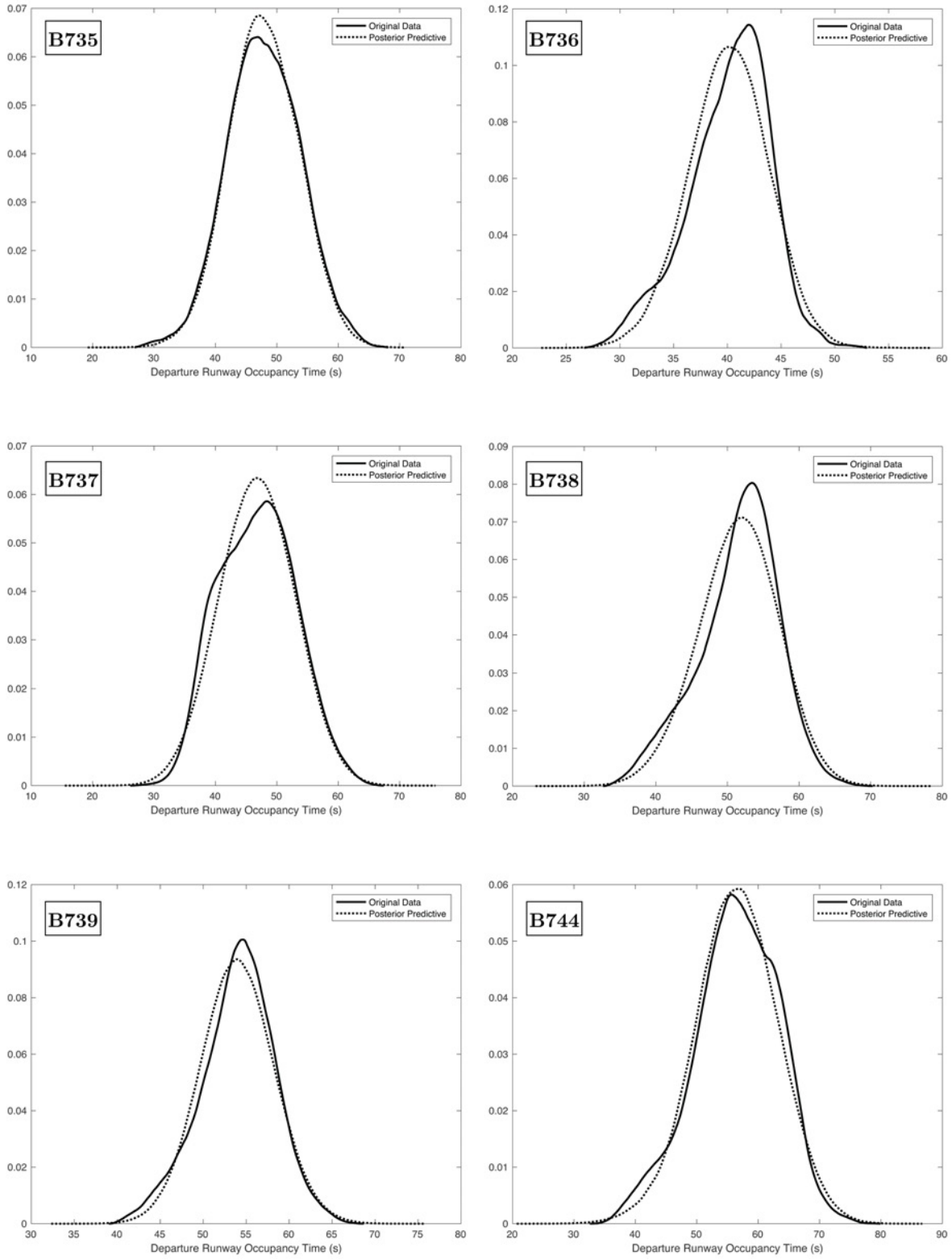

Figure B.4: Comparisons of Observed Data against Posterior Predictive Distributions of Model 5a, B735 - B744.

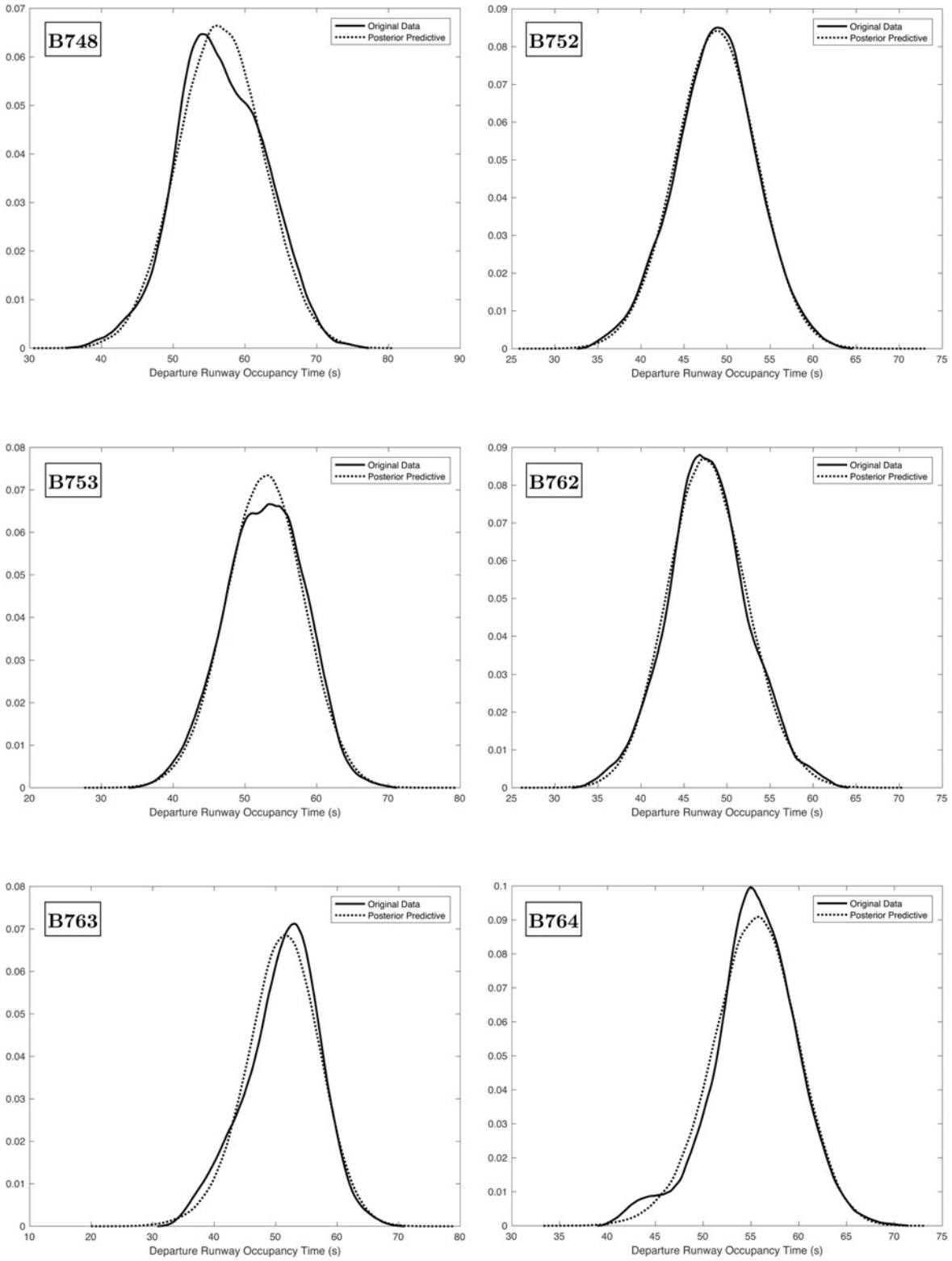

Figure B.5: Comparisons of Observed Data against Posterior Predictive Distributions of Model 5a, B748 - B764.

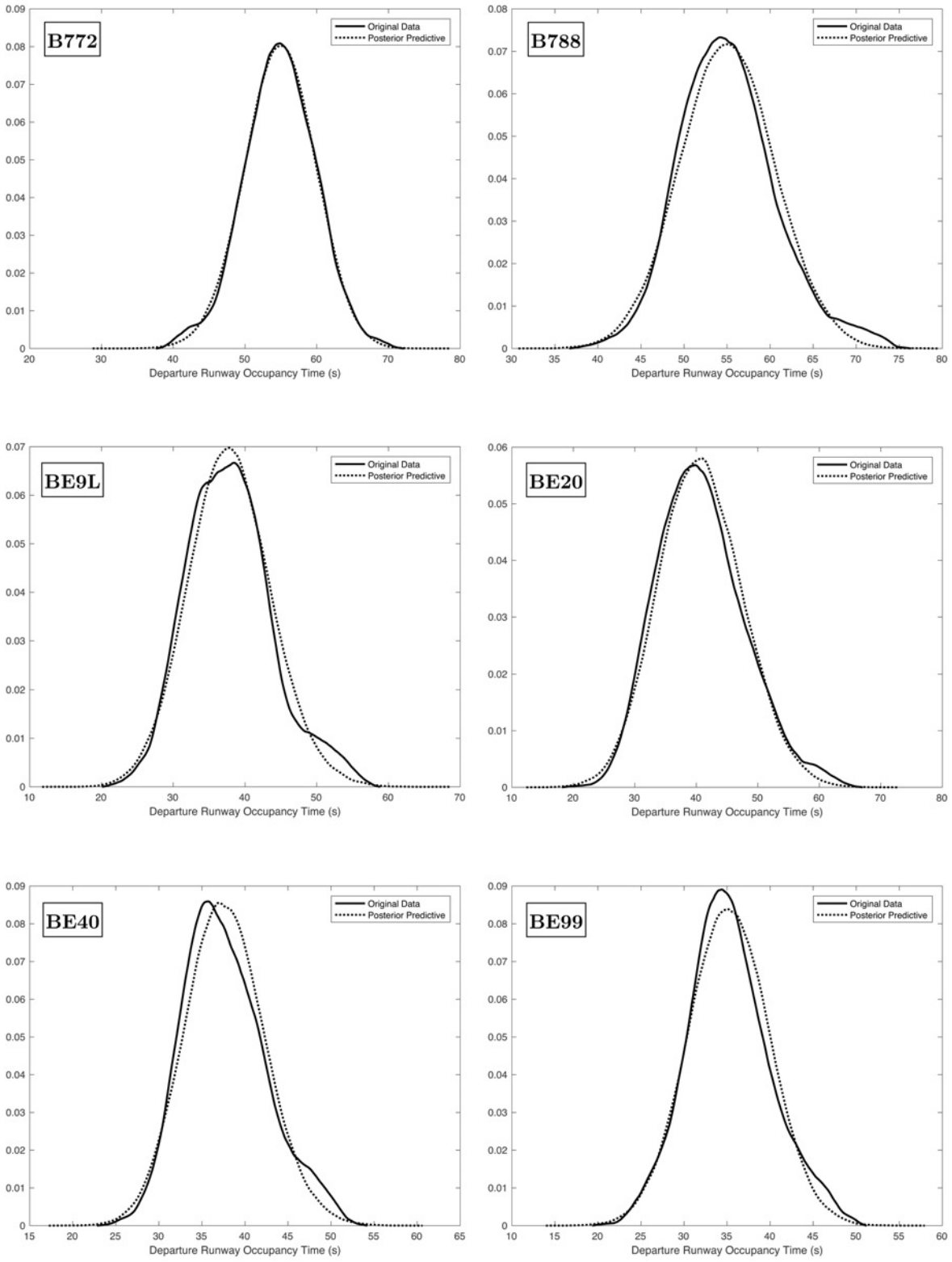

Figure B.6: Comparisons of Observed Data against Posterior Predictive Distributions of Model 5a, B772 - BE99.

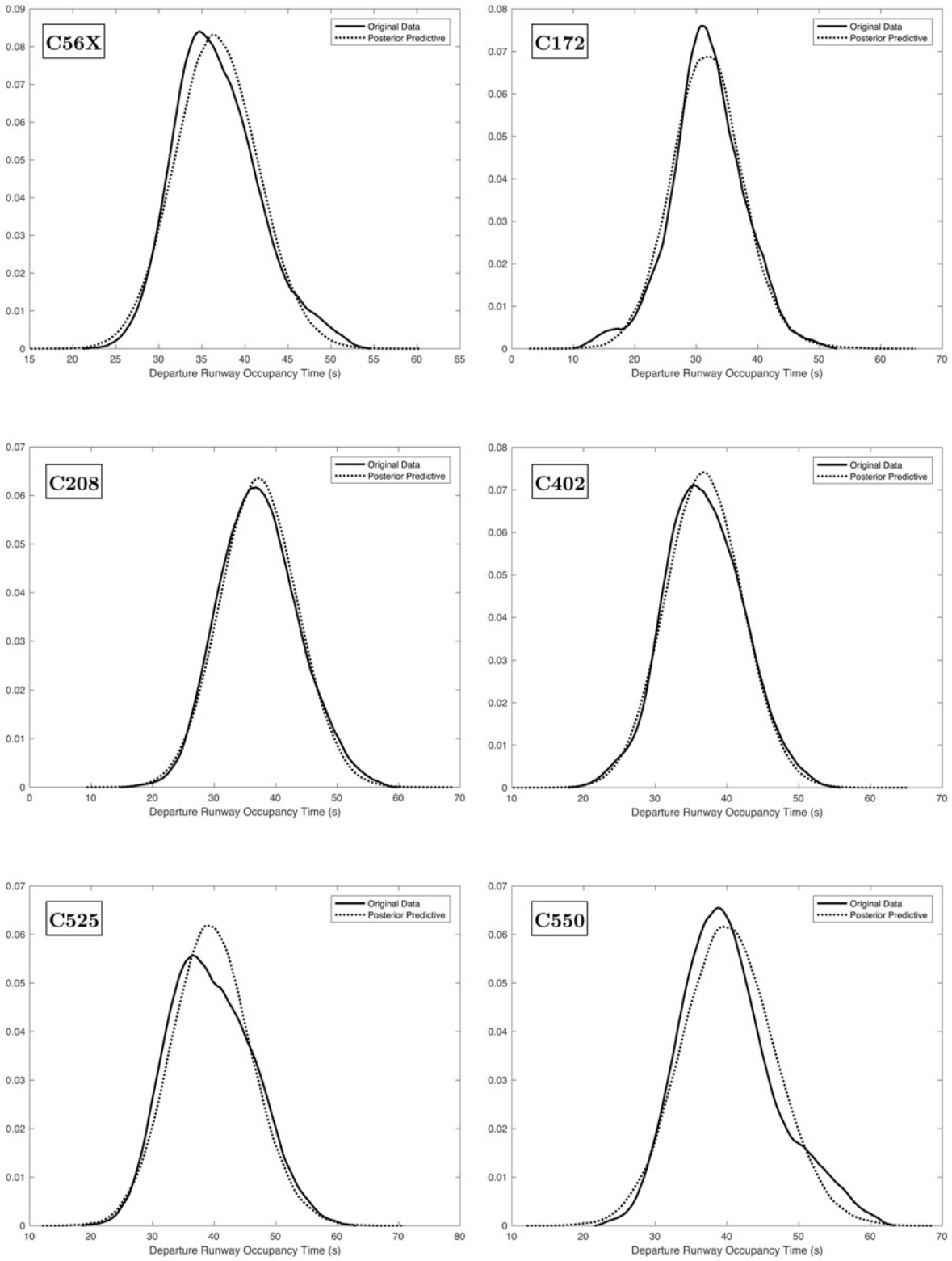

Figure B.7: Comparisons of Observed Data against Posterior Predictive Distributions of Model 5a, C56X - C550.

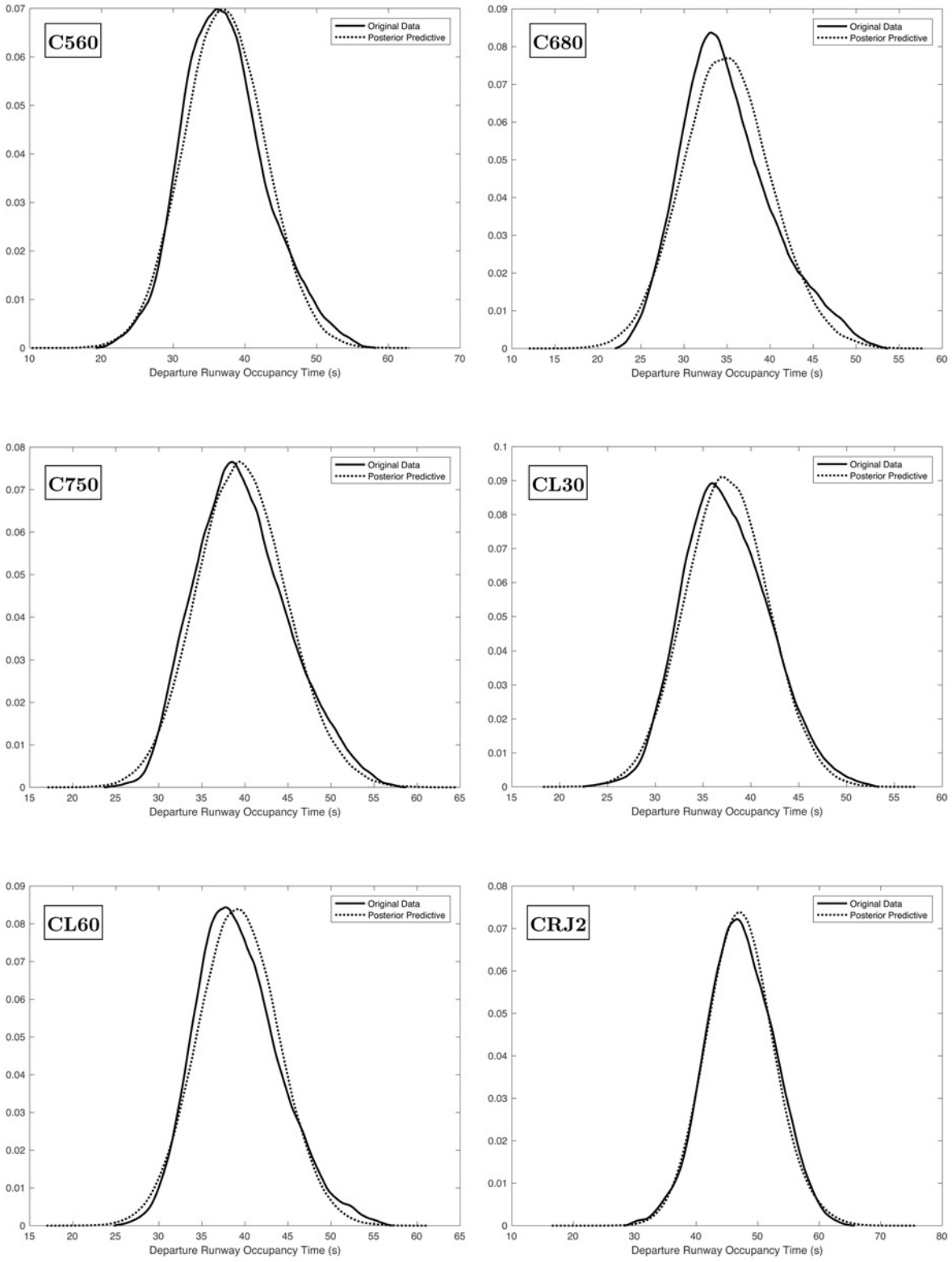

Figure B.8: Comparisons of Observed Data against Posterior Predictive Distributions of Model 5a, C560 - CRJ2.

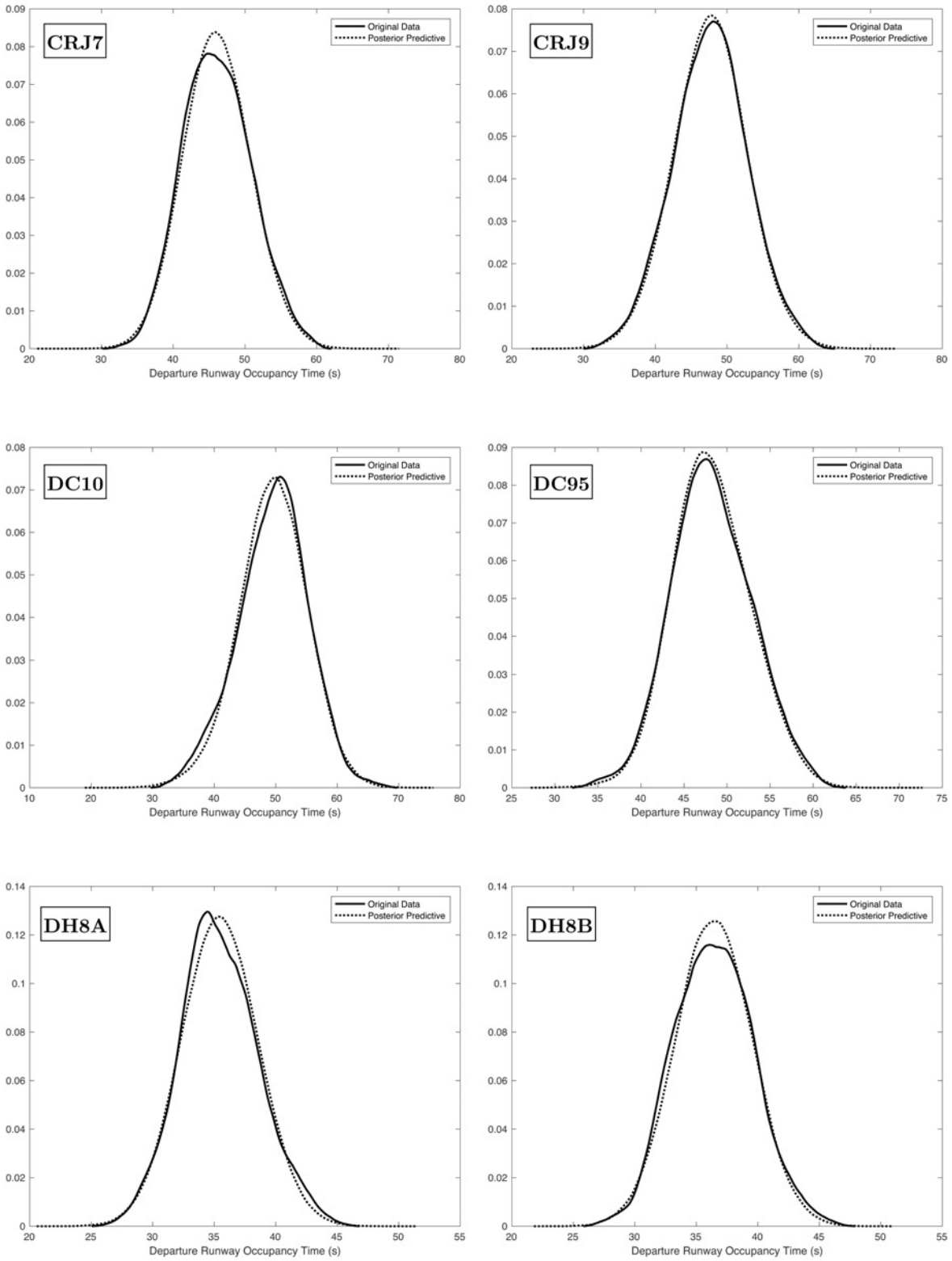

Figure B.9: Comparisons of Observed Data against Posterior Predictive Distributions of Model 5a, CRJ7 - DH8B.

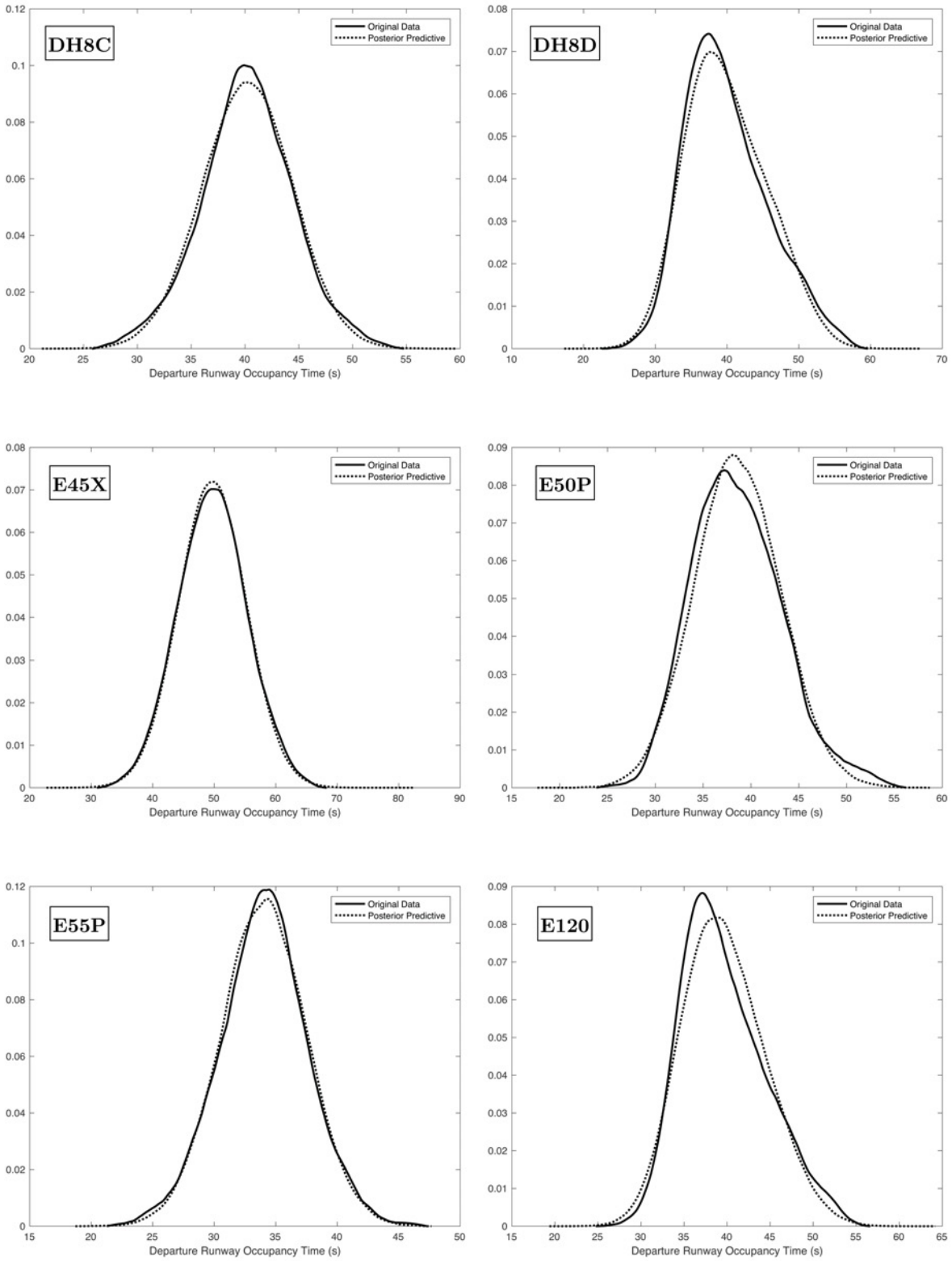

Figure B.10: Comparisons of Observed Data against Posterior Predictive Distributions of Model 5a, DH8C - E120.

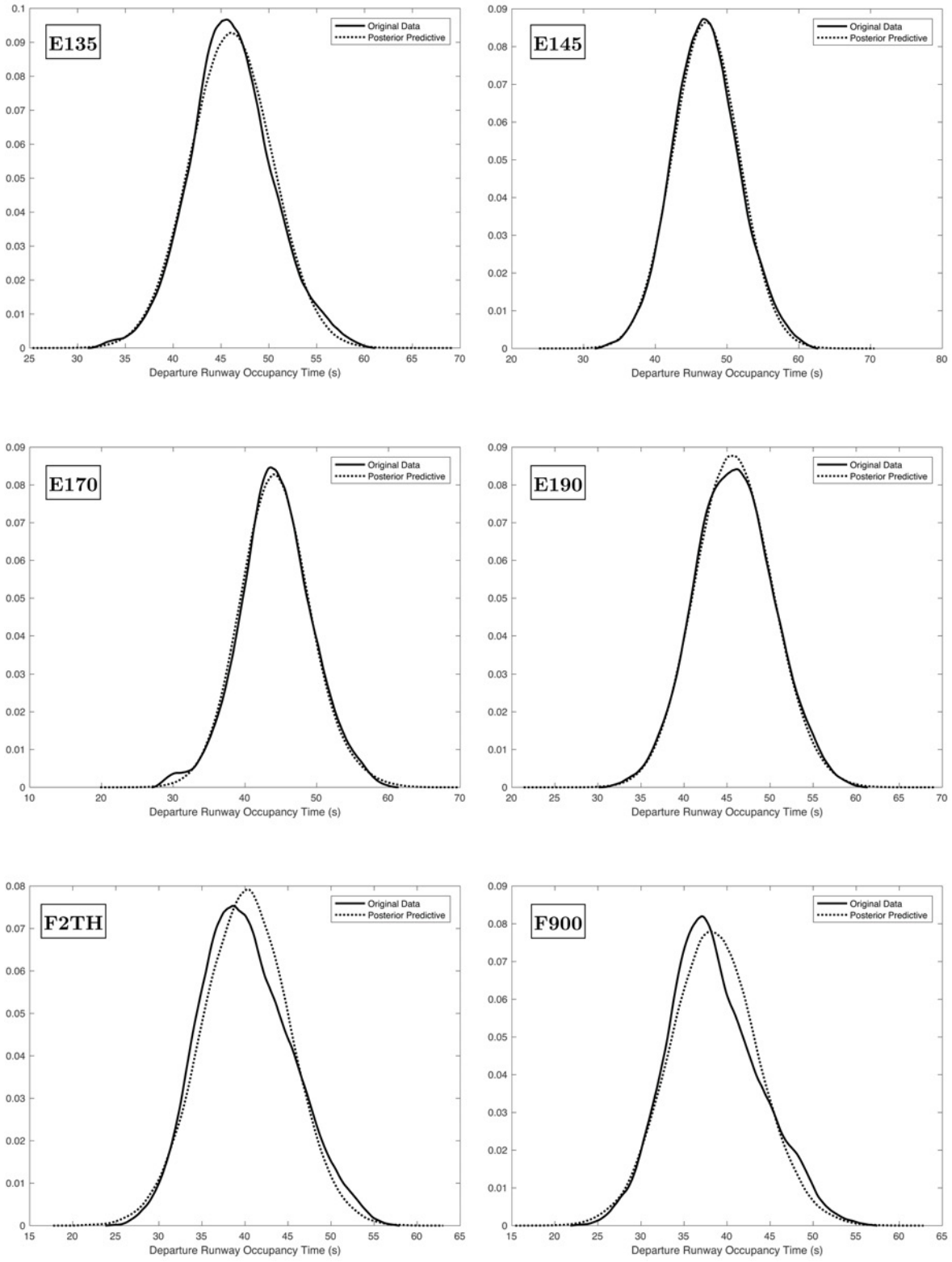

Figure B.11: Comparisons of Observed Data against Posterior Predictive Distributions of Model 5a, E135 - F900.

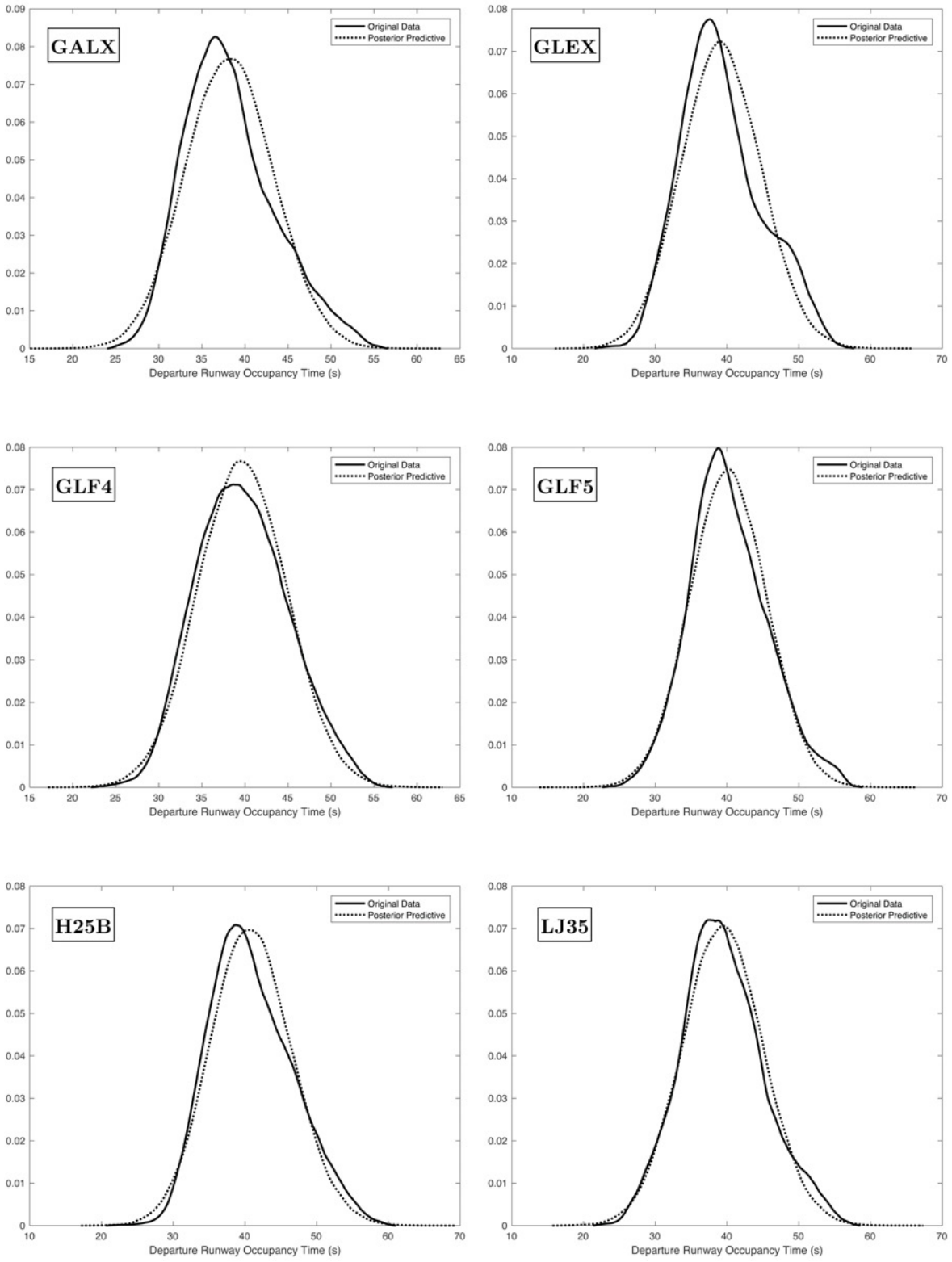

Figure B.12: Comparisons of Observed Data against Posterior Predictive Distributions of Model 5a, GALX - LJ35.

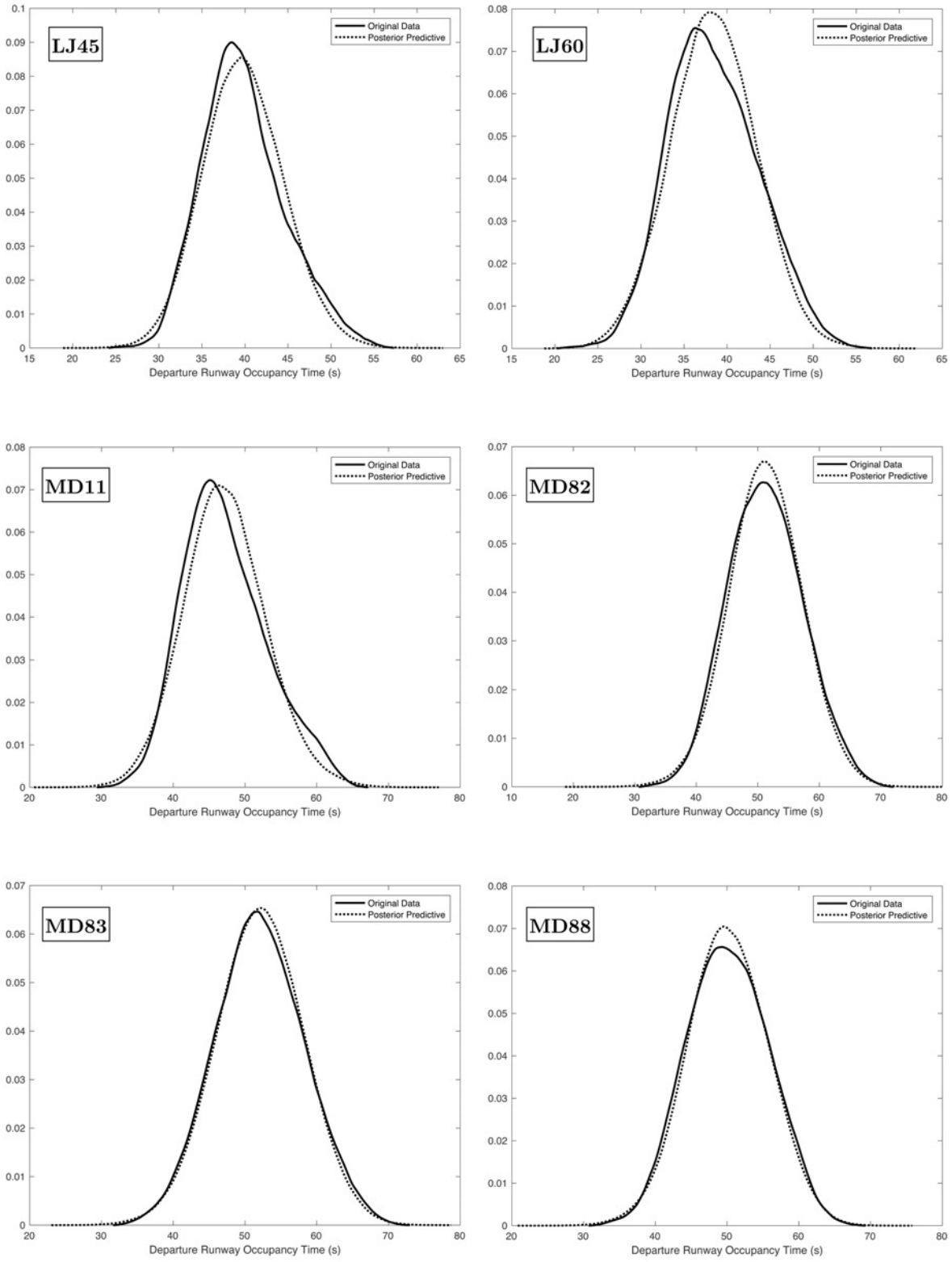

Figure B.13: Comparisons of Observed Data against Posterior Predictive Distributions of Model 5a, LJ45 - MD88.

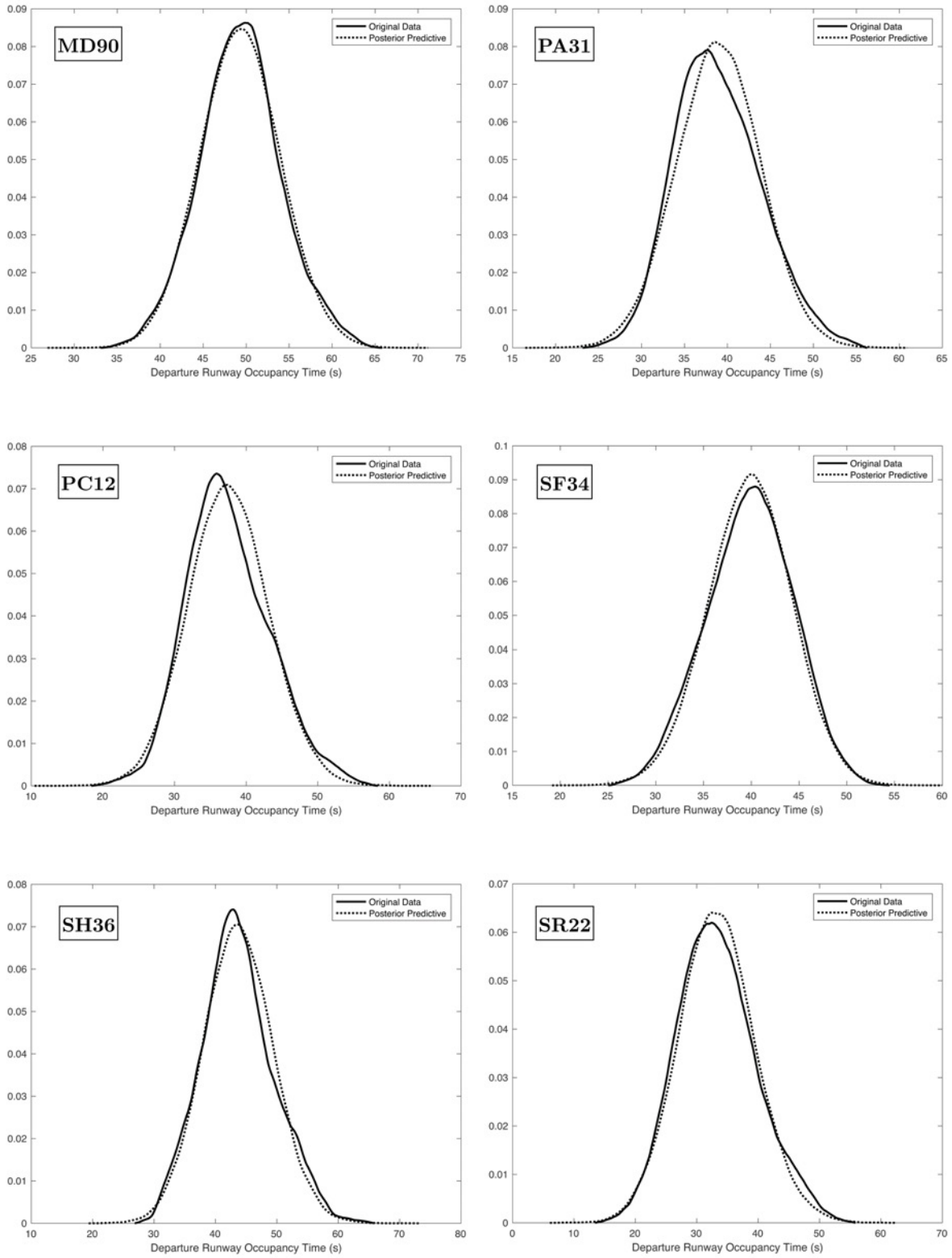

Figure B.14: Comparisons of Observed Data against Posterior Predictive Distributions of Model 5a, MD90 - SR22.

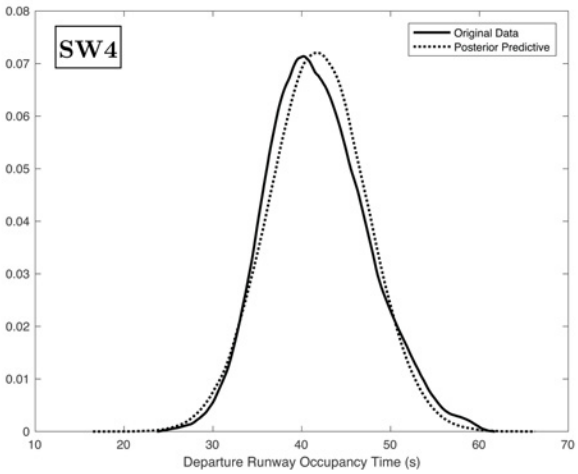

Figure B.15: Comparisons of Observed Data against Posterior Predictive Distributions of Model 5a, SW4.

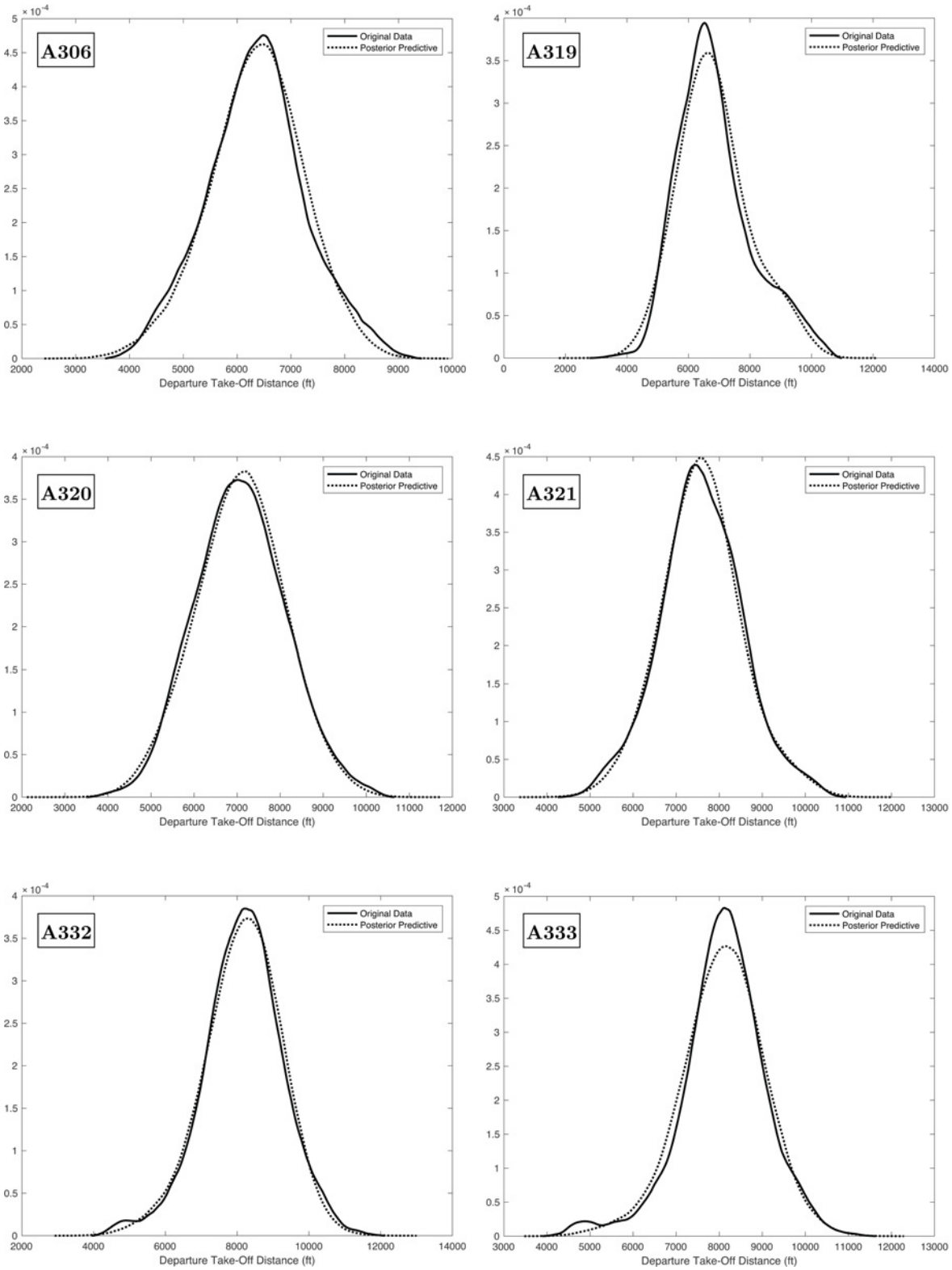

Figure B.16: Comparisons of Observed Data against Posterior Predictive Distributions of Model 5b, A306 - A333.

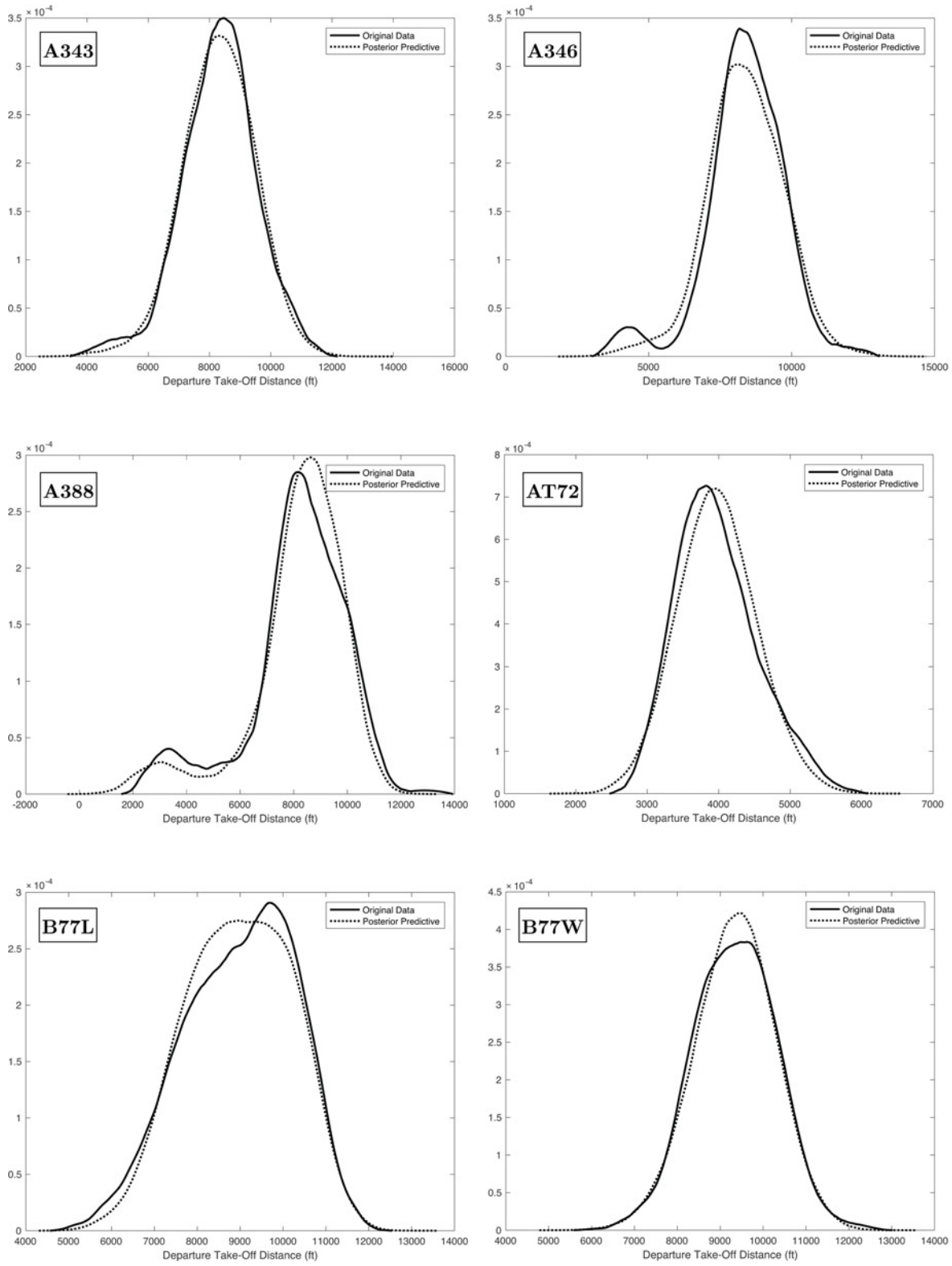

Figure B.17: Comparisons of Observed Data against Posterior Predictive Distributions of Model 5b, A343 - B77W.

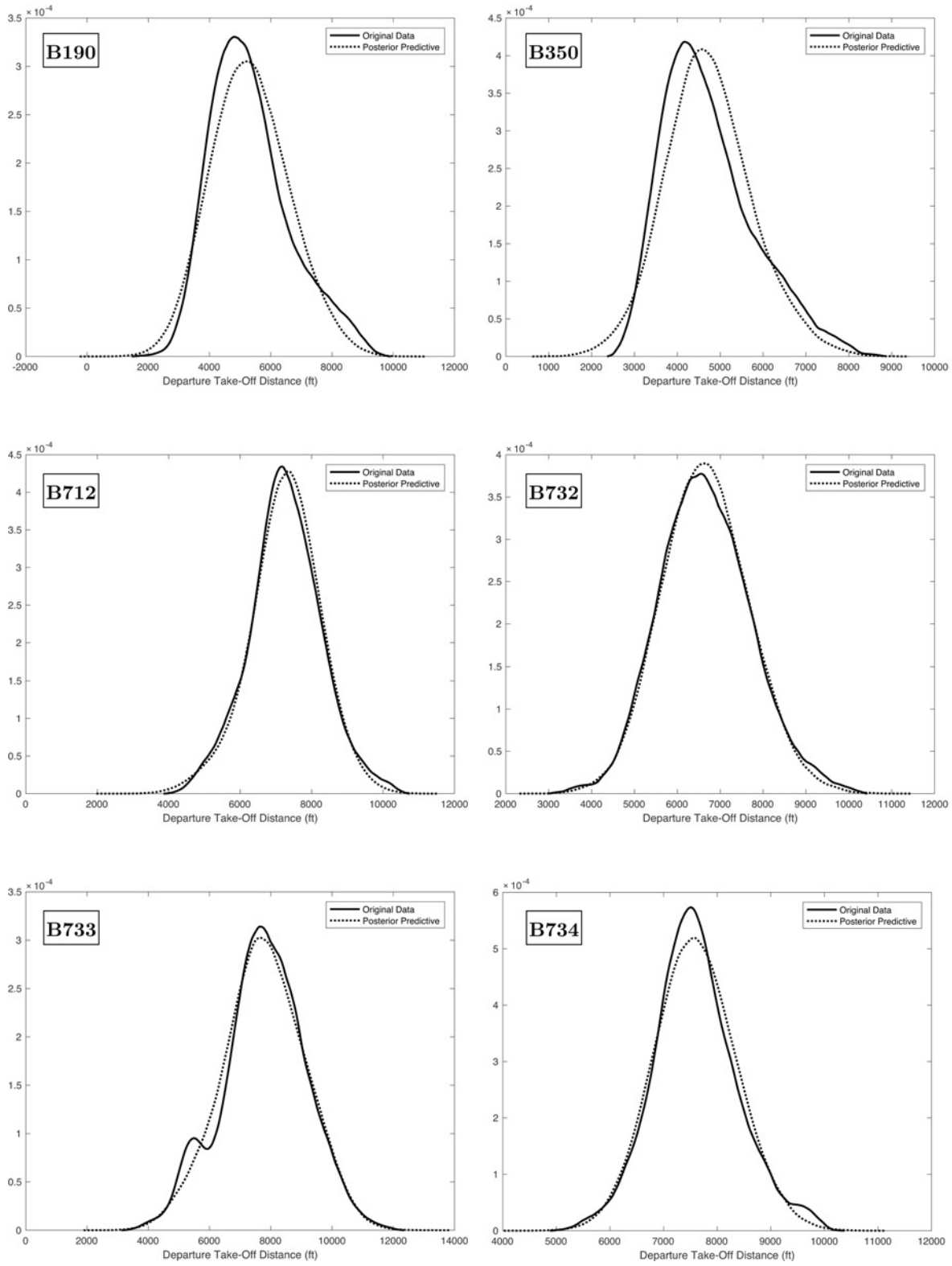

Figure B.18: Comparisons of Observed Data against Posterior Predictive Distributions of Model 5b, B190 - B734.

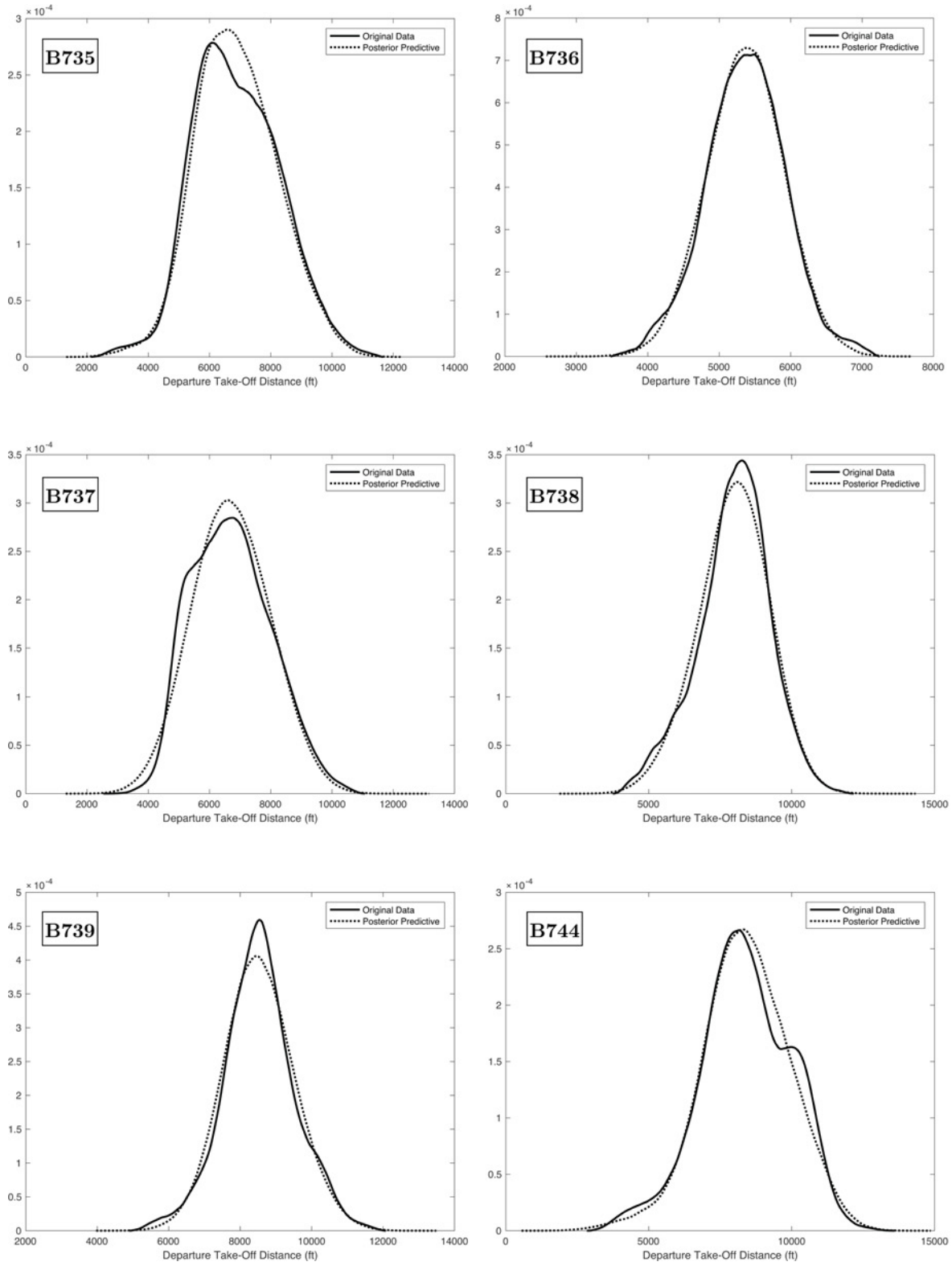

Figure B.19: Comparisons of Observed Data against Posterior Predictive Distributions of Model 5b, B735 - B744.

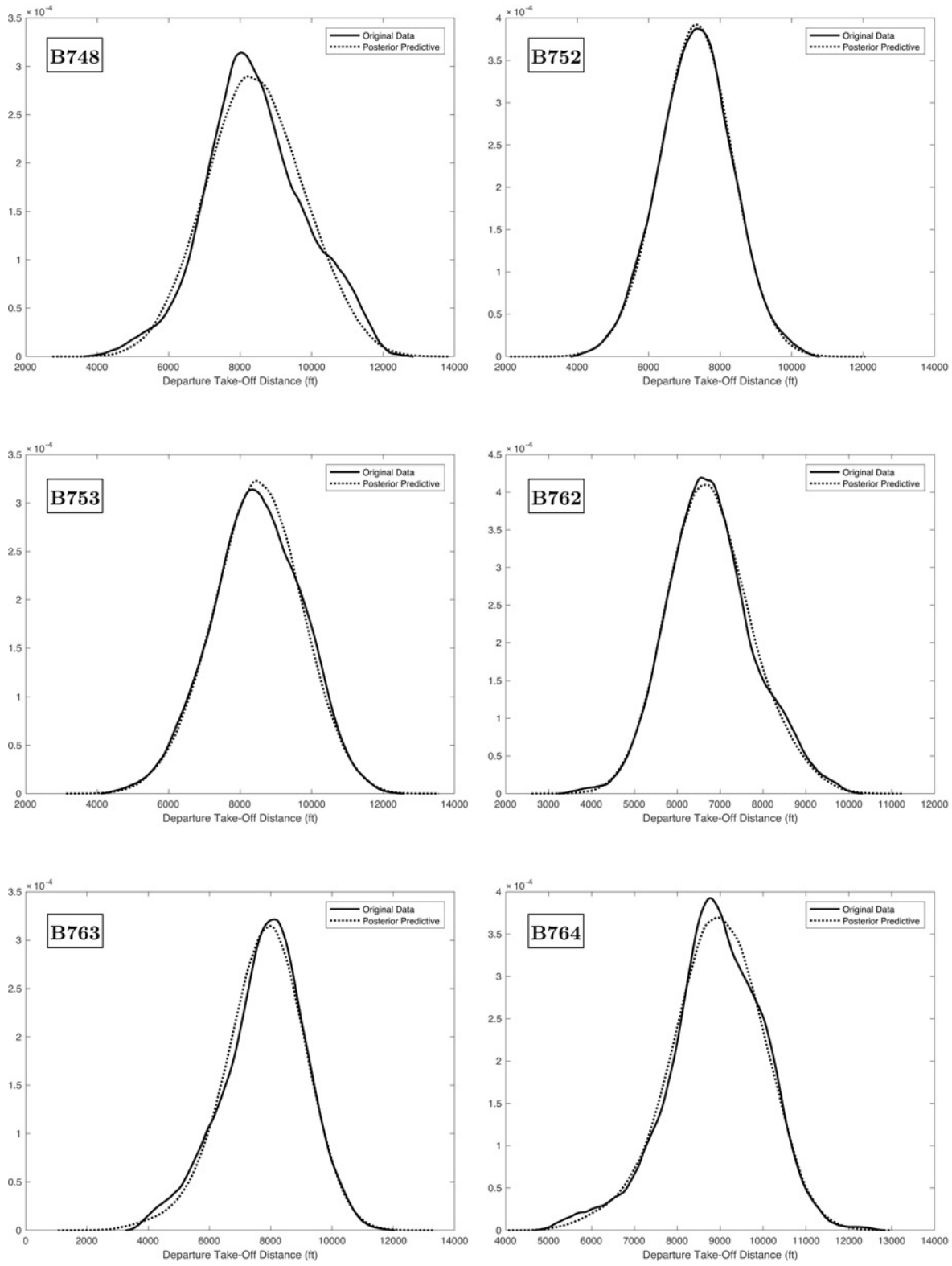

Figure B.20: Comparisons of Observed Data against Posterior Predictive Distributions of Model 5b, B748 - B764.

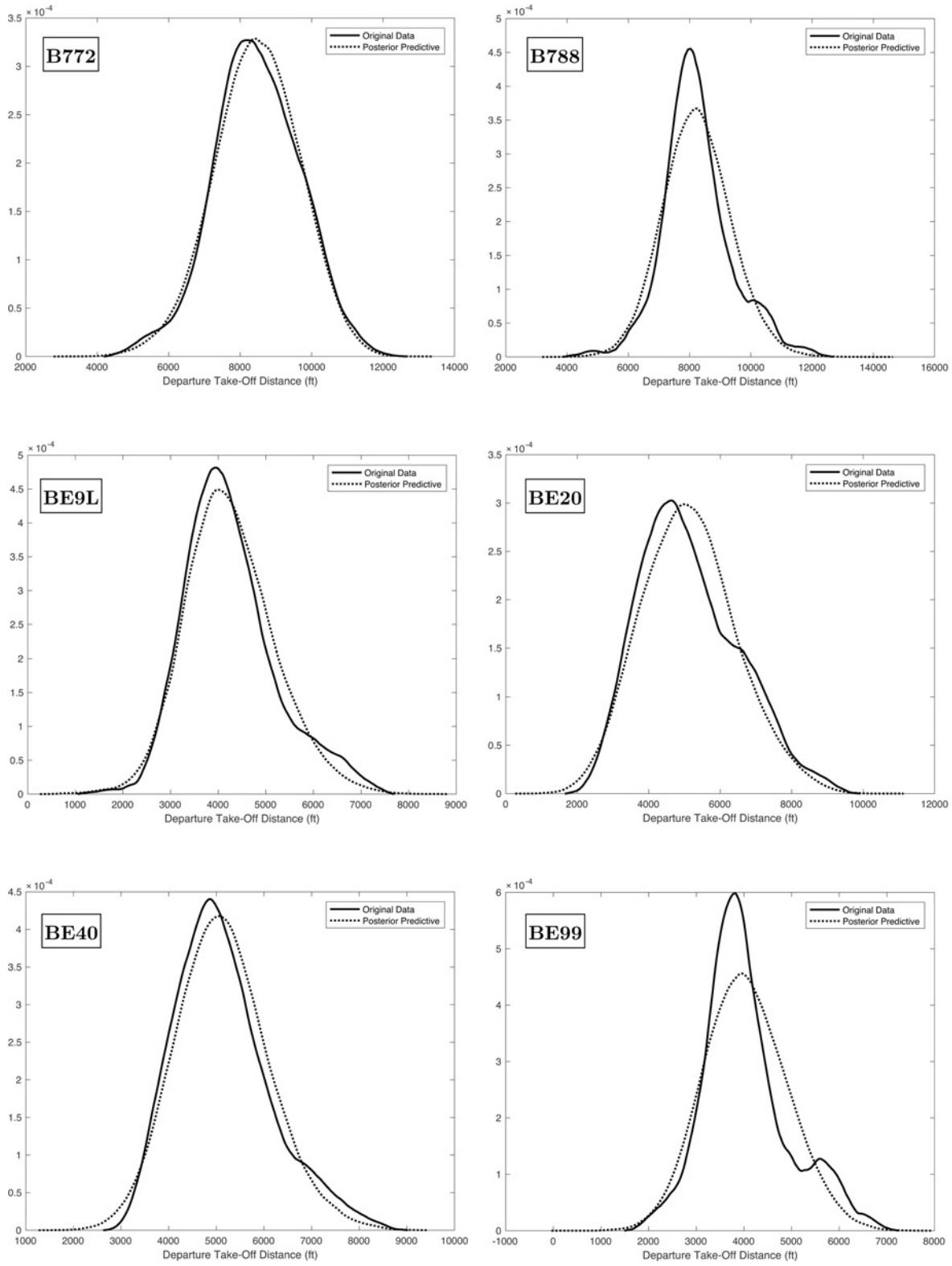

Figure B.21: Comparisons of Observed Data against Posterior Predictive Distributions of Model 5b, B772 - BE99.

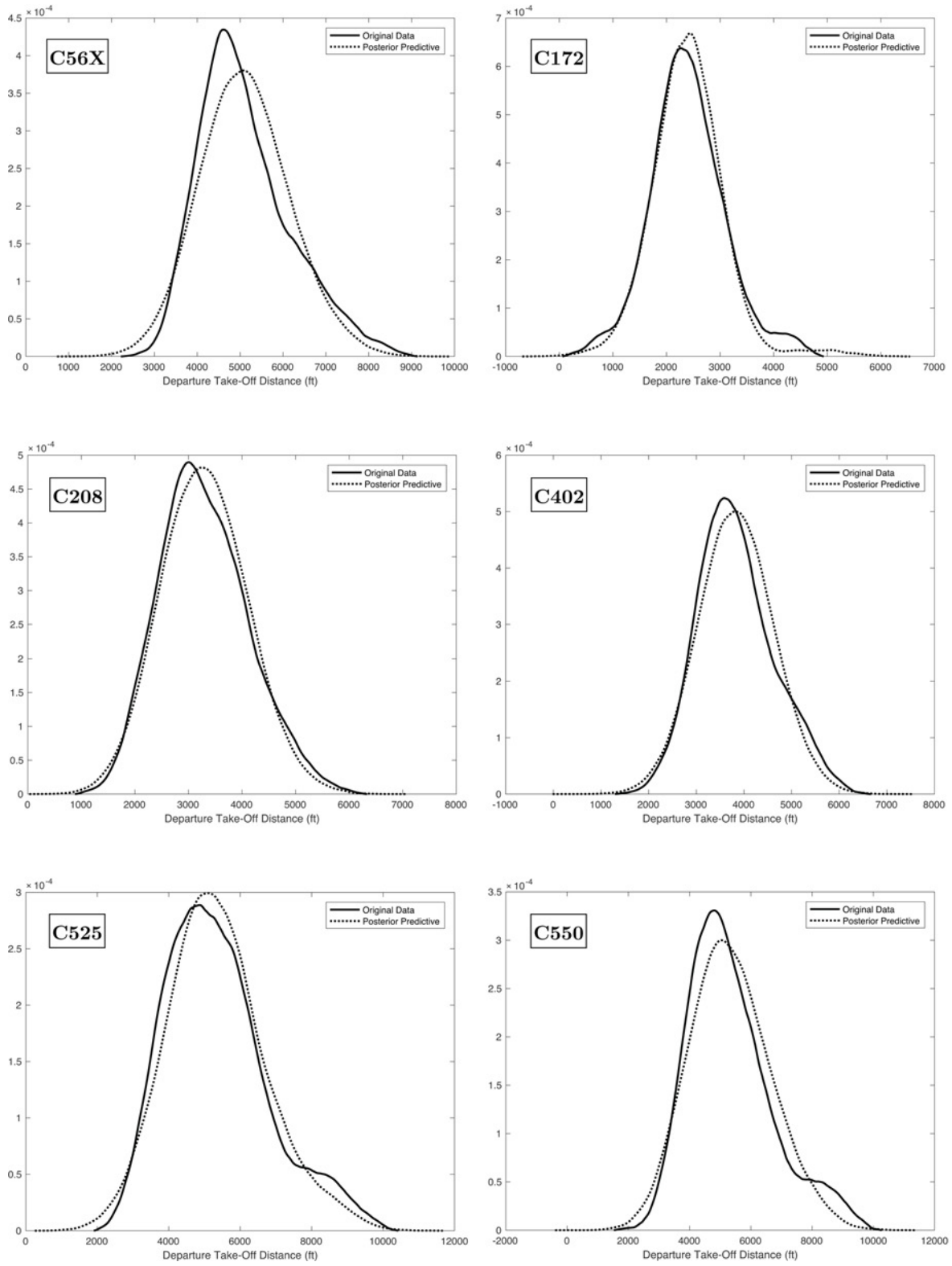

Figure B.22: Comparisons of Observed Data against Posterior Predictive Distributions of Model 5b, C56X - C550.

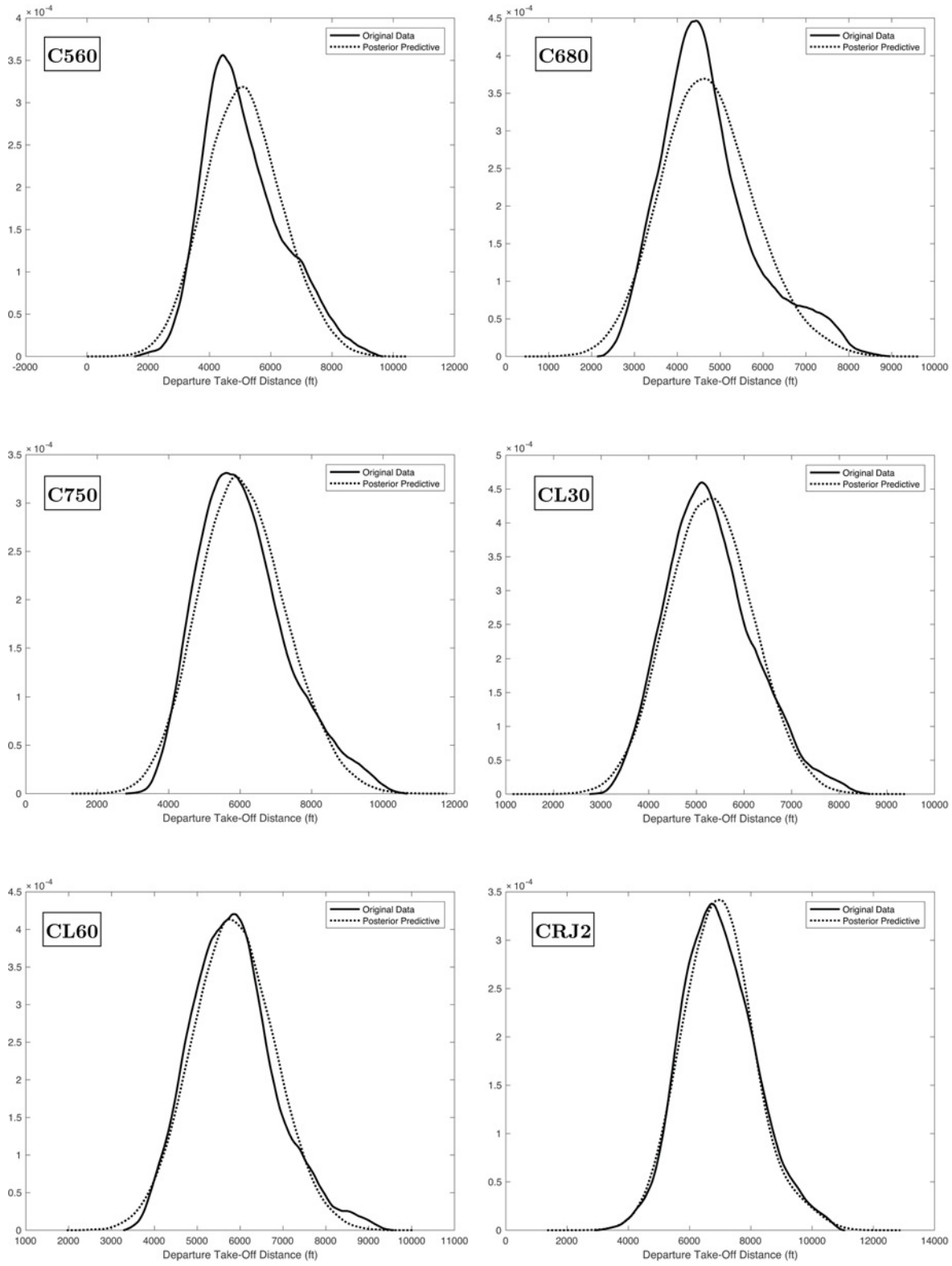

Figure B.23: Comparisons of Observed Data against Posterior Predictive Distributions of Model 5b, C560 - CRJ2.

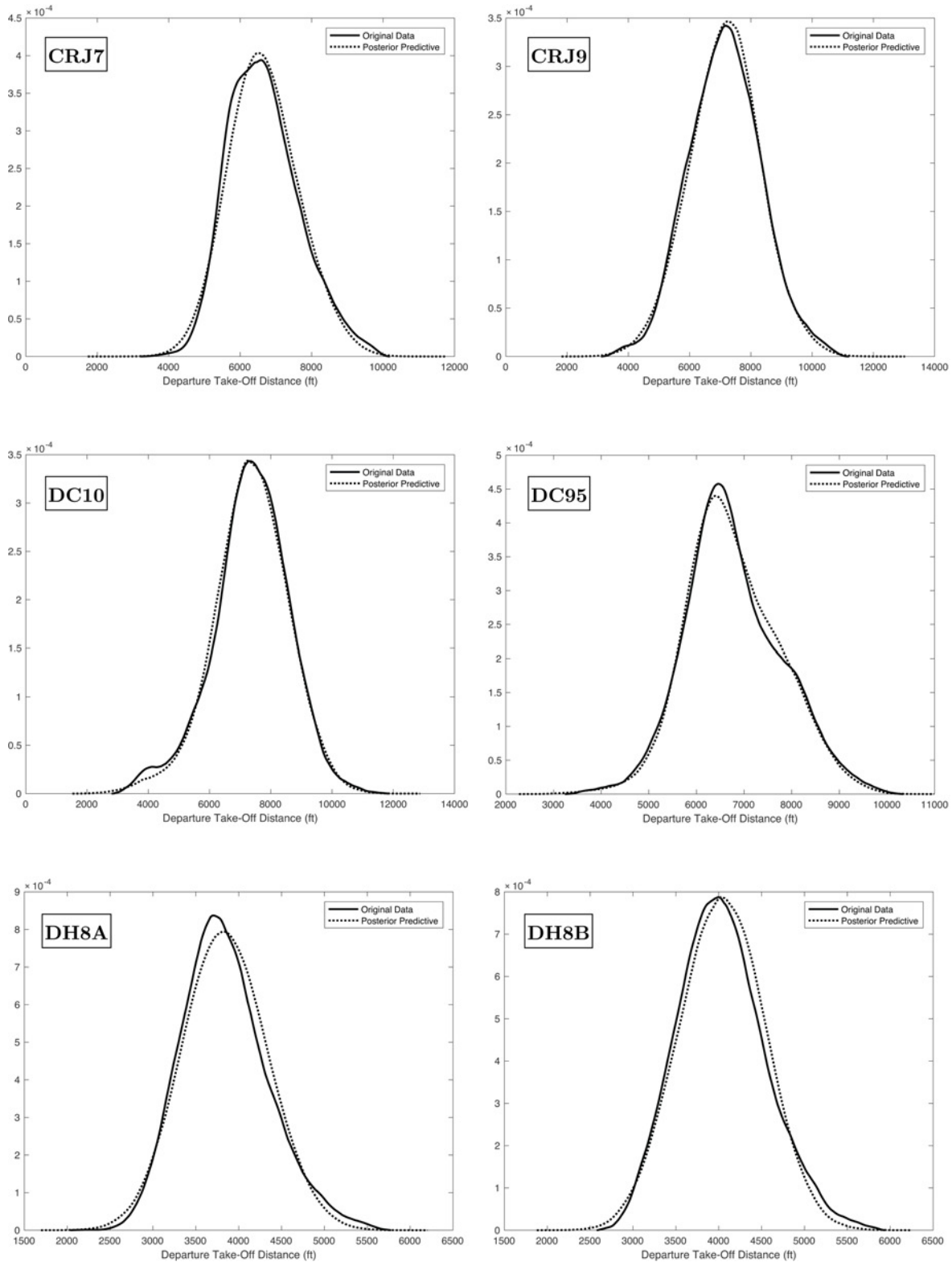

Figure B.24: Comparisons of Observed Data against Posterior Predictive Distributions of Model 5b, CRJ7 - DH8B.

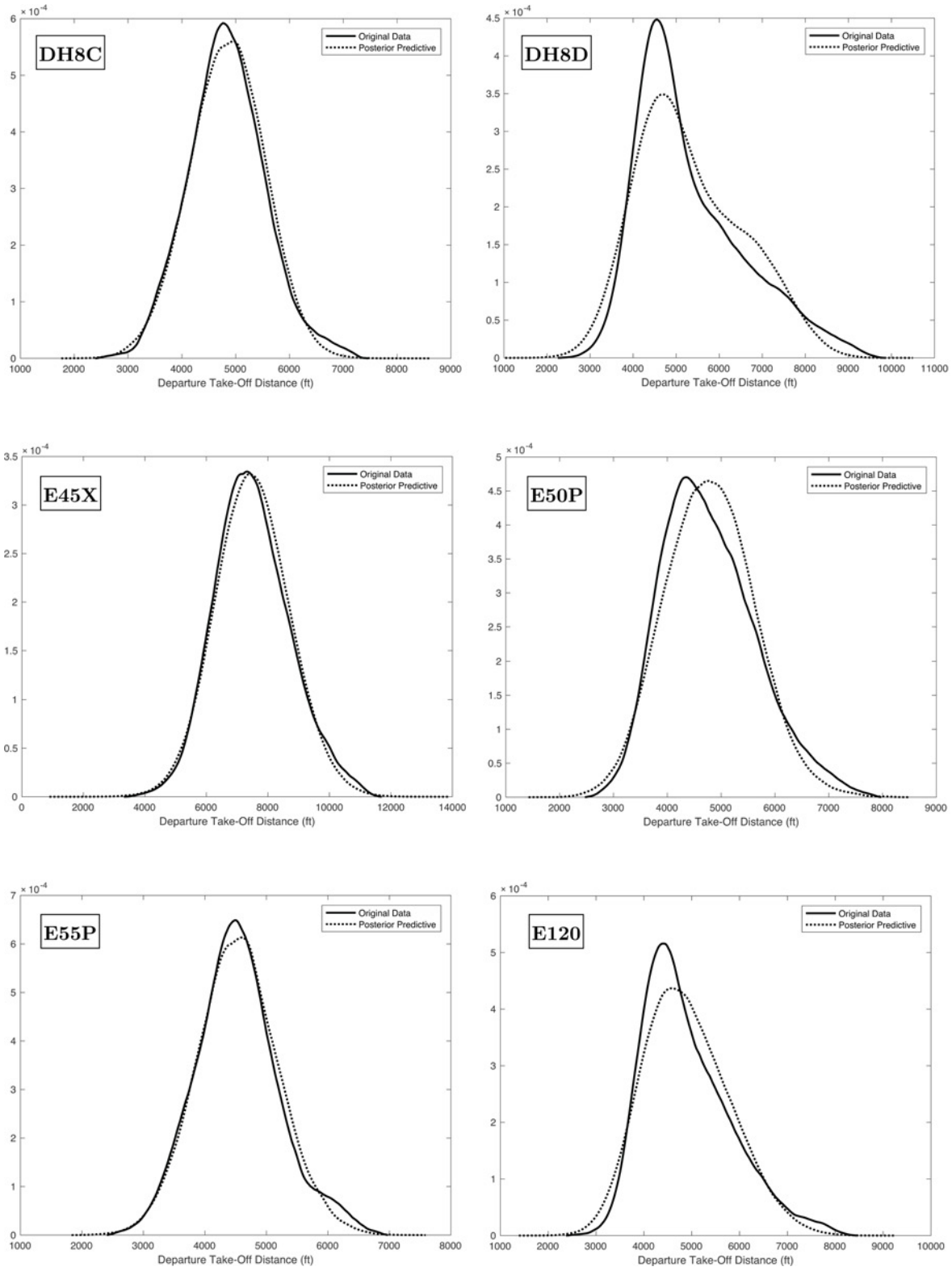

Figure B.25: Comparisons of Observed Data against Posterior Predictive Distributions of Model 5b, DH8C - E120.

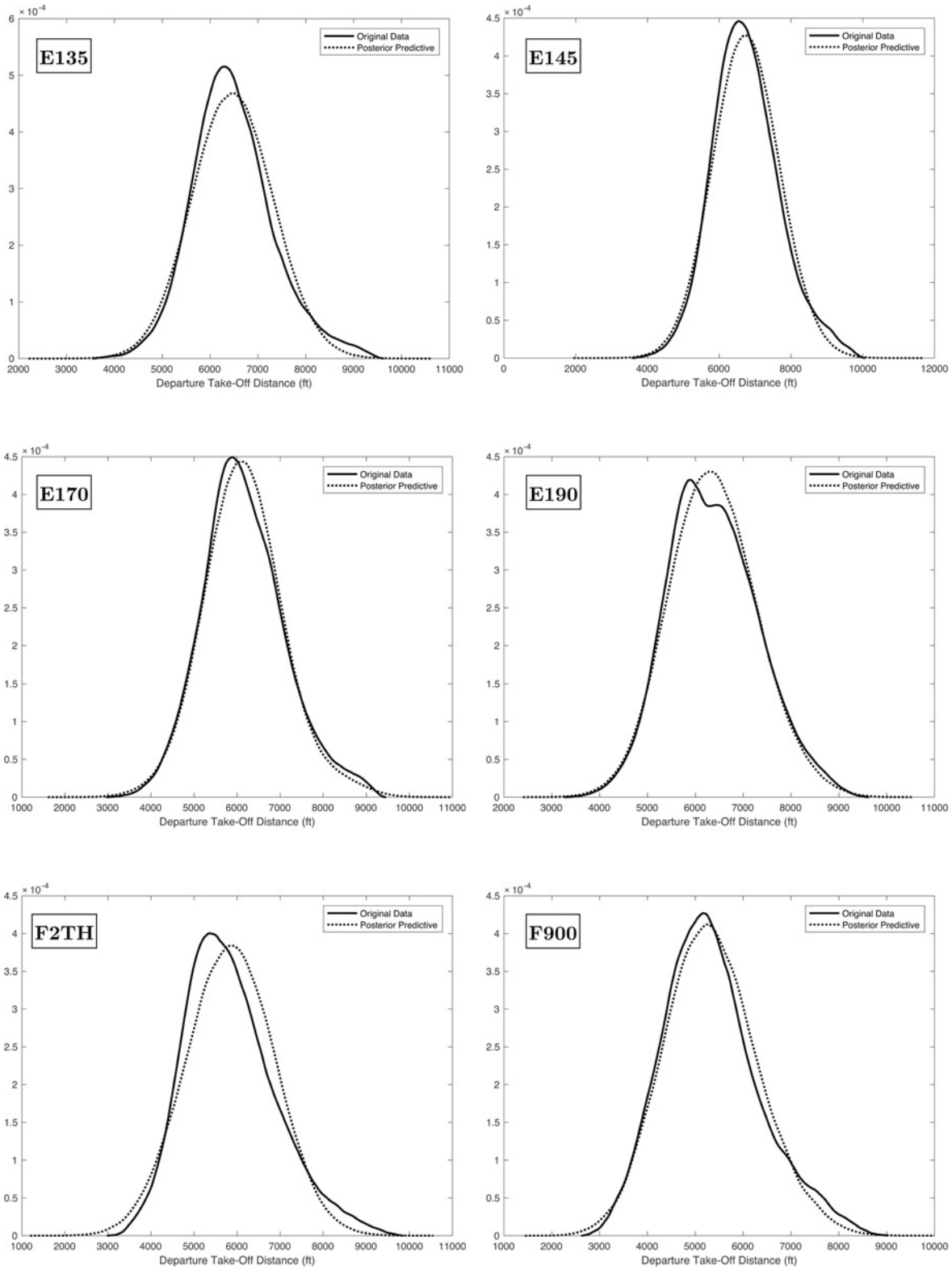

Figure B.26: Comparisons of Observed Data against Posterior Predictive Distributions of Model 5b, E135 - F900.

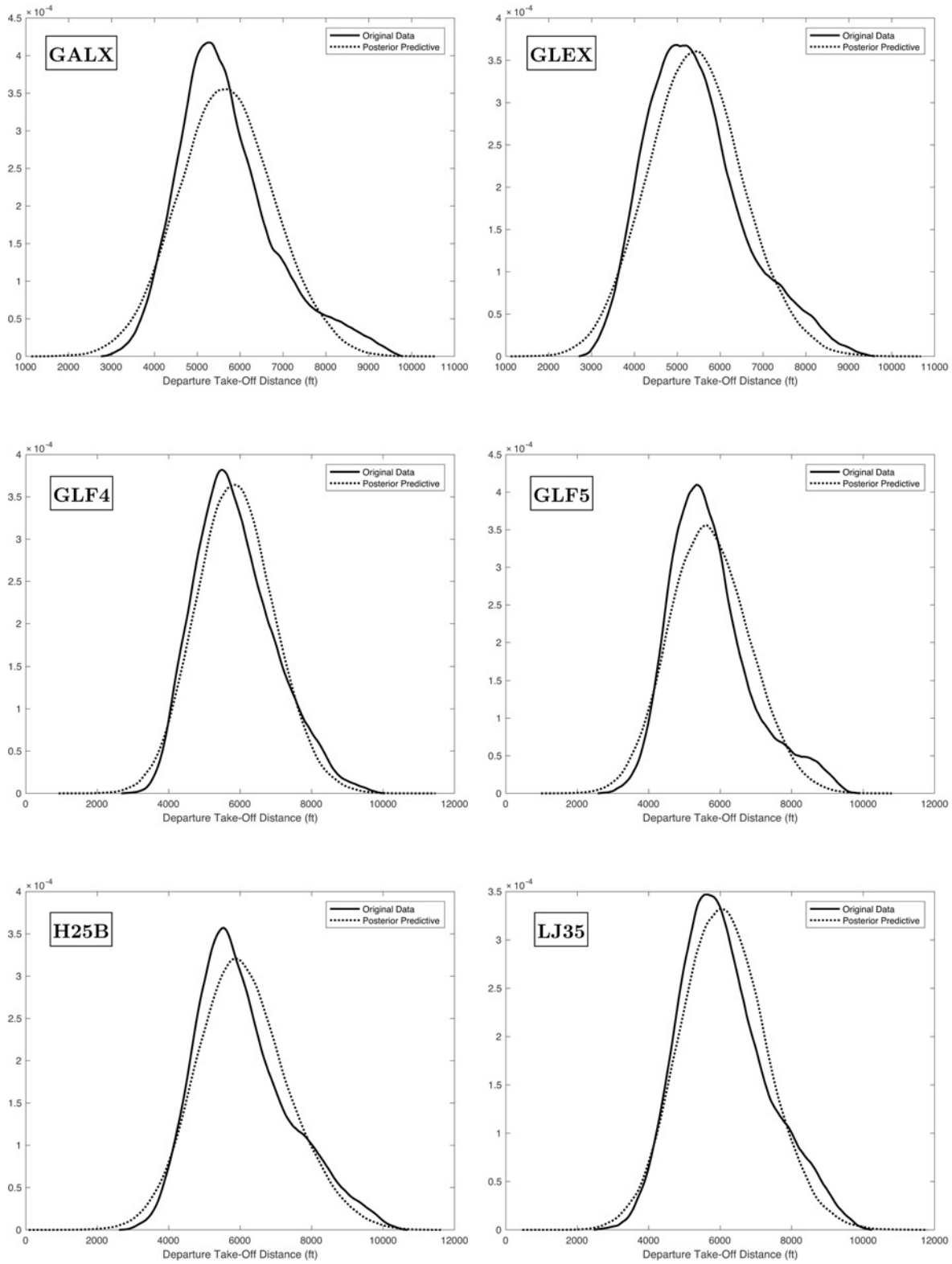

Figure B.27: Comparisons of Observed Data against Posterior Predictive Distributions of Model 5b, GALX - LJ35.

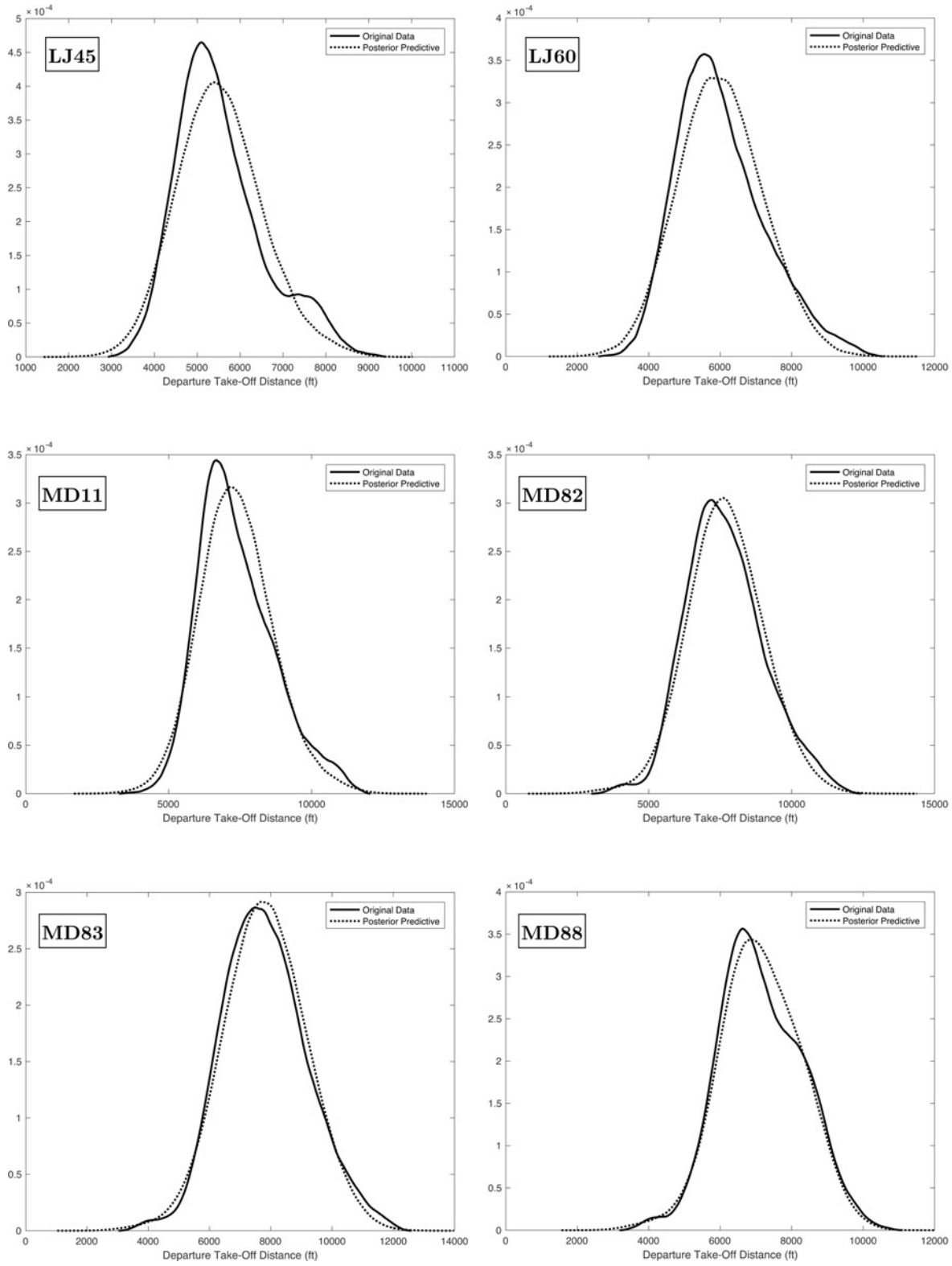

Figure B.28: Comparisons of Observed Data against Posterior Predictive Distributions of Model 5b, LJ45 - MD88.

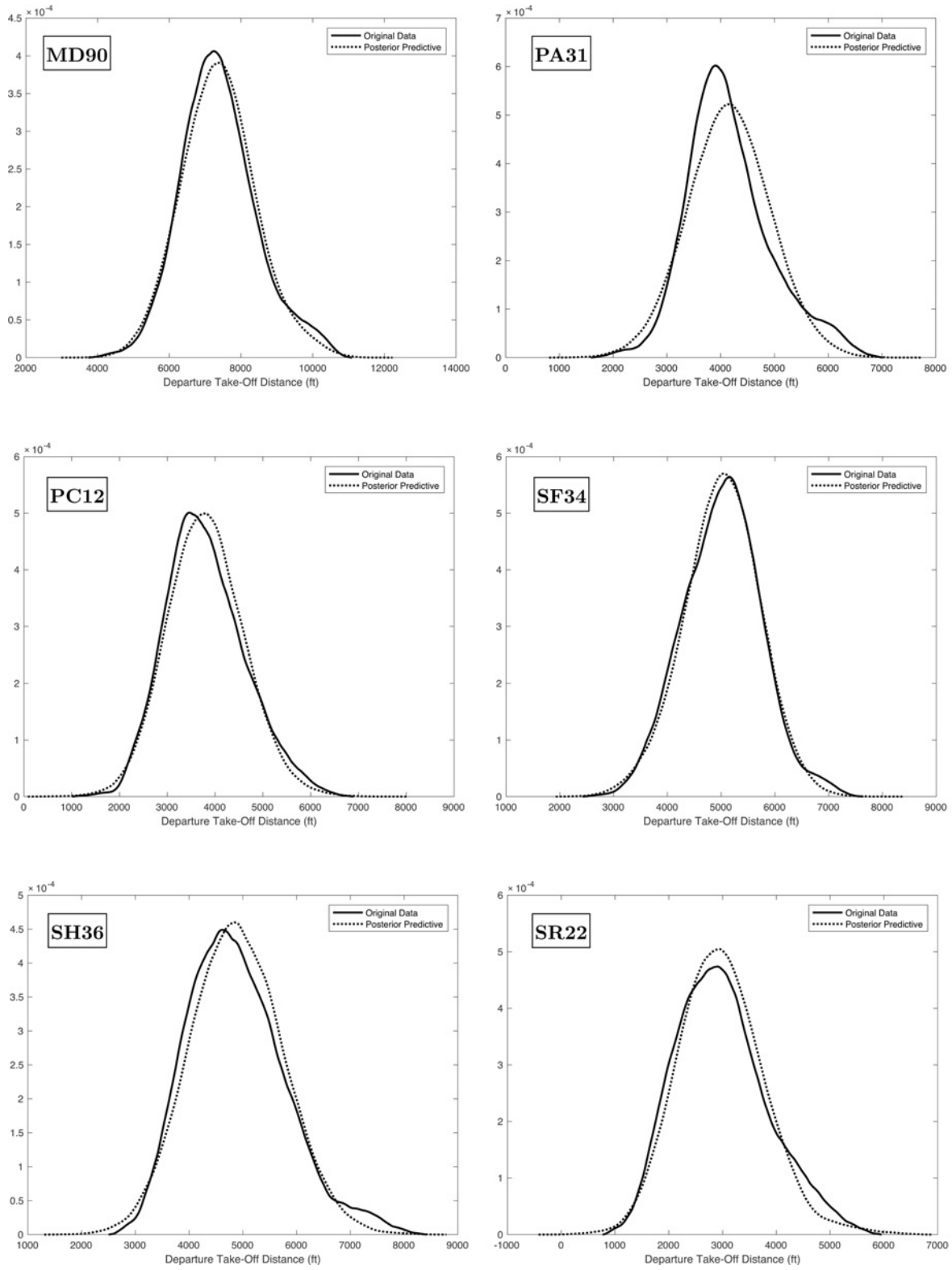

Figure B.29: Comparisons of Observed Data against Posterior Predictive Distributions of Model 5b, MD90 - SR22.

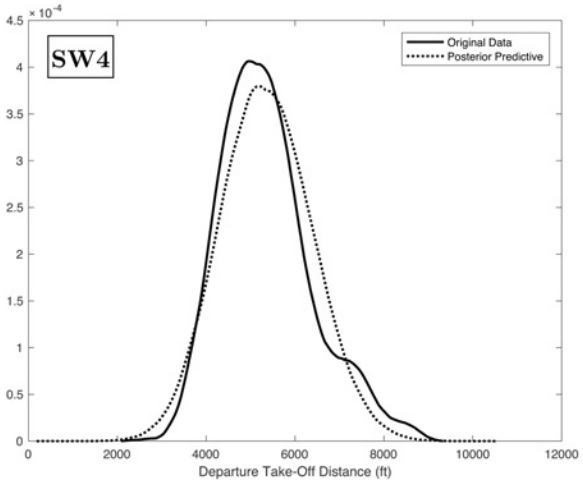

Figure B.30: Comparisons of Observed Data against Posterior Predictive Distributions of Model 5b, SW4.

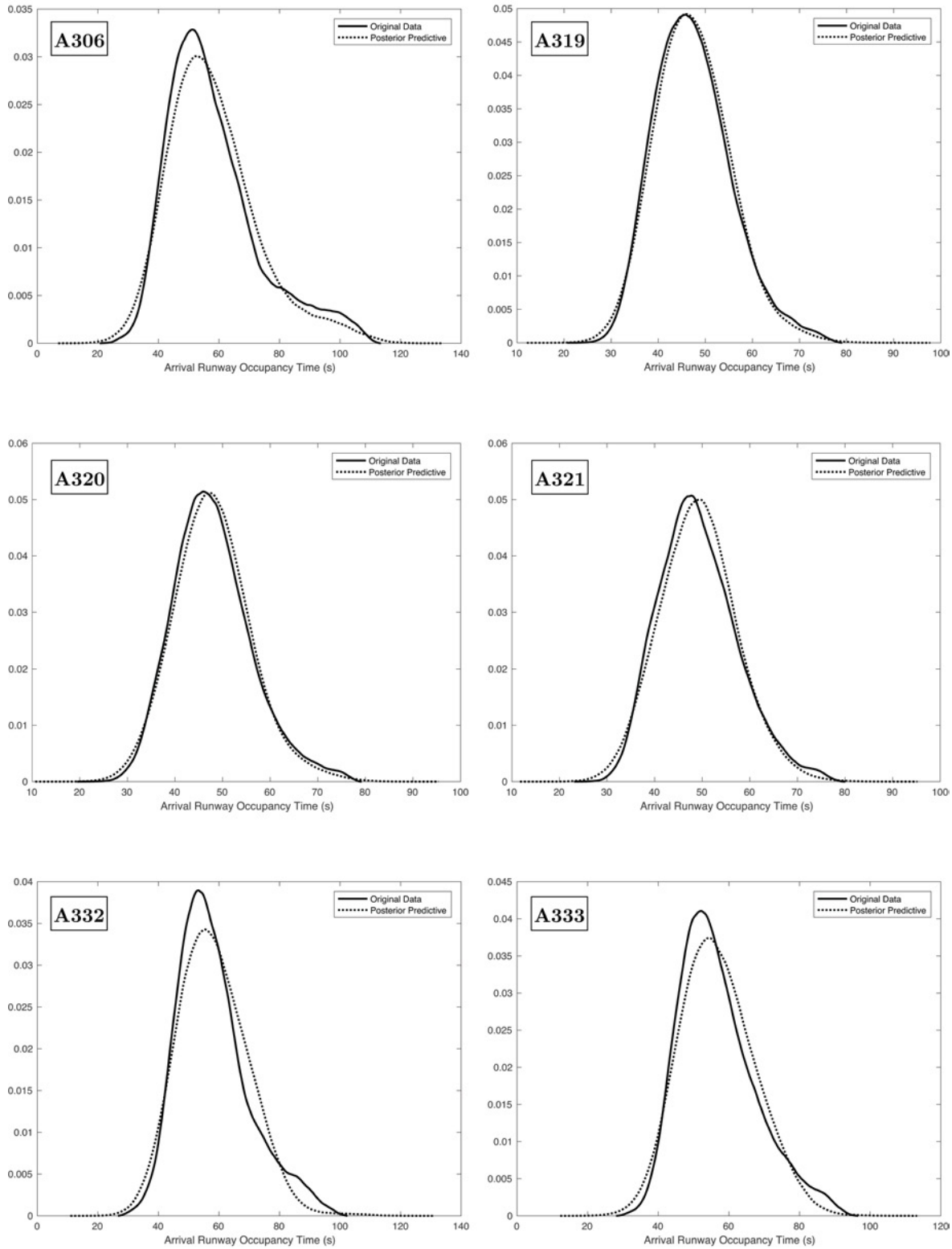

Figure B.31: Comparisons of Observed Data against Posterior Predictive Distributions of Model 5c, A306 - A333.

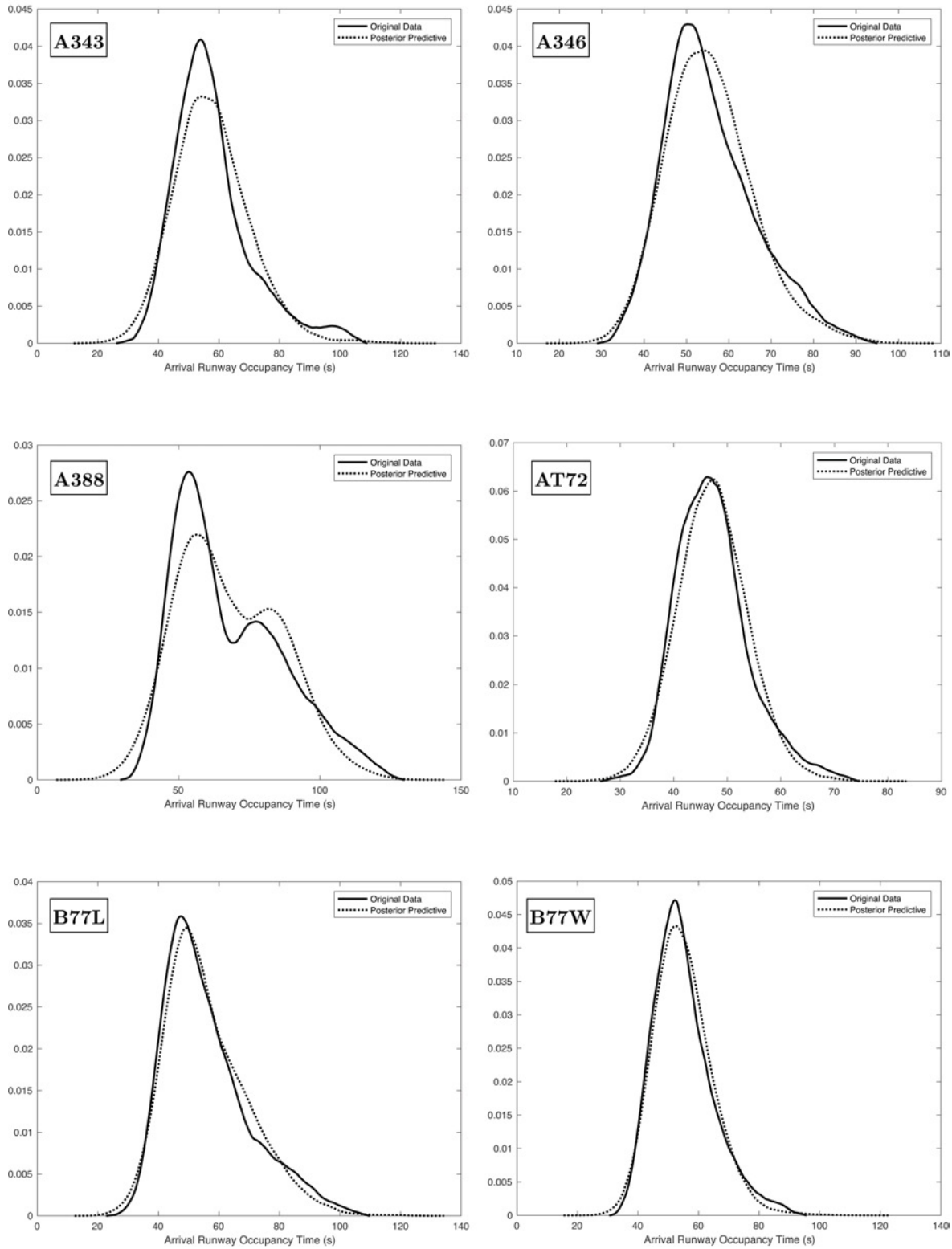

Figure B.32: Comparisons of Observed Data against Posterior Predictive Distributions of Model 5c, A343 - B77W.

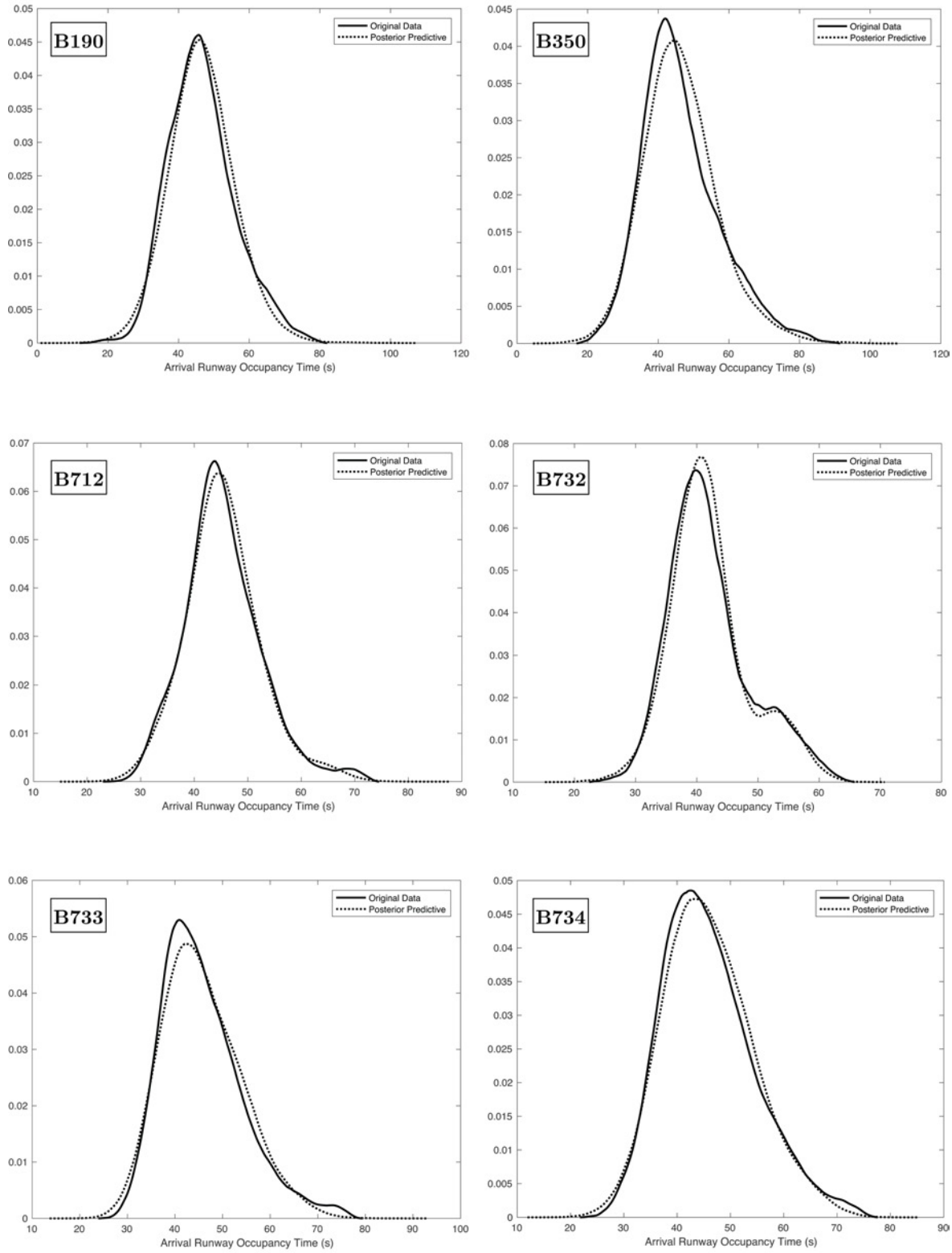

Figure B.33: Comparisons of Observed Data against Posterior Predictive Distributions of Model 5c, B190 - B734.

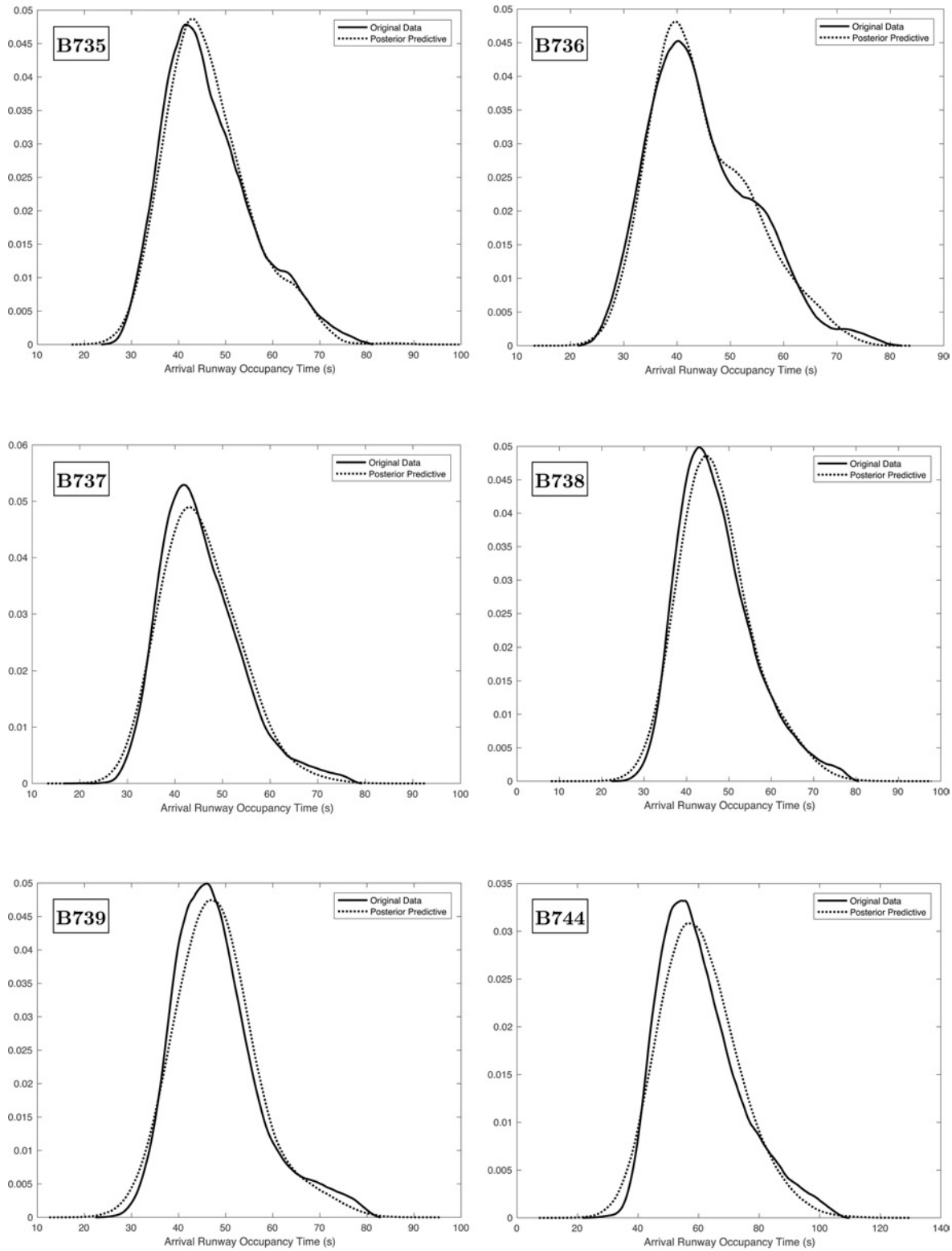

Figure B.34: Comparisons of Observed Data against Posterior Predictive Distributions of Model 5c, B735 - B744.

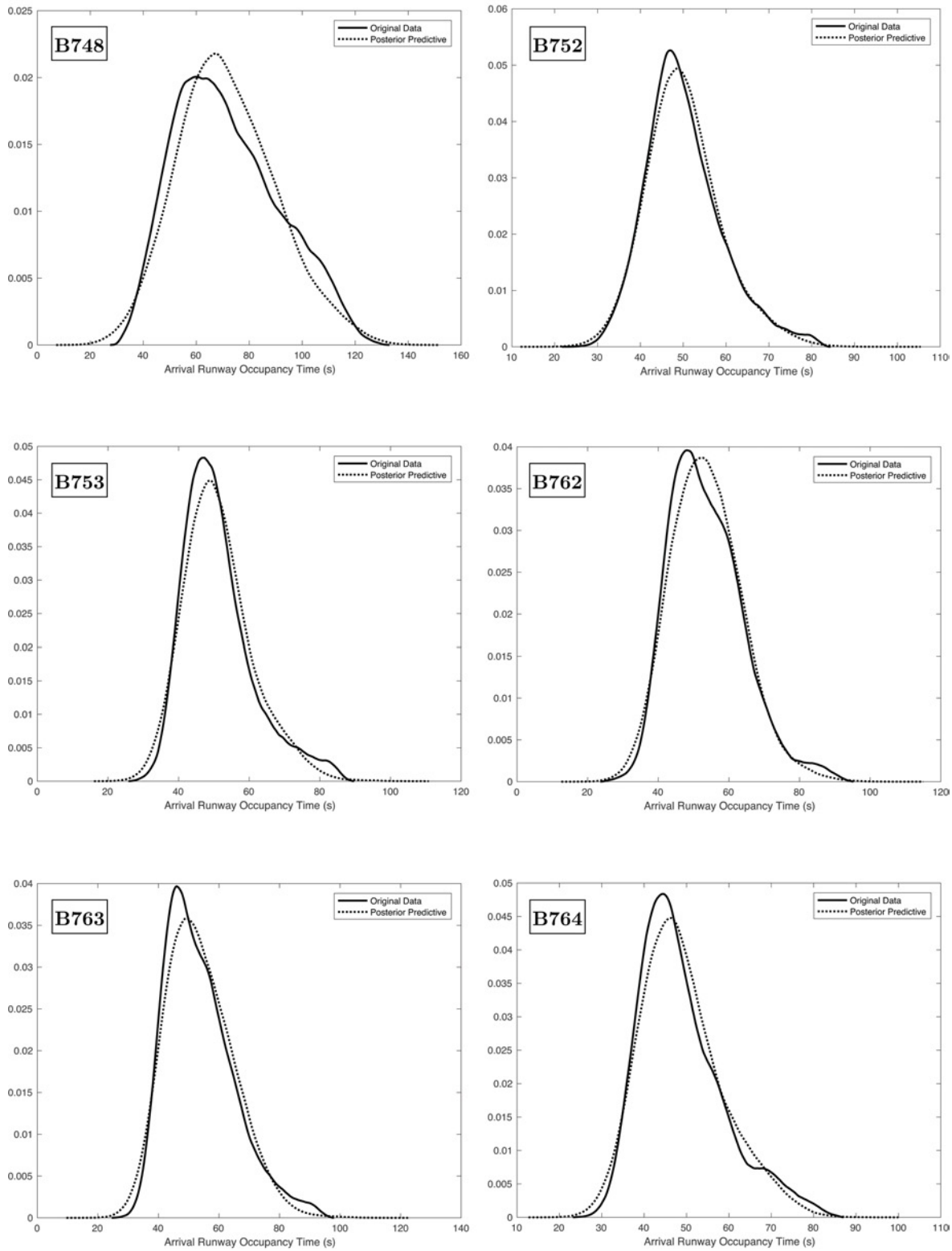

Figure B.35: Comparisons of Observed Data against Posterior Predictive Distributions of Model 5c, B748 - B764.

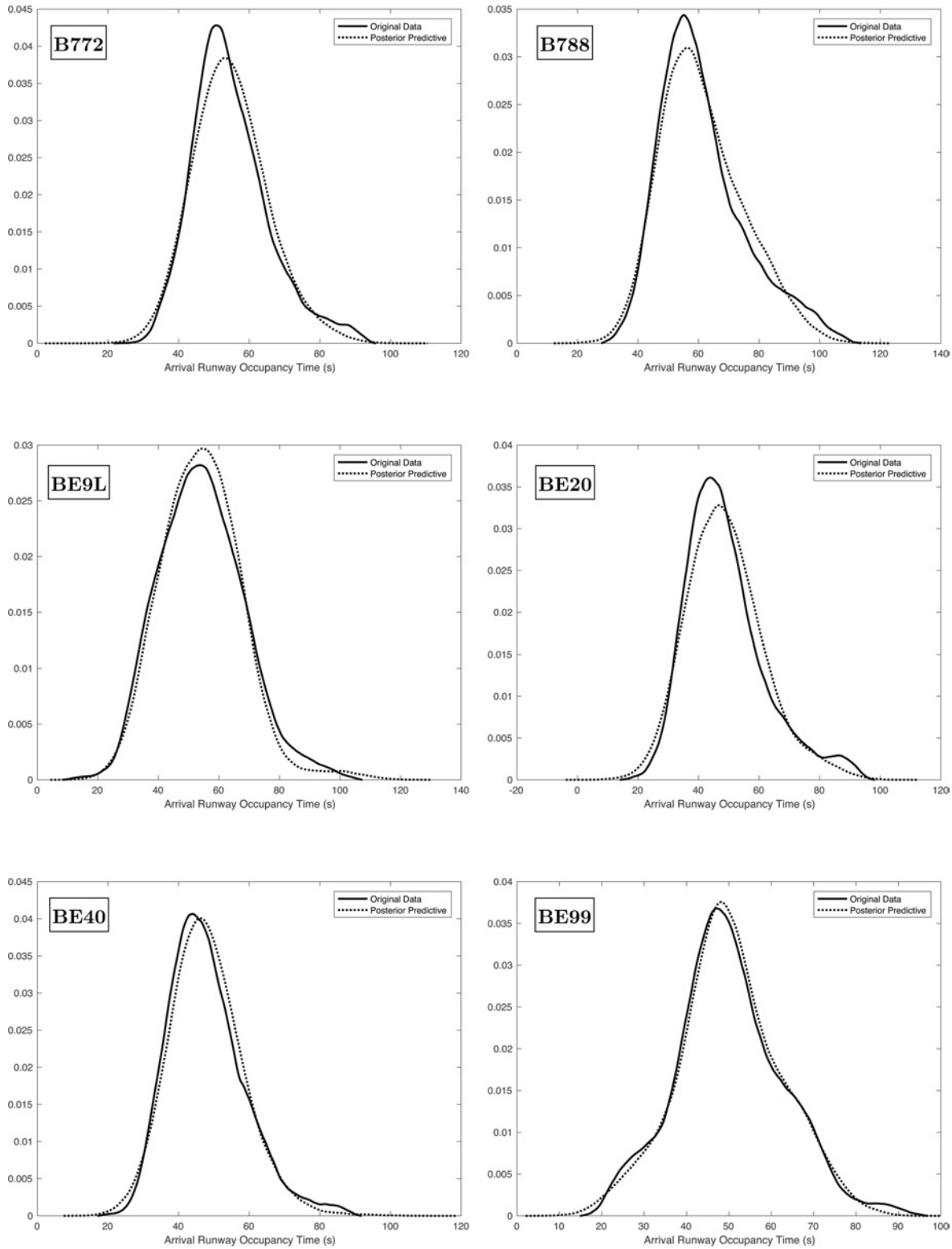

Figure B.36: Comparisons of Observed Data against Posterior Predictive Distributions of Model 5c, B772 - BE99.

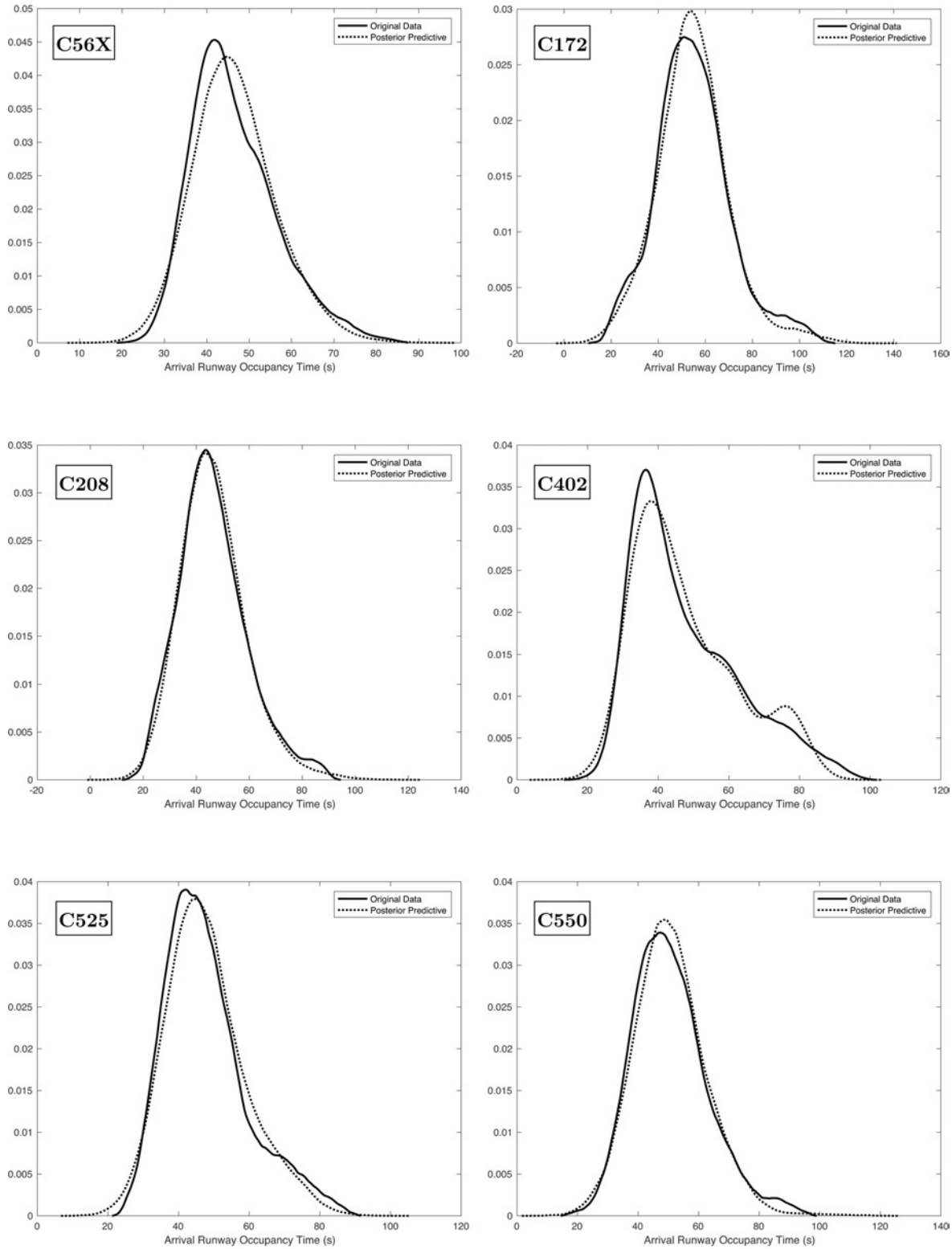

Figure B.37: Comparisons of Observed Data against Posterior Predictive Distributions of Model 5c, C56X - C550.

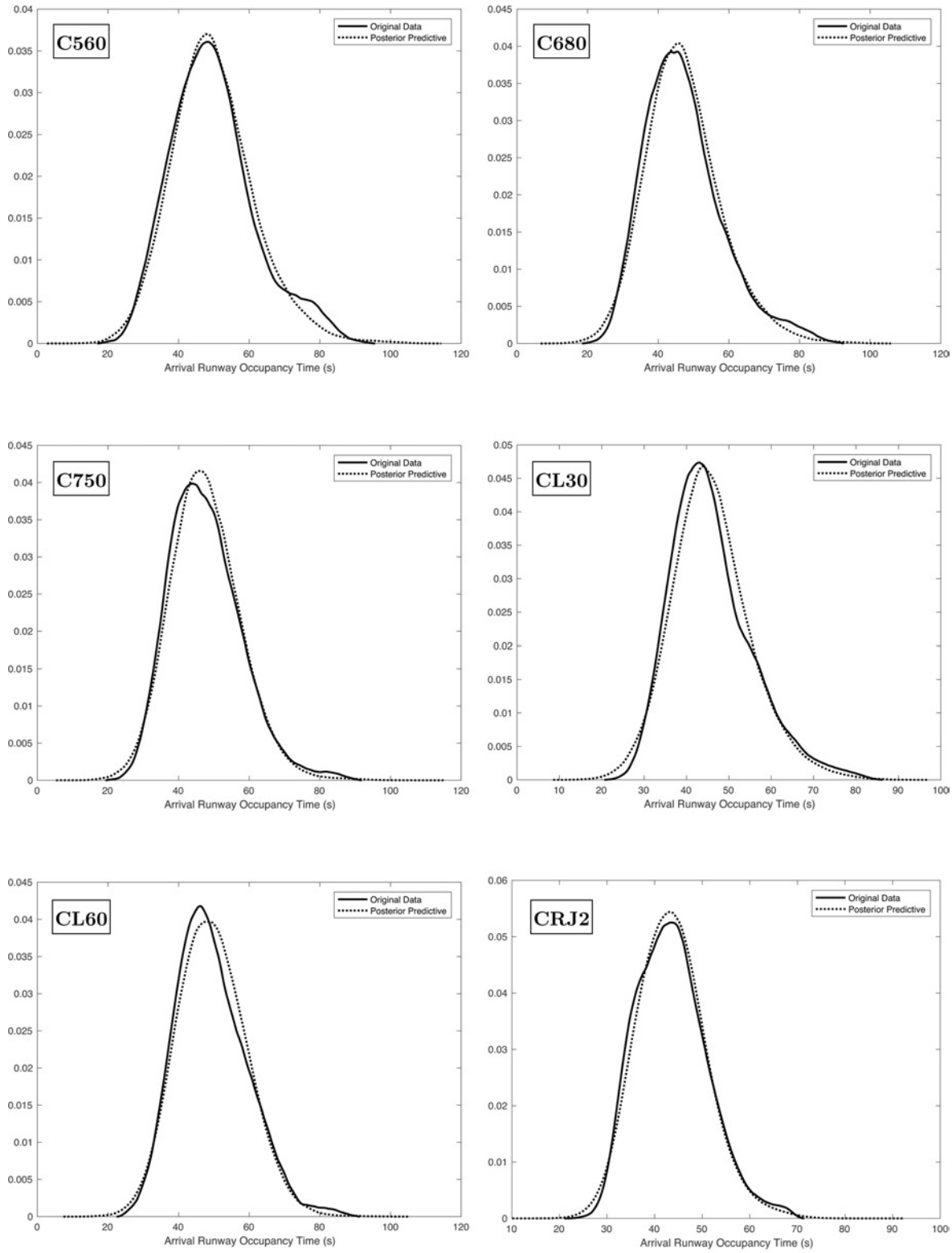

Figure B.38: Comparisons of Observed Data against Posterior Predictive Distributions of Model 5c, C560 - CRJ2.

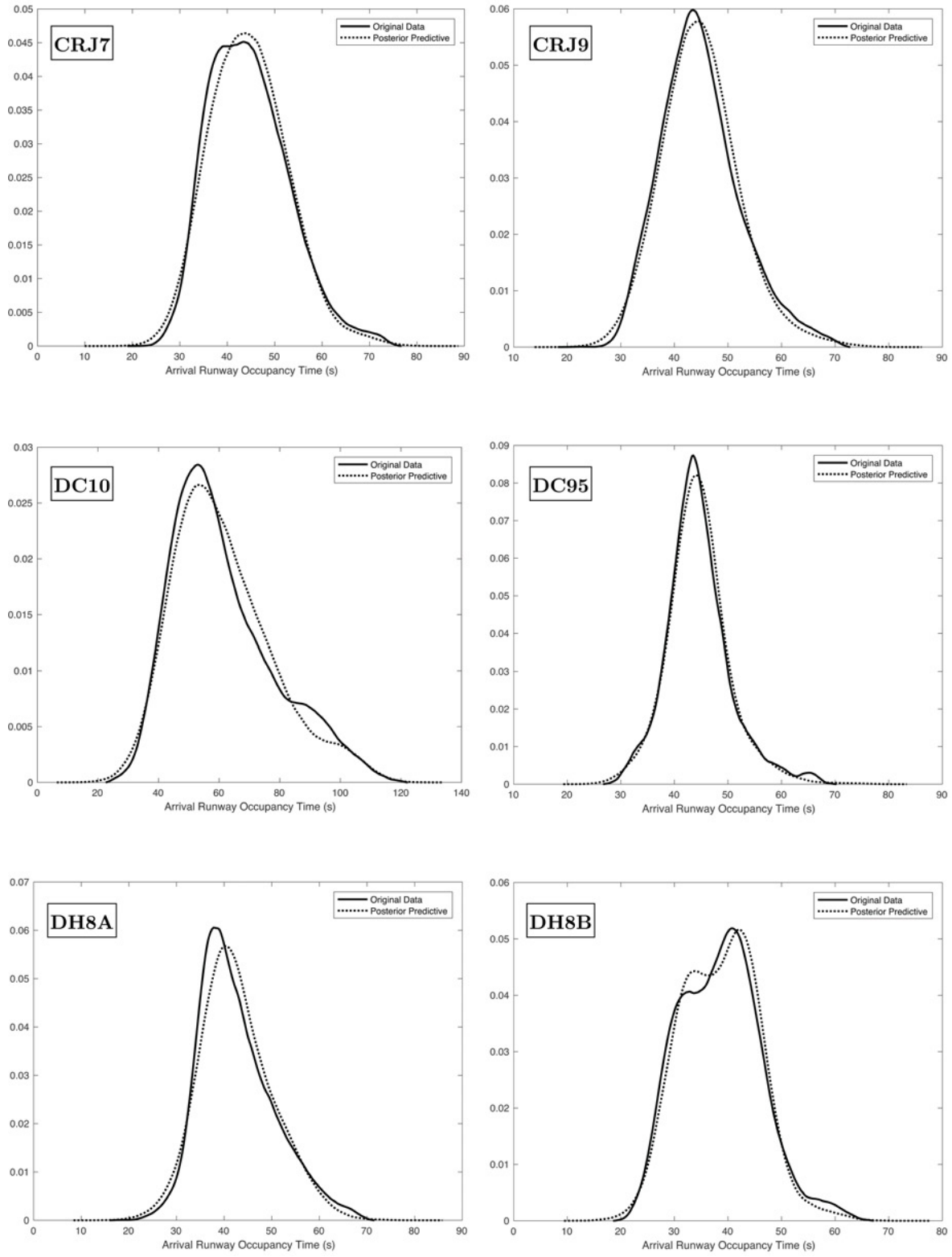

Figure B.39: Comparisons of Observed Data against Posterior Predictive Distributions of Model 5c, CRJ7 - DH8B.

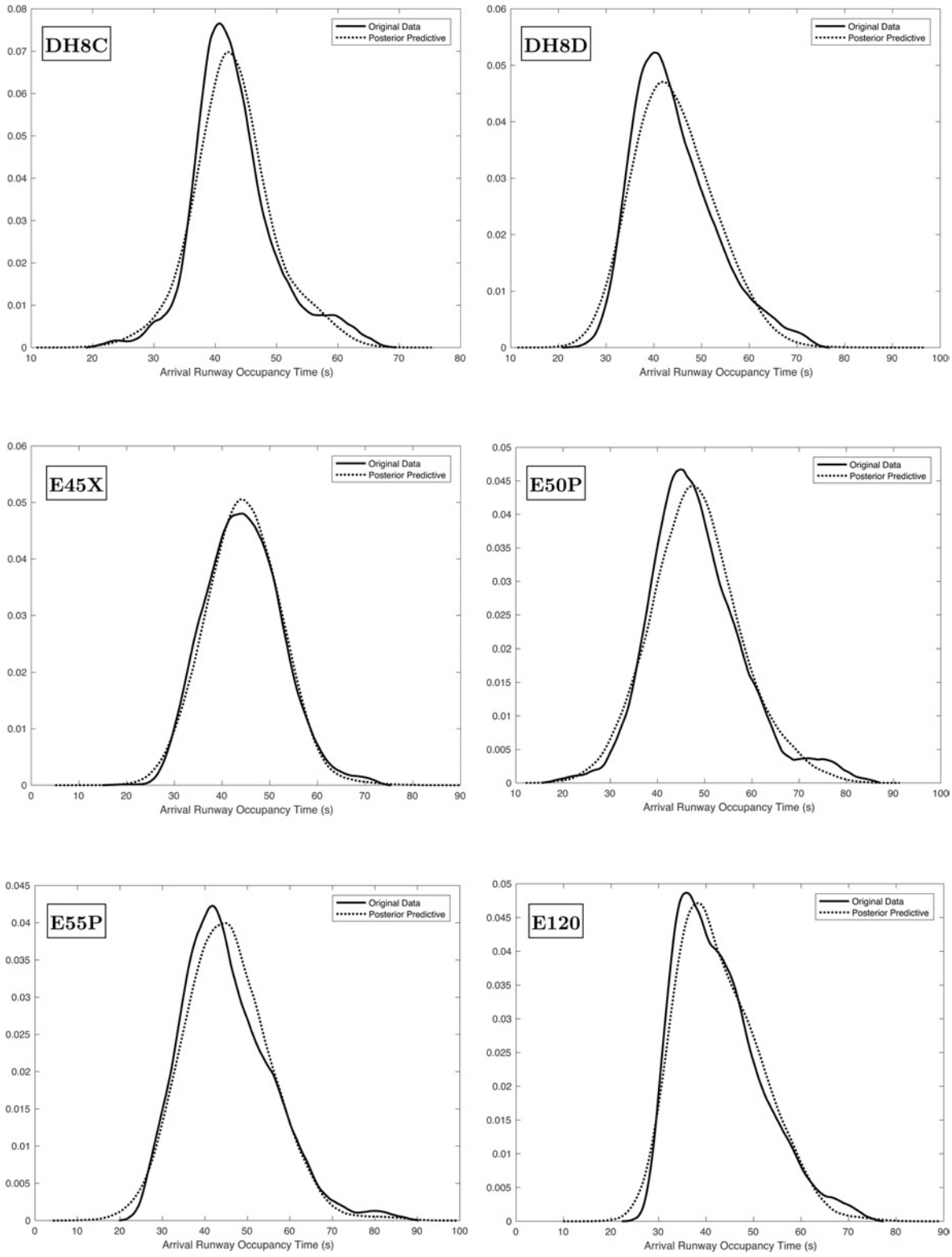

Figure B.40: Comparisons of Observed Data against Posterior Predictive Distributions of Model 5c, DH8C - E120.

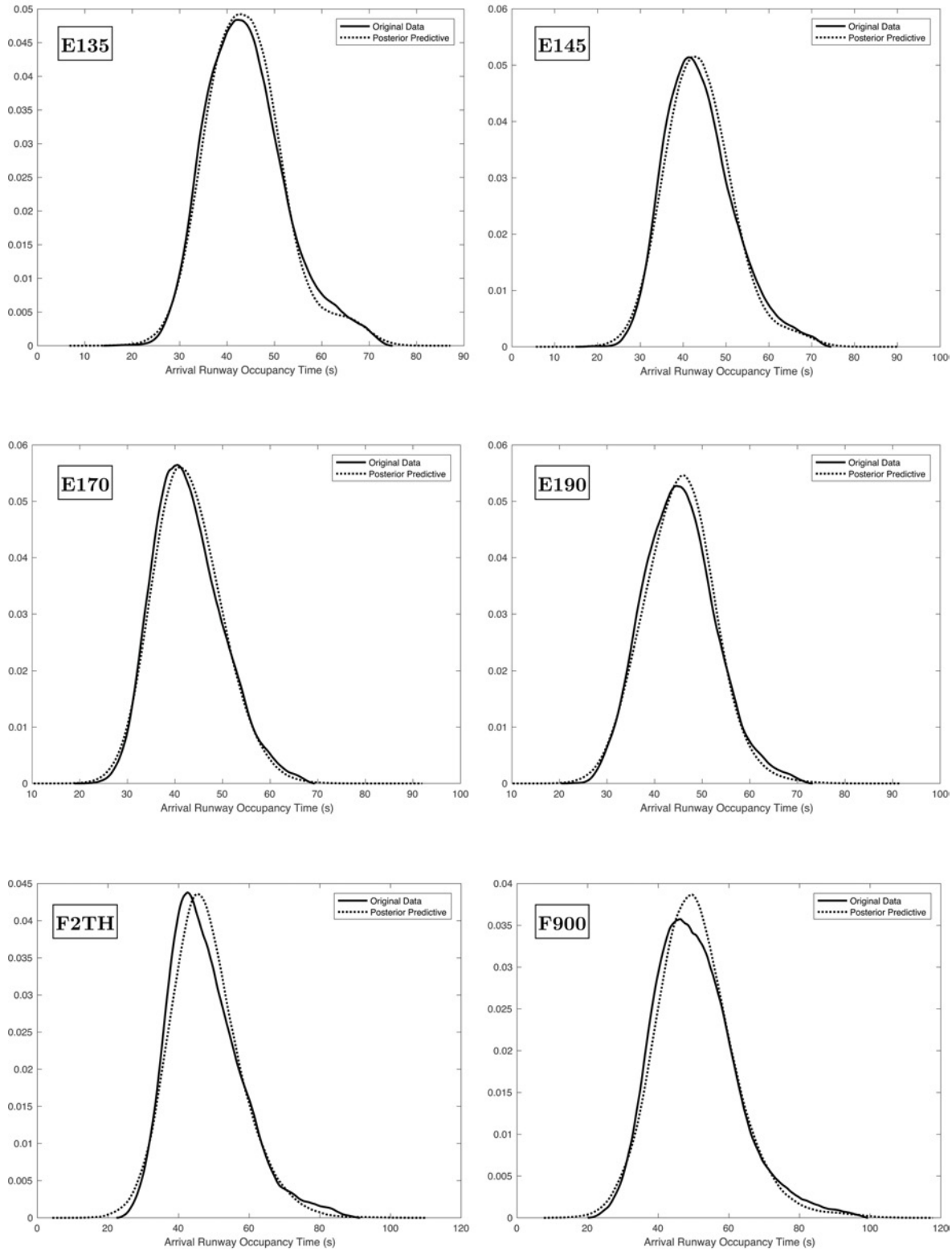

Figure B.41: Comparisons of Observed Data against Posterior Predictive Distributions of Model 5c, E135 - F900.

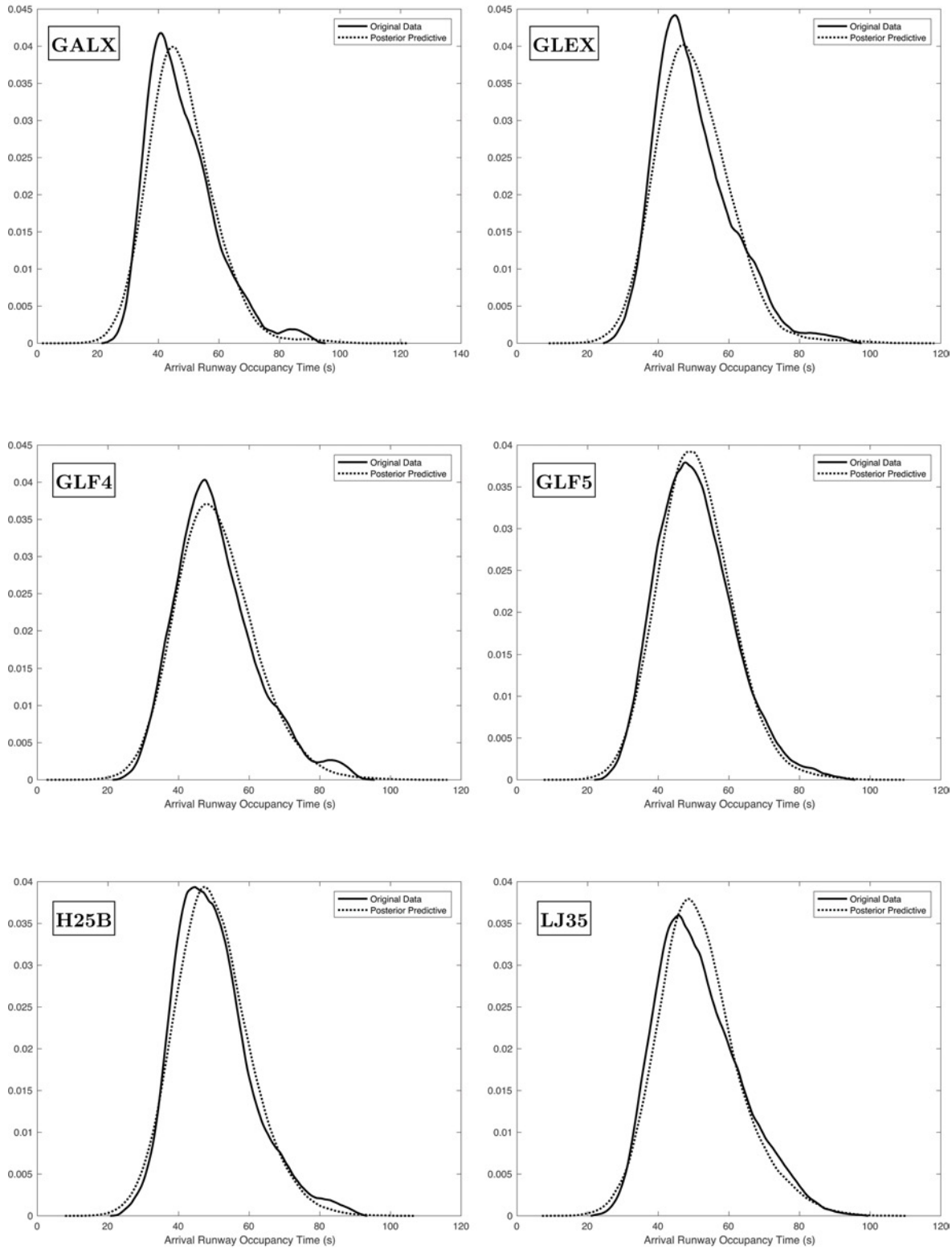

Figure B.42: Comparisons of Observed Data against Posterior Predictive Distributions of Model 5c, GALX - LJ35.

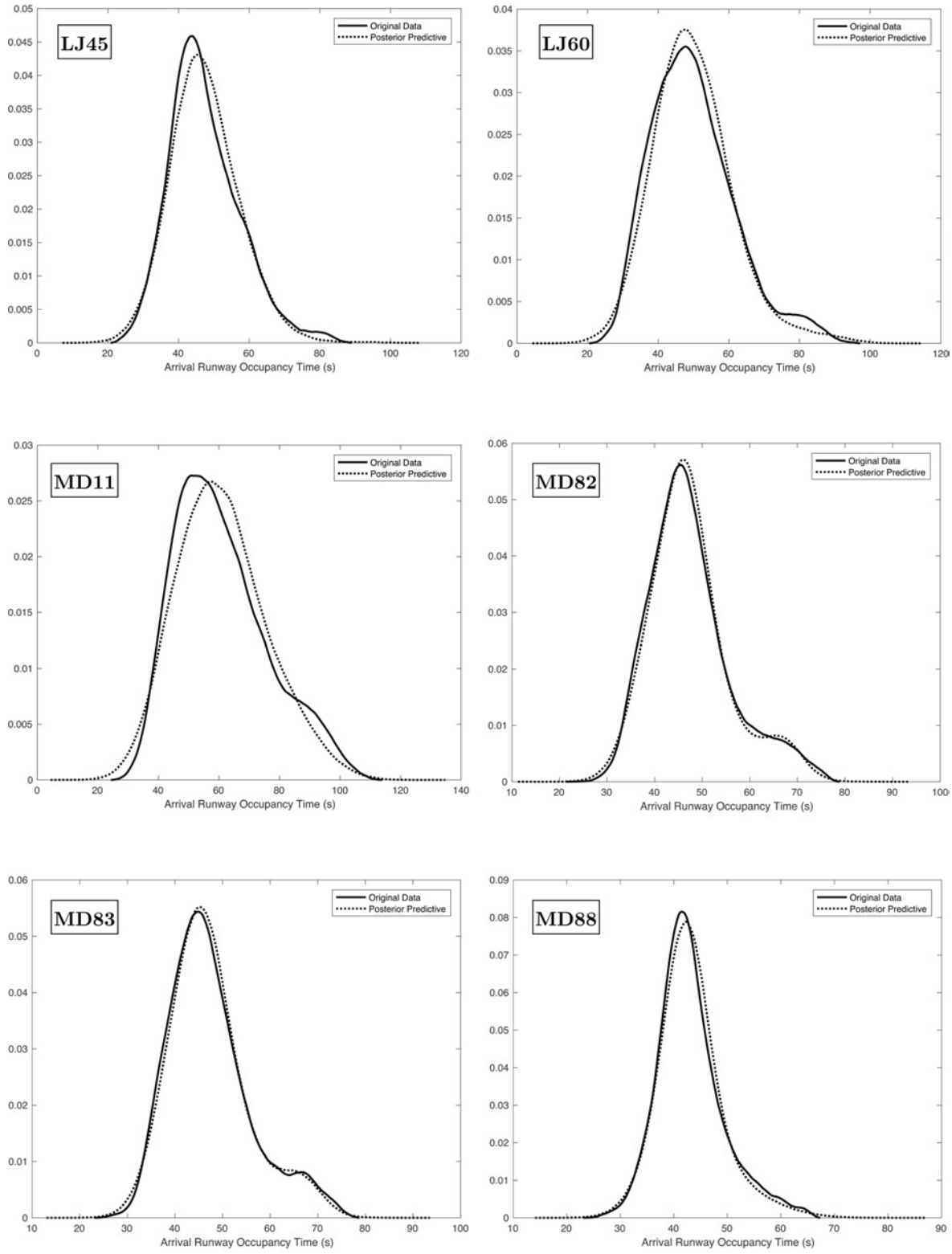

Figure B.43: Comparisons of Observed Data against Posterior Predictive Distributions of Model 5c, LJ45 - MD88.

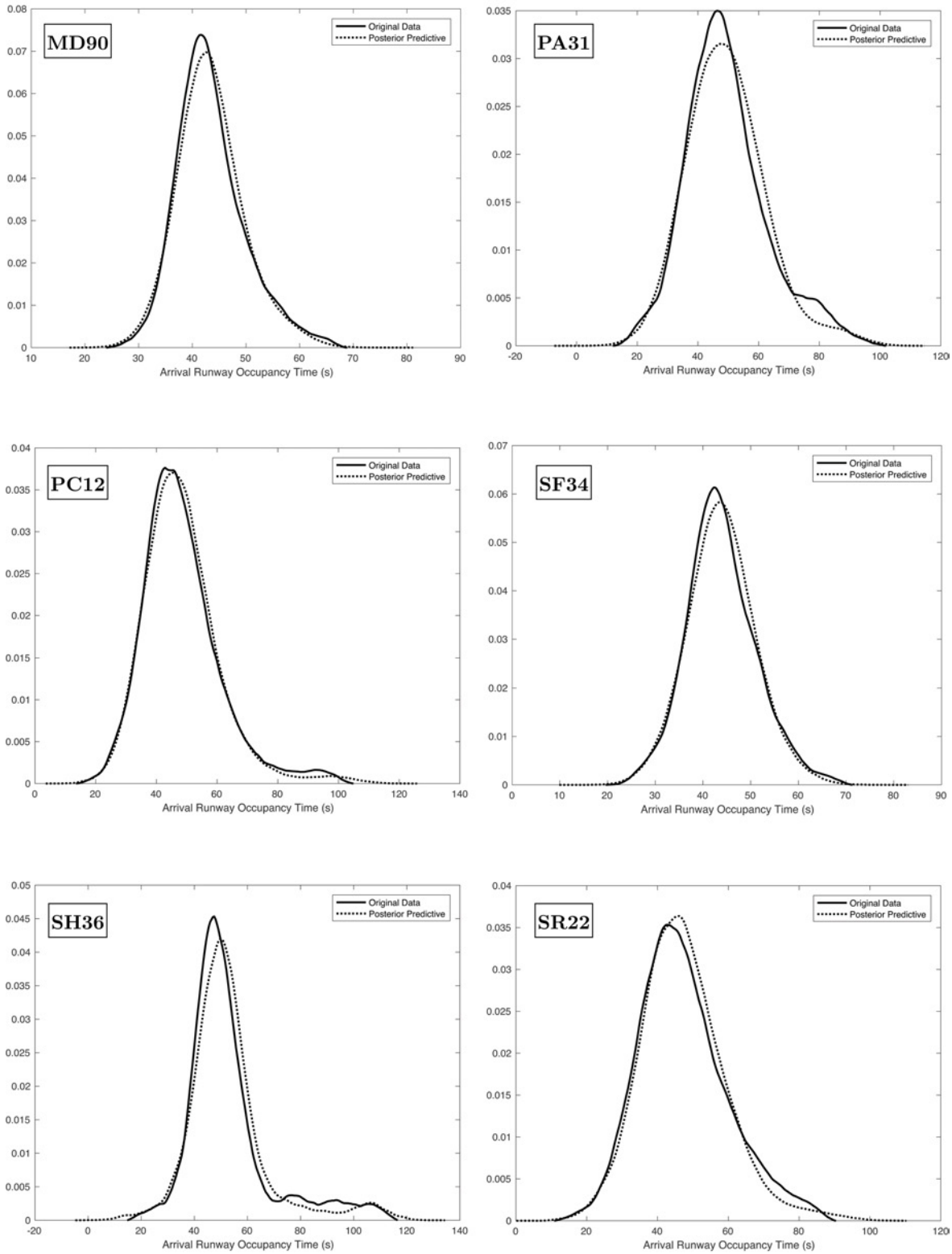

Figure B.44: Comparisons of Observed Data against Posterior Predictive Distributions of Model 5c, MD90 - SR22.

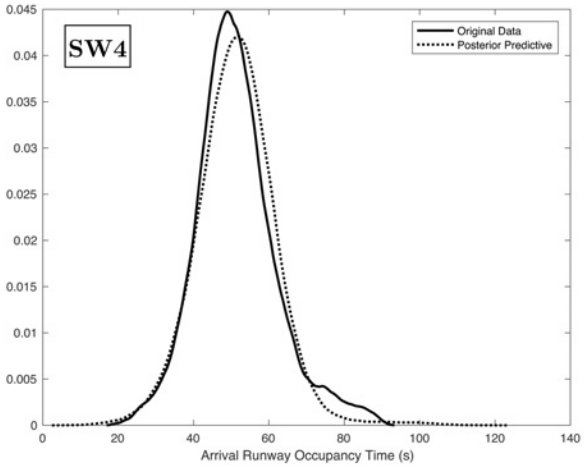

Figure B.45: Comparisons of Observed Data against Posterior Predictive Distributions of Model 5c, SW4.

Appendix C

Full Fuel Burn Results from Simulated Air Canada Domestic Network

Table C.1: Fuel Burn Results from Simulated Air Canada Domestic Network

Depart	Arrive	Aircraft Type	Daily Flights	Cruise Speed (Mach)	Time GC (s)	Fuel Burn GC (kg)	Time Wind (s)	Fuel Burn Wind (kg)	Daily Savings (kg)	Annual Savings (kg)
YYZ	YEG	A319	1	0.78	14230	9134.48	13870	8908.11	226.37	82625.05
YYZ	YHZ	A319	1	0.78	5323	3463.61	5253	3418.44	45.17	16487.05
YYZ	YUL	A319	2	0.78	2074	1356.56	2074	1356.56	0	0
YYZ	YQR	A319	1	0.78	10079	6510.13	10015	6469.42	40.71	14859.15
YYZ	YYT	A319	2	0.78	8359	5413.4	8220	5324.52	177.76	64882.4
YYZ	YWG	A319	2	0.78	7284	4725.07	7268	4714.81	20.52	7489.8
YUL	YYC	A319	1	0.78	14790	9486.17	14592	9361.88	124.29	45365.85
YUL	YEG	A319	2	0.78	15548	9961.33	15233	9763.99	394.68	144058.2
YUL	YHZ	A319	1	0.78	3277	2139.26	3230	2108.74	30.52	11139.8
YVR	YYC	A319	9	0.78	2340	1529.88	2340	1529.88	0	0
YVR	YEG	A319	5	0.78	2729	1783.09	2729	1783.09	0	0
YVR	YWG	A319	2	0.78	7023	4557.61	6860	4452.96	209.3	76394.5
YYT	YYZ	A319	4	0.78	10031	6479.6	9919	6408.35	285	104025
YWG	YYZ	A319	3	0.78	5499	3577.14	5482	3566.17	32.91	12012.15
YWG	YVR	A319	2	0.78	9247	5980.32	9063	5862.97	234.7	85665.5
YYC	YYZ	A319	1	0.78	9932	6416.62	9922	6410.25	6.37	2325.05
YYC	YVR	A319	7	0.78	3269	2134.06	3253	2123.67	72.73	26546.45
YOW	YYC	A319	1	0.78	14207	9120.03	13955	8961.58	158.45	57834.25
YQR	YYZ	A319	2	0.78	7458	4836.63	7456	4835.35	2.56	934.4
YEG	YVR	A319	5	0.78	3820	2491.57	3805	2481.84	48.65	17757.25
YEG	YHZ	A319	1	0.78	14224	9130.71	14133	9073.51	57.2	20878.0
YEG	YUL	A319	1	0.78	10972	7077.36	10956	7067.21	10.15	3704.75
YHZ	YEG	A319	2	0.78	18302	11679.49	18230	11634.73	89.52	32674.8
YHZ	YUL	A319	2	0.78	3486	2274.93	3486	2274.93	0	0
YHZ	YYZ	A319	1	0.78	5820	3784.04	5802	3772.44	11.6	4234.0
YYZ	YYC	A320	4	0.78	13490	9198.15	13081	8927.44	1082.84	395236.6
YYZ	YEG	A320	7	0.78	14230	9686.75	13870	9449.25	1662.5	606812.5
YYZ	YMM	A320	3	0.78	14276	9717.08	14076	9585.2	395.64	144408.6
YYZ	YHZ	A320	6	0.78	5323	3698.63	5253	3650.6	288.18	105185.7

Depart	Arrive	Aircraft Type	Daily Flights	Cruise Speed (Mach)	Time GC (s)	Fuel Burn GC (kg)	Time Wind (s)	Fuel Burn Wind (kg)	Daily Savings (kg)	Annual Savings (kg)
YYZ	YUL	A320	11	0.78	2074	1452.48	2074	1452.48	0	0
YYZ	YOW	A320	9	0.78	1236	867.39	1236	867.39	0	0
YYZ	YXE	A320	3	0.78	11236	7700.29	11198	7674.91	76.14	27791.1
YYZ	YYT	A320	7	0.78	8359	5766.69	8220	5672.64	658.35	240297.75
YYZ	YVR	A320	6	0.78	16553	11210.71	16250	11012.77	1187.64	433488.6
YYZ	YYJ	A320	4	0.78	16436	11134.31	16222	10994.46	559.4	204181.0
YYZ	YWG	A320	12	0.78	7284	5037.74	7268	5026.86	130.56	47654.4
YUL	YYC	A320	12	0.78	14790	10055.49	14592	9925.21	1563.36	570626.4
YUL	YEG	A320	3	0.78	15548	10553.21	15233	10346.57	619.92	226270.8
YUL	YYZ	A320	11	0.78	2190	1533.28	2190	1533.28	0	0
YUL	YVR	A320	10	0.78	18090	12211.02	17769	12002.62	2084.0	760660.0
YVR	YYC	A320	9	0.78	2340	1637.7	2340	1637.7	0	0
YVR	YEG	A320	5	0.78	2729	1908.13	2729	1908.13	0	0
YVR	YUL	A320	4	0.78	14194	9663.02	13896	9466.41	786.44	287050.6
YVR	YOW	A320	3	0.78	13668	9315.82	13322	9087.01	686.43	250546.95
YVR	YYZ	A320	5	0.78	12681	8662.22	12458	8514.17	740.25	270191.25
YYT	YYZ	A320	5	0.78	10031	6893.44	9919	6818.23	376.05	137258.25
YYJ	YOW	A320	1	0.78	13718	9348.86	13427	9156.49	192.37	70215.05
YYJ	YYZ	A320	1	0.78	12811	8748.47	12549	8574.6	173.87	63462.55
YWG	YYZ	A320	7	0.78	5499	3819.31	5482	3807.66	81.55	29765.75
YYC	YUL	A320	5	0.78	11476	7860.48	11384	7799.09	306.95	112036.75
YYC	YYZ	A320	10	0.78	9932	6826.96	9922	6820.25	67.1	24491.5
YYC	YVR	A320	8	0.78	3269	2282.7	3253	2271.62	88.64	32353.6
YOW	YYZ	A320	13	0.78	1374	963.91	1374	963.91	0	0
YOW	YVR	A320	4	0.78	17328	11715.88	17089	11560.26	622.48	227205.2
YOW	YYJ	A320	1	0.78	17381	11750.37	17061	11542.02	208.35	76047.75
YXE	YYZ	A320	2	0.78	7981	5510.78	7959	5495.87	29.82	10884.3
YEG	YYZ	A320	7	0.78	9684	6660.3	9644	6633.4	188.3	68729.5
YEG	YVR	A320	7	0.78	3820	2663.9	3805	2653.53	72.59	26495.35
YEG	YOW	A320	1	0.78	10409	7147.01	10401	7141.65	5.36	1956.4
YEG	YUL	A320	3	0.78	10972	7523.89	10956	7513.19	32.1	11716.5
YMM	YYZ	A320	2	0.78	9231	6355.39	9201	6335.17	40.44	14760.6
YHZ	YYZ	A320	6	0.78	5820	4039.17	5802	4026.85	73.92	26980.8
YYZ	YYC	A321	13	0.78	13490	10899.68	13081	10580.39	4150.77	1515031.05
YYZ	YEG	A321	4	0.78	14230	11475.72	13870	11195.75	1119.88	408756.2
YYZ	YHZ	A321	1	0.78	5323	4395.92	5253	4338.96	56.96	20790.4
YYZ	YUL	A321	4	0.78	2074	1728.51	2074	1728.51	0	0
YYZ	YOW	A321	1	0.78	1236	1032.58	1236	1032.58	0	0
YYZ	YVR	A321	6	0.78	16553	13270.66	16250	13037.67	1397.94	510248.1
YYZ	YWG	A321	1	0.78	7284	5983.03	7268	5970.15	12.88	4701.2
YUL	YEG	A321	1	0.78	15548	12496.58	15233	12253.18	243.4	88841.0
YUL	YYZ	A321	3	0.78	2190	1824.58	2190	1824.58	0	0
YUL	YVR	A321	1	0.78	18090	14447.41	17769	14202.35	245.06	89446.9
YVR	YYC	A321	2	0.78	2340	1948.72	2340	1948.72	0	0
YVR	YYZ	A321	5	0.78	12681	10267.51	12458	10092.8	873.55	318845.75
YWG	YYZ	A321	1	0.78	5499	4539.05	5482	4525.23	13.82	5044.3
YYC	YYZ	A321	11	0.78	9932	8100.08	9922	8092.14	87.34	31879.1
YYC	YVR	A321	2	0.78	3269	2715.22	3253	2702.05	26.34	9614.1
YOW	YYZ	A321	1	0.78	1374	1147.42	1374	1147.42	0	0
YOW	YVR	A321	1	0.78	17328	13865.07	17089	13681.99	183.08	66824.2
YEG	YYZ	A321	6	0.78	9684	7903.05	9644	7871.24	190.86	69663.9
YEG	YUL	A321	1	0.78	10972	8923.62	10956	8910.98	12.64	4613.6
YHZ	YYZ	A321	2	0.78	5820	4799.76	5802	4785.15	29.22	10665.3
YYZ	YUL	A333	3	0.82	1975	3408.45	1975	3408.45	0	0
YUL	YYZ	A333	2	0.82	2080	3588.97	2080	3588.97	0	0

Depart	Arrive	Aircraft Type	Daily Flights	Cruise Speed (Mach)	Time GC (s)	Fuel Burn GC (kg)	Time Wind (s)	Fuel Burn Wind (kg)	Daily Savings (kg)	Annual Savings (kg)
YUL	YVR	A333	2	0.82	17091	28740.9	16816	28291.06	899.68	328383.2
YVR	YUL	A333	2	0.82	13572	22955.41	13306	22515.47	879.88	321156.2
YYZ	YYC	B763	3	0.8	13090	19253.61	12711	18714.21	1618.2	590643.0
YYZ	YEG	B763	2	0.8	13790	20247.24	13466	19787.76	918.96	335420.4
YYZ	YHZ	B763	2	0.8	5195	7800.84	5131	7706.07	189.54	69182.1
YYZ	YUL	B763	4	0.8	2023	3064.18	2023	3064.18	0	0
YYZ	YOW	B763	2	0.8	1207	1832.35	1207	1832.35	0	0
YYZ	YVR	B763	3	0.8	16078	23471.56	15798	23078.87	1178.07	429995.55
YUL	YYZ	B763	4	0.8	2134	3231.31	2134	3231.31	0	0
YUL	YVR	B763	2	0.8	17576	25563.59	17280	25151.38	824.42	300913.3
YVR	YUL	B763	2	0.8	13876	20369.08	13595	19970.79	796.58	290751.7
YVR	YOW	B763	1	0.8	13361	19638.69	13033	19172.55	466.14	170141.1
YVR	YYZ	B763	3	0.8	12398	18267.97	12190	17971.05	890.76	325127.4
YYC	YYZ	B763	1	0.8	9716	14415.64	9708	14404.07	11.57	4223.05
YOW	YYZ	B763	2	0.8	1338	2030.48	1338	2030.48	0	0
YEG	YYZ	B763	2	0.8	9479	14072.71	9441	14017.68	110.06	40171.9
YHZ	YYZ	B763	2	0.8	5668	8500.26	5652	8476.63	47.26	17249.9
YYZ	YVR	B77L	1	0.84	15206	38334.61	14965	37749.62	584.99	213521.35
YVR	YYZ	B77L	1	0.84	11870	30176.09	11686	29722.22	453.87	165662.55
YYZ	YVR	B77W	3	0.84	15206	39480.51	14965	38879.84	1802.01	657733.65
YUL	YYZ	B77W	1	0.84	2029	5466.3	2029	5466.3	0	0
YVR	YYZ	B77W	3	0.84	11870	31098.36	11686	30631.73	1399.89	510959.85
YYZ	YYC	B788	2	0.84	12357	20383.09	12032	19857.85	1050.48	383425.2
YVR	YYZ	B788	3	0.84	11870	19595.82	11686	19298.05	893.31	326058.15
YYC	YYZ	B788	1	0.84	9312	15439.87	9305	15428.44	11.43	4171.95
YYZ	YVR	B789	3	0.84	15206	25836.56	14965	25437.67	1196.67	436784.55
YVR	YYZ	B789	4	0.84	11870	20286.15	11686	19978.18	1231.88	449636.2
YUL	YFC	CRJ2	2	0.77	2171	675.22	2152	669.34	11.76	4292.4
YUL	YHZ	CRJ2	1	0.77	3318	1029.36	3270	1014.58	14.78	5394.7
YUL	YQM	CRJ2	1	0.77	2799	869.33	2767	859.46	9.87	3602.55
YUL	YOW	CRJ2	3	0.77	539	168.25	539	168.25	0	0
YUL	YSJ	CRJ2	1	0.77	2441	758.74	2441	758.74	0	0
YUL	YHM	CRJ2	2	0.77	2219	690.07	2219	690.07	0	0
YHM	YUL	CRJ2	2	0.77	2100	653.24	2100	653.24	0	0
YOW	YYG	CRJ2	1	0.77	3951	1224.06	3886	1204.09	19.97	7289.05
YOW	YUL	CRJ2	3	0.77	490	152.97	490	152.97	0	0
YSJ	YUL	CRJ2	2	0.77	2636	819	2636	819	0	0
YDF	YHZ	CRJ2	4	0.77	4101	1270.12	4071	1260.91	36.84	13446.6
YYG	YUL	CRJ2	1	0.77	3548	1100.16	3548	1100.16	0	0
YYG	YOW	CRJ2	1	0.77	4240	1312.77	4240	1312.77	0	0
YFC	YUL	CRJ2	2	0.77	2282	709.57	2282	709.57	0	0
YQX	YHZ	CRJ2	2	0.77	4971	1536.69	4953	1531.18	11.02	4022.3
YHZ	YDF	CRJ2	4	0.77	2090	650.14	2090	650.14	0	0
YHZ	YQX	CRJ2	2	0.77	2599	807.57	2599	807.57	0	0
YHZ	YUL	CRJ2	1	0.77	3533	1095.55	3533	1095.55	0	0
YQM	YUL	CRJ2	2	0.77	2994	929.5	2994	929.5	0	0
YQM	YOW	CRJ2	1	0.77	3701	1147.23	3701	1147.23	0	0
YUL	YHZ	CRJ9	1	0.8	3197	1543.99	3153	1522.98	21.01	7668.65
YUL	YOW	CRJ9	1	0.8	517	252.19	517	252.19	0	0
YUL	YWG	CRJ9	6	0.8	8431	3996.41	8410	3986.74	58.02	21177.3
YVR	YYC	CRJ9	4	0.8	2290	1109.66	2290	1109.66	0	0
YVR	YEG	CRJ9	1	0.8	2670	1291.98	2670	1291.98	0	0
YVR	YXE	CRJ9	3	0.8	4205	2023.34	4205	2023.34	0	0
YVR	YXY	CRJ9	4	0.8	5801	2775.3	5779	2764.99	41.24	15052.6
YVR	YWG	CRJ9	5	0.8	6868	3273.36	6714	3201.7	358.3	130779.5

Depart	Arrive	Aircraft Type	Daily Flights	Cruise Speed (Mach)	Time GC (s)	Fuel Burn GC (kg)	Time Wind (s)	Fuel Burn Wind (kg)	Daily Savings (kg)	Annual Savings (kg)
YQY	YYZ	CRJ9	3	0.8	6746	3216.6	6727	3207.76	26.52	9679.8
YXY	YVR	CRJ9	4	0.8	6215	2968.99	6173	2949.36	78.52	28659.8
YWG	YYC	CRJ9	8	0.8	6027	2881.1	5793	2771.55	876.4	319886.0
YWG	YUL	CRJ9	4	0.8	6870	3274.29	6864	3271.5	11.16	4073.4
YWG	YOW	CRJ9	5	0.8	6270	2994.68	6262	2990.94	18.67	6825.5
YWG	YVR	CRJ9	5	0.8	8980	4248.57	8809	4170.13	392.2	143153.0
YYC	YVR	CRJ9	4	0.8	3172	1532.05	3157	1524.89	28.64	10453.6
YYC	YWG	CRJ9	7	0.8	4246	2042.76	4233	2036.6	43.12	15738.8
YOW	YUL	CRJ9	2	0.8	472	230.28	472	230.28	0	0
YOW	YWG	CRJ9	4	0.8	7838	3722.99	7805	3707.74	61	22265
YXE	YVR	CRJ9	3	0.8	5921	2831.5	5808	2778.58	158.76	57947.4
YQR	YVR	CRJ9	1	0.8	6499	3101.53	6391	3051.16	50.37	18385.05
YEG	YVR	CRJ9	2	0.8	3706	1786.47	3692	1779.82	13.3	4854.5
YHZ	YUL	CRJ9	1	0.8	3396	1638.9	3396	1638.9	0	0
YYZ	YQX	E170	1	0.7	8590	3492.2	8470	3444.5	47.7	17410.5
YYZ	YUL	E170	3	0.7	2304	952.9	2304	952.9	0	0
YYZ	YQR	E170	2	0.7	11465	4626.23	11365	4587.05	78.36	28601.4
YYZ	YXE	E170	4	0.7	12830	5159.05	12760	5131.81	108.96	39770.4
YUL	YHZ	E170	6	0.7	3639	1499.41	3579	1474.94	146.82	53589.3
YUL	YOW	E170	3	0.7	595	247.28	595	247.28	0	0
YUL	YYT	E170	4	0.7	6865	2803.78	6718	2744.83	235.8	86067.0
YUL	YYZ	E170	2	0.7	2448	1012.04	2448	1012.04	0	0
YYT	YUL	E170	5	0.7	8602	3496.96	8553	3477.49	97.35	35532.75
YOW	YUL	E170	3	0.7	536	222.8	536	222.8	0	0
YOW	YQR	E170	2	0.7	12228	4924.49	12157	4896.79	55.4	20221.0
YOW	YXE	E170	2	0.7	13632	5470.48	13459	5403.4	134.16	48968.4
YXE	YOW	E170	2	0.7	9685	3926.04	9669	3919.72	12.64	4613.6
YXE	YYZ	E170	4	0.7	8752	3556.53	8723	3545.02	46.04	16804.6
YQR	YOW	E170	2	0.7	9299	3773.38	9280	3765.86	15.04	5489.6
YQR	YXE	E170	1	0.7	1333	552.83	1333	552.83	0	0
YQR	YYZ	E170	1	0.7	8191	3333.51	8185	3331.12	2.39	872.35
YQX	YYZ	E170	1	0.7	10574	4276.51	10301	4169.05	107.46	39222.9
YHZ	YUL	E170	9	0.7	3899	1605.38	3899	1605.38	0	0
YYZ	YMM	E190	3	0.75	15025	7879.46	14769	7750.4	387.18	141320.7
YYZ	YHZ	E190	2	0.75	5527	2974.93	5449	2933.61	82.64	30163.6
YYZ	YUL	E190	2	0.75	2155	1171.43	2155	1171.43	0	0
YYZ	YOW	E190	5	0.75	1283	699.24	1283	699.24	0	0
YYZ	YQR	E190	6	0.75	10558	5603.32	10482	5564.14	235.08	85804.2
YYZ	YXE	E190	9	0.75	11785	6233.71	11737	6209.12	221.31	80778.15
YYZ	YYT	E190	1	0.75	8666	4623.27	8512	4543.06	80.21	29276.65
YYZ	YWG	E190	1	0.75	7625	4079.77	7605	4069.3	10.47	3821.55
YUL	YEG	E190	2	0.75	16315	8527.4	15947	8342.98	368.84	134626.6
YUL	YHZ	E190	1	0.75	3404	1843.56	3353	1816.21	27.35	9982.75
YUL	YOW	E190	1	0.75	554	302.6	554	302.6	0	0
YUL	YYT	E190	1	0.75	6447	3461.01	6322	3395.11	65.9	24053.5
YUL	YYZ	E190	3	0.75	2280	1238.92	2280	1238.92	0	0
YVR	YYC	E190	1	0.75	2420	1314.45	2420	1314.45	0	0
YYT	YHZ	E190	2	0.75	5076	2735.73	5063	2728.83	13.8	5037.0
YYT	YOW	E190	1	0.75	8610	4594.11	8554	4564.94	29.17	10647.05
YYT	YYZ	E190	8	0.75	10479	5562.59	10345	5493.48	552.88	201801.2
YWG	YYZ	E190	1	0.75	5691	3061.77	5673	3052.24	9.53	3478.45
YYC	YOW	E190	5	0.75	11251	5959.85	11171	5918.76	205.45	74989.25
YOW	YYC	E190	5	0.75	14872	7802.35	14584	7657.02	726.65	265227.25
YOW	YEG	E190	3	0.75	15760	8249.14	15314	8024.98	672.48	245455.2
YOW	YYT	E190	1	0.75	7142	3826.55	6992	3747.78	78.77	28751.05

Depart	Arrive	Aircraft Type	Daily Flights	Cruise Speed (Mach)	Time GC (s)	Fuel Burn GC (kg)	Time Wind (s)	Fuel Burn Wind (kg)	Daily Savings (kg)	Annual Savings (kg)
YOW	YYZ	E190	3	0.75	1433	780.64	1433	780.64	0	0
YXE	YYZ	E190	9	0.75	8254	4408.53	8229	4395.49	117.36	42836.4
YQR	YYZ	E190	5	0.75	7717	4127.93	7713	4125.84	10.45	3814.25
YEG	YVR	E190	1	0.75	4004	2164.7	3987	2155.62	9.08	3314.2
YEG	YOW	E190	2	0.75	10762	5708.41	10753	5703.77	9.28	3387.2
YEG	YYT	E190	1	0.75	16969	8854.35	16890	8814.91	39.44	14395.6
YMM	YYZ	E190	3	0.75	9536	5075.15	9504	5058.57	49.74	18155.1
YHZ	YUL	E190	1	0.75	3630	1964.65	3630	1964.65	0	0
YHZ	YYT	E190	1	0.75	3071	1664.84	3071	1664.84	0	0
YHZ	YYZ	E190	3	0.75	6064	3258.96	6042	3247.34	34.86	12723.9

Appendix D

BADA Files

```
CCCCCCCCCCCCCCCCCCCCCCCCCCCCCCCCCCCCCCCCCCCCCCCC HALE__.APF CCCCCCCCCCCCCCCCCCCCCCCCCCCCCCCCCCCCCCCCCCCCCCCC/
CC                                                                                                             /
CC                 AIRLINES PROCEDURES FILE                                                                    /
CC                                                                                                             /
CC      File_name: HALE__.APF                                                                                  /
CC                                                                                                             /
CC      Creation_date: Oct 01 2014                                                                             /
CC                                                                                                             /
CC      Modification_date: Oct 01 2014                                                                         /
CC                                                                                                             /
CC                                                                                                             /
CC                                                                                                             /
CC   LO= --.-- to --.--  /  AV= --.-- to --.--  /  HI= --.-- to --.--                                          /
CC                                                                                                             /
CC=============================================================================================================/
CC  COM CO    Company name ------climb-------  --cruise--  -----descent------  --approach-  model- /
CC                        mass  lo  hi              lo  hi         hi  lo            (unused)          /
CC    version engines  ma  cas cas mc xxxx xx  cas cas mc  mc cas cas xxxx xx  xxx xxx xxx  opf___ /
CC===:=======:=======::==::===:===:==:====:==::===:===:==::==:===:===:====:==::===:===:===::======:/
CD  *** **    Default Company                                                                           /
CD   HALE     ELECP    LO   30  60 20           35  45 20  20  35  40           0   0   0  HALE__ /
CD   HALE     ELECP    AV   35  60 20           35  45 20  20  35  40           0   0   0  HALE__ /
CD   HALE     ELECP    HI   38  60 20           35  45 20  20  35  40           0   0   0  HALE__ /
CC===:=======:=======::==::===:===:==:====:==::===:===:==::==:===:===:====:==::===:===:===::======:/
CC//////////////////////////////////  THE END  ////////////////////////////////////////////////////////
```

Figure D.1: BADA APF File for Assumed HALE Solar Hybrid Vehicle

BADA PERFORMANCE FILE Oct 01 2014

AC/Type: HALE__

SOURCE OPF FILE: Oct 01 2014
SOURCE APF FILE: Oct 01 2014

Speeds: CAS(LO/HI) Mach Mass Levels [kg] Temperature: ISA
climb - 40/ 50 0.20 low - 2000
cruise - 40/ 70 0.20 nominal - 2100 Max Alt. [ft]: 65000
descent - 45/ 60 0.20 high - 2200

FL	CRUISE				CLIMB					DESCENT		
	TAS [kts]	fuel [kg/min]			TAS [kts]	ROCD [fpm]			fuel [kg/min]	TAS [kts]	ROCD [fpm]	fuel [kg/min]
		lo	nom	hi		lo	nom	hi	nom		nom	nom
0					35	331	315	300	0.0	35	200	0.0
5					35	330	310	295	0.0	40	230	0.0
10					35	325	307	290	0.0	45	250	0.0
15					35	318	303	288	0.0	50	270	0.0
30					35	310	285	273	0.0	50	280	0.0
70	50	0.0	0.0	0.0	35	284	269	258	0.0	55	300	0.0
100	50	0.0	0.0	0.0	45	260	245	233	0.0	60	310	0.0
200	55	0.0	0.0	0.0	50	210	198	180	0.0	65	330	0.0
300	60	0.0	0.0	0.0	55	173	162	152	0.0	70	340	0.0
400	65	0.0	0.0	0.0	62	145	134	119	0.0	85	350	0.0
500	70	0.0	0.0	0.0	72	103	93	82	0.0	80	380	0.0
600	80	0.0	0.0	0.0	83	60	50	42	0.0	90	390	0.0
650	88	0.0	0.0	0.0	85	48	32	25	0.0	90	400	0.0

Figure D.2: BADA PTF File for Assumed HALE Solar Hybrid Vehicle

```
CCCCCCCCCCCCCCCCCCCCCCCCCCCCCCCCCCCCCCCCCCCCCCC HALE__.OPF CCCCCCCCCCCCCC/
CC                                                                        /
CC                AIRCRAFT PERFORMANCE OPERATIONAL FILE                   /
CC                                                                        /
CC                                                                        /
CC      File_name: HALE__.OPF                                             /
CC                                                                        /
CC      Creation_date: Oct 01 2014                                        /
CC                                                                        /
CC      Modification_date: Oct 01 2014                                    /
CC                                                                        /
CC                                                                        /
CC====== Actype ===========================================================/
CD   HALE__          2 engines    Piston                              S    /
CC   VT              HALE with 2  ELECP    engines          wake          /
CC                                                                        /
CC====== Mass (t) =========================================================/
CC    reference      minimum      maximum     max payload  mass grad  /
CD     .21000E+01   .18000E+01   .22000E+02   .04000E+01   .00000E+00 /
CC====== Flight envelope ==================================================/
CC     VMO(KCAS)       MMO        Max.Alt       Hmax       temp grad  /
CD     .10000E+03   .20000E+00   .65000E+05   .00000E+00  .00000E+00  /
CC====== Aerodynamics =====================================================/
CC Wing Area and Buffet coefficients (SIM)                                /
CCndrst Surf(m2)     Clbo(M=0)       k           CM16                     /
CD 5   .23800E+03   .13000E+01   .00000E+00   .00000E+00                  /
CC   Configuration characteristics                                        /
CC n Phase  Name    Vstall(KCAS)    CD0          CD2         unused     /
CD 1 CR   Clean     .20000E+02   .00150E+01   .14700E-01   .00000E+00 /
CD 2 IC   Clean     .18000E+02   .00000E+00   .00000E+00   .00000E+00 /
CD 3 TO   Clean     .17000E+02   .00000E+00   .00000E+00   .00000E+00 /
CD 4 AP   Clean     .17000E+02   .00000E+00   .00000E+00   .00000E+00 /
CD 5 LD   Clean     .17000E+02   .00000E+00   .00000E+00   .00000E+00 /
CC   Spoiler                                                             /
CD 1      RET                                                            /
CD 2      EXT                                .00000E+00   .00000E+00 /
CC   Gear                                                                /
CD 1      UP                                                             /
CD 2      DOWN                  .00000E+00   .00000E+00   .00000E+00 /
CC   Brakes                                                              /
CD 1      OFF                                                            /
CD 2      ON                                 .00000E+00   .00000E+00 /
CC====== Engine Thrust ====================================================/
CC         Max climb thrust coefficients (SIM)                            /
CD     .23000E+04   .68000E+05   .12000E+04   .00000E+00   .00000E+00 /
CC      Desc(low)    Desc(high)   Desc level   Desc(app)    Desc(ld)  /
CD     .10000E+00   .10000E+00   .16000E+05   .00000E+00   .00000E+00 /
CC      Desc CAS     Desc Mach    unused       unused       unused    /
CD     .35000E+02   .18600E+00   .00000E+00   .00000E+00   .00000E+00 /
CC====== Fuel Consumption =================================================/
CC   Thrust Specific Fuel Consumption Coefficients                        /
CD     .00000E+00   .00000E+00                                           /
CC   Descent Fuel Flow Coefficients                                      /
CD     .00000E+01   .00000E+00                                           /
CC   Cruise Corr.     unused       unused       unused       unused    /
CD     .00000E+01   .00000E+00   .00000E+00   .00000E+00   .00000E+00 /
CC====== Ground ===========================================================/
CC        TOL          LDL        span         length       unused    /
CD     .20000E+04   .80000E+03   0.3110E+03   .95000E+02   .00000E+00 /
CC=========================================================================/
FI                                                                        /
```

Figure D.3: BADA OPF File for Assumed HALE Solar Hybrid Vehicle